THE UNIVERSITY OF ADELAIDE
Department of Civil and Environmental Engineering

Strengthening of reinforced concrete beams by bolting steel plates to their sides

A Thesis

by

Marfique Ahmed

B. Sc. in Civil Engineering (BUET, Bangladesh)

Submitted to the Research and Graduate Studies Branch

for the Degree of **Master of Engineering Science**

October, 1996

Strengthening of Reinforced Concrete Beams by Bolting Steel Plates to their Sides

by Marfique Ahmed

Corrigenda

Page 14 line 12
As a linear behaviour of ....

Page 14 line 13
assumed, the longitudinal ...

Page 31 line 12
research on bolted plated beams which will ....

Page 35 line 6
axes in Fig. 3-2(b) as h_{na}, the magnitude of which is unknown at this stage.

Page 38 line 11
that a partial-shear-connection analysis always deals with partial interaction ...

Page 49 line 9
elastic but the shear connectors are plastic. These assumptions are ...

Page 77 line 22
beam is divided into a number of segments ....

Page 83 line 17 and 18
the ductility now increases with the increase of h/D; the strength and stiffness also increase as ....

Page 155 line 5
longitudinal shear force and vertical shear force. Eight beams were tested where two were ...

Page 226 line 7
reduces to 107.40 kN. The longitudinal force can be seen increasing ...

Page 243 line 26
the load started to drop off, and spalling was noticed at an applied load of ...

To my mother Feroza Ahmed,
father Dr. Mozaffar Ahmed and
wife Bulbuli Nishat

ABSTRACT

A preliminary study of the strengthening of existing reinforced concrete beams by bolting steel plates to their sides has been presented. The study shows that the elements in the plated beams slip relative to each other both longitudinally and vertically. Due to the vertical slip, the longitudinal shear force reduces relative to the value with no vertical slip and hence the rigid plastic ultimate strength also reduces. Mathematical models to quantify the vertical slip and the vertical shear forces have been developed and then a design procedure for plated beams is described. Furthermore, a suite of non-linear computer models are described that are used to analyse side plated beams with various degrees of longitudinal and vertical interaction.

Twenty-four push specimens with different types of bolted shear connectors have been tested to find a suitable connector for side plated beams. Two unplated and six plated beams were tested. The variations in the plated beams are the degrees of shear connection and the depth of the plates.

Publications

The following papers were published in **conference proceedings** based on the outcomes of this research project.

A) **Oehlers D. J. and Ahmed M., (1995),** *Design procedures for bolting steel plates to the sides of reinforced concrete beams*, Proceedings of the International Conference on Structural Stability and Design, Sydney, Australia, P333-336.

B) **Ahmed, M. and Oehlers D. J. (1995),** *Strengthening of RC Beams by Bolting Vertical Sandwich Plates*, Proceedings of the 14th Australasian Conference on the Mechanics of Structures and Materials, Tasmania, Australia, P12-17.

C) **Oehlers D. J. and Ahmed, M., (1996),** *Upgrading reinforced concrete beams by bolting steel side plates*, Bridge Management 3: Inspection, maintenance, assessment and repair, edited by Harding, J. E., Parke, G. A. R. and Ryall, M. J., Third International Conference on Bridge Management, UK.

D) **Ahmed, M and Oehlers D. J., (1996)** *Ultimate strength analysis procedures for reinforced concrete beams with externally attached side sheets or plates*, To be published in the proceedings of 3rd Asia-Pacific Conference on Computational Mechanics.

The following paper was submitted as a **journal** publication.

A) **Oehlers, D. J., Nguyen, N. T., Ahmed, M and Bradford, M. A., (1996),** *The effect of partial interaction in composite beams with mechanical shear connectors*, Submitted for publication in the Journal of Construction Steel and Research.

Statement of originality

This work contains no material which has been accepted for the award of any other degree or diploma in any university or other tertiary institution and, to the best of my knowledge and belief, contains no material previously published or written by another person, except where due reference has been made in the text.

I give my consent to this copy of my thesis, when deposited in the University Library, being available for loan and photocopying.

SIGNATURE..... **DATE** 30/10/96

ACKNOWLEDGMENTS

The project was supervised by Dr. D. J. Oehlers, Senior Lecturer in the Department of Civil and Environmental Engineering, the University of Adelaide. His advice, assistance and encouragement to accomplish the project is gratefully acknowledged. I express my deepest gratitude to him for his excellent guidance and enthusiastic supervision and, also for his review of the thesis.

I would like to thank Dr. N. Nguyen, Post Doctoral Fellow, who provided advice during the work of the project. Especially, I am grateful to Mr. M. J. Burnet, Ph. D. student, who kindly made his computer programme available which was the initial start of the computing work of this project. Also his assistance in using different software is appreciated. I am thankful to Mr. Stephen Carr, Computing Officer who always gave kind attention to me whenever there was a problem with the computer systems.

The experimental works of this project was funded from a part of a Large Australian Research Council grant which made this study possible. Mr. David Hale, Laboratory technician gave invaluable help in the preparation of the experimental work. It was impossible to do the experimental works without his sincerity and hard work. Mr. W. Eidam, Laboratory Manager, Mr. B. Kelman, Laboratory technician, and Mr. T. Sawosko also gave their support during different parts of the experimental work, which I would like to express my appreciation for.

I am also thankful to the academics, staff and post graduate students who provided friendship, advice and assistance. Especially, I would like to thank Nyugen, Abir Ghosh and M. Ali. Also, thanks to Mr. Paul Morgan for proof reading this thesis.

I remain indebted to my parents, brother and sister in Bangladesh who felt a long aching separation from me for the last two years and gave me moral support with the necessary boost during my hours of depression. The love and encouragement I received from my wife, Nishat has been a great source of strength to me when times were tough. I appreciate her worthy patience during many a puzzling time.

Finally, I am grateful to Mr. Q. I. Siddique, Chief Engineer, Local Goverment Engineering Department (LGED), Bangladesh for his kind approval on my deputation to

carry out this study at the University of Adelaide. I also remember all of the other officers and staff of LGED who wished me a successful study. Especially, thanks to Mr. A. K. Farhad Ahmed of LGED for his kind advice. Furthermore, I was supported by the Australian Agency for International Aid (AusAid) which is gratefully acknowledged.

Table of Contents

Page

Page

Page

Page

Page

ABBREVIATION

ACI	American Concrete Institute
ASCE	American Society of Civil Engineers
CL	centre line
LVDT	low voltage displacement transducer
n-a	neutral axis
N-E	North-East
NLA	non-linear analysis
N-W	North-West
RC	reinforced concrete
RPA	rigid plastic analysis
S-E	South-East
S-W	South-West
UDL	uniform distributed load

Principal notation

A_{conc} = cross-sectional area of concrete element;

A_m = area of moment diagram;

A_{plate} = area of plate element;

A_{rc} = area of compressive reinforcing bars;

A_r, A_{rt} = area of tensile refinforcing bars;

A_{sh} = area of axial force diagram;

A_{steel} = area of steel section;

A_{stud} = cross-sectional area of the shank of a stud shear connector;

a = depth of rectangular stress block in reinforced concrete beam;

b = width of reinforced concrete beam;

b_c = effective width of concrete slab;

c = characteristic strength; clearance in the plate hole;

D = Depth of reinforced concrete beam;

D_b = diameter of bolt;

D_{max} = dowel strength of shear connector;

$(D_{max})_{push}$ = dowel strength of shear connector when used in push specimen;

$(D_{max})_{beam}$ = dowel strength of shear connector when used in beam specimen;

d = effective depth of reinforced concrete beam;

d_{sh} = diameter of the shank of a stud shear connector;

dx = length of a segment in a beam;

$(EI)_c$ = flexural rigidity of concrete element;

$(EI)_p$ = flexural rigidity of plate element;

E = normalized strain;

E_c = elastic modulus of concrete;

E_p = elastic modulus of plate;

E_s = elastic modulus of steel;

e = ecentricity of load;

F = applied load; ductility factor; internal axial forces; force profile;

F_b = bond force;

$(F_b)_{fi,fsc}$ = full-shear-connection full-interaction bond force;

$(F_b)_{pi,fsc}$ = full-shear-connection partial-interaction bond force;

$(F_b)_{pi,psc}$ = partial-shear-connection partial-interaction bond force;

F_{con} = force in the concrete element;

F_{plate} = force in the plate element;

F_{reo}, $F_{reo,t}$ = force in the tesile reinforcement;

$F_{reo,c}$ = force in the compressive reinforcement;

F_{steel} = force in the steel element;

F_{shear} = longitudinal shear forces at steel/concrete interface;

$(F_{shear})_{c1}$ = longitudinal shear force in concrete element in segment 1;

$(F_{shear})_{p1}$ = longitudinal shear force in plate element in segment 1;

f_c = compressive cylinder strength of concrete;

f_{cb} = splitting tensile strength of concrete;

f_{cf} = modulus of rupture strength of concrete;

f_{cu} = compressive strength of concrete of cube specimens;

f_t = tensile strength of concrete;

f_u = tensile strength of stud material;

f_y = yield strength of steel;

f_{yp} = yield strength of plate;

f_{yr} = yield strength of reinforcing bars;

H = horizontal frictional force; force in a shear connector normal to the interface;

h = height of plate;

h_b = vertical position of bolts;

h_c = distance between the centroid of concrete element and the steel-concrete interface in a standard composite beam; distance between the centriod of concrete element and top of concrete element in a side plated beam;

h_{conc} = height of concrete slab in standard composite beam;

h_d = distance between mid-depth of plate and top of concrete element;

h_f = depth of plate that resist flexure due to vertical shear force;

h_{na} = distance between the neutal axis of concrete element and steel or plate element;

h_o = distance between the top of plate and top of reinforced concrete element;

h_p = distance between the centroid of plate element and top of concrete element;

h_s = distance between the centroid of steel element and the steel-concrete interface;

h_{steel} = height of steel I-section in standard composite beam;

I_c = second moment of area of concrete element;

I_p = second moment of area of plate element;

I_s = second moment of area of steel element;

K_{si} = initial modulus of load-slip curve;

K_{end} = modulus of load-slip curve at fracture;

L = length of shear span;

l =distance between resulatnt longitudinal force of shear connectors and resultant longitudinal internal force;

l_b = length of bolt;

M = applied moment;

M_{conc} = moment in concrete element;

$(M_{fi})_{fsc}$ = full-shear connection full-interaction moment capacity;

M_{max} = maximum moment;

$(M_{pi})_{fsc}$ = full-shear connection partial-interaction moment capacity;

M_{plate} = moment in the plate element;

M_{steel} = moment in the steel element;

m = total number of connectors in a shear span;

n = numbers of shear connectors in a group; numbers of shear connectors fail in a group;

$n_{v,end}$ = numbers of connector to resist vertical shear force at support end;

$n_{v,mid}$ = numbers of connector to resist vertical shear force at center of the beam;

P_{max} = ultimate load;

P, P_1 = resulatnt longitudinal shear force;

P_{bolt} = design vertical shear force in a bolted shear connector;

$(P_{bolt})_{shear}$ = maximum shear force in a bolted shear connector;

P_{shear} = strength of longitudinal shear connection in a shear span;

P_{split} = load to cause concrete element to split;

P_{comp} = compressive force in the plate element;

P_{plate} = resultant axial force in the plate element;

P_{ten} = tensile force in the plate element;

q = longitudinal shear force per unit length;

R = reaction at support;

S = normalized stress;

s = longitudinal spacing of connectors;

s_h = longitudinal slip;

$s_{h,max}$ = maximum longitudinal slip;

s_{h1} = longitudinal slip in segment 1;

s_{h2} = longitudinal slip in segment 2;

s_v = vertical slip;

s_{v1} = vertical slip in segment 1;

s_{v2} = vertical slip in segment 2;

$(s_v)_t$ = total vertical slip;

t = depth of slice;

t_p = thickness of plate;

V, V_1 = resultant vertical shear force;

y_c = deflection of concrete element;

y_p = deflection of plate element;

y_n = neutral axis position when full-interaction;

y_{nc} = neutral axis position in concrete element;

y_{np} = neutral axis position in plate element;

y_{n1} = neutral axis position in the top element;

y_{n2} = neutral axis position in the bottom element;

y_i, y_j = distance between the mid-depth of slice and the level of connectors;

y_{c1} = neutral axis in the concrete element in segement 1;

y_{p1} = neutral axis in the plate element in segment 1;

β = reduction factor of force in a bolted shear connector;

γ = neutral axis parameter;

γ_1 = define shape of loading portion of stress-strain curve of concrete;

γ_2 = define shape of unloading portion of stress-strain curve of concrete;

Δs_h = change in longitudinal slip;

Δs_{v1} = change in vertical slip;

ε = strain; strain profile

ε_c = strain in concrete;

ε_i = strain at i-th slice;

ε_p = strain in the plate element;

ε_s = strain in the steel element;

ε_{strain} = slip strain in composite beam;

ε_t = tensile failure strain of concrete;

ε_y = yield strain of steel element;

ε_{yp} = yield strain of plate;

η = degree of shear connection;

κ = curvature;

κ_c, κ_{cl} = curvature in the concrete element;

$(\kappa_{max})_c$ = curvature at maximum moment in concrete element;

κ_p, κ_{pl} = curvature in the plate element;

$(\kappa_{max})_p$ = curvature at maximum moment in plate element;

κ_u = curvature at maximum moment when full-interaction;

κ_y = curvature at first yield of tensile reinforcing bars;

σ = stress; stress profile;

σ_c = stress in concrete;

σ_u = cylinder strength of concrete;

Chapter One

Introduction

In practice, situations arise where existing concrete slabs are found to be inadequate and in need of strengthening (Van Gemert, 1981; Parkinson, 1978; Jones et al, 1988). A very common remedial procedure that can be applied in this situation is to glue steel plates to the tension face of the slabs (Oehlers, 1995). As this system is very prone to premature debonding, occasionally bolts are placed at the ends of the plate as shown in Fig. 1-1 (Oehlers and Burnet, 1994). This technique is relatively easy to use, fast, and can be applied effectively while the structure remains in use. Site disruption and reductions in room height are minimal with this technique. Furthermore, it is inexpensive and can be less than half the cost of alternative techniques (Wyatt and Oehlers, 1992; Oehlers and Wyatt, 1993).

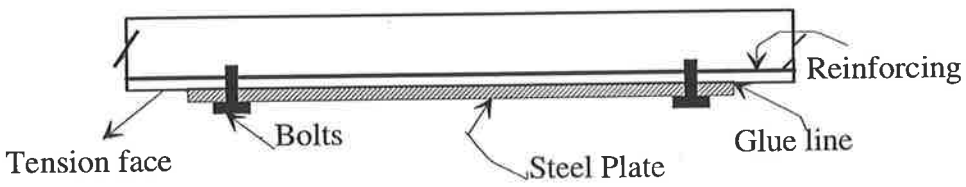

Fig. 1-1 Plated slab

The same technique can be applied to upgrading reinforced concrete beams as shown in Fig. 1-2, but premature debonding of the plate can occur due to flexural peeling (Oehlers and Moran, 1990) and shear peeling (Oehlers, 1992) as shown. Flexural peeling can be prevented by judicious design (Oehlers, 1995), however, shear peeling cannot be prevented as this occurs at the shear strength of the reinforced concrete beam without

stirrups and, therefore, this is not affected by the presence of stirrups (Oehlers, 1990). Hence, shear peeling is a major restriction in plated beam construction, as debonding will occur at relatively small shear loads. Besides peeling, some other minor problems are also found in soffit plated beams. The plate acts as tensile reinforcement and, therefore, the ductility requirements and the strength of the concrete section limit the area of plate that can be added. Also, the plate cannot prevent the occurrence of the diagonal crack in the unplated region as shown in Fig. 1-2.

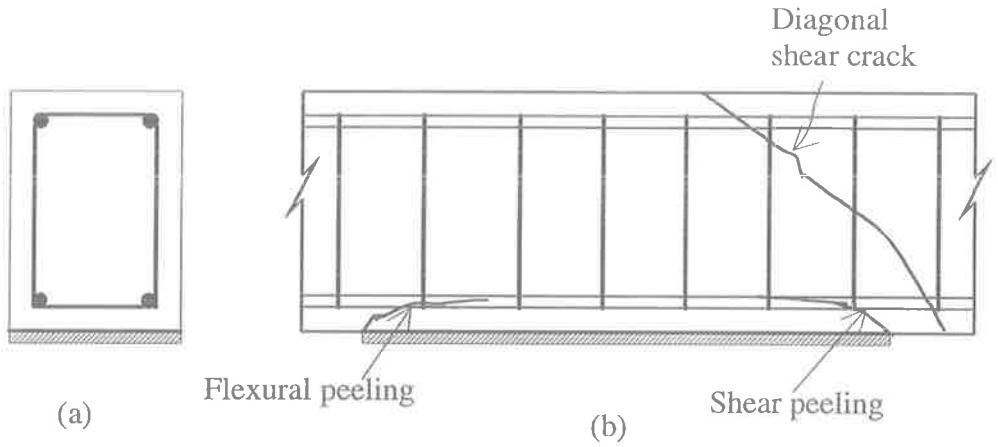

Fig. 1-2 Soffit plated beam

Premature shear peeling in soffit plated beams can be avoided by bonding steel plates to the sides of the reinforced concrete beam as shown in Fig. 1-3 (Luo, 1993; Al-Sulaimani et al, 1994). In this system, the soffit plate increases the flexural strength of the beam and the side plate inhibits shear peeling. As an alternative, the steel plate can be bolted to the sides of the reinforced concrete beam from end to end as shown in Fig. 1-4. This technique will be studied in this research. This system is not restricted by shear peeling, the plates do not reduce the ductility of the reinforced concrete section, and there is no theoretical limit to the increase in flexural strength. However, this system will have interface longitudinal slip and vertical slip which can effect the stiffness and strength of the side plated beam. The longitudinal slip induces slip strain, whereas the vertical slip induces a difference in curvatures between the concrete element and plate element. In this research, a preliminary study on both of these slips will be described and a design procedure will be given. The disposition of the thesis is given below.

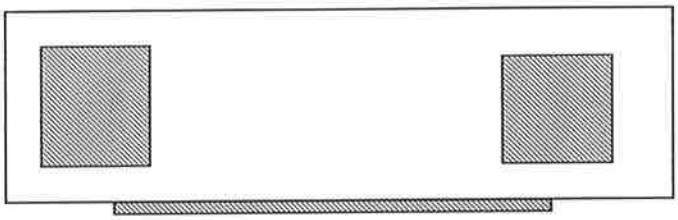

Fig. 1-3 Side plate to resist shear peeling

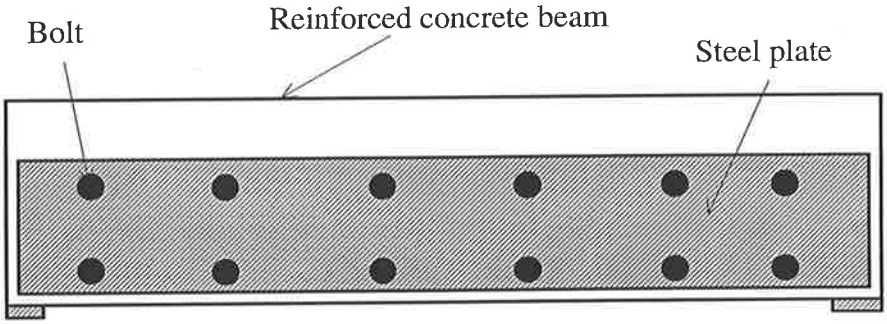

Fig. 1-4 Side plated beam

DISPOSITION OF THE THESIS

In Chapter 2 a literature review is presented on existing theory and computer models for standard composite beams that have been used in this research. Chapters 3 and 4 cover the basic theories for longitudinal shear forces and vertical shear forces, respectively, that are used in the development of the computer models in Chapter 5 to analyse the plated beams. The computer model is then used in its simplest form of full interaction to, firstly, study the ductility behaviour of plated beams, in Chapter 6, and, secondly to develop γ factors for use in determining the longitudinal bond force in plated beams in Chapter 7. Chapter 8 describes the experimental work on push tests of bolted shear connectors and plated beam tests. Chapter 9 describes the analysis and design procedure for vertical slips and the conclusions are given in Chapter 10.

Chapter Two

Literature Review

2.1 INTRODUCTION

No published literature is available on the strengthening of existing reinforced concrete (RC) beams by bolting plates to their sides. However, much research is available on the strengthening of RC beams by gluing steel plates to their tension face (Swamy et al, 1987; Mckenna and Ekri, 1994; Ziraba et al, 1994) and a small amount of research on gluing plates to the sides of RC beams (Luo, 1993; Smith, 1995). As glue is stiff and provides full-interaction between the bonded elements, no relative slip occurs at the interface between the elements. On the other hand, bolts are flexible and provide partial-interaction between the elements allowing slip at the interface. Therefore, the major difference between plated beams with glue and plated beams with bolts lies in their different composite actions due to differences in the bonding material properties. It follows that the theory of plated beams with glue is not applicable to plated beams with bolts. Instead, the behaviour and hence theory of standard composite beams with mechanical shear connectors and composite profiled beams with rib shear connectors are applicable because their behaviour depends on interface slip. Therefore, nothing will be discussed in this chapter on the existing research on the plated beams with glue. Only the theory and the models of both the standard composite beam and the composite profiled beam have been discussed in this literature review.

First, the rigid plastic ultimate flexural strength analysis procedures for standard composite beams and for composite profiled beams will be described. Then the serviceability behaviour of standard composite beams will be discussed by taking into account the interface slip. This will be followed by a procedure for determining the dowel strength of mechanical shear connectors and the splitting resistance of slabs as these are relevant to the design of bolted connections in plated beams. Finally, an existing computer model for the non-linear analysis of standard composite beams will be described as this model has been extended in this research to analyse the plated beams.

2.2 RIGID PLASTIC ANALYSIS

Rigid plastic analysis is a non-linear equilibrium analysis technique that is used to determine the maximum possible strength of a composite beam. This is a simple procedure and generally applied by assuming that the materials are at their plastic stage. First, the rigid plastic material properties and then the rigid-plastic analysis procedure of standard composite beam and composite profiled beam will be described in the following sections.

2.2.1 Rigid Plastic Material Properties

Rigid plastic material properties allow for the non-linearity in the materials by assuming idealised material properties as represented in Fig. 2-1, where, f_c is the compressive strength of the concrete, f_y is the yield strength of steel, and D_{max} is the dowel strength of the shear connectors.

2.2.1.1 Material properties of concrete

Rigid plastic analysis requires large curvatures κ in concrete as shown in Fig. 2-2(b) and therefore, the strain gradient is also very large. A typical example of the stress distribution is shown in (c) in which the concrete is in compression in region A, is in tension in region B and cracked through tension in region C. Because of the large curvature and hence the strain gradient, the tensile region B is very small compared to the compressive region A. Hence, the tensile strength of the concrete is assumed to be zero in rigid plastic analyses.

The steel element in the standard composite beam is not encased by the concrete element and as such there is no necessity to ensure that the steel element is fully yielded when the concrete crushes at a strain of about 0.003. This means that there is no need to define the real neutral axis by using the γ factor that is usually applied to reinforced concrete beam design. It is usually assumed in the rigid plastic analysis that the concrete in compression is fully yielded at a strength of $0.85f_c$ with an unlimited plastic plateau as shown in Fig. 2-1.

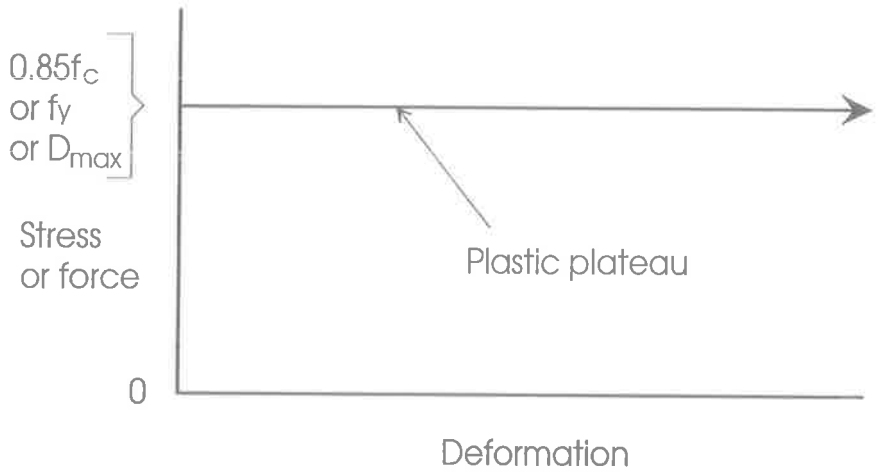

Fig. 2-1 Idealised material properties

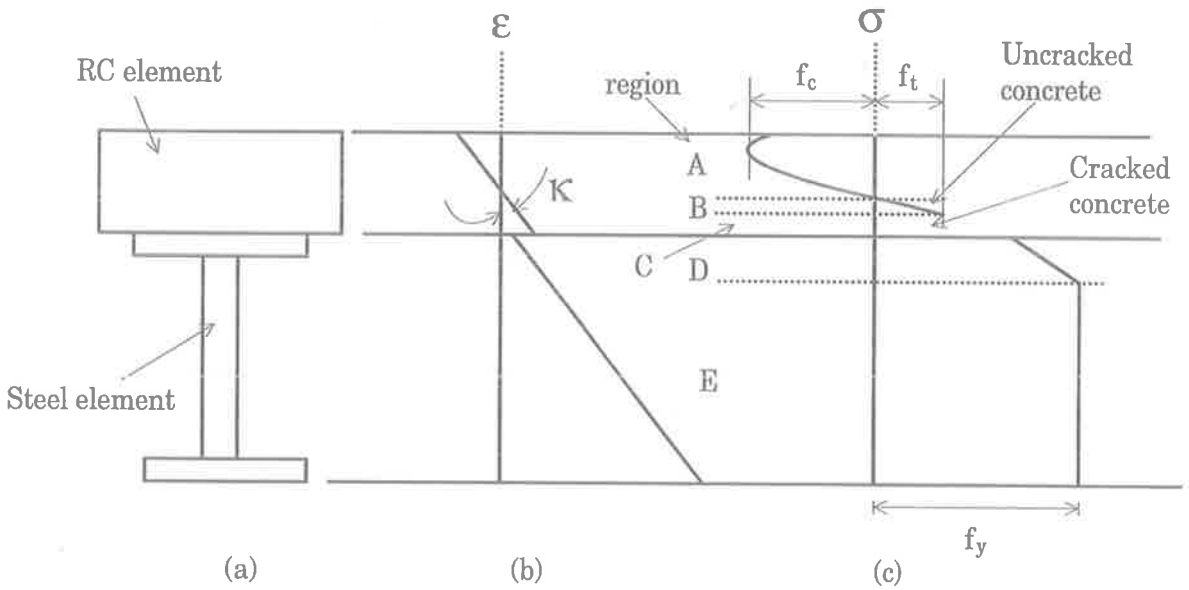

Fig. 2-2 Real behaviour of composite beams (Oehlers and Bradford, 1995)

2.2.1.2 Material properties of steel

Usually fracture of the concrete occurs much sooner than fracture of the steel. Thus the steel element is assumed to have an unlimited strain capacity, as in Fig. 2-1. Also, because of the large curvature in the steel element, the linear elastic zone D in the stress distribution in Fig. 2-2(c) would be very small and can be assumed to be fully yielded. Hence, the steel in compression and in tension are both assumed to be fully yielded at the yield strength of f_y.

2.2.1.3 Material properties of shear connectors

The rigid plastic analysis assumes that the shear connectors are always fully loaded at an effective yield load of D_{max}, as shown in Fig. 2-1, and that they have an unlimited slip capacity.

2.2.2 Analysis of Standard Composite Beam

The analysis of a standard composite beam in Fig. 2-3(a) depends on two important phenomena which are the degree of shear connection and the degree of interaction. The degree of shear connection deals with the strength of the shear connection in a composite beam, whereas the degree of interaction deals with the flexibility or the stiffness of the shear connection. Although there is no direct relation between them, both of them increase with the number of shear connectors in the shear span.

The degree of shear connection is generally expressed as either full-shear-connection or partial-shear-connection. Full-shear-connection is defined as the least number of connectors, above which the bending resistance of the beam will not be increased if more connectors were provided (Johnson and Molenstra, 1991). Conversely when the numbers of shear connectors in a shear span is less than that required for full-shear-connection then this is termed as partial-shear-connection.

The degree of interaction is generally expressed as either full-interaction or partial-interaction. Full interaction refers to the case when there is no slip at the interface of the

composite beam, whereas partial-interaction refers to the case when there is slip at the interface.

In the following sections, the analysis procedure for full-shear-connection with full interaction and with partial-interaction will first be described. This will be followed by the analysis procedure for partial-shear-connection that always assumes partial-interaction.

2.2.2.1 Full-shear connection analysis

The rigid-plastic full-shear-connection analysis of a standard composite beam is determined by finding a stress distribution that ensures equilibrium of the longitudinal forces. This will be described below for full-interaction and partial-interaction.

2.2.2.1.1 Full-interaction

A standard full-shear-connection full-interaction rigid-plastic analysis of the standard composite beam in Fig. 2-3(a) is summarised in (b) to (d). As we are dealing with full interaction, the strain profile is assumed to be uni-linear as shown in (b) i.e. the slip strain at the interface between the concrete element and the steel element is zero. The position of the neutral axis is determined by moving the strain profile in (b) up and down until we find a stress distribution as in (c) where the resultant compressive force F_{con} in (d) is equal to the tensile force F_{steel}. Once these forces and their positions are known, we can then take moments to determine the rigid-plastic full-shear-connection full-interaction flexural capacity. It can be seen that the analysis is extremely simple.

2.2.2.1.2 Partial-interaction

In reality, the condition of full-interaction cannot be achieved as mechanical shear connectors must slip across the interface to transfer forces between the elements. As such, a parallel bi-linear strain profile occurs as in Fig. 2-4(b). The step change in the strain profile across the interface is defined as the slip strain (ds/dx), which is equal to the derivative of the slip along the length of the beam (Johnson, 1994).

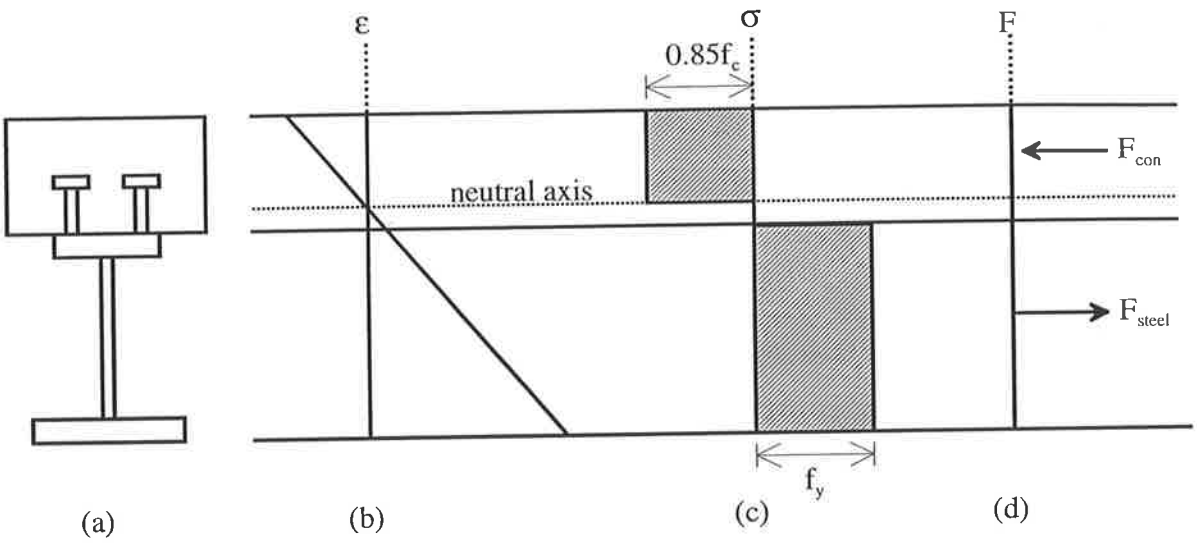

Fig. 2-3 Full-shear-connection full-interaction analysis

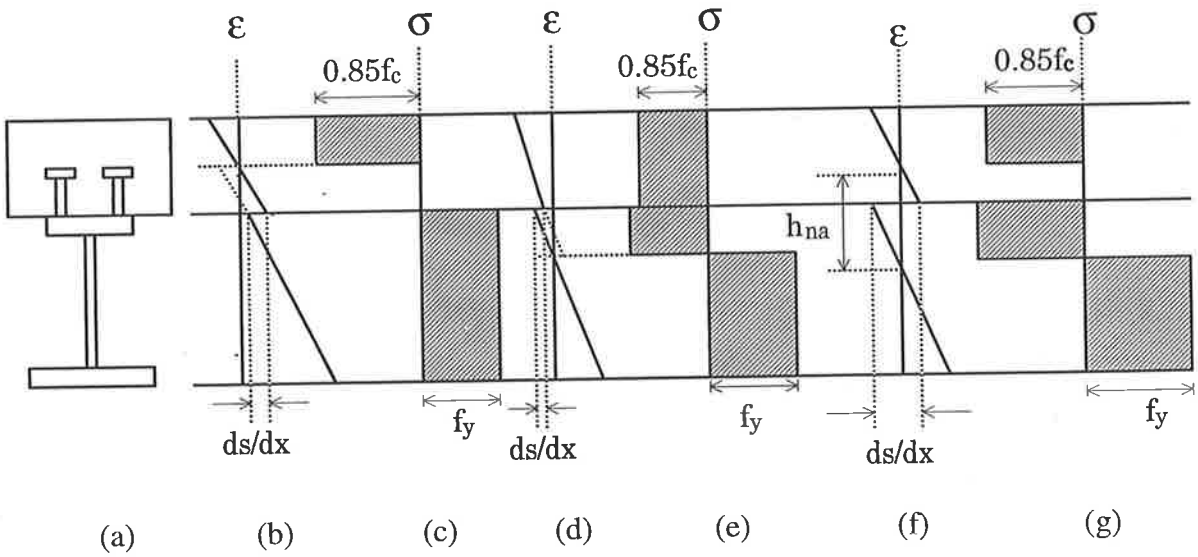

Fig. 2-4 Full-shear-connection partial-interaction analysis

It can be seen in Fig. 2-4 that the neutral axes of the strain profiles of both the concrete element and the steel element may lie either in the concrete element as in (b), in the steel element as in (d), or in the respective elements as in (f). The respective stress profiles are shown in (c), (e) and (g) respectively. However, and in all the cases, if we know the distance between the neutral axes h_{na}, then we can move the strain profiles up or down until we find a stress distribution in which the longitudinal forces are in equilibrium. We can then determine the rigid-plastic full-shear-connection partial-interaction flexural

capacity from the longitudinal forces. It can be seen that the strength of the shear connection is not used in these full-shear-connection analyses for both full-interaction and partial-interaction.

It is important to note that the full-shear-connection partial-interaction strength in Fig. 2-4(c) is the same as the full-shear-connection full-interaction strength in Fig. 2-3(c), because both neutral axes in Fig. 2-4(b) lie in the concrete element. The same can be said for the strain distribution in Fig. 2-4(d), when both neutral axes in (d) lie in the steel element. Hence, for standard composite beams in which one element is fully above the other, the partial-interaction strength is the same as the full-interaction strength when both neutral axes lie in the same element. In contrast, the full-shear-connection partial-interaction strength in Fig. 2-4(g) is less than the full-shear-connection full-interaction strength because the neutral axes in (f) lie in different elements. Therefore, it can be concluded that partial-interaction can, but does not necessarily always, reduce the full-shear-connection rigid-plastic strength.

2.2.2.2 Partial-shear-connection analysis

In order to ensure full-shear-connection in the standard composite beam, the strength of the shear connectors in the shear span P_{shear} must be greater than or equal to the force in the concrete element, F_{con}, or in the steel element, F_{steel}, as derived by a full-shear-connection analysis as in Fig. 2-3. Hence, the maximum strength of shear connection required for full-shear-connection $(P_{shear})_{fsc} = F_{con} = F_{steel}$. When $P_{shear} < (P_{shear})_{fsc}$, the degrees of shear connection, η, can be defined as the strength of the shear connection, P_{shear}, as a proportion of the full-shear-connection strength, $(P_{shear})_{fsc}$, so that $\eta = P_{shear}/(P_{shear})_{fsc}$ (Oehlers and Bradford, 1995). When $P_{shear} < (P_{shear})_{fsc}$, the resultant force in all of the components of the composite beam is equal to P_{shear}, as shown in Fig. 2-5(d). This is referred to as partial-shear-connection.

In a partial-shear-connection analysis, the shear forces control the axial forces in the composite beam. Therefore, neither the steel nor the concrete elements are fully stressed in one direction (Oehlers and Bradford, 1995). As P_{shear} is less than $(P_{shear})_{fsc}$, both elements will have a neutral axis as shown in Fig. 2-5(b) and hence partial-shear-connection is

always associated with partial-interaction. The position of the neutral axis in concrete element, y_{nc}, can be derived from

$$P_{shear} = 0.85 f_c b y_{nc} \quad \text{.....(2.1)}$$

The position of the neutral axis in the steel element, y_{np}, can be evaluated from the steel element in (b), by determining the level at which the resultant force in the steel is equal to the shear strength, P_{shear}. Having defined the neutral axes positions, we can now determine the magnitude and position of the axial forces. Then the flexural capacity can be derived by taking the moments of the axial forces.

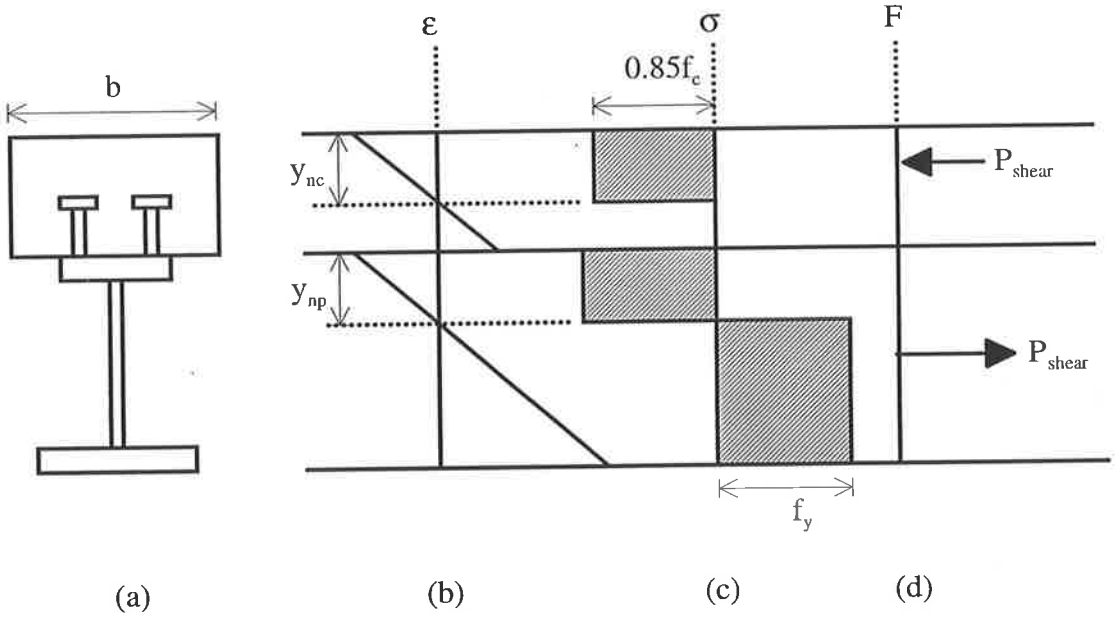

Fig. 2-5 Partial-shear-connection analysis

2.2.3 Analysis of Composite Profiled Beam

The composite profiled beams and the side plated beams are similar in the sense that they both have some sort of steel elements on their sides. Therefore, the rigid plastic analysis of composite profiled beam will be described in this section.

The rigid plastic analysis of the composite profiled beam in Fig. 2-6(a) is similar but not the same as the standard composite beam. In this case, the depth of the neutral axis in the concrete element is not assumed to be the same as the depth of the concrete compression block. The reason is that when the thickness of the profiled sheet in Fig. 2-

6(a) tends to zero, the analysis reverts to that of a normal RC beam and it is the common procedure in RC beam design to use the γ factor in determining the position of the neutral axis. Therefore, the depth of the concrete compression block in composite profiled beam is determined by taking into account the γ factor.

2.2.3.1 Full-shear-connection analysis

A full-shear-connection full-interaction analysis of an idealised composite profiled beam is shown in Fig. 2-6 (Oehlers et al, 1994). When there is full-shear-connection and full-interaction, the neutral axes of both the elements coincide as shown in (b), with the corresponding stress profiles of the concrete and the steel elements, occurring as shown in (c) and (d) respectively.

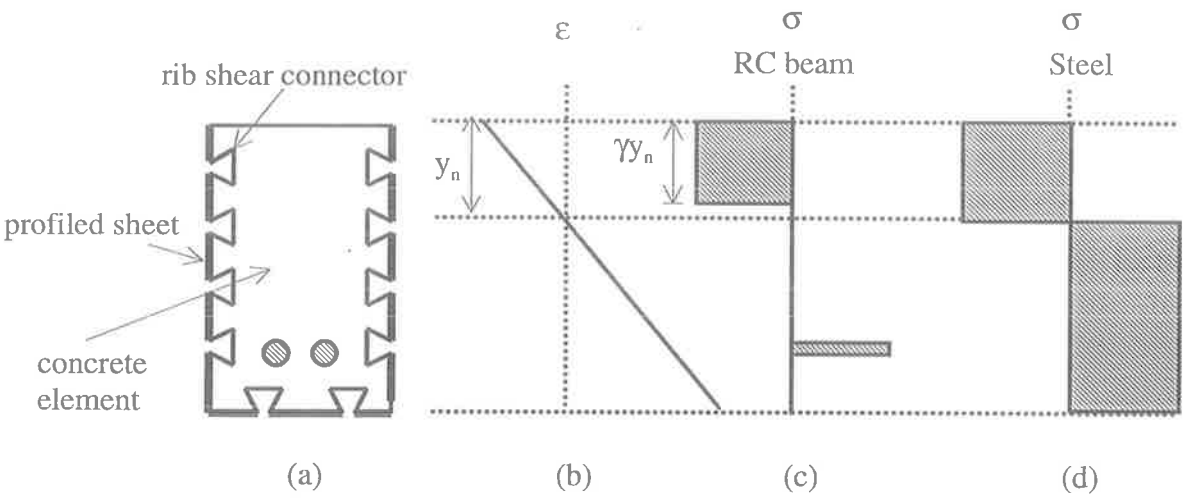

Fig. 2-6 Full-shear-connection full-interaction analysis

The position of the neutral axis, y_n in Fig. 2-6(b) is derived using the standard procedure of equating the compressive strength above the neutral axis to the tensile strength below the neutral axis. Having derived the position of the neutral axis, the stress distributions in each element shown in (c) and (d) are known, so the flexural capacity with full-shear-connection and full-interaction can be determined. The *bond strength* can then be derived from the resultant force in either of the elements in (c) or (d).

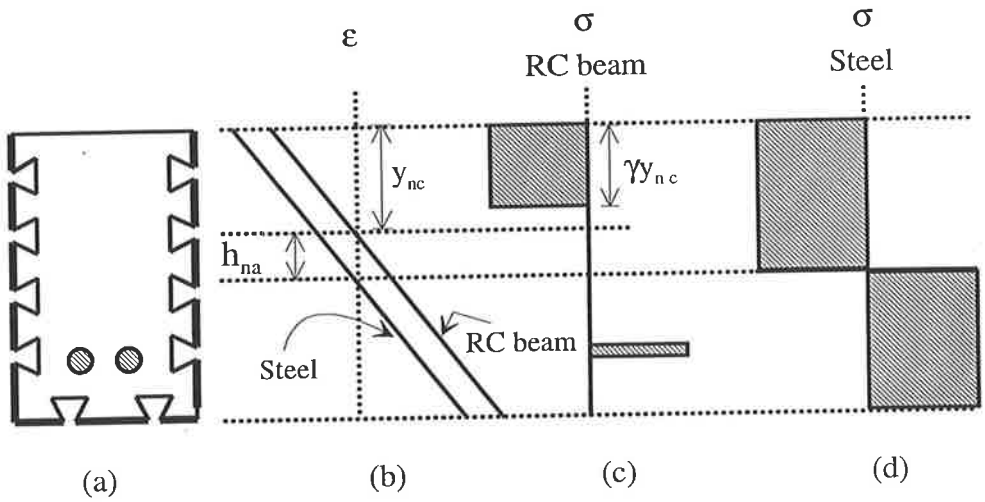

Fig. 2-7 Full-shear-connection partial-interaction analysis

When there is full-shear-connection but partial-interaction, then a parallel bi-linear strain profile in Fig. 2-7(b) is applicable. The situation is similar to that of the standard composite beam in Sect. 2.2.2.1.2. We can determine the flexural capacity for this situation if we can determine h_{na} in (b) and follow the same procedure as mentioned in Sect. 2.2.2.1.2. It can be seen that the bond force for partial-interaction will be less than that of the full-interaction.

2.2.3.2 Partial-shear-connection analysis

When the bond strength required for full-shear-connection cannot be provided in the beam then the analysis reverts to that of partial-shear-connection and the neutral axes of both the elements do not coincide, as shown in Fig. 2-7(b). In this case, the resultant force in each element will be controlled by the strength of the shear connection in the shear span. The neutral axis position in each element can be evaluated from the known resultant force that is the bond force, and thereby the flexural capacity can be determined.

2.3 LONGITUDINAL SLIP IN STANDARD COMPOSITE BEAMS

It is very important in standard composite beams to ensure that the shear connectors can withstand longitudinal slip. Vertical slip is assumed to be restricted in this type of structure by bearing of the elements at the interface. In the following section, the analysis procedure for longitudinal slip in standard composite beams will be described.

2.3.1 Linear Elastic Analysis

The linear elastic behaviour of composite beams was studied by Newmark, Seiss and Veist (1951) and assumed that

(a) The shear connection between the concrete and the steel is continuous along the length of the beam.

(b) The amount of slip permitted by the shear connection is directly proportional to the load transmitted.

(c) The distribution of strains throughout the depth of the concrete and the steel is linear.

(d) The steel and concrete elements deflect equal amounts at all points along their length.

As the linear behaviour of the load-slip relationship for a stud shear connection is assumed, so the longitudinal slip, s_h, is given by

$$s_h = \frac{D_{\max}}{K_{si}} \quad \text{.....(2.2)}$$

where, D_{max} is the shear force in the shear connection, and K_{si} is the initial modulus of load-slip curve. Hence, under a uniform spacing of the connectors over the length L, eqn. (2.2) can be written as

$$s_h = \frac{qL}{K_{si}} \quad \text{.....(2.3)}$$

in which q is the shear force transmitted per unit length of the beam, which is often referred as shear flow. When dealing with partial-shear-connection, the force in the concrete section, F_{con}, and the force in the steel section, F_{steel}, are equal to the force in the shear connector, F_{shear}, as shown in Fig. 2-8. Therefore,

$$F_{con} = F_{steel} = F_{shear} \quad \text{.....(2.4)}$$

The shear force per unit length q is equal to the rate of change in the force F_{shear} along the length of the beam. Therefore eqn. (2.3) can be written as

$$s_h = \frac{L}{K_{si}} \frac{dF_{shear}}{dx} \quad \text{.....(2.5)}$$

Differentiating eqn. (2.5) gives the rate of change of slip along the length of beam

$$\frac{ds_h}{dx} = \frac{L}{K_{si}} \frac{d^2 F_{shear}}{dx^2} \quad \text{.....(2.6)}$$

Consider the composite beam in Fig. 2-8(a). The axial forces F and moments M in each element of the composite beam and at any section are shown in (b). These actions act through the centroid of the concrete element at any distance h_c from the steel/concrete interface, as shown in (b), and at the centroid of the steel element at a distance h_s from the interface.

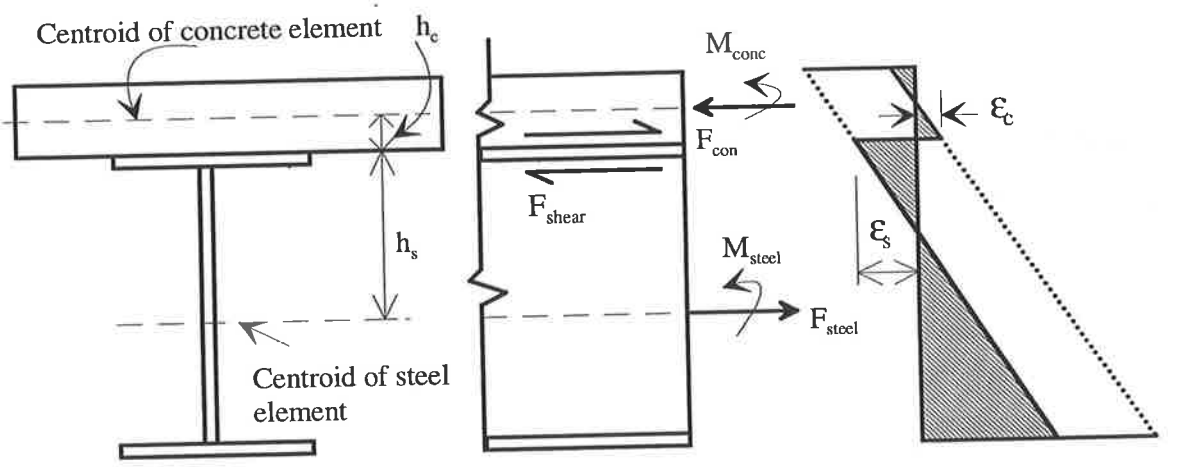

(a) cross-section (b) internal forces (c) strain distribution

Fig. 2-8 Linear elastic analysis

The elastic strain ε_c at the bottom of the concrete element in (c) is given by

$$\varepsilon_c = \frac{\sigma_c}{E_c} = \frac{1}{E_c}\left(\frac{M_{conc}h_c}{I_c} - \frac{F_{con}}{A_{conc}}\right) \quad \text{.....(2.7)}$$

where σ_c is the stress in concrete element, E_c is the elastic modulus of concrete, I_c is the second moments of area of concrete section about the centroidal axis and A_{conc} is the area of the concrete section. Then eqn. (2.7) can be written as

$$\varepsilon_c = \frac{M_{conc}h_c}{E_c I_c} - \frac{F_{con}}{E_c A_{conc}} \quad \text{.....(2.8)}$$

Similarly, the elastic strain ε_s at the top of the steel element is

$$\varepsilon_s = \frac{F_{steel}}{E_s A_{steel}} - \frac{M_{steel}h_s}{E_s I_s} \quad \text{.....(2.9)}$$

where E_s is the elastic modulus of steel, A_{steel} is the area of the steel elements and I_s is the second moments of area of the steel elements about the centroidal axes.

The rate of change of slip is equal to the difference between the strain in the concrete and the strain in the steel element at the level at which slip occurs. With the notation in Fig. 2-8(c) this is expressed by

$$\frac{ds_h}{dx} = \varepsilon_c - \varepsilon_s \quad \text{.....(2.10)}$$

Inserting eqn. (2.6), (2.8) and (2.9) in eqn. (2.10), gives

$$\frac{L}{K_{si}}\frac{d^2F_{shear}}{dx^2} = \left[\frac{M_{conc}h_c}{E_c I_c} + \frac{M_{steel}h_s}{E_s I_s}\right] - F_{shear}\left[\frac{1}{E_c A_c} + \frac{1}{E_s A_{steel}}\right] \quad \text{.....(2.11)}$$

The summation of the three internal moments M_{conc} and M_{steel} and the moment contribution of the axial force equals the applied moment M, that is

$$M = M_{conc} + M_{steel} + F_{shear}(h_c + h_s) \quad \text{.....(2.12)}$$

The assumption that the concrete and steel elements deflect equal amounts at all points along their length requires that the curvature κ of both the element is equal. This condition can be expressed as

$$\kappa = \frac{M_{conc}}{E_c I_c} = \frac{M_{steel}}{E_s I_s} = \frac{M - F_{shear}(h_c + h_s)}{E_c I_c + E_s I_s} \quad \text{.....(2.13)}$$

Equations (2.12) and (2.13) can be used in eqn. (2.11), so that we get the following differential equation.

$$\frac{d^2 F_{shear}}{dx^2} + F_{shear} \frac{K_{si}}{L} \frac{\overline{EI}}{\overline{EA} \sum EI} = \frac{K_{si}}{L} \frac{(h_c + h_s)}{\sum EI} M \quad \text{.....(2.14)}$$

where

$$\sum EI = E_c I_c + E_s I_s \quad \text{.....(2.15)}$$

$$\frac{1}{\overline{EA}} = \frac{1}{E_c A_{conc}} + \frac{1}{E_s A_{steel}} \quad \text{.....(2.16)}$$

$$\overline{EI} = \sum EI + \overline{EA}(h_c + h_s)^2 \quad \text{.....(2.17)}$$

The differential eqn. (2.14) is a general expression for the force F_{shear}. As the external moment varies along the beam and depends on the type of loading, eqn. (2.14) must be solved separately for each type of load. With F_{shear} thus found, all internal forces acting on any cross section of the beam will be known and expressions for longitudinal slip, shear between the interacting elements, strains and deflections can easily be derived.

2.3.2 Linear Elastic-Plastic Analysis

A linear elastic-plastic analysis has been developed by Oehlers and Sved (1995) to determine longitudinal slip in a standard composite beam. This is an extension of Newmark's (1951) linear elastic analysis which has been described in the previous section. The assumption of linear elastic-plastic analysis is that the steel and concrete elements remain linear elastic whereas the shear connectors are fully plastic.

In this analysis, F_{shear} in eqn. (2.4) is equal to P_{shear}, where P_{shear} is the strength of the shear connection in the shear span, as it is assumed that all the connectors are fully loaded. Hence, substituting eqn. (2.6) into eqn. (2.11) gives

$$\frac{ds_h}{dx} = \left[\frac{M_{conc}h_c}{E_cI_c} + \frac{M_{steel}h_s}{E_sI_s}\right] - P_{shear}\left[\frac{1}{E_cA_c} + \frac{1}{E_sA_{steel}}\right] \quad \text{.....(2.18)}$$

Rearranging eqn. (2.18) and then using the abbreviations of eqns. (2.15) and (2.16), gives

$$\frac{ds_h}{dx} = \frac{M(h_c+h_s)}{\sum EI} - P_{shear}\left[\frac{1}{\overline{EA}} + \frac{(h_c+h_s)^2}{\sum EI}\right] \quad \text{..... (2.19)}$$

Integrating eqn. (2.19) gives the change in longitudinal slip Δs_h as follows,

$$\Delta s_h = K_1 \int_{\Delta L} M dx - K_2 \int_{\Delta L} P_{shear} dx \quad \text{.....(2.20)}$$

where

$$K_1 = \frac{h_c+h_s}{\sum EI} \quad \text{.....(2.21)}$$

and

$$K_2 = \frac{(h_c+h_s)^2}{\sum EI} + \frac{1}{\overline{EA}} \quad \text{.....(2.22)}$$

In order to determine the maximum longitudinal slip $s_{h,max}$, we can integrate eqn. (2.19) up to the point of zero slip, which occurs at the position of maximum moment due to reversal of longitudinal slip (Oehlers and Bradford, 1995).

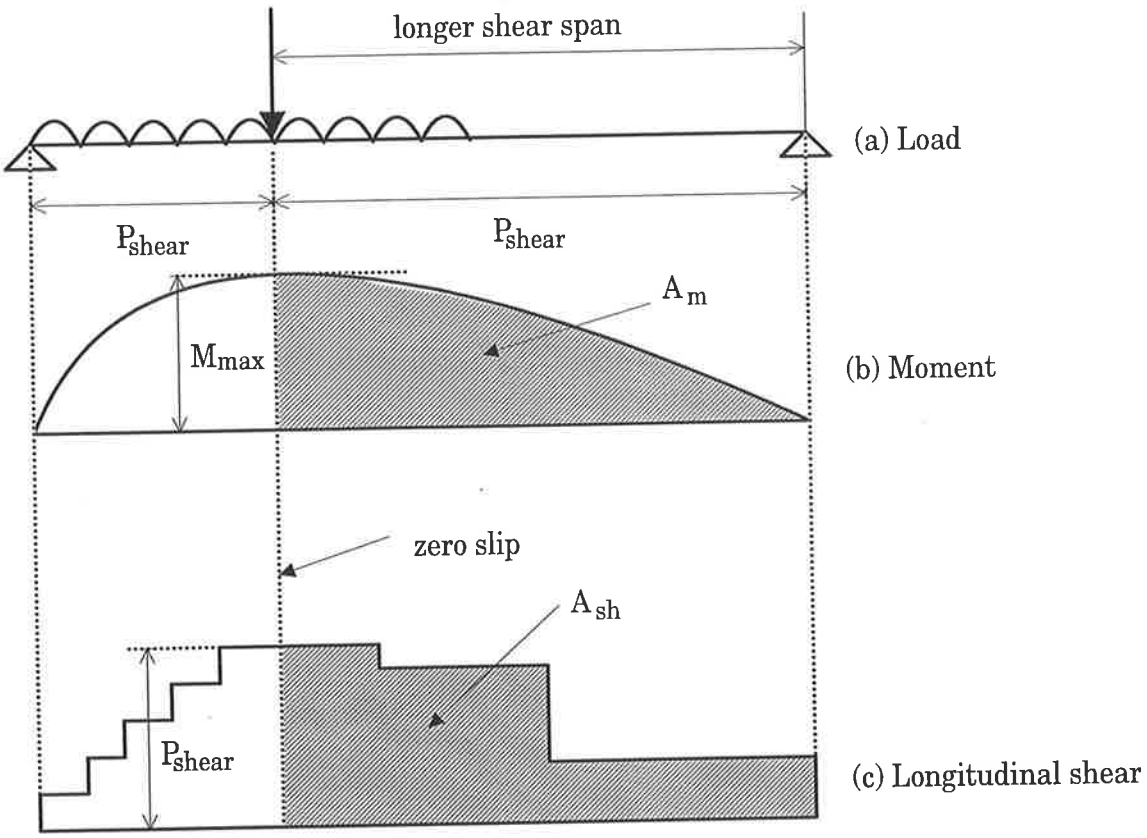

Fig. 2-9 Linear elastic-plastic analysis (Oehlers and Bradford, 1995)

Equation (2.20) can be generalised for maximum longitudinal slip by considering the illustration in Fig. 2-9, where P_{shear} is longitudinal shear strength in the shear span. The maximum longitudinal slip will normally occur at the end of the longest shear span, so the areas A_m and A_{sh}, shown in the Fig. 2-9, can be determined from both the applied moment distribution and the shear connector distribution. Hence $s_{h,max}$ can be calculated from

$$s_{h,\max} = A_m K_1 - A_{sh} K_2 \quad \text{..... (2.23)}$$

The first parameter in eqn. (2.23) is the maximum slip when there are no connectors and the second parameter is the reduction of slip due to the shear connectors. It is necessary in

the composite beam that the connectors have a slip capacity that is more than $s_{h,max}$, so that the ultimate strength can be achieved.

2.4 MECHANICAL SHEAR CONNECTOR

There are many types of mechanical shear connectors among which the stud shear connectors are most commonly used in composite construction. Also, stud shear connections are similar to the bolted shear connectors that have been used in the experimental work of this research in plated beams. Furthermore, the push specimen test set up used for rib shear connectors is similar to the push specimen test set up that has been used in this research for bolted shear connectors. Therefore, stud shear connectors and rib shear connectors will be examined in this section.

2.4.1 Stud Shear Connector

The stud shear connector is a steel dowel that is embedded into a concrete medium. The load is transferred from one element to the other through the dowel action of the connector. The resistance of a connector to this dowel action is referred to as the dowel strength. Because of the complexity of the dowel action, the strength and ductility of shear connectors are always determined experimentally by push tests which will be described in the following sections.

2.4.1.1 Push specimen of stud shear connector

An example of a push specimen is shown in Fig. 2-10 (Oehlers and Bradford, 1995). It can be seen in (b) that the steel section is sandwiched by the concrete sections. When vertical displacement is applied to the steel element, a load of $2F$ is induced as shown in (b). This load is transferred to the base of the concrete element through the dowel action of the shear connectors. Therefore, a force F is induced in the shear connector at an eccentricity e as shown in (a). This eccentricity is much less than the depth of the concrete slab h_2. Therefore, it can be assumed that the force F acts at the surface of the concrete element and is dispersed to the base of the element at a distance $h_2/2$ from the surface. The external force F forms a couple $Fh_2/2$, which is resisted by a horizontal frictional force H that is

induced in the base and in the shear connection as shown in (a). This causes an opposing couple Hh_1, where h_1 is the height of the connection from the base. Hence the horizontal component H is given by

$$H = F\frac{h_2}{2h_1} \quad \text{..... (2.24)}$$

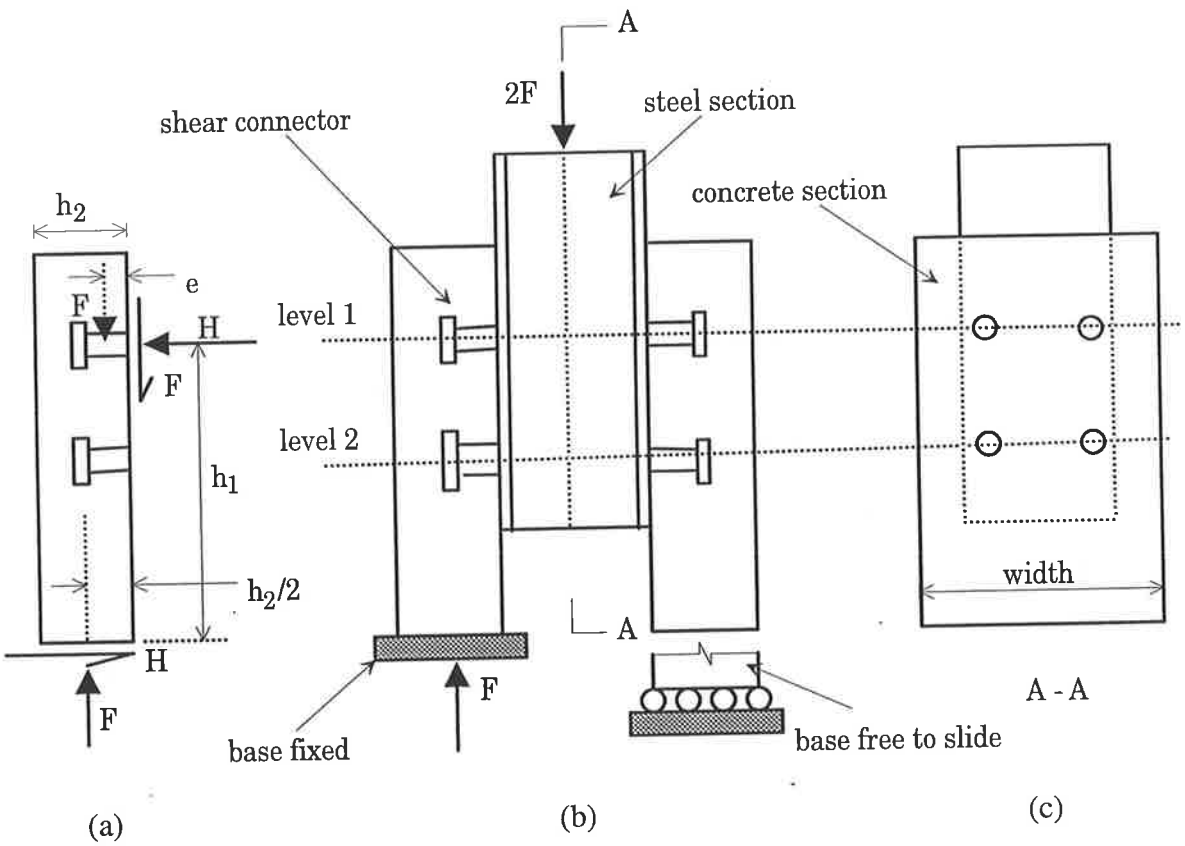

Fig. 2-10 Push specimen of stud shear connector (Oehlers and Bradford, 1995)

As dowel failure is caused by the tensile stresses in the shank of the stud, the compressive force H will increase the dowel strength. The horizontal force H does not occur in the beams as the connectors are loaded indirectly from the flexural forces within the beam. Hence, the dowel strength determined from the push tests are greater than those in composite beams. Therefore, the magnitudes of the dowel strengths from push tests need to be reduced before they are used in beam analyses. Alternatively, the push specimen could be allowed to slide using rollers as shown in Fig. 2-10(b), so that the resultant force across the steel/concrete interface is zero (Oehlers and Bradford, 1995).

2.4.1.2 Mechanism of failure in push specimens

It is always desired in push tests that the connectors on both sides of the push specimen fracture at an average strength. This is not possible unless the shear connections have an adequate rotational stiffness and have a plastic plateau in the load-slip curve (Oehlers and Johnson, 1987). The required rotational stiffness can be achieved using two levels of connectors as shown in Fig. 2-10.

2.4.1.3 Dowel strength of stud shear connector

Oehlers and Johnson (1987) derived the following semi-empirical equation to predict the dowel strength of stud shear connectors in push tests from a statistical analysis of experimental data.

$$(D_{\max})_{push} = \left[5.3 - \frac{1.3}{\sqrt{n}}\right] A_{stud} f_u^{0.65} f_c^{0.35} \left[\frac{E_c}{E_s}\right]^{0.40} \quad \text{.....(2.25)}$$

where, n is the number of connectors in a group, A_{stud} is the cross-sectional area of the shank of the stud, f_u is the tensile strength of the stud material, f_c is the compressive strength of concrete, E_c is the elastic modulus of concrete and E_s is the elastic modulus of steel.

It can be seen in eqn. (2.25) that the dowel strength depends on the strength of the shank and the properties of the materials. When dealing with beams, Oehlers and Johnson (1987) found that the dowel strength in beams is 81% of that in push specimens and provided the following equation to describe their strength.

$$(D_{\max})_{beam} = \left[4.3 - \frac{1.1}{\sqrt{n}}\right] A_{stud} f_u^{0.65} f_c^{0.35} \left[\frac{E_c}{E_s}\right]^{0.40} \quad \text{.....(2.26)}$$

2.4.1.4 Splitting forces due to stud shear connector

Stud shear connectors transfer the longitudinal shear forces between the steel and concrete elements by imposing concentrated loads on the concrete element. These concentrated loads can cause the concrete to fail in tension by ripping or by splitting as illustrated in Fig.

2-11. The splitting crack can affect the ability of the shear connections to transfer the shear in which case the dowel strength will be reduced (Oehlers, 1989), whilst the ripping crack still allows shear transfer. The splitting crack frequently occurs in composite beams that have limited side cover to the shear connector (Johnson and Oehlers, 1982; Toprac and Dale, 1967; Teraszkiewicz, 1968) and is a form of failure that can occur in plated beams.

The highly concentrated dowel force exerted by the shear connectors is dispersed laterally into the concrete element, as shown by the arrows marked C in Fig. 2-11. In order to maintain equilibrium, transverse tensile stresses are induced in the concrete that have a resultant force shown as T. If these transverse tensile stresses induced by T exceed the splitting tensile strength of the concrete f_{cb}, a longitudinal crack will occur as shown in the concrete element that is in line with the shear connectors. This crack will propagate through the bearing zone of the shear connection and hence release the triaxial restraint, so that the concrete will crush at a reduced bearing pressure. This means that the dowel strength will reduce.

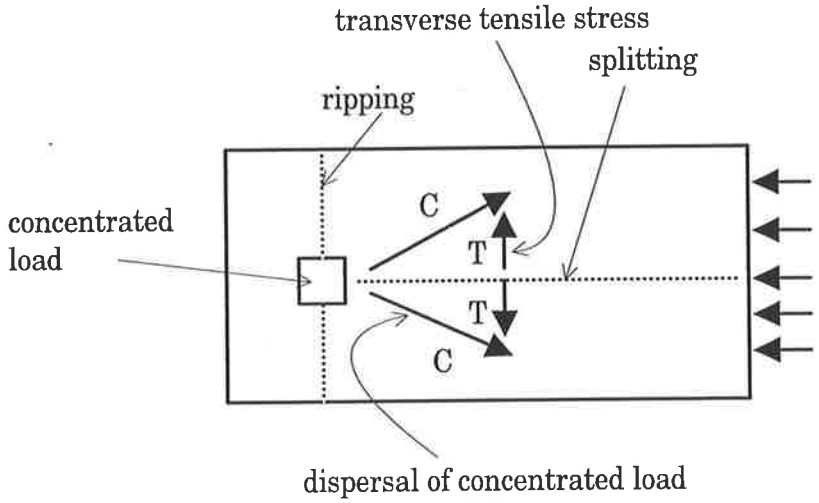

Fig. 2-11 Tensile cracking due to connector force (Oehlers and Bradford, 1995)

Oehlers (Oehlers and Bradford, 1995) provided the following equation to determine the splitting resistance of the concrete element to a line of connectors. They assumed that for normal density concrete $f_{cb} = 0.5\sqrt{f_c}$.

$$P_{split} = \left(\left(\left(1 - \frac{0.9 d_{sh}}{h_{conc}} \right)^2 \frac{0.9 d_{sh}}{h_{conc}} \right)^{-1} + \frac{b_c}{d_{sh}\left(1 - \frac{d_{sh}}{b_c} \right)} \right) c d_{sh}^2 \sqrt{f_c} \quad \text{..... (2.27)}$$

where, d_{sh} is the diameter of the shank of the stud, h_{conc} is the height of concrete slab, b_c is the effective width of concrete slab, c is the characteristic strength; which is usually given by $c = 1 - \frac{0.25}{\sqrt{n}}$, where n is the number of connectors that fail as a group; and f_c is the cylinder strength of concrete. The dowel strength should be less than the splitting strength of concrete.

2.4.2 Rib Shear Connector

Rib shear connectors are another type of mechanical shear connector that is used in the profiled sheeting of composite profiled beams or slabs. The bond characteristics of rib shear connectors are determined from push specimens that will be described in the following section.

2.4.2.1 Push specimen of rib shear connector

An example of a push specimen for rib shear connectors is shown in Fig. 2-12 (Burnet, 1996). It can be seen that the concrete block is sandwiched between two profiled sheets.

The forces and the restraints that occur in the rib shear connector push specimen are the same as those in the push specimen for stud shear connectors in Fig. 2-10. Therefore, eqn. (2.24) for the horizontal force H is applicable. In the rib shear connector push specimen, the thickness of the sheet h_2 in Fig. 2-12 is much less than the distance h_1 to the centre of the concrete block. Hence, the magnitude of the horizontal force H that can be derived from eqn. (2.24) is very small. As such there will be practically no increase in the bond strength due to the external force H. Therefore, the behaviour of the bond in this type of push specimen should be close to that in a profiled composite beam.

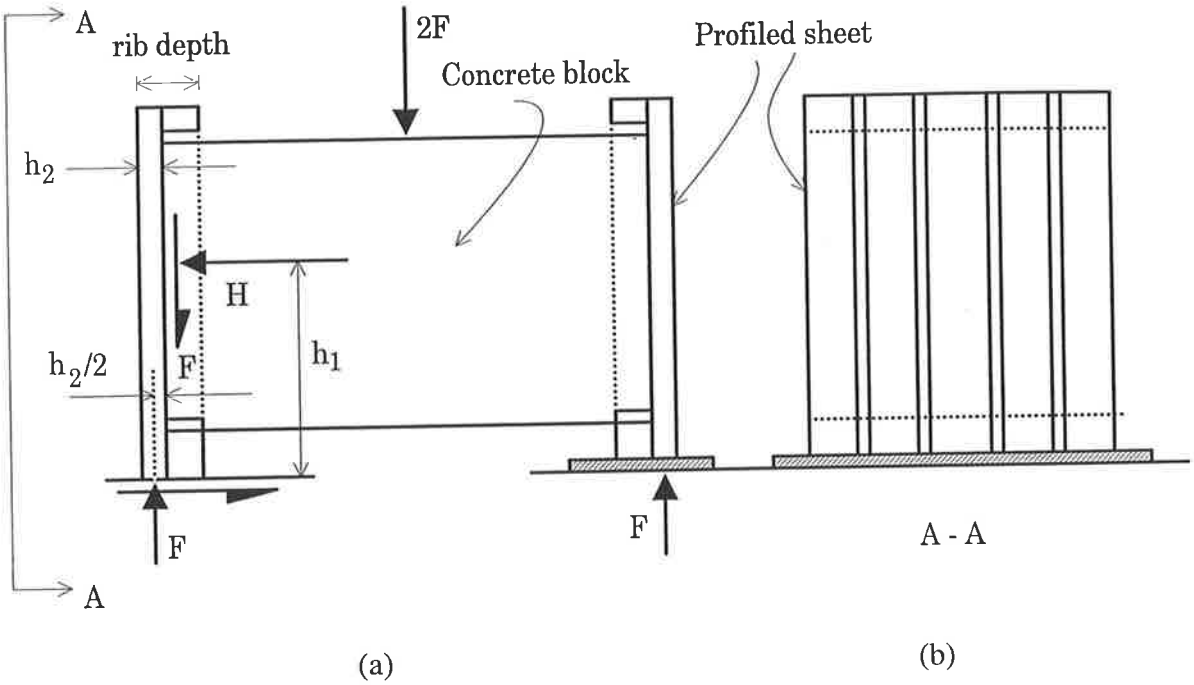

Fig. 2-12 Rib shear connector push specimen (Burnet, 1996)

2.5 NON-LINEAR COMPUTER MODEL

The analysis of a section of standard composite beam has been described in Sects. 2.2.2 and 2.3 by considering that the materials either plastic or elastic or a combination of elastic-plastic. In this section, a non-linear computer model of Burnet (1996) will be described, which determines the bond force and the longitudinal slip at the interface. This model consists of two parts: a full-interaction analysis that produces a general moment-curvature diagram as well as the bond strength; and a partial-interaction analysis that produces the variation of longitudinal slip along the length of a member as well as the moment-curvature diagram at discrete points.

2.5.1 Full-Interaction Analysis

A full-interaction analysis of a typical composite beam in Fig. 2-13(a) will be presented in this section. The elementary theory and then the procedure of analysis will be described.

2.5.1.1 Elementary theory of full-interaction analysis

A full-interaction analysis is carried out by first dividing the cross-section into a series of slices as shown in Fig. 2-13(a). A strain distribution is assumed as shown in (b) where the coordinate axes are set at the top of the cross-section and strain is evaluated at the mid-height of each slice as shown.

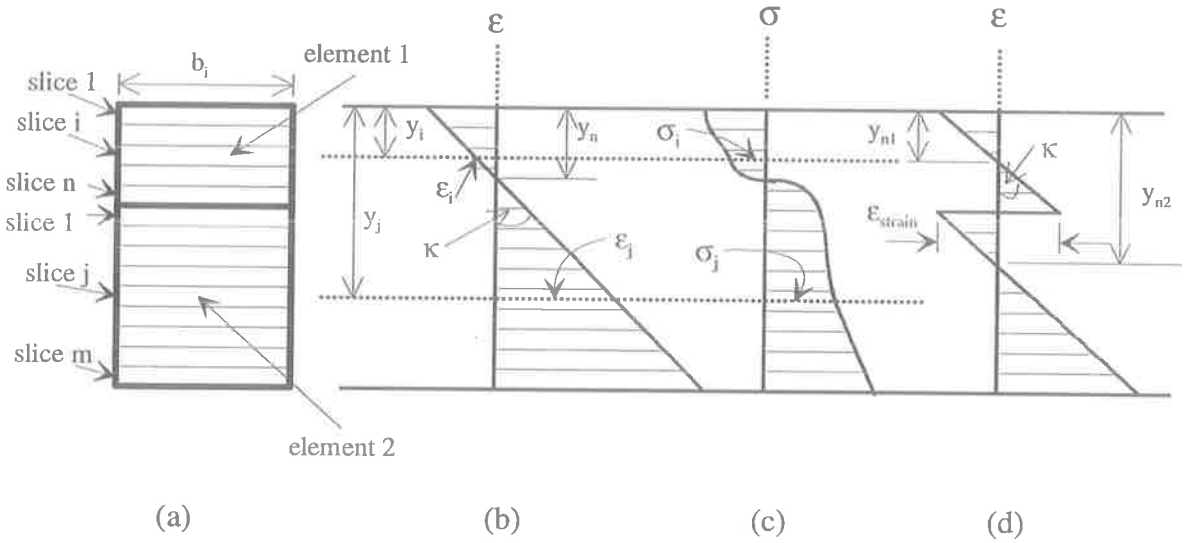

Fig. 2-13 Idealised cross-section using slices (Burnet, 1996)

The strain at the i-th slice is given by

$$\varepsilon_i = \kappa(y_n - y_i) \quad \text{.....(2.28)}$$

where ε_i is the strain at the mid-height of i-th slice, y_i is the location of the mid-height of the i-th slice, y_n is the neutral axis location in the composite cross-section and κ is the curvature in the cross-section.

The stress profile in Fig. 2-13(c) is evaluated from the known stress-strain relationships of the material. It is assumed in the analysis that the stress at the mid-height of each slice acts throughout the depth of the slice. Then the axial force in the slice is given by

$$F_i = \sigma_i b_i t \quad \text{.....(2.29)}$$

where σ_i is the stress in the i-th slice, b_i is the width of the i-th slice and t is the depth of the slices. The summation of all the axial forces in the cross-section should be zero, that is

$$\sum_{i=1}^{n} F_i + \sum_{j=1}^{m} F_j = 0 \quad \text{.....(2.30)}$$

where n is the total numbers of slices in the top element and m is the total number of slices in the bottom element. The summation of the moment contribution of each slice at top of the cross-section is the total applied moment M, that is

$$\sum_{i=1}^{n} y_i F_i + \sum_{j=1}^{m} y_j F_j = M \quad \text{.....(2.31)}$$

The axial force transferred at the interface between the two elements can be found by summing the axial forces in either of the elements. This is known as the bond force F_b and is given by the following equations.

$$F_b = \sum_{i=1}^{n} F_i \quad \text{.....(2.32)}$$

$$F_b = -\sum_{j=1}^{m} F_j \quad \text{.....(2.33)}$$

2.5.1.2 Procedure of full-interaction analysis

The analysis starts with an estimate of the neutral axis location y_n for a given curvature in Fig. 2-13(b). Then eqn. (2.28) is used to determine the strain distribution in each slice from which the stress in each slice is determined. The stress in each slice is used in eqn. (2.29) to determine the slice forces which in turn are summed in eqn. (2.30). In the computer model, the right hand part of eqn. (2.30) is not considered as zero but very close to zero to allow for an acceptable error. The location of the neutral axis is adjusted until the sum of the forces in the cross-section from eqn. (2.30) falls within the acceptable error. Once the neutral axis position is ascertained, the moment in the cross-section is determined by summing the moment contributions of each slice about any point as given by eqn. (2.31).

This iterative procedure produces one point in the moment-curvature diagram. The curvature is then incremented and the procedure repeated to produce a complete moment-curvature behaviour based on full-interaction.

2.5.2 Partial-Interaction Analysis

When there is partial-interaction as shown in Fig. 2-13(d), the slip strain varies uniquely with the magnitude of the bond force. Therefore, it is necessary to know either the bond force or the slip strain as well as the externally applied moment to determine the strain distribution throughout the cross-section. The model developed by Burnet (1996) is based on known variation of bond force with the applied moment, that is, F_b in eqn. (2.32) and (2.33) and M in eqn. (2.31) are known. First the procedure of analysis at a cross-section and then the same along the length of a member will be described in the following sections.

2.5.2.1 Analysis of cross-section with partial-interaction

In this analysis, the two elements in the cross-section are considered separately. For a given bond force and given curvature, an initial estimate is made of the neutral axis position in the top element. Then eqn. (2.28) is used to determine the strains in the slices throughout the element, from which the stresses in each slice can be determined. This is substituted into eqn. (2.29) to get the axial force in each slice, which in turn is substituted into eqn. (2.32) to derive the bond force. This bond force is compared with the initially given bond force. The neutral axis location is then varied until the derived bond force is within a specified tolerance of the given bond force. Thus, the neutral axis location is fixed in the top element for a given curvature and given bond force. The same procedure is repeated for the bottom element until its neutral axis location is found for the same given curvature and bond force. The internal moment can then be found by summing the moment contributions for each slice from both elements about any point, as given in eqn. (2.31). If the internal moment is not within an acceptable error of the externally applied moment, then the curvature is adjusted and the whole procedure is repeated for the same value of bond force. The slip strain in Fig. 2-13(d) can be determined from the following equation.

$$\varepsilon_{strain} = \kappa\left(y_{n2} - y_{n1}\right) \quad \text{.....(2.34)}$$

where y_{n1} is the neutral axis location in the top element and y_{n2} is the neutral axis location in the bottom element.

2.5.2.2 Analysis of member with partial-interaction

The cross-section analysis in Sect. 2.5.2.1 will be used in the following member analysis. This is done by dividing the member into a number of segments of length dx as shown in Fig. 2-14.

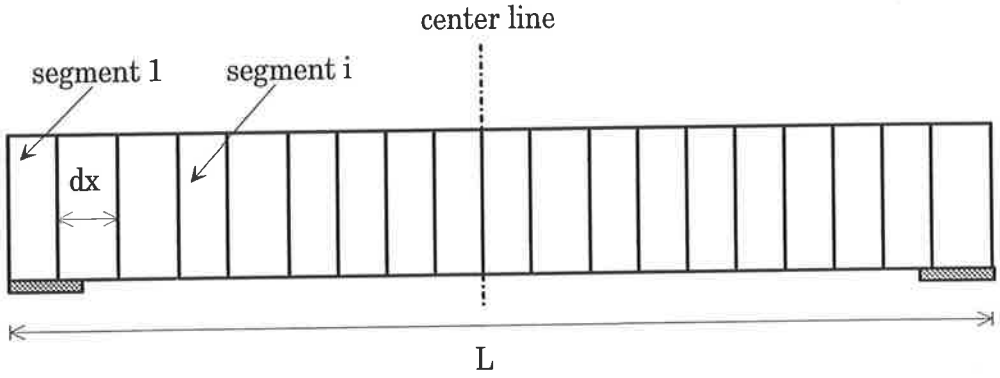

Fig. 2-14 Member analysis

In this analysis, the connectors are modelled as being uniformly distributed over the segment in which they are situated. If the spacing of connectors is s, then the longitudinal shear load in the i-th segment $P(i)$ is calculated as follows

$$P(i) = f(s_h(i))\frac{dx}{s} \quad \text{.....(2.35)}$$

where $f(s_h(i))$ is the longitudinal shear load in a connector for the slip $s_h(i)$ in i-th segment which can be determined from the known load-slip curve. The bond force acting at i-th segment can then be found by summing the loads in the connectors for each of the preceding segments, that is

$$F_b(i) = \sum_{j=1}^{i} P(j) = F_b(i-1) + P(i) \quad \text{.....(2.36)}$$

The first step in the member analysis is to estimate the slip in Segment 1. The load in the connector for the segment can be determined from eqn. (2.36), where i =1 and

hence $F_b(1) = 0$, and then the bond force in segment 1 is equal to the force in the connectors. This bond force is considered equal over the length of the segment. Then the external moment at this segment is known from the distribution of the imposed load. Thus the external moment in the first segment is known as well as the bond force. These values can be used in eqns. (2.30), (2.31) and (2.33) so that the neutral axis position and the curvature can be determined by following the procedure as described in Sect. 2.5.2.1.

When the correct values of the neutral axis positions and curvature are known, then the slip-strain in Segment 1 is determined from eqn. (2.34) which is assumed to be constant over the length of the segment. As slip strain is the rate of change of longitudinal slip, then by integrating it, we can get the change of longitudinal slip $\Delta s_h(i)$ over the segment under consideration as follows.

$$\Delta s_h(i) = \varepsilon_{strain} dx \quad \text{.....(2.37)}$$

This can then be used to estimate the slip at the next segment as follows

$$s_h(i+1) = s_h(i) - \Delta s_h(i) \quad \text{.....(2.38)}$$

where $s_h(i)$ is the slip at the i-th segment and $\varepsilon_{strain}(i)$ is the slip strain at the i-th segment.

With the value of slip derived in the previous paragraph, the load in the connectors for the second segment can be determined. Hence the bond force as well as the external moment at this segment are now known. The procedure as described for segment 1 can be repeated to determine the neutral axis position, the curvature and hence the slip strain in Segment 2. The latter is then used to estimate the slip in Segment 3 and the analysis proceeds in this way until the point where a boundary condition is known is reached. For a simply supported symmetrically loaded beam as shown in Fig. 2-14, this is at the centre of the beam where the slip is zero. If the centre slip is not within acceptable error of zero, then the initial estimate of the slip at segment 1 is changed, and the whole procedure is repeated. This means that successive iterations will be required to satisfy the boundary condition.

It can be seen that the algorithm given above can be used to determine the variation of longitudinal slip in the composite beam.

2.6 SUMMARY

It has been mentioned in this literature review that the theory of glued plated beams cannot be used in this research on bolted plated beams as their interface behaviour is not the same. However, the theory of composite structures with mechanical shear connectors can be used. As such, this literature review has looked at the theories of composite structures that are directly applicable to bolted plated beams. Rigid plastic analyses, procedures to determine longitudinal slip and the procedure to determine the dowel strength of stud shear connectors that have been developed for standard composite beams have been described. Also, an existing non-linear computer model which can determine the partial-interaction behaviour of standard composite beams has been described. All these theories and the computer model, either in their original or extended forms, have been used directly in this research on bolted plated beams will be described in the following chapters.

Chapter Three

Basic Theories for Longitudinal Shear Forces in Side Plated RC beams

3.1 INTRODUCTION

The bolts in side plated beams transfer both longitudinal shear forces and vertical shear forces between the plate and the reinforced concrete (RC) elements. This chapter deals with the basic theories that govern longitudinal shear force which will be used in the development of computer models in Chapter 5 and in the experimental work in Chapter 8. Firstly, the ultimate strength rigid plastic analysis in Sect. 2.2 will be adapted for side plated beams as this will be used in the design of the plated beams in Chapter 8. Then it will be shown that the same mathematical model that is used to determine the maximum longitudinal slip in the standard composite beam in Sect. 2.3.2 can be used in side plated beams.

3.2 ULTIMATE STRENGTH RIGID PLASTIC ANALYSIS

The rigid plastic ultimate strength analysis of standard composite beams and composite profiled beams has been described in Sect. 2.2. These basic procedure will be adapted to analyse the side plated beam in Fig. 3-1(a). The γ factor will be used to calculate the depth of the neutral axis in the concrete element for the same reason as mentioned in Sect. 2.2.3. Like the composite beams in Sects. 2.2.2 and 2.2.3, the strength of the side plated beam depends on the degree of shear connection and the degree of interaction. These parameters

will be taken into account in describing the rigid plastic analysis of side plated beam in the following section.

3.2.1 Full-Shear-Connection Full-Interaction Analysis

A full-shear-connection full-interaction analysis of a typical side plated beam is shown in Fig. 3-1. When there is full-shear-connection and full-interaction, the neutral axes of both the elements coincide as shown in (b), from which the stress profiles can be determined in both the concrete element and the steel element, as shown in (c) and (e) respectively. It can be seen in (e) that no stress is taken into consideration at the plate bolt holes.

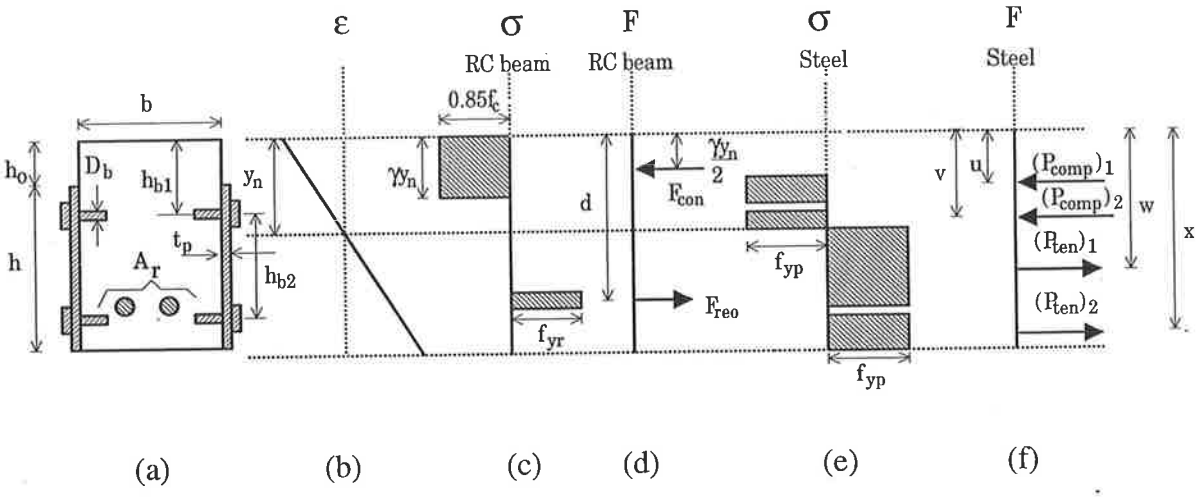

Fig. 3-1 Full shear connection full interaction analysis

The position of the neutral axis, y_n, in Fig. 3-1(b) can be derived from the equilibrium of the axial forces in (d) and (f) and hence we can write

$$F_{con} + (P_{comp})_1 + (P_{comp})_2 = F_{reo} + (P_{ten})_1 + (P_{ten})_2 \quad \text{..... (3.1)}$$

where F denotes the forces in the reinforced concrete element and P denotes the forces in the plate element. Using the notations in Fig. 3-1 and inserting the respective parameters for the forces in eqn. (3.1), we get

$$0.85 f_c \gamma y_n b + 2(y_n - h_o - D_b) t_p f_{yp} = A_r f_{yr} + 2(h_o + h - y_n - D_b) t_p f_{yp} \quad \text{.....(3.2)}$$

y_n can be calculated from eqn. (3.2) as all the other parameters are known. It is worth noting that we are dealing with rectangular stress blocks, so the resultant force in a block will act at the mid-depth of the block. The distances of the stress resultants from the top of the RC element are shown in (d) and (f). The flexural capacity $\left(M_{fi}\right)_{fsc}$ (the sub-script fsc denotes to full-shear-connection and fi denotes to full interaction) is given by the following equation.

$$\left(M_{fi}\right)_{fsc} = F_{con}\frac{\gamma y_n}{2} - F_{reo}d + (P_{comp})_1 u + (P_{comp})_2 v - (P_{ten})_1 w - (P_{ten})_2 x \quad \text{.....(3.3)}$$

The bond force $(F_b)_{fi,fsc}$ can then be derived from the resultant force in either of the elements in (d) or (f). For the reinforced concrete element

$$\left[\left(F_b\right)_{fi,fsc}\right]_{RC} = F_{con} - F_{reo} \quad \text{.....(3.4)}$$

and for the plate element

$$\left[\left(F_b\right)_{fi,fsc}\right]_{plate} = P_{comp} - P_{ten} \quad \text{.....(3.5)}$$

where, P_{comp} is the resultant compressive force in the plate element, and P_{ten} is the resultant tensile force in the plate. It needs to be mentioned here that the bond shear forces acting on the concrete element and the plate element are in opposite directions, so,

$$\left[\left(F_b\right)_{fi,fsc}\right]_{RC} = -\left[\left(F_b\right)_{fi,fsc}\right]_{plate} \quad \text{.....(3.6)}$$

3.2.2 Full-Shear-Connection Partial-Interaction Analysis

A full-shear-connection partial-interaction analysis of the side plated beam in Fig. 3-1(a) is shown in Fig. 3-2. Due to partial interaction, the neutral axes of the elements do not coincide as shown in (b). However, the respective stress profiles can be derived as shown in (c) and (e).

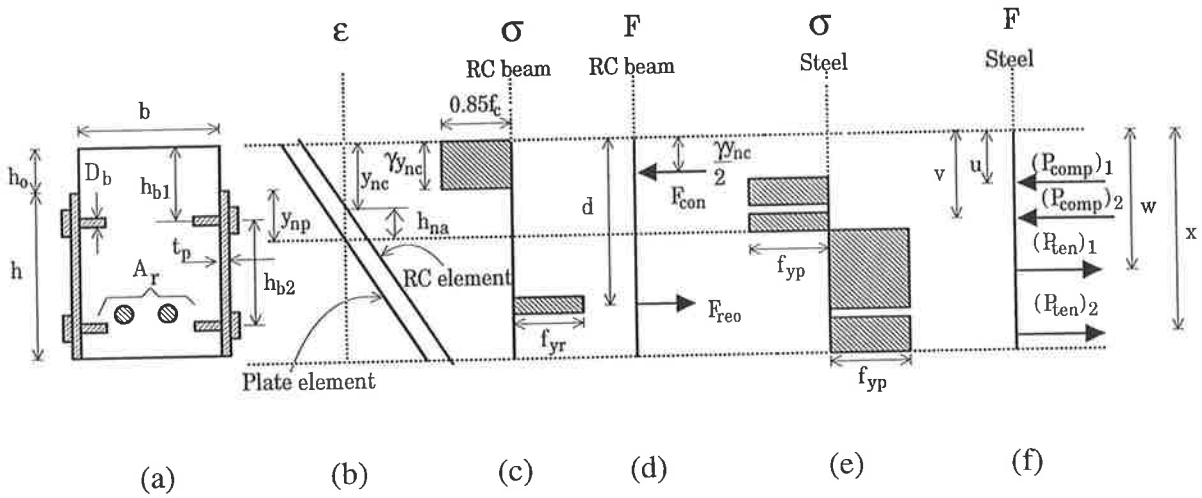

Fig. 3-2 Full-shear-connection partial-interaction analysis

Equation (3.2) can now be rewritten as

$$0.85f_c\gamma y_{nc}b+2(y_{np}-D_b)t_pf_{yp}=A_rf_{yr}+2(h-y_{np}-D_b)t_pf_{yp} \quad \text{.....(3.7)}$$

where y_{nc} and y_{np} are the neutral axes positions in the RC element and the plate element respectively, as shown in Fig. 3-2(a). Let us now denote the distance between the neutral axes in Fig. 3-2(b) as h_{na}. Inserting this into eqn. (3.7) we get

$$0.85f_c\gamma y_{nc}b+2(y_{nc}+h_{na}-h_o-D_b)t_pf_{yp}=A_rf_{yr}+2(h_o+h-y_{nc}-h_{na}-D_b)t_pf_{yp}$$

$$\text{.....(3.8)}$$

Equation (3.8) now can be solved for y_{nc}, as all the other parameters are known, and thereby y_{np} can be known. The axial forces and their locations in (d) and (f) can then be obtained and, hence the partial-interaction full-shear-connection moment $\left(M_{pi}\right)_{fsc}$ and bond force $(F_b)_{pi,fsc}$ can be calculated (the sub-script pi denotes to partial interaction).

A comparison of the full-shear-connection full-interaction analysis with the full-shear-connection partial-interaction analysis is shown in Fig. 3-3. In this example, the full-interaction neutral axis lies in the concrete element as shown in (b) and this produces the stress distribution in (c). When there is a small reduction in the degree of interaction as shown by the small separation of the neutral axes in (d), then this will lead to the same

stress profile in (c) and, therefore, the flexural strength of the plated beam will not reduce. The same situation was shown in the case of the standard composite beam in Sect. 2.2.2.1.2.

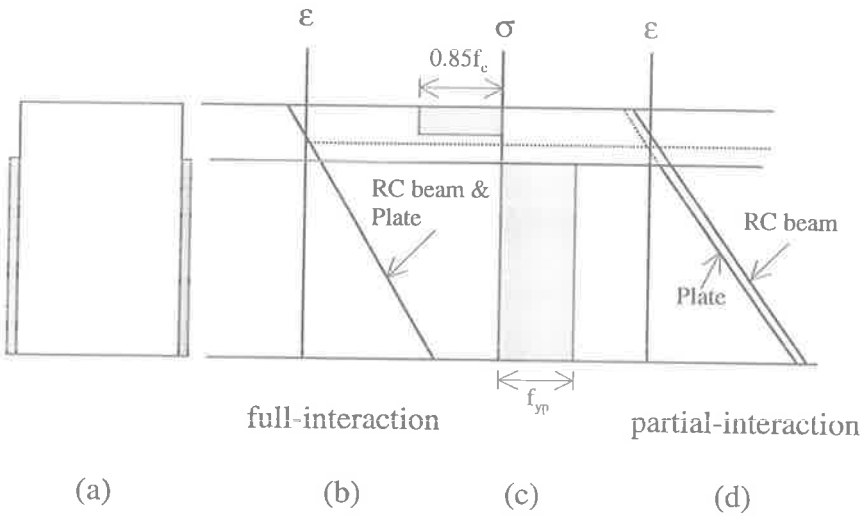

Fig. 3-3 Flexural strength due to partial interaction

Now, let us assume that the full-interaction neutral axis lies in the plate element as shown in Fig. 3-4(b), which has the stress profile in (c). In this case, a small reduction in the degree of interaction in (d) will lead to the stress profile in (e) where the net axial strength is less than that in (c). Therefore, the flexural strength of the beam will reduce due to partial interaction even though there is still full-shear-connection. This reduction in flexural strength can be seen in Fig. 3-5 where the partial-interaction full-shear-connection strength $\left(M_{pi}\right)_{fsc}$ is given as a proportion of the full-interaction full-shear-connection strength $\left(M_{fi}\right)_{fsc}$, and h_{na} is given as a proportion of h_d; where h_d is the distance between the mid-depth of plate and the top of the RC beam. It is evident from Fig. 3-5 that the increase of h_{na} can significantly reduce the flexural strength of plated beam. It is to be noted that in a standard composite beam, there is no change in flexural strength for this situation, as described in Sect. 2.2.2.1.2, because in the standard composite beam the elements lie above each other whereas in the plated beam they lie side by side.

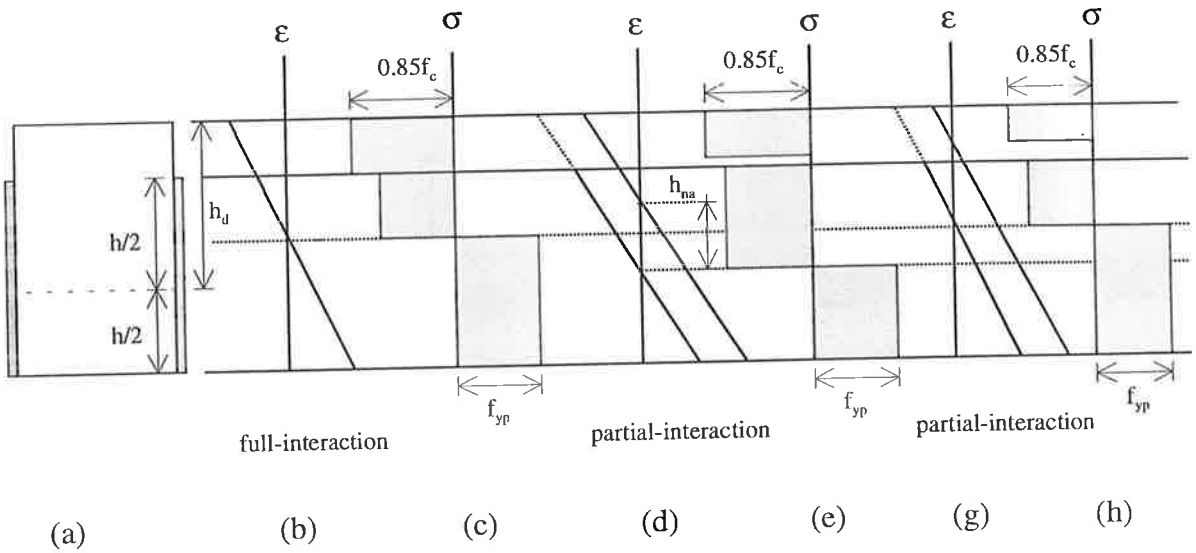

Fig. 3-4 Flexural strength analysis

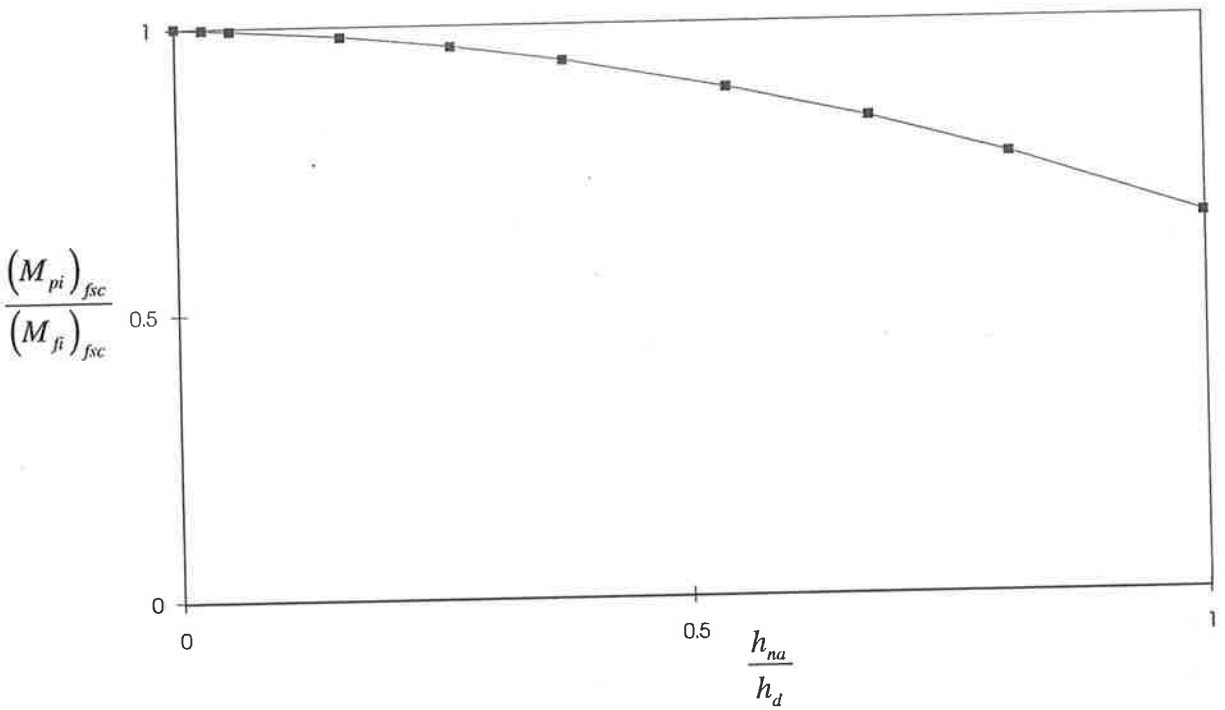

Fig. 3-5 Partial interaction flexural strength

In a third situation, let us assume that the partial-interaction full-shear-connection neutral axes lie in their respective elements as shown in Fig. 3-4(g) which has the stress profile in (h). The flexural strength for this situation will be less than that of the full-shear-connection full-interaction flexural strengths in 3-3(c) and 3-4(c) as the bond force will be

less. The same situation occurs in the case of the standard composite beam, as explained in Sect. 2.2.2.1.2.

3.2.3 Partial-Shear-Connection Partial-Interaction Analysis

Let us consider the side plated beam in Fig. 3-6(b) in which each row of bolts has the longitudinal shear force of $F_{shear}/2$. The degree of shear connection can be determined from Sect. 2.2.2.2, that is

$$\eta = \frac{F_{shear}}{(F_b)_{fi,fsc}} \quad \text{.....(3.9)}$$

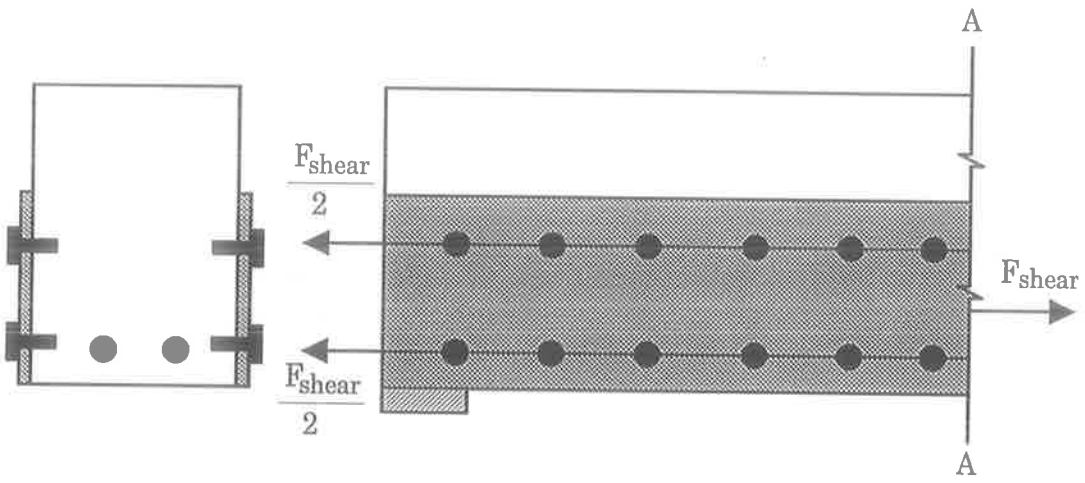

Fig. 3-6 Side plated RC beam

When $\eta \geq 1$, the side plated beam has a full-shear-connection strength. However, when $\eta < 1$, a partial-shear-connection analysis applies. It has been described in Chapter 2 that a partial-shear-connection analysis always deals partial interaction and hence with a bi-linear strain profile as shown in Fig. 3-7(b). The bond force for this situation is referred to as $(F_b)_{pi,psc}$ (where the sub-script psc is the partial-shear-connection) and is equal to the resultant force of the shear connection in the shear span F_{shear}, i.e.

$$(F_b)_{pi,psc} = F_{shear} \quad \text{.....(3.10)}$$

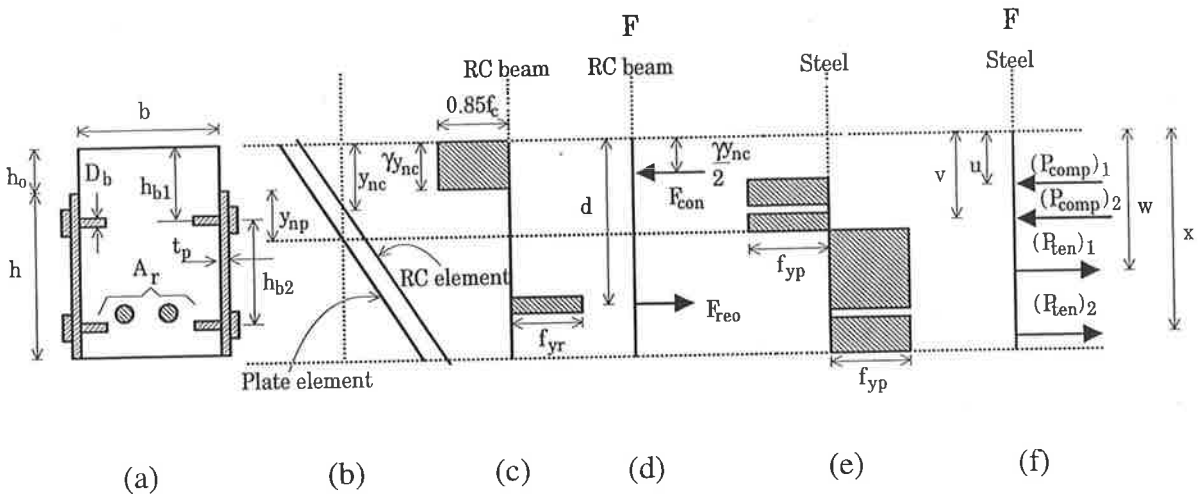

Fig. 3-7 Partial-shear-connection analysis

Then, for the reinforced concrete element

$$F_{shear} = 0.85 f_c \gamma y_{nc} b - A_r f_{yr} \quad \text{.....(3.11)}$$

This can be used to derive the neutral axis position of concrete element y_{nc}. Similarly for the plate element,

$$F_{shear} = 2\left(h - y_{np} - D_b\right) t_p f_{yp} - 2\left(y_{np} - D_b\right) t_p f_{yp} \quad \text{.....(3.12)}$$

Hence the neutral axis position of the plate element y_{np} can also be derived. Now, as we know the neutral axes positions, the magnitudes and the locations of the forces in Fig. 3-7(d) and (f) can be determined and the flexural capacity $\left(M_{pi}\right)_{psc}$ can be determined by following a similar procedure to that in Sect. 3.2.1. In partial-shear-connection analysis, the flexural capacity always reduces from that of the full-shear-connection flexural capacity as the bond strength reduces.

3.3 VARIATION IN FLEXURAL STRENGTH DUE TO DEGREE OF SHEAR CONNECTION AND DEGREE OF INTERACTION

The variation in the flexural strength of side plated beams for different degrees of shear connection and with different degrees of interaction is illustrated in Fig. 3-8. It can be derived from a simple partial-shear-connection analyses, as described in Sect. 3.2.3, that as

the strength of the shear connection P_{shear} is increased, the flexural capacity of the plated beam gradually increases from the flexural strength of the plate M_{plate} to the full-interaction full-shear-connection strength $\left(M_{fi}\right)_{fsc}$ which can be derived from Sect. 3.2.1. The strength of the shear connection at G is $\left(P_{fi}\right)_{fSC}$ and any further increase in the strength of the shear connection above G in Fig. 3-8 will not affect the flexural capacity as shown by the horizontal line C-D. The variation in the flexural strength with partial interaction is given by A-B-E. Hence, the variation in strength initially follows the same path as that for partial-interaction partial-shear-connection until point B is reached, which is given by a partial-interaction full-shear-connection rigid plastic analysis as described in Sect. 3.2.2. Any increase in the shear strength above $\left(P_{pi}\right)_{psc}$ after point F will not increase the flexural capacity above $\left(M_{pi}\right)_{fsc}$. It can therefore, be seen that the partial-interaction full-shear-connection strength simply places an upper bound to the partial-shear-connection strength.

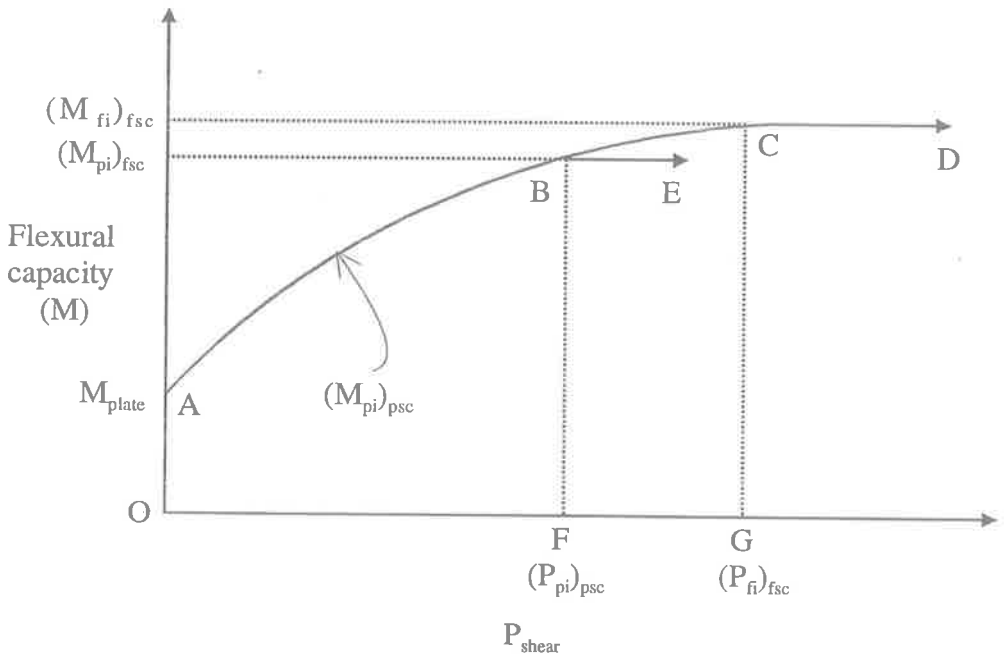

Fig. 3-8 Variation of flexural capacity in side plated beam

3.4 DETERMINATION OF MAXIMUM LONGITUDINAL SLIP

The elastic-plastic analysis outlined in Sect. 2.3.2 which is used to determine the maximum longitudinal slip in standard composite beams can be applied to side plated beams. Even though the standard composite beam and the side plated beams do not have the same shape, it will be seen that the same general eqn. (2.23) can be applied to side plated beams.

Let us consider the side plated beam in Fig. 3-9. The axial forces F and moments M in each of the elements are shown in (b). The concrete stress resultants act through the elastic centroid of the concrete element at the distance h_c from the top of the RC beam as shown in (b), and the steel stress resultants act at the centroid of the steel element at the distance, h_p, from the top of the RC beam. As we are dealing with an equal curvature in both the elements, the slip strains are the same throughout the height of the plated beam as shown in (c). Considering the slip strain at the level of the top of the RC beam, where the strain in the RC element is ε_c and the strain in the plate is ε_p, then from elementary mechanics,

$$\varepsilon_c = -\frac{M_{conc} h_c}{E_c I_c} - \frac{F_{con}}{E_{conc} A_{conc}} \quad \text{.....(3.13)}$$

$$\varepsilon_p = \frac{F_{plate}}{E_p A_{plate}} - \frac{M_{plate} h_p}{E_p I_p} \quad \text{.....(3.14)}$$

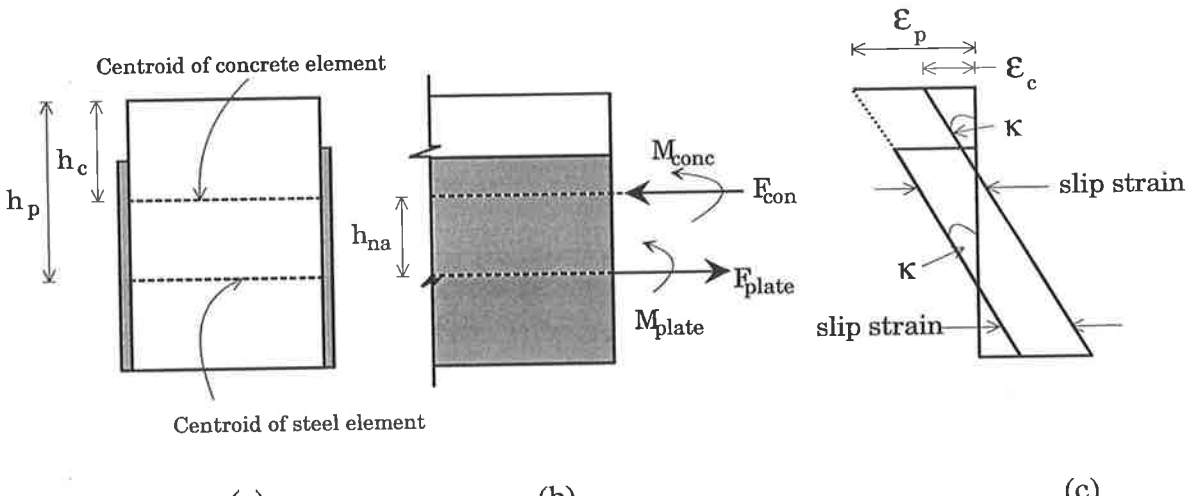

Fig. 3-9 Elastic-plastic analysis for longitudinal slip

According to the definition of slip strain in Sect. 2.3.1, we can write

$$\frac{ds_h}{dx} = \varepsilon_c - \varepsilon_p \quad \text{.....(3.15)}$$

It has been described in Sect. 2.3.2 that $F_{con} = F_{plate} = P_{shear}$. Substituting these values into eqns. (3.13) and (3.14) and substituting these into eqn. (3.15), we get

$$\frac{ds_h}{dx} = \left(\frac{M_{plate} h_p}{E_p I_p} - \frac{M_{conc} h_c}{E_c I_c} \right) - P_{shear} \left(\frac{1}{E_c A_{conc}} + \frac{1}{E_p A_{plate}} \right) \quad \text{.....(3.16)}$$

From equilibrium of the forces in Fig. 3-9(b),

$$M = M_{conc} + M_{plate} + P_{shear}(h_p - h_c) \quad \text{.....(3.17)}$$

Furthermore, from the assumption of equal curvatures in eqn. (2.13),

$$\kappa = \frac{M_{conc}}{E_c I_c} = \frac{M_{plate}}{E_p I_p} = \frac{M - P_{shear}\left(h_p - h_c\right)}{E_c I_c + E_p I_p} \quad \text{.....(3.18)}$$

Substituting eqn. (3.18) into eqn. (3.16), we get

$$\frac{ds_h}{dx} = \frac{M}{E_p I_p + E_c I_c}\left(h_p - h_c\right) - P_{shear}\left(\frac{\left(h_p - h_c\right)^2}{E_p I_p + E_c I_c} + \frac{1}{E_c A_{conc}} + \frac{1}{E_p A_{plate}} \right) \quad \text{.....(3.19)}$$

For simplification of eqn. (3.19), eqns. (2.15) and. (2.16) can be modified as follows

$$\sum EI = E_p I_p + E_c I_c \quad \text{.....(3.20)}$$

$$\frac{1}{\overline{EA}} = \frac{1}{E_c A_{conc}} + \frac{1}{E_p A_{plate}} \quad \text{.....(3.21)}$$

Inserting eqns. (3.20) and (3.21) into eqn. (3.19), then gives

$$\frac{ds_h}{dx} = \frac{M}{\sum EI}\left(h_p - h_c\right) - P_{shear}\left(\frac{(h_p - h_c)^2}{\sum EI} + \frac{1}{\overline{EA}}\right) \quad \text{.....(3.22)}$$

It can be seen in eqn. (3.22) that the term (h_p-h_c) is the distance between the centroidal axes of the RC element and the plate element. This was (h_c+ h_s) in the case of the standard composite beam in Fig. 2-8. Therefore, the eqn. (2.19) for standard composite beam is the same as the eqn. (3.22) of the side plated beam. Hence, eqns. (2.20) and (2.23) are generic equations that can be used to evaluate the maximum longitudinal slip in the side plated beams.

3.5 SUMMARY

In this chapter, both rigid plastic ultimate strength analyses and the longitudinal slip analysis for standard composite beams have been adapted for side plated beams for use in the analysis of both the experimental work and the computer simulations.

Chapter Four

Basic Theories for Vertical Shear Forces in Side Plated Beams

4.1 INTRODUCTION

In the theories for standard composite beams in Chapter 2, the implicit assumption is that there is no separation or relative vertical movement between the concrete and the steel elements. The reason is that the vertical movement of the two elements relative to each other is severely restricted by bearing of the two elements at the interface and by the axial tensile forces induced in the studs in regions where there is separation. Accordingly, in the development of the basic theories of longitudinal shear forces in side plated beams in Chapter 3, it is assumed that there is no vertical slip between the elements; hence the curvatures in the two elements are considered as equal. In practice, the assumption of no vertical slip is not applicable to side plated beams. The reason is that the only way that longitudinal forces can be induced in the bolted shear connectors is by applying vertical forces to the steel plates and these can only be transmitted to the steel plates through vertical shear forces in the bolted shear connectors. Therefore, it is essential to consider vertical partial-interaction due to vertical shear forces as well as longitudinal shear forces in side plated beams.

In this chapter, it will first be shown qualitatively that the rigid plastic ultimate strength of side plated beams in Sect. 3.2 reduces due to the presence of vertical slip. Then the distribution of the vertical slip will be described qualitatively and quantified for the

simple linear elastic case which will be used in chapter 9 to provide a design rules for vertical slip in side plated beams.

4.2 EFFECT OF VERTICAL SLIP ON RIGID-PLASTIC FLEXURAL STRENGTH

In this section, the effect of vertical slip on the rigid plastic flexural strength of side plated beams will be described. Let us consider the situation of no vertical slip as in the plated beam in Fig. 4-1(a). The curvature in the concrete element κ_c is equal to the curvature in the plate element κ_p in (c). The slip strain at the level of the top bolts $(ds/dx)_t$ is equal to the slip strain at the level of the bottom bolts $(ds/dx)_b$. Therefore, as the slip is derived by integrating the slip strain along the length of the beam, the slip distribution along the shear span is the same at each level so that the force in the shear connectors at each level $(P_{shear}/2)$ is the same as shown in (b). Hence, the axial force in the plate is P_{shear} from which the flexural capacity can be determined.

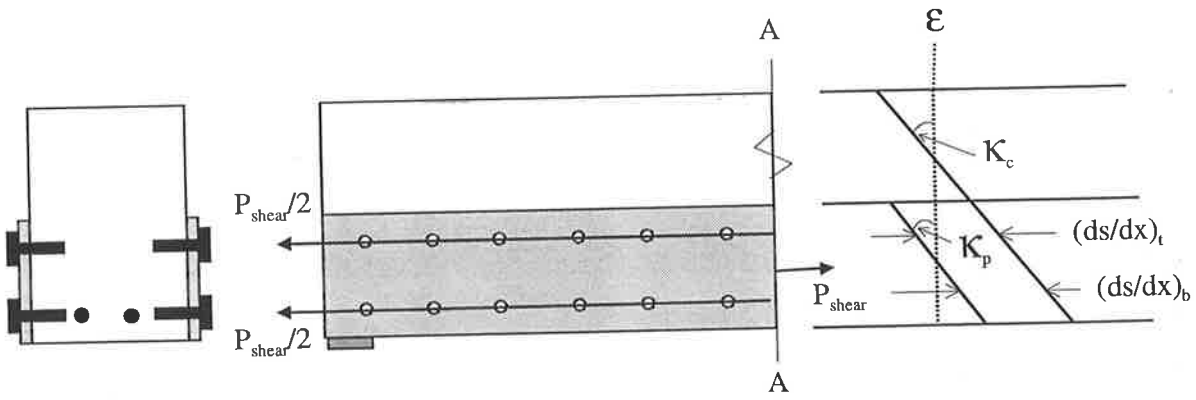

Fig. 4-1 No vertical slip

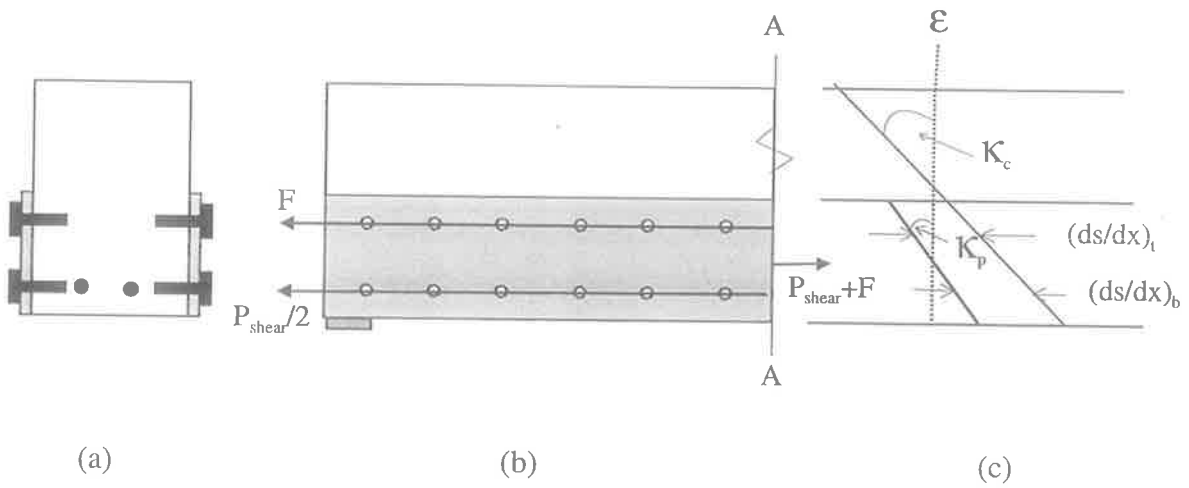

Fig. 4-2 Vertical slip

When there is vertical slip between the plate element and the reinforced concrete element in side plated beams, as shown in Fig. 4-2(a), the deflection of the two elements must be different. As deflection is obtained by integrating the curvature twice, so the only way to have vertical slip, which is the difference in element deflection, is to have different curvatures in the elements, as shown in (c). The different curvatures also means that the slip strains at the two levels of shear connectors have different magnitudes, as shown in (c). Hence, the slip at the bottom level may be greater than that at the top from which the longitudinal force at the top, F, is less than the bottom level. This can cause a considerable reduction in the tensile force in the plate from P_{shear} in 4-1(b) to $P_{shear}/2 + F$ in 4-2(b) and hence a reduction in the rigid plastic flexural capacity. Therefore, it is clear from this example that the vertical slip can reduce the ultimate strength of a side plated beam.

4.3 GENERAL DISTRIBUTION OF VERTICAL SLIP

In this section, the distribution of vertical slip along the length of the beam will be described. Let us consider the simply supported plated beam in Fig. 4-3(a) and assume that there is no shear connection between the elements. In this case, when a load, F, is applied to the RC element, no vertical shear load is transferred into the plate element so that the RC element deflects in contrast to the plate element as shown in (b).

Now, consider the plated beam in Fig. 4-3(a) as a cantilever, as shown in (c). Also, let us assume that there are bolted connections between the elements. In this case, vertical shear loads will be transferred by the bolts into the plate element. The direction of the shear forces acting on the plates is shown in (c). As the concrete element deflects, these forces drag the plate element down as well, but as slip is required to induce these shear forces the deflection of the plate lags behind that of the concrete element. Therefore, a relative vertical slip s_v between elements will occur, as shown in (d), where the deflection of the plate lags behind that of the concrete when the load is applied to the reinforced concrete cantilever.

Now let us consider the plated beam in Fig. 4-3(c) as simply supported instead of a cantilever, as shown in (e). When a load F is applied to the concrete element, vertical shear loads are transferred into the plate element, as shown. At the support, the vertical shear load in the plate element acts upwards and this causes a relative vertical slip s_v at the support, as shown in (f). At mid-span, the vertical shear load in the plate element acts downwards and this causes a relative vertical slip s_{v1} in the mid-span, as shown in (f). From this qualitative analysis it can be seen that the vertical slip of the plate element relative to concrete element reverses direction from the support to the mid-span. Therefore, there will be no vertical slip at some point within the shear span of the plated beam as shown in (f). Also, the maximum vertical slip can be expected to occur at either end of a shear span.

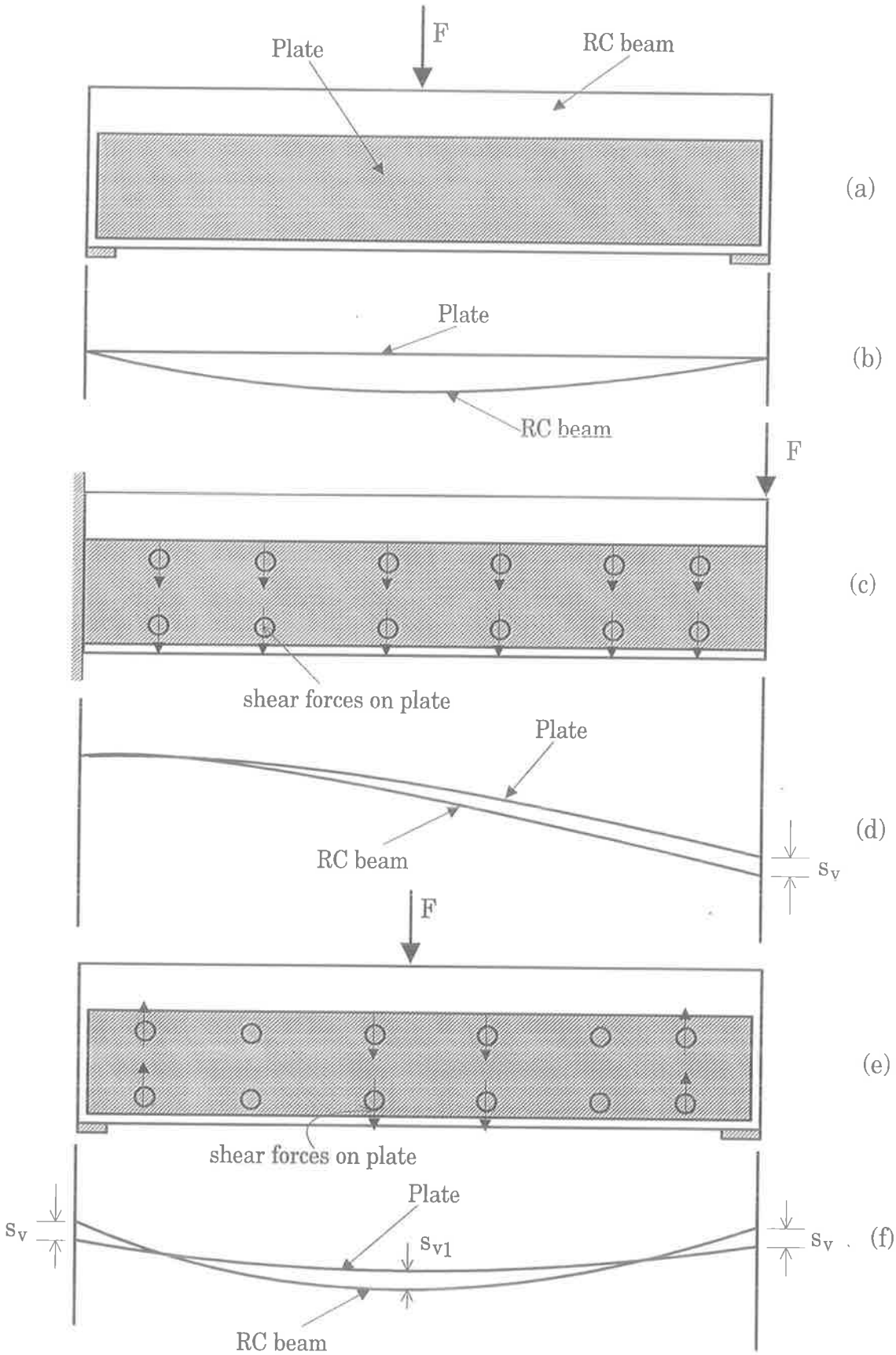

Fig. 4-3 Vertical slip in plated beam

4.4 VERTICAL SHEAR FORCE AND VERTICAL SLIP

In this section, the vertical shear forces that have been discussed in the previous section will be quantified. First, an analysis procedure will be described for vertical full-interaction and it will be followed by the analysis procedure for vertical partial-interaction.

4.4.1 Vertical Full-Interaction

Vertical full-interaction refers to the situation at which no vertical slip occurs in the side plated beam. Hence, it is assumed in the following analysis that both of the elements deflect the same amount. It is also assumed that the concrete and plate elements are linear elastic but the shear connectors are plastic. These assumption are the same as elastic-plastic analysis in Sect. 2.3.2.

Consider the plated beam in Fig. 3-9. As the elements deflect the same amount the curvatures are equal, so that

$$\frac{M_{conc}}{(EI)_c} = \frac{M_{plate}}{(EI)_p} \quad \text{.....(4.1)}$$

The equilibrium equation for the plated beam in Fig. 3-9 is

$$M = M_{conc} + M_{plate} + P_{shear} h_{na} \quad \text{.....(4.2)}$$

where the consideration is that $F_{con} = F_{plate} = P_{shear}$ as described in Sect. 2.3.2.

Solving eqn. (4.1) for M_{conc}, gives

$$M_{conc} = M_{plate} \frac{(EI)_c}{(EI)_p} \quad \text{.....(4.3)}$$

Inserting eqn. (4.3) into eqn. (4.2) gives

$$M = M_{plate}\frac{(EI)_c}{(EI)_p} + M_{plate} + P_{shear}h_{na} \quad \text{.....(4.4)}$$

Solving eqn. (4.4) for M_{plate}, gives

$$M_{plate} = \frac{M - P_{shear}h_{na}}{\left(1 + \frac{(EI)_c}{(EI)_p}\right)} \quad \text{.....(4.5)}$$

Hence, eqn. (4.5) can be used to derive M_{plate} when there is no vertical slip. Considering now the side plated beam in Fig. 4-4, a point load of 2F is applied at the mid-span of the concrete element as shown. It is assumed that the connectors between the ends of a shear span resist longitudinal shear forces as shown and are also fully loaded longitudinally. Furthermore, it is assumed that the bolts near the ends of shear span resist the vertical shear forces as shown. Considering this idealisation, we can view the plate element separately, as shown in Fig. 4-5, where V and P are the resultant vertical and longitudinal shear forces, respectively.

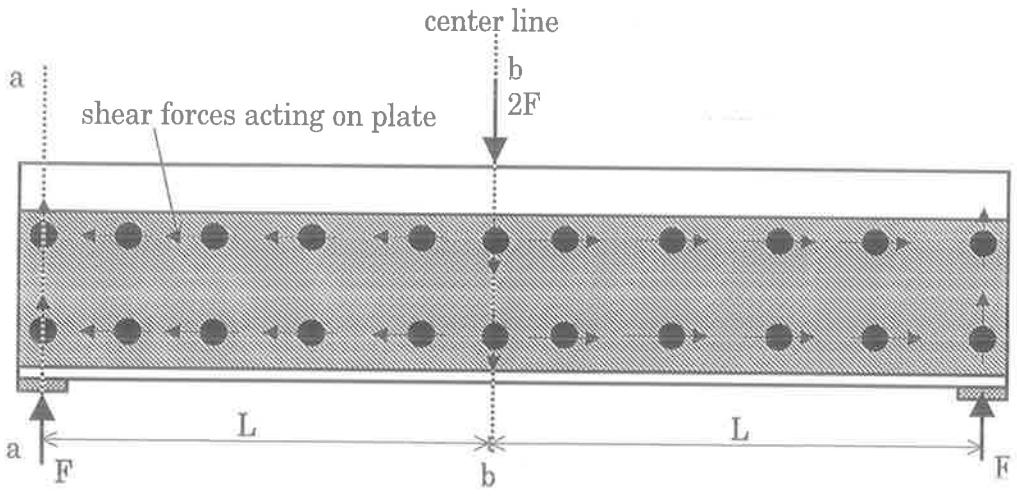

Fig. 4-4 Side plated beam

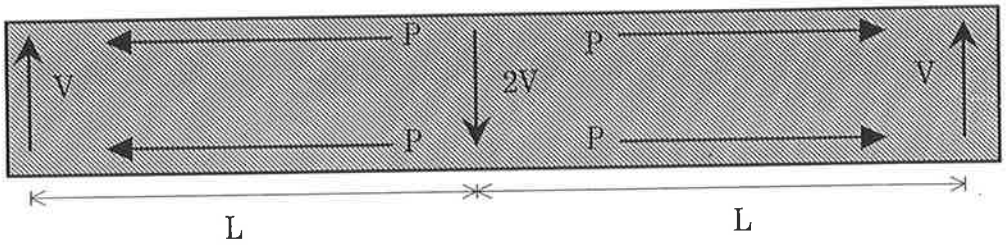

Fig. 4-5 Plate element

From Fig. 4-5 it can be seen that

$$M_{plate} = VL \quad \text{.....(4.6)}$$

Inserting eqn. (4.6) into eqn. (4.5) gives

$$V = \frac{M - P_{shear} h_{na}}{\left(1 + \frac{(EI)_c}{(EI)_p}\right) L} \quad \text{.....(4.7)}$$

Therefore, eqn. (4.7) can be used to derive the vertical shear force, V, when there is no vertical slip that is, when the vertical stiffness of the connectors is very large and hence this calculation can be considered to give an upper bound to the vertical shear forces at the condition of point load in the beam as shown in Fig. 4-4.

4.4.2 Vertical Partial-Interaction

Vertical partial-interaction refers to the situation in which vertical slip occurs in the side plated beam. In this case, the RC element and the plate element do not have the same deflection and hence the curvatures of the elements are not the same. This can be expressed as

$$\frac{M_{conc}}{(EI)_c} \neq \frac{M_{plate}}{(EI)_p} \quad \text{.....(4.8)}$$

As a first approximation, we shall assume a linear variation in the moment distribution in the plate element as shown in Fig. 4-6 for the side plated beam in Fig. 4-4. Selecting the origin at the left end as shown, the moment in the plate element at any point x is

$$M_{plate}(x) = Vx \quad \text{.....(4.9)}$$

Then, the moment in the concrete element at any point x can be derived from eqn. (4.2) as follows

$$M_{conc}(x) = M(x) - M_{plate}(x) - P_{shear}(x)h_{na} \quad \text{.....(4.10)}$$

Inserting the respective parameters in eqn. (4.10), we get

$$M_{conc}(x) = Fx - Vx - qxh_{na} \quad \text{.....(4.11)}$$

where F is the shear load as shown in Fig. 4-4 and q is the longitudinal shear force per unit length of the beam.

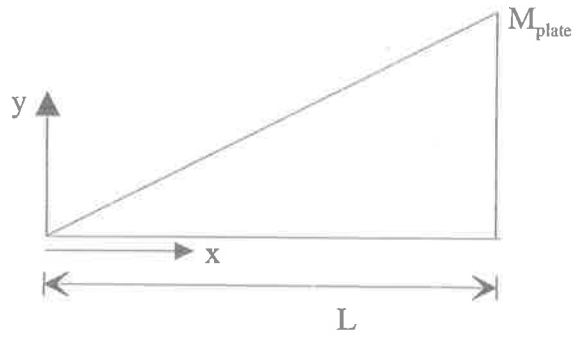

Fig. 4-6 Linear variation in moment distribution in plate

From elementary mechanics, we know that the relationship between the curvature and the moment is

$$\frac{d^2y}{dx^2} = \frac{M_{conc}(x)}{(EI)_c} \quad \text{.....(4.12)}$$

Inserting eqn. (4.11) into eqn. (4.12), gives

$$\frac{d^2y}{dx^2} = \frac{1}{(EI)_c}\left(Fx - Vx - qxh_{na}\right) \quad \text{.....(4.13)}$$

Integrating once gives,

$$\frac{dy}{dx} = \frac{1}{(EI)_c}\left(F - V - qh_{na}\right)\frac{x^2}{2} + C_1 \quad \text{.....(4.14)}$$

The constant in eqn. (4.14) may be evaluated by noting that the slope is zero at the mid-span of the plated beam in Fig. 4-4. That is at x = L, dy/dx = 0 in eqn. (4.14), so

$$C_1 = -\frac{1}{(EI)_c}\left(F - V - qh_{na}\right)\frac{L^2}{2} \quad \text{.....(4.15)}$$

Substituting eqn. (4.15) into eqn. (4.14) gives,

$$\frac{dy}{dx} = \frac{1}{2(EI)_C}\left(F - V - qh_{na}\right)\left(x^2 - L^2\right) \quad \text{.....(4.16)}$$

Integrating eqn. (4.16), gives

$$y_{c(x)} = \frac{1}{2(EI)_c}\left(F - V - qh_{na}\right)\left(\frac{x^3}{3} - L^2x\right) + C_2 \quad \text{.....(4.17)}$$

The constant in eqn. (4.17) can be evaluated at the support of the plated beam in Fig. 4-4 where at x = 0, $y_c = 0$ and hence $C_2 = 0$. Substituting this into eqn. (4.17), gives

$$y_{c(x)} = \frac{1}{2(EI)_c}\left(F - V - qh_{na}\right)\left(\frac{x^3}{3} - L^2x\right) \quad \text{.....(4.18)}$$

The deflection of the concrete element at a distance x = L in Fig. 4-4 is

$$y_{c(x=L)} = -\frac{1}{(EI)_c}(F - V - qh_{na})\frac{L^3}{3} \quad \text{.....(4.19)}$$

Similarly, the deflection in the plate element at a distance x =L in Fig. 4-4 is given by

$$y_{p(x=L)} = -\frac{1}{(EI)_p}\frac{VL^3}{3} \quad \text{.....(4.20)}$$

when the vertical slip at the support is zero, as shown in Fig. 4-7(c). The total vertical slip of the plate element relative to the concrete element, $(s_v)_t$ (sub-script t denotes total), in the shear span, L, is the algebraic difference between the vertical slips at sections a-a and b-b in Fig. 4-4 and is given by

$$\left|y_{c(x=L)}\right| - \left|y_{p(x=L)}\right| = (s_v)_t \quad \text{.....(4.21)}$$

Inserting eqn. (4.19) and (4.20) into eqn. (4.21), gives the total vertical slip, $(s_v)_t$ as

$$\frac{L^3}{3}\left(\frac{F - V - qh_{na}}{(EI)_c} - \frac{V}{(EI)_p}\right) = (s_v)_t \quad \text{.....(4.22)}$$

The distribution of the total vertical slip $(s_v)_t$ in eqn. (4.22) depends on the boundary restraints applied to the plate element. For example, when the ends of the plate are not restrained by the support as shown in Fig. 4-7(a) then for the slip in the shear span L as shown in (b), $(s_v)_t = s_{v1} + s_{v2}$, which is the algebraic difference between the slip at each end of the shear span. However, when the end of the plate is restrained by the support as shown in (c), then $s_{v1} = 0$, as shown in (d), so that $(s_v)_t = s_{v2}$. A similar procedure can be applied when the plate is terminated short of the support as shown in (e). In this case, the distribution of curvatures in the concrete and plate elements are shown in (g) and the difference which is shown shaded in (g) can be used to determine $(s_v)_t$ in (f).

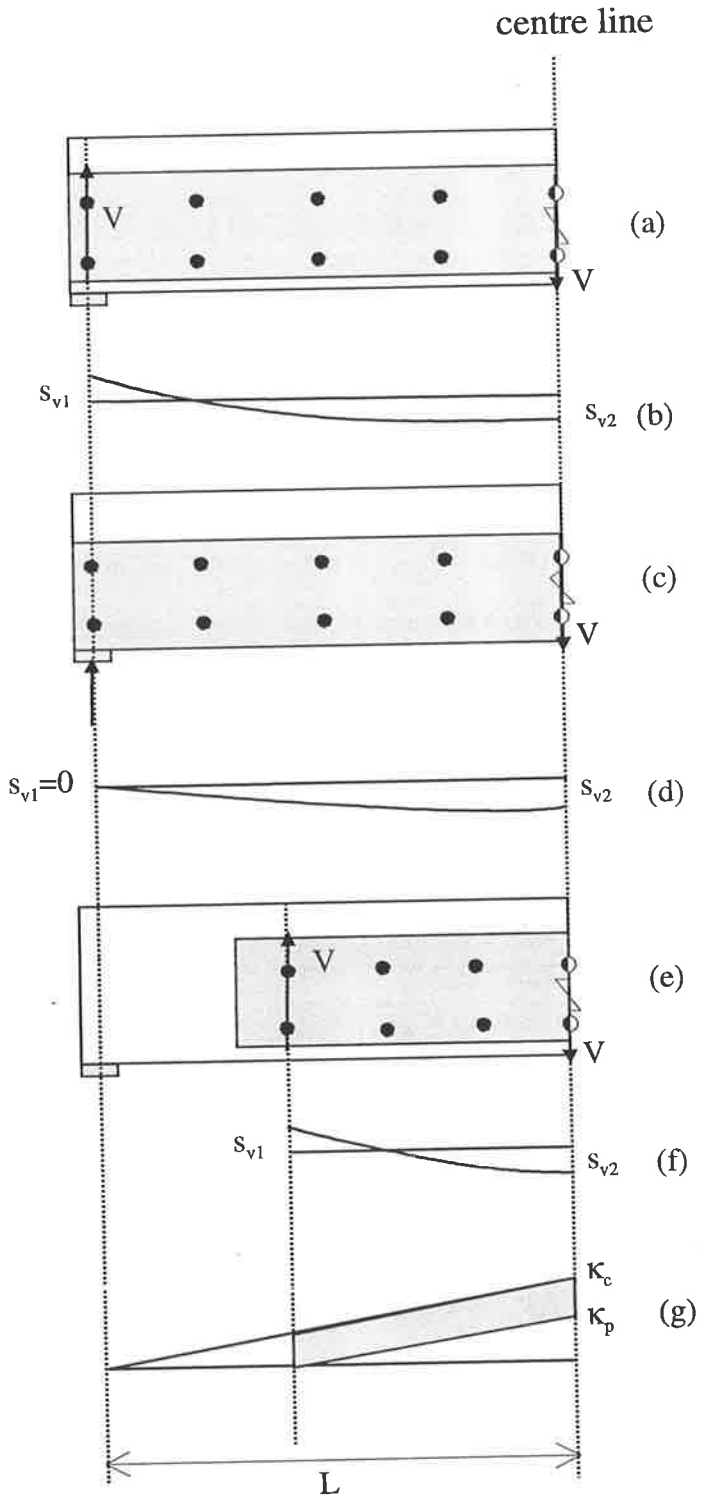

Fig. 4-7 Distribution of vertical slip

In this vertical partial-interaction analysis, it is assumed that the bolted shear connectors which resist the vertical shear forces are linear elastic. The vertical slip, s_v, is then given by

$$s_v = \frac{P_{bolt}}{K_{si}} \quad \text{.....(4.23)}$$

where, K_{si} is the initial modulus of load-slip curve of the bolted shear connector and P_{bolt} is the design vertical force that an engineer requires in one bolt. Alternatively, P_{bolt} can be expressed in the following equation, where β is the reduction factor of the strength of the bolted shear connectors, $(P_{bolt})_{shear}$.

$$P_{bolt} = \beta(P_{bolt})_{shear} \quad \text{.....(4.24)}$$

Hence eqn.(4.23) can be written as

$$s_v = \frac{P_{bolt}}{K_{si}} = \frac{\beta(P_{bolt})_{shear}}{K_{si}} \quad \text{.....(4.25)}$$

For the boundary conditions of the plate element in Fig. 4-7(c), it can be seen in (d) that $(s_v)_t = s_{v2}$. This leads to $(s_v)_t = P_{bolt} / K_{si}$ from eqn.(4.25). Inserting this value of $(s_v)_t$ into eqn. (4.22) we get

$$\frac{L^3}{3}\left(\frac{F - V - qh_{na}}{(EI)_c} - \frac{V}{(EI)_p}\right) = \frac{P_{bolt}}{K_{si}} \quad \text{.....(4.26)}$$

However, for the boundary condition of the plate element in Fig. 4-7(a), $(s_v)_t = s_{v1} + s_{v2} = 2P_{bolt}/K_{si}$, as $s_{v2} = s_{v1}$, because V is applied at each end of the shear span as shown. Hence eqn. (4.26) becomes

$$\frac{L^3}{3}\left(\frac{F - V - qh_{na}}{(EI)_c} - \frac{V}{(EI)_p}\right) = \frac{2P_{bolt}}{K_{si}} \quad \text{.....(4.27)}$$

Therefore, depending on the boundary conditions, eqns. (4.26) or (4.27) may be solved to derive the vertical shear force V for a specific value of P_{bolt}. Hence, the vertical shear force V may be derived when there is vertical partial-interaction. Once V is known then the numbers of bolt that are required to resist the vertical shear force at support end, $n_{v,end}$, can be determined by

$$n_{v,end} = \frac{V}{P_{bolt}} \quad \text{.....(4.28)}$$

The numbers of bolt that are required to resist the vertical shear force at the center of the beam, $n_{v,mid}$ is equal to $2n_{v,end}$ as 2V is applied at mid-span as shown in Fig. 4-5.

Alternatively, the engineer may simply wish to limit $(s_v)_t$ in eqn. (4.22) to some proportion of the slip of the bolted shear connection in order to restrict the difference in curvature between the elements.

In the previous analysis, eqn. (4.22) was derived for a concentrated load at the mid-span as shown in Fig. 4-4. A similar approach can be applied when the beam in Fig. 4-4 is subjected to a uniform distributed load of w per unit length. Then the total vertical slip in the shear span L is expressed by the following equation, a detailed derivation of which is given in Appendix-A.

$$\frac{L^3}{3}\left(\frac{0.625wL - V - qh_{na}}{(EI)_c} - \frac{V}{(EI)_p}\right) = (s_v)_t \quad \text{.....(4.29)}$$

For the case of the beam in Fig. 4-8 which is the type of beam used in the experimental tests in Chapter 8, the total vertical slip in the shear span L is given by the following equation, a detailed derivation of which is given in the Appendix-A.

$$\left(\frac{F - V - qh_{na}}{(EI)_c} - \frac{V}{(EI)_p}\right)\left(\frac{L^3}{6} + \frac{L^3 - 2L^2L_1}{2}\right) = (s_v)_t \quad \text{.....(4.30)}$$

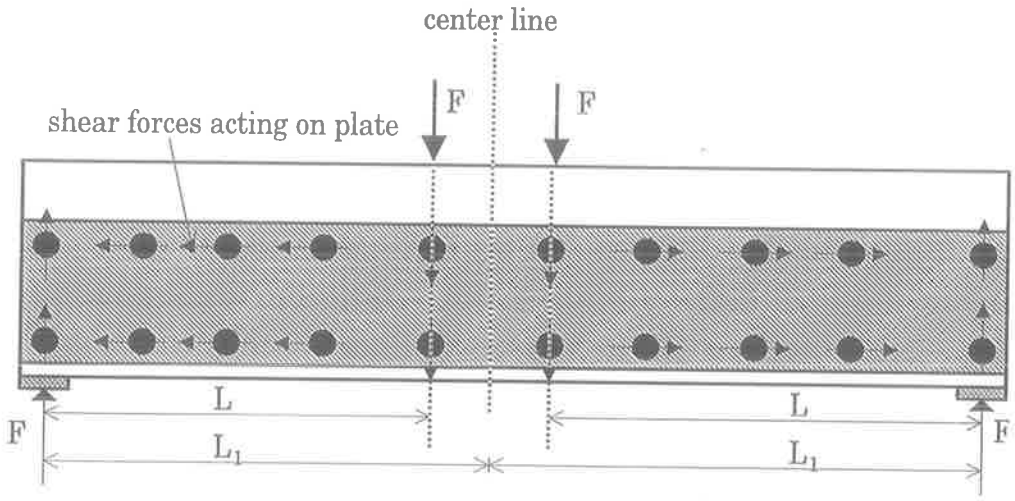

Fig. 4-8 Side plate beam

4.5 MOMENT IN PLATE DUE TO VERTICAL SHEAR FORCE

In this section, the flexure induced in the plate element due to vertical shear force will be discussed. Let us consider the side plated beam in Fig. 4-9(a), where one row of bolts is placed at the mid-depth of the plate. We shall assume the rigid plastic stress profile in the plate as shown in (c), from which the resultant axial force P_{plate} can be determined that acts at a distance l from the center of the plate as shown in (b).

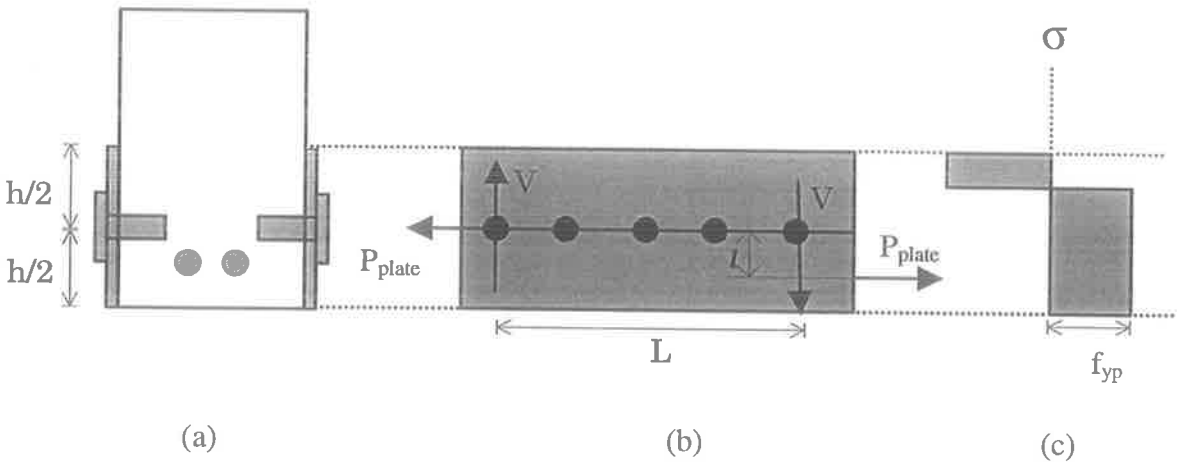

Fig. 4-9 Side plated beam

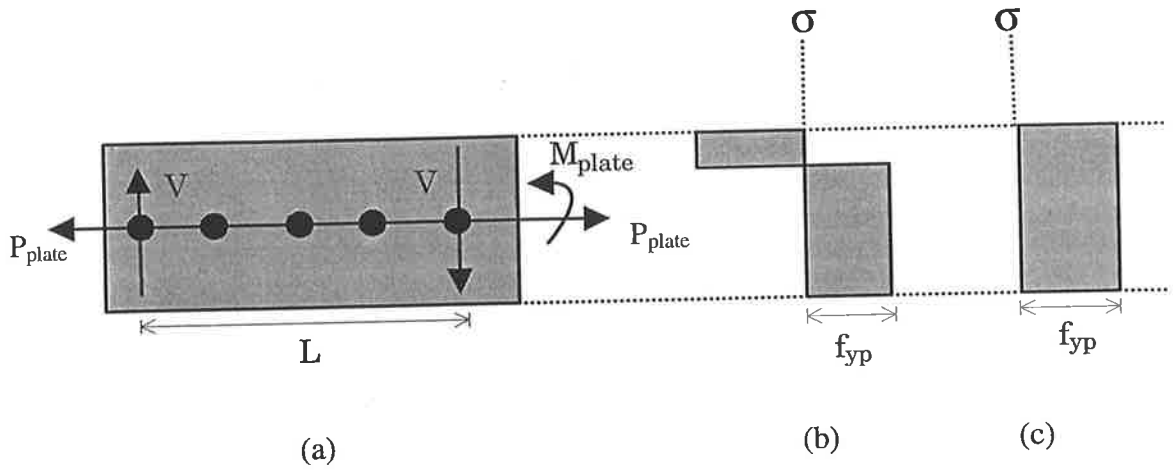

Fig. 4-10 Side plated beam

The forces in the plate element in Fig. 4-7(b) are equivalent to those in Fig. 4-10(a), where the axial force P_{plate}, along with the moment M_{plate}, acts at the mid-depth of the plate element in line with the bolts. Then

$$M_{plate} = P_{plate} l \quad \text{.....(4.31)}$$

and

$$VL = M_{plate} \quad \text{.....(4.32)}$$

Equating eqn. (4.31) and (4.32), gives

$$VL = P_{plate} l \quad \text{.....(4.33)}$$

The above analysis can now be considered for the situation, where the plate element is fully yielded, as shown in 4-10(c). In this case, the resultant axial force P_{plate} must lie at the mid-depth of the plate and so, M_{plate} is equal to zero as $l = 0$ in eqn. (4.31). Therefore, eqn. (4.33) becomes

$$VL = 0 \quad \text{.....(4.34)}$$

This shows that rotational equilibrium cannot be maintained and the fundamental equation for the vertical shear force is also not obtained. Therefore, it can be concluded that the

plate element can not be fully yielded when the connectors lie in the center line of the plate. However, full yielding of the plate element can be obtained by finding a suitable position and distribution of the connectors so that the resultant shear force does not lie at the center line of the plate. In the case of two lines of connectors as in Fig. 4-2(a), the resultant longitudinal force will not be at the center line of the plate as the slip varies between the top and bottom rows of bolts and hence, full yielding of the plate can be achieved.

4.6 SUMMARY

The presence of vertical slip in side plated beams has a significant effect on the rigid plastic flexural strength. A simple procedure to determine the vertical slip and thereby the vertical shear force has been described and it has been shown qualitatively that both the position and distribution of the bolts over the shear span have a significant effect on rigid plastic strength of side plated beams.

Chapter Five

Computer Model

5.1 INTRODUCTION

The bolts in side plated beams are subjected to both longitudinal shear forces and vertical shear forces. As such, they are prone to longitudinal slip and vertical slip. Longitudinal slip has been discussed in Chapter 3 and vertical slip in Chapter 4, where rigid-plastic, linear-elastic and linear elastic-plastic theory have been used. In this chapter, non-linear computer models will be described to quantify both longitudinal slip and vertical slip.

The non-linear computer model for standard composite beams described in Sect. 2.5 deals with two situations: one with full interaction; and the other with partial interaction. In the full interaction situation, the assumption is that the shear connectors are infinitely stiff in both the longitudinal direction and vertical direction, so the shear connectors do not slip in any direction. In the partial interaction situation, the shear connectors are assumed to be infinitely stiff in the vertical direction but flexible in longitudinal direction. Therefore, the shear connectors slip only in the longitudinal direction. This computer model for both of these situations will be adapted for side plated beams. Furthermore, an analysis technique for side plated beams will be presented that assumes that the bolts do not slip in the longitudinal direction but slip in the vertical direction. That is, the bolts are infinitely stiff in longitudinal direction but flexible in vertical direction. This will be followed by the analysis technique that assumes that the bolts are flexible in both the longitudinal and vertical directions. That is, the bolts slip in both the longitudinal and vertical direction which is what occurs in reality.

First, the material properties of the elements of side plated beams used in the computer model will be described. This will be followed by the analysis of the equilibrium of forces in the side plated beams and description of different computer models.

5.2 MATERIAL PROPERTIES

In this section, material properties of different elements of the side plated beams that will be used in the computer model in Sect. 5.4 will be presented.

5.2.1 Plate and Reinforcement

The stress-strain curve for the plate elements and reinforcing bars are assumed to be initially a straight line from zero stress to the yield strength f_{yp} at a slope equal to the modulus of elasticity E_p as shown in Fig. 5-1, where E_p is 200 GPa. The strain is assumed to increase, thereafter, at a constant stress ignoring any strain-hardening. Hence the plate exhibits linear elastic-plastic behaviour as shown in Fig. 5-1. For the computer modelling, the stress-strain curve for tension and compression are considered to be identical.

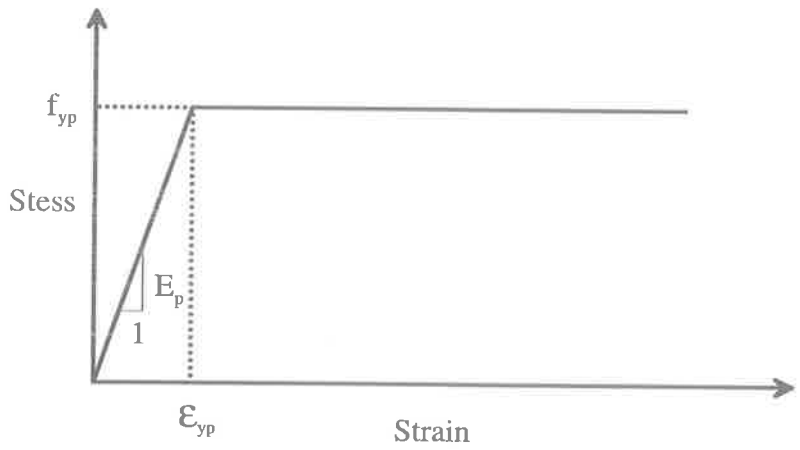

Fig. 5-1 Stress-strain relation of plate and reinforcement

5.2.2 Compressive Concrete

The stress-strain relationship adopted for compressive concrete is that recommended by Warner (1969) for normal-density concrete. This relationship is represented by using a non-dimensionalized stress, S, and a normalized strain, E. The non-dimensionalised stress, S, is given by

$$S = \frac{\sigma}{\sigma_u} \qquad \text{.....(5.1)}$$

where σ is the strength in concrete and σ_u is the cylinder strength of the concrete. The normalized strain, E, is given by

$$E = \frac{\varepsilon}{\varepsilon_c} \qquad \text{.....(5.2)}$$

where ε is the strain in concrete and ε_c is the strain in concrete at σ_u; where $\varepsilon_c = 0.0041 - 0.000026\sigma_u$ (Oehlers and Bradford, 1995). The following equations are used to represent the relationship between the strain and stress for monotonically increasing strain.

$$0 \le E \le 1.0 \qquad S = \gamma_1 E + (3 - 2\gamma_1)E^2 + (\gamma_1 - 2)E^3 \qquad \text{(5.3a)}$$

$$1.0 \le E \le \gamma_2 \qquad S = 1 - \frac{1 - 2E + E^2}{1 - 2\gamma_2 + \gamma_2^2} \qquad \text{(5.3b)}$$

$$E > \gamma_2 \qquad S = 0 \qquad \text{(5.3c)}$$

Where the parameters γ_1 and γ_2 are shown in Fig. 5-2 and define the shape of the loading and unloading portions of the curve respectively.

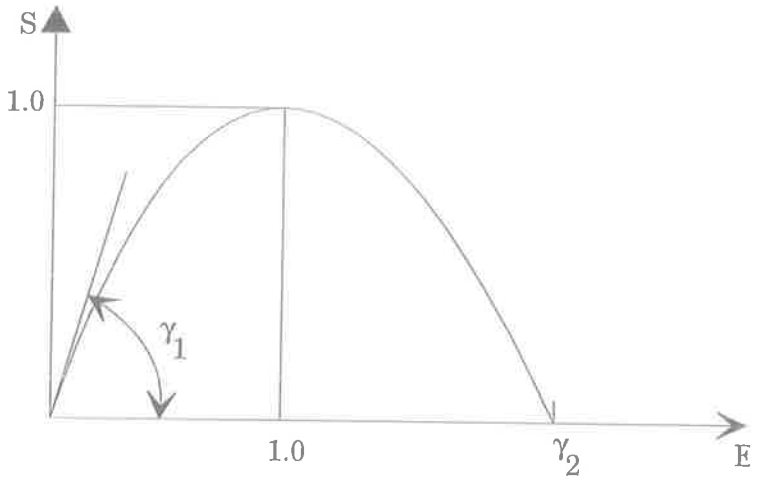

Fig. 5-2 Stress and strain of concrete in compression

Thc initial slope parameter γ_1 is fixed by the initial elastic modulus of concrete E_c and is given by

$$\gamma_1 = \frac{E_c \varepsilon_c}{\sigma_u} \quad \text{.....(5.4)}$$

There is no rational value for γ_2 and no physical significance has been given to this point (Warner 1969). However, a value of 3.0 has been used in different numerical calculations (Warner and Lambert, 1974; Kotsovos, 1984; Burnet, 1996) which has, therefore, also used in the present computer model.

5.2.3 Tensile Concrete

The stress-strain curve for concrete in tension (Bazant and Oh, 1984; Burnet, 1996) is shown in Fig. 5-3. This shows that the concrete behaves linearly up to the tensile strength of concrete, f_t, with a slope equal to that in compression in Sect. 5.2.2. The tensile strength of concrete, f_t, is the modulus of rupture strength and is given by

$$f_t = 0.6\sqrt{f_c} \quad \text{.....(5.5)}$$

where both strengths are in N/mm^2. Once the concrete tensile failure strain, ε_t, in Fig. 5-3 has been exceeded, the stress in the concrete diminishes to zero at $10\varepsilon_t$ (Gilbert and Warner, 1978), as shown in Fig. 5-3. This allows for the decreasing effect of tension stiffening with strain.

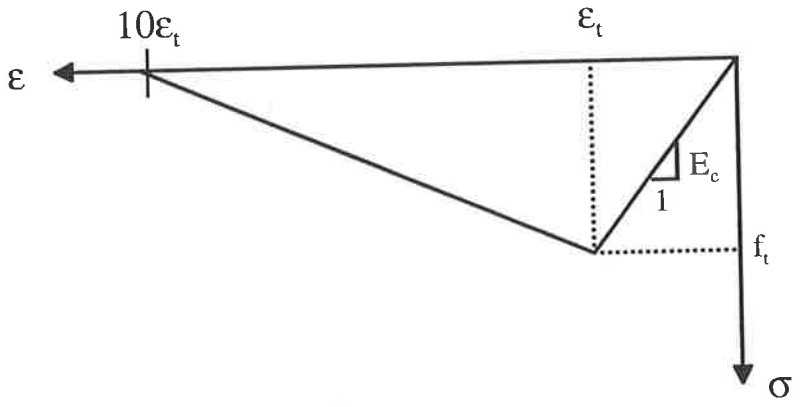

Fig. 5-3 Tensile properties of concrete

5.2.4 Bolted Shear Connection

The shear load-slip curve of bolted shear connections is shown in Fig. 5-4. This shows that the variation of shear load and slip is linear up to the maximum shear load, D_{max}, at slip s_{si} where the initial modulus is K_{si}. The slip then increases to s_{end} at a constant shear load of D_{max}, after which the strength diminishes to zero with a slope of K_{end}. This linear elastic-plastic behaviour of bolted shear connection will be shown in Chapter 8, where the push test results will be presented.

5.3 ANALYSIS OF EQUILIBRIUM OF FORCES

In this section, the distribution of longitudinal and vertical shear forces in the elements of side plated beams will be described and hence, equilibrium equations will be presented as this will be used in the computer model in Sect. 5.4.

Consider the simply supported plated beam in Fig. 5-5. A point load, F, is applied at the mid-span of the beam that induces both longitudinal and vertical shear forces at the

bolted connections and a reaction at the support of *0.5F*, as shown. Now, consider the shear forces in the concrete element and the plate element separately in the shear span of length, *b*, by cutting the beam at section a-a as follows.

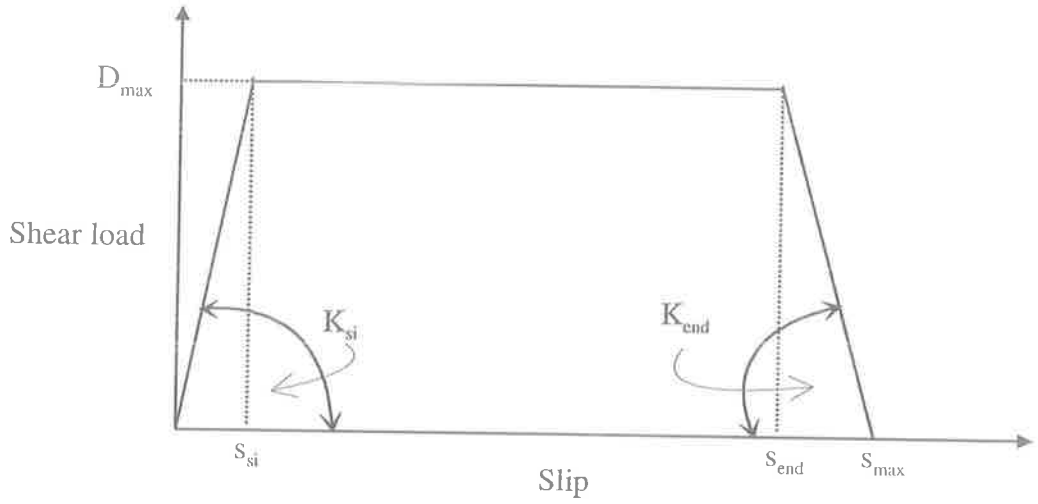

Fig. 5-4 Bolted shear connection

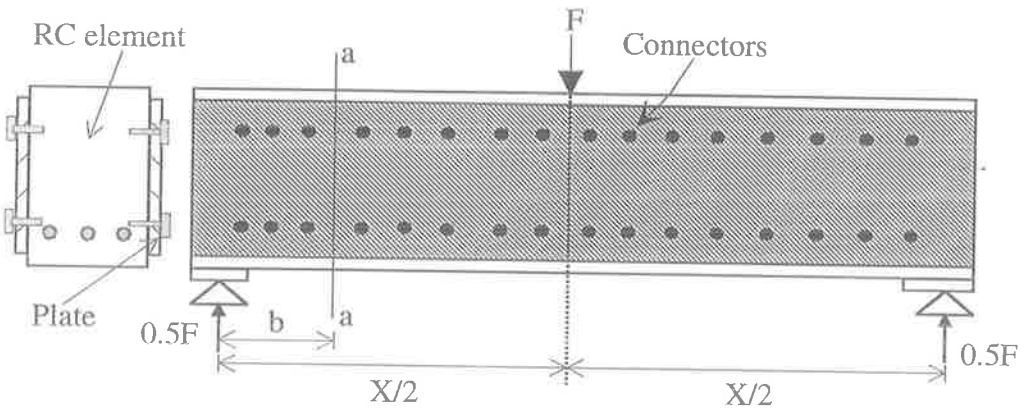

Fig. 5-5 Plated beam

5.3.1 Forces in Plate Element

The longitudinal and vertical shear forces that occur at the bolt positions in the plate element are shown in Fig. 5-6(a) and then the stress distribution at cut a-a is shown in (b).

The resultant of all the longitudinal shear forces, P, is acting at a distance, l, from an arbitrary point O on the cut and the resultant of all the vertical shear forces V is acting at a distance L from point O as shown in (c). The internal forces on the plate acting at the cut about point O are shown in (c) where M_{plate} is the internal moment of the plate. Considering rotational equilibrium about point O, gives

$$M_{plate} - VL + Pl = 0 \quad \text{.....(5.6)}$$

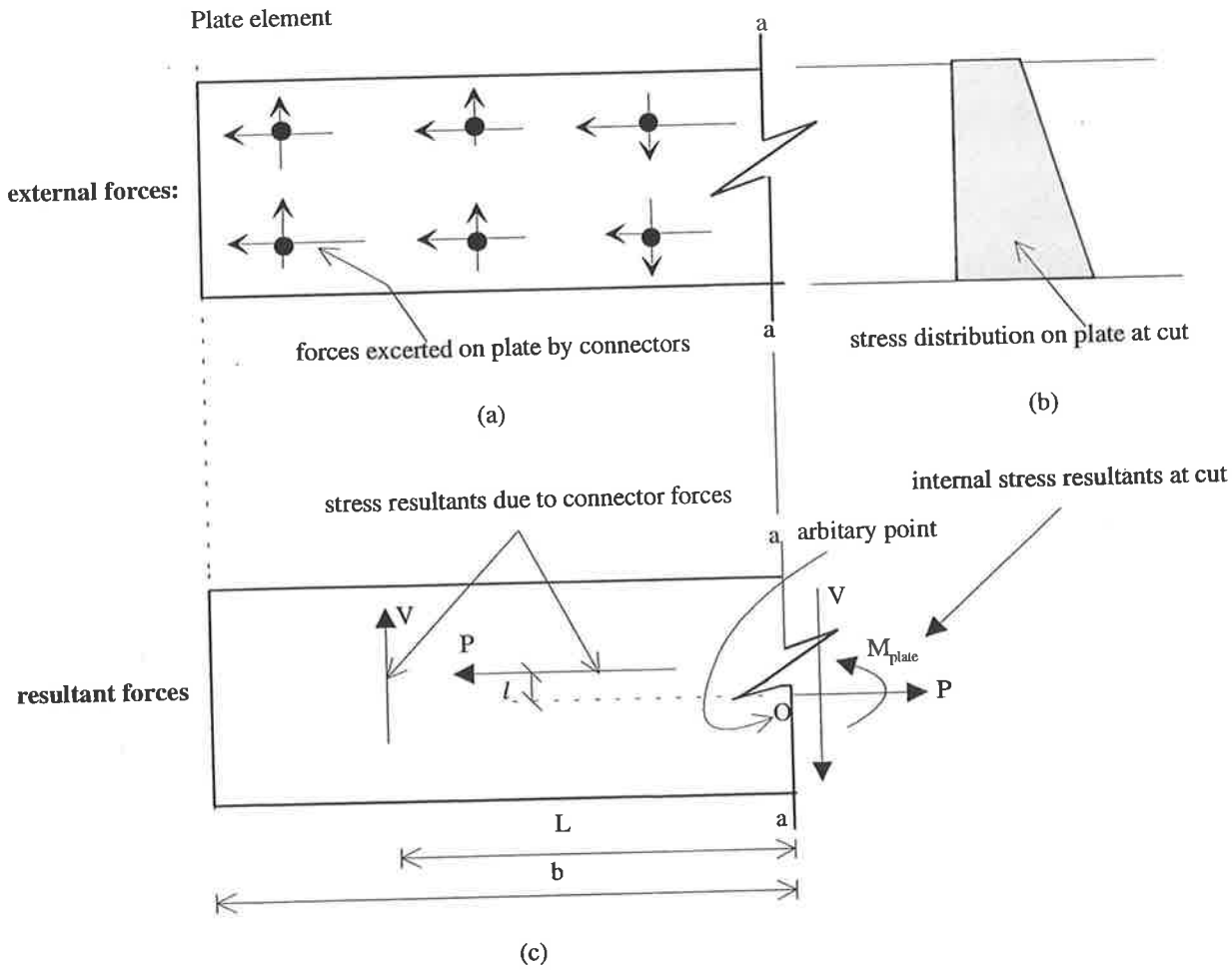

Fig. 5-6 Forces in plate

5.3.2 Forces in Concrete Element

The longitudinal and vertical shear forces that occur at the bolt positions in the concrete element are shown in Fig. 5-7(a). Their resultant forces P and V respectively are shown in (c). These forces act at the same position as those shown in the plate element in Fig. 5-6(c). The internal forces acting at the cut of the concrete element are shown in Fig. 5-7(c), where M_{conc} is the moment in the concrete element. Considering rotational equilibrium about point O, gives

$$M_{conc} + VL - Pl - \frac{F}{2}b = 0 \quad \text{.....(5.7)}$$

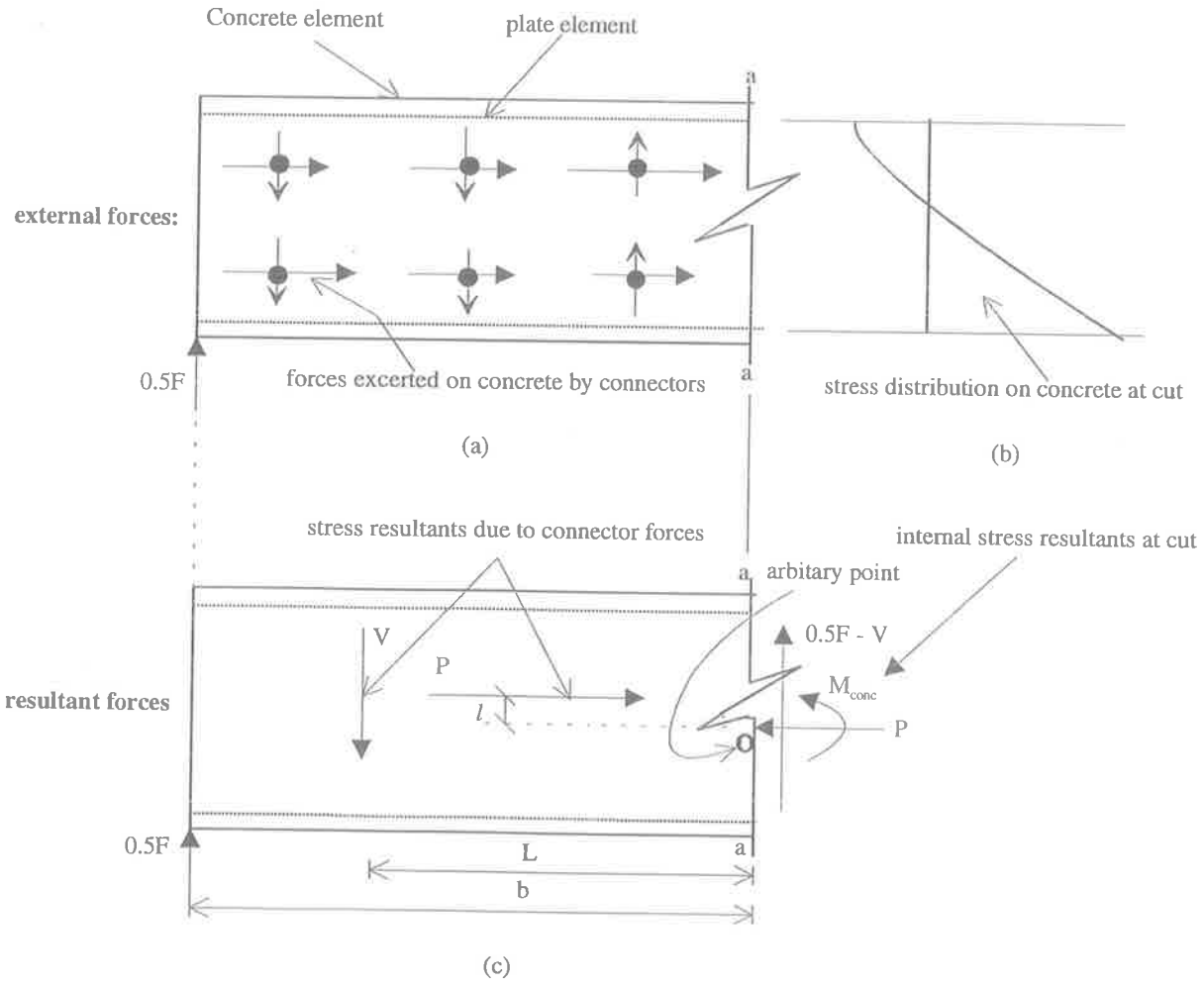

Fig. 5-7 Forces in RC element

Adding equation (5.6) and (5.7), gives

$$M_{conc} + M_{plate} = \frac{F}{2}b \quad \text{.....(5.8)}$$

The applied moment, M, at section a-a, in Fig. 5-5, due to the point load, F, on the plated beam is given by

$$M = \frac{F}{2}b \quad \text{.....(5.9)}$$

Inserting eqn. (5.9) into eqn. (5.8) gives,

$$M_{conc} + M_{plate} = M \text{.....(5.10)}$$

Thus, the summation of the moment contribution of the plate and the concrete element at any particular point along a section is equal to the applied moment at the same section. This elementary theory will be used in the computer model in the next section.

5.4 COMPUTER MODELS

Four computer models will be described in this section which are given in Table 5.1. The equilibrium of forces in the plate element and in the concrete element in Figs. 5-6 and 5-7 have been used to develop the algorithms of the computer models in the following sections.

Table 5.1 Description of different computer model of side plated beams

Computer model	Purpose
1	2
Computer Model 1	to analysis for longitudinal and vertical full-interaction
Computer Model 2	to analysis for longitudinal partial-interaction but vertical full-interaction
Computer Model 3	to analysis for vertical partial-interaction but longitudinal full-interaction.
Computer Model 4	to analysis for longitudinal and vertical partial-interaction

5.4.1 Computer Model 1: Longitudinal and Vertical Full-Interaction Analysis

This computer model assumes that the bolted shear connectors are stiff in both the longitudinal and vertical direction; therefore, longitudinal and vertical full interaction occurs at the interface of the plated beams. A full interaction analysis procedure of a standard composite beam has been fully described in Sect. 2.5.1. This procedure, which was developed for standard composite beams in which the elements lie one above the other, has been adapted for side plated beams in which the elements lie side to side. This adaptation is very simple and, therefore, this will not be described in this chapter.

5.4.2 Computer Model 2: Longitudinal Partial-Interaction and Vertical Full-interaction Analysis

This computer model assumes that the bolts are stiff in the vertical direction and flexible in the longitudinal direction, that is, that the bolts experience no vertical slip but do experience longitudinal slip. As vertical slip is zero, the curvatures in the concrete and plate elements are equal and, therefore, the strain profile of both the elements are parallel, as shown in Fig. 3-2. This situation has been dealt with fully in Sect. 2.5.2 for standard

composite beams and this procedure has been adapted for side plated beams. As with the 'full interaction analysis' of Sect. 5.4.1, the existing programme was simply adapted to analysis elements that were side by side.

5.4.3 Computer Model 3: Longitudinal Full-interaction and Vertical Partial-interaction Analysis

In order to study the effect of vertical partial-interaction by itself, an analysis procedure will be presented in this section that assumes that the bolted shear connectors can slip in the vertical direction but not in the longitudinal direction.

Figure 5-8 shows a half span of a simply supported beam with a single row of bolts. The analysis technique will be described for a point load at the mid-span, however the same procedure can be applied to other type of loadings. Again, in this analysis, the bolts are assumed to be equally spaced over the length of the beam and are located at the mid-length of each segment as shown; however the procedure can be applied to any distribution of connectors. For the purpose of this analysis, the half span of the beam is divided into numbers of segments equally spaced at a distance dx apart, as shown in Fig. 5-8. The analysis proceeds by considering the segments sequentially, i.e. first Segment 1 up to point 2, then Segment 1 and 2 up to point 3 and so on, which is similar to the computer model in Sect. 2.5. At each section, the elements are separated as described in Sect. 5.3 (i.e. Figs. 5-6 and 5-7) and first rotational equilibrium and then longitudinal equilibrium of forces are established by trial and error method as described in the following section.

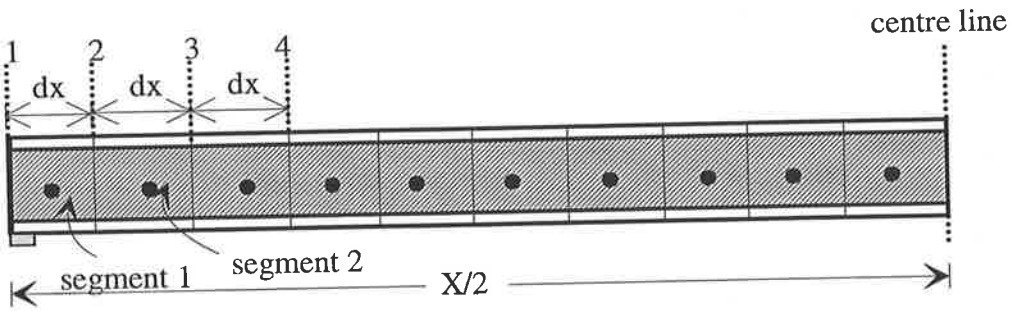

Fig. 5-8 Plated RC beam

5.4.3.1 Concrete element

Figure 5-9 shows the RC element of segment 1 in Fig. 5-8. Let us assume that the bolts in this segment experience a longitudinal shear force P_1 and a vertical shear force V_1 (sub-script 1 denotes the segment number) when the support has a reaction R as shown in Fig. 5-9(a). There will then be a strain distribution at a-a, as shown in (b), that has the curvature κ_{c1} and a neutral axis that is located at a distance y_{c1} from the top fiber of the concrete element (sub-script c denotes the concrete element and sub-script 1 denotes Segment 1). The corresponding stress distribution is shown in (c). The element is divided into a number of slices so that the procedure in the computer model in Sect. 2.5 is followed to calculate the strain, stress and force in each of the slices. Then the following equation can be derived from the rotational equilibrium about point O that lies at the level of shear connectors.

$$Rdx - V_1 \frac{dx}{2} + \sum_{i=1}^{n} y_i F_i = 0 \quad \text{.....(5.11)}$$

where n is the number of the slice in the concrete element, y is the distance between the mid-depth of a slice and the level of bolted shear connectors as shown in Fig. 5-9(b) and F is the force in the slice as shown in (d). Equation (5.11) is solved by using the trial and error method. However, it would be tedious to get an unique solution and as such, the following approximation is used in the computer model.

$$\frac{\left|Rdx - V_1 \frac{dx}{2}\right| - \left|\sum_{i=1}^{n} y_i F_i\right|}{\left|Rdx - V_1 \frac{dx}{2}\right| + \left|\sum_{i=1}^{n} y_i F_i\right|} \leq 0.0005 \quad \text{.....(5.12)}$$

The numerator in eqn. (5.12) is the difference between the magnitudes of the external moment and internal moment at the cut whereas the denominator is the sum of both the magnitudes. Therefore, the left hand side of eqn. (5.12) can determine an error between the external moment and the internal moment in the segment in question as a proportion of approximately twice the external moment. In this computer model, an error of 0.05% has been adopted which is shown in the right hand side of eqn. (5.12).

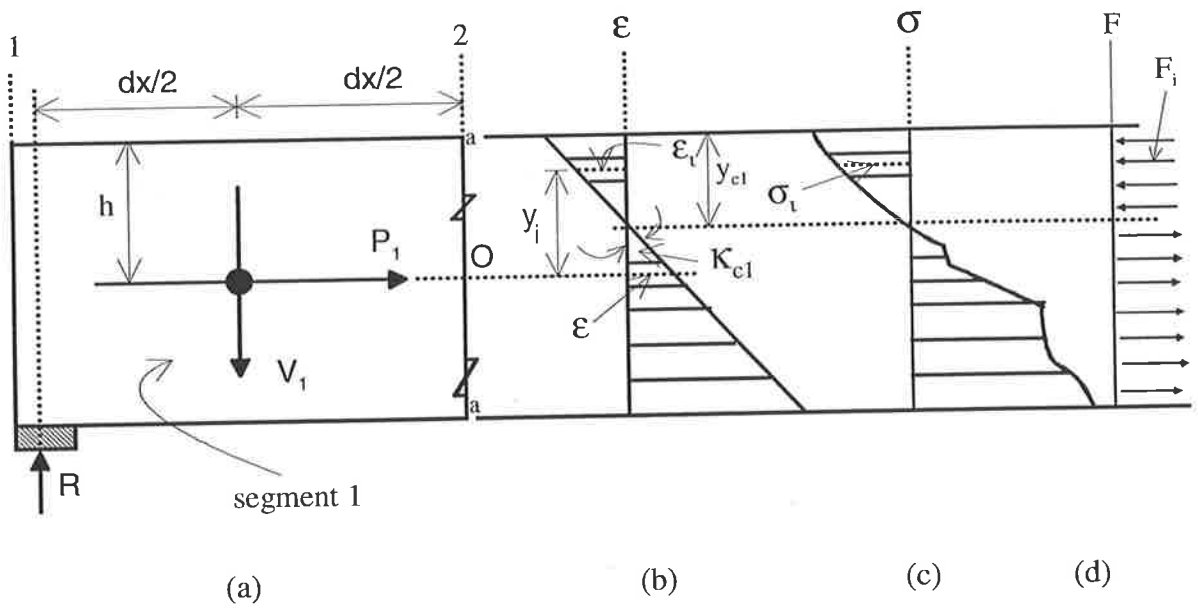

Fig. 5-9 RC element

It is worth mentioning at this stage that we are dealing with longitudinal full interaction, that is no longitudinal slip between the elements at the level of shear connectors. This can be achieved when the strain in the concrete and plate element at the level of shear connector is equal. Hence eqn. (5.12) can be solved for an estimated strain ε in Fig. 5-9(b). This will be kept equal in the analysis of the plate element in the same segment.

First, an estimate of the vertical slip s_{v1} (sub-script v1 denotes vertical slip in Segment 1) is made, which is used to evaluate the vertical shear force V_1 from the known load-slip curve of the bolted shear connector. Then, for a given curvature κ_{c1}, the neutral axis position y_{c1} is determined from the estimated strain ε at the level of shear connectors as shown in Fig. 5-9(b). These are used to determine the strain distribution and thereby the stress distribution in (c) from the known stress-strain relationships of the materials. Then the forces in each slice in the concrete element F in (d) are evaluated. At this stage, eqn. (5.12) is checked. If it is not satisfied, a new value of curvature is chosen and the above procedure is repeated until eqn. (5.12) is satisfied.

Having obtained a solution, the longitudinal shear force in segment 1 is determined by summing the forces in (d), that is

$$\left(F_{shear}\right)_{c1} = \sum_{i=1}^{n} F_i \quad \text{.....(5.13)}$$

Furthermore, the moment in the concrete element at the level of the shear connectors at point O can be derived from eqn. (5.11) as

$$\left(M_{conc}\right)_1 = Rdx - V\frac{dx}{2} \quad \text{.....(5.14)}$$

Equation. (5.13) and (5.14) are now used in the following analysis of plate element. It is worth noting that the vertical slip of the first segment s_{v1} and estimated strain ε in the concrete element at the level of shear connectors are guessed. Both of these parameters are yet to be determined.

5.4.3.2 Plate element

Figure 5-10 shows the plate element in segment 1. The longitudinal shear force P and vertical shear force V are now known from the analyses of the concrete element in the previous section. Also the moment in the plate element M_{plate} is known from eqns. (5.10) and (5.14) as M_{conc} in eqn. (5.10) is $(M_{conc})_1$ in eqn. (5.14) and M in eqn. (5.10) is the externally applied moment at section a-a in Figs. 5-11 and 5-12.

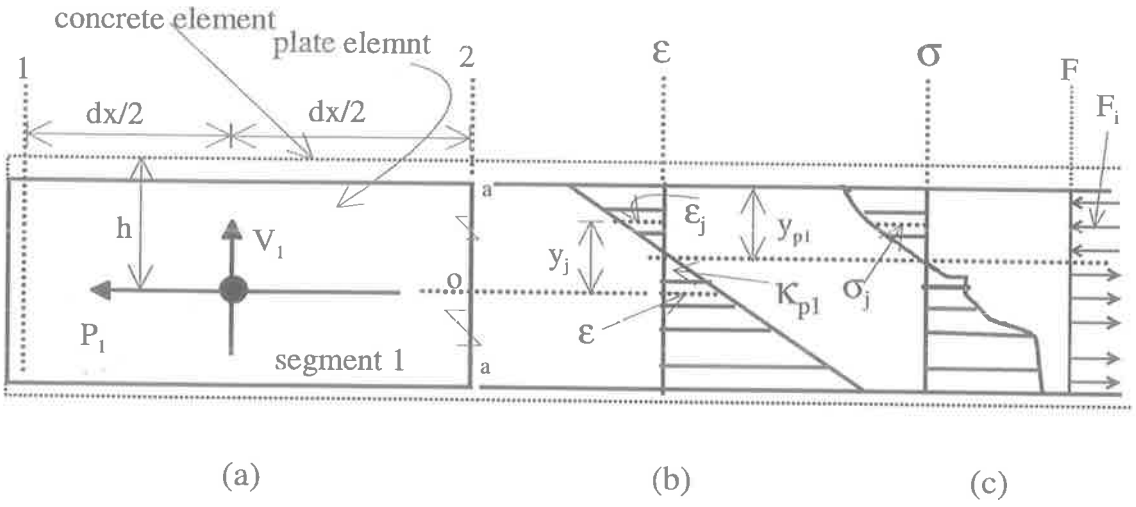

Fig. 5-10 Plate element

As we are dealing with longitudinal full interaction, the strain at the level of longitudinal shear force in the concrete element and plate element must be equal, as shown by ε in both Figs. 5-9(b) and 5-10(b). Therefore, for a given curvature κ_{p1} in the plate element in Fig. 5-10(b) (sub-script p1 denotes the plate element in Segment 1), the location of the neutral axis y_{p1} is fixed by the estimated strain, ε, at the level of the longitudinal shear force in the plate element. A check is now made for rotational equilibrium at point O in Fig. 5-10, which gives

$$V_1 \frac{dx}{2} - \sum_{j=1}^{m} y_j F_j = 0 \quad \text{.....(5.15)}$$

As for the concrete element, the following approximation is used for the plate element which can determine an error between the external moment and internal moment in the segment in question as a proportion of approximately twice the external moment. The acceptable error is 0.05% as shown in the right hand side of eqn. (5.16).

$$\frac{\left|V_1 \frac{dx}{2}\right| - \left|\sum_{j=1}^{m} y_i F_i\right|}{\left|V_1 \frac{dx}{2}\right| + \left|\sum_{j=1}^{m} y_i F_i\right|} \leq 0.0005 \quad \text{..... (5.16)}$$

If eqn. (5.16) is not satisfied, then a new value of curvature is chosen and the above procedure is repeated.

Once the curvature and the neutral axis position, y_{p1}, in Fig. 5-10(b) is fixed, the longitudinal shear force is obtained in the usual way from the following summation of the forces in the slices from (d).

$$\left(F_{shear}\right)_{p_1} = \sum_{j=1}^{m} F_j \quad \text{.....(5.17)}$$

where m is the number of slices in the plate element. A check is then made whether the longitudinal shear force in plate element in eqn. (5.17), is the same as that in the concrete

element in eqn. (5.13). The following approximation is used in the computer model to make this check in order to maintain longitudinal equilibrium.

$$\frac{\left|(F_{shear})_{c1}\right| - \left|(F_{shear})_{p1}\right|}{\left|(F_{shear})_{c1}\right| + \left|(F_{shear})_{p1}\right|} \leq 0.0005 \quad \text{.....(5.18)}$$

Equation (5.18) determines the error between the longitudinal force in the concrete element and in the plate element as a proportion of twice the longitudinal force in the concrete element. If eqn. (5.18) is not satisfied, a new value of strain in the concrete element is chosen for ε in Fig. 5-9(b) and the analysis re-start from the concrete element. The above procedures are repeated for this new strain profile until eqn. (5.18) is satisfied. At this stage we have horizontal equilibrium as P1 in the plate element in Fig. 5-9 is equal to P_1 in the concrete element in Fig. 5-10.

When eqn. (5.18) is satisfied, the change in vertical slip Δs_{v1} over segment 1 is evaluated by twice integrating the difference between the curvature in the concrete element and in the plate element. It is assumed that the difference between curvatures is constant between the mid-sections of adjacent elements. The change in vertical slip Δs_{v1} from the bolt groups in segment 1 to that in segment 2 is given by

$$\Delta s_{v1} = (\kappa_{c1} - \kappa_{p1})\frac{(dx)^2}{2} + (\nu'_{c1} - \nu'_{p1})dx \quad \text{.....(5.19)}$$

where ν'_{c1} is the slope in the concrete element and ν'_{p1} is the slope in the plate element, which depends on the initial estimate of the difference in slope, which also depends on the boundary condition. This can then be used to estimate the vertical slip in Segment 2 as

$$s_{v2} = s_{v1} - \Delta s_{v1} \quad \text{.....(5.20)}$$

The analysis procedure described above for a section of the plated beam comprising of segment 1 in Fig. 5-8 can now be applied to a section of the beam comprising of segments 1 and 2. Hence, the beam is now cut at section 3 and equilibrium over a shear span of length 2dx is considered to determine the vertical slip in Segment 2. This way the analysis proceeds up to the segment at mid-span where the following boundary condition is checked

$$V_1 + V_2 + V_3 + \cdots\cdots\cdots + V_n = 0 \quad \text{.....(5.21)}$$

as well as the slope at mid-span being zero. The left hand side of eqn. (5.21) is the summation of vertical shear forces along the length of the beam. If eqn. (5.21) is not satisfied, a new estimate of vertical slip s_{v1} is made at the Segment 1 and the whole procedure described before is repeated until eqn. (5.21) is satisfied.

This computer model can only be applied to a single row of connectors as we can only get zero slip strain at one level when the curvatures of the elements are different. Hence, we can only get longitudinal full interaction at one level only when there is vertical slip.

5.4.4 Computer Model 4 : Longitudinal Partial-Interaction and Vertical Partial-Interaction Analysis

In this section, an analysis technique is presented that represents the real behaviour of the bolted shear connector, that is the shear connector slips in both the longitudinal and vertical direction. The analysis is similar but not the same as that described in Sect. 5.4.3.

The same beam in Fig. 5-8 will be used in describing the algorithm of Model 4. The beam is divided into a numbers of segments as in the previous analysis. The analysis starts with an initial estimate of the longitudinal and vertical slip at segment 1 in Fig. 5-8, from which the corresponding vertical and longitudinal shear loads are evaluated from the defined load-slip curve. The elements are separated as in the previous analysis.

5.4.4.1 Concrete element:

The longitudinal shear force P_1 and the vertical shear force V_1 in Fig. 5-9(a) are known. For a given curvature κ_{c1} in (b), an estimate is made of the neutral axis position y_{c1} so that we know the strain distribution and can determine the strain, stress and force in each slice as described in the Model 3. The longitudinal equilibrium is then checked by the following equation.

$$\frac{|P_1| - \left|\sum_{i=1}^{n} F_i\right|}{|P_1| + \left|\sum_{i=1}^{n} F_i\right|} \leq 0.0005 \qquad \text{.....(5.22)}$$

Equation (5.22) can determine an error between the external longitudinal force and internal longitudinal force as a proportion of approximately twice the external longitudinal shear force. If eqn. (5.22) is not satisfied, the neutral axis position y_{c1} in Fig. 5-9(b) is varied and the above procedure is repeated. When eqn. (5.22) and hence longitudinal equilibrium is satisfied, a check is made of the rotational equilibrium; and this can be made at any level such as at point O at section a-a in Fig. 5-11 using eqn. (5.12). If eqn. (5.12) is not satisfied, a new curvature κ_{c1} is chosen and the neutral axis position y_{c1} is varied until eqn. (5.22) is satisfied and then eqn. (5.12) is checked for rotational equilibrium; this procedure is repeated until κ_{c1} satisfies rotational equilibrium. In this way, the curvature κ_{c1} and neutral axis position y_{c1} in Fig. 5-9(b) are determined for the estimated longitudinal slip and vertical slip in Segment 1 which gave V_1 and P_1.

5.4.4.2 Plate element:

The analysis for the plate element in Fig. 5-10 is similar to that of the RC element. For a given curvature κ_{p1}, an estimate of the neutral axis position y_{p1} is made and then a check is made for longitudinal equilibrium using the following equation.

$$\frac{|P_1| - \left|\sum_{i=1}^{m} F_j\right|}{|P_1| + \left|\sum_{i=1}^{m} F_j\right|} \leq 0.0005 \quad \text{.....(5.23)}$$

The neutral axis position y_{p1} in Fig. 5-10(b) is varied until eqn. (5.23) is satisfied. Then a check is made of the rotational equilibrium using eqn. (5.16) and if it is not satisfied, the curvature κ_{p1} is varied and the above procedure is repeated until eqn. (5.18) is satisfied and hence eqn (5.23) is satisfied. This gives the curvature κ_{p1} and the neutral axis position y_{p1} in the plate element for the estimated longitudinal and vertical slip. The next step in the analysis is to estimate the longitudinal slip and vertical slip in the next segment.

5.4.4.3 Estimate of longitudinal slip in the following segment

The curvatures and neutral axis positions in both the concrete and plate elements at Segment 1 in Fig. 5-11 are now known. The slip strain [ε_{strain}] at the level of the bolts as shown is

$$\left[\varepsilon_{strain}\right]_1 = \varepsilon_{p1} + \varepsilon_{c1} \quad \text{.....(5.24)}$$

It is assumed that this slip strain is constant between the bolt position of the adjacent segments. Hence, the integration of this slip strain over dx will give the change in the longitudinal slip from the bolts group of Segment 1 to that of Segment 2 which can be expressed as follows:

$$\Delta s_{h1} = \left[\varepsilon_{strain}\right]_1 dx \quad \text{.....(5.25)}$$

This is used to estimate the longitudinal slip in Segment 2 as follows:

$$s_{h2} = s_{h1} - \Delta s_{h1} \quad \text{.....(5.26)}$$

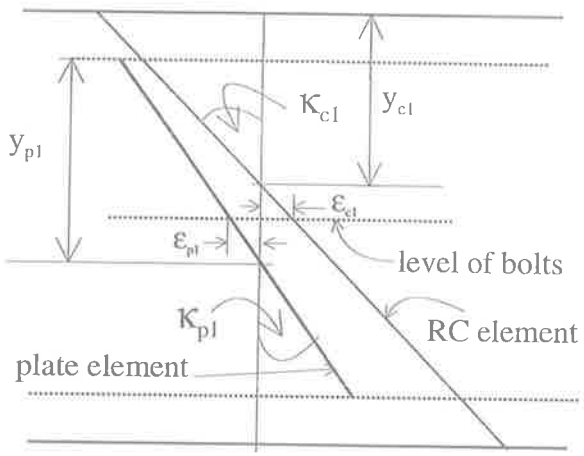

Fig. 5-11 Strain distribution in Segment 1

5.4.4.4 Estimate of vertical slip in the following segment

The change in the vertical slip and thereby an estimate of the vertical slip in Segment 2 can be determined from eqns. (5.19) and (5.20) respectively.

Knowing the longitudinal slip and vertical slip in the Segment 2 as well as in segment 1, the whole procedure is repeated for a section comprising Segment 1 and 2 to determine the slips in segment 3. In this way, the analysis proceeds along the beam up to the segment at the mid-span after which the following boundary conditions are checked.

5.4.4.5 Checking the boundary condition

As only simply supported beams with symmetric loadings are considered, the longitudinal slip at the mid-span is zero. However, if this boundary condition is not satisfied, the initial estimate of the longitudinal slip in Segment 1 is adjusted and the whole analysis procedure is repeated. When the boundary condition for the longitudinal slip is satisfied, a check is then made on the vertical slip as well as the slope at mid-span being zero. The boundary condition for vertical slip is given by eqn. (5.21). If this not satisfied, the vertical slip in Segment 1 is adjusted and the analysis repeated. The adjustments of both longitudinal slip and vertical slip are continued until both of the boundary conditions are satisfied.

Although the analysis in this section has been presented for one row of bolts, it can be used for more than one row of bolts. In that case, the initial estimate of longitudinal slip and vertical slip at Segment 1 will be made for each row of bolts and the same procedure will be followed.

5.5 SUMMARY

Several non-linear computer analysis techniques for side plated beams have been described in this chapter. An existing computer model has been adapted for the full interaction analysis and the longitudinal partial interaction analysis of side plated beams. In the longitudinal partial interaction analysis, the bolts do not slip in the vertical direction but are allowed to slip in the longitudinal direction.

New computer models have been described to study vertical partial interaction. In one model the bolts are allowed to slip in the vertical direction but not in the longitudinal direction. The other computer model simulates the real situation where the bolts can slip in both the longitudinal and vertical directions.

Chapter Six

Ductility of Side Plated Beams with Full Interaction

6.1 INTRODUCTION

Ductility is an important structural property because it ensures that large deformations and deflections will occur under overload conditions. A beam segment is ductile if it undergoes large plastic deformations prior to failure and it is characterised by an extended flat plateau in the moment curvature relationship of the beam (Warner et al, 1989).

Side plated beams are similar to composite profiled beams (Sect. 2.2.3) as they both have some sort of steel element along their sides. It has been established by Uy and Bradford (1995) that profiled composite beams have an improved ductility compared to their reinforced concrete counterparts. The reason is that the side profiled sheeting in profiled composite beams reduces the requirement of tensile reinforcing bars and increases the compressive reinforcement area which improves the ductility of the beam. It will be shown through a parametric study that a similar response occurs in side plated beams. The full interaction computer model in Sect. 5.4.1 has been used to develop the moment curvature relationships for the parametric study.

6.2 PARAMETRIC STUDY

The side plated beam in Fig. 6-1 was chosen for the parametric study. The depth of the RC beam D = 370 mm and the thickness of the plate t_p = 6 mm. The compressive strength of

concrete f_c = 35 MPa, the yield strength of reinforcement f_{yr}= 400 MPa and the yield strength of plate f_{yp} = 285 MPa. The height of the plate h was varied with respect to D for values of h/D of 0.1, 0.2, 0.3, 0.6, 0.9 and 1.0. It is to be noted that the bottom of the plate is in line with the bottom of the RC beam in all cases.

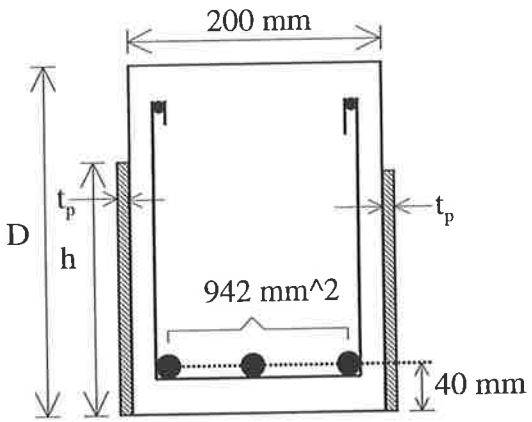

Fig. 6-1 Side plated RC beam

6.2.1 Moment-Curvature Plot

The moment curvature relationships are shown in Fig. 6-2. The moment curvature plots of the beams with $h / D \leq 0.6$ in Fig. 6-2 show that the ductility decreases as h/D increases whereas the strength and the stiffness increases with the increase of h/D. It is clear from the figure that the ductility of the beam with h/D = 0.6 is much less than that of the unplated beam but the strength and initial stiffness are nearly double than that of the unplated beam. The reason is that increasing the plate height increases the tensile reinforcing area which increases both the stiffness and the strength but reduces the ductility. This is similar to the normal RC beam and the standard composite beam where the increase in the tensile reinforcement reduces the ductility of the beam.

The moment curvature plots for the beams with $h / D \geq 0.6$ in Fig. 6-2 shows that the ductility now increases with the increase of h/D; the strength and the stiffness are increases as to be expected. The ductility of the beam with h/D=1.0 is similar to the unplated beam. The reason is that increasing the plate height above h/D = 0.6 increases the

compression reinforcing area which increases both the stiffness and the strength without a loss of ductility. This is also similar to profiled composite beams, and also to normal RC beams where compressive steel is occasionally added to maintain ductility when the strength is increased by the addition of tensile steel (Uy and Bradford, 1995).

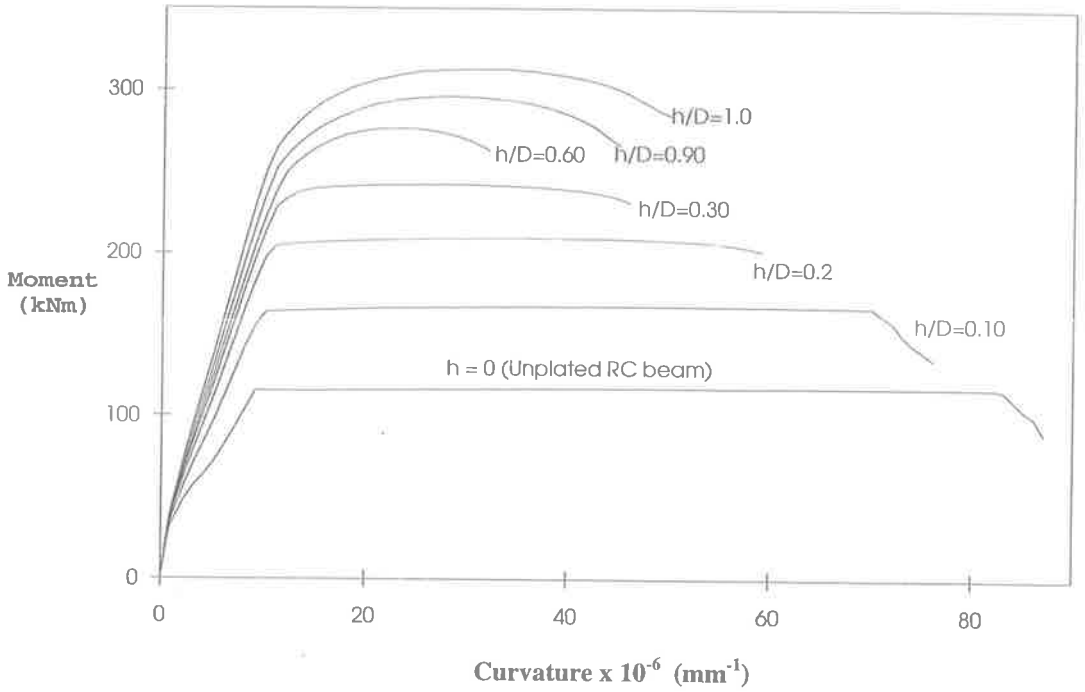

Fig. 6-2 Moment-curvature plot

A quantitative measure of the ductility of a beam section is provided by the ductility factor F, which is defined as (Warner et al, 1989)

$$F = \frac{\kappa_u}{\kappa_y} \qquad \text{.....(6.1)}$$

where, κ_u is the curvature at the maximum moment and κ_y is the curvature at first yield of the reinforcing bars. Figure 6-3 shows the ductility factor F for different h/D ratios. It is evident from the figure that the ductility of the side plated beam decreases as the plate height increases up to the middle of the RC beam after which the ductility increases with further increase in plate height.

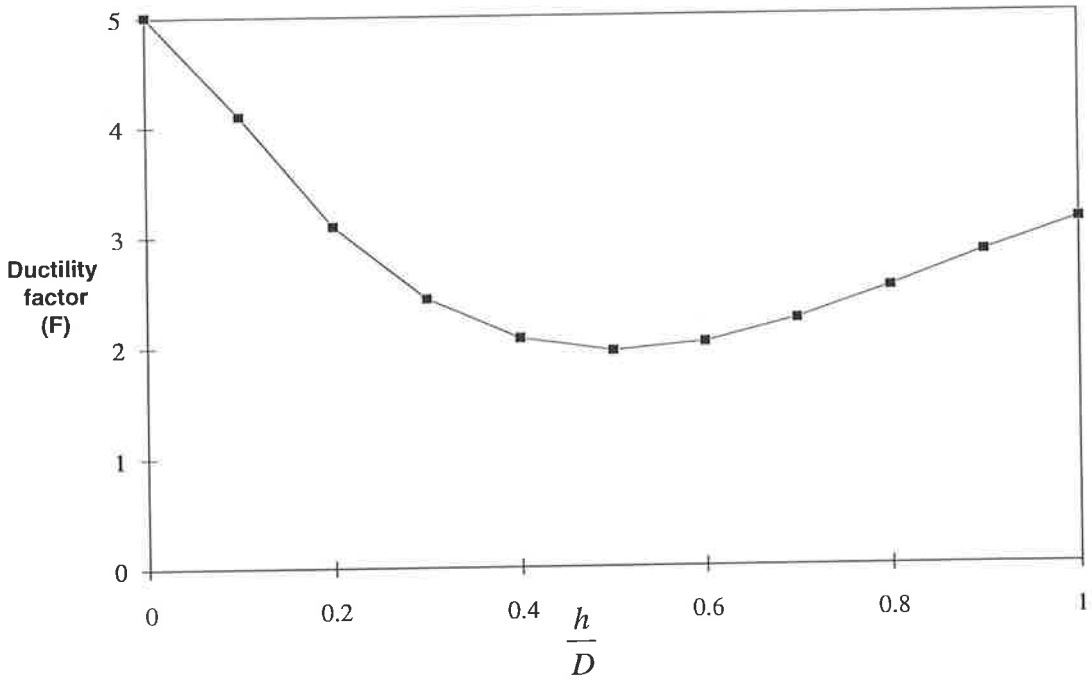

Fig. 6-3 Variation of ductility factor

The ductility of side plated beams can be affected by different properties such as: the yield strength of the plate, compressive strength of the concrete, thickness of the plate and cross-section of the beam. In the following sections, the effect of both the plate thickness and the yield strength of the plate will be discussed.

6.2.2 Effect of Plate Thickness, t_p on Ductility

To determine the effect of plate thickness on ductility, the beam in Fig. 6-1 with h/D = 1.0 used in the parametric study was examined. The moment curvature plots for various plate thicknesses are shown in Fig. 6-4. It can be seen that increasing the thickness of the plate increases both the stiffness and the strength significantly but with a somewhat decreased ductility. When compared with the unplated beam (t_p=0), it is found that the ductility of the plated beam is fairly large.

6.2.3 Effect of Plate Yield Stress, f_{yp} on Ductility

The beam in Sect. 6.2.2. was used to study the effect of the yield strength of the plate on ductility and the results are shown in Fig. 6-5. The effect of increasing the yield strength of the plate is an increase in strength with a decrease in curvature of maximum moment, that is a reduced ductility. The figure also shows that the ductile failure is obtainable as for as unplated beam.

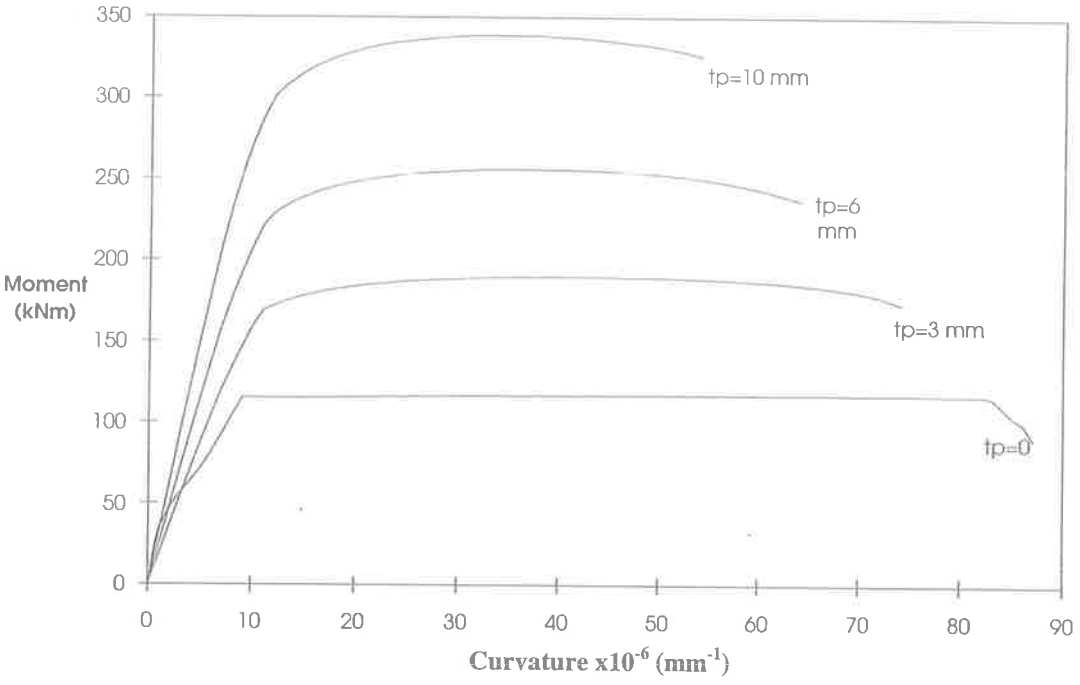

Fig. 6-4 Effect of plate thickness, t_p on ductility for h/D = 1.0

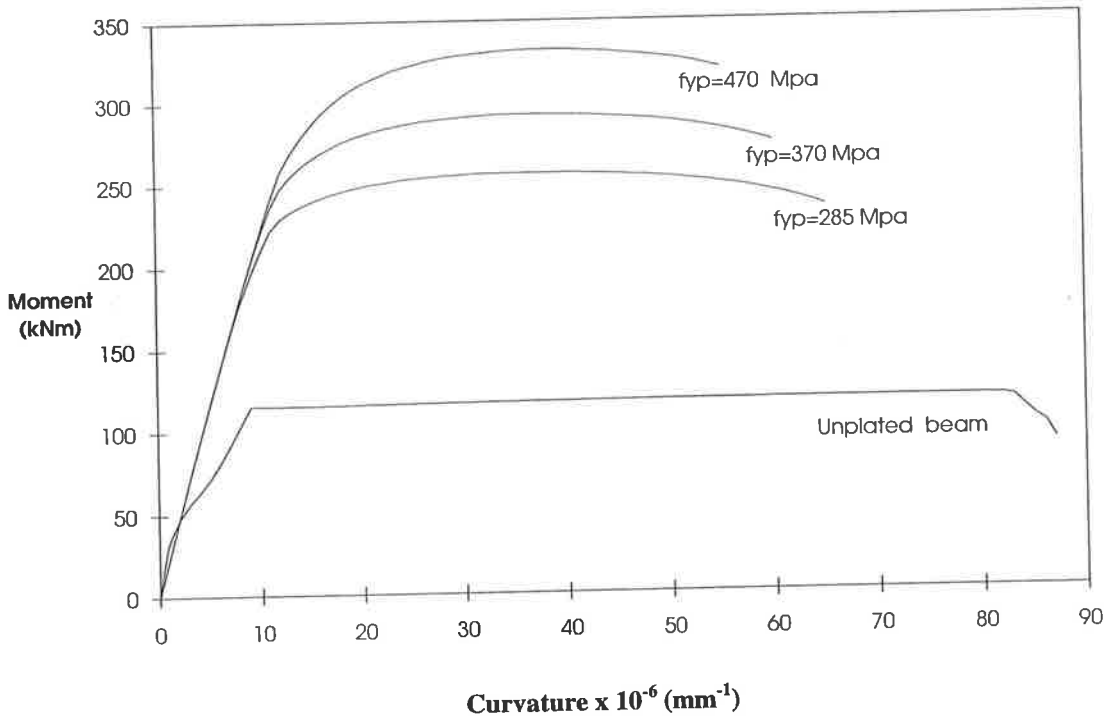

Fig. 6-5 Effect of plate yield stress, f_{yp} for h/D = 1.0

6.3 SUMMARY

It is evident from this brief parametric study of side plated beam that although the increase in strength of the cross-section may affect the ductility, the latter may still remain fairly large compared to an unplated RC beam (Fig. 6-2, 6-4 and 6-5) for all reasonable variations of the plate height, the thickness of the plate and the strength of the plate.

Chapter Seven

γ Factor in Design of Side Plated Beams with Full Interaction

7.1 INTRODUCTION

The γ factor, that is commonly used in ultimate strength reinforced concrete beam design (AS 3600, 1988), is used to relate the real stress distribution in a reinforced concrete beam with the idealised rectangular stress distribution. It is generally expressed as the following empirically derived equation.

$$\gamma = 0.85 - 0.007(f_c - 28) \leq 0.85 \text{ and } \geq 0.65 \quad \text{..... (7.1)}$$

The γ factor is not normally used in the rigid plastic analysis of standard composite beams but it has been used in the analyses of profiled composite beams which has been discussed in Sect. 2.2.3. Furthermore, it has been discussed in Sect. 3.2 that the γ factor should be used in the rigid plastic analysis of side plated beams.

In this chapter, it will be shown that the use of eqn. (7.1) in the analysis of plated beams with full interaction can produce an unconservative estimate of the bond force; and this will be demonstrated by a parametric study. A new equation for γ is then derived that can be used in a rigid plastic analysis of side plated beams which will not produce an unconservative bond force.

7.2 PARAMETRIC STUDY

The rigid plastic full interaction analysis (RPA) in Sect. 3.2.1 and the non-linear full interaction analysis (NLA) in Sect. 5.3.1 have been used to determine both the flexural capacities and the bond forces of the beams in Figs. 7-1(a) and (b). The reinforced concrete (RC) part is the same in both sections whereas the height of the plate is different. The heights have been chosen deliberately to keep the plate in (a) below the neutral axis position and to keep the plate in (b) in both the tension and compression regions. The yield stress of the plate f_{yp} was chosen as 285 MPa and the compressive strength of concrete f_c was varied as 28, 30, 35, 40, 45, 50, and 55 MPa.

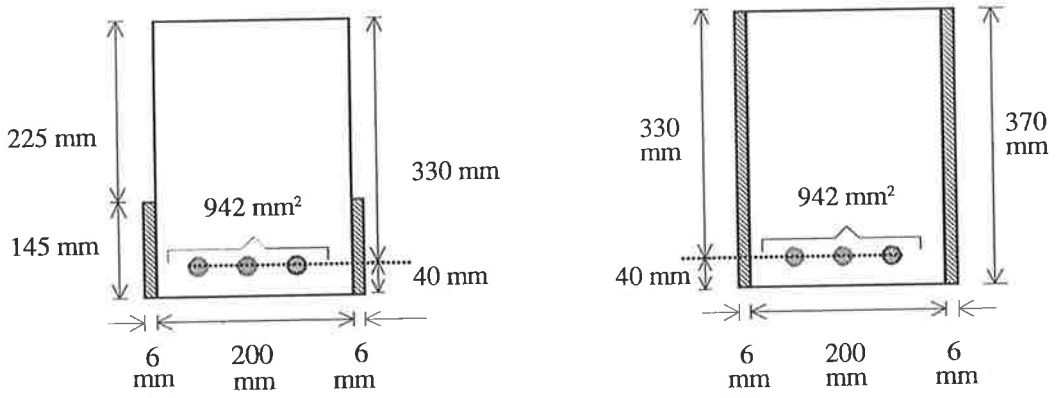

Fig. 7-1 Parametric study of the beam cross-section

The results of the analysis of the cross-section in Fig. 7-1(a) are given in Table 7.1. It is to be noted that neutral axis position has been measured from the top of the RC element. The bond forces from the NLA and the RPA technique are compared in Col. 8 where the mean value is 1.0 and the range is 1.01-1.03. Again the same for moment capacities in Col. 9 has the mean value of 0.971 and the range is 0.959-0.982. These comparisons suggest a good correlation between the results of the NLA and the RPA for the beam in Fig. 7-1 (a).

The results of the analysis of the cross-section in Fig. 7-1(b) are given in Table 7.2. The bond force from the NLA and the RPA technique are compared in Col. 8 where the mean value is 0.792 and the range is 0.747-0.823. The same comparison for moment

capacities in Col. 9 has the mean value of 0.981 and the range is 0.976-0.985. These comparisons suggest that there is good correlation between the moment capacities from the NLA and the RPA, but there exists a big difference in bond force for the beam in Fig. 7-1(b).

Table 7.1 Results of parametric study on beam in Fig. 7-1(a)

	Non-Linear Analysis			Rigid Plastic Analysis $\gamma = 0.85 - 0.007(f_c-28)$			Comparison	
f_c (MPa)	Bond force (kN)	n-a position (mm)	Moment M (MPa)	Bond force (kN)	n-a position (mm)	Moment M (MPa)	Bond force col.5 (RPA) / col.2 (NLA)	Moment col.7 (RPA) / col.4 (NLA)
1	2	3	4	5	6	7	8	9
28	483	187	200	496	216	192	1.03	0.959
30	491	178	205	496	205	197	1.01	0960
35	496	157	215	496	183	208	1.00	0.967
40	496	139	222	496	168	216	1.00	0.973
45	496	124	227	496	156	222	1.00	0.977
50	496	113	232	496	148	227	1.00	0.980
55	496	103	235	496	141	231	1.00	0.982

Table 7.2 Results of parametric study of beam in Fig. 7-1(b)

	Non-Linear Analysis			Rigid Plastic Analysis $\gamma = 0.85 - 0.007(f_c-28)$			Comparison	
f_c (MPa)	Bond force (kN)	n-a position (mm)	Moment M (MPa)	Bond force (kN)	n-a position (mm)	Moment M (MPa)	Bond force col.5 (RPA) / col.2 (NLA)	Moment col.7 (RPA) / col.4 (NLA)
1	2	3	4	5	6	7	8	9
28	284	143	245	234	151	241	0.823	0.985
30	310	140	249	254	148	245	0.816	0.985
35	366	131	256	298	141	252	0.813	0.984
40	418	124	263	333	136	258	0.796	0.982
45	460	117	268	362	132	263	0.786	0.980
50	502	111	274	385	129	268	0.766	0.978
55	539	107	278	403	126	272	0.747	0.976

The comparisons of moment capacities and bond forces from the NLA and RPA are presented in Fig. 7-2 and 7-3 respectively. It can be seen in Fig. 7-2 that the variation in moment between the two methods is very minimal and that the moment is always lower in the RPA than in the NLA. Hence, the RPA slightly underestimates the flexural capacity and gives a conservative design. It is evident from Fig. 7-3 that the method of analysis does not affect the bond force when the plate is bonded in the tensile region of the RC beam as in Fig. 7-1(a). This is because, in general, the plate is fully yielded and hence the bond force is equal to the plate strength. However, the RPA gives a much lower bond force than the NLA when the plate height extends into the compression region in (b). This means that the RPA will underestimate the bond force when plate height covers the compression as well as tension regions. The reasons for this discrepancy are discussed in the following section.

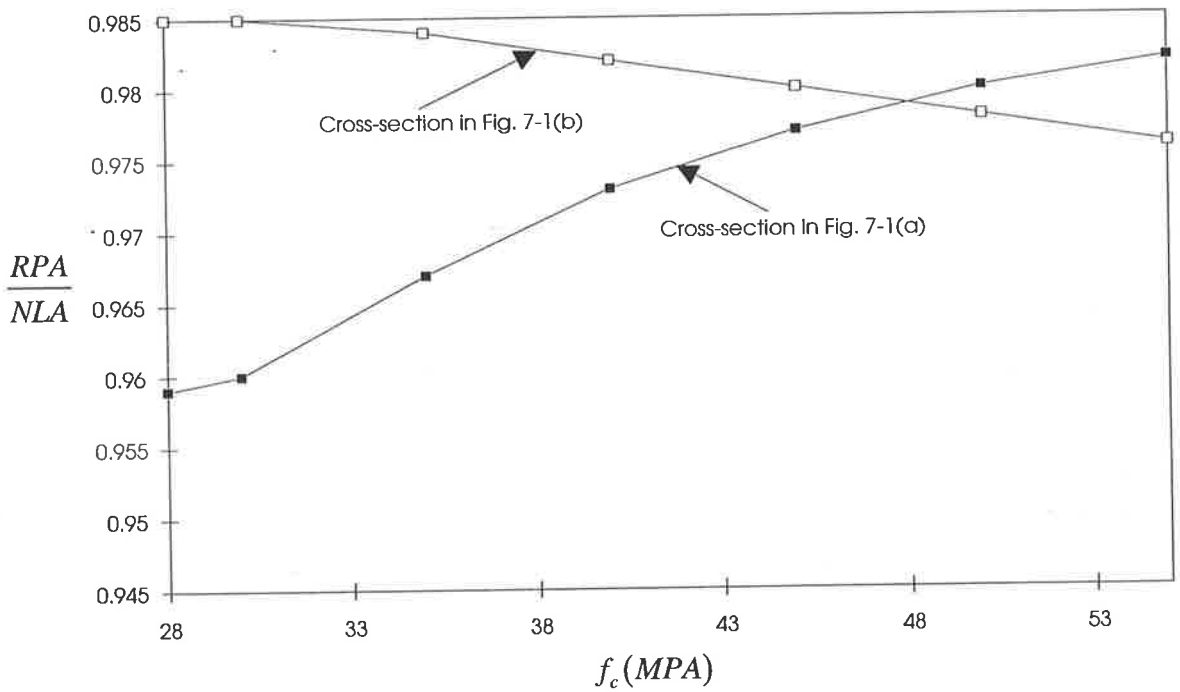

Fig. 7-2 Comparison of moment capacities from NLA and RPA

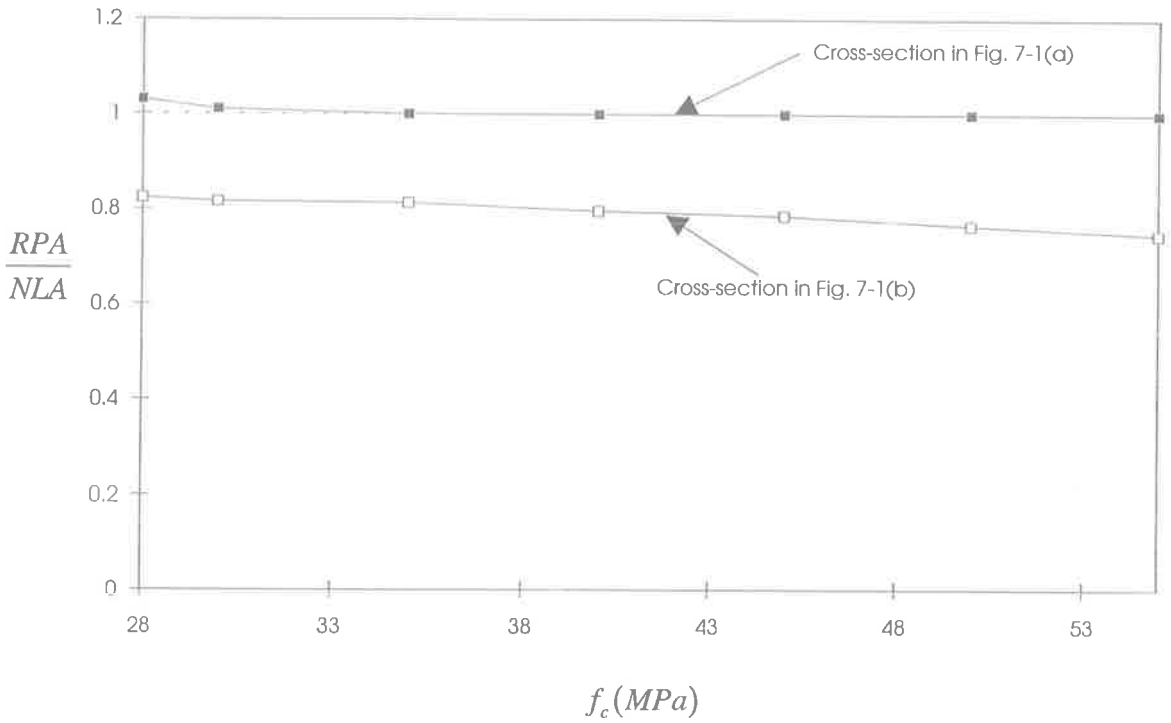

Fig. 7-3 Comparison of bond forces from NLA and RPA

7.2.1 REASON OF DIFFERENCE IN BOND FORCE BETWEEN THE RPA AND NLA

In the previous section, it was shown that RPA underestimates the bond force. Let us consider the beam in Fig. 7-1(b) with f_c=30 MPa. The forces that are found by the NLA in both the plate and RC elements are shown in Fig. 7-4(a) and (b) respectively, and the forces that are found by the RPA in the plate and RC elements are shown in Fig. 7-5(a) and (b) respectively.

A comparison of the forces between the NLA in Fig. 7-4 and the RPA in Fig. 7-5 show that there is no difference in the reinforcement tensile force as it is fully yielded in both cases. However, there are differences in the compressive forces in both the concrete and the plate elements and the tensile force in the plate element. This is due to the difference in the neutral axis positions in the two methods. This variation in the neutral axes position causes very large differences in the bond force. In order to find out the reason for the difference in the neutral axis position, the following studies were implemented.

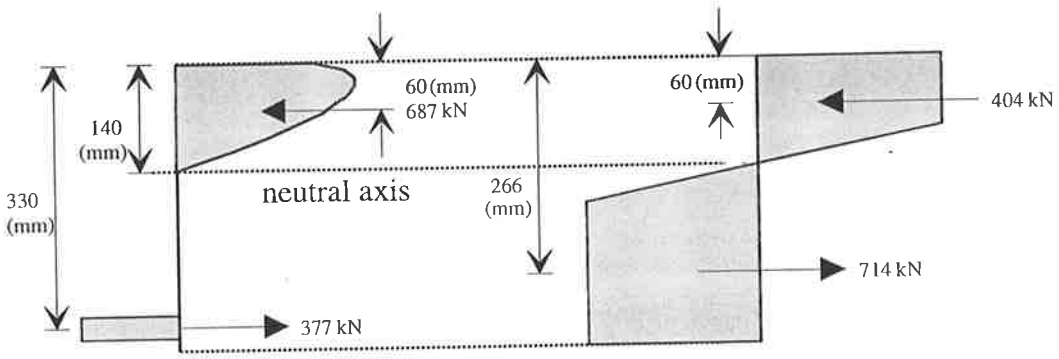

(a) concrete element (b) plate element

Fig. 7-4 Non-linear analysis (NLA)

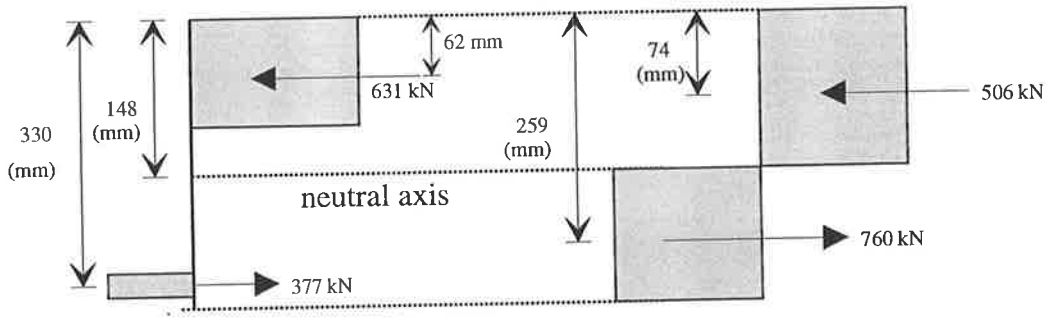

(a) concrete element (b) plate element

Fig. 7-5 Rigid plastic analysis (RPA)

7.2.2 Study of Stress Profile of Plate Section

First, we shall look at the stress profile of the plate section at ultimate load. The non-linear material properties of the plate are such that a non-rectangular stress block occurs, as shown in Fig. 7-4(b), instead of the rectangular stress block, as in Fig. 7-5(b), as the portions of the plate that are close to the neutral axis in Fig. 7-4(b) are not fully yielded. Let us consider the trapezoidal stress block (shaded area) in Fig. 7-6, which represent the difference in the stress distributions between Fig. 7-4(b) and 7-5(b) adjacent to the neutral axis. In Fig. 7-6, the area of triangle OAB in the compression zone is equal to the area of triangle OEF in the tension zone. By symmetry, triangles OAB and OEF are equal and so

their exclusion from the rectangular block, in Fig. 7-5(b), will not produce any change in the resultant force in the plate which is also the bond force of the plated beam. Furthermore, the amount of moment contribution of the triangular area in Fig. 7-6, that is $2Fl_a$, is much smaller than the total moment in the rectangular stress block distribution in Fig. 7-5(b), as the lever arm $2l_a$ in Fig. 7-6 is very small. Therefore, the elastic stress zone adjacent to the neutral axis in Fig. 7-4(b) has little effect on the bond force or on the flexural capacity.

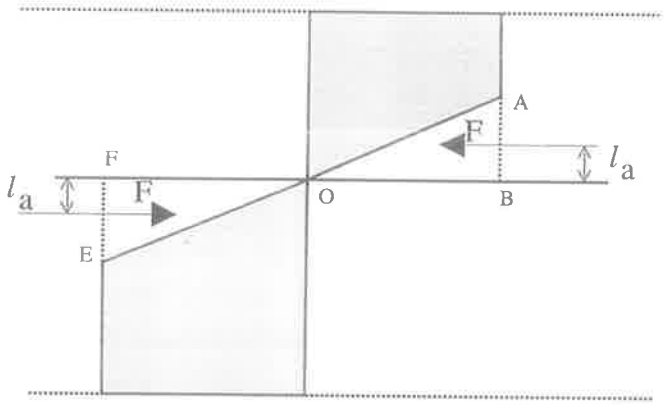

Fig. 7-6 Trapezoidal stress profile of plate

As an example, the beam in Fig. 7-1(b) with f_c=30 MPa was analysed using a trapezoidal stress block in the plate and the results are shown in Fig. 7-7. The strain at top fiber of the RC section and hence, the strain at this level of the plate is taken as the concrete crushing strain 0.003, as shown in (a). This is used to determine the portion of the plate that is yielded and the portion that is elastic as shown in (c). The forces and their position in both the RC beam and plate are shown in (b) and (c), respectively. As it has been shown that the trapezoidal section does not affect the resultant axial forces in the elements and hence, the neutral axis in the concrete element is unchanged at 148 mm in (b) from that shown in Fig. 7-5(a).

It can be derived from Figs. 7-7(b) and (c) that the bond force is 254 kN and the moment is 239 kNm. These were 254 kN and 245 kNm respectively in the case of the rectangular stress block in Fig. 7-5. Therefore, as discussed before, there is no change in bond force but the moment capacity has decreased by 2.34%. Hence for simplicity, the

assumption of a rectangular stress block in the plate section is quite acceptable and not responsible for the discrepancy in bond force.

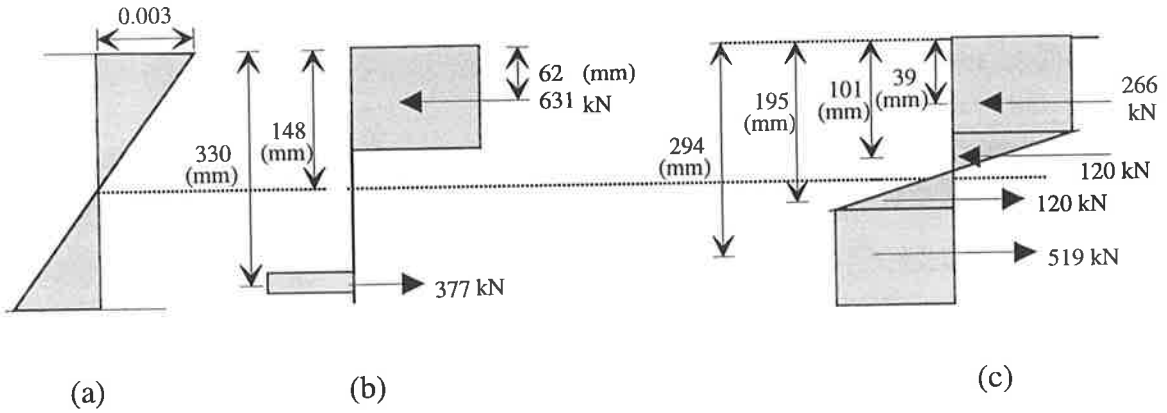

Fig. 7-7 Analysis of beam using trapezoidal stress block in plate element

7.2.3 Study of stress profile of RC beam with t_p=0

In this section, an unplated RC beam will be analysed using both the RPA and the NLA in order to compare the neutral axis positions from the two methods. Three different RC beams B1, B3 and B5 that have the cross-sections defined in Fig. 7-8 and Table 7.3 were analysed. The results of the analysis are presented in Tables 7.4, 7.5 and 7.6. It is to be noted that the neutral axis position has been measured from the top of the beam.

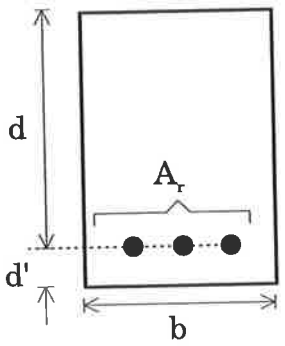

Fig. 7-8 Beam section for parametric study

Table 7.3 Parametric study cross-sections

Section number	Width of beam, b (mm)	Effective depth, d (mm)	Clear cover, d' (mm)	Area of tensile reinforcement A_r (mm^2)	Yield stress of reinforcement, f_{yr} (MPa)
1	2	3	4	5	6
B1	200	330	40	942	400
B3	300	500	30	2480	400
B5	500	700	40	1964	325

The flexural capacities from the RPA and the NLA are compared in Col. 8 in the respective tables of the beams. It can be seen that the mean value is 0.013 and the range is 0.0-0.02 for beam B1, 0.0128 and 0.01-0.02 for beam B3 and 0.002 and 0.002-0.002 for beam B5. This suggests very good correlation between the results of flexural capacity from NLA and RPA.

The neutral axis position from the NLA and the RPA are compared in Col. 9 of the respective tables of the beams. The mean value is 0.224 and the range is 0.12-0.38 for beam B1, 0.22 and 0.12-0.36 for beam B3 and 0.215 and 0.13-0.39 for beam B5. This suggests that there is big variation between the neutral axis position from the NLA and the RPA. It can therefore, be seen from the comparison of the results between RPA and NLA in Col. 9 that RPA over estimates the neutral axis (n-a) position. This is due to the value of γ that is used in the rigid plastic analysis (AS 3600, 1988). The percentage of over estimation increases with the increase of the compressive strength of concrete, f_c, as shown in Fig. 7-9.

Table 7.4 Analysis of beam section B1

	Rigid Plastic Analysis (RPA)			Non-Linear Analysis		Comparison	
f_c (MPa)	Rectangular stress block depth (mm)	n-a position by γ=0.85-0.007(fc-28) (mm)	moment capacity (kNm)	n-a position (mm)	moment capacity (kNm)	Moment $\frac{Col.5 - Col.7}{Col.7}$	n-a $\frac{Col.4 - Col.6}{Col.6}$
1	2	4	5	6	7	8	9
28	79.2	93.1	109	83.2	111	0.02	0.12
30	73.9	88.4	110	78.0	112	0.02	0.13
35	63.3	79.1	112	67.9	114	0.02	0.17
40	55.1	72.3	114	59.7	115	0.01	0.21
45	49.6	67.4	115	53.9	116	0.01	0.25
50	44.3	63.7	116	48.6	117	0.01	0.31
55	40.3	60.9	117	44.2	117	0.0	0.38

Table 7.5: Analysis of Beam section B3

	Rigid Plastic Analysis (RPA)			Non-Linear Analysis (NLA)		Comparison	
f_c (MPa)	Rectangular stress block depth (mm)	n-a position by γ=0.85-0.007(fc-28) (mm)	moment capacity (kNm)	n-a position (mm)	moment resistance (kNm)	Moment $\frac{Col.5 - Col.7}{Col.7}$	n-a $\frac{Col.4 - Col.6}{Col.6}$
1	2	4	5	6	7	8	9
28	139	163	427	146	435	0.02	0.12
30	130	155	432	137	439	0.02	0.13
35	111	139	441	119	447	0.01	0.16
40	97.2	127	448	105	453	0.01	0.21
45	86.4	118	453	94.0	458	0.01	0.25
50	77.8	112	457	85.3	461	0.01	0.31
55	70.7	107	461	78.9	464	0.01	0.36

Table 7.6 Analysis of Beam section B5

	Rigid Plastic Analysis			Non-Linear Analysis (NLA)		Comparison	
f_c (MPa)	Rectangular stress block depth (mm)	n-a position by γ=0.85-0.007(fc-28) (mm)	moment capacity (kNm)	n-a position (mm)	moment capacity (kNm)	Moment $\frac{Col.5 - Col.7}{Col.7}$	n-a $\frac{Col.4 - Col.6}{Col.6}$
1	2	4	5	6	7	8	9
28	53.6	63.1	430	55.7	431	0.002	0.13
30	50.0	59.9	431	53.1	432	0.002	0.13
35	42.9	53.6	433	45.2	434	0.002	0.18
40	37.5	49.0	435	40.0	436	0.002	0.22
45	33.3	45.7	436	37.4	437	0.002	0.22
50	30.0	43.2	437	34.9	438	0.002	0.24
55	27.3	41.3	438	29.8	439	0.002	0.39

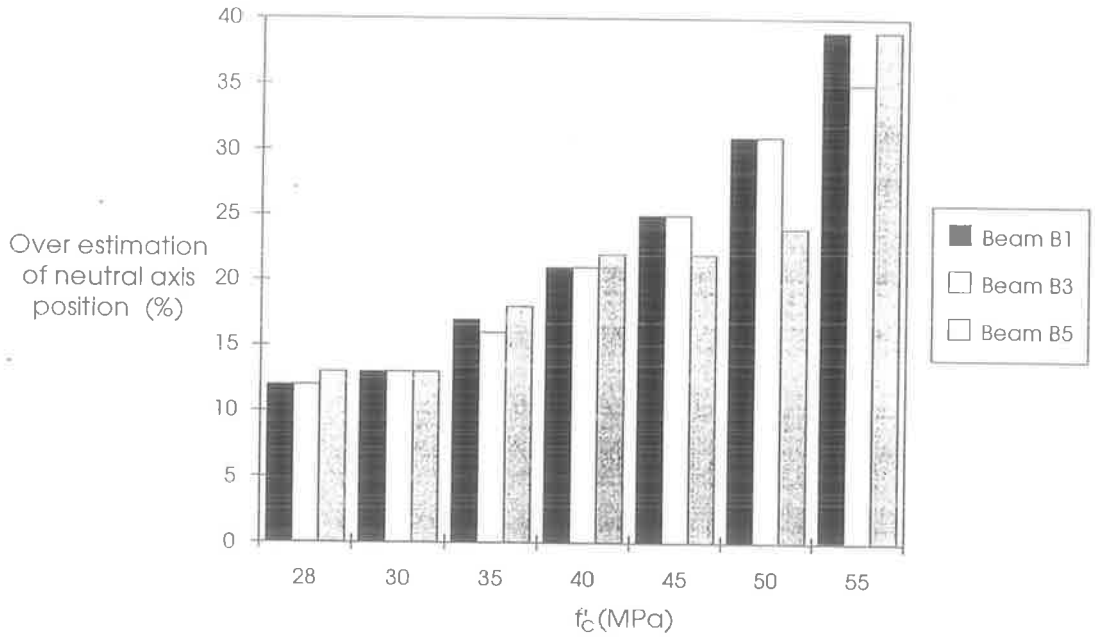

Fig. 7-9 Over estimation in neutral axis position in rigid plastic method

The over-estimation of the neutral axis position in Beam B1 is 12% for f_c=28 MPa and 39% for f_c=55 MPa Col. 9 of Table 7.4. However, the difference in moment capacities is only 1.56% and 0% respectively. The reason is that the γ factor that is used to determine

the rigid plastic neutral axis position does not come into the calculation of the moment capacity of the RC beam. Therefore, it can be deduced that the existing values of γ used in codes does not give a correct neutral axis (n-a) position and thereby can under estimate the bond force in the rigid plastic analysis of a side plated beam. It may be worth mentioning that the γ in codes is primarily there to ensure that the steel reinforcement has yielded in which case the γ in codes is conservative. However, when applied to the bond strength in plated beams, it is unconservative.

7.2.4 Using γ=1 in Side Plated Beams

It needs to be mentioned here that the γ factor is usually not considered in the analysis of a standard composite beam where one element does not encase the other. Therefore, it is not necessary in the standard composite beam to ensure that the steel element has fully yielded when the concrete crushes at a strain of 0.003. If we adopt this situation for side plated beams, then the discrepancy in the bond force between the rigid plastic method (RPA) and the non-linear analysis (NLA) can be much reduced.

For example, the side plated beam in Fig. 7-1(b) was analysed using a RPA in which γ=1 and compared with the results of NLA in Table 7.7. A comparison of the bond forces and the moment capacities between the two methods is shown in Cols. 8 and 9 and in Fig. 7-10. It is evident from the figure that the use of γ=1 in rigid plastic analysis of the RC section can prevent the large error in the bond force, as mentioned in section 7.2. For example, for the beam in Fig. 7-1(b) with f_c=30 MPa, RPA over estimates the bond force by 4.7% (Table 7.7) when γ=1 whereas it under estimates the bond force by 18% when $\gamma \neq 1$(Table 7.2).

But we cannot use γ=1 in the rigid plastic analysis of the RC element of a side plated beam because when the plate thickness tends to zero, then the analysis reverts to that of a normal RC beam in which case the usual practice is to consider the γ factor. Therefore in order to overcome this problem, the existing γ factor is calibrated in the following section.

Table 7.7 Analysis of cross-section in Fig. 7-1(b) using γ=1

	Non-linear analysis (NLA)			Rigid plastic analysis (RPA) with γ = 1			Comparison	
f_c (MPa)	Bond force (KN)	n-a position (mm)	Moment M (MPa)	Bond force (KN)	n-a position (mm)	Moment, M (MPa)	Bond force col.5 / col.2	Moment col.7 / col.4
1	2	3	4	5	6	7	8	9
28	283.8	142.9	245.1	297.0	141.6	242.2	1.046	0.988
30	309.9	139.6	249.0	324.6	137.5	245.5	1.047	0.986
35	365.9	131.4	256.0	387.1	128.4	253.0	1.057	0.988
40	418.4	123.8	262.6	441.8	120.4	259.6	1.056	0.988
45	460.3	117.2	268.5	490.2	113.3	265.4	1.065	0.988
50	502.3	111.3	273.5	533.1	107.1	270.5	1.061	0.989
55	538.9	106.6	278.3	571.6	101.4	275.2	1.060	0.989

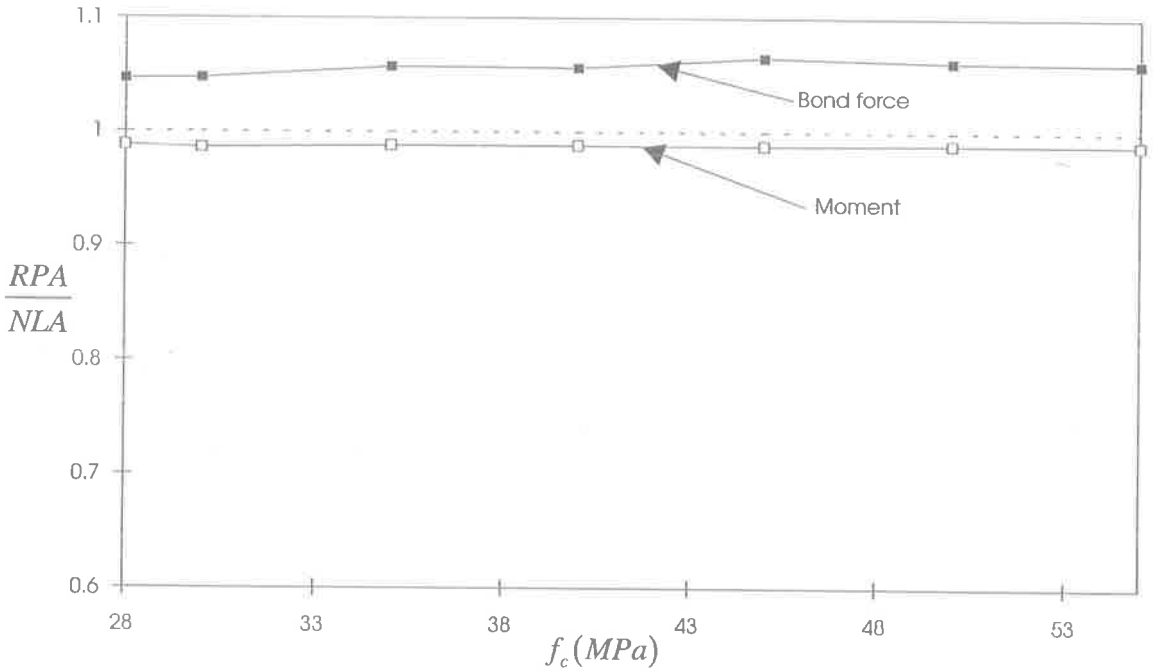

Fig. 7-10 comparison of RPA and NLA for γ=1

7.3 CALIBRATION OF γ FACTOR

In this section, a new equation for γ will be proposed for the use in side plated beams by following an analytical procedure. The procedure will be described in the following sections. In doing this, two types of beams were used: one without an external plate to the side of RC beam i.e. $t_p = 0$; and the other with external plates to the sides of the RC beam i.e. $t_p>0$. The procedure is described in the following sections.

7.3.1 Case-1; when $t_p=0$

As there is no plate to the sides, we are simply dealing with normal RC beams. The stress and strain profiles of the RC beam are shown in Fig. 7-11 for the NLA and RPA. We first find the neutral axis position y_{nc} in (b) by using the non-linear analysis (NLA). This is then used to determine the γ factor for the rigid plastic analysis in (d) as follows.

Using the notations in Fig. 7-11(a) and (d), the compressive force, F_{con}, in (d) is

$$F_{con} = 0.85 f_c ab \quad \text{.....(7.2)}$$

and the tensile force, F_{reo}, in (d) is

$$F_{reo} = A_r f_{yr} \quad \text{.....(7.3)}$$

Equating eqns. (7.2) and (7.3), we can determine the depth of the stress block, 'a' in Fig. 7-11(d). The non-linear analysis in (b) gives the neutral axis position y_{nc} of the RC section and is used in the following equation to calculate γ.

$$\gamma = \frac{a}{y_{nc}} \quad \text{.....(7.4)}$$

The beams defined in Table 7.3 and Fig. 7-8 do not have any external plate to their sides and, hence, have been used to determine γ for different compressive strengths of concrete, f_c. The results are given in Table 7.9.

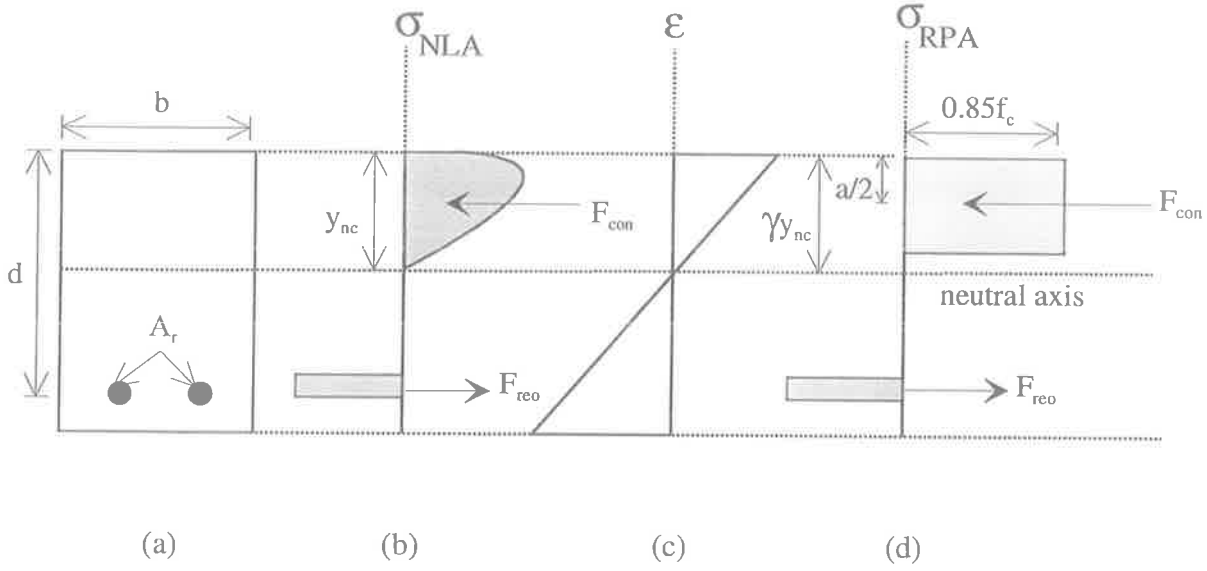

Fig. 7-11 Stress and strain profile

7.3.2 Case-2; When t_p>0

The stress distributions within the RC section and within the plate section from rigid plastic analyses are shown in Figs. 7-12(a) and (b) respectively. From equilibrium of the forces gives,

$$F_{con} + P_{comp} = P_{ten} + F_{reo} \quad \text{.....(7.5)}$$

Inserting the respective parameters from Fig. 7-12 into eqn. (7.5), gives

$$0.85 f_c b \gamma y_n + 2 y_n f_{yp} t_p = 2(D - y_n) f_{yp} t_p + A_r f_{yr} \quad \text{.....(7.6)}$$

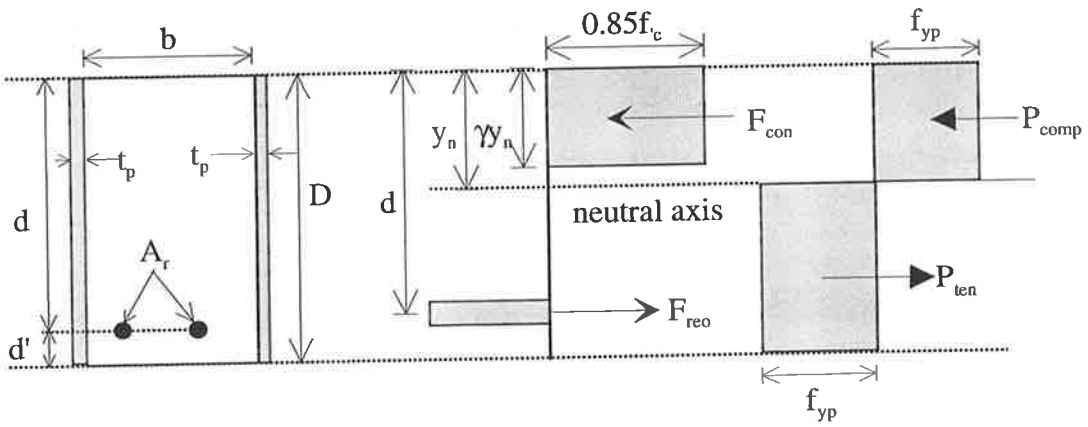

(a) Plated beam (a) Concrete element (c) Plate element

Fig. 7-12 Rigid plastic analysis of plated beam

From the non-linear analysis, we can derive the neutral axis (n-a) position y_n. This is used in equation (7.6) to calculate γ for the RC section. The externally plated beams in Table 7.8 were used for this analysis. Their results are given in Table 7.9 for different value of f_c.

Table-7.8: Cross-section of plated beams

Beam number	Width of beam, b (mm)	Effec-tive depth, d (mm)	Clear cover, d' (mm)	Area of reinforce-ment A_r (mm^2)	Yield strength of reinforce-ment f_{yr} (MPa)	Thick-ness of plate, t_p (mm)	Yield stress of plate, f_{yp} (MPa)
1	2	3	4	5	6	7	8
B2	200	330	40	942	400	6	285
B4	300	500	30	2480	400	3	370
B6	500	700	40	1964	325	1	210

Table-7.9: Calculated γ values

	Calculated γ for beams without external plate ($t_p = 0$)			Calculated γ for beams with external plate ($t_p > 0$)		
	Beam number			Beam number		
f_c	B1	B3	B5	B2	B4	B6
1	2	3	4	5	6	7
28	0.952	0.954	0.964	0.977	0.973	0.958
30	0.948	0.948	0.943	0.971	0.964	0.958
35	0.934	0.933	0.950	0.950	0.951	0.915
40	0.928	0.926	0.939	0.945	0.939	0.941
45	0.914	0.919	0.893	0.938	0.930	0.908
50	0.913	0.912	0.860	0.931	0.923	0.930
55	0.911	0.895	0.918	0.916	0.922	0.926

7.3.3 Variation of γ

The values of γ in Table 7.9 are plotted in Fig. 7-13 against (f_c-28). A linear regression analysis gave the following equation for the mean line,

$$\gamma = 0.958 - 0.00191(f_c - 28) \quad \text{.....(7.7)}$$

which has the mean of 0.934 and standard deviation of 0.023.

The degrees of freedom of this regression analysis is (42-2) = 40. Using the table of probability points of the t-distribution (single-sided) as described by Davies and Goldsmith (1980), we get the 5% confidence limit as $t_{0.05}$= 1.68 standard deviations. Therefore, the 90% confidence limits occur at 0.958 ± 1.68x0.023. Hence, the upper bound characteristic value for γ is

$$\gamma = 0.997 - 0.00191(f_c - 28) \quad \text{.....(7.8)}$$

nd the lower bound characteristic value is

$$\gamma = 0.919 - 0.00191(f_c\text{-}28) \quad \text{.....(7.9)}$$

Both eqns. (7.8) and (7.9) are shown in Fig. 7-13 along with eqn. (7.10) from codes (AS 3600, 1988).

$$\gamma = 0.85 - 0.007(f_c - 28) \quad \text{.....(7.10)}$$

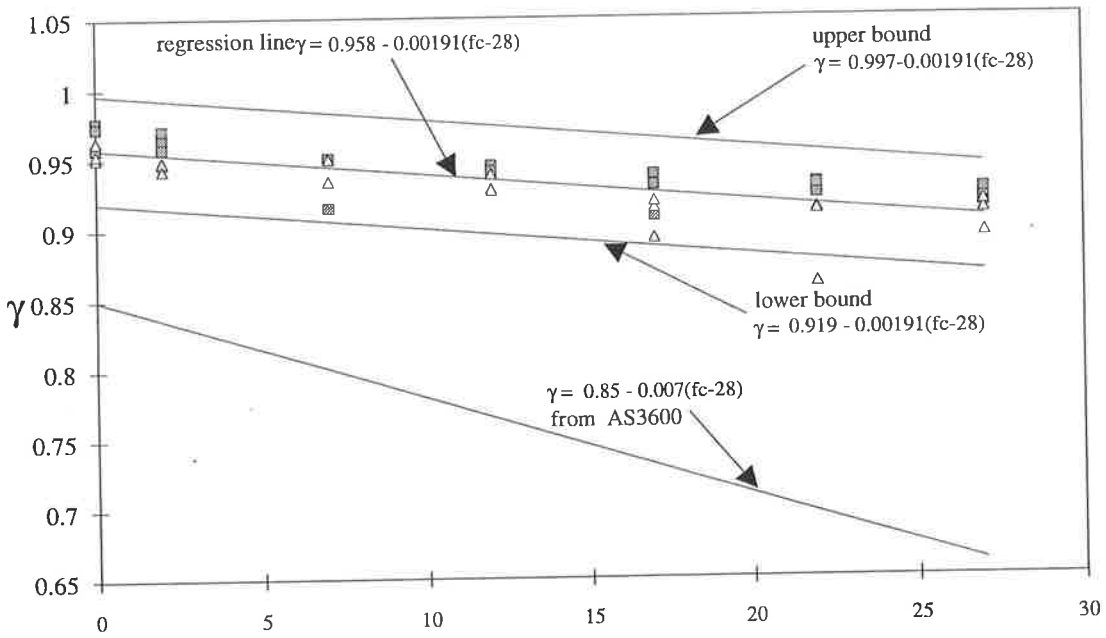

Fig. 7-13 Linear regression analysis for calculated γ

7.3.4 Use of new γ in rigid plastic analysis

In order to ensure a safe design, over estimation of the bond force is necessary rather than under estimation. Therefore, the characteristic γ at the upper confidence limit in eqn. (7.8) should be used. This was used in the RPA of beams B2, B4 and B6 in Table 7.8. These results are compared with the results from the NLA and also, from the RPA using γ from the code (eqn. (7.10)) in Tables 7.10, 7.11 and 7.12, respectively.

Table 7.10 Analysis of Beam B2

	Non-linear analysis			Rigid Plastic Analysis $\gamma=0.85-0.007(f_c-28)$			Rigid Plastic Analysis $\gamma=0.997-0.00191(f_c-28)$		
f_c (MPa)	neutral axis position (mm)	bond force (kN)	moment (kNm)	neutral axis position (mm)	bond force (kN)	moment (kNm)	neutral axis position (mm)	bond force (kN)	moment (kNm)
1	2	3	4	5	6	7	8	9	10
28	142.92	283.85	245.07	150.85	233.56	241.48	141.77	295.68	242.20
30	139.28	311.09	248.43	147.89	253.78	244.65	137.97	321.69	245.51
35	131.43	365.94	255.95	141.49	297.56	251.76	129.41	380.22	253.01
40	123.81	418.41	262.64	136.30	333.14	257.85	122.00	430.90	259.58
45	117.16	460.32	268.47	132.09	361.88	263.10	115.53	475.19	265.38
50	111.60	502.39	273.54	128.74	384.82	267.64	109.82	514.21	270.49
55	106.58	538.93	278.26	126.13	402.70	271.55	104.77	548.81	275.09

Table 7.11 Analysis of Beam B4

	Non-linear analysis			Rigid Plastic Analysis $\gamma=0.85-0.007(f_c-28)$			Rigid Plastic Analysis $\gamma=0.997-0.00191(f_c-28)$		
f_c	neutral axis position (mm)	bond force (kN)	moment (kNm)	neutral axis position (mm)	bond force (kN)	moment (kNm)	neutral axis position (mm)	bond force (kN)	moment (kNm)
1	2	3	4	5	6	7	8	9	10
28	190.47	327.25	613.94	206..36	260.38	603.43	187.68	343.22	604.74
30	183.54	359.84	622.41	200.14	287.98	611.79	180.21	376.49	613.30
35	167.76	428.90	640.40	187.13	345.76	629.81	164.11	447.96	631.85
40	154.68	485.46	655.45	176.98	390.79	644.53	150.91	506.58	647.16
45	143.49	538.91	668.05	169.05	426.02	658.74	139.89	555.49	660.01
50	133.79	580.69	678.35	162.88	459.41	666.97	130.56	596.90	670.96
55	124.86	623.79	687.63	158.17	474.32	675.61	122.57	632.39	680.38

Table 7.12: Analysis of Beam B6

	Non-linear analysis			Rigid Plastic Analysis $\gamma=0.85-0.007(f_c-28)$			Rigid Plastic Analysis $\gamma=0.997-0.00191(f_c-28)$		
f_c	neutral axis position (mm)	bond force (kN)	moment (kNm)	neutral axis position (mm)	bond force (kN)	moment (kNm)	neutral axis position (mm)	bond force (kN)	moment (kNm)
1	2	3	4	5	6	7	8	9	10
28	77.55	244.81	530.12	86.64	238.02	526.39	74.94	248.02	526.45
30	72.67	249.45	531.97	82.54	241.47	528.59	70.32	251.73	528.66
35	65.68	254.67	536.00	74.41	248.29	533.06	61.38	259.25	533.15
40	56.38	262.98	538.74	68.47	253.29	536.46	54.58	264.96	536.56
45	52.14	268.57	541.40	64.04	257.006	539.126	49.24	269.44	539.25
50	46.07	277.85	543.24	60.723	259.793	541.279	44.93	273.06	541.42
55	42.23	279.79	544.69	58.26	261.862	543.05	41.39	276.03	543.20

A comparison of the bond forces and moments between the two methods, for beam B2, B4 and B6, is shown in Figs. 7-14 and 7-15 respectively. Figure 7-14 shows that when the new equation of γ is used the bond force in all the beams is somewhat higher in the RPA than the NLA. Figure 7-15 shows that when new γ values are used the moment capacities of all the beams is somewhat less in the RPA than in the NLA, which gives a conservative design. Therefore, it can be concluded that the use of the new characteristic γ for RC section in a rigid plastic analysis can prevent under estimation of the bond force in a RPA of side plated beams.

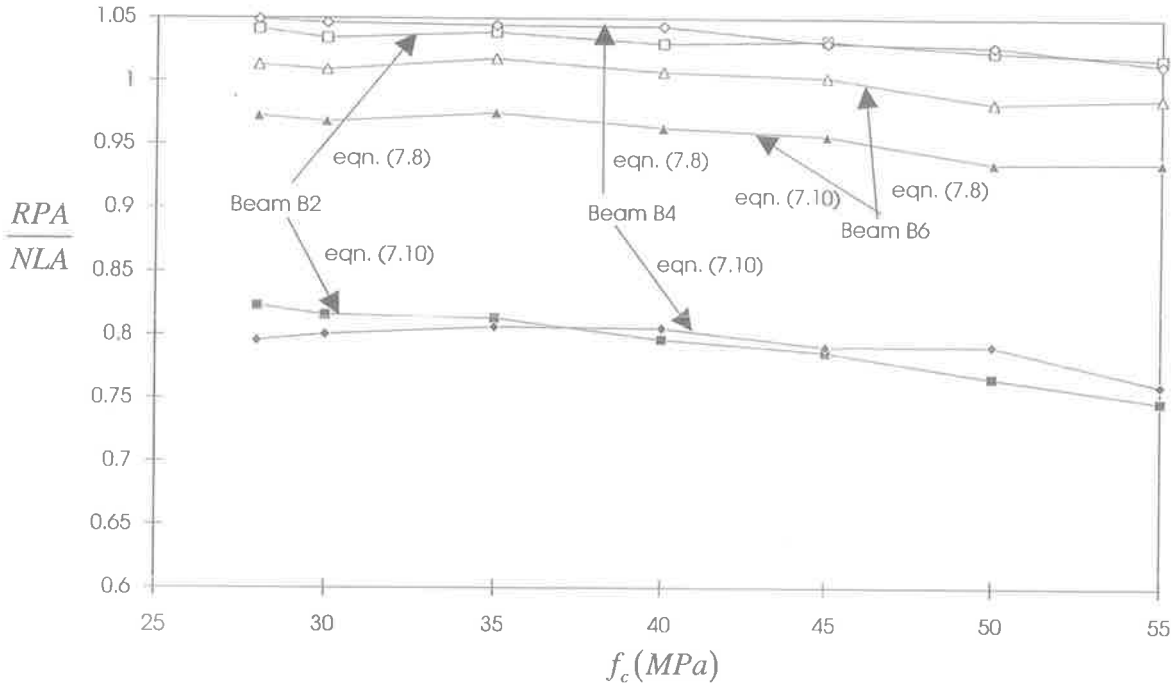

Fig. 7-14 Comparison of bond forces

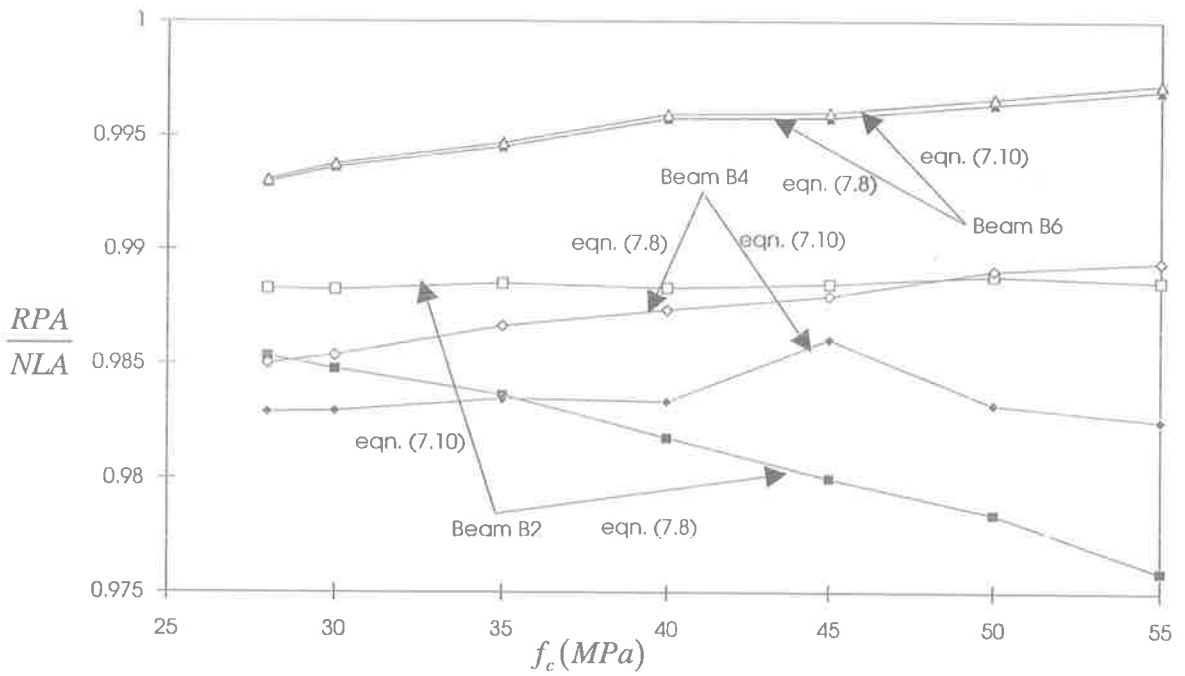

Fig. 7-15 Comparison of moment capacities

7.5 SUMMARY

In this chapter, it has been shown that the use of the existing γ in the rigid plastic analysis under estimates the bond forces in the side plated beams. The reason is that the use of the existing γ over-estimates the neutral axis depth in the rigid plastic analysis. A parametric study was used to determine a value of γ that give the same neutral axis depth in the rigid plastic analysis as in the non-linear analysis. This γ will be used in the analysis of the experimental plated beams in Chapter 8.

Chapter Eight

Experimental work

8.1 INTRODUCTION

The work presented in this chapter is divided into three sections. Section 1 deals with the material properties of the concrete, reinforcement and plate, as determined experimentally and the material properties of bolt, as given by the manufacturer. Section 2 deals with the properties of bolted shear connectors, where the objective of the tests was to find a suitable bolt for plated beams. Section 3 describes plated beams tested in flexure; the major variations were the depths of the plate and the degree of shear connection. The aims of the beam tests were: to get an understanding of the problems that are encountered when reinforced concrete beams are strengthened for flexure by bolting plates to their sides; to validate the computer model in Chapter 5; and to validate the mathematical models for vertical shear force in Chapter 9.

8.2 SECTION 1: MATERIAL PROPERTIES

This section describes the material properties of the concrete, reinforcement, plate and bolt. The material properties of the concrete were obtained by the cylinder compression test (f_c), the cube compression test (f_{cu}), the indirect tensile test (f_t), the flexural strength test (f_{cf}) and the elastic modulus test (E_c). The material properties of the reinforcement and plate were obtained from tensile tests. All these tests were performed according to the Australian Standards. The material properties of the bolts were supplied by the manufacturer.

8.2.1 Concrete

Five pours were required to cast the concrete specimens for the push tests and plated beam tests. The respective pour numbers for the push and beam specimens are shown in Table 8.1.

Table 8.1 Concrete Pours

Pour number	Push specimen	Beam specimen
(1)	(2)	(3)
1	Push series 1	-
2	Push series 2	-
3	Push series 3	-
4	Push series 4 and 5 (excluding specimens P23 & P24)	Beam series 1 to 3 excluding beam A21 and B24
5	Push specimens P23 & P24	Beam B24 and Beam A21

For each pour, the concrete tests were performed at different ages of concrete according to the Australian Standard AS1012 (1993). Details of the individual test results are given in Appendix-B. The mean strengths at different ages and the overall averages (i.e the strengths irrespective of age) are given in Tables 8.2 and 8.3 respectively.

Table 8.2 Average material properties of the different pours

Pour number	Cylinder specimen			Cube specimen	Beam specimen	Age
	Average compressive strength, f_c (MPa)	Average indirect tensile strength, f_t (MPa)	Elastic modulus, E_c (MPa)	Average compressive strength, f_{cu} (MPa)	Average flexural tensile strength, f_{cf} (MPa)	(days)
(1)	(2)	(3)	(4)	(5)	(6)	(7)
1	51.9	5.50	42600	56.0	-	133
	-	-	-	-	6.30	835
2	44.9	4.00	32700	49.9	-	111
	-	-	-	-	5.70	832
3	45.0	4.10	42300	37.7	5.70	605
4	-	4.10	-	-	6.10	53
	49.6	-	39900	-	-	121
	48.8	-	42500	55.8	-	143
	-	4.10		-	6.50	144
5	46.6	-	33200	53.0	-	109
	44.4	4.50	35200	-	6.41	117

Table 8.3 Overall average concrete material properties

Pour number	Cylinder specimen			Cube specimen	Beam specimen
	Average compressive strength, f_c (MPa)	Average tensile strength, f_t (MPa)	Elastic modulus, E_c (MPa)	Average compressive strength, f_{cu} (MPa)	Average flexural strength, f_{cf} (MPa)
(1)	(2)	(3)	(4)	(5)	(6)
1	51.9	5.50	42600	56.0	6.30
2	44.9	4.00	32700	49.9	5.70
3	45.0	4.10	42300	37.7	5.70
4	49.2	4.10	41200	55.8	6.30
5	45.5	4.50	34200	53.0	6.40

8.2.2 Reinforcement

The tensile strength of the 20 mm diameter (Y20) reinforcement was tested according to the Australian Standard AS 1391 (1991). The average yield strength and ultimate strength of Y20 bar used in beam Series 1-3 (except beam A21 and B24) were 443 MPa and 528 MPa respectively. That of beam A21 and B24 was 432 MPa and 527 MPa respectively. The individual test results are described in Appendix-B.

8.2.3 Plate

The tensile strength of the plate was tested in accordance with the Australian Standard AS 1391 (1991). The average strengths are given in Table 8.4. The individual test results are given in Appendix-B.

Table 8.4 Material Properties of Plate

Plated beam Series	Push specimen Series	Yield strength, f_{yp} (MPa)	Ultimate strength, f_{up} (MPa)
(1)	(2)	(3)	(4)
Beam Series 2 and 3	-	377	442
-	Push Series 3 to 5 (except P22)	368	464
-	Push test P22	320	437

8.2.4 Bolts

Four different types of bolts, as shown in Figure 8-1, were used in the tests. The bolt in (a), (c) and (d) are mechanical anchors and the bolt in (b) is an adhesive anchor.

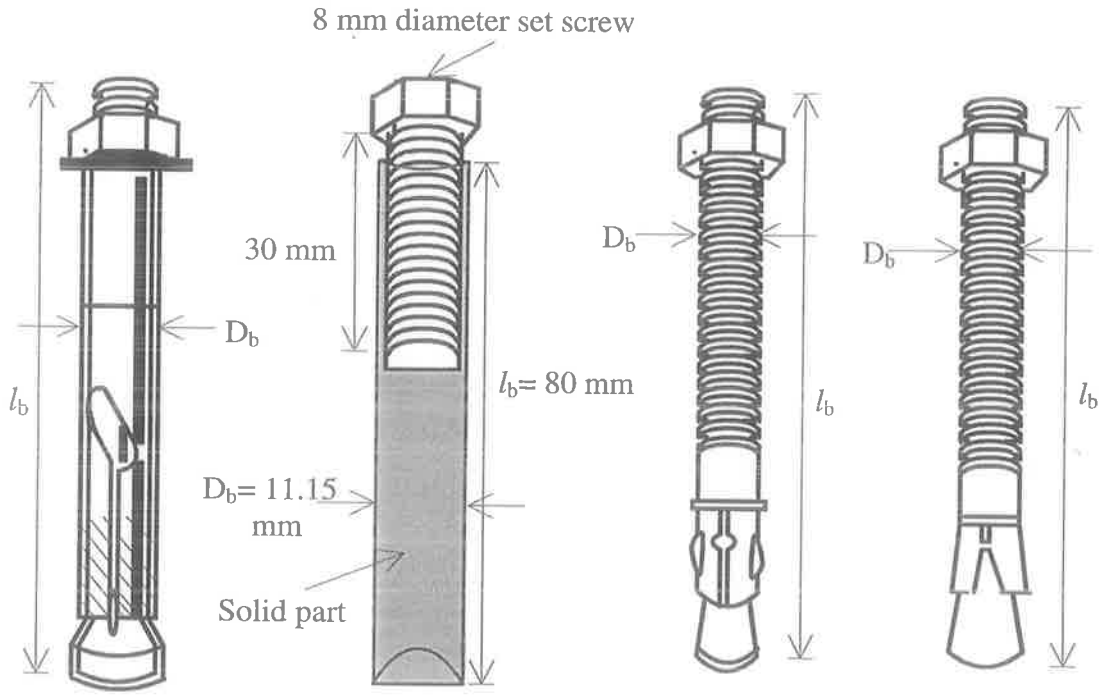

(a) Dynabolt (b) HIS adhesive bolt (c) Trubolt (d) HSA bolt

Fig. 8-1 Bolts

The Dynabolt in (a) is a sleeve anchor with a torque induced setting action; the HIS in (b) is an internally threaded anchor, used with a set screw as a fastener; the Trubolt in (c) is a stud anchor, with a torque induced setting action; and the HSA in (d) is also a stud anchor with a force controlled expansion of three wedges. The mechanical properties of the bolts were not measured in the laboratory; the manufacturer's specifications [Hilti manual (1993a,1993b); Ramset manual (1992a,1992b)] are presented in Table 8.5.

Table 8.5 Parameters and mechanical properties of bolts

General Name	Manufacturer's Specification	Name of company	Outside diameter D_b (mm)	Length of sleeve l_b (mm)	Yield strength (MPa)	Ultimate strength (MPa)
(1)	(2)	(3)	(4)	(5)	(6)	(7)
mecha-nical anchor	Dynabolt Dynabolt Dynabolt	Ramset Ramset Ramset	6.00 6.00 6.00	26.0 38.0 58.0	550.0 550.0 550.0	750.0 750.0 750.0
Adhe-sive anchor	HIS	Hilti	11.15	80.0	440.0	540.0
mecha-nical anchor	HSA	Hilti	7.82	75.0	530.0	740.0
Set screw	Ajax bolt	Ajax	8.00	30.0	640.0	800.0
mecha-nical anchor	Trubolt T8090	Ramset	7.88	90.0	590.0	740.0

8.2.5 Glue

The glue used in the bolted connections was a medium setting two part epoxy paste; one part was preblended resin and fillers and the other part was a hardener. Two different company's glue were used; they were Hilti and Ramset company.

8.3 SECTION 2 : PUSH TEST

The purpose of the push tests was to determine an ideal shear connector for the plated beams. Different shear connectors were developed with the bolts in Fig. 8-1. A total of 24 tests were performed, where the variations were the type of push specimen and the shear connector.

8.3.1 Design of Push Specimen

The push specimen in Fig. 8-2 consisted of three material: the concrete block, the plate and the shear connector. The length of the concrete block is very small as compared with the width and the depth so that no bending occurs, and so no reinforcement was used in the concrete block.

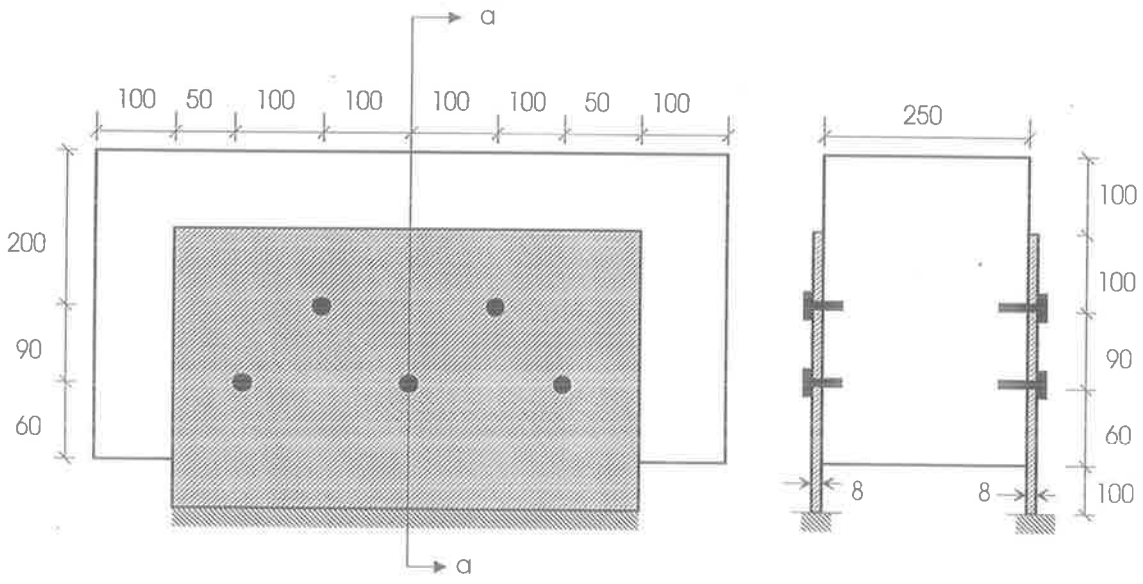

(a) Longitudinal view (b) Section a-a

Note: All dimensions are in millimetres

Fig. 8-2 Push specimen of Type 1

Two types of push specimens were designed as shown in Figs. 8-2 and 8-3 respectively. The dimension of the concrete block in both types was the same whereas the dimensions of the plates were different. There were five shear connectors per side in Type 1 and three shear connectors per side in Type 2 as shown in Figs. 8-2 and 8-3, respectively. The bolt positions were selected according to Sect. 2.4.1.4 to ensure that the splitting of concrete would not occur before the dowel strength was achieved. The push specimen of Type 1 was used in the Series 1 and 2 and Type 2 was used in Series 3 to 5.

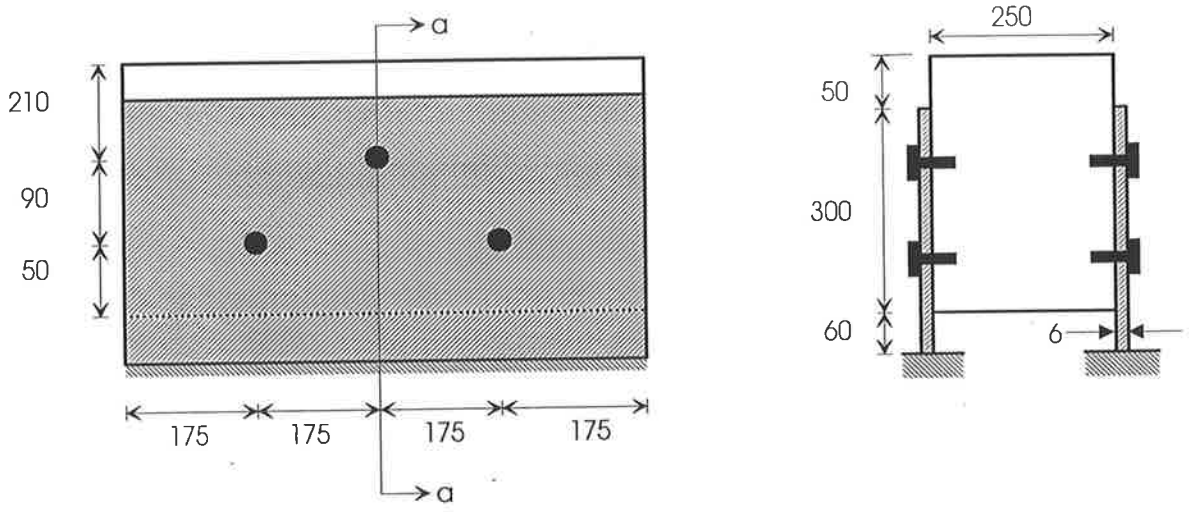

(a) Longitudinal view

(b) Section a-a

Note: all dimensions are in millimetres

Fig. 8-3 Push specimen of Type 2

8.3.1.1 Design of shear connection

Five different shear connectors were designed using the bolts in Fig. 8-1 and they are shown in Fig. 8-4. It can be seen that the same Trubolt in (b) was used in (c) with glue and the 'HIS adhesive bolt' in (e) was also glued. The shear connectors in Fig. 8-4 were tested in five series. The respective series, diameter of the hole in the concrete and in the plate, and the thickness of glue (when used) are given in Table 8.6.

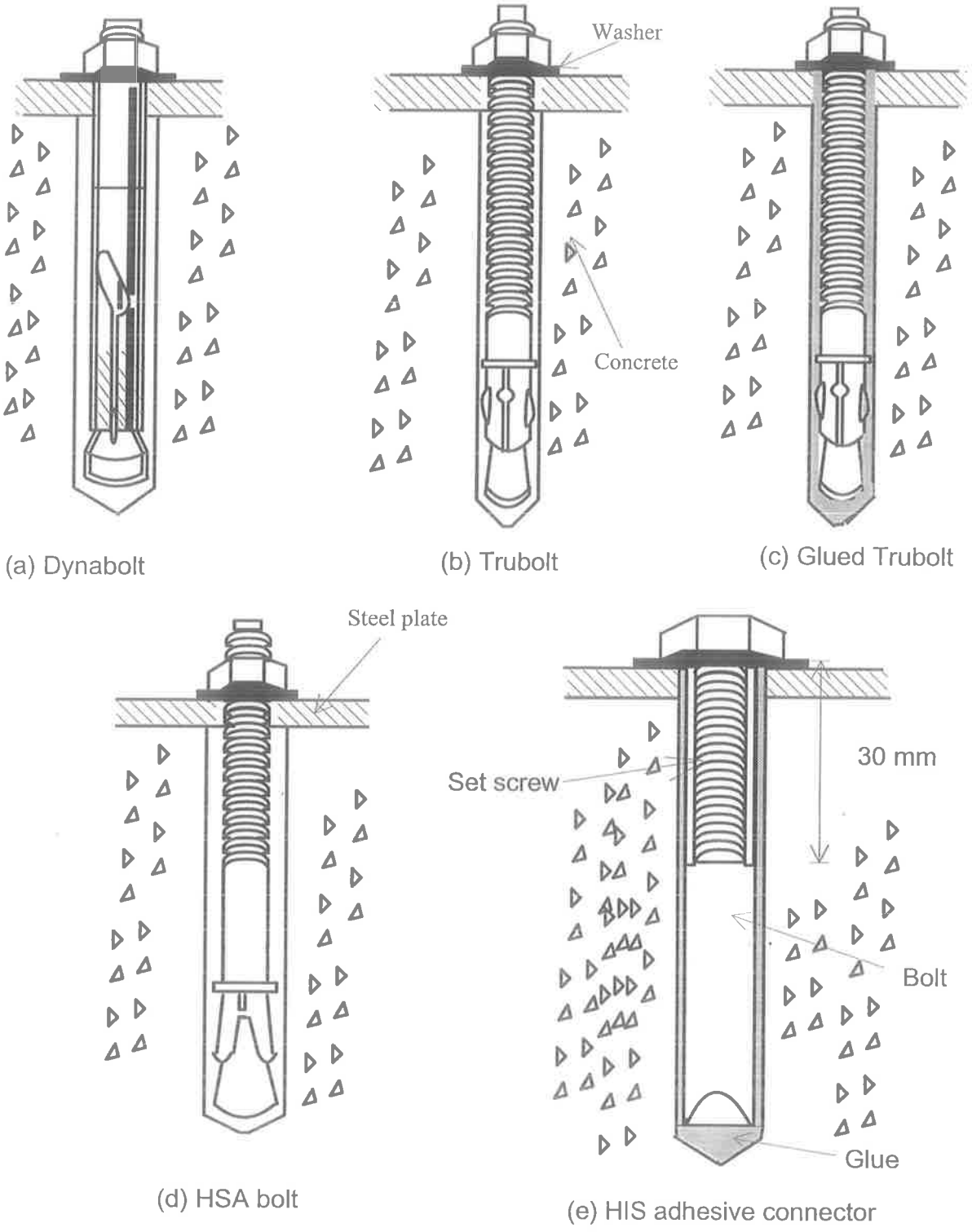

Fig. 8-4 Shear connectors

Table 8.6 Design of shear connector

Shear connector	Push Series	No. of tests	Diam-eter of bolt (mm)	Hole dia-meter in concrete (mm)	Hole dia-meter in plate (mm)	Thickness of glue (mm)	Length of bolt (mm)
(1)	(2)	(3)	(4)	(5)	(6)	(7)	(8)
Dynabolt	Push Series 1	2	6.0	6.5	6.5	-	26
		2	6.0	6.5	6.5	-	38
		2	6.0	6.5	6.5	-	58
	Push Series 2	2	6.0	6.5	8.5	-	38
		2	6.0	6.5	9.5	-	38
		2	6.0	6.5	10.5	-	38
Trubolt	Push Series 3	1	7.88	8.00	8.00	-	90.0
Glued Trubolt	Push Series 3	1	7.88	8.00	8.00	0.12	90.0
HSA bolt	Push Series 3	1	7.82	7.95	7.95	-	75.0
HIS adhesive bolt	Push Series 3, 4 & 5	9	11.15	12.5	12.5	1.35	80.0

8.3.2 Description of Series of Push Tests

There were five series of push tests. The first three series of tests were designed to find a suitable shear connector from those shown in Fig. 8-4. The comparison of the test results in Sect. 8.3.5.3.1 showed that the HIS adhesive shear connector in (e) would be suitable for the plated beams. The fourth series of tests was used to find a suitable glue for the HIS

adhesive shear connectors from which the Ramset glue was found to be suitable. Having thus ascertained the best type of shear connection and glue, these were used in the manufacture of plated beams. The subsequent series of push specimens were poured with the plated beams. This was done with a view to determining the behaviour of the shear connection for the beams from the push tests. A detailed description of each series is given in the following sections.

8.3.2.1 Series 1: Different length of Dynabolt

The aim of Series 1 was to investigate the load-slip behaviour of the Dynabolt in Fig. 8-4(a) for different lengths, l_b, in Figure 8-5. The lengths used were 26mm, 38 mm and 58 mm. The clearance in the hole of the plate, c in Figure 8-5, was 0.5 mm in all the tests. A detailed description of the tests in this series are given in Table 8.7.

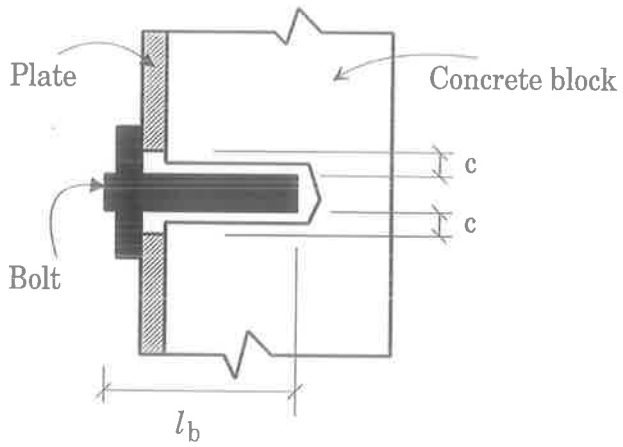

Fig. 8-5. Definition of l_b and c

8.3.2.2 Series 2: Dynabolt with different clearance

The main aim of Series 2 in Table 8.7 was to investigate the load-slip behaviour of the Dynabolt in Fig. 8-4(a) for three different clearances between the bolt and the plate, c in Figure 8-5. The three clearances used were 2.5 mm, 3.5 mm and 4.5 mm. The length of the bolt, l_b, was kept constant at 38 mm.

Table 8.7 Description of Push Series 1 and 2

Series	Test no.	Height of bolt l_b (mm)	Clearance in the hole of plate c (mm)	Pour number of concrete block	Age of concrete block at testing (days)
(1)	(2)	(3)	(4)	(5)	(6)
Series 1	Test P1	26.0	0.5	1	106
	Test P2	26.0	0.5	1	106
	Test P3	38.0	0.5	1	106
	Test P4	38.0	0.5	1	106
	Test P5	58.0	0.5	1	106
	Test P6	58.0	0.5	1	106
Series 2	Test P7	38.0	2.5	2	108
	Test P8	38.0	2.5	2	108
	Test P9	38.0	3.5	2	108
	Test P10	38.0	3.5	2	108
	Test P11	38.0	4.5	2	108
	Test P12	38.0	4.5	2	108

8.3.2.3 Series 3: Different type of bolt

The main purpose of series 3, the test descriptions for which are given in Table 8.8, was to investigate the load-slip behaviour of four different types of shear connectors. They were the Trubolt in 8-4(b), glued Trubolt in (c), HSA bolt in (d) and HIS adhesive bolt in (e).

8.3.2.4 Series 4: HIS adhesive bolt with different glue

Series 4, the test descriptions for which are provided in Table 8.8, was used to find a suitable glue for the HIS adhesive bolt. Two different glues were used: the Hilti glue and the Ramset glue. Moreover, one test was done to see the variation in load-slip characteristics when no glue was used. The push specimens of this series were poured with the beams; so the results were used to determine the load-slip characteristics of the HIS adhesive bolt in the beams.

Table 8.8 Description of Series 3, 4, 5 and 6

Series name	Test name	Adhesive type	Bolt type	Concrete pour number	Age of concrete block
(1)	(2)	(3)	(4)	(5)	(6)
Series 3	Test P13	-	Trubolt	3	605
	Test P14	Ramset glue	Trubolt	3	605
	Test P15	-	HSA	3	605
	Test P16	Hilti glue	HIS adhesive	3	605
Series 4	Test P17	Ramset glue	HIS adhesive	4	62
	Test P18	Ramset glue	HIS adhesive	4	62
	Test P19	Hilti glue	HIS adhesive	4	62
	Test P20	-	HIS adhesive	4	62
Series 5	Test P21	Ramset glue	HIS adhesive	4	152
	Test P22	Ramset glue	HIS adhesive	4	219
	Test P23	Ramset glue	HIS adhesive	5	137
	Test P24	Ramset glue	HIS adhesive	5	142

8.3.2.5 Series 5: HIS adhesive bolt with Ramset glue

The aim of Series 5, the test description for which are given in Table 8.8, was to investigate the load-slip behaviour of the HIS adhesive bolt with the Ramset glue. This was done by using push specimens which were poured with the beams.

8.3.3 Preparation of Push Test Specimens

The preparation of the specimens was very straight forward. Firstly, the plate was clamped to the concrete block and the holes for the bolts were created by drilling through the plate into the concrete. In the case of the shear connector without glue, they were screwed into the hole by applying the necessary torque. In case of shear connectors with glue, all the loose material and dust were removed from the hole in the concrete. The glue was then injected into the hole and the bolt was pressed into it by finger. The specimen was kept for 48 hours to allow for hardening of the glue. The nut into the Trubolt and the set screw into the HIS adhesive bolt were tightened, after adhesive was fully cured.

8.3.4 Test Rig and Instrumentation

The general arrangement of the test rig is shown in Fig. 8-6 and in the photograph P8.1. It can be seen that the thickness of the plate is much less than its height. For this reason, the horizontal force that is induced at the base and thereby the resultant forces across the steel/concrete interface, as described in Sect. 2.4.2, will be nearly zero. Thus, the dowel strength of the shear connections in the push specimens will not be greater than those in the plated beam. As such, no rollers were used at the base of the plate to reduce the interface forces. Instead, the bottoms of the plate were simply bedded to the base using a dental paste as shown.

A spreader beam was kept at the mid-width over the top of the concrete block which was bonded by dental paste, as shown in Fig. 8-6. The length of the spreader beam was the same as the length of the concrete block. The purpose of this arrangement was to

ensure even distribution of displacement. The displacement was applied at the middle of the push specimen.

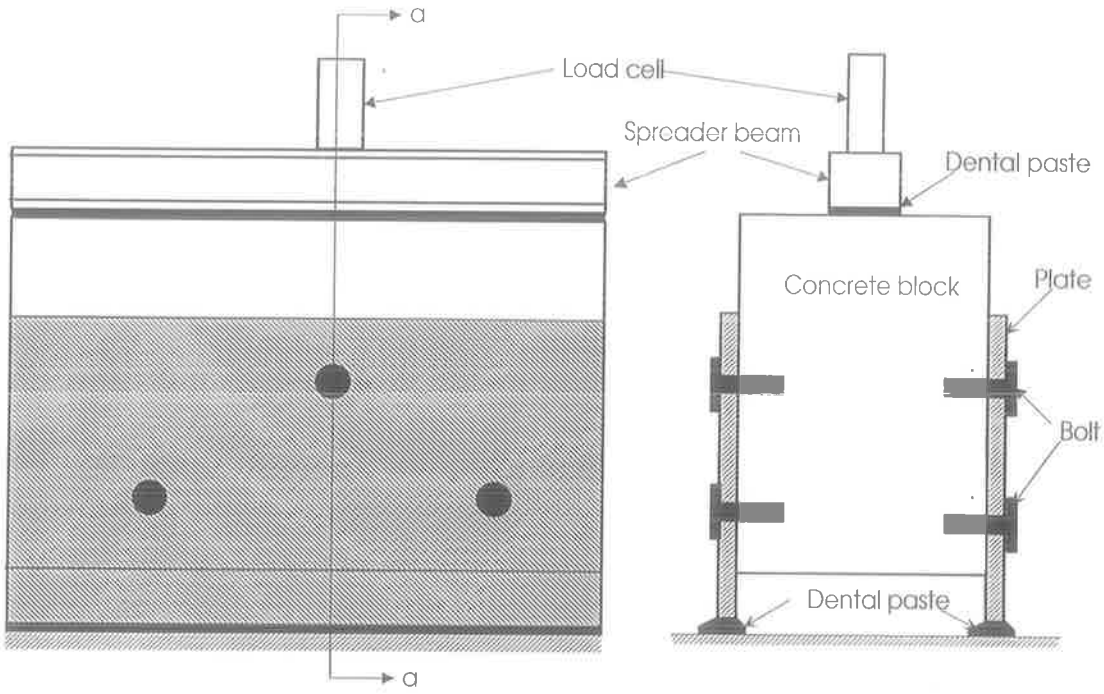

(a) Side elevation (b) Section a-a

Fig. 8-6 Test rig

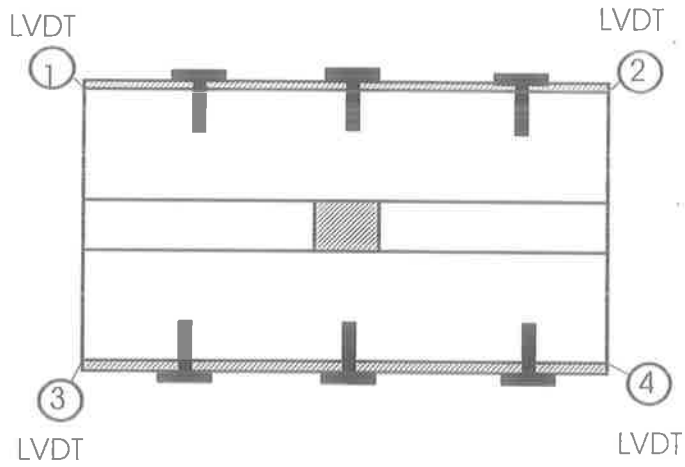

Fig. 8-7 Plan of push specimen showing instrumentation

Four LVDTs were placed at the four corner of the push specimen, as shown in Fig. 8-7, to measure the relative slip between the plate and the concrete element. The reference numbers of the respective LVDTs is encircled.

8.3.5 Description of Push Tests and Results

8.3.5.1 Series 1: Different length of Dynabolt

The aim of this series was to investigate the load-slip behaviour of shear connections with the Dynabolts in Fig. 8-4(a) for three different bolt lengths of 26 mm, 38 mm and 58 mm. Six push specimens of Type 1 in Fig. 8-2 were tested. Tests P1 and P2 were done with 26 mm length bolt, Test P3 and P4 with 38 mm length bolt and Tests P5 and P6 with 58 mm length bolt. The material properties of the concrete are given in Sect. 8.2.1.

The average slip against load/bolt for 26 mm, 38 mm and 58 mm length bolts are shown in Fig. 8-8 to Fig. 8-10 respectively. These were derived from the slip at the four corners of the push specimen, which is shown in Appendix-C. It can be seen in Figs. 8-8 to Fig. 8-10 that almost no slip occurs at the beginning in the tests P2, P3, P4, P5 and P6, possibly due to friction being overcome. In the test P1, there was slip. There was linear variation up to point A after which a gradual reduction in the stiffness of the push specimens occurs up to the maximum load at point B. A small plastic plateau of constant load occurs at this stage up to point C, after which the strength of the push specimen reduces rapidly, which is possibly caused by the pull out of the bolts. The load and slip at the start of non-linearity at point A, at the beginning of plateau near point B and at the end of the plateau near point C are given in Table 8.9. The shape of the bolt after pull out is shown in P8.2. At the end of the tests, the concrete surrounding the bolt was found to be crushed, as shown in P8.3.

It can be seen in Table 8.9 that the length of the plateau from B to C is very small in all the tests except test P5. Although there was no variation between tests P5 and P6, much variation occurs in the length of the plateau for which no reason was found. The maximum load in the push specimens varied from 5 to 10 kN/bolt.

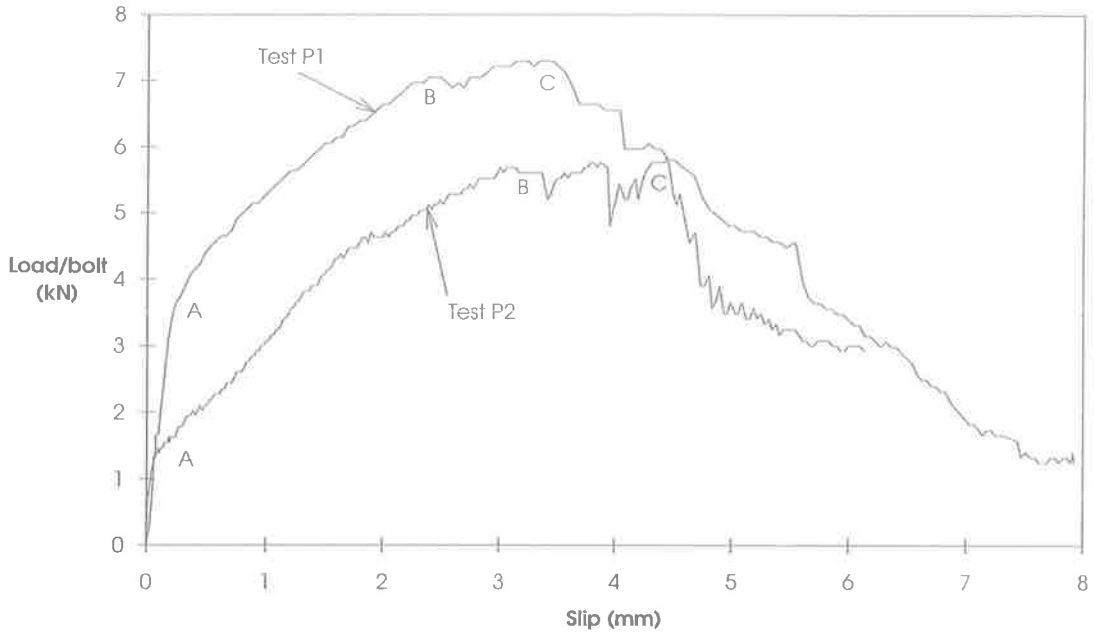

Fig. 8-8. Dynabolt of 26 mm length

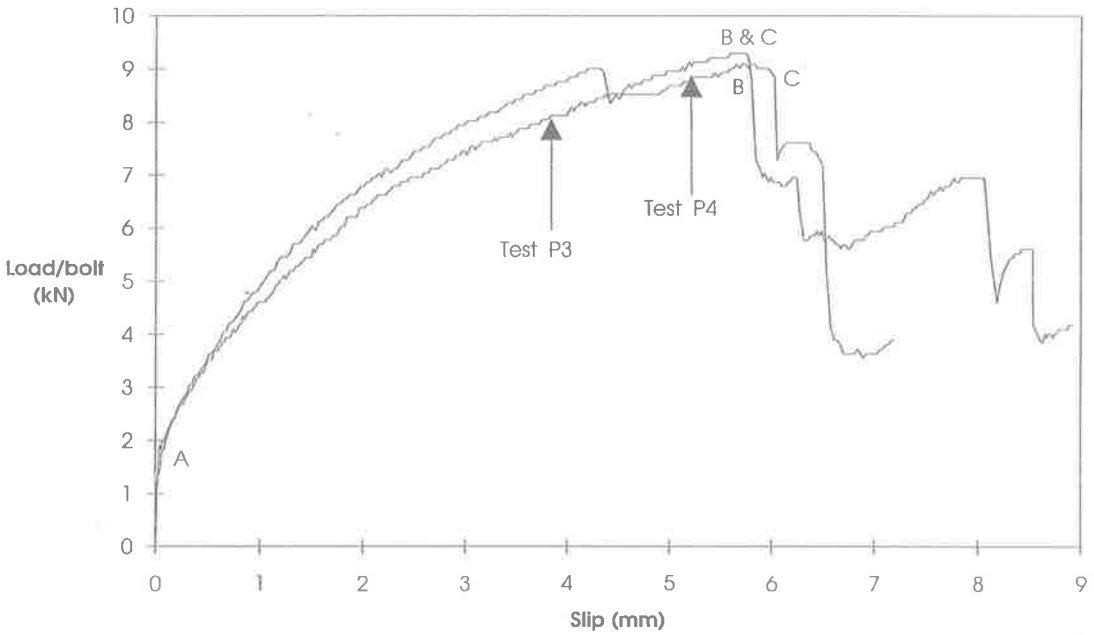

Fig. 8-9 Dynabolt of 38 mm length

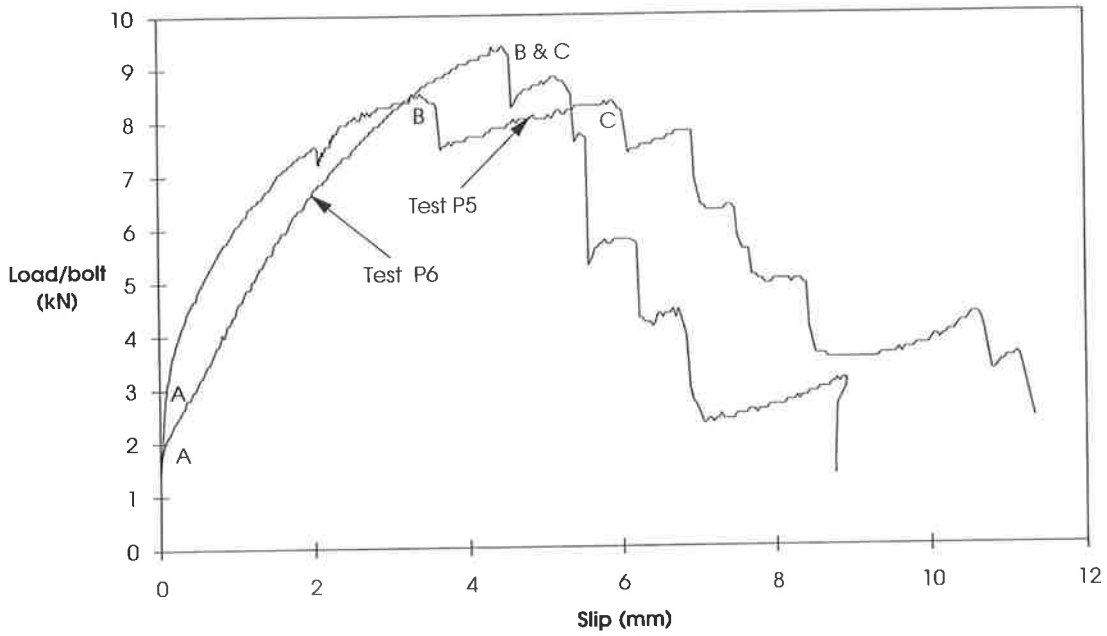

Fig. 8-10 Dynabolt of 58 mm length

Table 8.9 Results of Push test Series 1: Different length of Dynabolt

Test name	Length of bolt (mm)	Linear variation (Point A)		Beginning of plateau (Point B)		End of plateau (Point C)	
		Load (kN/bolt)	Slip (mm)	Load (kN/bolt)	Slip (mm)	Load (kN/bolt)	Slip (mm)
(1)	(2)	(3)	(4)	(5)	(6)	(7)	(8)
Test P1	26.0	3.60	0.25	6.80	2.25	7.30	3.45
Test P2	26.0	1.55	0.18	5.60	3.25	5.80	4.25
Test P3	38.0	1.90	0.10	9.30	5.58	9.30	5.74
Test P4	38.0	1.80	0.08	9.00	5.59	9.10	5.82
Test P5	58.0	3.00	0.08	8.50	3.29	8.35	5.91
Test P6	58.0	1.89	0.05	9.40	4.32	9.40	4.47

8.3.5.1.1 Comparison of Push test Series 1: Different length of Dynabolt

Two tests were done for each length of bolt in Series 1. The mean load-slip curves for each length of bolt are shown in Fig. 8-11 and summarised in Table 8.10. It can be seen that the stiffness and the strength of 26 mm length bolts is considerably less than that of both the 38 mm and 58 mm length bolts. The strength and the stiffness of 38 and 58 mm length bolt is very close to each other. This suggests that there is a limit to the increase in the strength and stiffness of the push specimen as the length of the bolt is increased. It is the general characteristic of these bolts that they pulled out as soon as the maximum load was achieved. Therefore, these Dynabolts are not suitable for use in plated beams as they do not have a significant plateau in the load-slip curve.

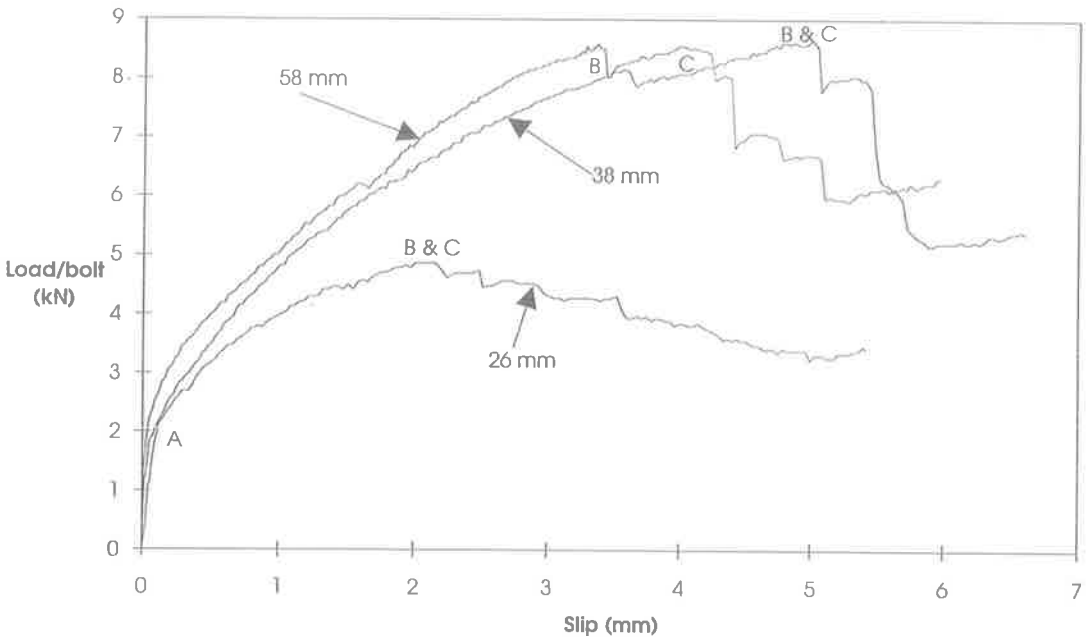

Fig. 8-11 Push tests in Series 1: Dynabolt of different length

Table 8.10 Mean results of Push test Series 1: Different length of Dynabolt

Length of bolt (mm)	Linear variation (Point A)		Beginning of plateau (Point B)		End of plateau (Point C)	
	Load (kN/bolt)	Slip (mm)	Load (kN/bolt)	Slip (mm)	Load (kN/bolt)	Slip (mm)
(1)	(2)	(3)	(4)	(5)	(6)	(7)
26.0	1.80	0.09	4.87	2.00	4.87	2.15
38.0	2.10	0.10	8.61	4.77	8.65	5.00
58.0	2.10	0.04	8.59	3.37	8.51	4.12

8.3.5.2 Series 2: Dynabolt (38 mm length) with different clearance

The aim of Series 2 was to investigate the load-slip behaviour of the Dynabolt in Fig.8-4(a) for three different amounts of clearance in the plate hole. The clearances were 2.5 mm, 3.5 mm and 4.5 mm and hence the corresponding diameters of the holes in the plates were 8.5 mm, 9.5 mm and 10.5 mm respectively. Six push specimens of Type 1 in Fig. 8-2 were tested and two tests were done for each amount of clearance. Tests P7 and P8 had a 2.5 mm clearance, Tests P9 and P10 had a 3.5 mm clearance, and Tests P11 and P12 had a 4.5 mm clearance. The properties of the concrete were given earlier in Sect. 8.2.1.

The average slip against load/bolt is shown in Figs. 8-12 to Fig. 8-14. These were derived from the slip at the four corners of the push, which are given in Appendix-C. It can be seen in Fig. 8-12 that there is no slip up to point A. Also, there is no linear variation in the load-slip curve. The stiffness of the push specimen decreases gradually from point A to point C, where the maximum strength of the push specimen is reached. The load then drops slightly at an almost constant slip before increasing again up to point D, after which rapid reduction of strength occurs as the bolts were being pulled out. There is also no slip up to point A in Figs. 8-13 and Fig. 8-14, after which there occurs a some what different shape in the curve up to point B that was not seen in the previous tests. This might happen due to large clearances that have to be overcome by the slip before bearing of the bolt against the plate. The stiffness then gradually decreases from point B to the maximum load at point C, after which there occurs a slight drop of load at almost constant slip after which the load increases up to point D. The strength of the push specimen reduces very rapidly soon after the point D. The load and slip at points C and D are given in Table 8.11. It can be seen in Table 8.11 that the maximum strength of the push specimen varies from 7 to 10 kN/bolt. Also the slip between C and D is very small.

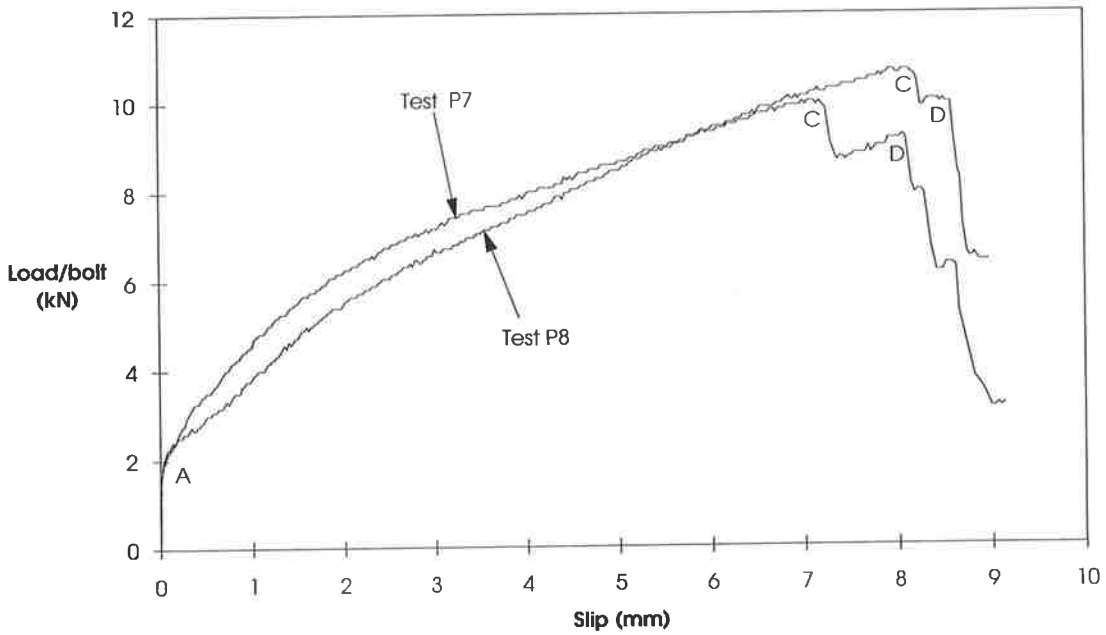

Fig. 8-12 Dynabolt (38 mm length) with 2.5 mm clearance

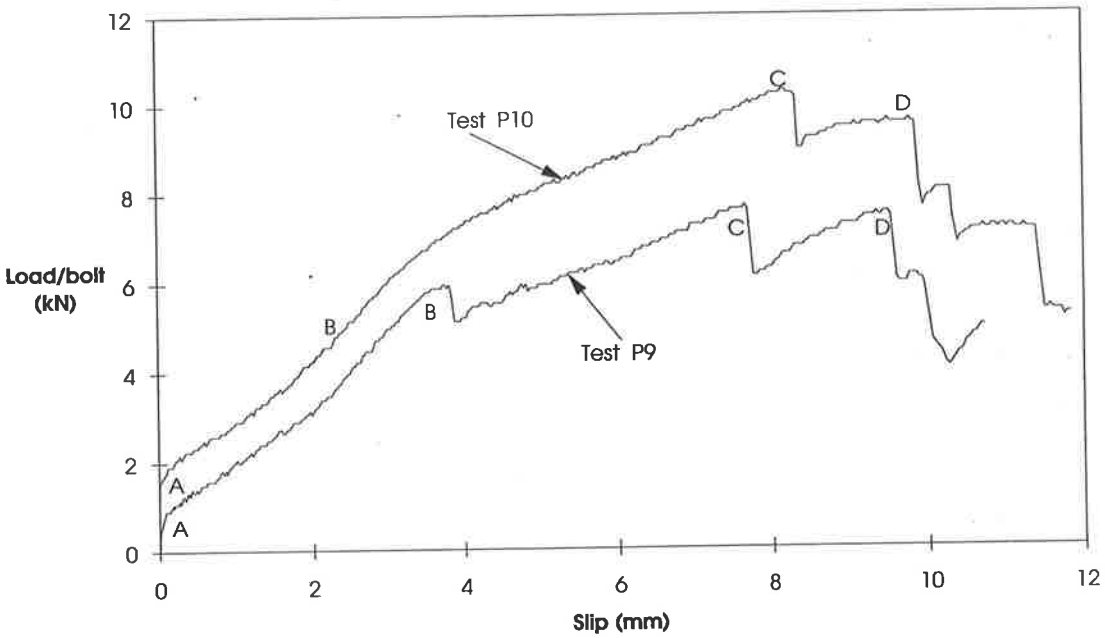

Fig. 8-13 Dynabolt (38 mm length) with 3.5 mm clearance

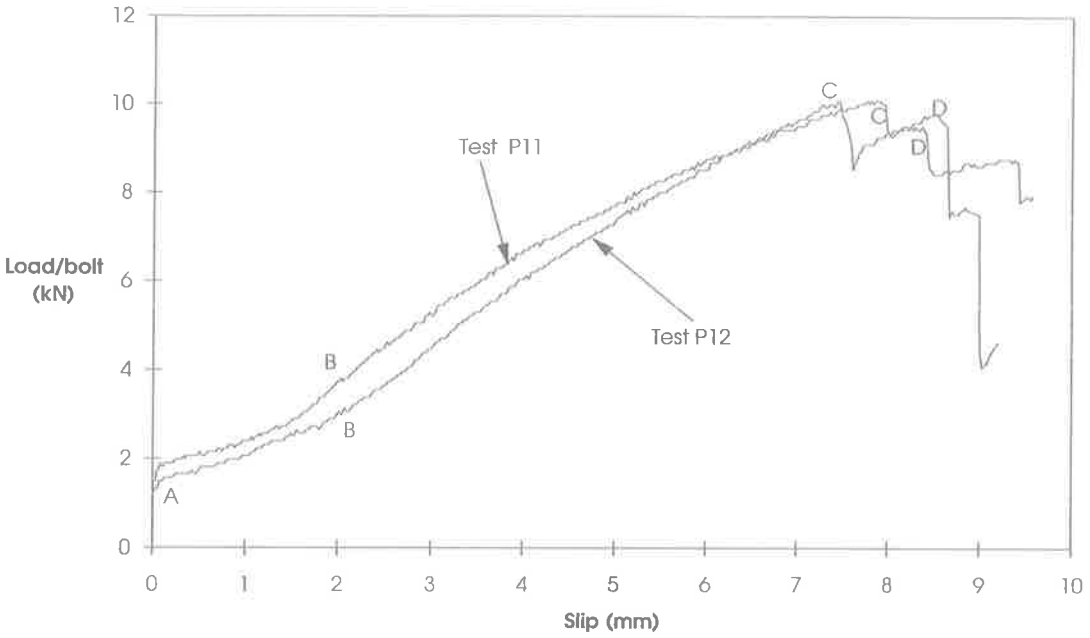

Fig. 8-14 Dynabolt (38 mm length) with 4.5 mm clearance

Table 8.11 Push test Series 2: Dynabolt (38 mm length) with different clearance

Test name	Clearance of plate hole (mm)	Linear variation (Point A)		Point C		Point D	
		Load (kN/bolt)	Slip (mm)	Load (kN/bolt)	Slip (mm)	Load (kN/bolt)	Slip (mm)
(1)	(2)	(3)	(4)	(5)	(6)	(7)	(8)
Test P7	2.5	1.90	0.0	9.7	7.20	8.05	8.10
Test P8	2.5	1.90	0.0	10.45	8.10	9.70	8.60
Test P9	3.5	0.50	0.0	7.7	7.66	7.54	9.50
Test P10	3.5	1.50	0.0	10.3	8.08	9.90	9.90
Test P11	4.5	1.70	0.0	10.1	7.80	10.0	8.00
Test P12	4.5	1.70	0.0	10.1	7.43	9.8	8.54

8.3.5.2.1 Comparison of Push test Series 2: Dynabolt (38 mm length) with different clearance

The main variation in Series 2 was the amount of clearance in the hole of the plate. The mean load-slip curve for each clearance is shown in Figure 8-15. These were determined from the test results described in the previous section. It can be seen in Fig. 8-15 that the bolt with the 2.5 mm clearance in the plate has the highest strength and stiffness. Also the strength of the bolt having a 4.5 mm clearance is higher than that of the bolt with a 3.5 mm clearance. The point to be noted in all of the cases is that there was a drop of load immediately after C. The load and slip at points C and D are given in Table 8.12. It can be seen in Fig. 8-15 that there is no significant plateau of slip and the push specimens failed soon after the maximum load was achieved. Therefore, it can be concluded that this type of shear connection that is Dynabolt with different clearance would not be suitable for the plated beams.

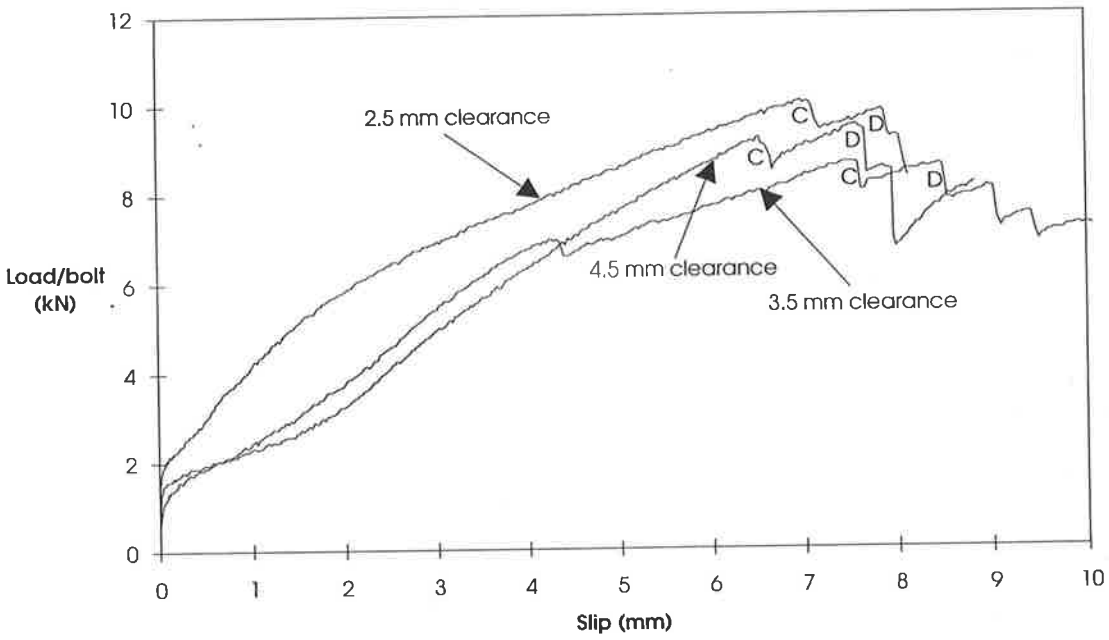

Fig. 8-15 Push tests Series 2: Dynabolt (38 mm length) with different clearance

Table 8.12 Mean results of Push test Series 2: Dynabolt (38 mm) with different clearance

Clearance of plate hole (mm)	Linear variation (Point A)		At maximum (Point C)		At dropping (Point D)	
	Load (kN/bolt)	Slip (mm)	Load (kN/bolt)	Slip (mm)	Load (kN/bolt)	Slip (mm)
(1)	(2)	(3)	(4)	(5)	(6)	(7)
2.5	1.90	0.0	10.0	6.90	9.84	7.84
3.5	1.00	0.0	8.66	7.43	8.62	8.46
4.5	1.70	0.0	9.22	6.50	9.52	7.56

8.3.5.3 Series 3: Different type of bolts

The main purpose of Series 3 was to determine the load-slip behaviour of the shear connectors in Figs. 8-4(b) to (e). Four push specimens of Type 2 in Fig. 8-3 were tested in this series. Test P13 had the Trubolt in Fig. 8-4(b), P14 the glued Trubolt in (c), Test P15 the HSA bolt in (d) and Test P16 the HIS adhesive bolt in (e). The different parameters of the shear connectors are given in Table 8.6 and the properties of the concrete and the plate are given in Sects. 8.2.1 and 8.2.3 respectively.

The average slip against load/bolt is shown in Fig. 8-16 for the Trubolt, in Fig. 8-17 for the glued Trubolt, in Fig. 8-18 for the HSA bolt and in Fig. 8-19 for the HIS adhesive bolt. The slip at each of the LVDTs is given in Appendix-C.

The load-slip curves of the connectors other than the HIS adhesive connectors in Figs. 8-16 to Fig. 8-18 are similar. There is linear variation up to point A. A gradual reduction in the stiffness of the push specimen then occurs up to the maximum load at point B. A small plateau can be seen at this stage up to point C, after which the strength of the push specimen reduces very rapidly. The load and slip at point A, B and C are given in Table 8.13. It can be seen in the table that the strength of the Trubolt is somewhat higher than that of the glued Trubolt. The reason is that the glue in the glued Trubolt was not sufficiently hard due to some unknown reason and this may have had a detrimental effect on the performance of the shear connector.

The load-slip behaviour of the HIS adhesive bolt can be seen in Fig. 8-19. There is a linear variation up to point A (4.8 kN of load/bolt as given in Table 8.13). The stiffness then reduces up to the maximum load of 21.42 kN/bolt at point B, where the slip is 1.65 mm. The load then drops to 19.7 kN/bolt at a slip of 2.29 mm, after which the load increases again to 21.3 kN/bolt at point C, where the slip is 3.45 mm. The load then drops gradually as the bolts were being broken. It can be seen in P8.4 that the sleeve broke at the end of the set screw, which is 30 mm from top of the bolt, as shown in Fig. 8-4(e). At the end of the test, the concrete surrounding the bolt was found to be crushed, as shown in P8.5.

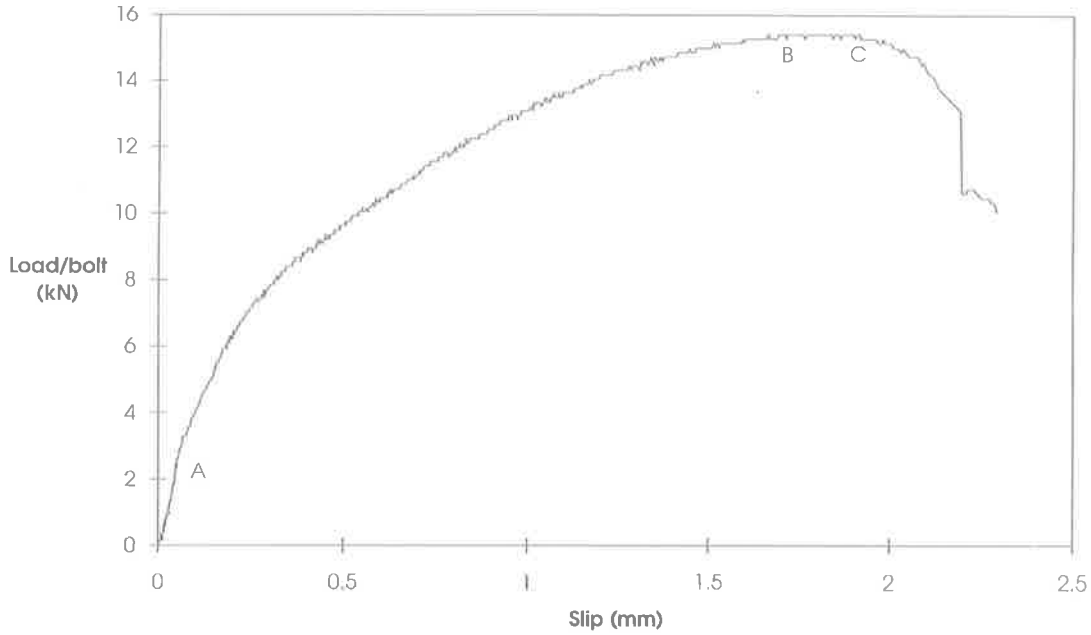

Fig. 8-16 Push test P13 with Trubolt

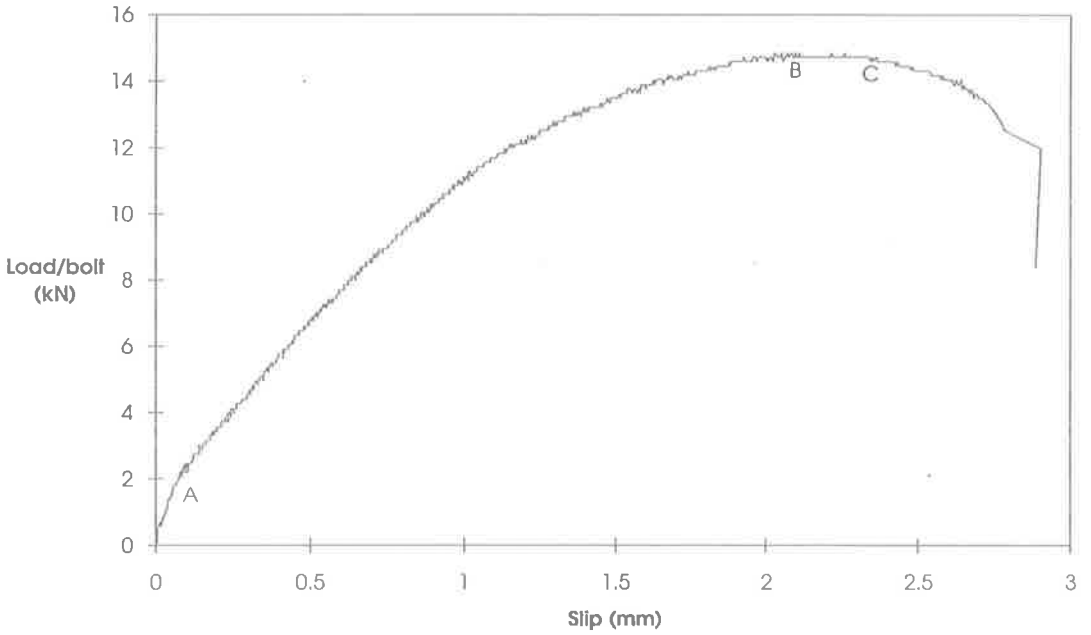

Fig. 8-17 Push test P14 with Glued Trubolt

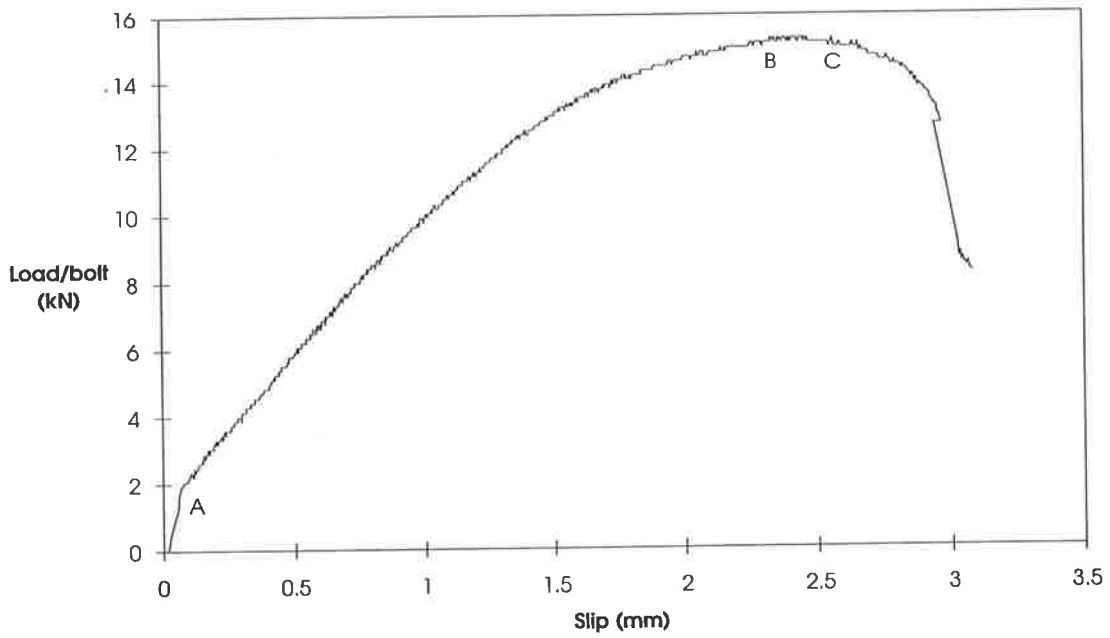

Fig. 8-18 Push test P15 with HSA bolt

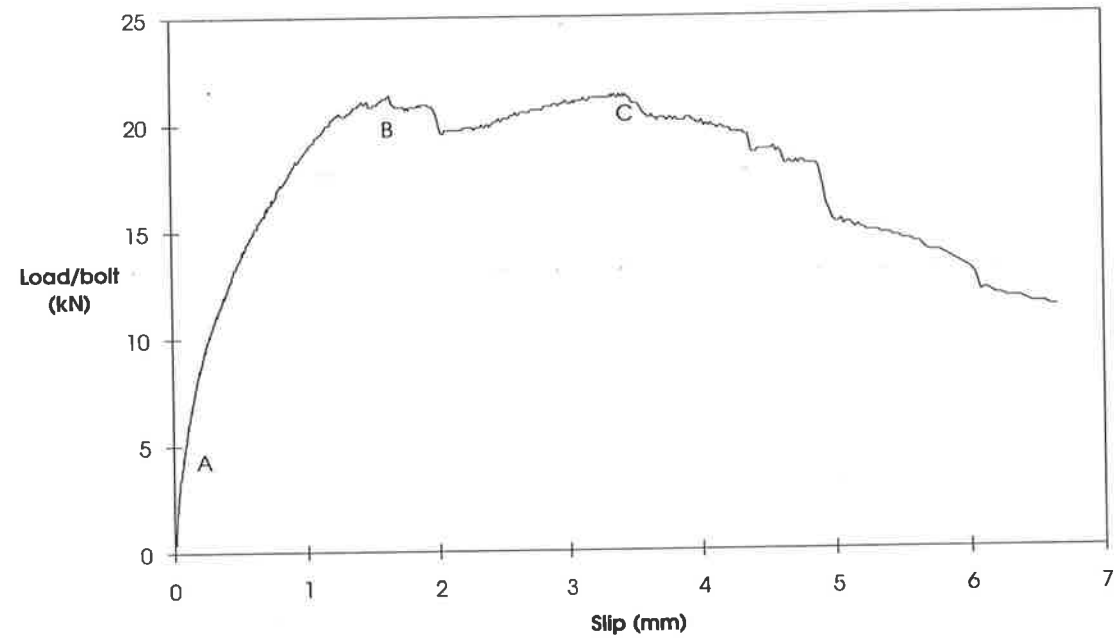

Fig. 8-19 Push test P16 with Adhesive HIS bolt

It can be seen in Table 8.13 that except for the HIS adhesive connector, all connectors had strengths around 15 kN/bolt and failed as soon as they achieved the maximum load. The HIS adhesive bolt had the largest strength of about 21 kN/bolt and had a large plateau of slip.

Table 8.13 Results of Push test Series 3: Different type of bolt

Test name	Bolt type	Adhesive Type	Linear variation Point A		Beginning of plateau Point B		End of plateau Point C	
			Load (kN/bolt)	Slip (mm)	Load (kN/bolt)	Slip (mm)	Load (kN/bolt)	Slip (mm)
(1)	(2)	(3)	(4)	(5)	(6)	(7)	(8)	(9)
Test P13	Trubolt	none	3.00	0.07	15.41	1.70	15.41	1.92
Test P14	Glued Trubolt	Ramset	1.90	0.07	14.86	2.02	14.73	2.36
Test P15	HSA bolt	none	1.92	0.07	15.28	2.33	15.28	2.56
Test P16	HIS adhesive bolt	Hilti	4.81	0.09	21.42	1.65	21.42	3.45

8.3.5.3.1 Comparison of Push test Series 3: Different type of bolt

In this series, the different shear connectors in Figs. 8-4(c) to (e) were tested. Their load-slip behaviours are compared in Fig. 8-20. The stiffness and the strength of HIS adhesive bolt is found to be much higher than that of the other bolts. Also, there occurs a large plateau of slip in the HIS adhesive bolt before failure whereas the other bolts failed as soon as they achieved their maximum strength. It can be seen in Fig. 8-20 that the reduction in strength in the HIS adhesive bolt is very gradual whereas it is very rapid in the other bolts. It was, therefore, decided to use the HIS adhesive bolt as the shear connection for the plated beam tests, as ductile failure of connector is a fundamental requirement of a plated beam.

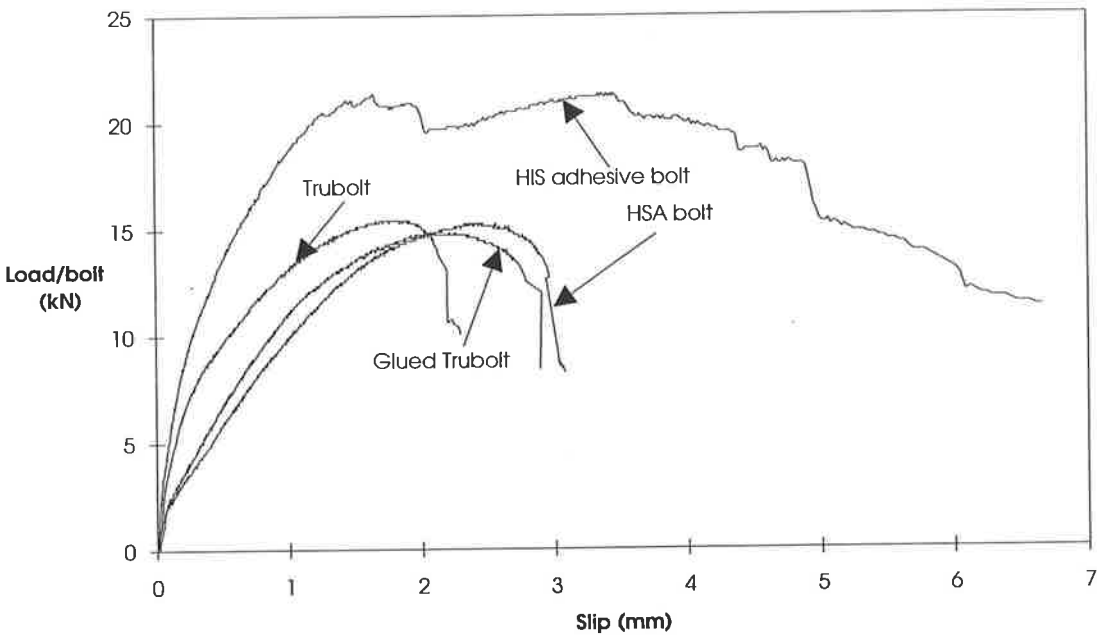

Fig. 8-20 Push test Series 3: Different type of bolt

8.3.5.4 Series 4: HIS adhesive bolt with different glue

This series consisted of four tests of the push specimen of Type 2 in Fig. 8-3. The main purpose was to study the load-slip characteristics of the HIS adhesive bolt in Fig. 8-4(e) for different types of glue and without glue. Furthermore, these specimens were poured with the beams in Series 1 to 3 (excluding beam B24 in Series 2), so that we could determine the load-slip characteristics of the HIS adhesive bolt in the beams from the push tests. The properties of the concrete and the plate are given in Sect. 8.1.2 and 8.2.3.

Specimens P17 and P18 used Ramset glue, P19 used Hilti glue and specimen P20 was not glued. The average slip against the load/bolt for the tests are shown in the Figs. 8-21 to 8-24 respectively. The slip at the four corners of the push specimen for all the tests are given in Appendix-C. It can be seen in Figs. 8-21 to 8-24 that the general form of the load-slip curve is similar to Test P16 in the previous Sect. 8.3.5.3. The load and slip at the end of linear variation, and at the beginning and end of the plateau are given in Table 8.14.

The failure mechanism of the push specimens was the same as in the previous test P16 with the same bolt in Sect. 8.3.5.3. The crushing of the surrounding concrete of the bolt is same as shown in P8.5.

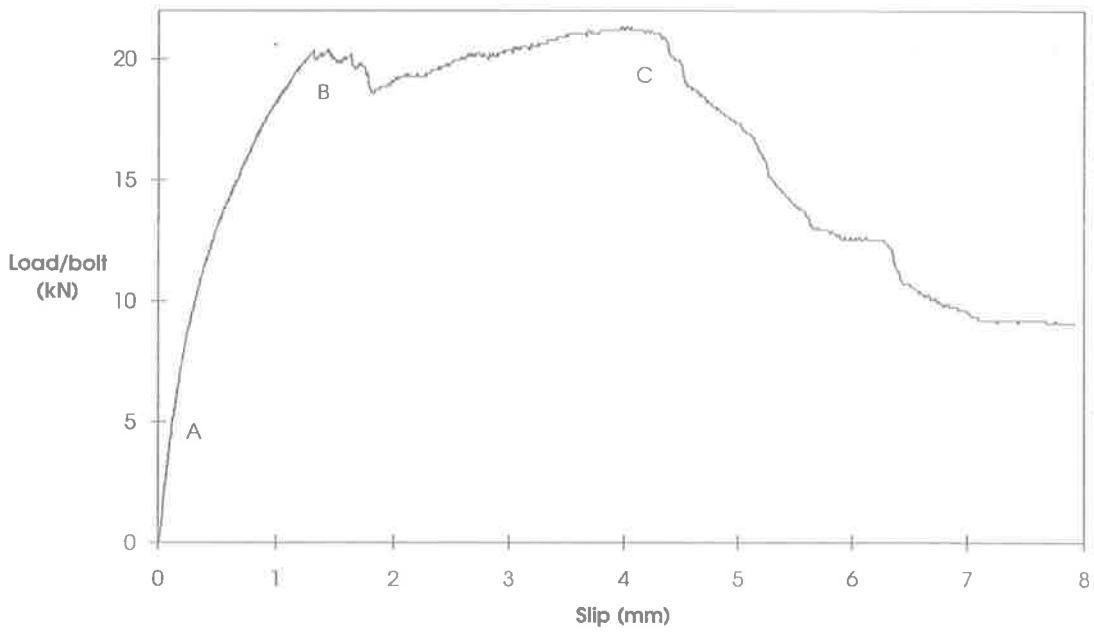

Fig. 8-21 Push test P17, HIS adhesive bolt with Ramset glue

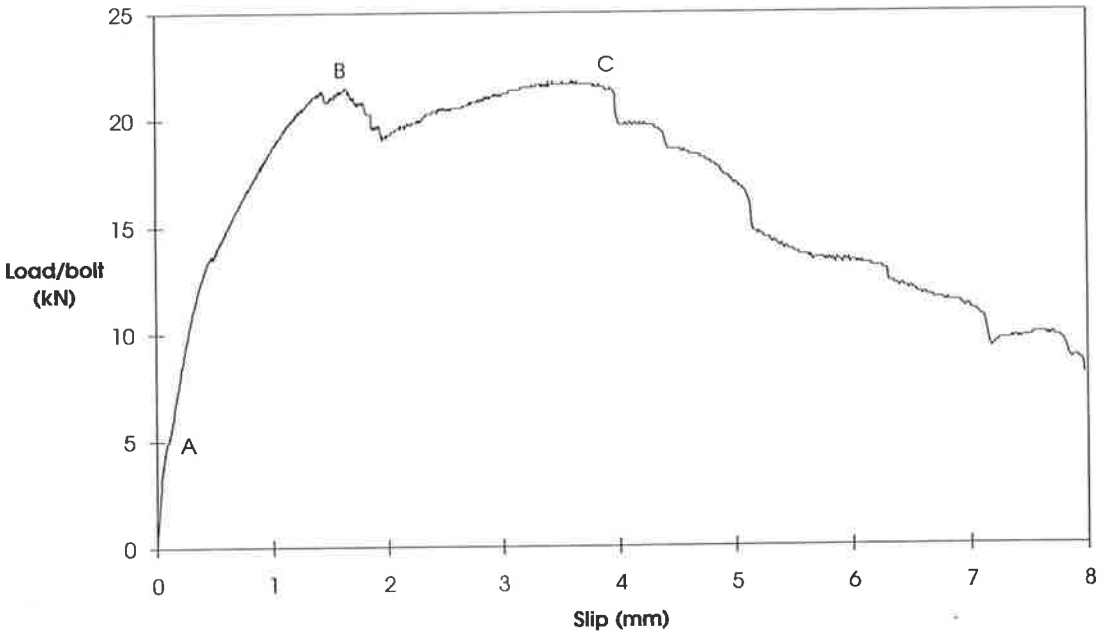

Fig. 8-22 Push test P18, HIS adhesive bolt with Ramset glue

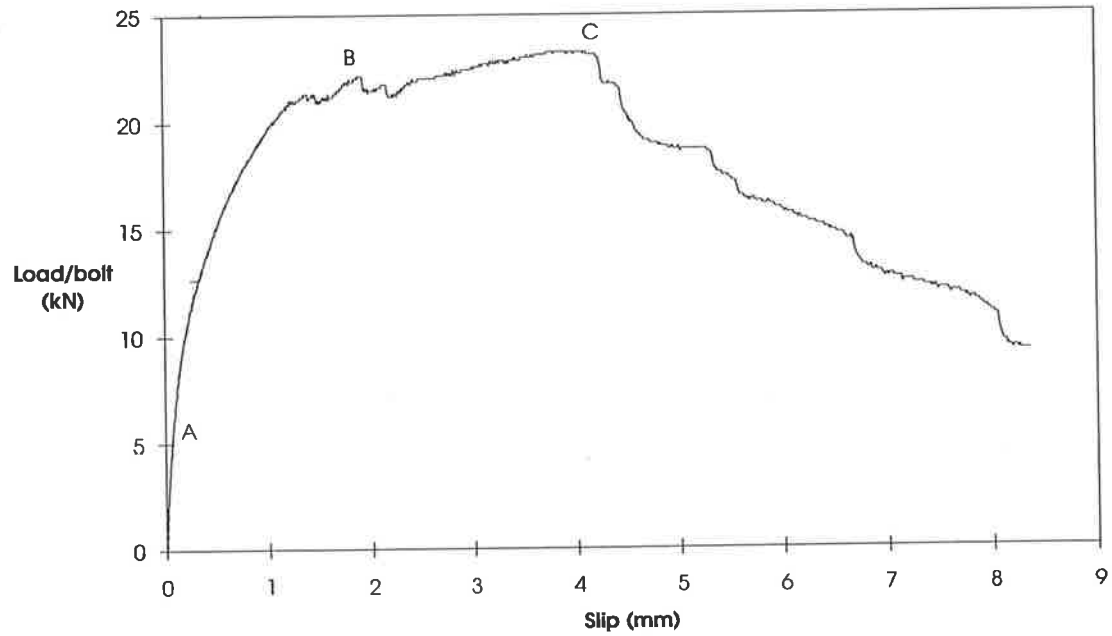

Fig. 8-23 Push test P19, HIS adhesive bolt with Hilti glue

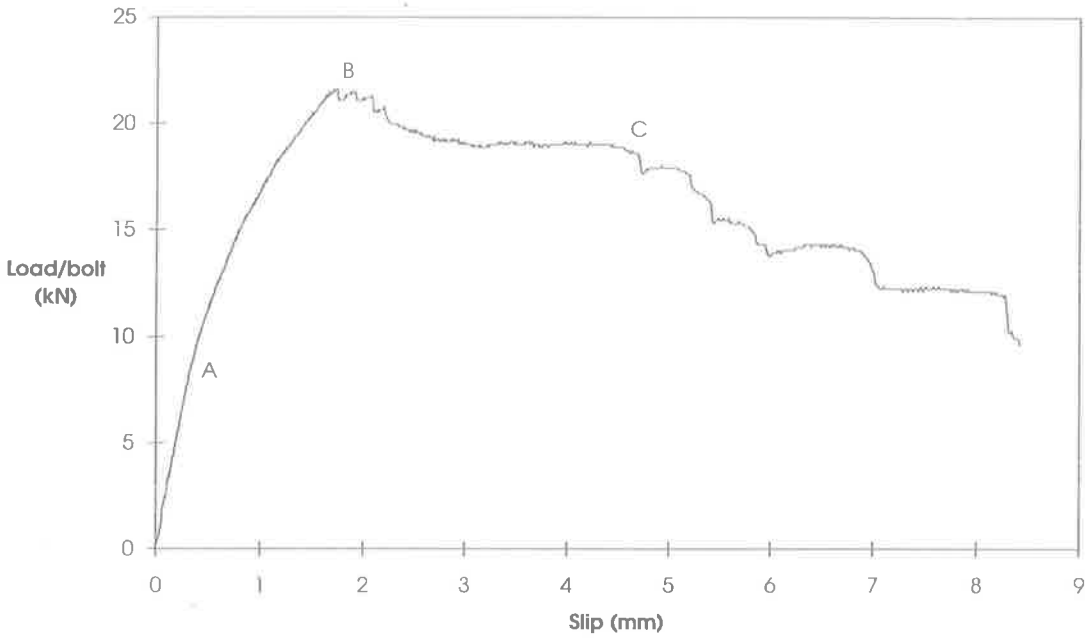

Fig. 8-24 Push test P20, HIS adhesive bolt without glue

Table 8.14 Push test Series 4: HIS adhesive bolt with different glue

Test name	Adhesive Type	Linear variation Point A		Start of plateau Point B		End of plateau Point C	
		Load (kN/bolt)	Slip (mm)	Load (kN/bolt)	Slip (mm)	Load (kN/bolt)	Slip (mm)
(1)	(3)	(4)	(5)	(6)	(7)	(8)	(9)
Test P17	Ramset glue	5.20	0.12	20.38	1.32	21.35	4.06
Test P18	Ramset glue	5.20	0.12	21.48	1.63	21.77	3.64
Test P19	Hilti glue	5.20	0.07	22.16	1.93	23.26	4.12
Test P20	no glue	7.56	0.29	21.61	1.72	17.90	5.08

8.3.5.4.1 Comparison of Push test Series 4: HIS adhesive bolt with different glue

The main variation in this series was the adhesive material. Two tests were performed with Ramset glue, one with Hilti glue and one without glue. The results are compared in Fig. 8-25. It can be seen in the figure that the shapes of all the load-slip curves are similar. This behaviour can be divided into three distinct parts: a linear variation from point O to B; a plastic plateau from point B to C; and failure from point C to D. A minor difference can be noticed in the load-slip behaviour in the plastic plateau region; the load gradually decreases from A to B when no glue is used, whereas the load gradually increases when some sort of glue is used. However, the maximum load and the length of plateau is almost identical. It needs to be mentioned here that the use of HIS adhesive bolts without glue is not practical as the glue is required to prevent the bolt pulling out. It was, therefore, decided to use the HIS adhesive bolt with Ramset glue as the shear connectors for the plated beams.

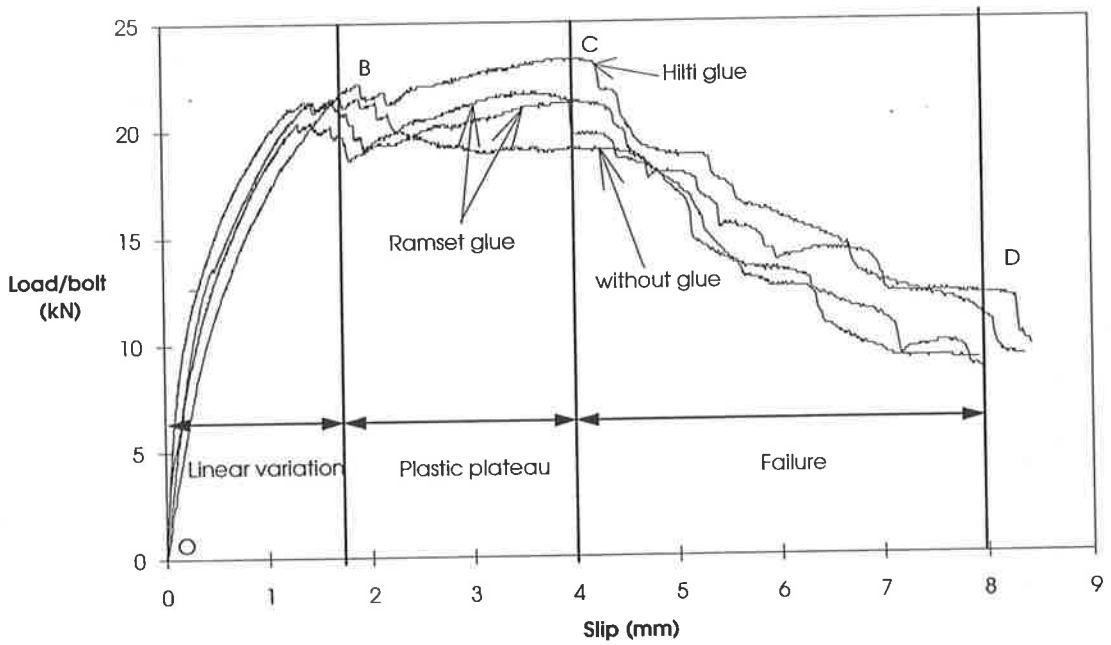

Fig. 8-25 Push test Series 4: HIS adhesive bolt with different glue

8.3.5.5 Series 5: HIS adhesive bolt with Ramset glue

Having finished the push tests of Series 1 to 4, the HIS adhesive bolt with Ramset glue was found to be suitable for the plated beams. Series 5 was designed to determine the load-slip characteristics of the bolts for the beams. Four push specimens of Type 2 were tested in this series. Push specimens P21 and P22 were poured with the beams in Series 1-3 except for beam B24. Push specimens P23 and P24 were poured with the beam B24. The properties of the concrete and the plate are given in Sect 8.2.1 and 8.2.3 respectively.

The average slip against the load/bolt for each of the tests are shown in Figs. 8-26 to 8-29 respectively. The variation of the slip at the four corners of the push specimens are given in Appendix-C. It can be seen in Figs. 8-26 to Fig. 8-29 that the load -slip behaviours are similar to the previous tests with the same bolt, as described in Sect. 8.3.5.4. The load and slip at the end of the linear variation at A and at points B and C are given in Table 8.15. The results are not compared for this series as the behaviour of the load-slip curve is now already established.

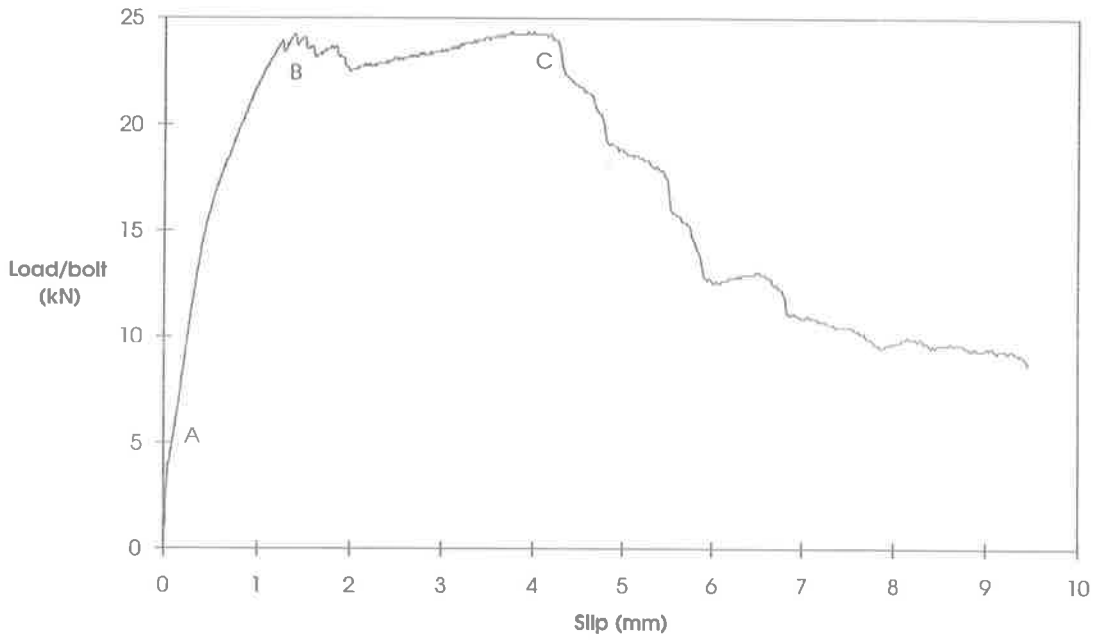

Fig. 8-26 Push test P21, HIS adhesive bolt with Ramset glue

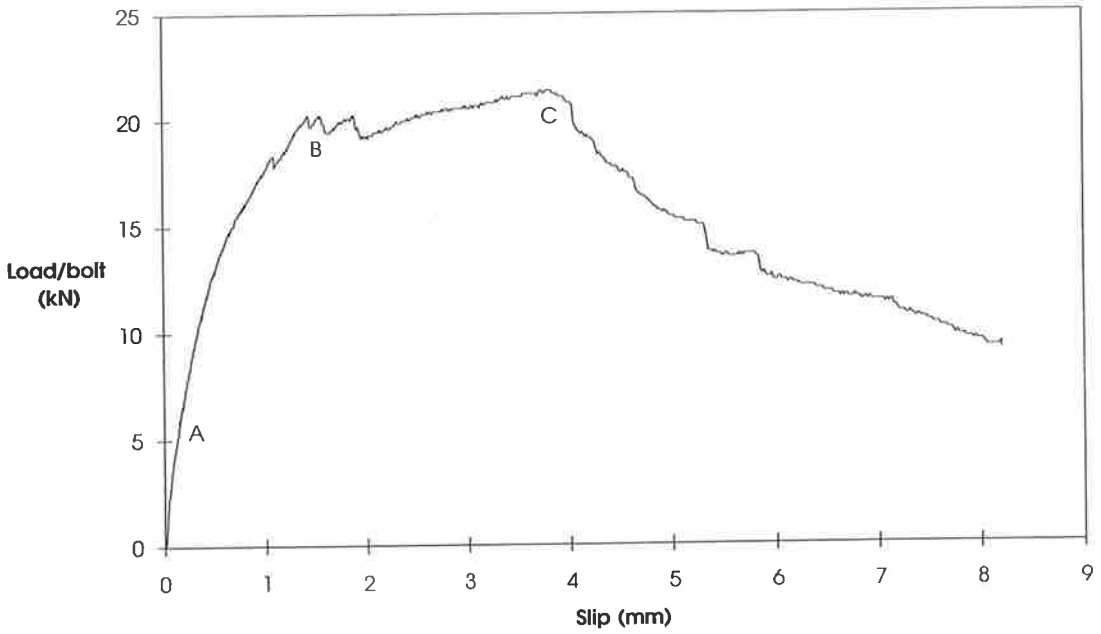

Fig. 8-27 Push test P22, HIS adhesive bolt with Ramset glue

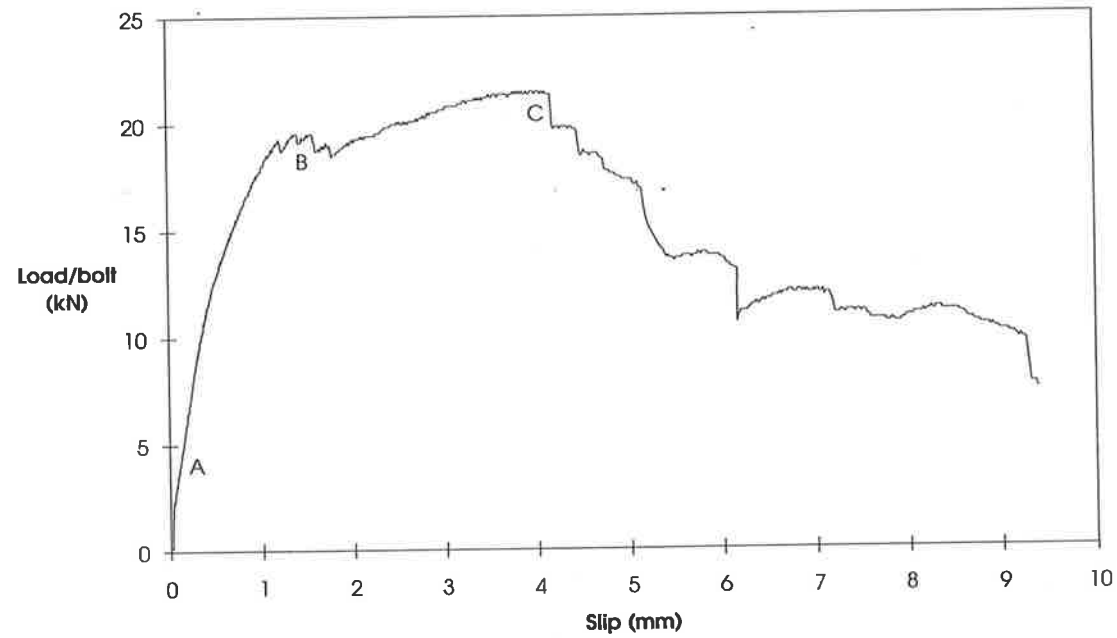

Fig. 8-28 Push test P23, HIS adhesive bolt with Ramset glue

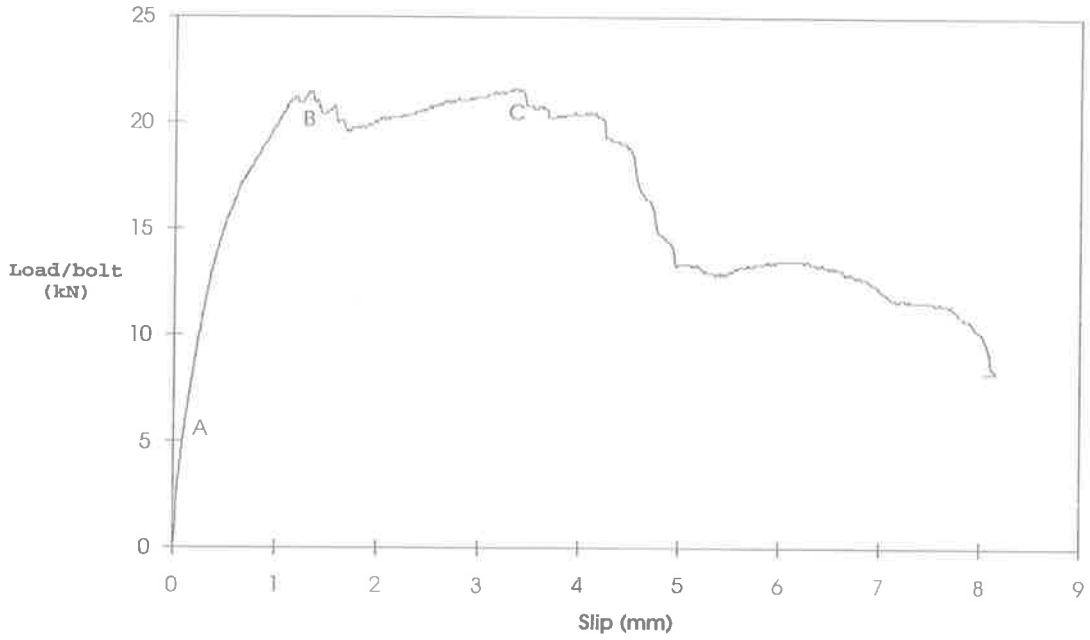

Fig. 8-29 Push test P24, HIS adhesive bolt with Ramset glue

Table 8.15 Push test Series 5: HIS adhesive bolt with Ramset glue

Test name	Pour number	Linear variation Point A		Start of plateau Point B		End of plateau Point C	
		Load (kN/bolt)	Slip (mm)	Load (kN/bolt)	Slip (mm)	Load (kN/bolt)	Slip (mm)
(1)	(3)	(4)	(5)	(6)	(7)	(8)	(9)
Test P21	4	5.20	0.10	24.23	1.38	24.23	4.19
Test P22	4	5.20	0.14	20.25	1.87	21.35	3.83
Test P23	5	4.40	0.12	19.55	1.36	21.5	4.10
Test P24	5	5.20	0.09	21.48	1.30	21.60	3.40

8.3.5.6 Summary of push test results and analysis

A total of five types of mechanical shear connectors were tested with further variations of length of bolt, clearance in the plate hole and types of glue. A comparison of the test results showed that the HIS adhesive bolt can produce greater stiffness and strength with a large plateau of slip at failure as compared to the other bolts. The behaviour of the load-slip curve of the HIS adhesive bolt can be divided into three distinct parts of constant stiffness, plastic plateau and the failure, as shown in Fig. 8-25.

In order to determine the load-slip characteristics of the bolts in the beams, the push specimens which were poured with the beams were tested in Series 4 and 5. All the results from the push specimen which were poured with the beam Series 1 to 3 (excluding beam B24) are shown in Fig. 8-30 and those were poured with beam B24 are shown in Fig. 8-31. The mean load and slip at different points for respective beams are given in Table 8.16

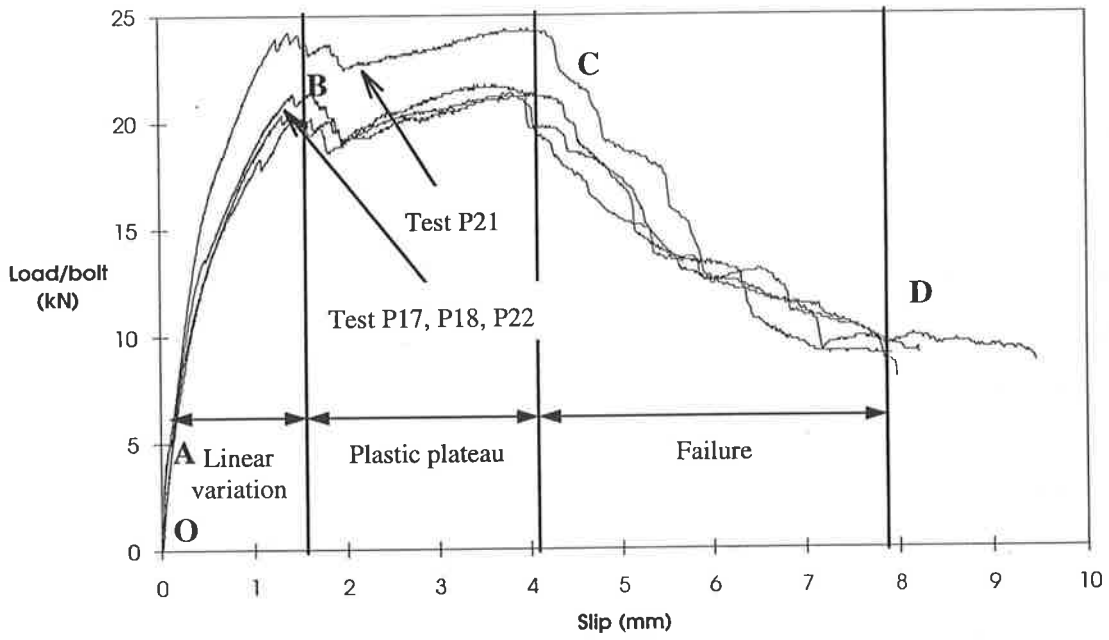

Fig. 8-30 Push tests for beam Series 1-3 (excluding Beam B24)

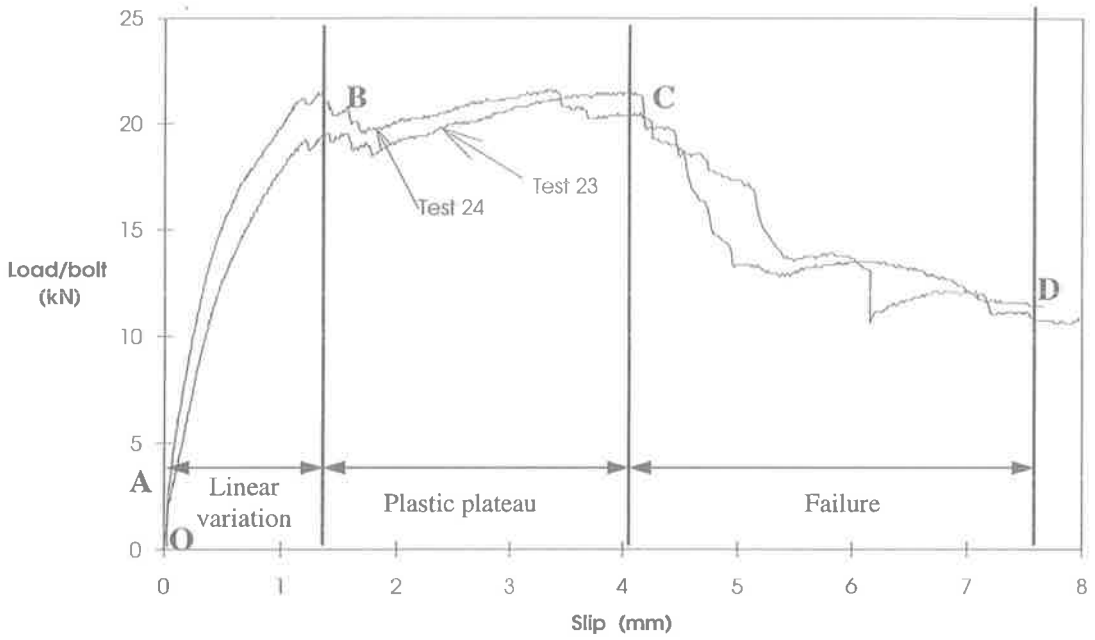

Fig. 8- 31 Push tests for Beam B24

Table 8.16 Mean result of push tests for beam specimen

Linear variation (Point A)		Beginning of plateau (Point B)		End of plateau (Point C)		Failure (Point D)	
Load (kN/bolt)	Slip (mm)	Load (kN/bolt)	Slip (mm)	Load (kN/bolt)	Slip (mm)	Load (kN/bolt)	Slip (mm)
(1)	(2)	(3)	(4)	(5)	(6)	(7)	(8)
Beam Series 1-3 (excluding beam B24): Push tests P17,P18,P21 & P22							
5.20	0.12	21.59	1.55	22.18	3.93	9.0	7.90
Beam B24: Push tests P23 and P24							
4.80	0.11	20.52	1.33	21.55	3.75	11.5	7.75

The bolted shear connector is similar to the stud shear connector. Hence, the bolted shear connectors which were tested were used in eqn. (2.25) to determine their theoretical

dowel strength. The results have been compared in Fig. 8-32, where $(D_{max})_{expt}$ is the dowel strength obtained by push test and $(D_{max})_{cal}$ is the dowel strength obtained from eqn. (2.25). This shows that all the theoretical dowel strengths are much larger than the experimental result. This suggests that the equation which was derived for the stud shear connector cannot be used for bolted shear connectors.

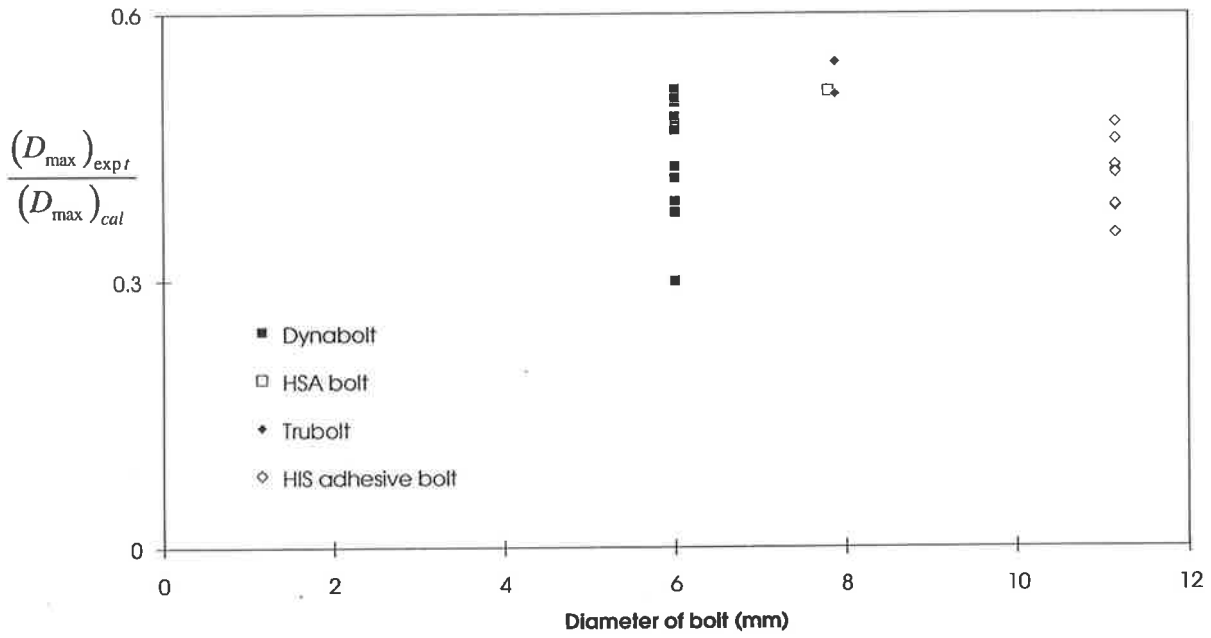

Fig. 8-32 Dowel strength of bolted shear connector

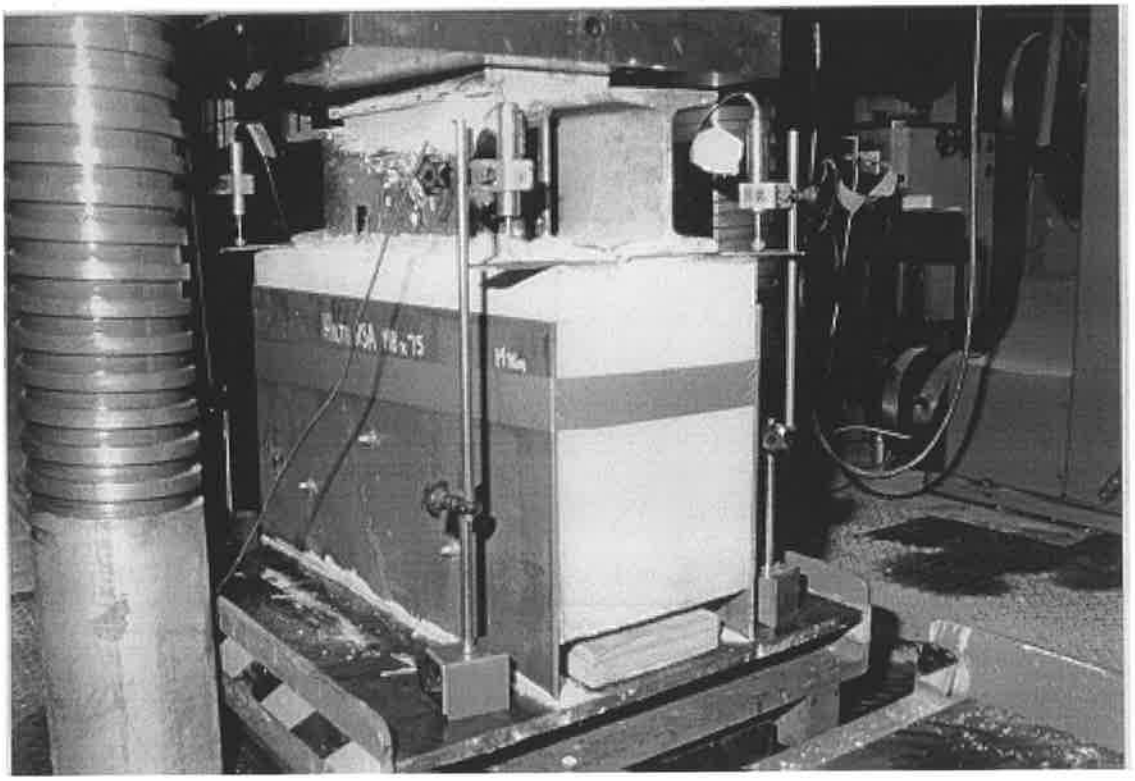

P8.1 Push test set up

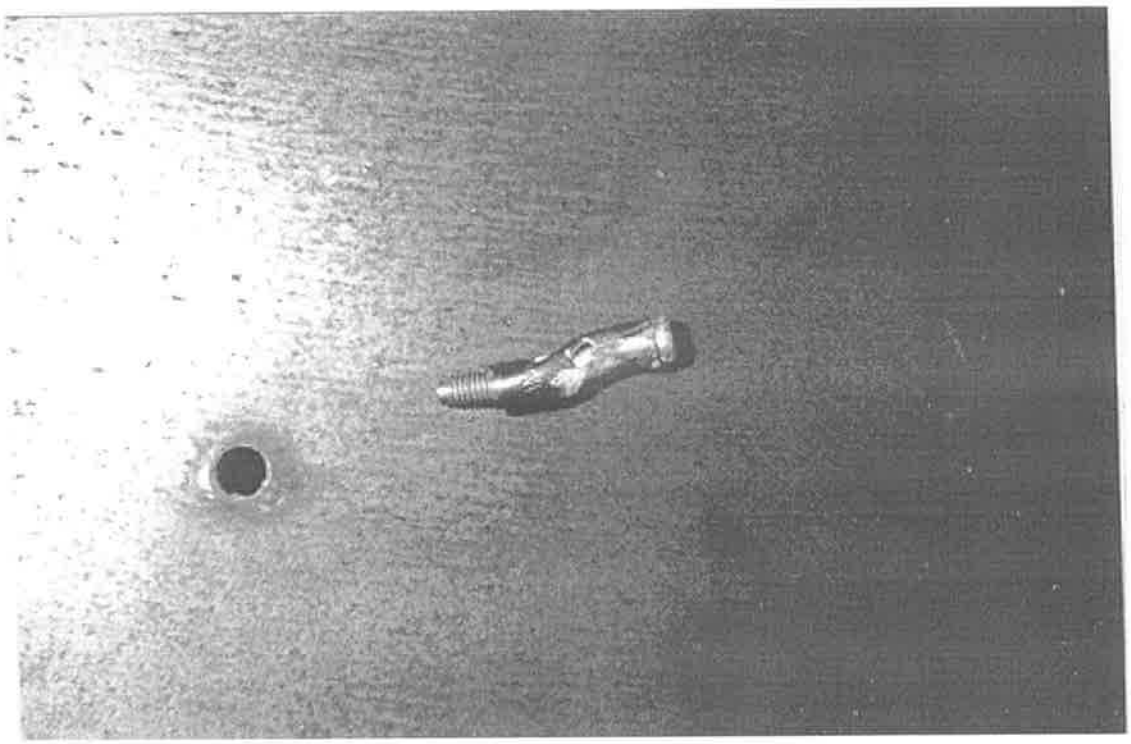

P8.2 Shape of Dynabolt after pull out

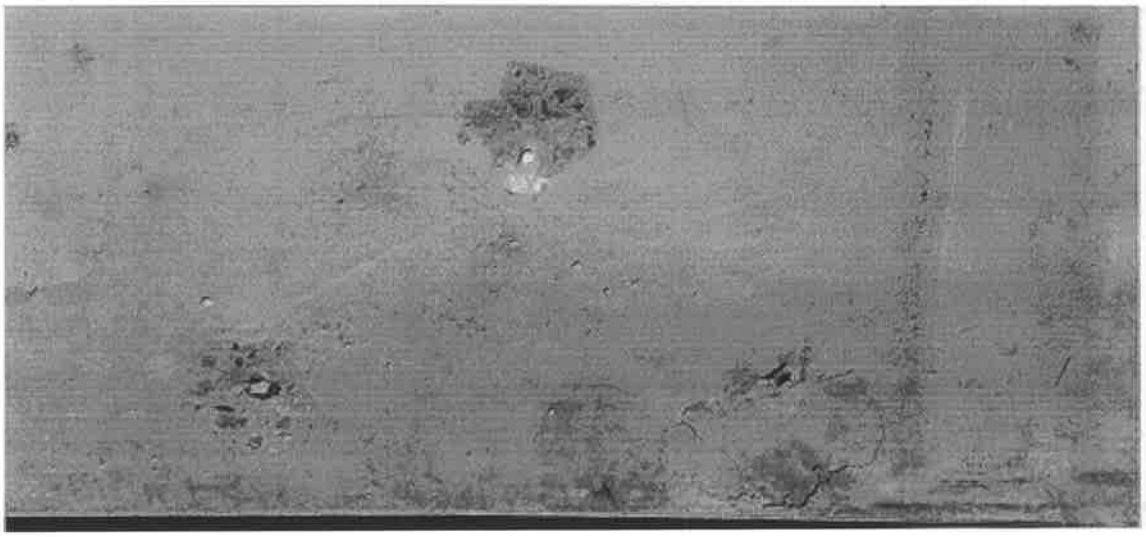

P8.3 Crushing of surrounding concrete of Dynabolt

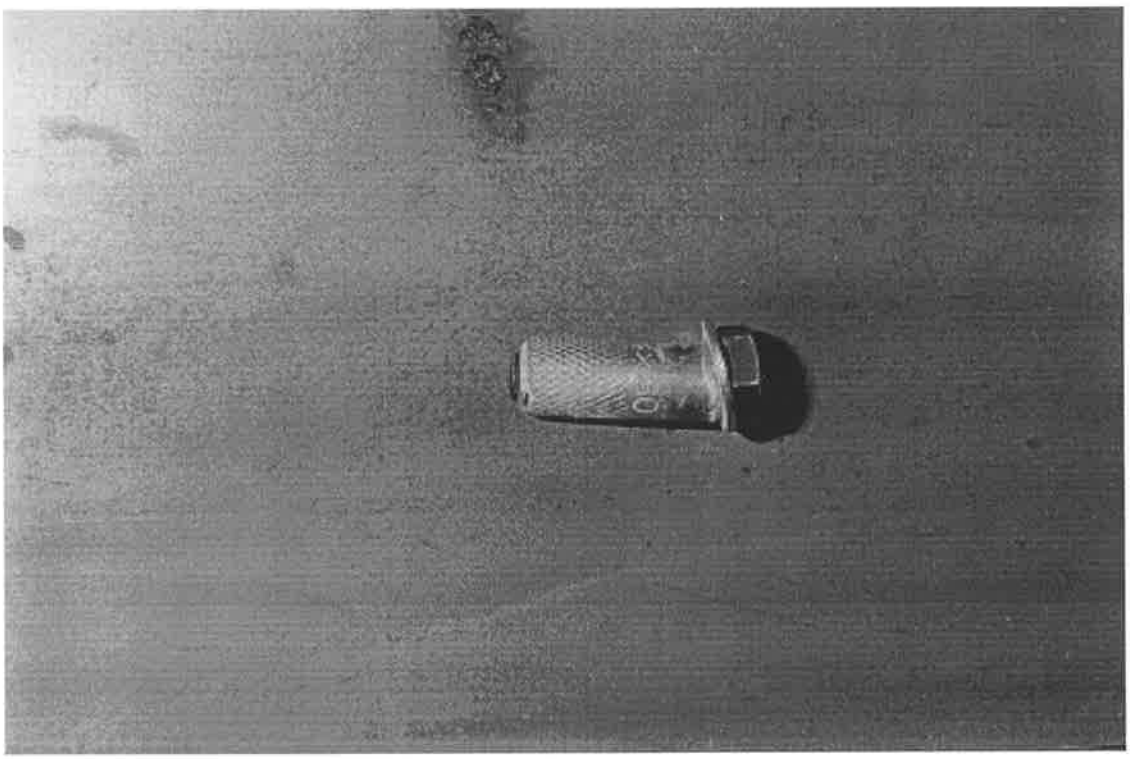

P8.4 Broken part of HIS adhesive bolt

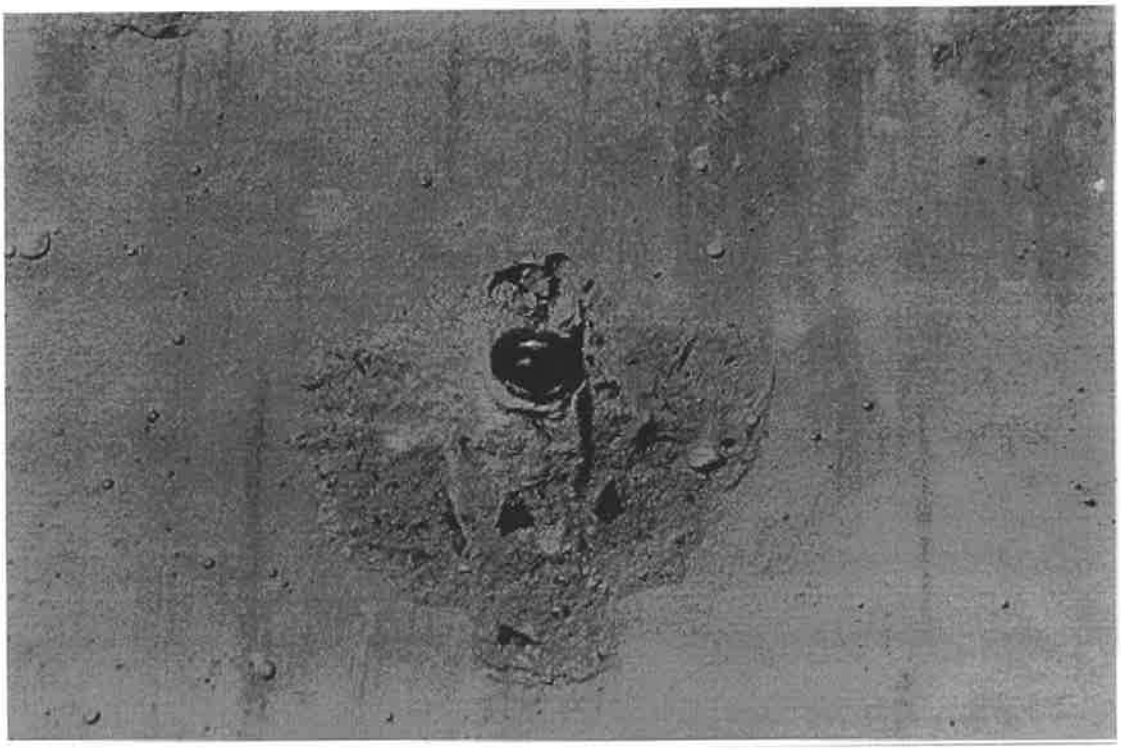

P8.5 Crushing of surrounding concrete of HIS adhesive bolt

8.4 SECTION 3: BEAM TESTS

The purpose of the plated beam tests was: to get an understanding of the problems that are encountered when reinforced concrete beams are strengthened for flexure; to validate the computer model in chapter 5; and to validate the mathematical models for both the longitudinal shear force and vertical shear force. Eight beams were tested where two was unplated and the other six were plated. The unplated beams were tested as reference beam to compare the flexural capacity and deflection with the plated beams. The parameters varied in the plated beam tests were the depths of the plate and the degree of shear connection. The HIS adhesive bolt with Ramset glue was used as the shear connector in the plated beams.

8.4.1 Design of Specimens

The beams were divided into three series. Series 1 consisted of two unplated RC beams A11 and A21, as shown in Fig. 8-33. Series 2 consisted of four plated beams, B11, B12, B13 and B24, that had shallow depths of plate as shown in Figs. 8-34 to 8-37. Series 3 consisted of two plated beams, C11 and C12, that had almost full depth plates, as shown in Figs. 8-39 and 8-40 respectively. Their design details are described in the following sections.

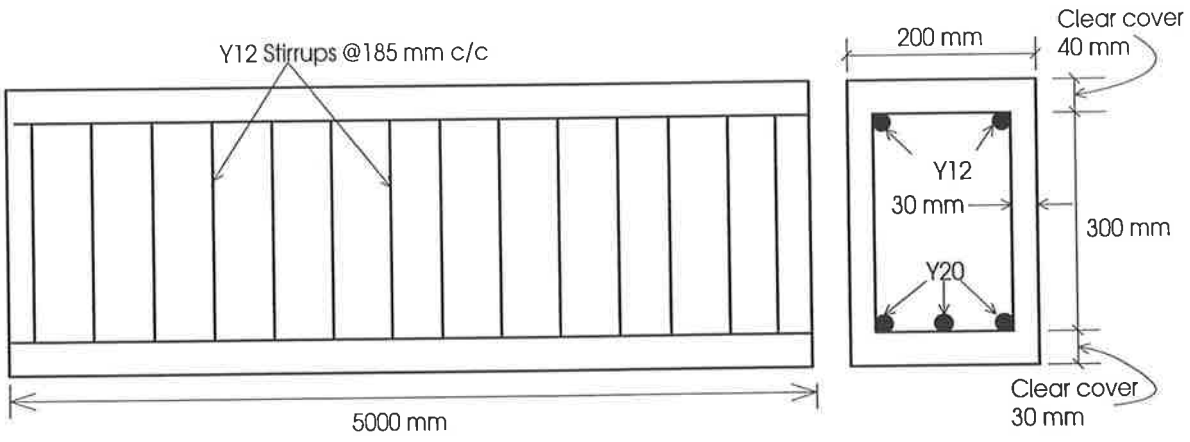

(a) Longitudinal section (b) Cross-section

Fig. 8-33 Series 1: Reinforced concrete beam (A11 and A21)

8.4.1.1 Series 1: Unplated beam

The dimensions and the reinforcement of the reinforced concrete (RC) beams A11 and A21 are shown in Fig. 8-33. The calculation of the theoretical flexural capacity of the beams is shown in Appendix-D, the results of which are given in Table 8.17.

8.4.1.2 Series 2: Shallow depth plated beam

This series consisted of four shallow depth plated beams B11, B12, B13 and B24. Their longitudinal sections are shown in Figs. 8-34 to 8-37 respectively and their cross-sections are shown in Fig. 8-38. The same RC beam in Series-1 (Fig. 8-33) was used in Series 2 to determine the effect of bonding plates. The size of the plate at both sides of the beam was 6 mm x 145 mm x 5000 mm.

The cross-section in Fig. 8-38 was analysed assuming full interaction in order to determine the full-shear-connection bond force. The number of shear connectors was then calculated for different degrees of shear connection. The strength of the shear connectors was determined from the push tests in Sect. 8.3. The numbers of bolts and the degrees of shear connection for each beam are listed in Table 8.17 and the detailed calculations are given in Appendix-D. It can be seen in Table 8.17 that the beams B12 and B13 had equal numbers of connectors, but their degree of shear connection are not the same. This happened as the beam B12 had two rows of connectors and beam B13 had one row of connectors, as shown in Fig. 8-38, and for this reason they had different full-shear-connection full-interaction bond force, which is used in the calculation of the degree of shear connection. The purpose of this arrangement was to investigate the difference in behaviour of the plated beams due to a different number of rows of connectors.

It can be seen in Fig. 8-38 that the bolts were placed in two rows in beams B11, B12 and B24 and in one row in beam B13. The position of the rows were chosen according to Sect. 2.4.1.4 in order to ensure that splitting in the concrete would not occur before the dowel strength was reached.

The longitudinal spacing of the bolts was chosen to ensure that their dowel strength would not be affected by the presence of the stirrups in the RC section. These spacings

were kept the same at each side of a shear span of the beam. The longitudinal spacing of the bolts are given in Figs. 8-34 to 8-37 respectively.

The rigid plastic flexural capacity of the beams were calculated by full-shear-connection and partial-shear-connection analysis, as shown in Appendix-D. The calculated flexural capacities are shown in Table 8.17.

Table 8.17 Degree of shear connection of the beams

Beam Series	Beam no	Plate dimension (mm x mm x mm)	Degree of shear connection	Nos of bolts in a shear span per side	Nos of rows of connectors	Longitudinal force in plate (kN)	Rigid plastic flexural capacity (kNm)
(1)	(2)	(3)	(4)	(5)	(6)	(7)	(8)
Series 1	A11	-	-	-	-	-	131.90
	A21	-	-	-	-	-	128.30
Series 2	B11	6 x 145 x 5000	1.75	22	2	542.88	233.50
	B12	6 x 145 x 5000	0.48	6	2	259.08	200.80
	B13	6 x 145 x 5000	0.43	6	1	259.08	202.00
	B24	6 x 145 x 5000	0.91	12	2	492.48	226.00
Series 3	C11	6 x 290 x 5000	0.70	10	2	431.80	260.90
	C12	6 x 290 x 5000	0.42	6	2	259.08	249.24

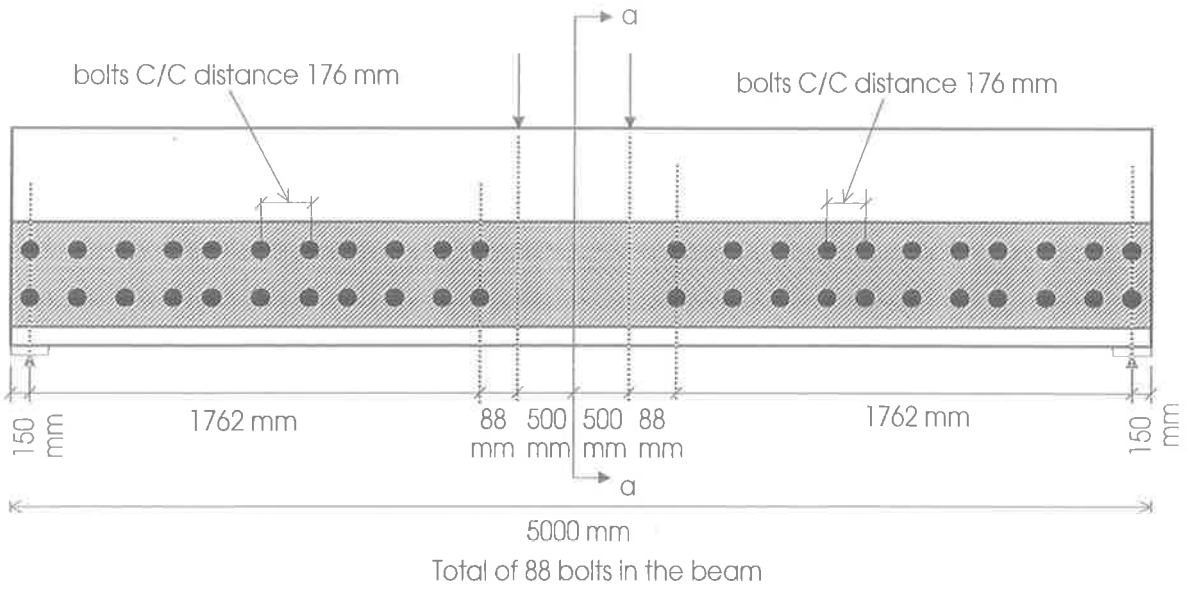

Fig. 8-34 Beam B11

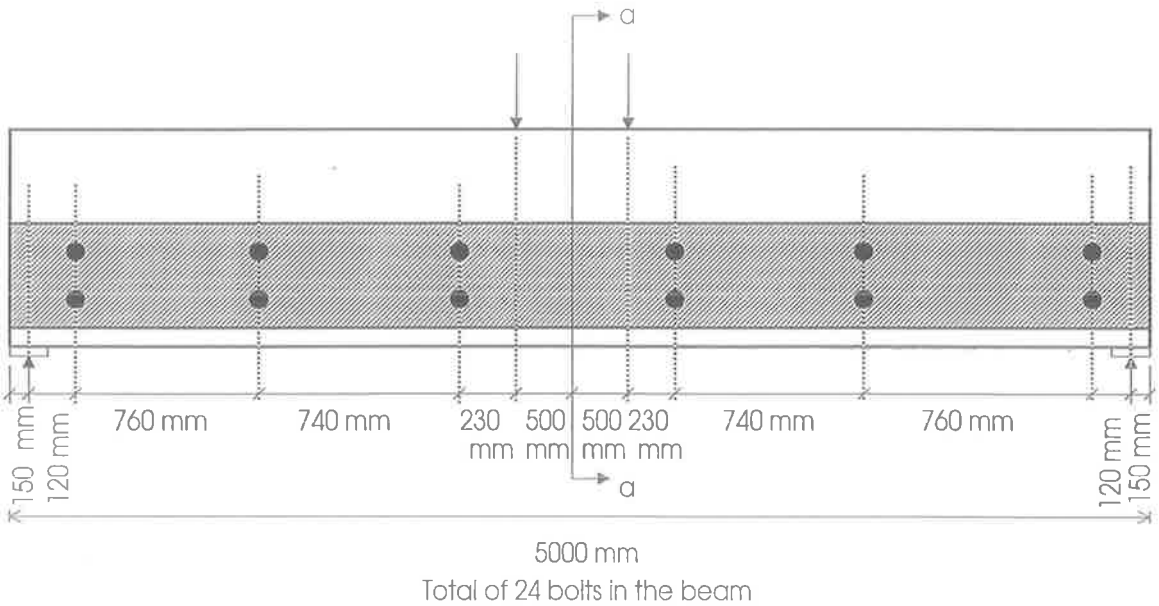

Fig. 8-35 Beam B12

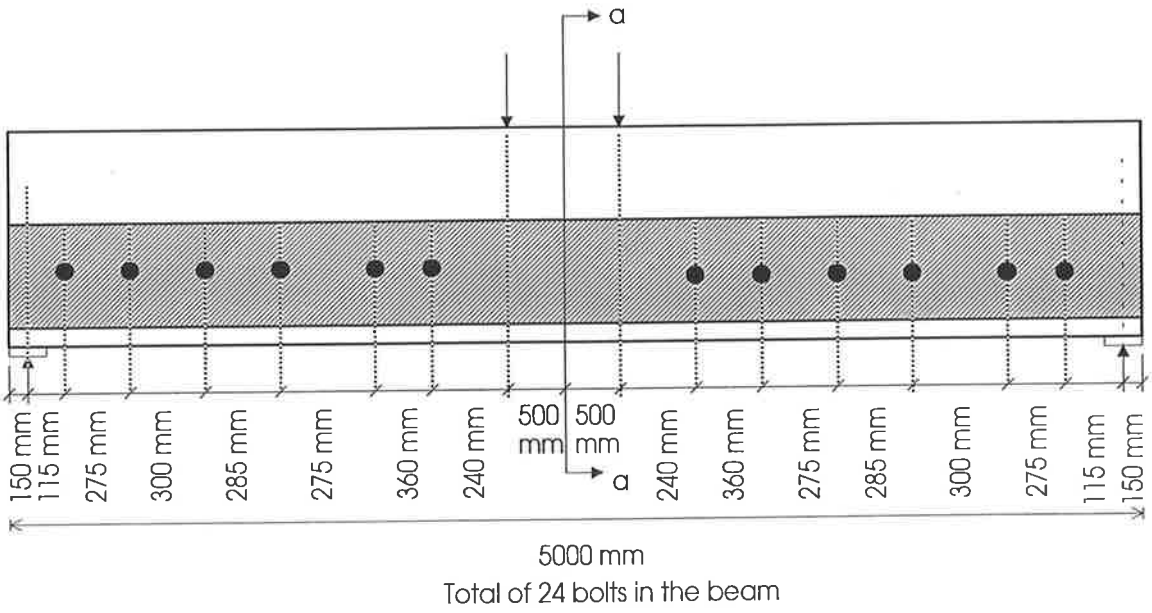

Fig. 8-36 Beam B13

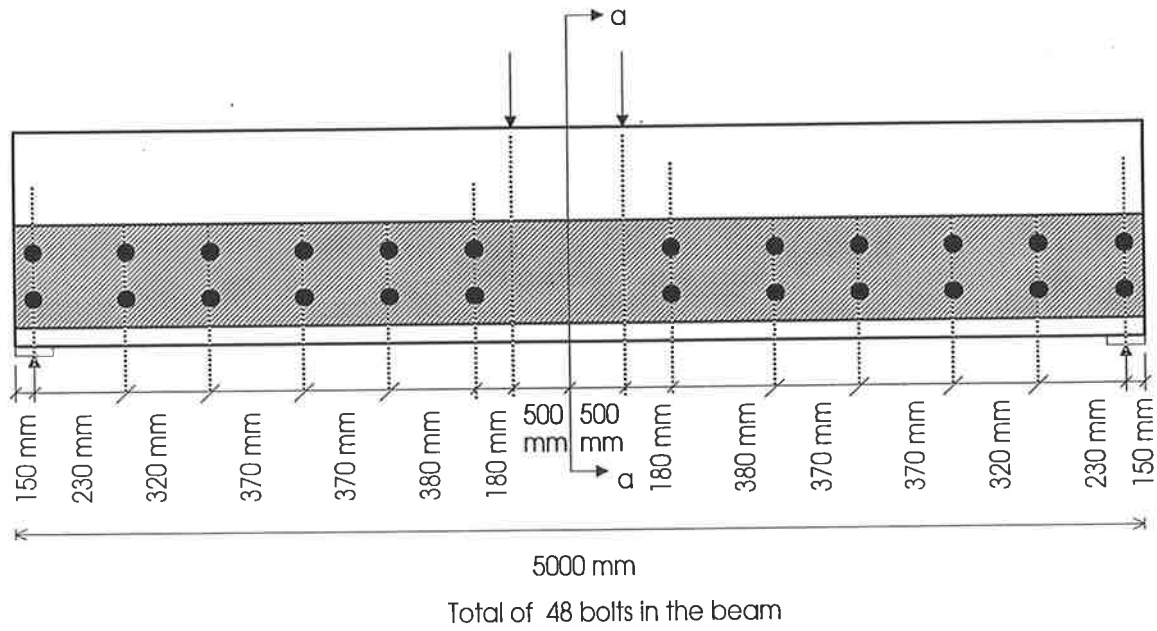

Fig. 8-37 Beam B24

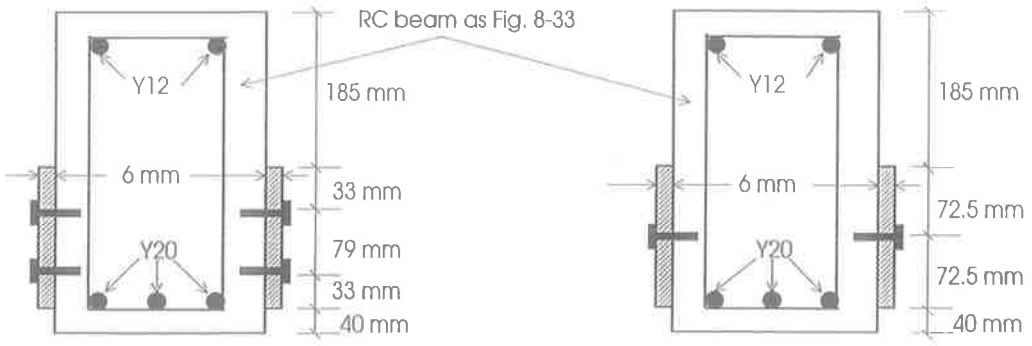

(a) Beam B11, B12 and B24 (b) Beam B13

Fig. 8-38 Cross-section of shallow plated beam

8.4.1.3 Series 3: Full depth plated beam

Series 3 consisted of two plated beams C11 and C12 that had almost full depth plates. Their longitudinal sections are shown in Figs. 8-39 and 8-40 respectively and their cross-section in Fig. 8-41. The same RC beam in Series-1 (Fig. 8-33) was uesd in Series 3, and the size of the plate at both sides of the beam was 6 x 290 x 5000 mm. The position of the bolts is shown in Figs. 8-39 to 8-41. The longitudinal positions were kept the same in each shear span. The calculations of the number of bolts for different degrees of shear connection and the rigid plastic flexural capacities are shown in Appendix-D, a summary of these being given in Table 8.17.

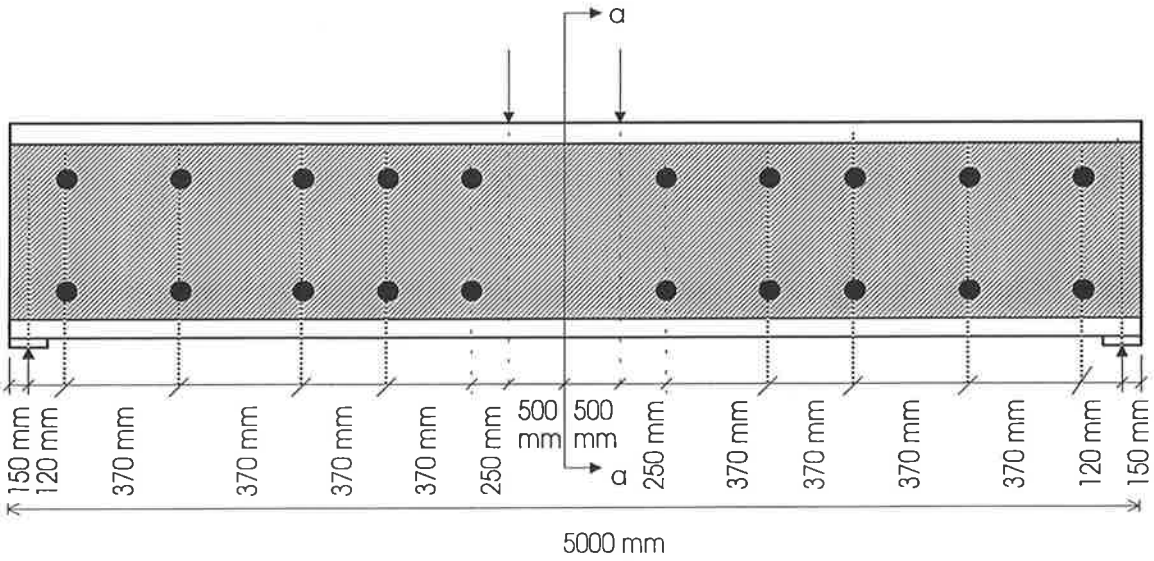

Fig. 8-39 Beam C11

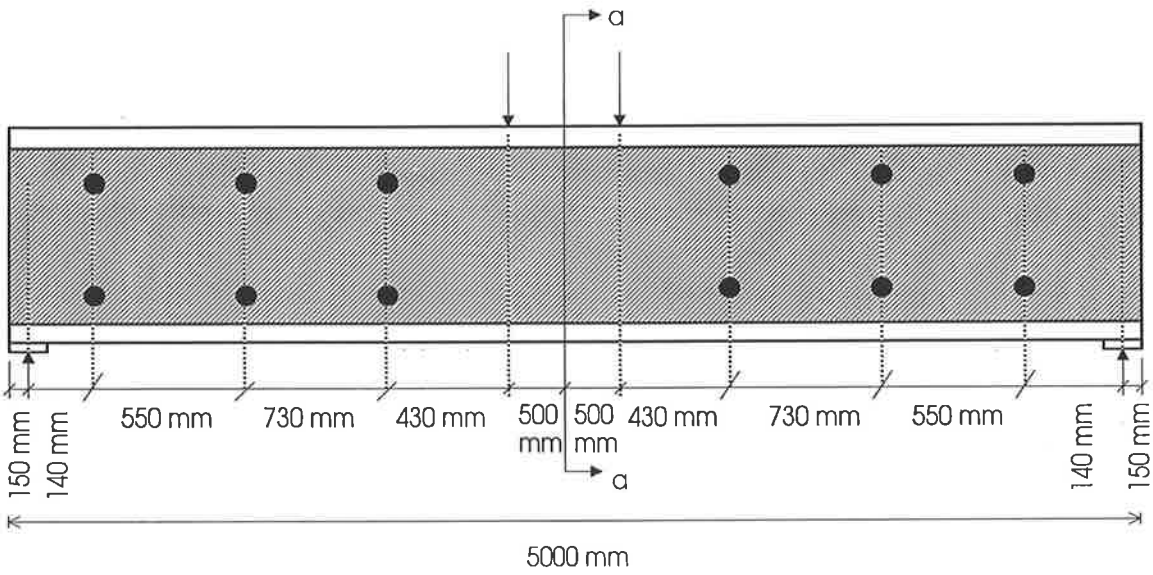

Fig. 8-40 Beam C12

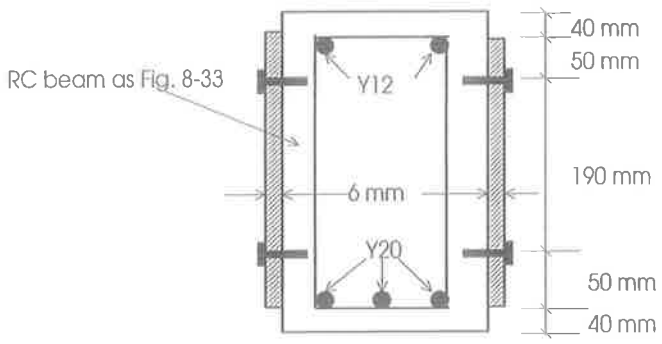

Fig. 8-41 Cross-section of beam C11 and C12

8.4.2 Aims of beam tests

8.4.2.1 Series 1: Unplated beams

Two unplated RC beam A11 and A21 were tested to determine the experimental flexural capacity and ductility of the beam in order to compare the results with the plated beams in Series 2 and 3.

8.4.2.2 Series 2: Shallow depth plated beam

The aim of this series was to investigate the flexural capacity and ductility and to study the longitudinal and vertical slip in the shallow depth plated beams. Four plated beams, B11, B12, B13 and B24, were designed where the variation was the degree of shear connection. Furthermore, all the beams had two rows of connectors except for beam B13 which had one row of connectors for the reasons given in Sect. 8.4.1.2.

8.4.2.3 Series 3: Full depth plated beam

The aim of this series was to investigate the flexural capacity and the ductility and to study the longitudinal and vertical slip in beams with almost full depth plates. Two beams C11 and C12 were designed with different degrees of shear connection.

8.4.3 Preparation of the plated beams

The preparation of the plated beam specimens was much straight forward and simple. The plate was clamped to the RC beam and then the holes were drilled, as shown in P8.6 for the bolts. The hole in the concrete beam was cleaned by spraying air into the hole, as shown in P8.7. Glue was inserted into the hole by using a pumping machine, as in P8.8. The bolt was then pressed into the hole by hand pressure, as in P8.9. Any surplus glue was ground off after hardening, as shown in P8.10. At this stage, the beam was kept for 48 hours to allow hardening of the glue, as shown in P8.11, after which the set screws was inserted and tightened as in P8.12.

8.4.4 Instrumentation

The instrumentation for the unplated beam and for the plated beams was not the same. In the unplated beam, only the deflection of the beam and the strains in the concrete were measured. In the plated beam, the deflection, strains in concrete and in the plate and longitudinal and vertical slips were measured. The position of the instrumentation is described in the following sections.

8.4.4.1 Beam A11 and A21

The instrumentation is shown in Fig. 8-42. The arrow signs with label P are the position of the applied load and that with label L is the position of the LVDT to measure deflections. Demec gauges, as shown by the squares were installed at the mid-span on both sides of the RC beam to measure the strain.

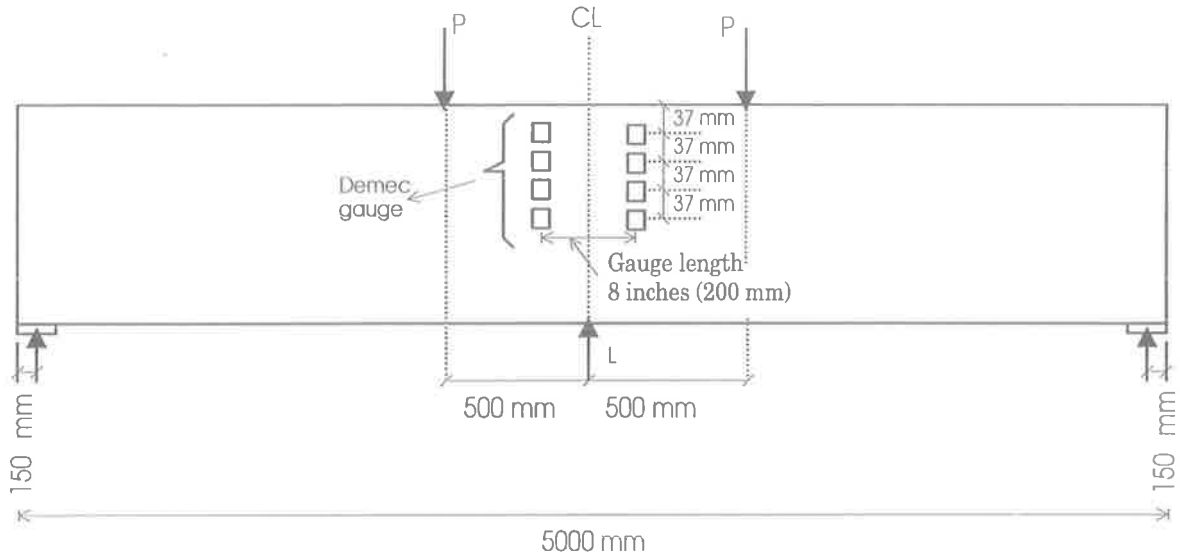

Fig. 8-42 Instrumentation in beam A11 and A21

8.4.4.2 Beam B11

Figures 8-43(a) and (b) show the instrumentation of the beam in the north and south sides respectively. The numbers which are circled at the top of the plates are the reference numbers of the LVDTs used to measure vertical slip. The circles with cross hairs represent the LVDTs used to measure the longitudinal slip. The rectangles in Fig. 8-43(a) are the electrical strain gauges used to measure the longitudinal strain in the plate near the mid-shear span. The strain at the mid-span in the concrete and in the plate were measured by using demec gauges, as shown in (c) at the both sides of the beam.

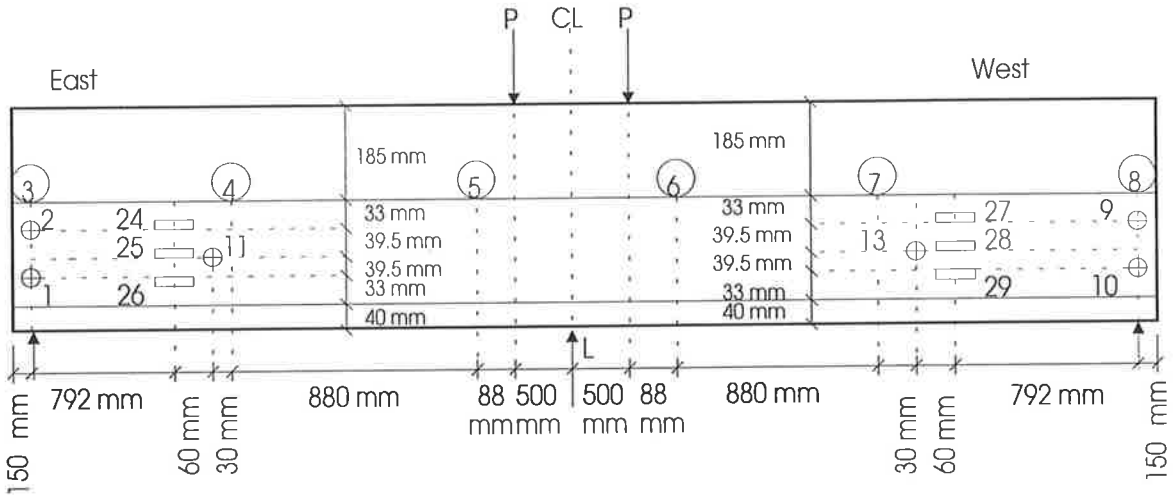

(a) North side

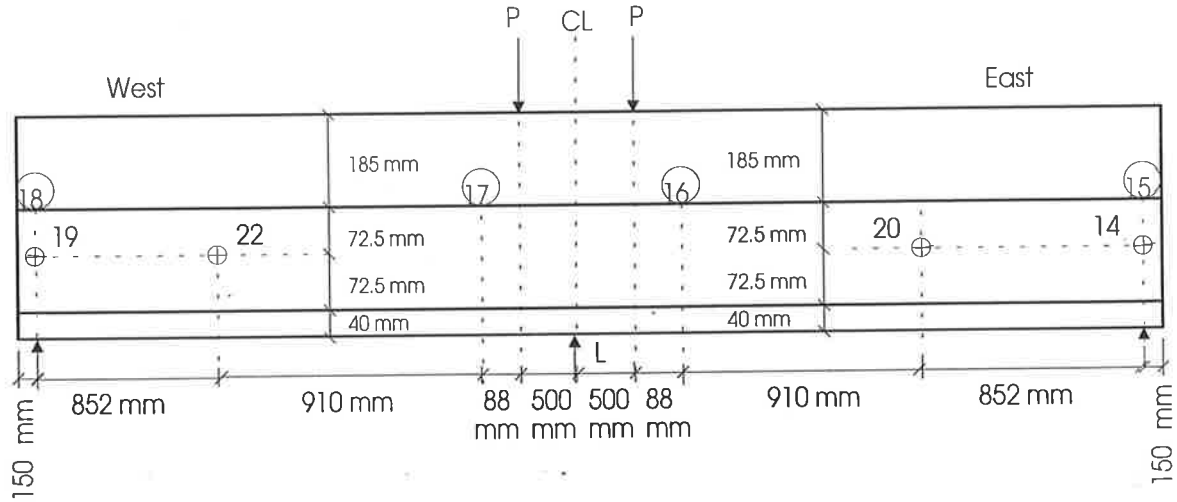

(b) South side

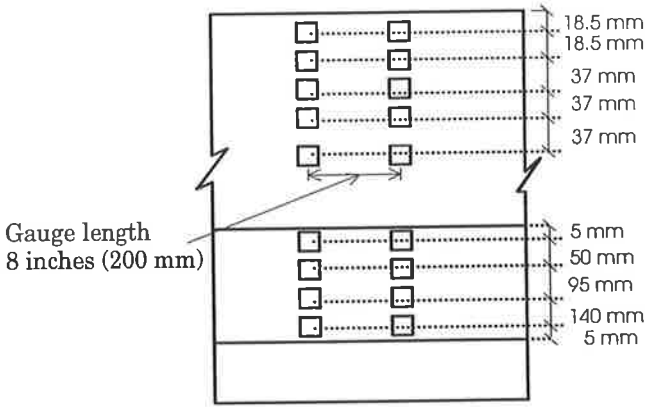

(c) Mid-span

Fig. 8-43 Instrumentation of beam B11

8.4.4.3 Beam B12

The instrumentation of beam B12 at the north and south sides are shown in Figs. 8-44(a) and (b) respectively. The strains in the concrete and in the plate at mid-span were measured using demec gauges and electrical strain gauges respectively, as shown in (c).

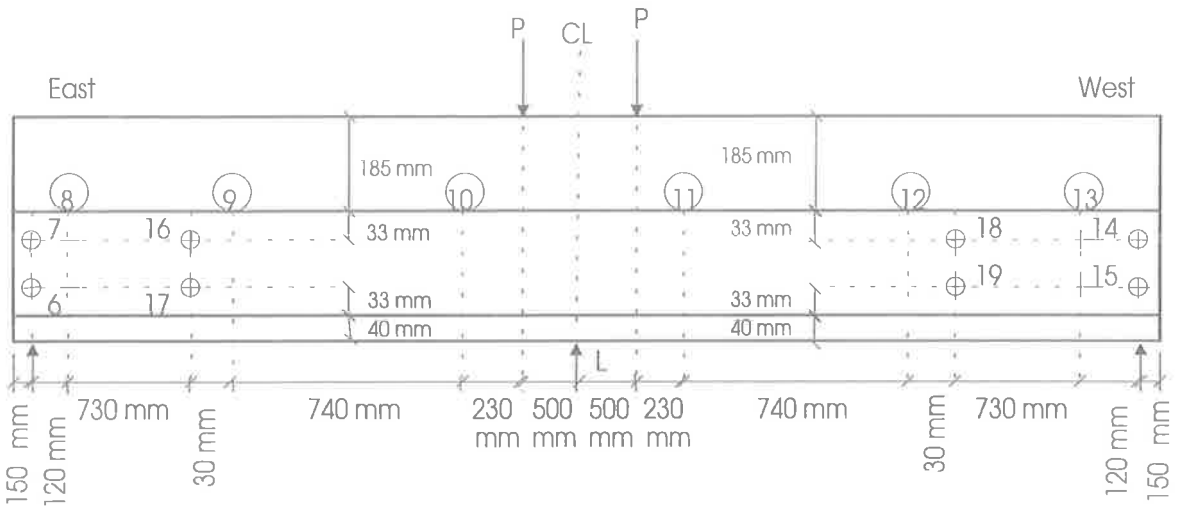

(a) North side

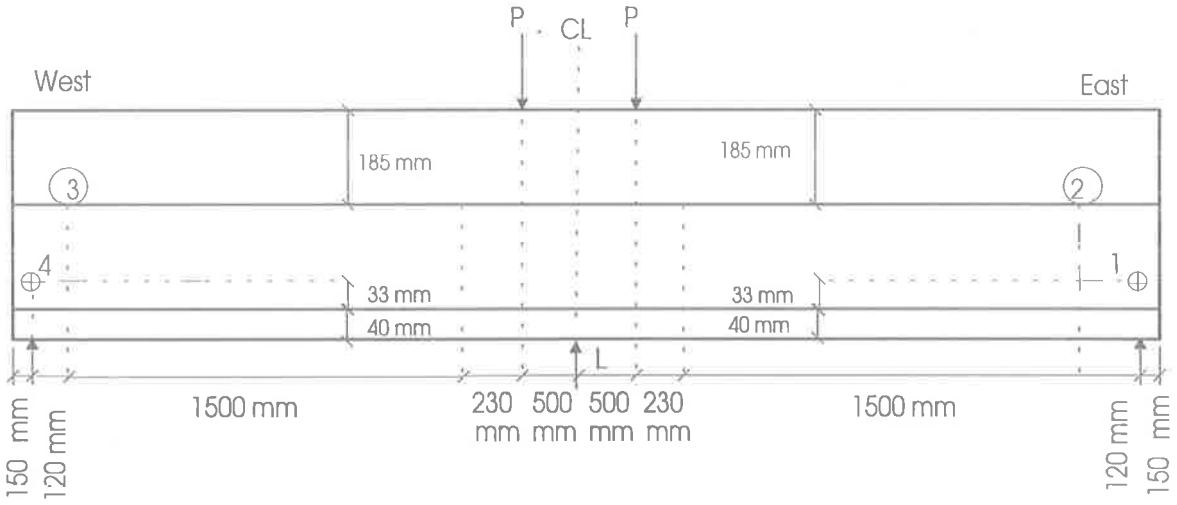

(b) South side

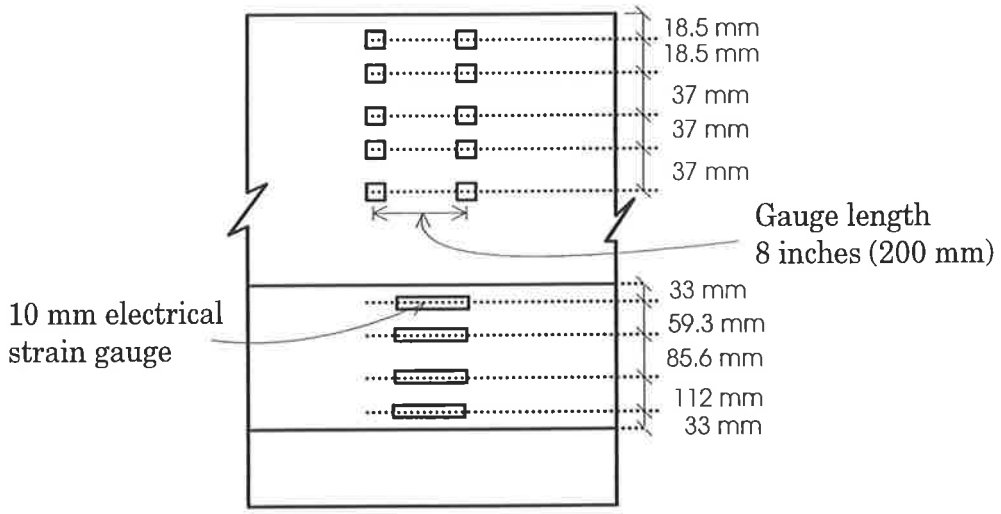

(c) mid-span

Fig. 8-44 Instrumentation in Beam B12

8.4.4.4 Beam B13

The instrumentation for beam B13 is shown in Fig. 8-45.

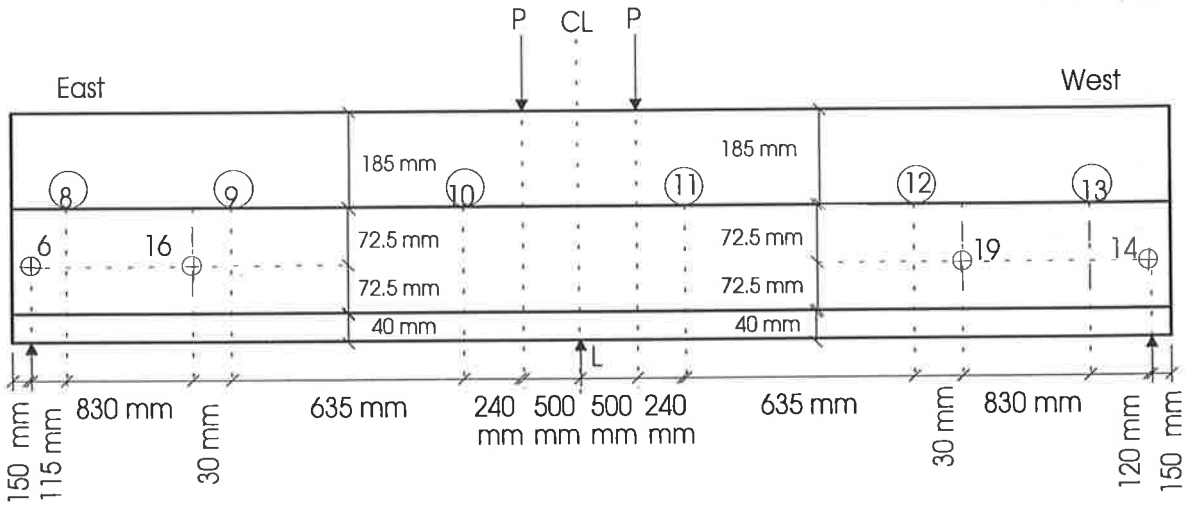

(a) North side

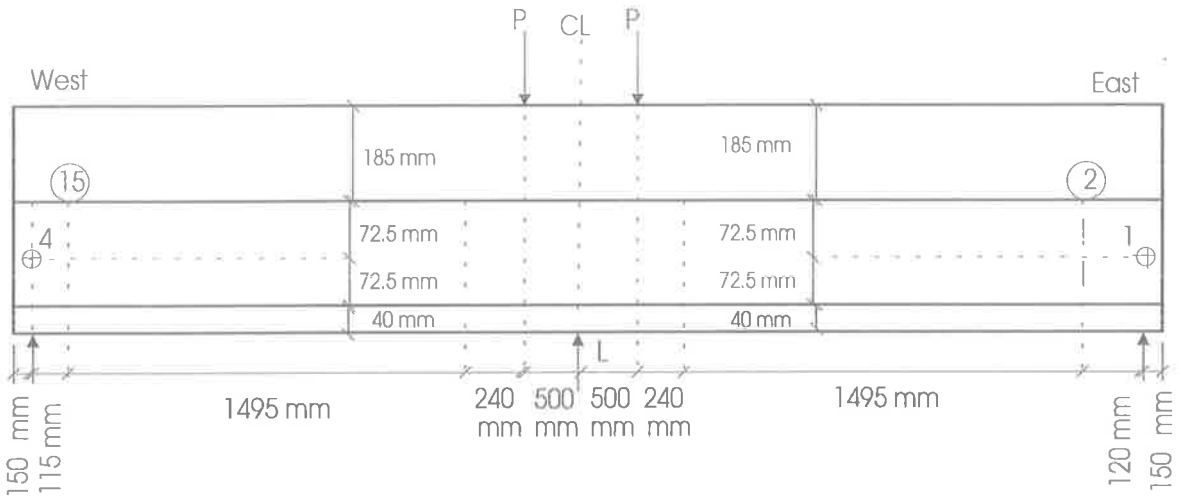

(b) South side

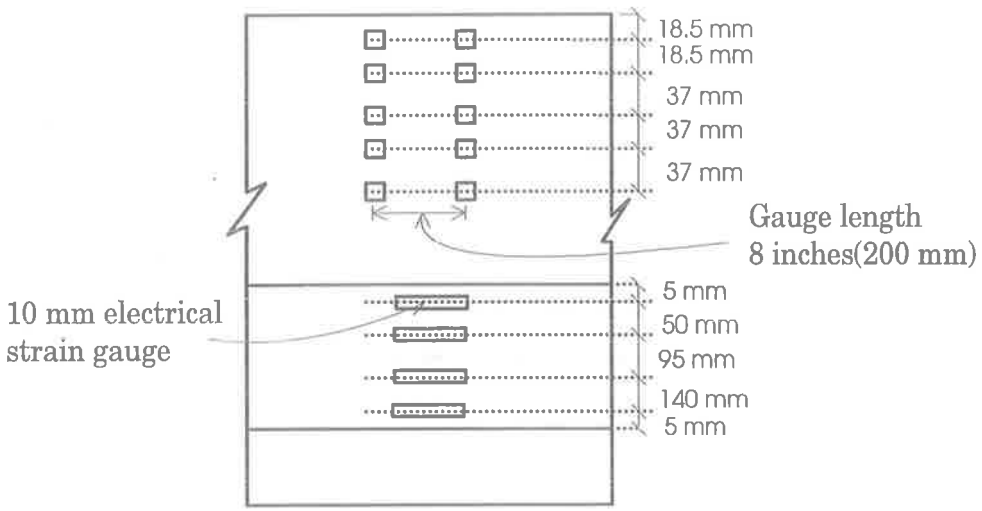

(c) mid-span

Fig. 8-45 Instrumentation in Beam B13

8.4.4.5 Beam B24

The instrumentation for beam B24 is shown in Fig. 8-46.

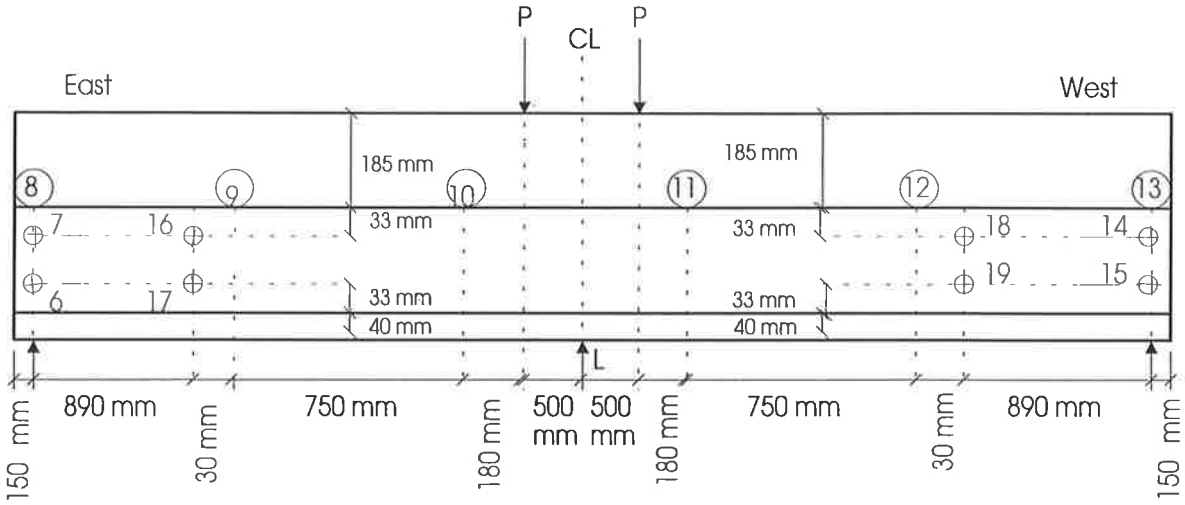

(a) North side

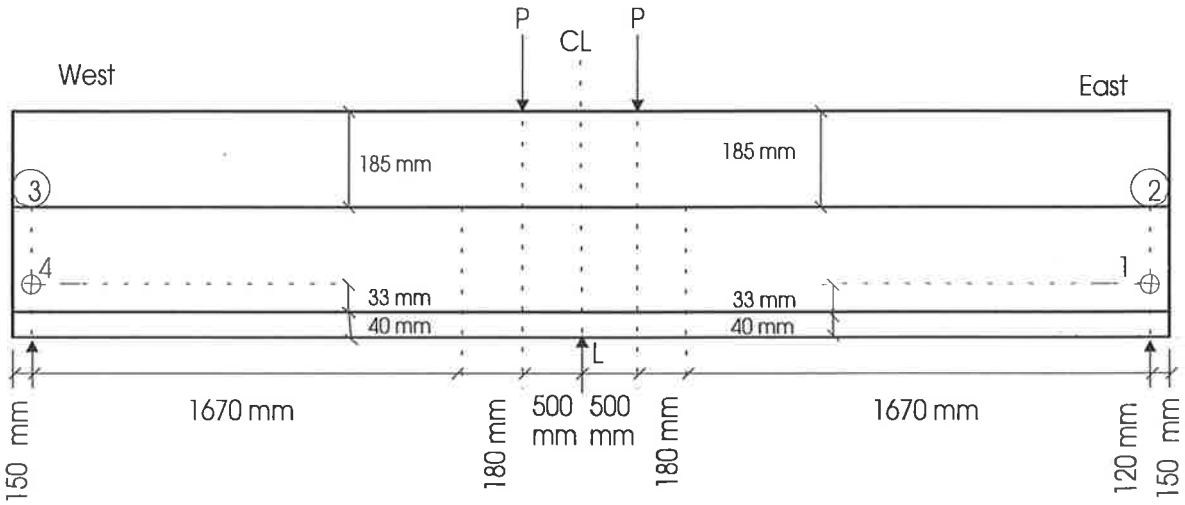

(b) South side

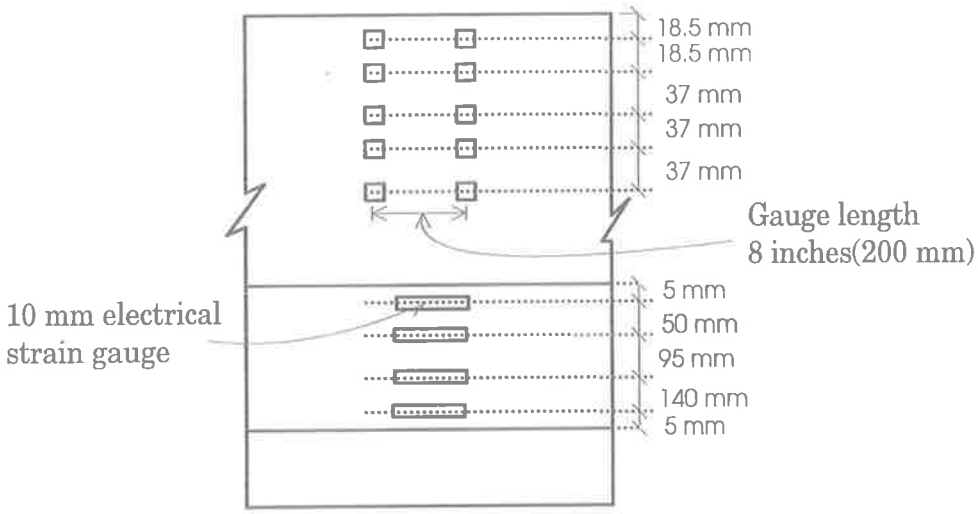

(c) mid-span

Fig. 8-46 Instrumentation of Beam B24

8.4.4.6 Beam C11

The instrumentation of the beam C11 is shown in Fig. 8-47.

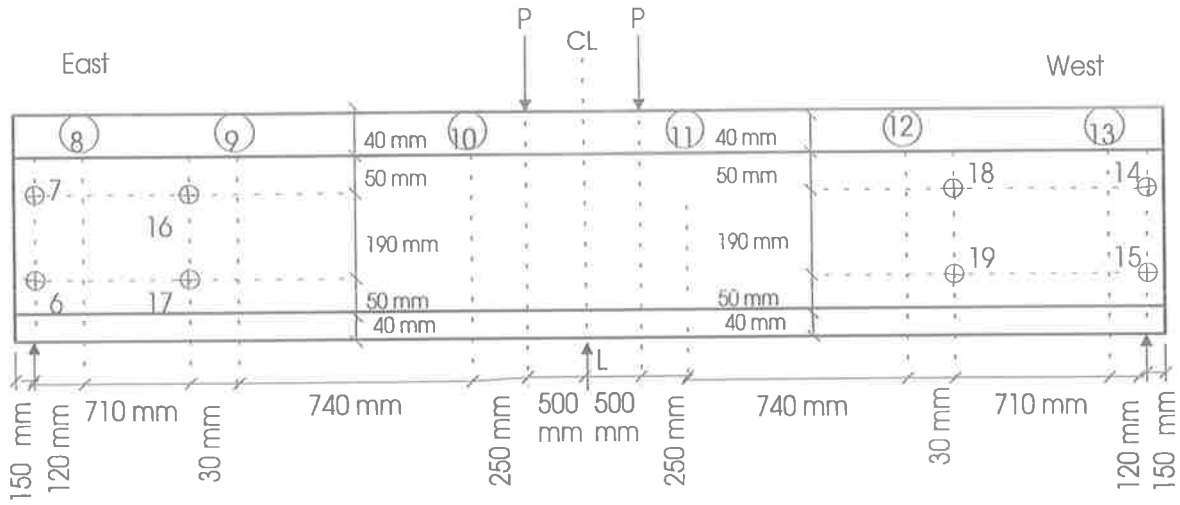

(a) North side

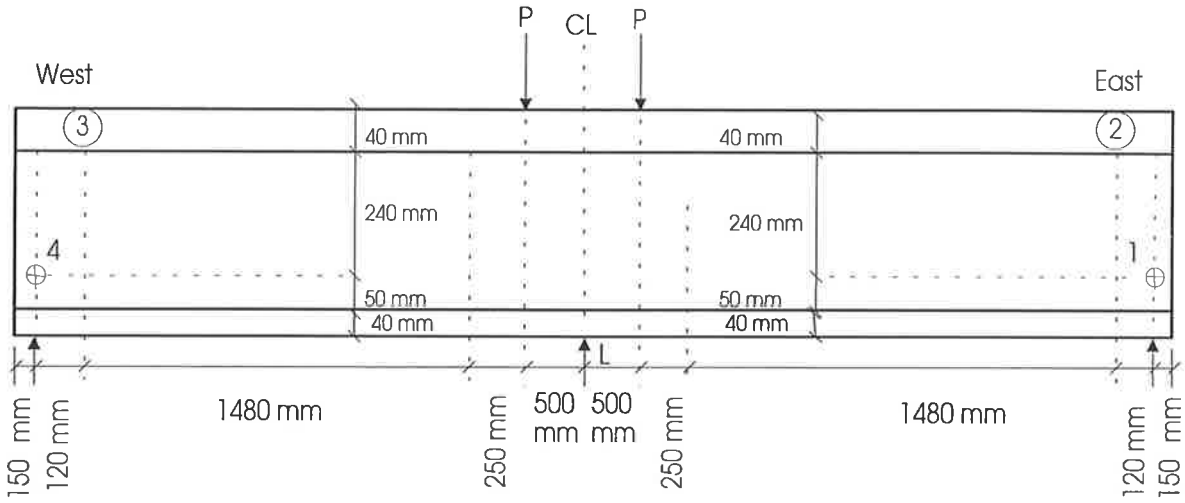

(b) South side

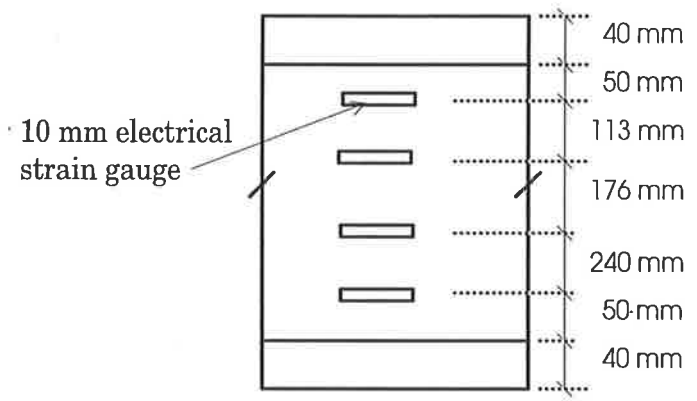

(c) mid-span

Fig. 8-47 Instrumentation of Beam C11

8.4.4.7 Beam C12

The instrumentation of beam C12 is shown in Fig. 8-48.

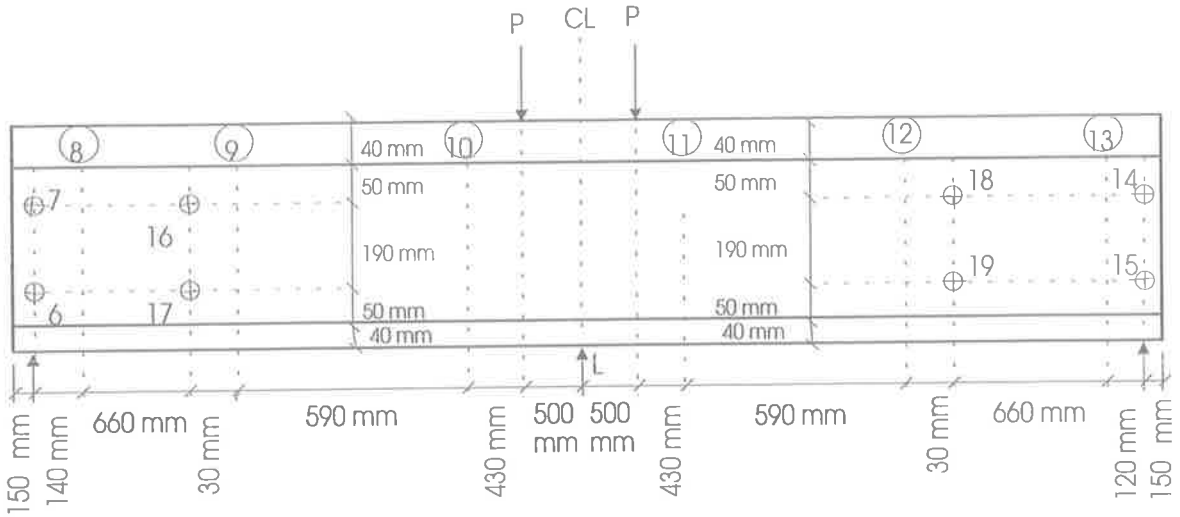

(a) North side

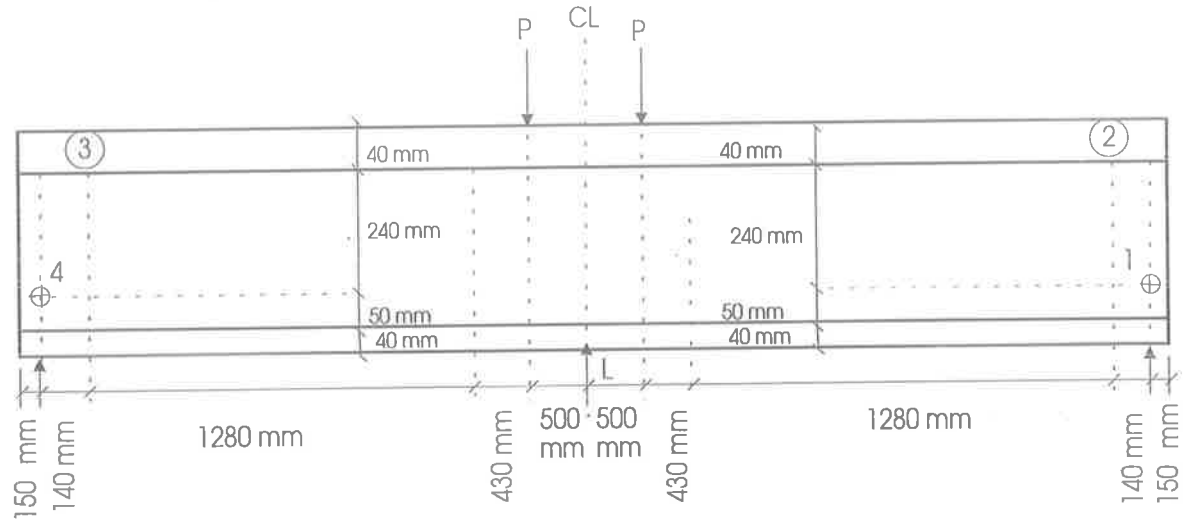

(c) South side

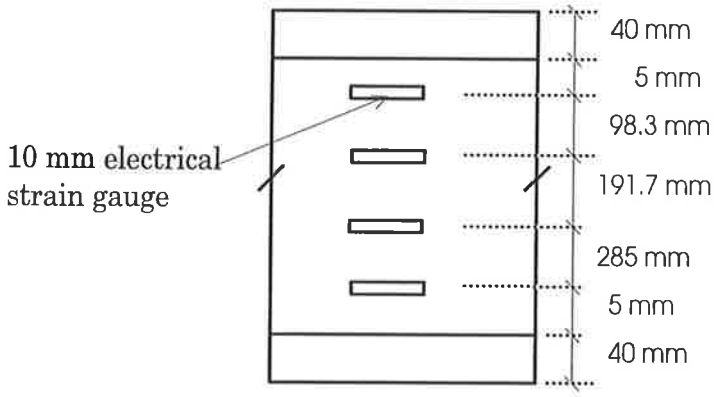

(c) mid-span

Fig. 8-48 Instrumentation of Beam C12

8.4.5 Test rig

The test rig was same for all of the beam tests and is shown in Fig. 8-49. All the beams were tested as simply supported beams with four point loads.

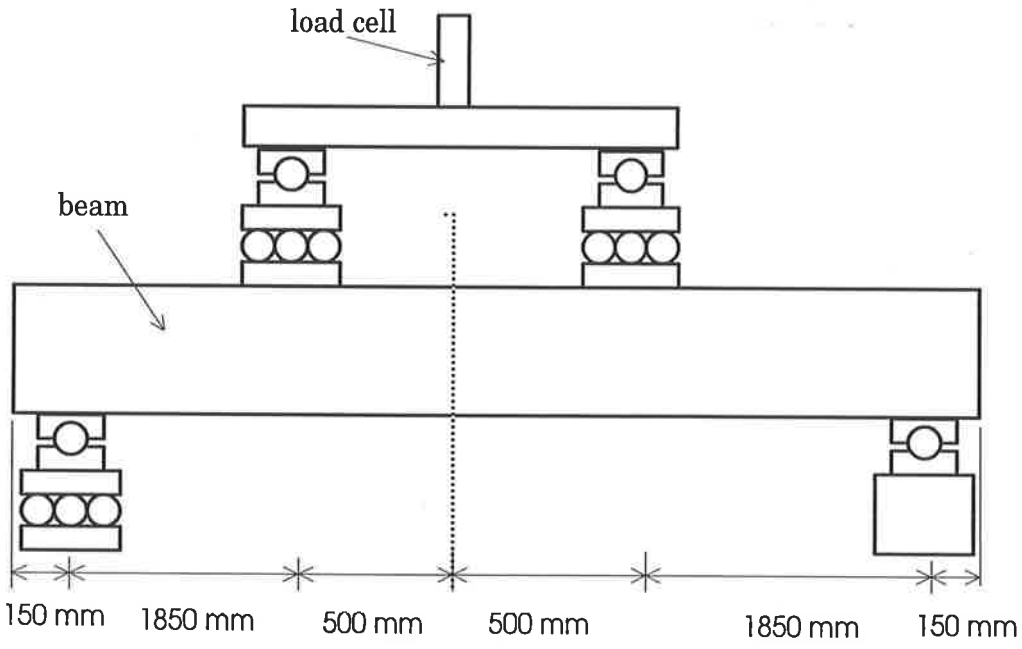

Fig. 8-49 Test rig

8.4.6 Description of test results

8.4.6.1 Series 1: Test 1: Unplated beam A11 and A21

This series consisted of two reinforced concrete beams without plates on their sides. The dimensions and reinforcement are shown in Fig. 8-33 and the properties of the concrete and the reinforcement are given in Sect. 8.3.1 and 8.3.2.

The beams were initially loaded in increments of 10 kN of applied load. The first flexural crack was formed at about 10 kN of shear load (applied load of 20 kN). As the load increased further, the cracks propagated almost vertically. Spalling at the mid-span in beam A11 was noticed at a shear load of 62 kN (applied load of 124.0 kN) and in beam A21 at a shear load of 60 kN (applied load of 120 kN). They then failed in flexure at a shear load of 64.9 kN and 61.3 kN respectively. Photograph of beam A11 at failure is shown in P8.13.

The relationship between the shear load and the deflection is shown in Fig. 8-50. It can be seen that the variation of deflection and shear load is linear up to point A. Then the deflection increases at almost constant shear load up to point B after which the strength of the beam reduces and failure in flexure occurred.

The measured strains in the concrete at mid-span at different load steps were used to find the strain profiles by regression analyses from which the curvatures were determined. The relationship between the curvature and moment are plotted in Fig. 8-51. It can be seen in Fig. 8-51 that the plateau part is missing as recordings of strain in the concrete was stopped at this stage due to spalling. The maximum moment in beam A11 was 120.06 kNm and in beam A21 was 113.41 kNm.

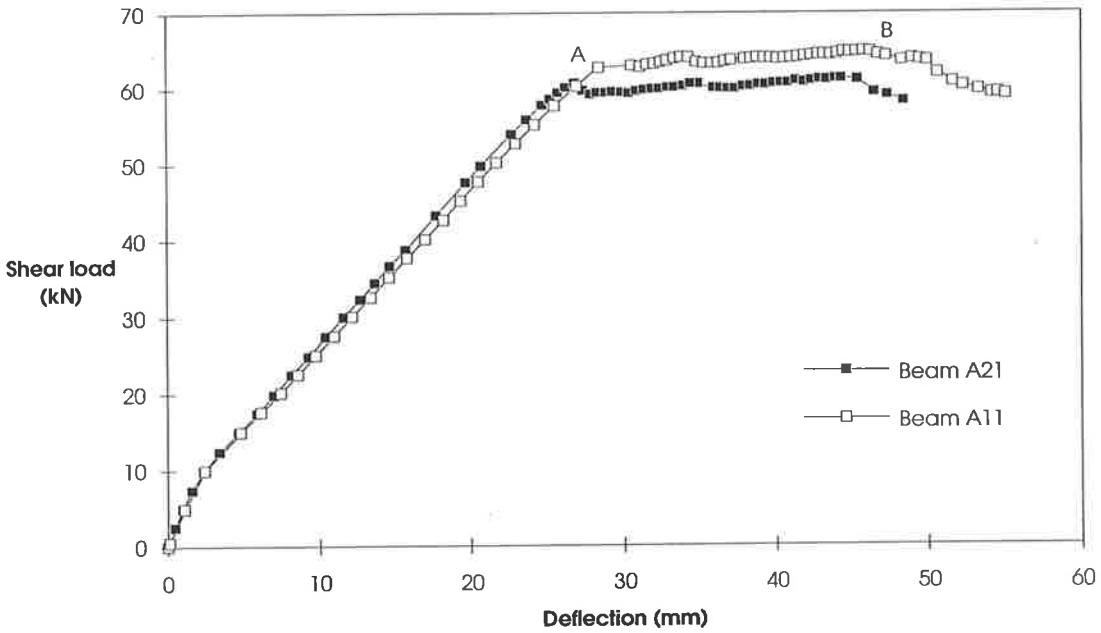

Fig. 8-50 Load deflection curve (Beam A11 and A21)

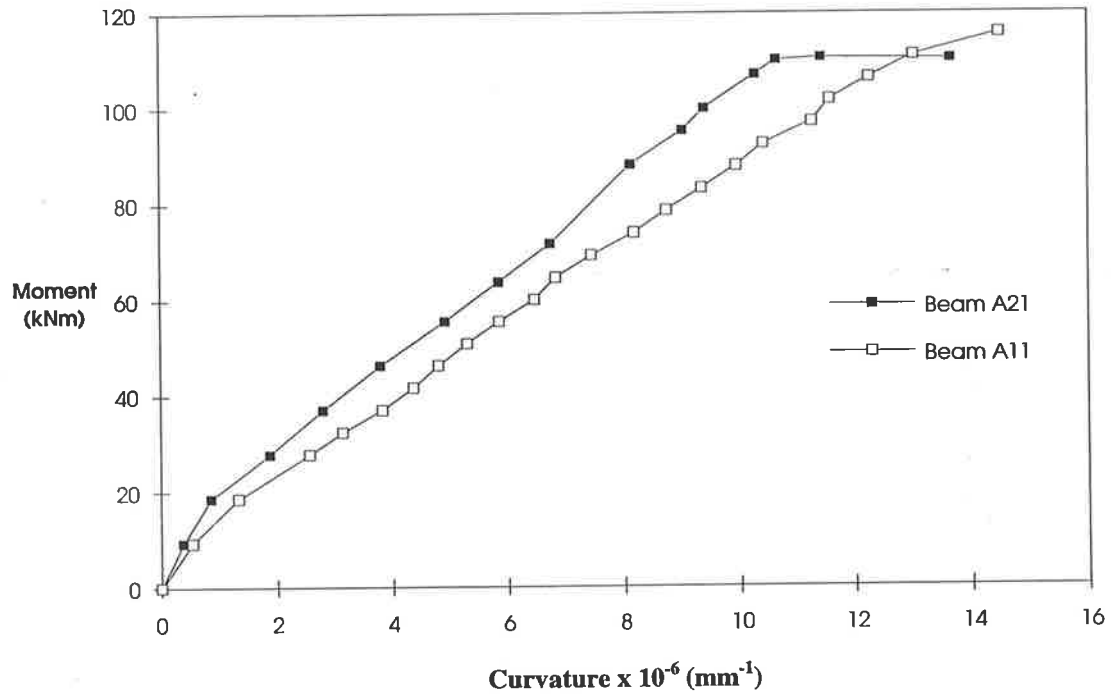

Fig. 8-51 Moment curvature curve (Beam A11 and A21)

8.4.6.2 Series 2: Shallow depth plated beam

This series consisted of four plated beams. The design of the beams was described in the Sect. 8.4.1.2. The main variation in this series was the degree of shear connection. The positions of the bolts are shown in Figs. 8-34 to 8-38. The instrumentation are shown in Figs. 8-43 to 8-46 and the test rig is shown in Fig. 8-49 respectively. The material properties of the concrete, the reinforcement and the plate were described in Sects. 8.2.1 to 8.2.3 respectively.

8.4.6.2.1 Test 2 : Shallow plated Beam B11

The set up of the beam is shown in P8.14. Load was applied to the beam in three cycles. In the first cycle, the increment of applied load was 5 kN. During this cycle the first flexural crack was noticed at the bottom of the RC beam at an applied load of 20 kN (shear load of 10 kN) and this was almost vertical. As the load was increased further, more vertical cracks were formed and propagated behind the plate, as shown in P8.15. These cracks were formed between the bolt positions. At 50 kN of applied load (shear load of 25 kN) the first cycle was finished and load was taken off gradually to zero.

In the second cycle, the increment of the applied load was 10 kN. More flexural cracks were formed after 50 kN (shear load of 25 kN). At an applied load of 100 kN (shear load of 50 kN) some cracks were noticed at the position of the bolts due to ripping action. At this stage, the second cycle of loading was complete and load was taken off to zero gradually.

In the final cycle, the beam was first loaded in increments of 25 kN until 100 kN, then in increments of 10 kN, after which it was loaded in displacement control. At 120 kN of applied load (shear load of 60 kN), the cracks had extended above the top of the plate. These propagated vertically as the load was further increased. After 198 kN of applied load (shear load of 99 kN), the load increments were replaced by 3 mm increments in deflection. This raised the applied load to the maximum of 203 kN (shear load of 101.5 kN). As the deflection was being increased by a further 3 mm, the beam failed in flexure through crushing of the concrete, as shown in P8.16, and the load dropped to 176 kN (shear load of 88 kN).

(a) Load-deflection behaviour

Figure 8-52 shows the relationship between the shear load and deflection. It can be seen in the figure that the variation is almost linear up to about 45 kN of shear load after which the stiffness of the beam reduces until the shear load reaches its maximum of 101.5 kN. The beam then failed in flexure and the shear load dropped very rapidly to 88 kN.

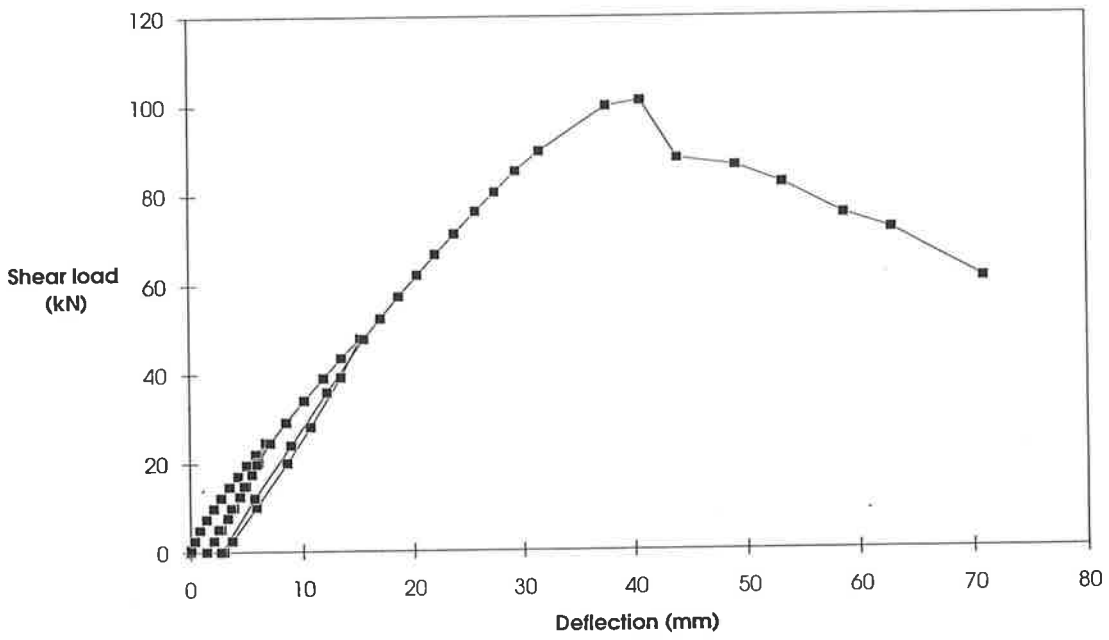

Fig. 8-52 Shear load-deflection curve (Beam B11)

(b) Vertical slip

The variation of the vertical slip at the supports is shown in Fig. 8-53, where the positions of the LVDTs is shown in Fig. 8-43. The LVDT 3 and 8 were found to be not working and as such they are not shown in Fig. 8-53. It can be seen in Fig. 8-53 that the vertical slip in LVDT 18 is initially positive which is defined as the plate moving upwards relative to the concrete. This is unrealistic, according to the theoretical investigation in Sect. 4.3. The vertical slip in LVDT 18 then gradually becomes negative, as the load increases with the plate moving downwards relative to the concrete. This situation is realistic, but almost no

increment in vertical slip can be seen at high load levels in LVDT 18, which suggests that LVDT 18 did not work properly.

The vertical slip in LVDT 15 in Fig. 8-53 is negative throughout the loading history, that is the plate moves downward relative to the concrete. The magnitude of the maximum vertical slip recorded in LVDT 15 was 0.040 mm at about 100 kN of shear load; then it reduces to 0.031 mm at the maximum shear load of 101.5 kN, and again increases to 0.04 mm at 88 kN of shear load, soon after failure of the beam. The vertical slip gradually reduces as the shear load reduces.

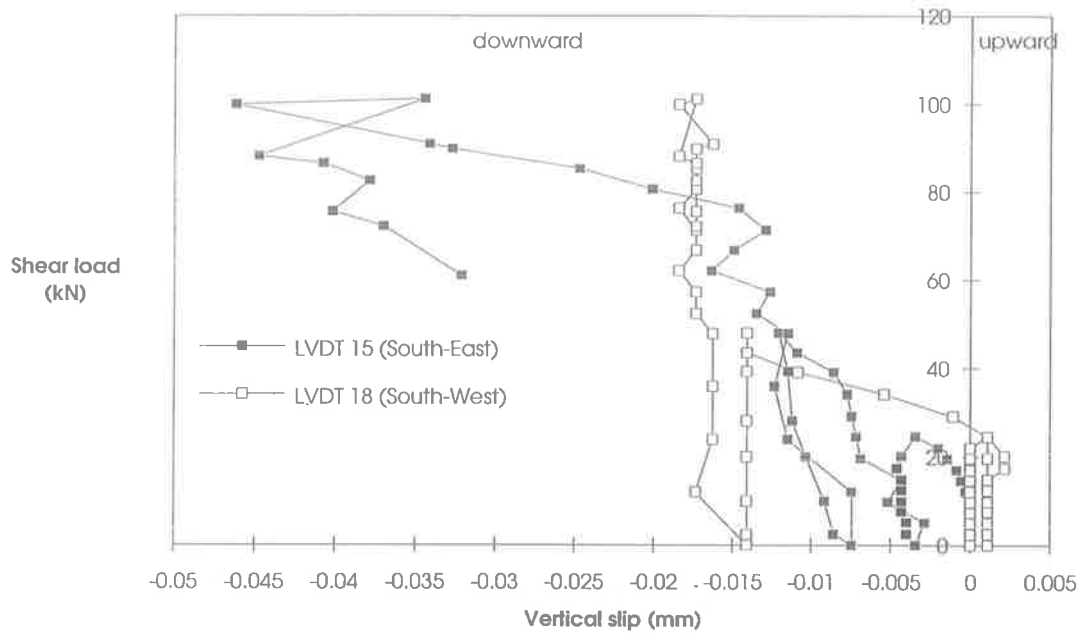

Fig. 8-53 Vertical slip at support (Beam B11)

Figure 8-54 shows the variation of vertical slip near the middle of the shear span, where the position of the LVDTs was shown in Fig. 8-43. It can be seen in the Fig. 8-54 that there is zero vertical slip up to about 55 kN and 25 kN of shear load in LVDTs 4 and 7, respectively. The vertical slip then increases gradually with the shear load. The vertical slips at the maximum shear load are given in Table 8.18. It can be seen in Fig. 8-54 that the vertical slip reduces gradually as load drops.

Figure 8-55 shows the variation of vertical slip at the bolt nearest to the mid-span, where the position of the LVDTs was shown in Fig. 8-43. It can be seen that the increment

of vertical slip is very small but linear up to about 50 kN of shear load, after which the rate increases gradually with the shear load. The vertical slip at the maximum shear load is given in Table 8.18. It can be seen in Fig. 8-55 that the vertical slip increases in LVDTs 5, 6 and 16 as the shear load decreases after failure, whereas vertical slip stays almost constant in LVDT 17.

It can be seen in Table 8.18 that the vertical slip is maximum at the position of the end bolt of the shear span. Also, the direction of vertical slip changes from downward at the support to upward at the end bolt of the shear span.

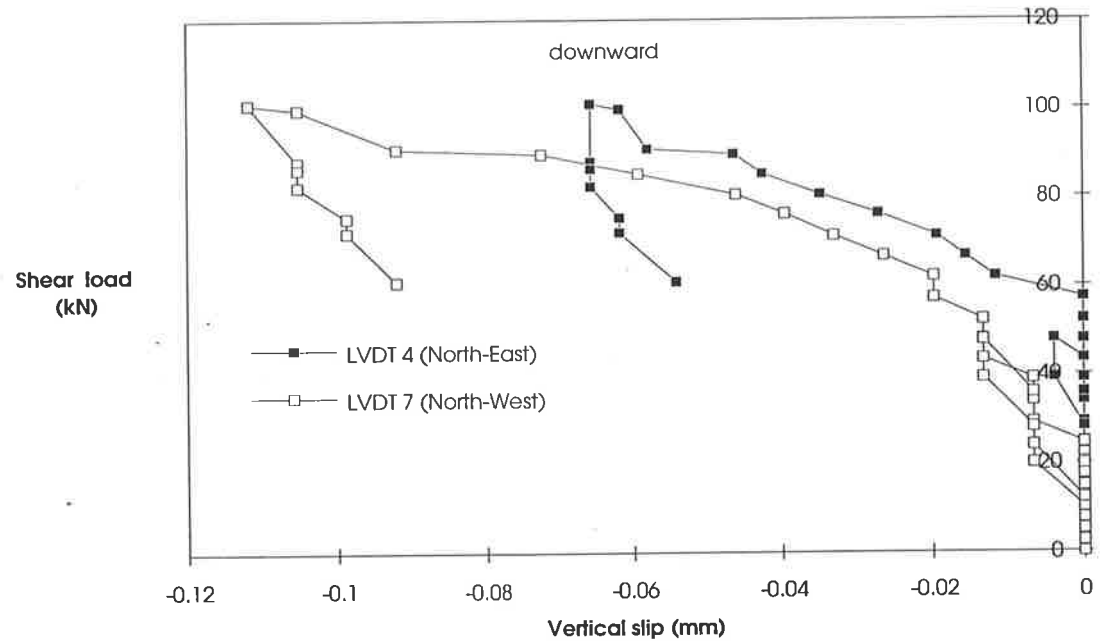

Fig. 8-54 Vertical slip near mid-shear span (Beam B11)

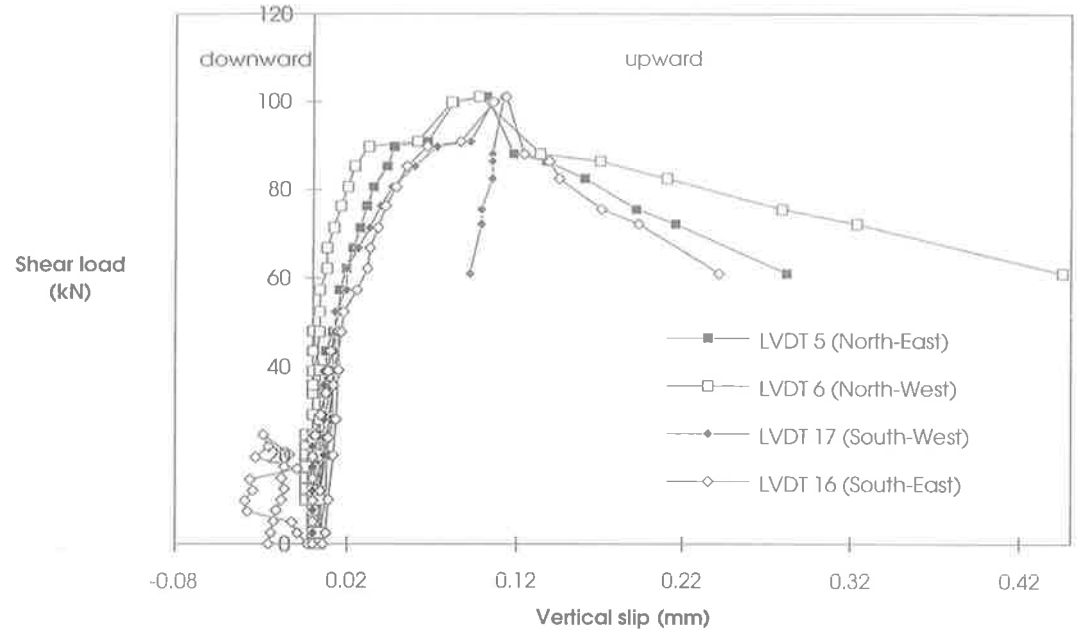

Fig. 8-55 Vertical slip at end bolt of the shear span (Beam B11)

Table 8.18 Vertical slip at the maximum shear load (Beam B11)

Direction	East shear span (Distance from East end support)			West shear span (Distances from West end support)		
	At 0 mm	At 882 mm	At 1762 mm	At 0 mm	At 882 mm	At 1762 mm
	(mm)	(mm)	(mm)	(mm)	(mm)	(mm)
(1)	(2)	(3)	(4)	(5)	(6)	(7)
North side	-	-0.066	+0.102	-	-0.112	+0.097
South side	-0.031	-	+0.113	-	-	+0.079

(c) Longitudinal slip

Figure 8-56 shows the variation of the longitudinal slip at the level of the top bolts and over the supports in Fig. 8-43(a). It can be seen that the longitudinal slip is positive throughout the loading history, positive being defined as when the longitudinal movement

of the plate relative to the concrete is inwards, that is towards the centre of the beam. There is almost zero longitudinal slip up to about 25 kN of shear loads and then it varies almost linearly up to the maximum load, after which it stays almost constant. The magnitude of longitudinal slip at the maximum shear load is given in Table 8.19.

Figure 8-57 shows the variation of the longitudinal slip at the level of the bottom bolts and over the supports. The behaviour is similar to the previous case of the top bolts and will not be discussed further. The longitudinal slip at the maximum shear load is given in Table 8.19.

Figure 8-58 shows the variation of the longitudinal slip at the level of the mid-depth of the plate and over the support points and on the south side of the beam. The behaviour is similar to the bolts near the supports. The longitudinal slip at the maximum shear load is given in Table 8.19.

Figure 8-59 shows the variation of the longitudinal slip at the level of the mid-depth of the plate and near mid shear span. The behaviour is similar to the other positions. It can be seen that the increment of longitudinal slip with shear load in LVDT 13 is reduced after about 60 kN whereas the increment stays the same in LVDT 11. The longitudinal slip at the maximum shear load is given in Table 8.19.

The longitudinal slip at the mid-span is shown in Fig. 8-60. The longitudinal slip was found to be increasing with the loads which is unexpected. Due to symmetry, the longitudinal slip at the mid-span must be zero. In the experiment, this was not achieved due to flexural cracks which were located at or near the LVDT.

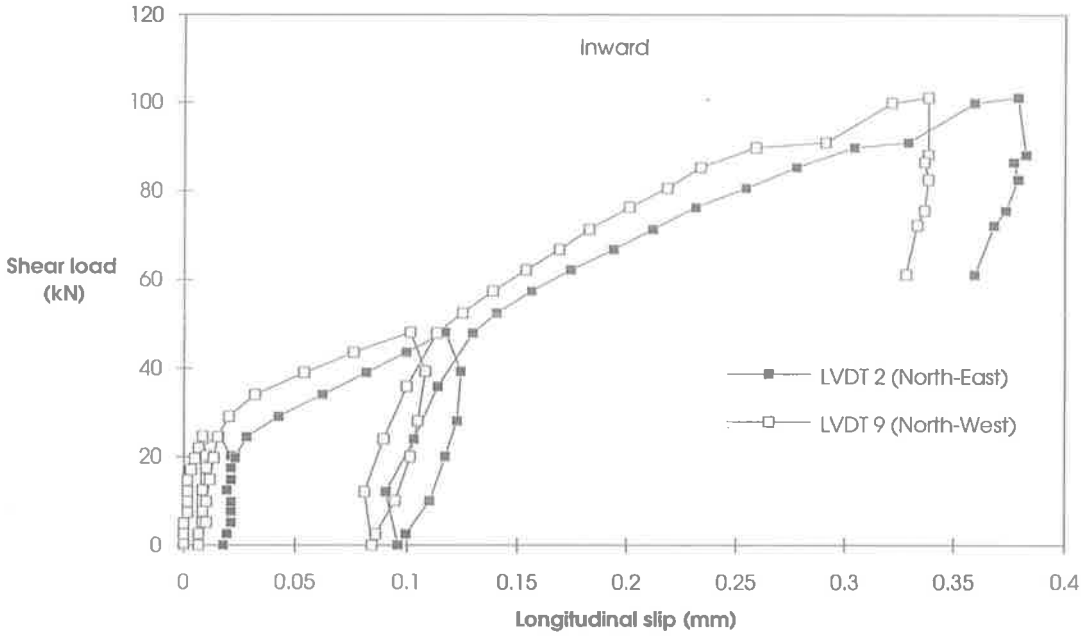

Fig. 8-56 Longitudinal slip at top bolt level over the support (Beam B11)

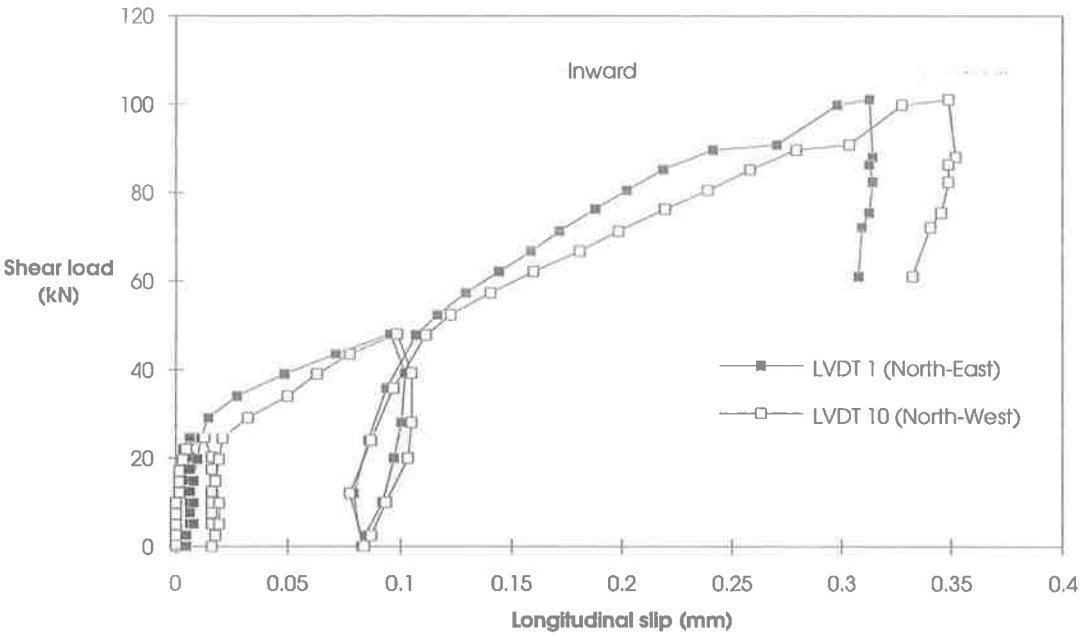

Fig. 8-57 Longitudinal slip at bottom bolt level and the support (Beam B11)

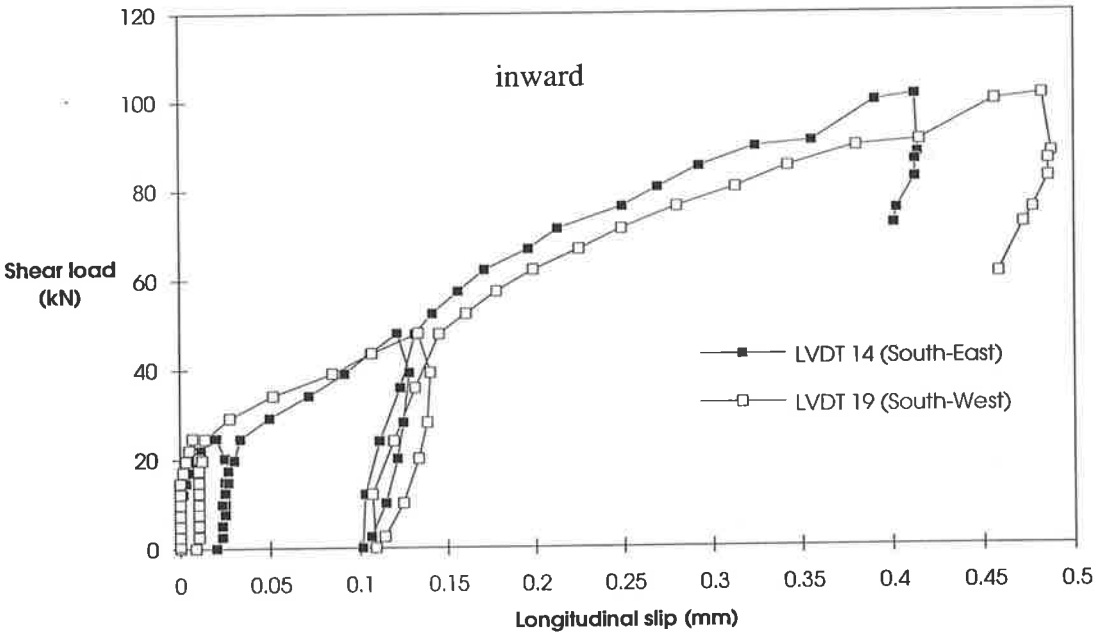

Fig 8-58 Longitudinal slip at mid-depth of plate over the support (Beam B11)

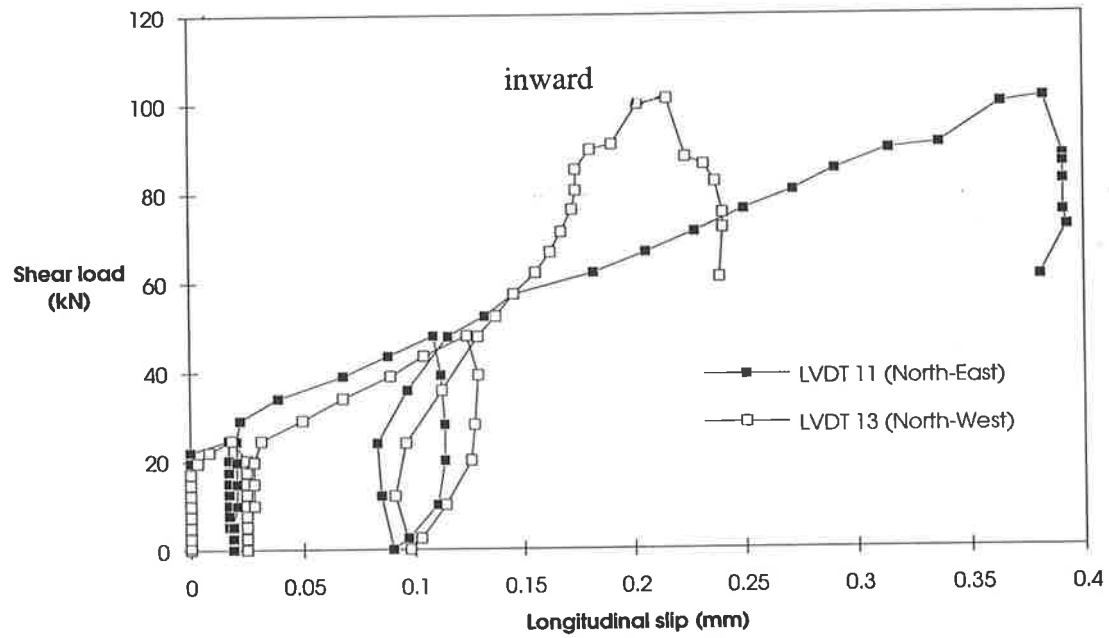

Fig. 8-59 Longitudinal slip at mid-depth of plate near mid-shear span (Beam B11)

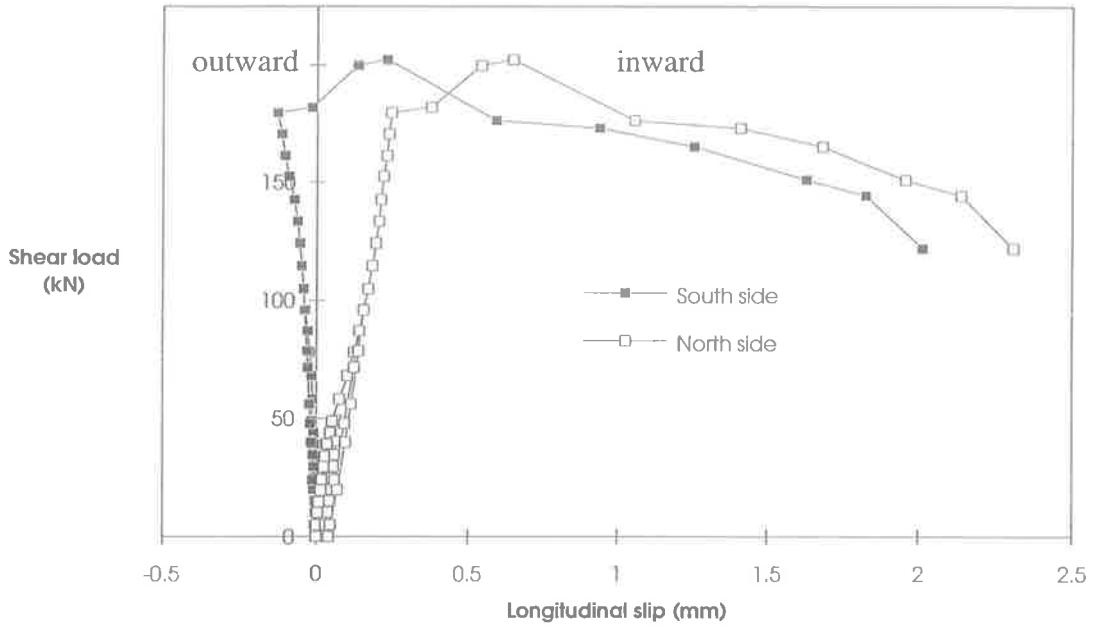

Fig. 8-60 Longitudinal slip at mid-span (Beam B11)

It can be seen in Table 8.19 that the longitudinal slip over the support at the bottom bolt level is less than that of the top. The longitudinal slip at the mid-depth of the plate over the support in the south side of the beam is higher than that of both the top and bottom bolt levels in the north side. Also, the longitudinal slips at the middle depth of the plate near mid-shear span are found to be more than at the support of north-east side of shear span. These results contradict what we expect from the strain profile in Fig. 8-73. It is clear from Fig. 8-73 that the slip strain increases towards the bottom of the beam; hence longitudinal slip is greater towards the bottom as it is found from the integration of the slip strain. Therefore, it would appear that the magnitudes of longitudinal slip were affected by the measurement error of the instrumentation or the positions of flexural cracks.

Table 8.19 Longitudinal slip at the maximum shear load (Beam B11)

Direction and vertical position	East side shear span		West side shear span	
	Position from East end support		Position from West end support	
	At 0 mm	At 852 mm	At 0 mm	At 852 mm
	(mm)	(mm)	(mm)	(mm)
(1)	(2)	(4)	(5)	(6)
North top	+0.33	-	+0.36	-
North mid	-	+0.36	-	+0.19
North bottom	+0.31	-	+0.33	-
South mid	-	+0.39	+0.47	-

(d) Longitudinal strain in plate at mid-shear span

Longitudinal strains were measured at the mid-shear-span of the north side plate of the beam, as shown in Fig. 8-43(a). The variations at different depths of the plate are shown in Figs. 8-61 to 8-63 respectively. It can be seen in the figures that the strain is positive at all load levels, where positive is defined as a tensile strain. Also, it can be seen that the variation is almost linear up to the maximum shear load. Moreover, the strain at the North-East shear span and the North-West shear span are very close which confirm symmetry of loading about mid-span of the beam and hence symmetry of slip. The strain at the maximum shear load is given in Table 8.20.

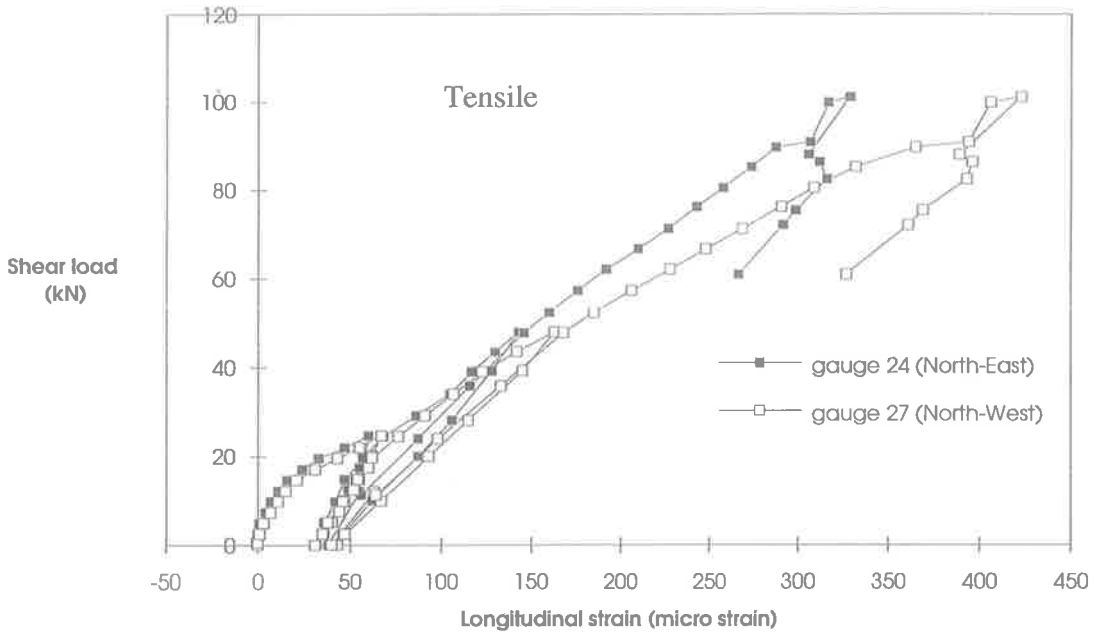

Fig. 8-61 Longitudinal strain at top bolt level near mid-shear span (Beam B11)

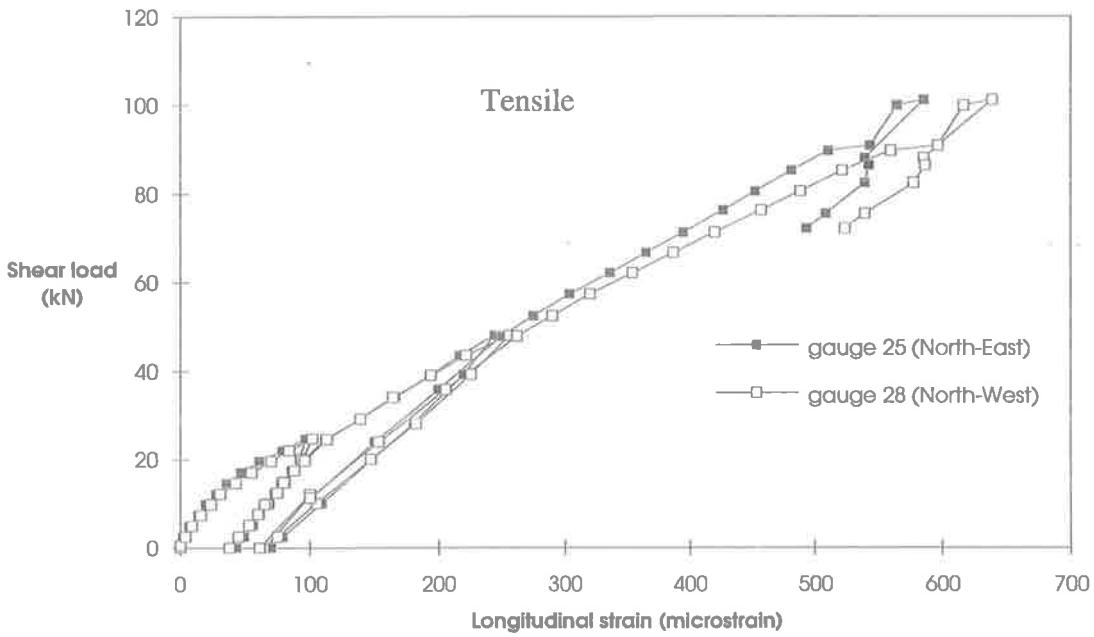

Fig. 8-62 Longitudinal strain in plate at mid depth of plate near mid-shear span (Beam B11)

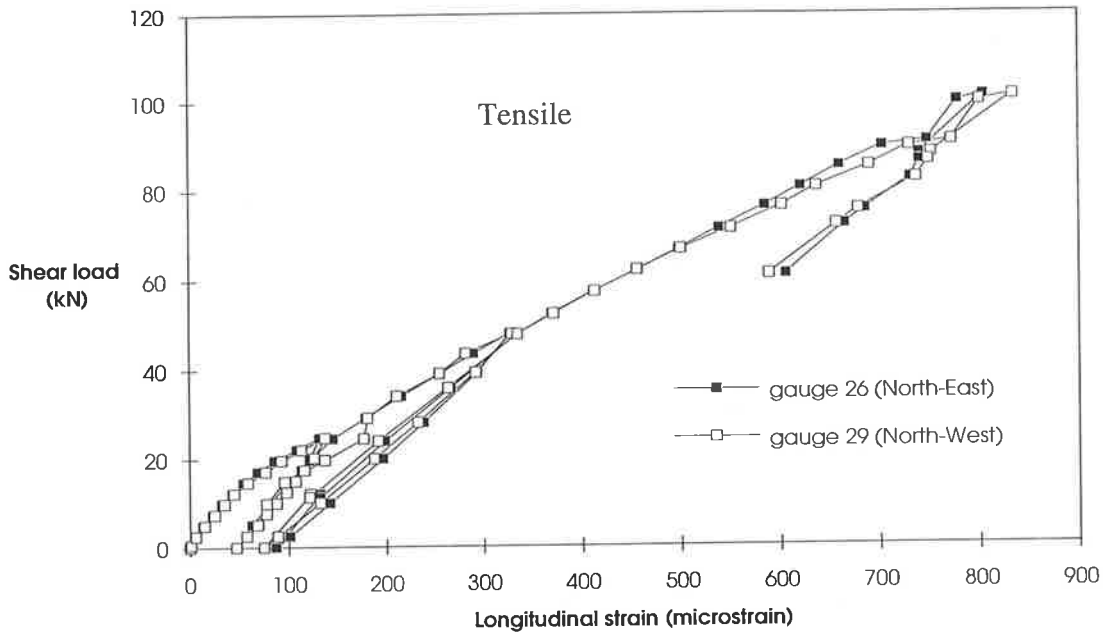

Fig. 8-63 Longitudinal strain at bottom bolt level near mid-shear span (Beam B11)

Table 8.20 Longitudinal strain in plate at mid-shear span (Beam B11)

Location from top of the plate	At East end (microstrain)	At West end (microstrain)
(1)	(2)	(3)
33 mm	+317	+406
67.50 mm	+586	+639
112 mm	+804	+834

The above strains in the plate were used to determine the forces at different load levels. A linear regression analysis of the strains at a given load level gave the distribution of strain in the plate. This was then used to determine the stress distribution by using the stress-strain relationship of the plate, as shown in Appendix-E. The forces in one side plate were calculated following the procedure described in Appendix-E. The forces in one side plate at a few load steps are given in the Table 8.21, where the notations are defined in Fig.

8-64, in which h = 145 mm. A negative sign in Col. 2 means the neutral axis position is above the plate.

Table 8.21 Forces in one side plate at mid-shear span (Beam B11)

Applied Load (kN)	n-a position y_{np} (mm)	Compressive force		Tensile force		Resultant force	
		P_{comp} (kN)	x (mm)	P_{ten} (kN)	y (mm)	P_{plate} (kN)	z (mm)
1	2	3	4	5	6	7	8
10	-65.10	0	0	9.11	85.23	9.11	85.23
50	-22.91	0	0	20.04	90.86	20.04	90.86
100	-36.62	0	0	43.38	88.56	43.38	88.56
150	-32.24	0	0	69.63	89.22	69.63	89.22
203	-31.46	0	0	104.84	89.35	104.84	89.35

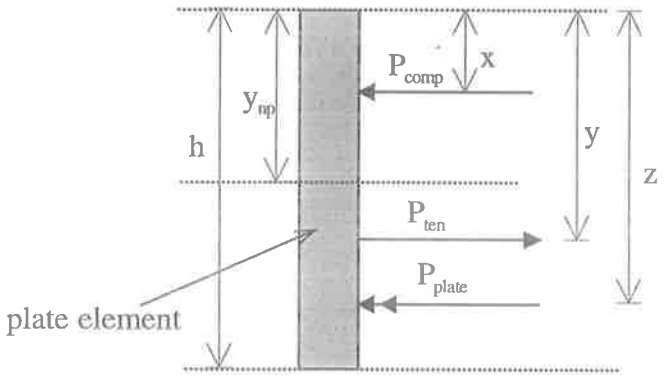

Fig. 8-64 Forces in the plate element

(e) Longitudinal strain in the plate at mid-span

Demec gauges were used to measure the strains in the plate at the mid-span, as was shown in Fig. 8-43(c). The measurements were taken at both the sides. The longitudinal strain at different depths of the plate are shown in Figs. 8-65 to 8-68.

Figure 8-65 shows that the strain at the top of the plate is close to zero initially. This suggests that the neutral axis position at low load levels was near the top of the plate. As the load increases further, the strain becomes increasingly tensile which suggests that the neutral axis position gradually moves towards the top of the beam. Obviously the strains at the other positions in the plate are tensile, as can be seen in Figs. 8-66 to 8-68. The longitudinal strain distribution is linear up to about 90 kN of shear load, after which it increases non-linearly. The longitudinal strain at the maximum shear load at the different depths of the plate are given in Table 8.22.

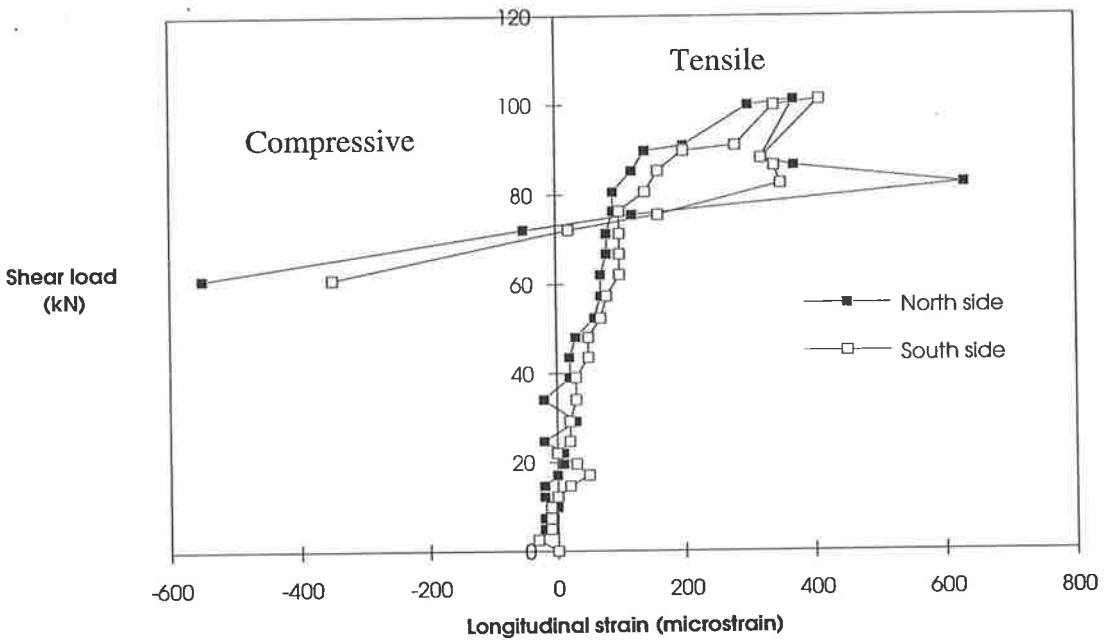

Fig. 8-65 Longitudinal strain at 5 mm level (Beam B11)

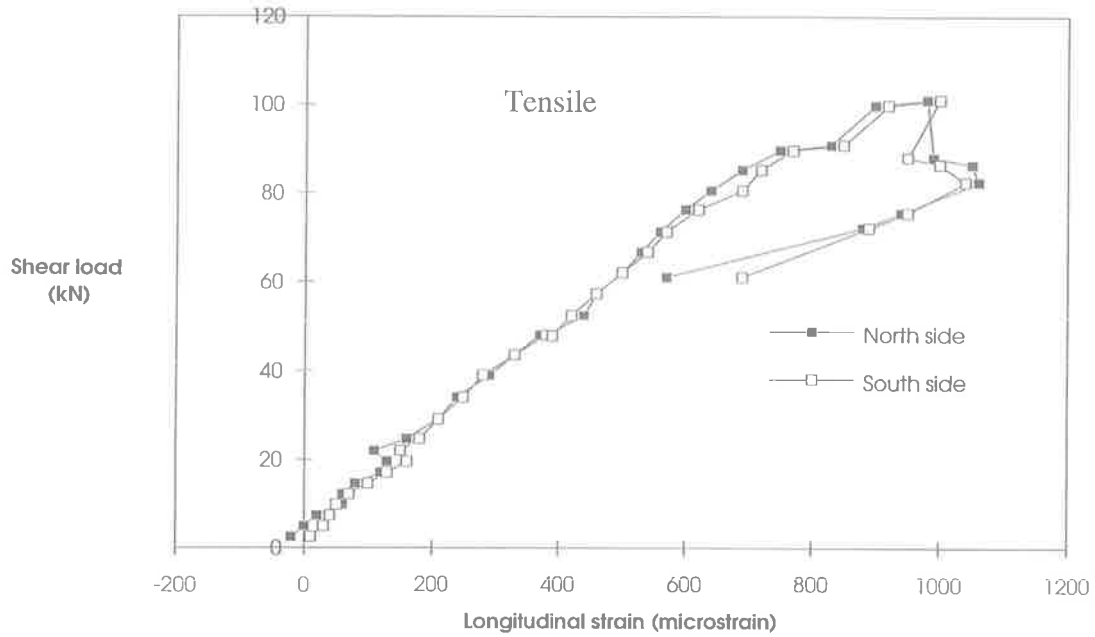

Fig. 8-66 Longitudinal strain at 50 mm level (Beam B11)

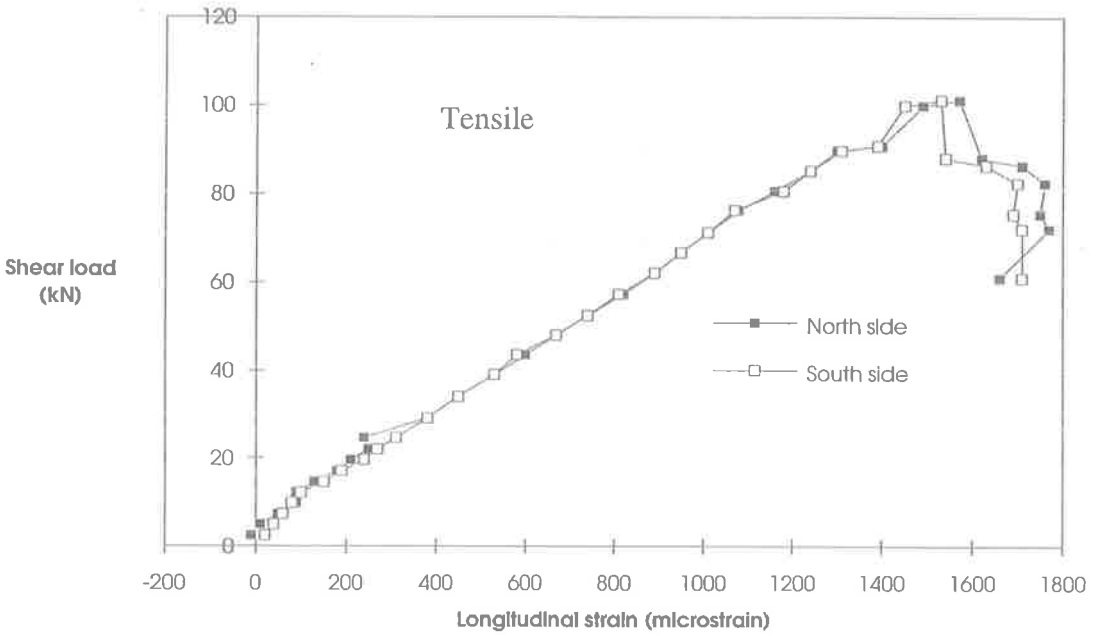

Fig. 8-67 Longitudinal strain at 95 mm level (Beam B11)

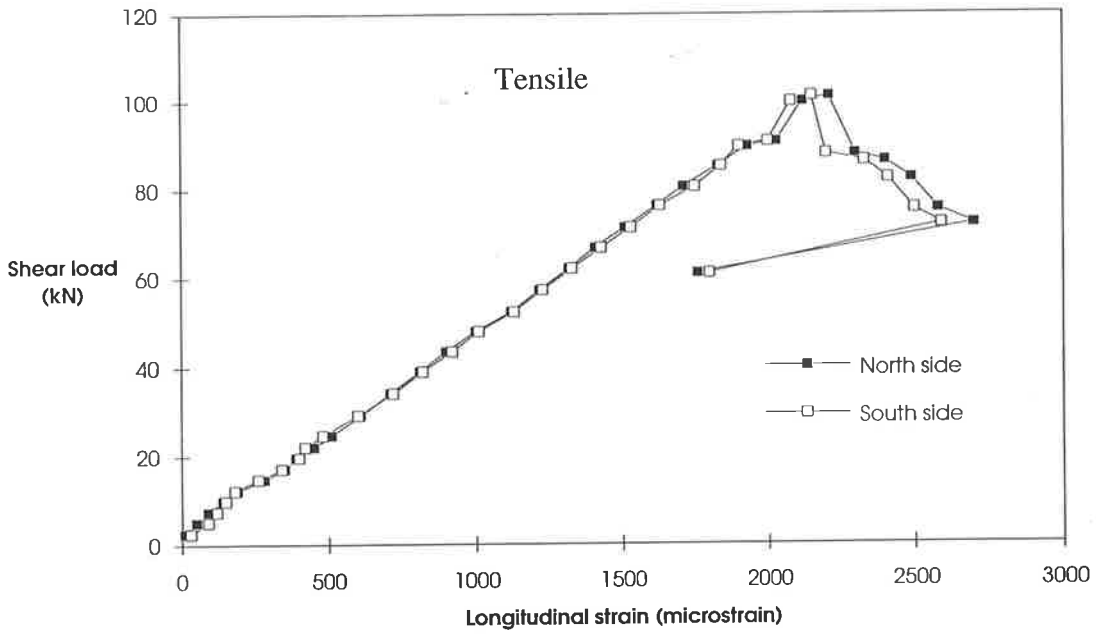

Fig. 8-68 Longitudinal strain at 140 mm level (Beam B11)

Table 8.22 Strain in plate at mid-span (B11)

Location from plate top	North side (microstrain)	South side (microstrain)
(1)	(2)	(3)
5 mm	+370	+410
50 mm	+980	+1000
95 mm	+1570	+1530
140 mm	+2210	+2150

(f) Strain profiles in the concrete and plate at mid-span

The longitudinal strains in the concrete and in the plate were measured at the mid-span and at various depths, as shown in Fig. 8-43(c). The strains at a specific load stage were used to find the strain profiles in the plate and in the concrete by regression analyses. These are shown in Figs. 8-69 to 8-73 for a few of the load steps.

Figure 8-69 shows the strain distribution in the plate and in the concrete at an applied load of 10 kN. It can be seen in the figure that the curvature in the plate is higher than that in the RC beam. At such a low load levels, this is very unlikely and cannot be true and is probably due to the large scatter of the experimental results, as shown in Fig. 8-69. However, as the load increases further, the curvature in both elements increases but the curvature in the RC beam increases more rapidly than that of the plate, as can be seen in Figs. 8-70 to 8-73, due to the vertical slip.

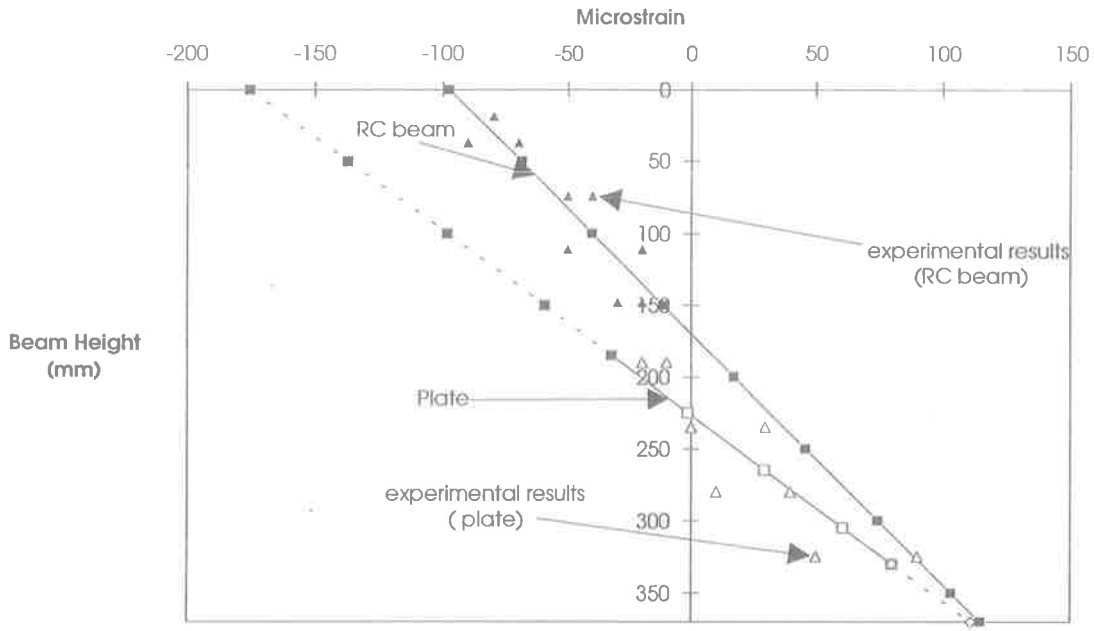

Fig. 8-69 Strain profiles at applied load of 10 kN (Beam B11)

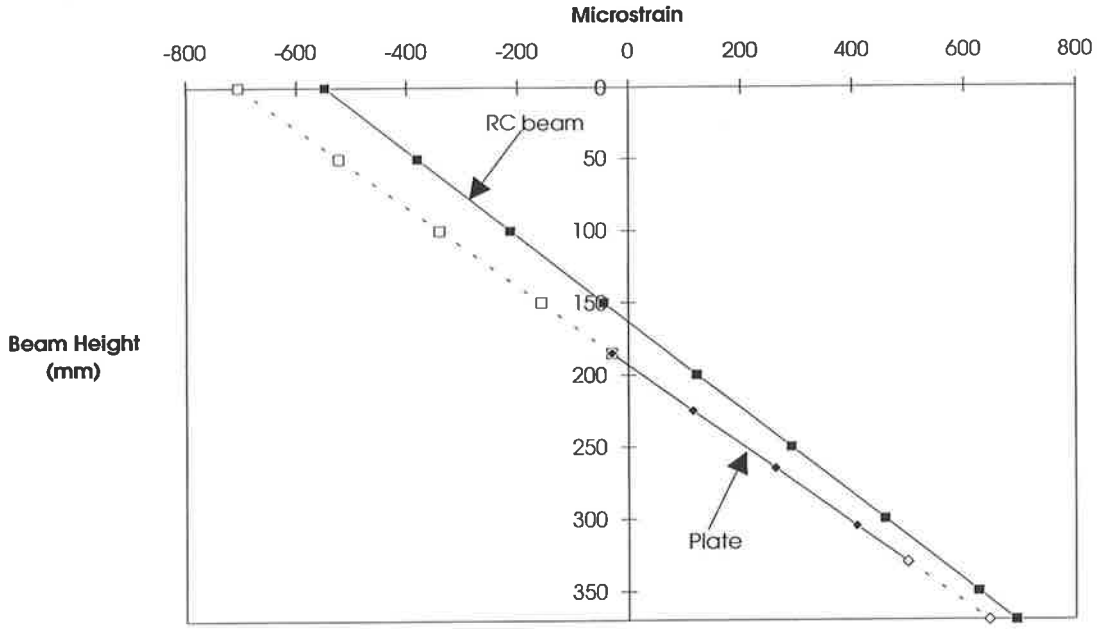

Fig. 8-70 slip strain at applied load of 50 kN (Beam B11)

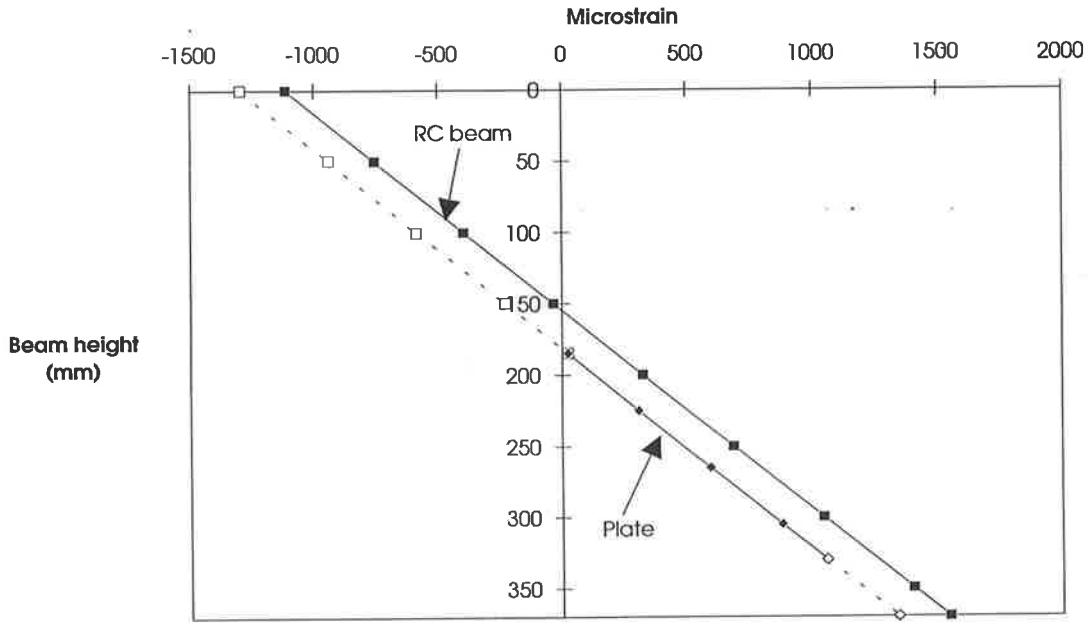

Fig. 8-71 Strain profile at applied load of 100 kN (Beam B11)

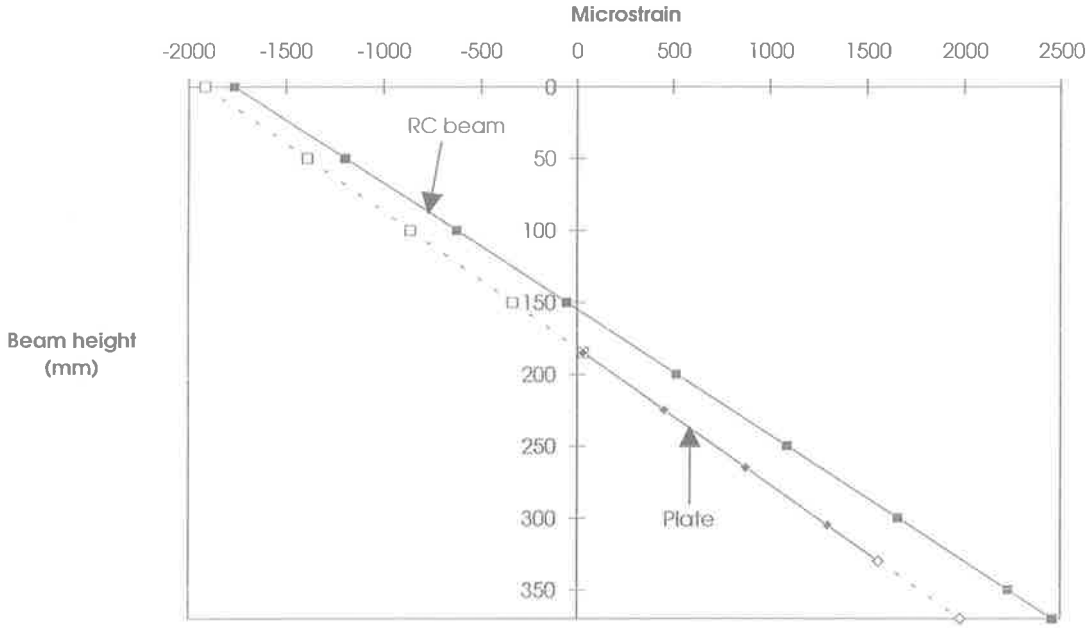

Fig. 8-72 Strain profile at applied load of 150 kN (Beam B11)

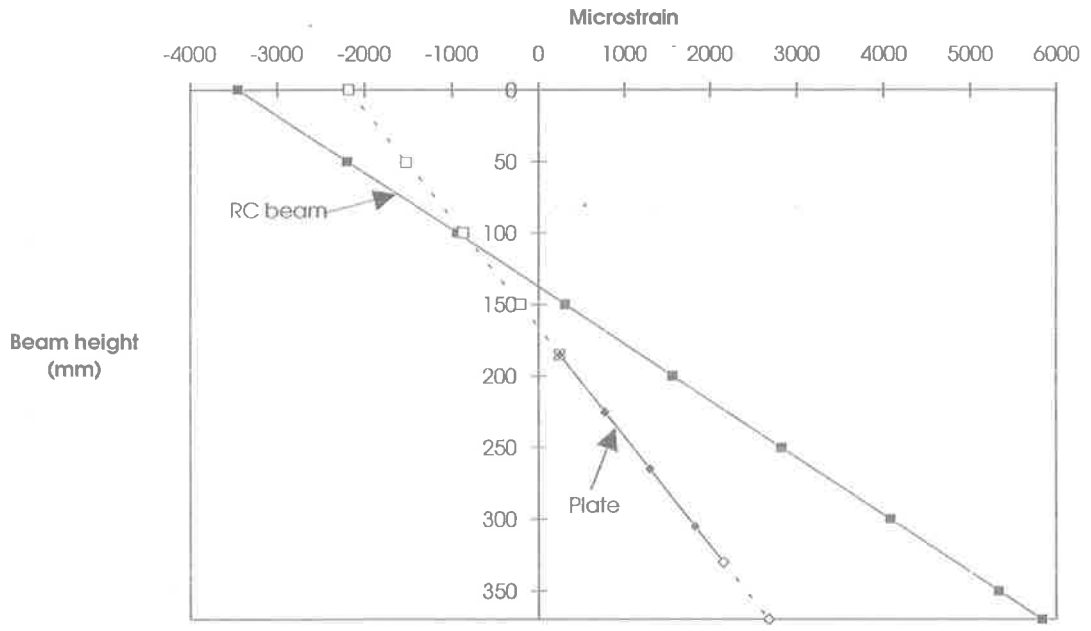

Fig. 8-73 Strain profile at applied load of 198 kN (Beam B11)

(g) Longitudinal forces in each of the side plate at mid-span

The strain distribution in the plate at various load steps was determined by linear regression analysis, as described in the last section. This is then used to determine the stress distribution in the plate by using the stress-strain relationship of the plate as shown in Appendix-E. The forces in one side plate were then calculated following the procedure described in Appendix-E. The forces in one side plate at a few load steps are given in the Table 8.23, with corresponding notation in Fig. 8-64. It can be seen that the resultant force in Col. 7 are almost double than those in Col. 7 of Table 8.21 which were found at almost mid-shear span of the plate.

The strain and stress distribution in the plate at the mid-span of the beam and at the maximum shear load is shown in Fig. 8-74. It can be seen in Fig. 8-74(b) that the full depth of the plate is in tension and 26.46 mm from the bottom of the plate is fully yielded. The position of the resultant force in the plate is shown in (c).

Table 8.23 Forces in one side plate at mid-span (Beam B11)

Applied Load (kN)	n-a position y_{np} (mm)	Compressive force		Tensile force		Resultant force	
		P_{comp} (kN)	x (mm)	P_{ten} (kN)	y (mm)	P_{plate} (kN)	z (mm)
1	2	3	4	5	6	7	8
10	14.54	0.02	4.84	16.15	101.51	16.13	100.45
50	1.01	0.002	0.36	45.46	97.00	45.46	97.00
100	-3.36	0	0	94.18	95.59	94.18	95.59
150	-3.11	0	0	138.55	95.67	138.55	95.67
203	-24.30	0	0	216.74	89.43	216.74	89.43

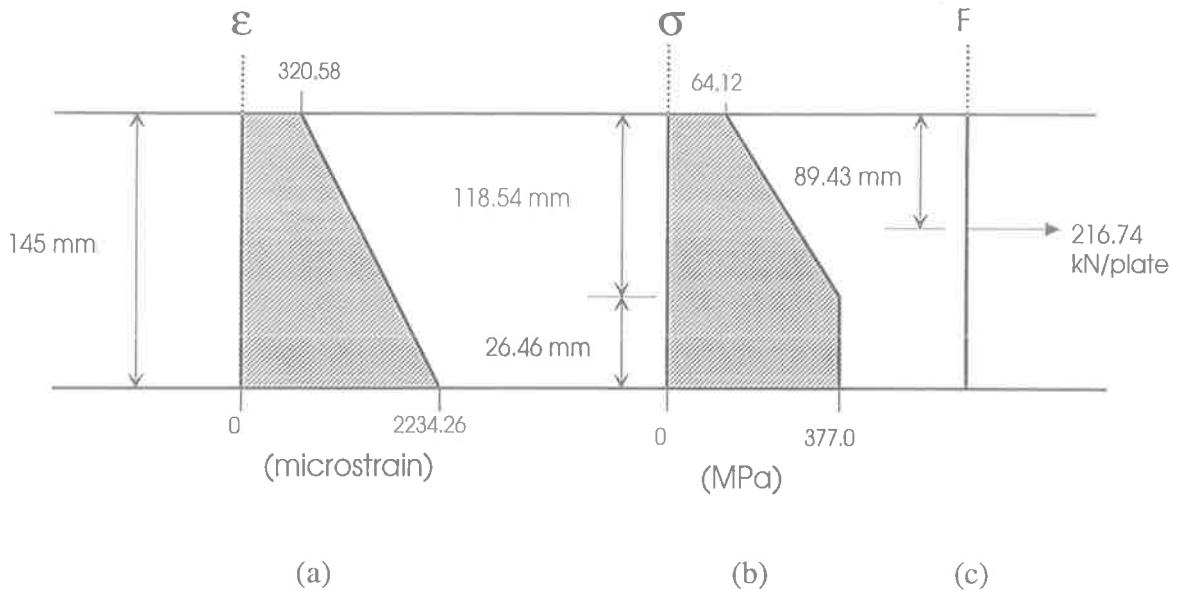

Fig. 8-74 Strain-stress-force in plate (Beam B11)

Figure 8-75 shows the relationship between the longitudinal force in the plate per side and the shear load. The variation is almost linear up to about 90 kN of shear load. The longitudinal force then increases in a non-linear manner up to the maximum shear load. The longitudinal shear force in each of the side plates at the maximum shear load is 216.74 kN. This force increased as the shear load reduced, up to a maximum of 248 kN per plate.

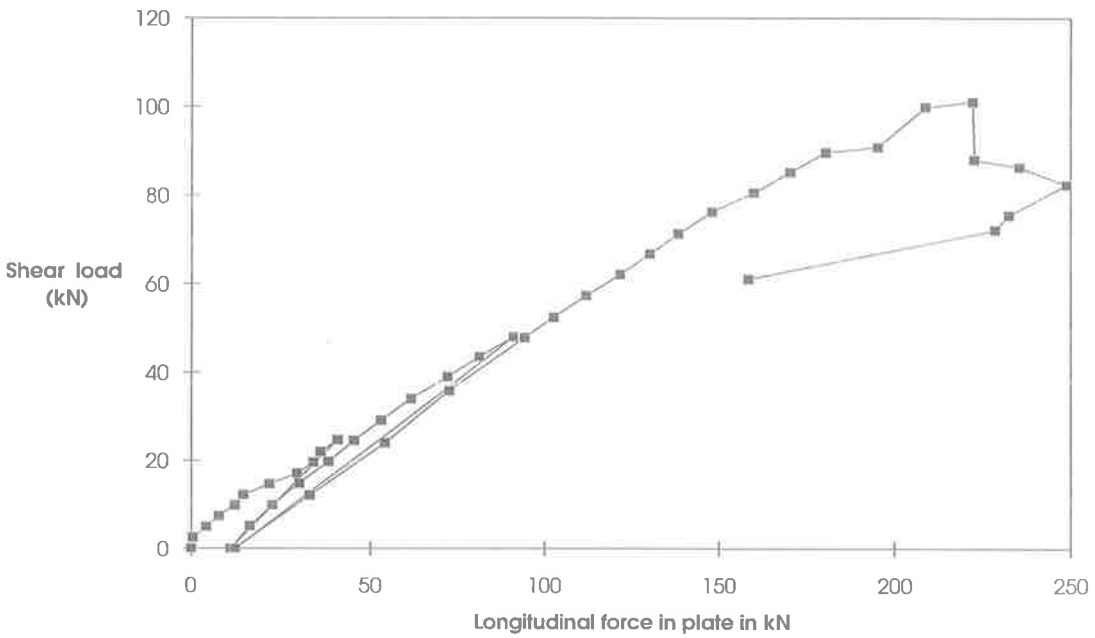

At each of the side plate

Fig. 8-75 Longitudinal force in plate/side at mid-span (Beam B11)

(h) Moment curvature relationship

The curvatures in the plate and in the RC beam were determined from their respective strain profiles. Figure 8-76 shows relationship between the curvatures and the moment. It can be seen that the curvature in the RC beam increases faster than that of the plate. Near the maximum moment, the curvature of the concrete element increases but the curvatures of the plate stays almost constant. The maximum moment is 187.78 kNm.

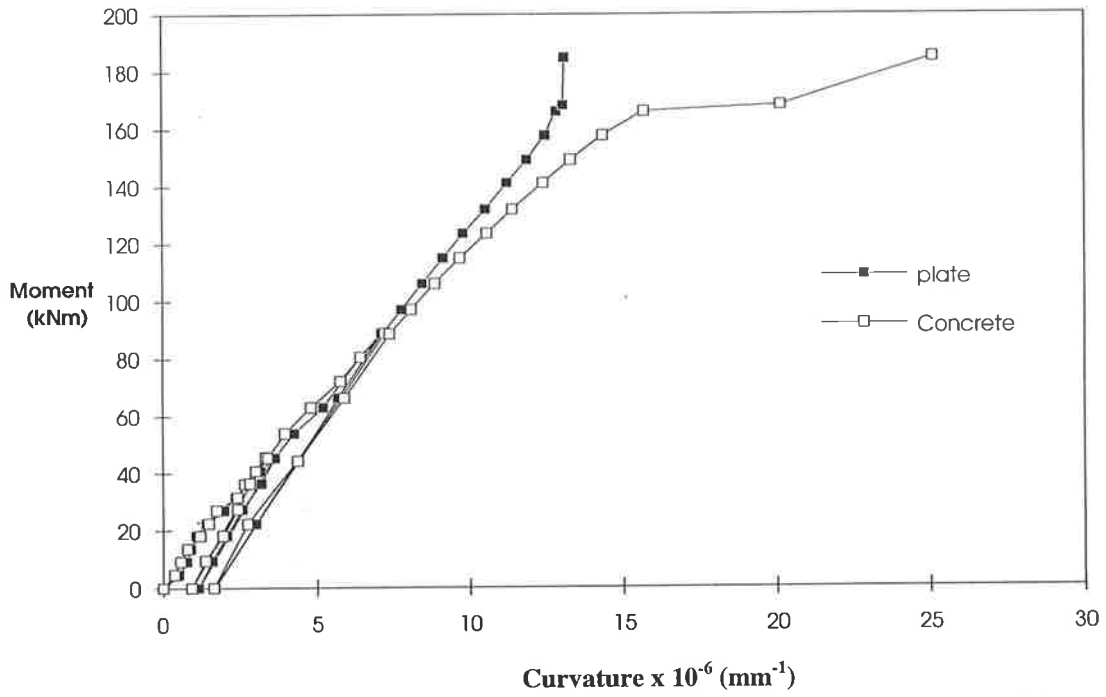

Fig. 8-76 Moment curvature curve (Beam B11)

8.4.6.2.2 Test 3 : Shallow depth plated beam B12

The set up of the beam is shown in P8.17. Load was applied to the beam in two cycles. In the first cycle, the increment of applied load was 10 kN. In this cycle, the flexural cracks appeared at the bottom of the beam at 30 kN of applied load (shear load of 15 kN). These cracks were almost vertical and occurred in between the bolt positions as shown in P8.18. The first cycle of loading was completed at 80 kN of applied load (shear load of 40 kN) and load was gradually taken off to zero.

In the second cycle, the increment of applied load was 10 kN up until 100 kN, after which the load was increased by following a 1 mm displacement at each load step. Cracks appeared above the plate at 90 kN of applied load (shear load of 45 kN), as shown in P8.18. At an applied load of 130 kN (shear load of 65 kN), cracks appeared at the position of the bolts. These were formed in between the existing flexural cracks due to ripping action, as shown in P8.19. At an applied load of 160 kN (shear load of 80 kN), cracks appeared through the bolt position near the supports, as shown in P8.20. At an applied load of 177 kN (shear load of 88.5 kN), buckling was noticed at top of the South West (S-W) part of the plate. At 182.8 kN of applied load (shear load of 91.4 kN), spalling occurred and the load started to drop. As load was dropping, much buckling in the S-W part of the plate was noticed. When the load dropped to 149.10 kN (shear load of 74.5 kN), the plate at S-W corner pulled out from the RC beam as all of the three pairs of bolt in that side were broken, as shown in P8.21. The concrete surrounding the bolts was crushed in the same way, as was seen in the push tests with the same bolt. At the end of the test, the plate was unscrewed and photographs were taken at each end of the RC beam, which are presented in P8.22 to P8.33.

(a) Load-deflection behaviour

Figure 8-77 shows the relationship between the shear load and deflection. The variation is almost linear up to point A (at 80 kN of shear load). The stiffness of the beam then reduces up to point B, after which the deflection increases at almost the maximum shear load up to point C. The strength of the beam then reduces after the beam failed in flexure.

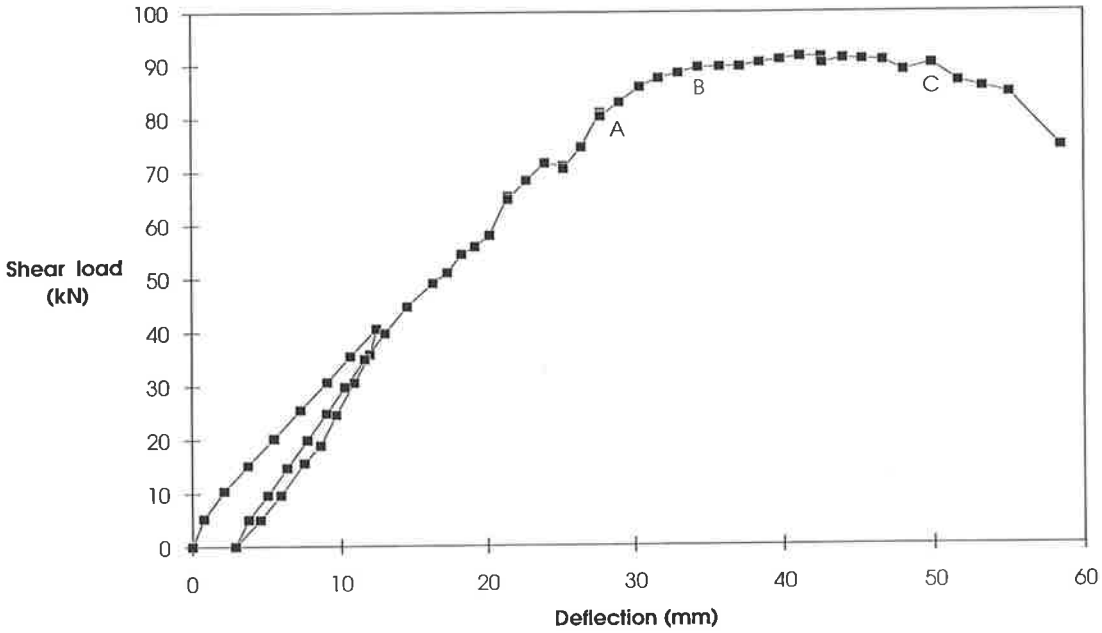

Fig. 8-77 Shear load deflection curve (Beam B12)

(b) Vertical slip

The variation of the vertical slip near the supports is shown in Figure 8-78. The variation is similar in all the LVDTs. It can be seen that at LVDT 3, the vertical slip is continuously increasing with larger increments than that of the others, as the load drops due to breaking of the bolt. The vertical slip at the maximum shear load is recorded in Table 8.24.

The variation of vertical slips near the mid-shear spans is shown in Fig. 8-79. The variation is similar to the previous shear load-vertical slip curve. It can be seen in Fig. 8-79 that the vertical slip is higher at LVDT 12 than at LVDT 9. The vertical slip at the maximum shear load is given in Table 8.24.

Figure 8-80 shows the variation of vertical slip at the bolt near to the mid-span. It can be seen that at LVDT 11, the vertical slip is close to zero at the maximum shear load, which suggests that the change of the direction of vertical slip in the N-W shear span occurred at or near to LVDT 11. The vertical slip at the maximum shear load at LVDT 10 is not as close to zero as at LVDT 11 at the maximum shear load, but is still very small. Therefore, we can assume that the change of direction of vertical slip in the N-E shear span

occurred at a point near to LVDT 10. The vertical slip at the maximum shear load is given in Table 8.24.

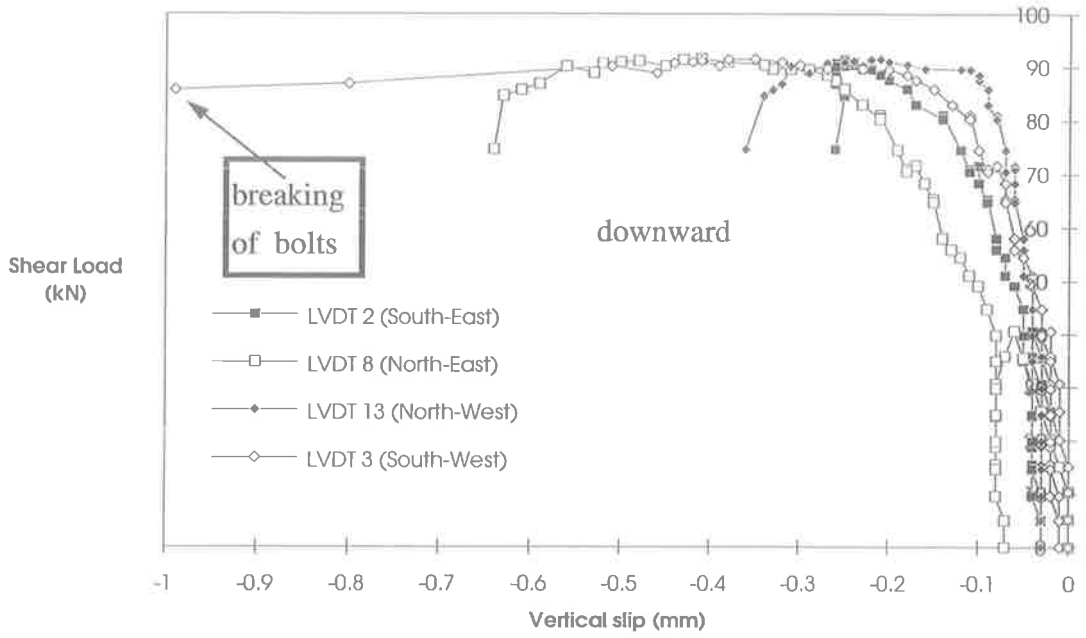

Fig. 8-78 Vertical slip at bolt near support (Beam B12)

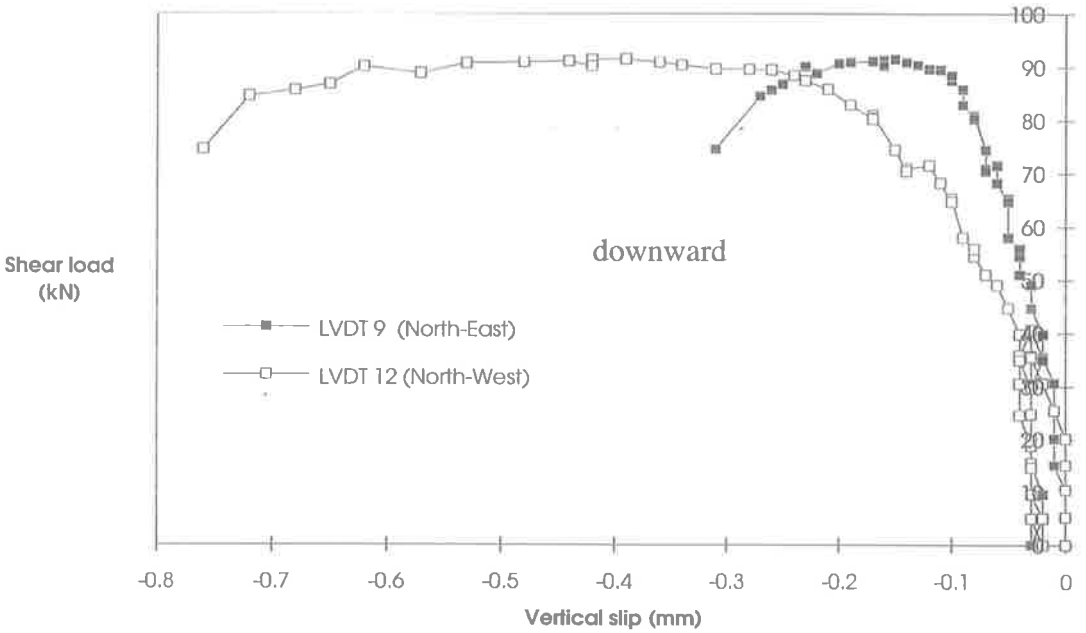

Fig. 8-79 Vertical slip at mid-shear span (Beam B12)

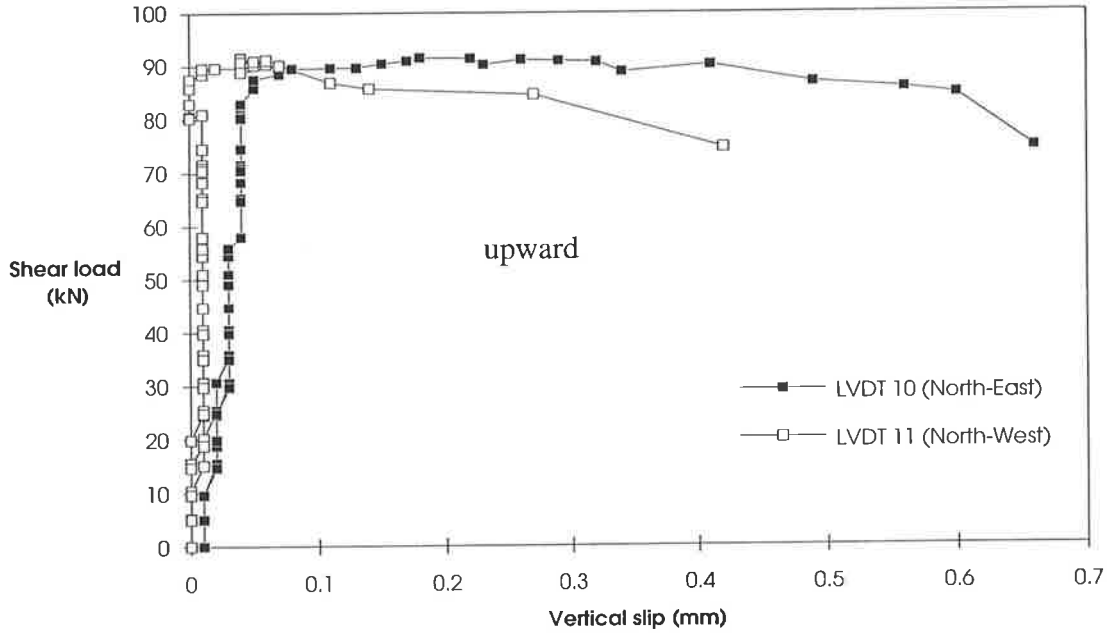

Fig. 8-80 Vertical slip at end bolt of the shear span (Beam B12)

It can be seen in Table 8.24 that the vertical slip is maximum at the bolt near the support in the N-E shear span whereas it is maximum at the bolt near the mid-shear-span in the N-W shear span. It is not possible to give a reason for this variation at this stage.

Table 8.24 Vertical slip at the maximum shear load (Beam B12)

Direction	East shear span (Distance from East end support)			West shear span (Distances from West end support)		
	At 120 mm	At 880 mm	At 1620 mm	At 120 mm	At 880 mm	At 1620 mm
	(mm)	(mm)	(mm)	(mm)	(mm)	(mm)
(1)	(2)	(3)	(4)	(5)	(6)	(7)
North side	-0.41	-0.15	+0.18	-0.21	-0.39	+0.04
South side	-0.25	-	-	-0.35	-	-

(c) Longitudinal slip

The variations of longitudinal slip at the support and at the levels of the top and bottom bolts are shown in Figs. 8-81 and 8-82 respectively. They all showed the usual ductile plateau. It can be seen in Fig. 8-81 that the longitudinal slip in LVDT 4 is continuously increasing. This was due to failure of the bolt. It is felt that bolt failure was induced by the lateral (buckling) displacement of the plate causing tensile axial forces in the bolt.

The variations of the longitudinal slip near the mid-shear span are shown in Figs. 8-83 and 8-84 for the top and bottom bolts respectively. The longitudinal slip at the maximum shear load is given in Table 8.25.

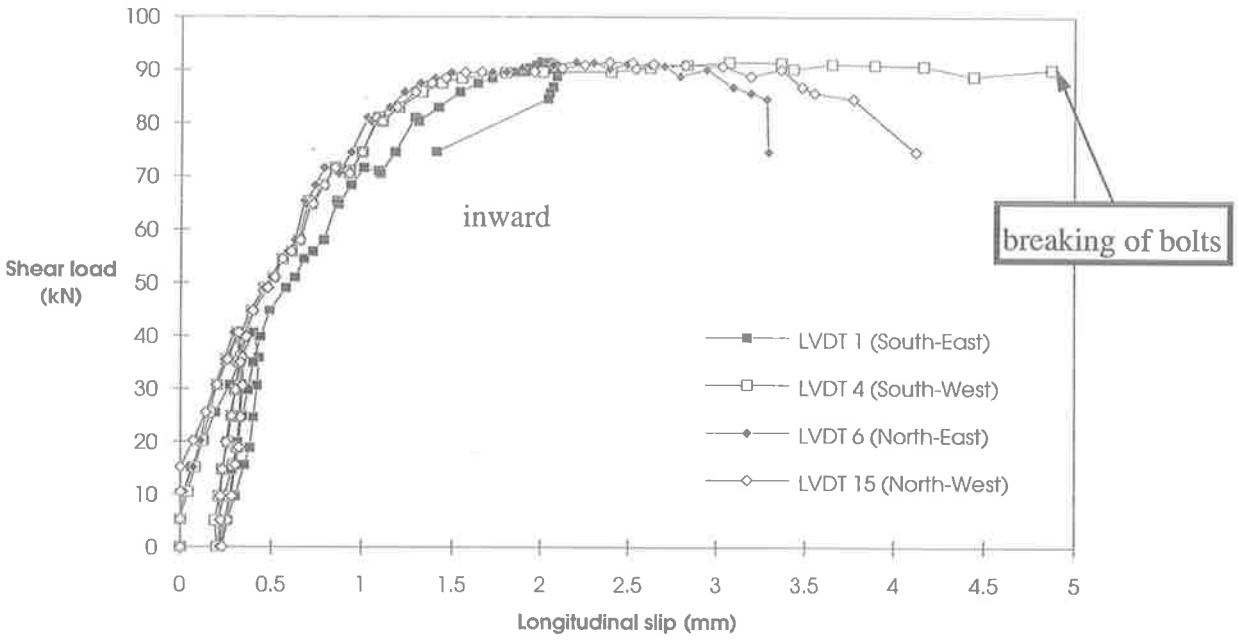

Fig. 8-81 Longitudinal slip at support at the level of bottom bolts (Beam B12)

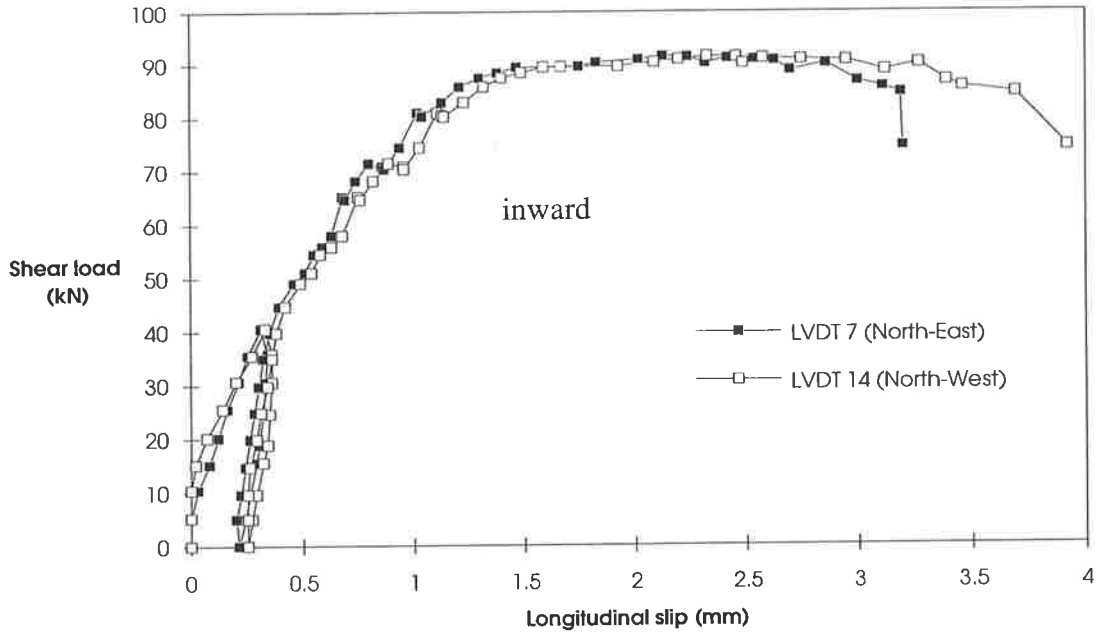

Fig. 8-82 Longitudinal slip over the supports at top bolt level (Beam B12)

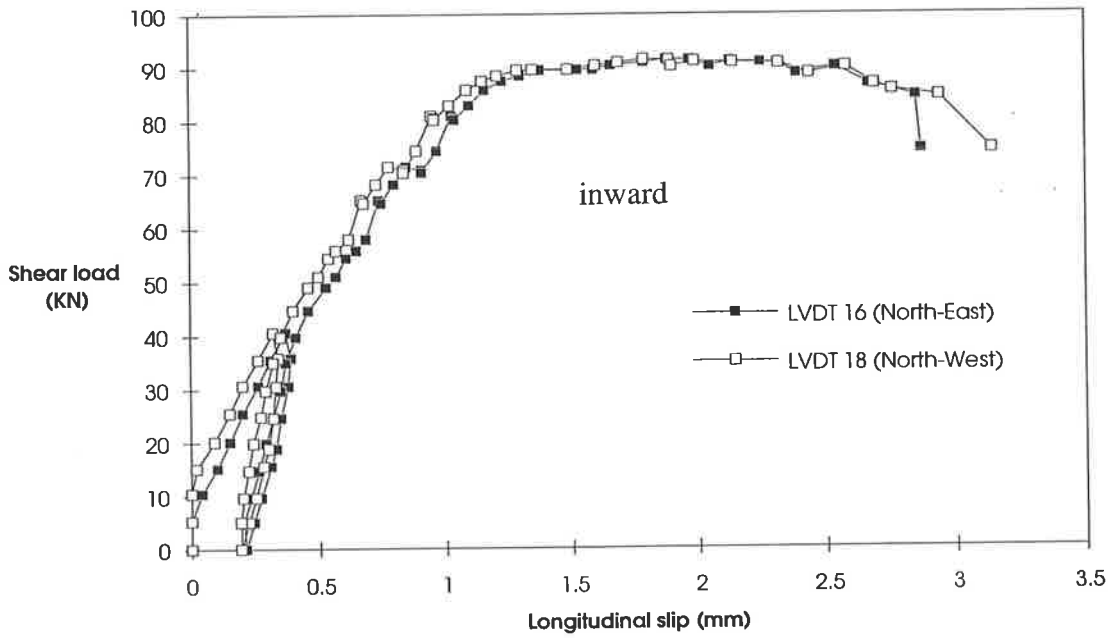

Fig. 8-83 Longitudinal slip at the level of top bolt near mid-shear span (Beam B12)

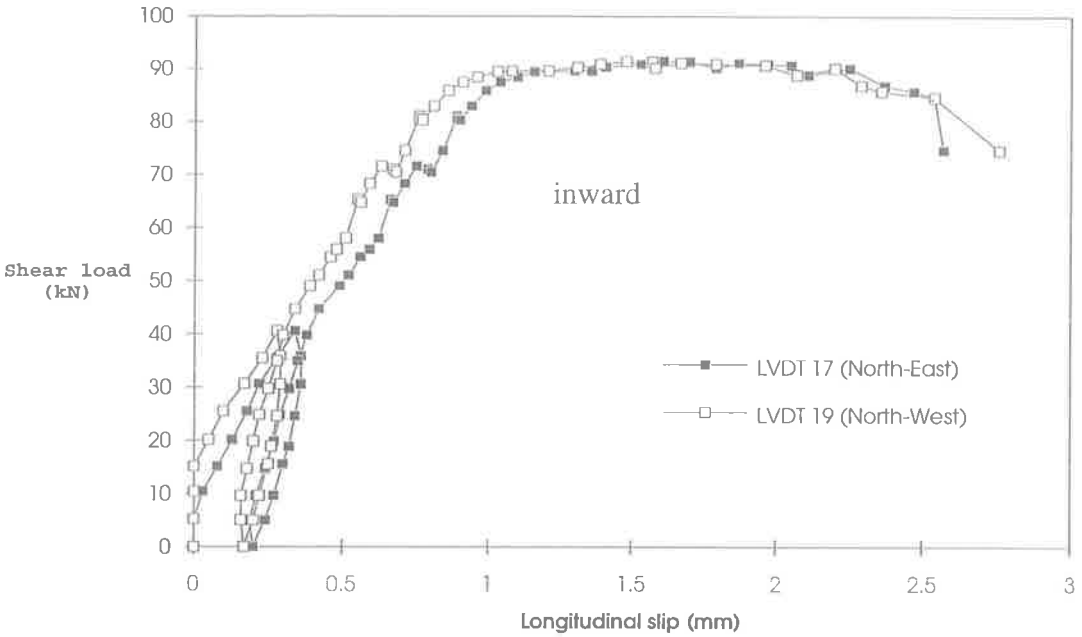

Fig. 8-84 Longitudinal slip at bottom bolt level near mid-shear span (Beam B12)

It can be seen in Table 8.25 that the longitudinal slip is a maximum at the supports and then gradually decreases towards the mid-span near mid-shear-span, where it is found to be less at the bottom bolt than that at the top bolts. This suggests that the slip strain at the bottom of the plate at mid shear-span is smaller than that of the top of the plate.

Table 8.25 Longitudinal slip at the maximum shear load (Beam B12)

Direction and vertical position	East side shear span		West side shear span	
	Position from East end support		Position from West end support	
	At 0 mm (mm)	At 880 mm (mm)	At 0 mm (mm)	At 880 mm (mm)
(1)	(2)	(4)	(5)	(6)
North top	+2.13	+1.88	+2.33	+1.79
North bottom	+2.20	+1.61	+2.39	+1.48
South bottom	+2.00		+3.07	-

(d) Longitudinal strain in plate at mid-span

The longitudinal strain in the plate at the mid-span was measured at both sides of the beam. The location of the electrical strain gauges are shown in Fig. 8-44(c). The variation of the longitudinal strain at different levels of the plate are shown in Figs. 8-85 to 8-88.

It can be seen in Fig. 8-85 that the strain is initially negative, that is compressive. The strain then becomes positive that is tensile and increases up to about 70 kN of shear load, after which it decreases to zero at about 90 kN of shear load. The strain then becomes compressive at almost constant shear load and increases as the load drops.

The strains at the other positions in the plate, in Figs. 8-86 to 8-88 are tensile throughout the loading history. The strains at the maximum shear load at the different levels are given in Table 8.26.

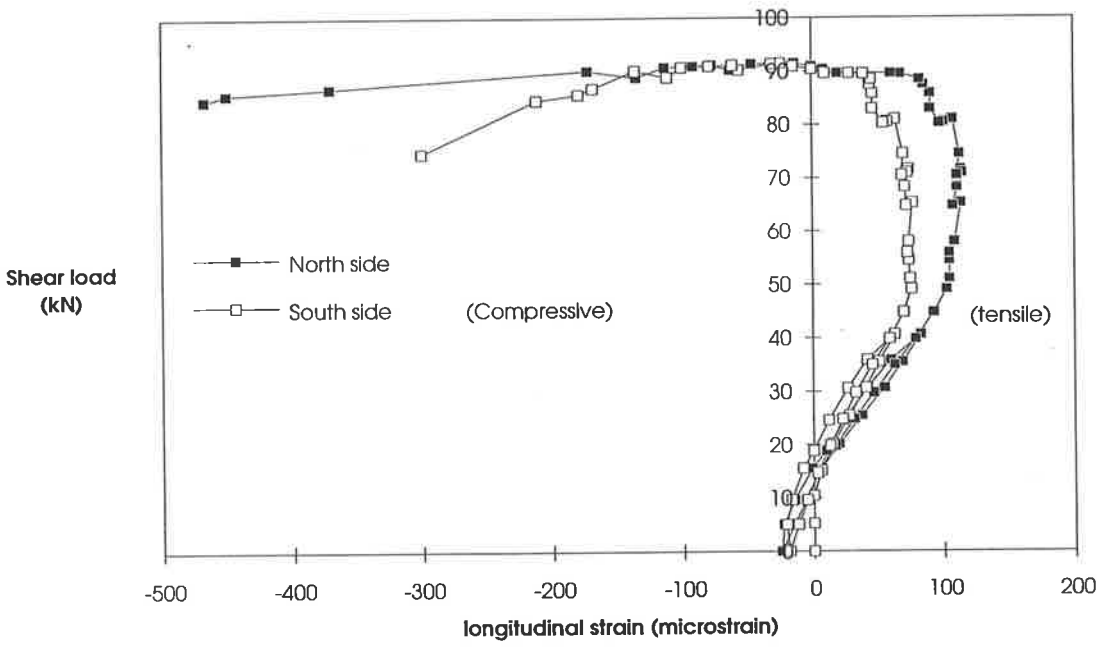

Fig. 8-85 Longitudinal strain at 33 mm level from plate top (Beam B12)

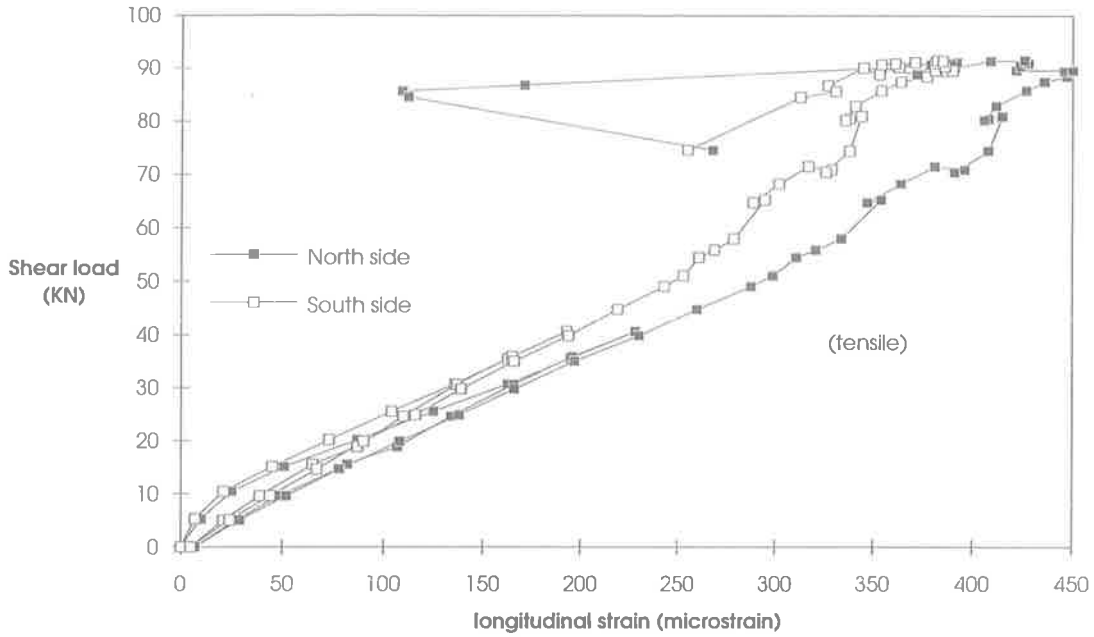

Fig. 8-86 Longitudinal strain at 59.3 mm level from plate top (Beam B12)

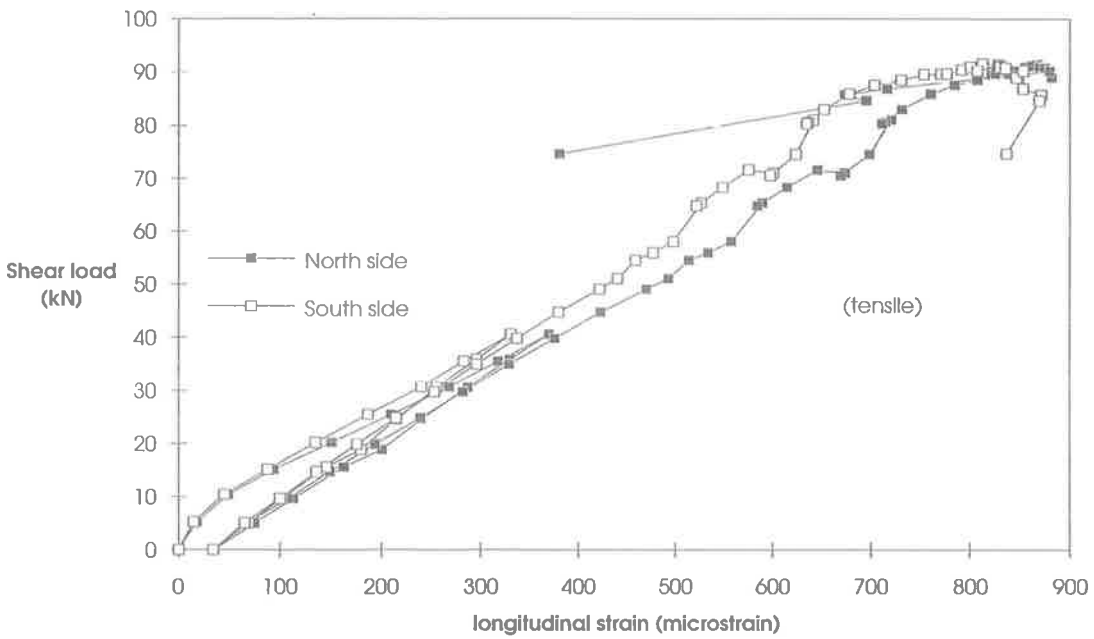

Fig. 8-87 Longitudinal strain at 85.6 mm level from plate top (Beam B12)

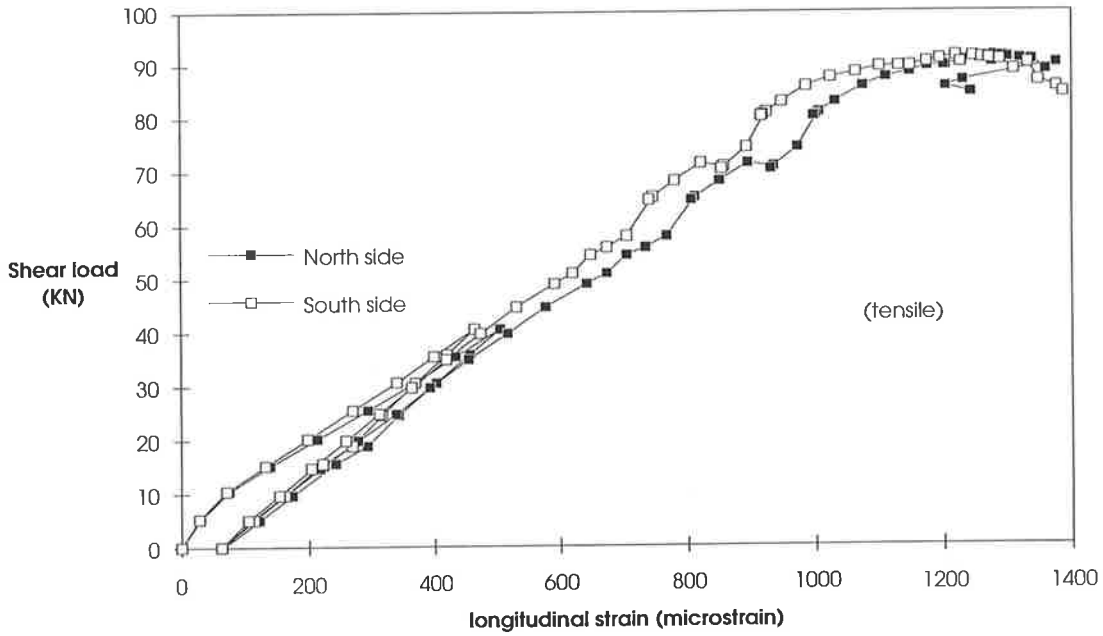

Fig. 8-88 Longitudinal strain at 112 mm level from plate top (Beam B12)

Table 8.26 Strain in plate at mid-span (Beam B12)

Location from plate top	North side (microstrain)	South side (microstrain)
(1)	(2)	(3)
33 mm	-13	-24
59.3 mm	+426	+382
85.6 mm	+868	+813
112 mm	+1279	+1246

(e) Strain profiles in both the RC beam and the plate at mid-span

The strain profiles in the RC beam and in the plate were determined by regression analysis, as discussed in Sect. 8.4.6.2.1, and are shown in Figs. 8-89 to 8-92 for a few load steps. It can be seen that the curvature in the RC beam is always larger than that of the plate. They both increase with the load but the curvature in the RC beam increases more rapidly.

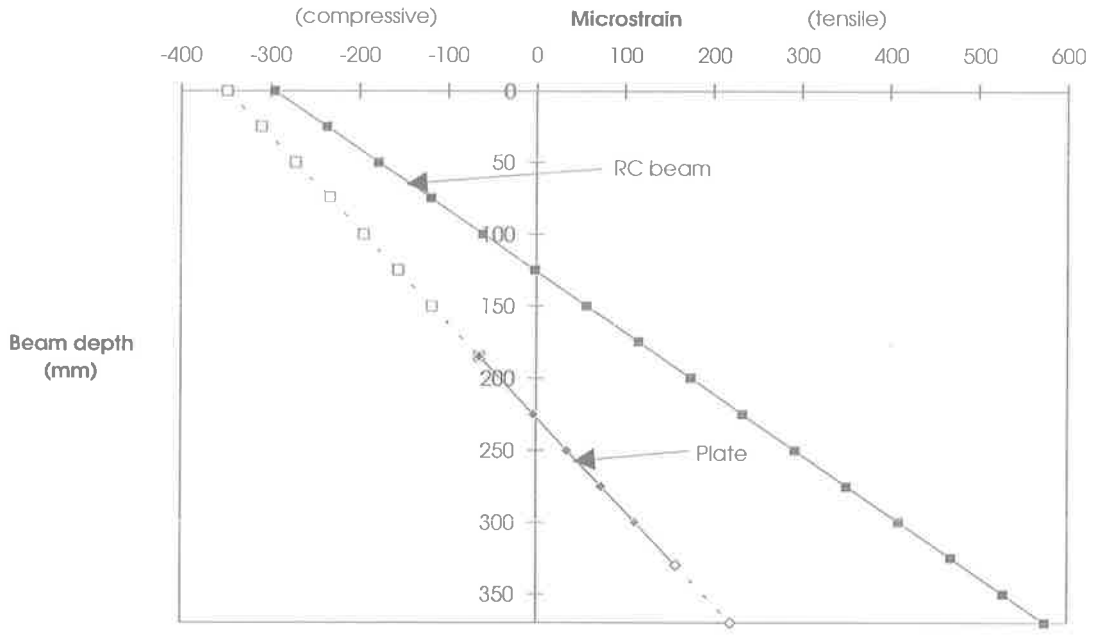

Fig. 8-89 Strain profiles at applied load of 10 kN (Beam B12)

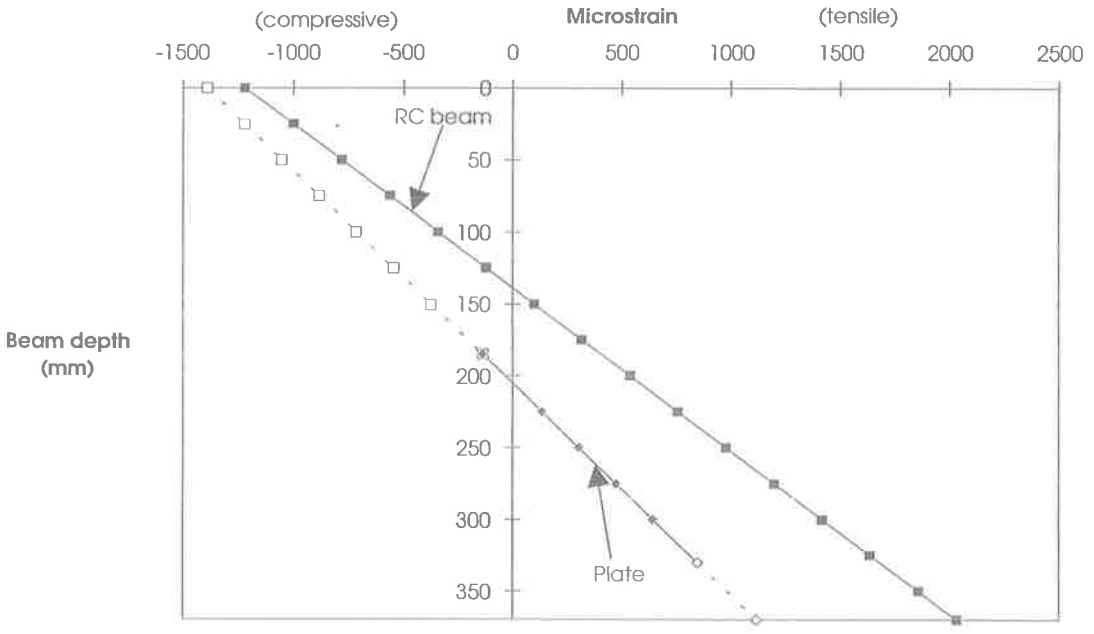

Fig. 8-90 Strain profiles at applied load of 100 kN (Beam B12)

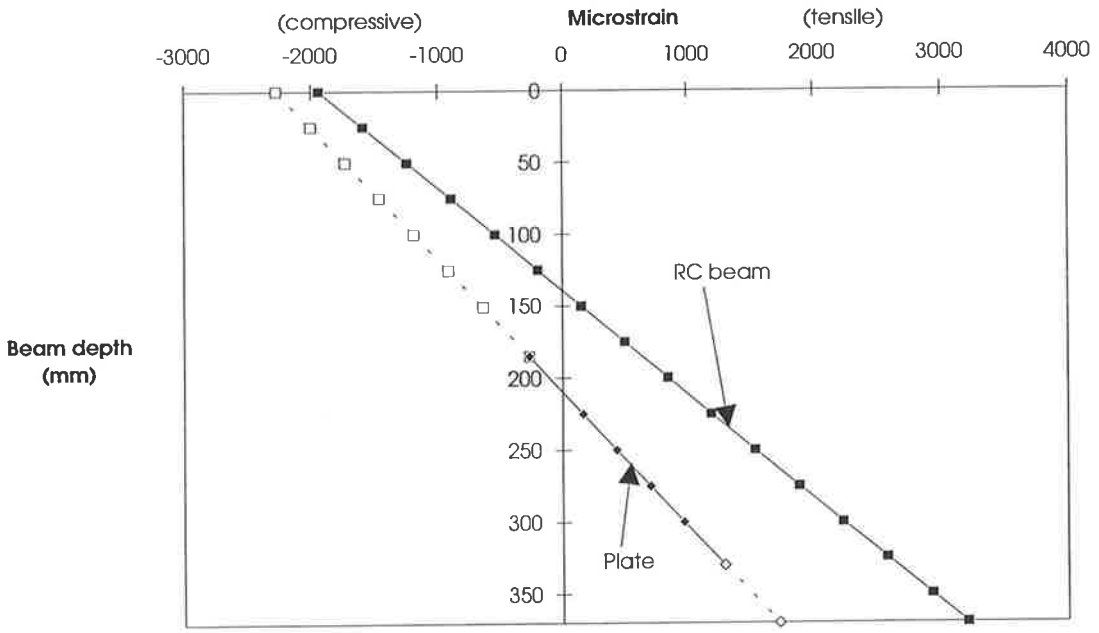

Fig 8-91 Strain profiles at applied load of 148 kN (Beam B12)

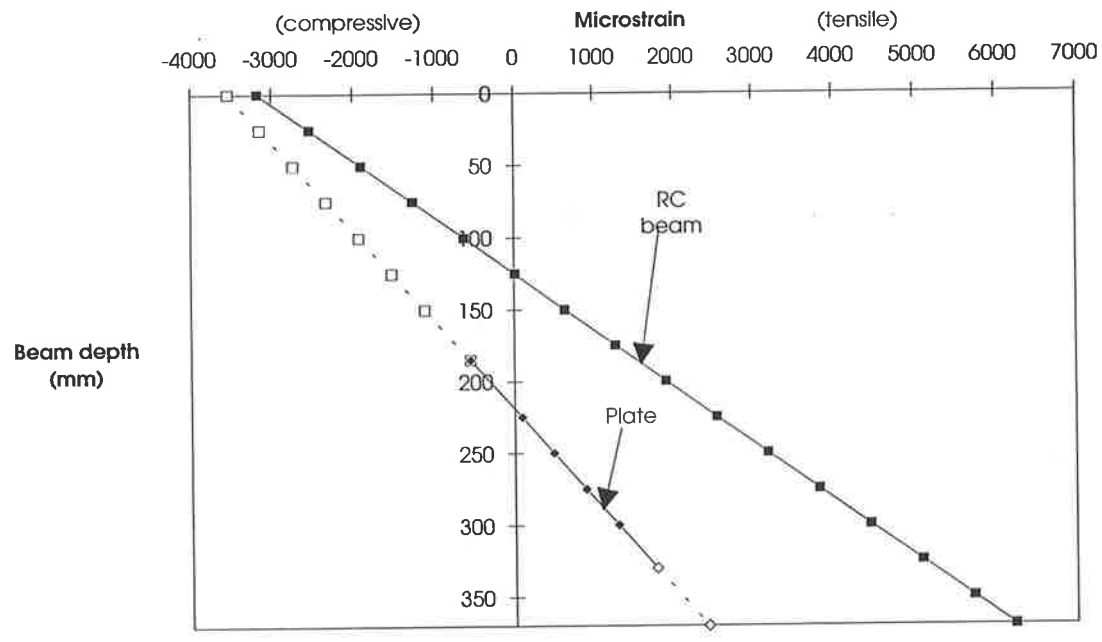

Fig. 8-92 Strain profiles at applied load of 183 kN (Beam B12)

(f) Longitudinal forces in each of the side plate at mid-span

The compressive and tensile forces in one side plate and their locations at various load steps are given in Table 8.27, with the notation are defined in Fig. 8-64. These forces were calculated following the same procedure as described in Sect. 8.4.6.2.1(d). It can be seen in Col. 2 that the neutral axis depth in the plate increases with the increase of applied load, for which the compressive forces in the plate also increase and causes lateral displacement in the plate as described before.

Figure 8-93 shows the strain and stress distribution in the plate at mid-shear span and at the maximum shear load. It can be seen in (b) that about one-fourth of the plate depth is in compression and the remainder is in tension; but that no portion of the plate is found to be fully yielded. The magnitudes and the positions of the resultant compressive force and tensile force in each of the side plate are shown in (c).

Table 8.27 Forces in one side plate (Beam B12)

Applied Load (kN)	n-a position y_{np} (mm)	Compressive force		Tensile force		Resultant force	
		P_{comp} (kN)	x (mm)	P_{ten} (kN)	y (mm)	P_{plate} (kN)	z (mm)
1	2	3	4	5	6	7	8
10	35.95	0.29	11.98	2.64	108.65	2.35	120.51
50	24.14	1.51	8.05	37.97	104.71	36.46	108.73
100	20.19	1.66	6.73	63.34	103.40	61.68	105.99
148	24.88	4.02	8.29	93.59	104.96	89.57	109.29
183	34.16	11.31	11.38	119.00	108.05	107.70	118.20

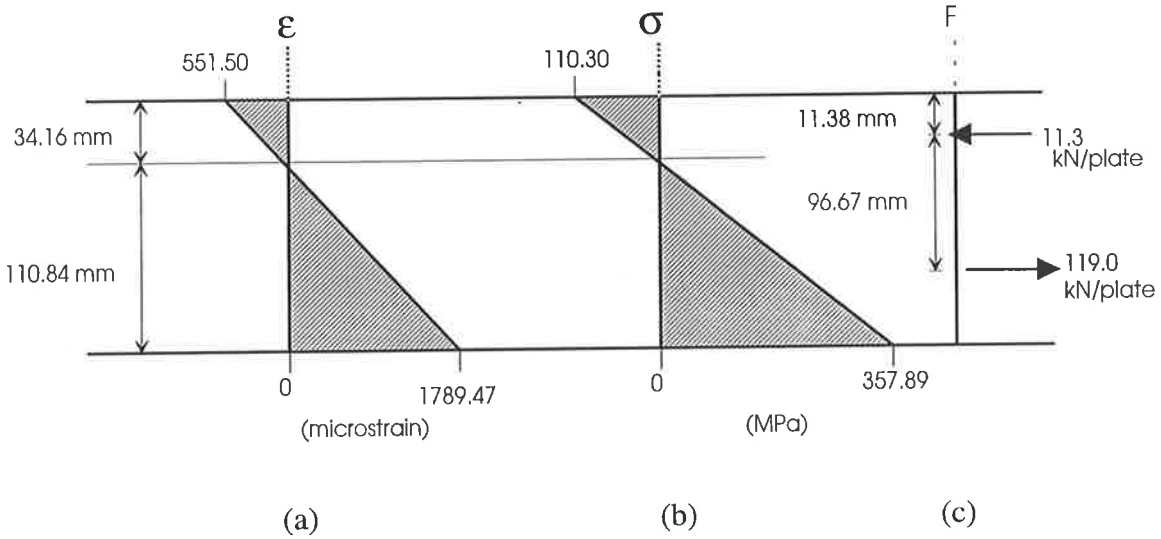

Fig. 8-93 Strain-stress-force distribution in plate at mid-span (Beam B12)

Figure 8-94 shows the relationship between the longitudinal force in the plate per side and the shear load. It can be seen in the figure that the variation is almost linear up to the maximum shear load of 91.5 kN. The maximum longitudinal shear force in the plate was 107.70 kN/side at the maximum shear load. It stays the same at the plateau of the shear load and then reduces as the shear load drops.

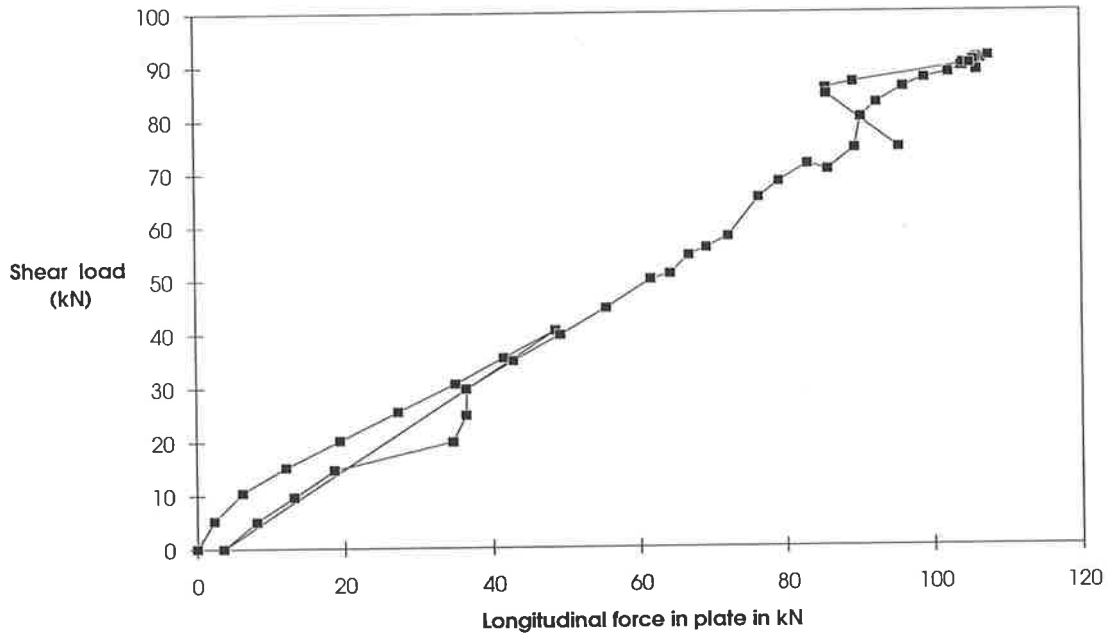

At each of the side plate

Fig. 8-94 Shear load vs longitudinal force in plate (Beam B12)

(g) Moment curvature relationship

The curvatures in both the RC beam and in the plate in Fig. 8-95 were determined from their respective strain profiles. It can be seen in the figure that the curvature in the plate is less than that of the concrete throughout the loading history of the beam. The curvature in the concrete increases rapidly after the maximum shear load due to the reduction of the strength of the RC beam. The maximum moment of 169.28 kNm was achieved in the beam at the maximum shear load.

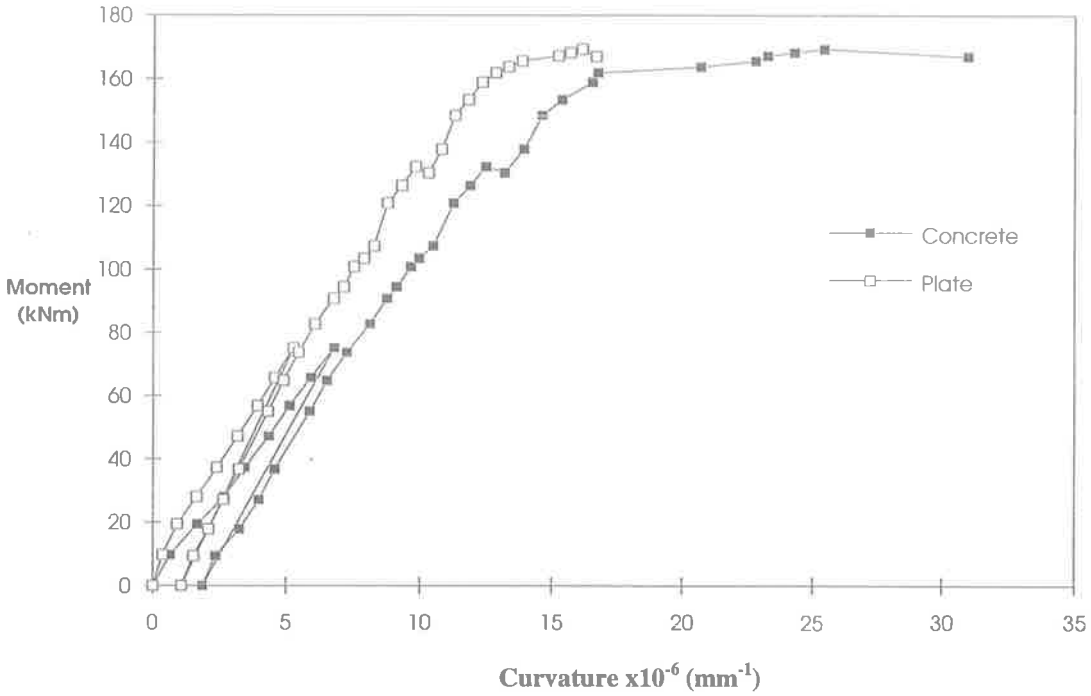

Fig. 8-95 Moment curvature curve (Beam B12)

8.4.6.2.3 Test 4 : Shallow depth plated beam B13

The set up of the beam is shown in P8.34. The load was applied to the beam in two cycles. In the first cycle, the increment of applied load was 10 kN. The flexural cracks in P8.35 were first formed at 20 kN of applied load (shear load of 10 kN). These cracks occurred in between the bolt positions and propagated almost vertically as the load increased. At 90 kN of applied load (shear load of 45 kN), the first cycle was completed and load was taken off gradually to zero.

In the second cycle, the increment of applied load was 20 kN up to 110 kN, then 10 kN until 160 kN, and then the load increments were replaced by 1 mm increments of deflection. Cracks propagated above the plate at 118 kN of applied load (shear load of 59 kN), as shown in P8.35. At one stage, the load dropped slightly at 179.5 kN of applied load (shear load of 89.8 kN), and then increased again. Spalling was noticed at 183 kN of applied load (shear load of 91.5 kN) and then the beam failed in flexure at 191.0 kN (shear load of 95.2 kN), as shown in P8.35.

At the end of the test, the plate was unscrewed from the RC beam and it was found that the bolt nearest to the mid span on the N-W shear span was sheared off, as shown in P8.36. It can be seen in P8.37 that the concrete surrounding the broken bolt was crushed due to dowel action.

The photographs of the other side and the shear spans can be seen in P8.38 to P8.40, where the ripping crack is visible in the latter. It is shown in P8.41 that the concrete surrounding the bolt was damaged even when the bolt was not sheared off.

(a) Shear load deflection Behaviour

Figure 8-96 shows the relationship between the shear load and deflection. It can be seen that the variation is almost linear up to point A (at about 80 kN of shear load) after which the stiffness of the beam reduces up to point B. The shear load then increases only a very small amount up to point C (at maximum shear load of 95.5 kN), after which the load drops as the beam fails in flexure.

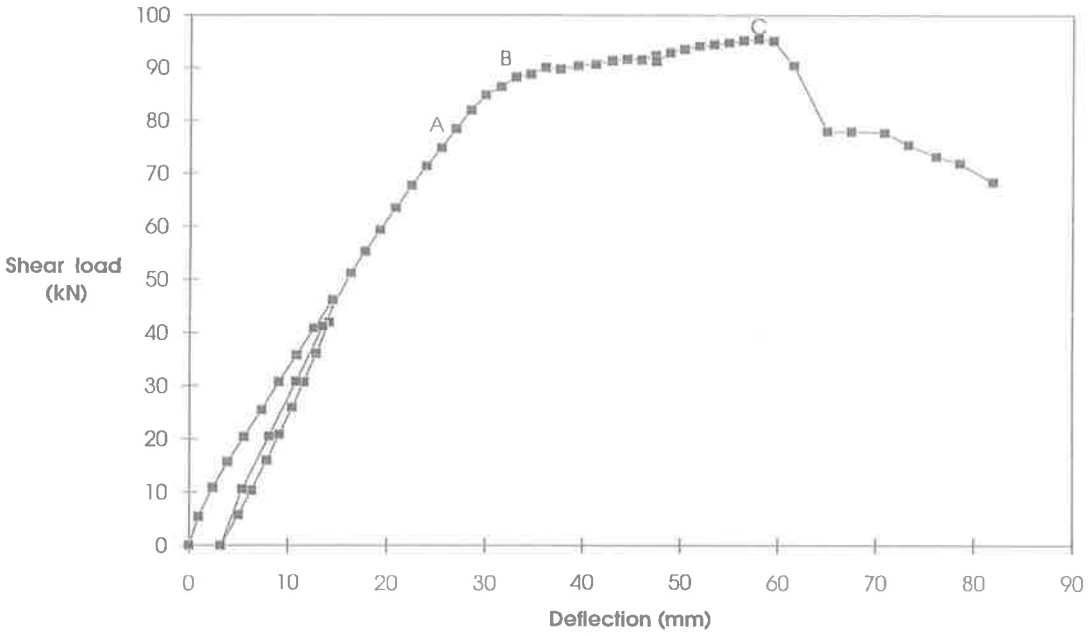

Fig. 8-96 Load deflection curve (Beam B13)

(b) Vertical slip

The instrumentation to measure vertical slip was shown in Fig. 8-45. It was measured at the bolt near the support, at the bolt near the mid-shear-span and at the bolt nearest to mid-span. The variations at these positions are shown in Figs. 8-97 to 8-99 respectively.

At the supports, the plate moves downward relative to the concrete and vertical slip increases rapidly at about 70 kN, as shown in Fig. 8-97. At mid-shear-span, the plate tends to move upwards slightly but then moves rapidly downwards, as shown in Fig. 8-98. Near mid-span, the plate tends to move upwards all the time, as shown in Fig. 8-99. Furthermore, in all the three positions, rapid increases in vertical slip occur almost at the same time at about 70 kN. Vertical slips at the maximum shear load are given in Table 8.28.

It can be seen in Table 8.28 that the vertical slip is maximum at the bolt nearest mid-span. Also, the vertical slip changes direction from downwards near the support to upwards near mid-span.

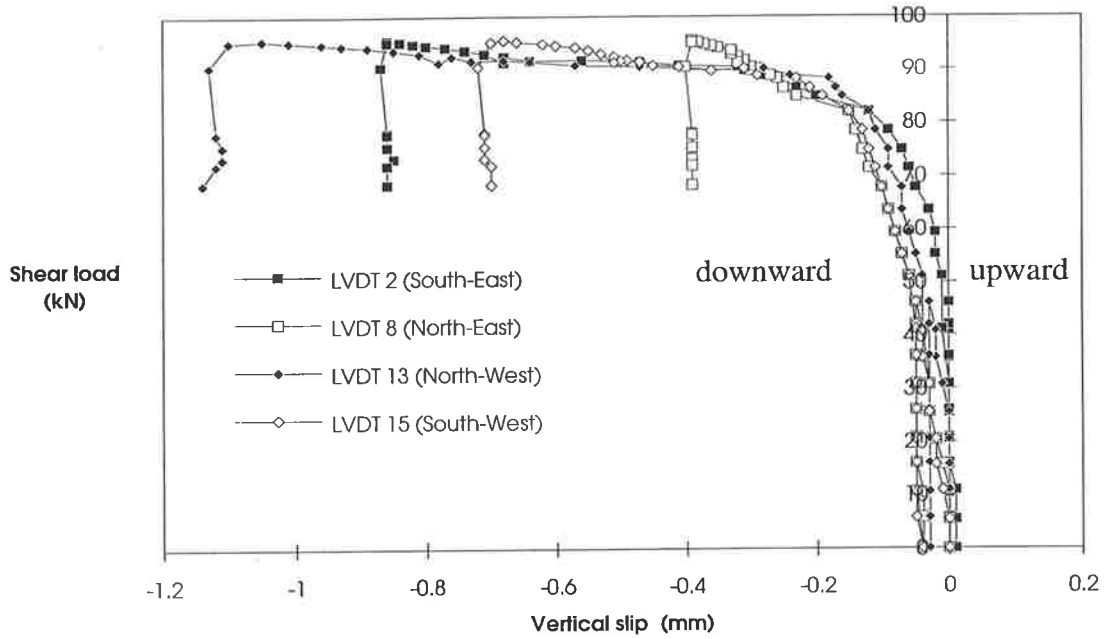

Fig. 8-97 Vertical slip at the bolt near the support (Beam B13)

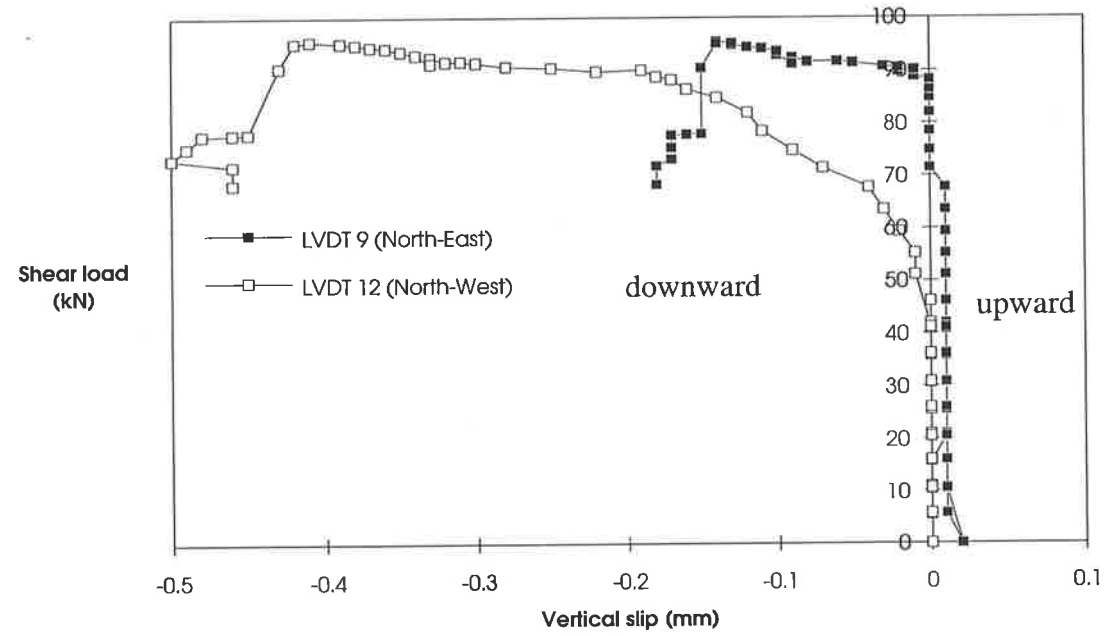

Fig. 8-98 Vertical slip near mid-shear-span (Beam B13)

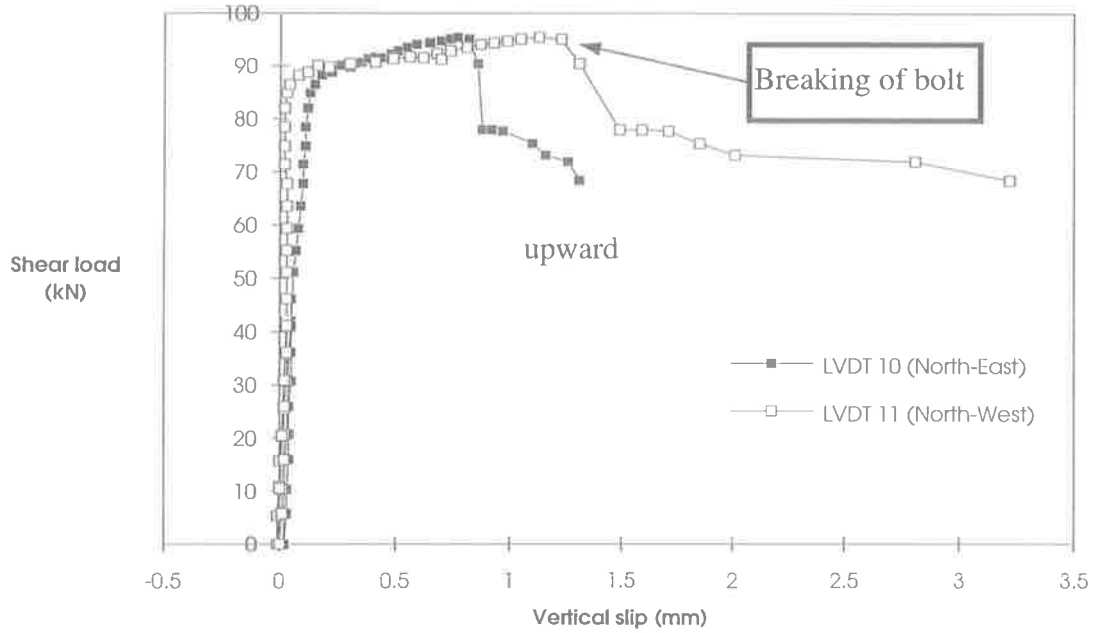

Fig. 8-99 Vertical slip at bolt nearest to mid-span (Beam B13)

Table 8.28 Vertical slip at the maximum shear load (Beam B13)

Direction	East shear span (Distance from East end support)			West shear span (Distances from West end support)		
	At 115 mm (mm)	At 975 mm (mm)	At 1610 mm (mm)	At 115 mm (mm)	At 975 mm (mm)	At 1610 mm (mm)
(1)	(2)	(3)	(4)	(5)	(6)	(7)
North side	-0.39	-0.14	+0.77	-1.05	-0.41	+1.13
South side	-0.86	-	-	-0.68	-	-

(c) Longitudinal slip

The instrumentation to measure longitudinal slip is shown in Fig. 8-45. The longitudinal slip was measured at the level of the bolts both over the supports and near mid-shear-span. They are shown in Figs. 8-100 and 8-101 respectively. The variation of longitudinal slip is similar to those found in the previous tests. The longitudinal slips at the maximum shear load are given in Table 8.29.

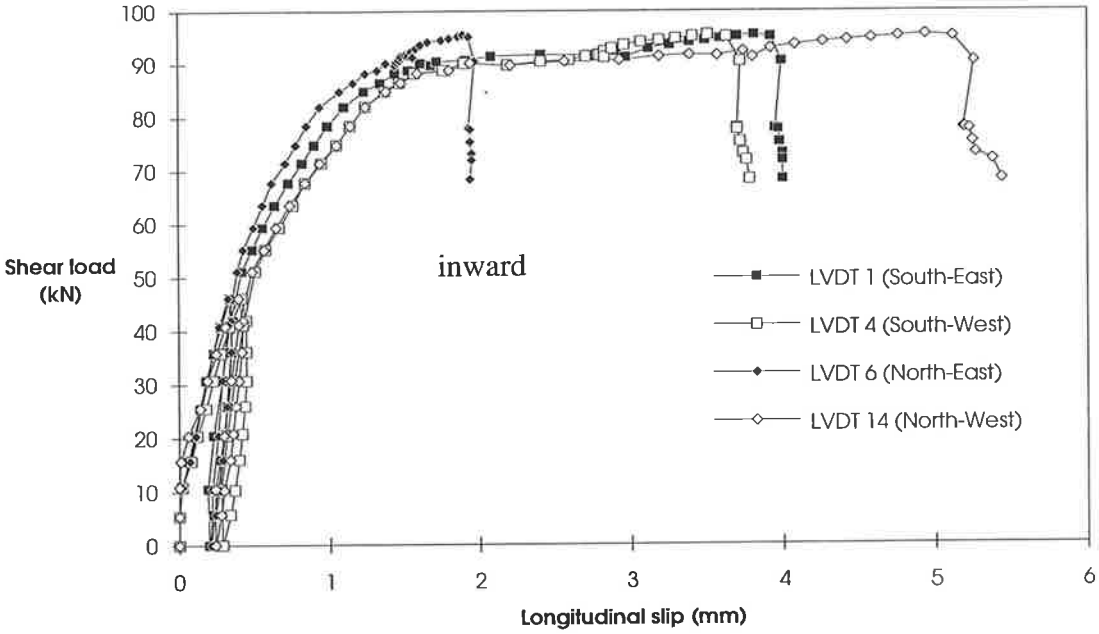

Fig. 8-100 Longitudinal slip at support end (Beam B13)

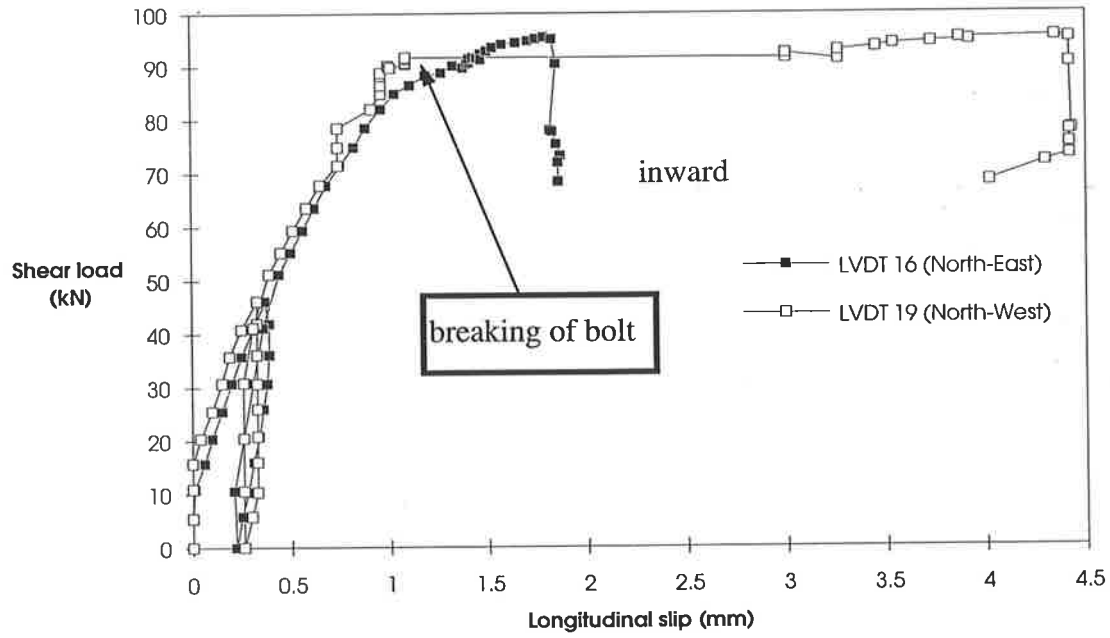

Fig. 8-101 Longitudinal slip at mid shear span (Beam B13)

It can be seen in Table 8.29 that the longitudinal slip at supports and mid-shear-span are almost the same, being a little larger at the supports. Also, the longitudinal slip at the support of the N-W shear span is found to be maximum where one bolt was sheared off.

Table 8.29 Longitudinal slip at maximum shear load (Beam B13)

Position	East side shear span		West side shear span	
	Position from East end support		Position from West end support	
	At 0 mm	At 945 mm	At 0 mm	At 945 mm
	(mm)	(mm)	(mm)	(mm)
(1)	(2)	(3)	(4)	(5)
North mid	+1.89	+1.79	+4.94	+4.35
South mid	+3.81	-	+3.51	-

(d) Longitudinal strain in plate at mid-span

Longitudinal strain was measured at different depths of the plate, as was shown in Fig. 8-45(c). The variation of longitudinal strains at different depths are shown in Fig. 8-102 to 8-105. It can be seen in Fig. 8-102 that the strains are negative, that is compressive throughout the loading history, whereas they are positive, that is tensile at the other positions in Figs. 8-103 to 8-105. The longitudinal strains at the maximum shear load are given in Table 8.30.

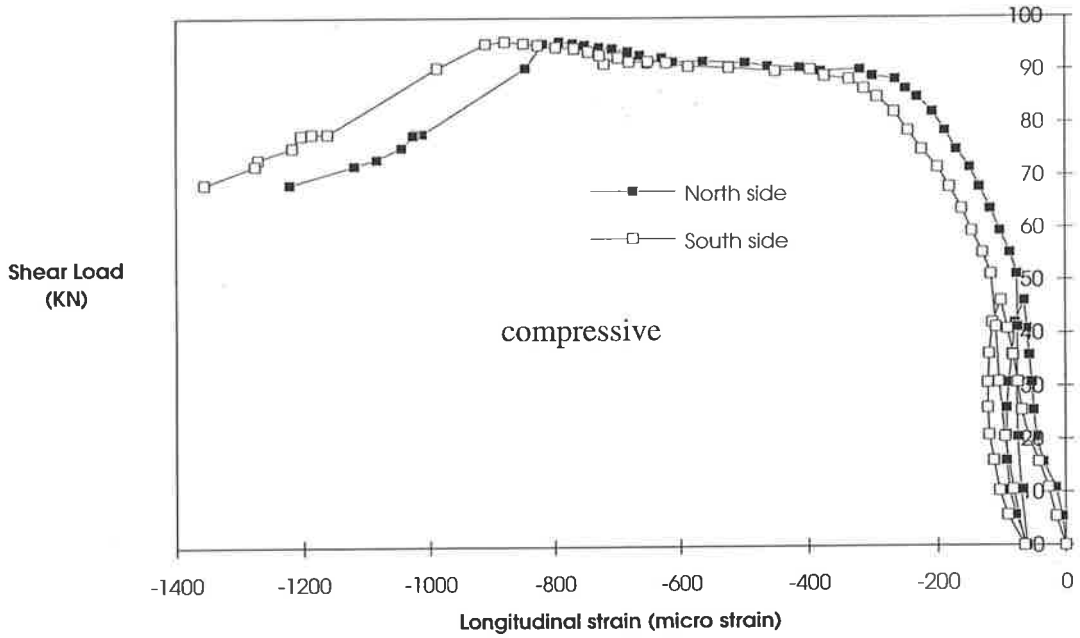

Fig. 8-102 Longitudinal strain in plate at 5mm level from top of plate (Beam B13)

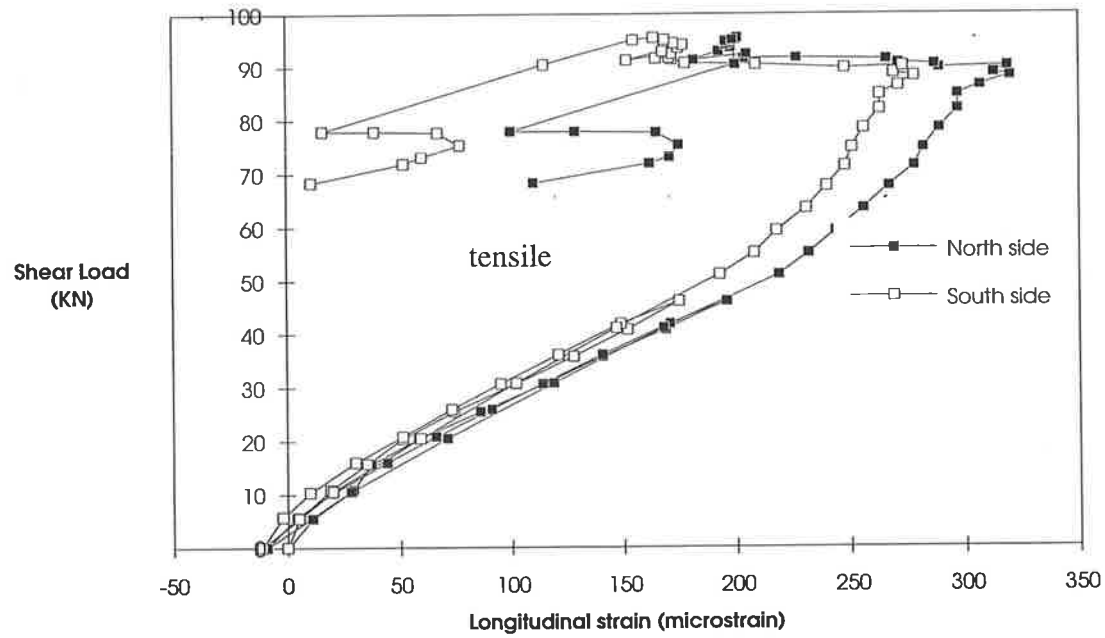

Fig. 8-103 Longitudinal strain in plate at 50 mm level from top of plate (Beam B13)

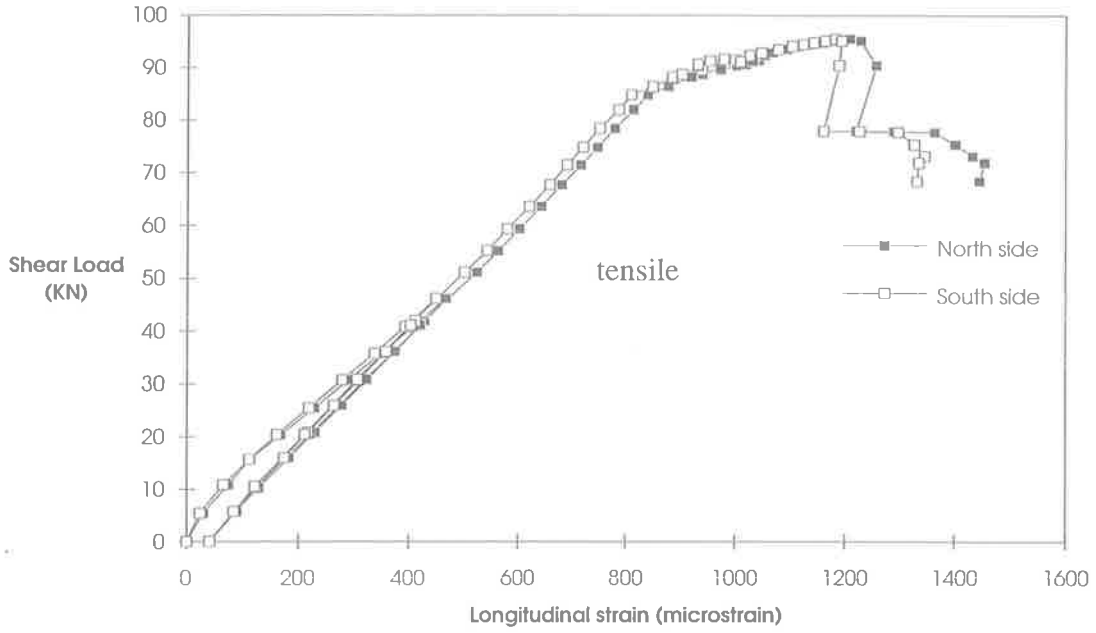

Fig. 8-104 Longitudinal strain in plate at 95 mm level from top of plate (Beam B13)

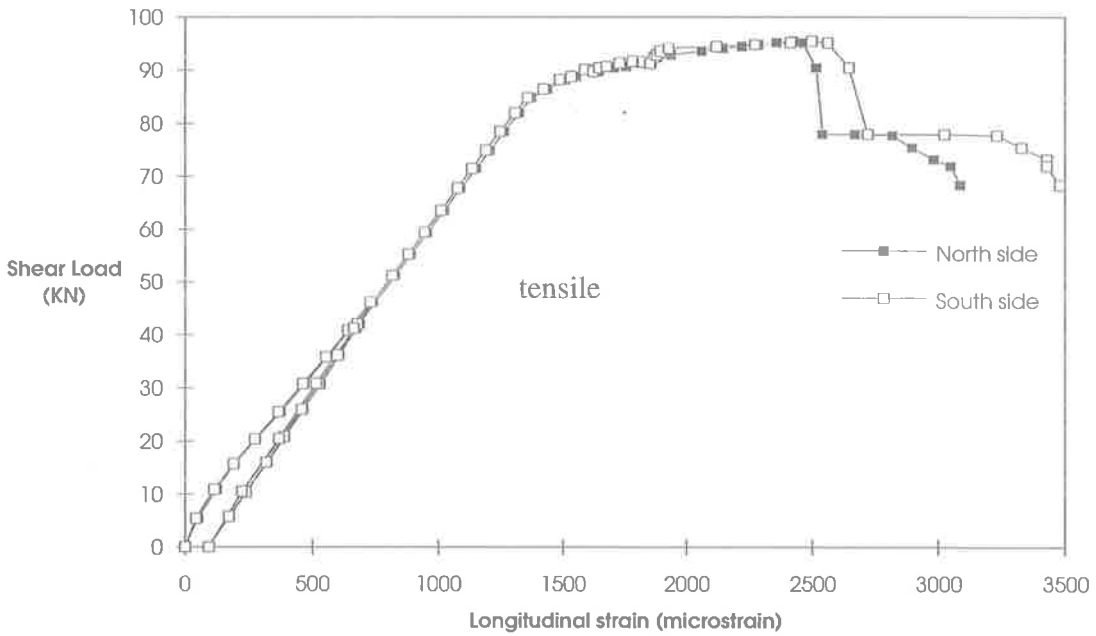

Fig. 8-105 Longitudinal strain in plate at 140 mm from top of plate (Beam B13)

Table 8.30 Strain in plate at mid-span at maximum shear load (Beam B13)

Location from plate top	North side (microstrain)	South side (microstrain)
(1)	(2)	(3)
5 mm	-792	-879
50 mm	+201	+164
95 mm	+1208	+1182
140 mm	+2423	+2498

(e) Strain profiles in the concrete and plate at mid-span

The strain profiles in the RC beam and the plate for various load levels are shown in Figs. 8-106 to 8-111. It can be seen in Fig. 8-106 that the curvature in the RC beam is higher than that of the plate. As the load increases, the curvatures in both the elements increases but its increment in the RC beam is higher, as can be seen in Figs. 8-107 to 8-111.

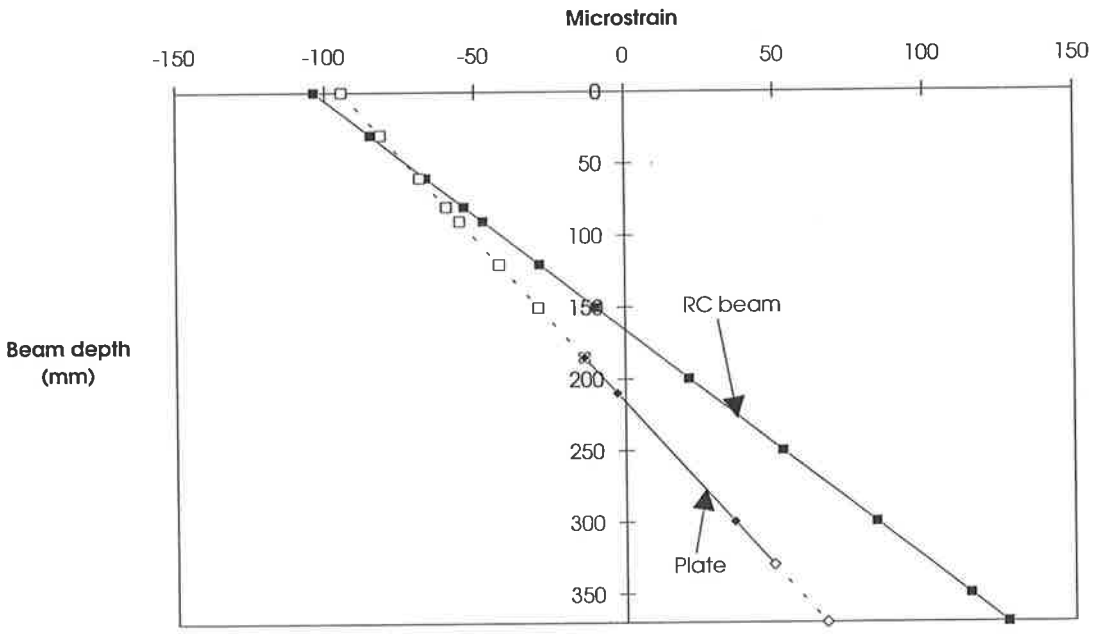

Fig. 8-106 Strain profiles at an applied load of 10.90 kN (Beam B13)

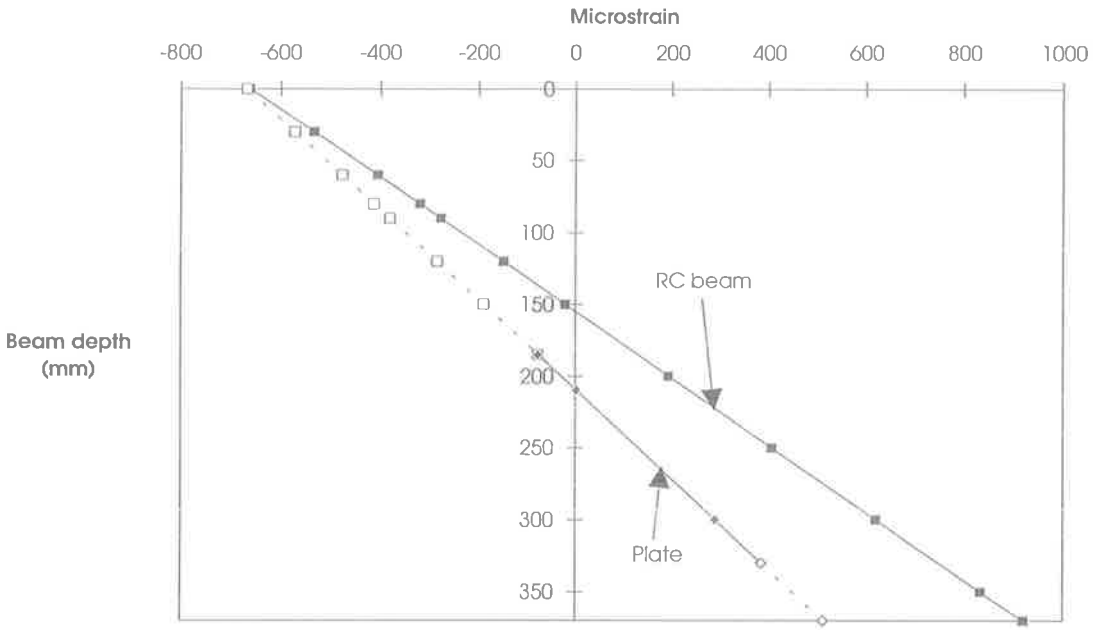

Fig. 8-107 Strain profiles at an applied load of 51 kN (Beam B13)

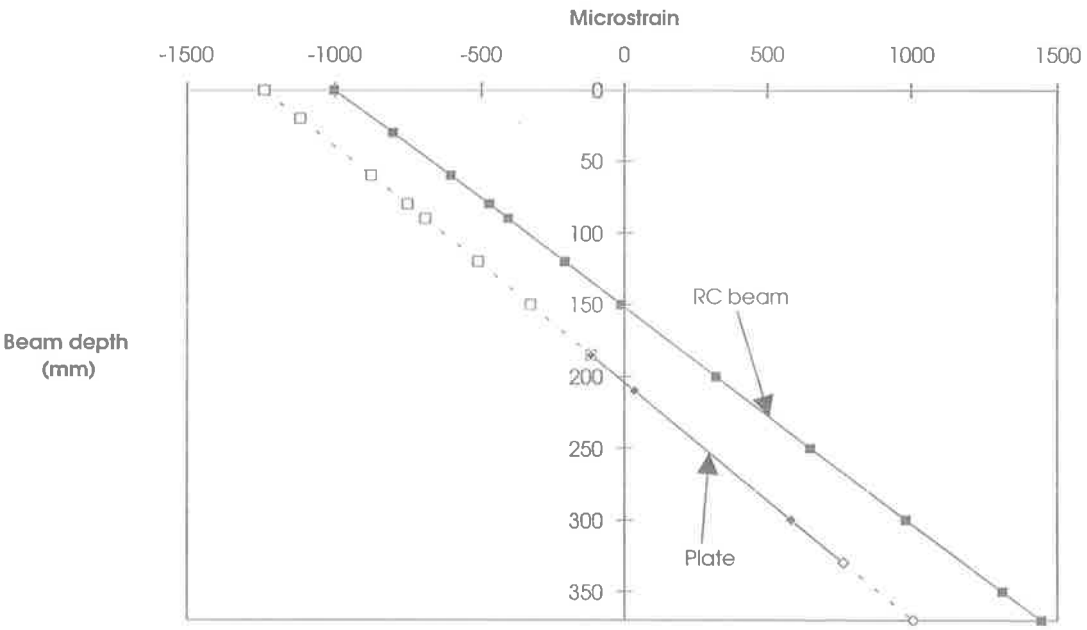

Fig. 8-108 Strain profiles at an applied load of 92.30 kN (Beam B13)

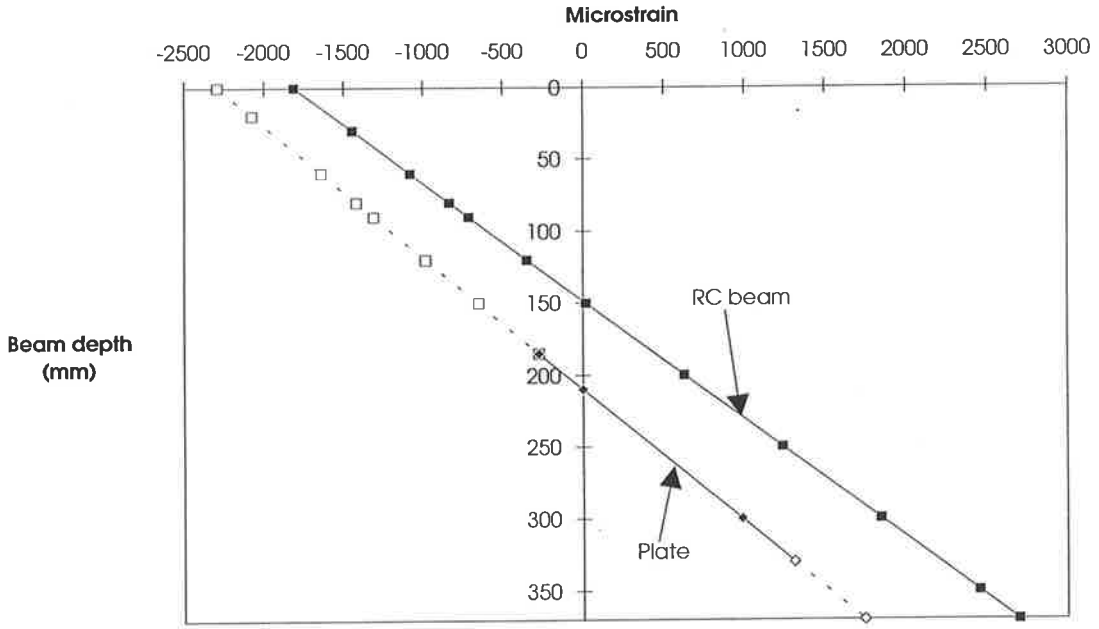

Fig. 8-109 Strain profiles at an applied load of 156 kN (Beam B13)

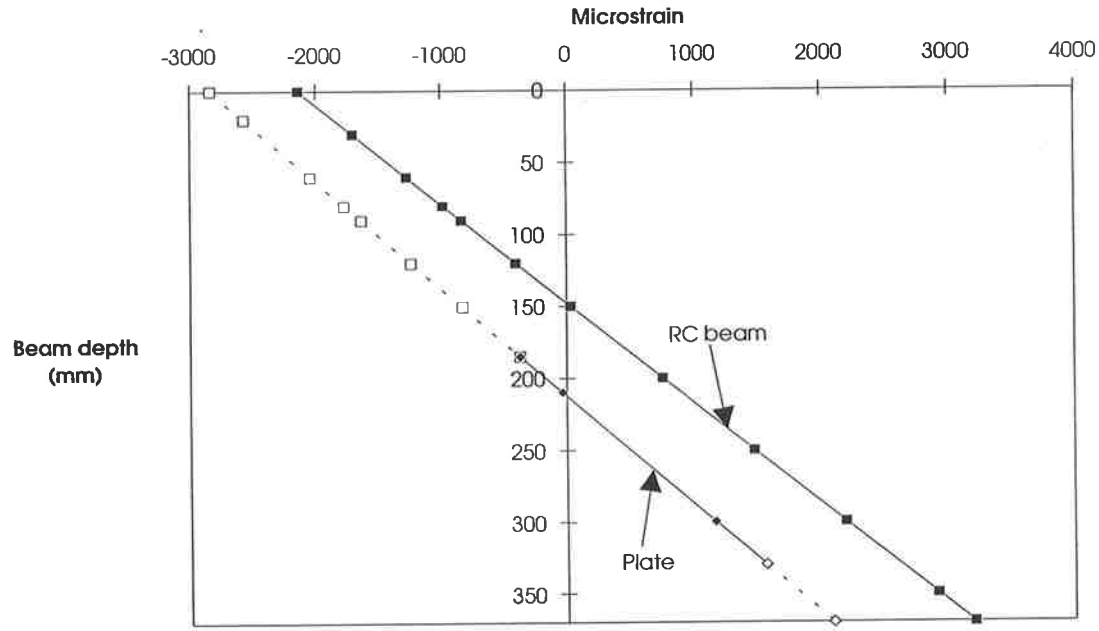

Fig. 8-110 Strain profiles at an applied load of 176 kN (Beam B13)

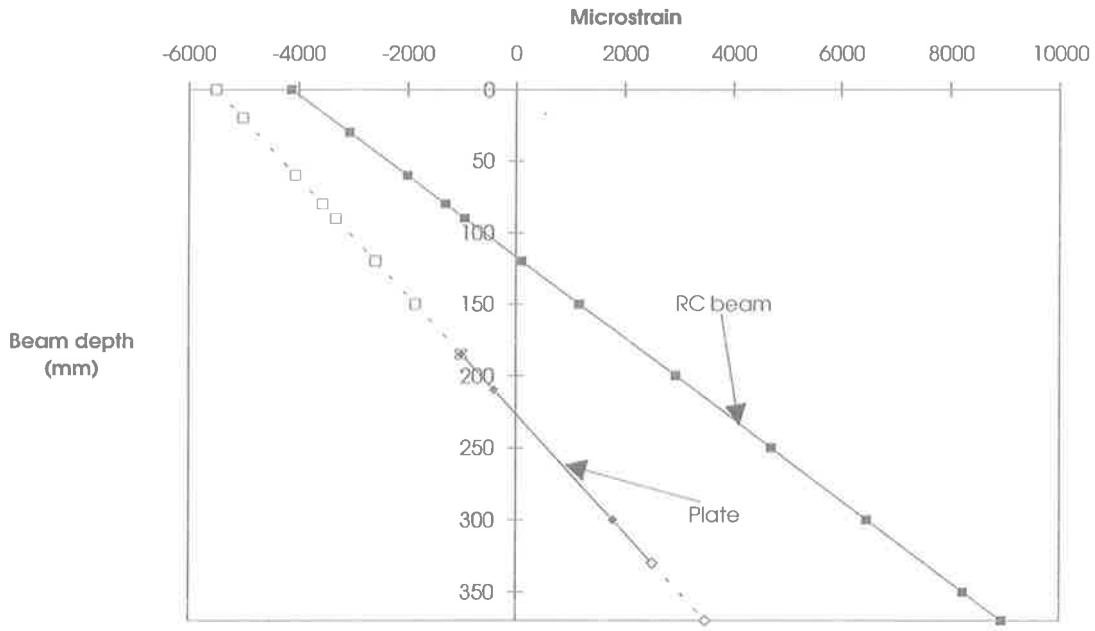

Fig. 8-111 Strain profiles at applied load of 191 kN (Beam B13)

(f) Longitudinal forces in each of the side plate at mid-span

The compressive and tensile forces in one side plate and their locations are given in Table 8.31. It can be seen in Col. 2 that the depth of neutral axis from the top of the plate is less than the vertical position of the bolt which was 75 mm. This means that the bolt did not fall in the compression region of the plate and that is why the plate was not buckled, as it was for beam B12.

The strain and stress distributions in the plate at the mid-span and at the maximum shear load are shown in Fig. 8-112. It can be seen in (b) that about one-fourth of the plate depth is in compression whereas the remainder is in tension. Also, only one-sixth of the plate depth is fully yielded in tension. The resultant compressive force and the tensile force are shown in (c).

Table 8.31 Forces in one side plate at mid span (Beam B13)

Applied Load (kN)	n-a position y_{np} (mm)	Compressive force		Tensile force		Resultant force	
		P_{comp} (kN)	x (mm)	P_{ten} (kN)	y (mm)	P_{plate} (kN)	z (mm)
1	2	3	4	5	6	7	8
10.90	31.24	0.26	10.41	3.39	107.08	3.13	114.96
51.0	24.34	1.13	8.11	27.89	104.78	26.75	108.88
92.3	19.11	1.33	6.37	57.75	103.04	56.42	105.32
156.9	24.95	4.08	8.32	94.43	104.98	90.35	109.34
176.5	27.57	6.09	9.19	110.55	105.86	104.76	111.50
191.0	41.63	25.28	13.88	146.14	108.82	120.86	128.68

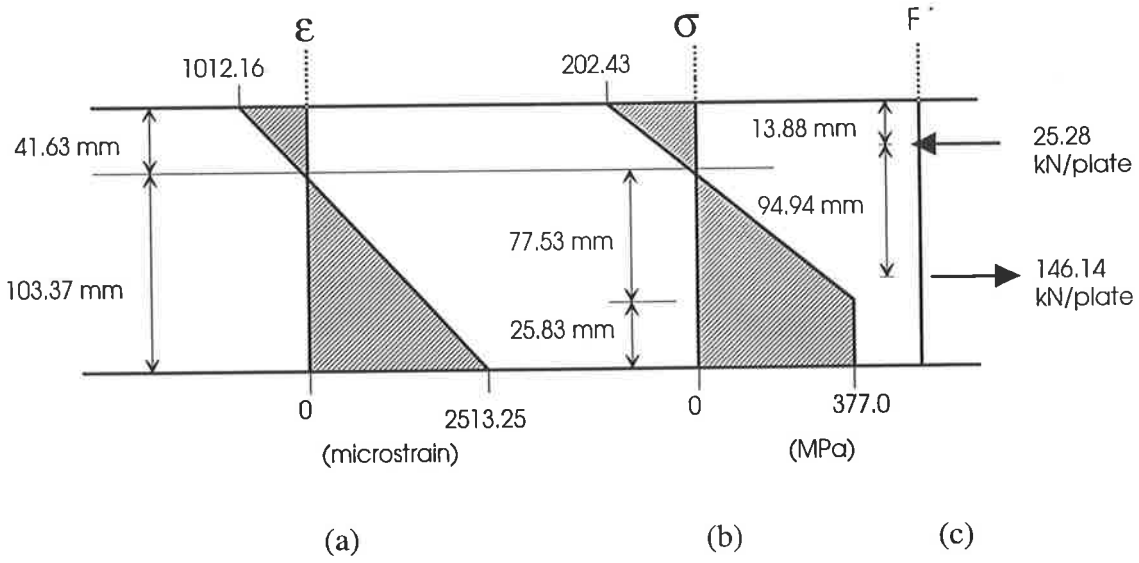

Fig. 8-112 Strain-stress-force distribution in plate (Beam B13)

Figure 8-113 shows the relationship between the longitudinal force in the plate per side and the shear load. The variation is almost linear up to about 90 kN of shear load, at which level plateau of shear load occurs as was shown in Fig. 8-96. At this plateau level, the longitudinal force in the plate stays almost same. However, the longitudinal force then increases to the maximum of 120.86 kN, when the shear load reaches to the maximum of 95.5 kN. As then the shear load drops up to 74 kN, the longitudinal force in the plate reduces to 107.40 kN. The longitudinal force can be seen increases thereafter with reduction of the shear loads.

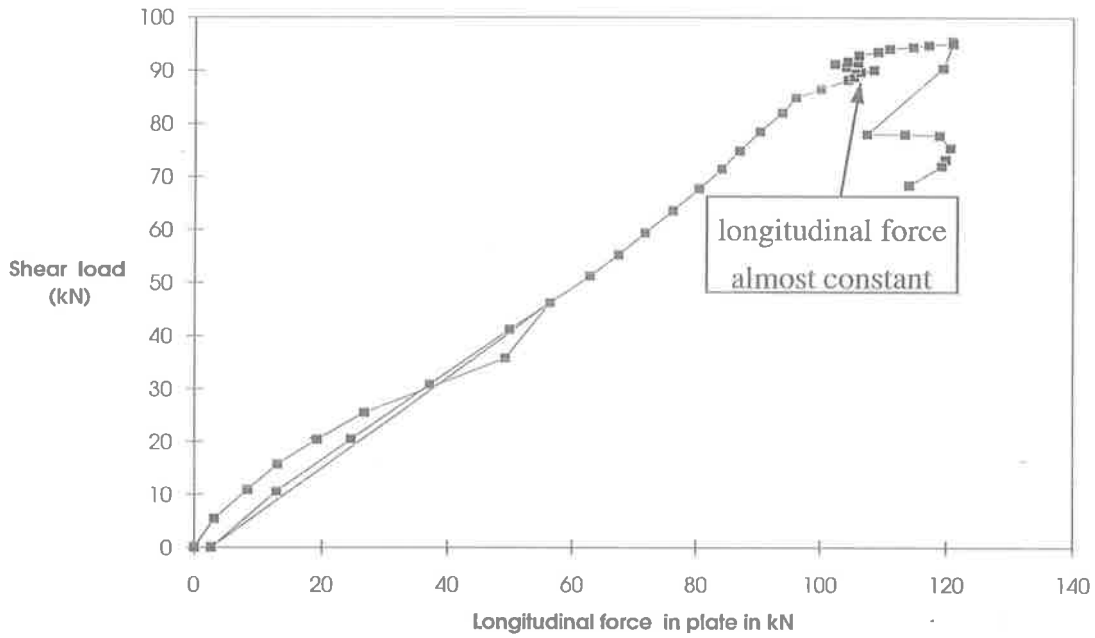

At each of the side plate

Fig. 8-113 Shear load vs longitudinal force in plate per side (Beam B13)

(g) Moment curvature relationship

Figure 8-114 shows the relationship between the moment and the curvature of the plate and the concrete element. The variation is similar to the previous tests. The maximum moment is 176.68 kNm.

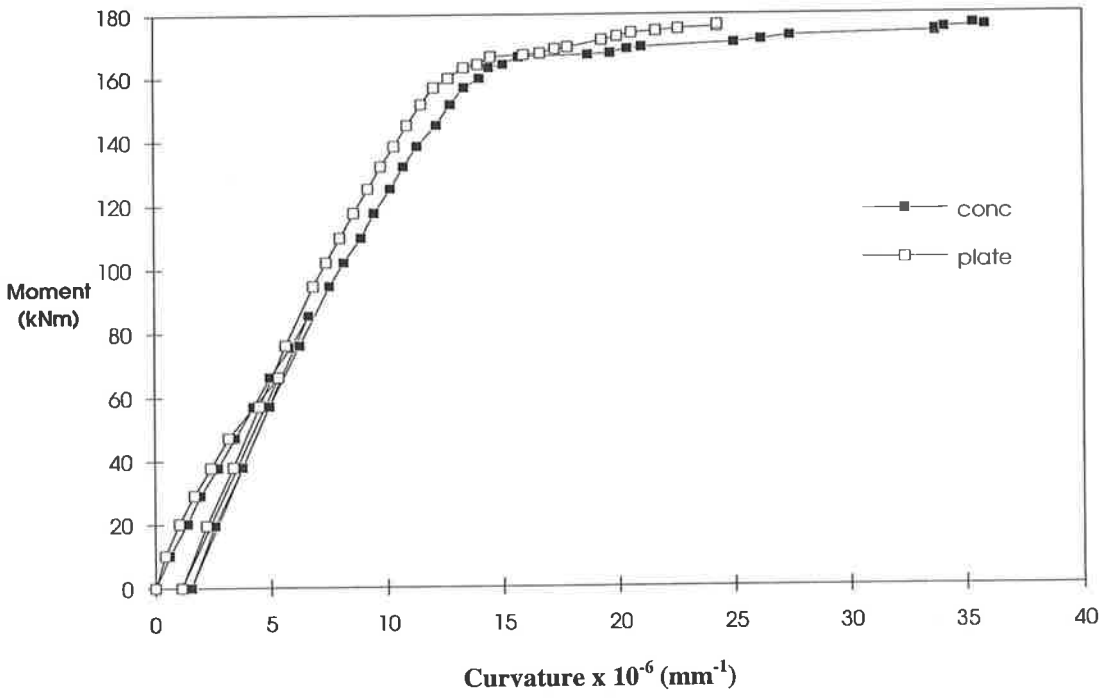

Fig. 8-114 Moment-curvature curve (Beam B13)

8.4.6.2.4 Test 5 : Shallow depth plated beam B24

The set up of the beam is shown in P8.42. The load was applied in two cycles. In the first cycle, the increment of applied load was 10 kN. The first flexural cracks were noticed at 20 kN of applied load (shear load of 10 kN), as shown in P8.43. As load was increased further, the flexural cracks formed between the bolt positions. At 100 kN of applied load the first cycle of loading was finished and load was taken off to zero gradually.

In the second cycle, the increment of applied load was 25 kN up to a total of 100 kN, then increments of 10 kN up to a total load of 160 kN, after which the load increments were replaced by 1 mm increments of deflection. Cracks propagated above the plate at 113 kN of applied load (shear load of 56.5 kN), as shown in P8.43. Ripping cracks were noticed through the bolt positions at 120 kN of applied load (shear load of 60 kN). Spalling in the concrete was noticed at 196.20 kN of applied load (shear load of 98.1 kN), after which load dropped to 195 kN (shear load of 97.5 kN). A photograph at this stage can be seen in P8.44. At 185.3 kN of applied load (shear load 92.7 kN), there occurred a large amount of concrete crushing, as shown in P8.45, and then the load dropped to 154.0 kN.

At the end of the test, the plate was unscrewed from the RC beam and photographs were taken at all the shear spans, which are presented in P8.46 to P8.52. In all the photographs, the ripping crack is visible. It can be seen in P8.53 that the concrete surrounding a bolt was damaged, although the bolt did not shear off.

(a) Load-deflection behaviour

Figure 8-115 shows the relationship between the load and the deflection. It can be seen that the variation is almost linear up to point A (at about 80 kN of shear load), after which the shear load increases gradually up to the maximum at point B. The strength of the beam then reduces and the beam failed in flexure at point C.

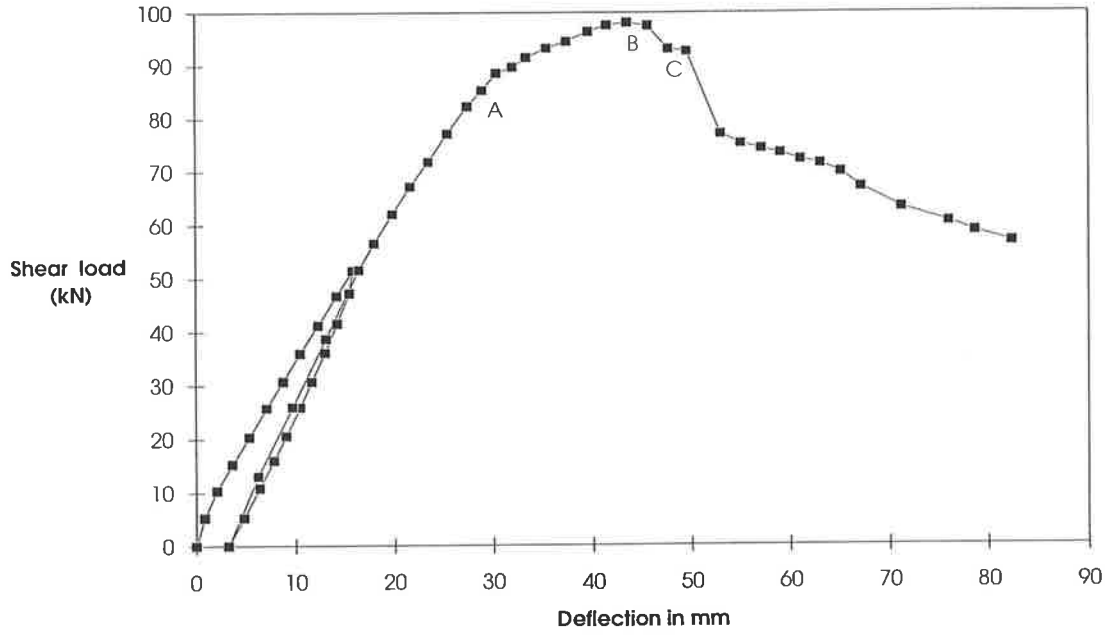

Fig. 8-115 Load deflection curve (Beam B24)

(b) Vertical slip

The variation of vertical slip with the shear load near the support bolt, near the mid-shear-span bolt and at the bolt nearest mid-span are shown in Figs. 8-116 to 8-118. It can be seen in Fig. 8-116 that the magnitude of the vertical slip is very small and hence the variation is not clear. As the vertical slip is higher towards the mid-span, the variation becomes clearer in Figs. 8-117 and 8-118. The vertical slips at the maximum shear load are given in Table 8.32.

It can be seen in Table 8.32 that the vertical slip is maximum at the nearest bolt of the mid- span. Also, the vertical slip changes direction from downwards near the supports to upwards near mid-span.

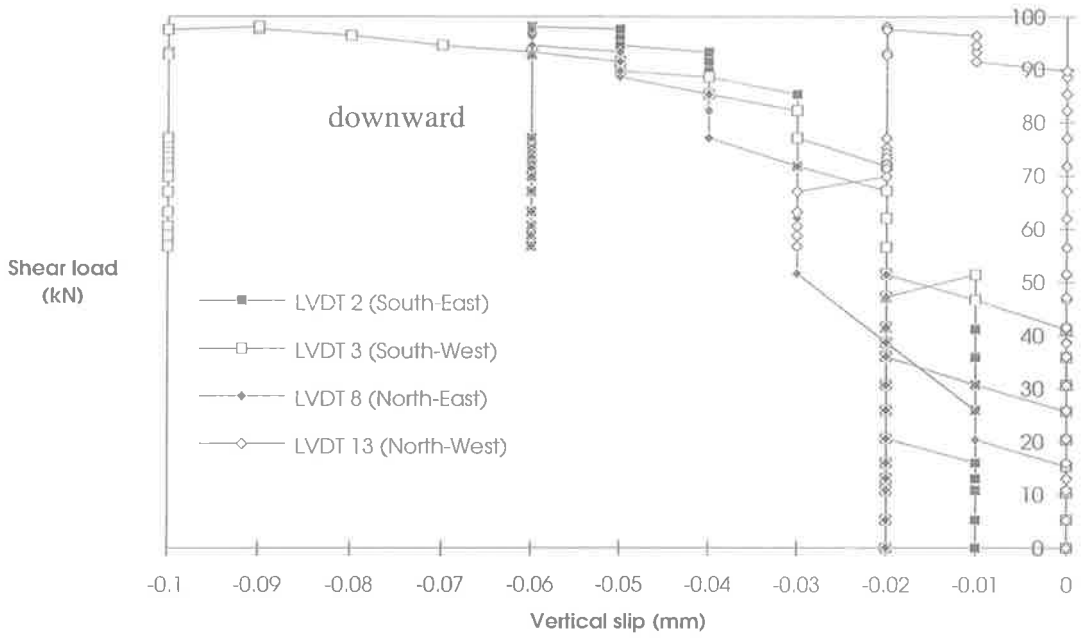

Fig. 8-116 Vertical slip at the bolt near support (Beam B24)

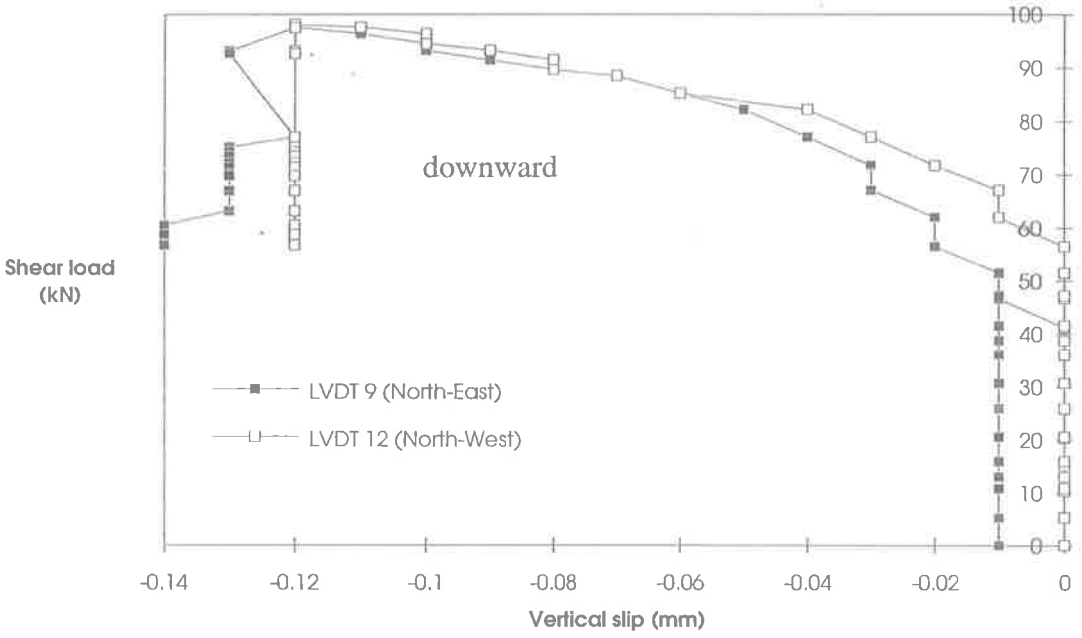

Fig. 8-117 Vertical slip near mid-shear span (Beam B24)

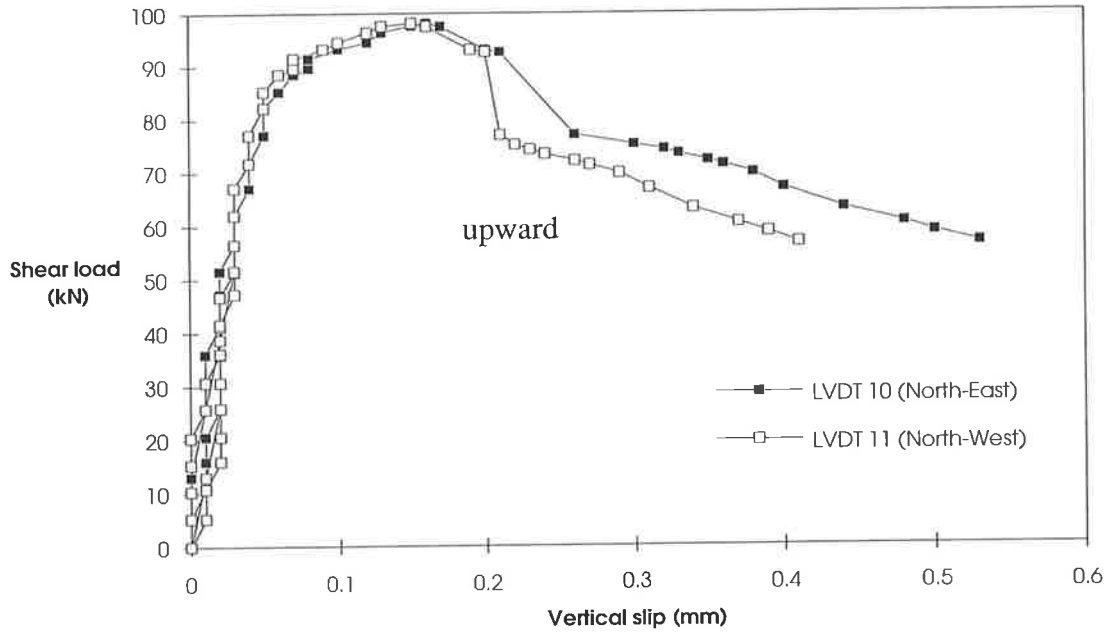

Fig. 8-118 Vertical slip at the end bolt of the shear span (Beam B24)

Table 8.32 Vertical slip at the maximum shear load (Beam B24)

Direction	East shear span (Distance from East end support)			West shear span (Distances from West end support)		
	At 0 mm (mm)	At 920 mm (mm)	At 1670 mm (mm)	At 0 mm (mm)	At 920 mm (mm)	At 1670 mm (mm)
(1)	(2)	(3)	(4)	(5)	(6)	(7)
North side	-0.06	-0.12	+0.16	-0.02	-0.12	+0.15
South side	-0.06			-0.09		

(c) Longitudinal slip

The longitudinal slip at the levels of the bottom and top bolts over the supports are shown in Figs. 8-119 and 8-120 respectively. It can be seen that there is no slip at the low load levels, after which the longitudinal slip increases gradually up to the maximum shear load. The longitudinal slip is found to be almost constant as the applied load reduces. A similar

variation can be seen at the other positions, as shown in Figs. 8-121 and 8-122. The longitudinal slips at the maximum shear load are given in Table 8.33.

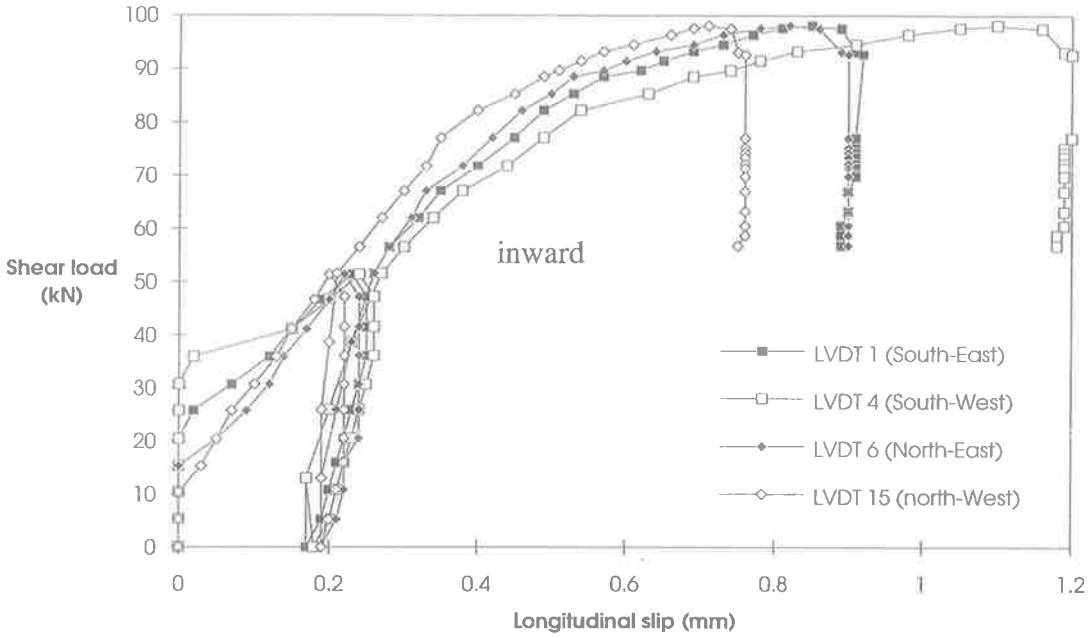

Fig. 8-119 Longitudinal slip at bottom bolt level over the support (Beam B24)

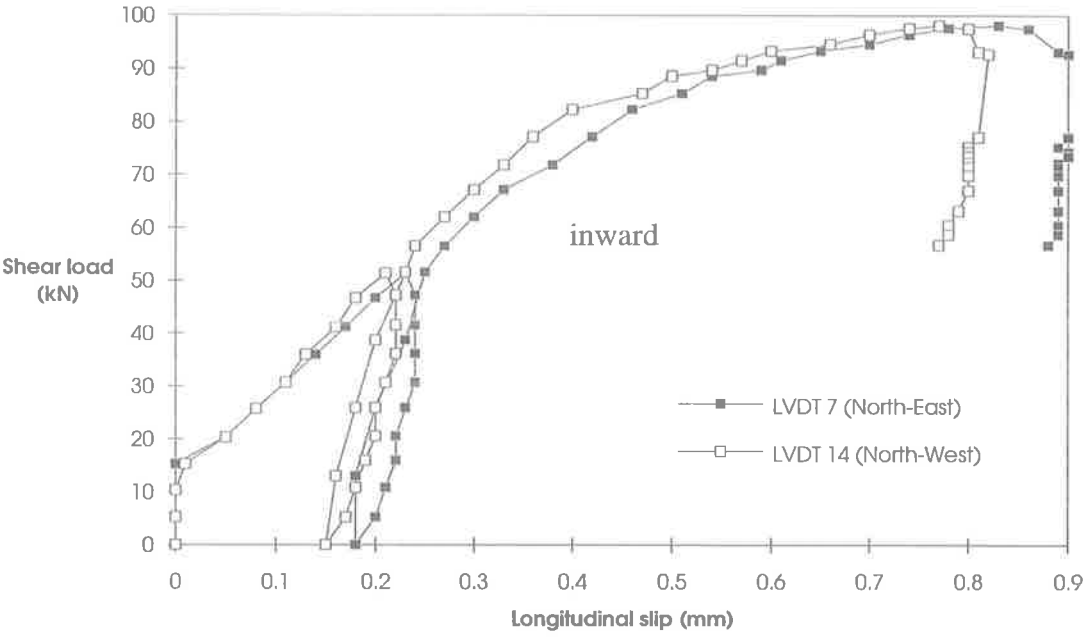

Fig. 8-120 Longitudinal slip at the top bolt level over the support (Beam B24)

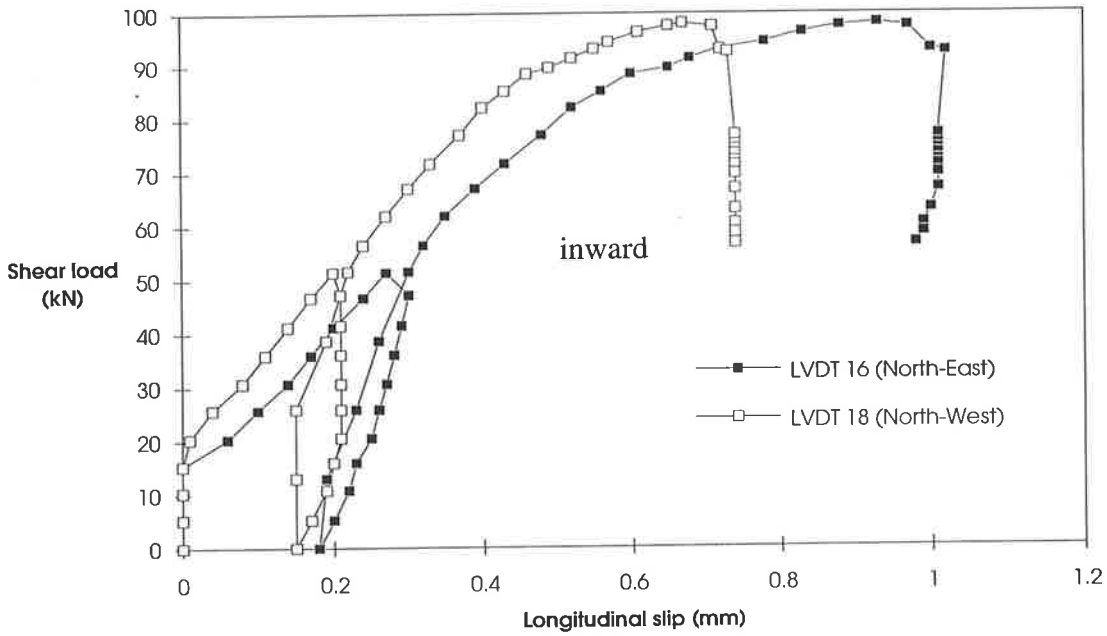

Fig. 8-121 Longitudinal slip at top bolt level near mid-shear span (Beam B24)

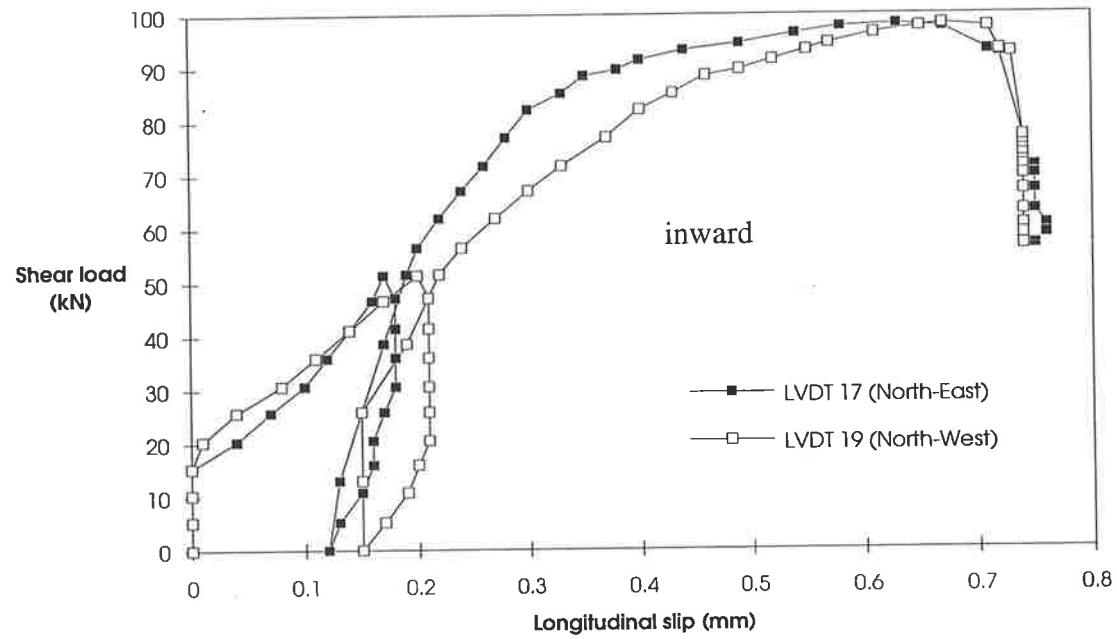

Fig. 8-122 Longitudinal slip at bottom bolt level near mid-shear span (Beam B24)

It can be seen in Table 8.33 that the longitudinal slip at the bottom bolt at the support is slightly larger than the top. In the case of the bottom bolt near mid-shear span, the longitudinal slip is smaller than the top.

Table 8.33 Longitudinal slip at the maximum shear load (Beam B24)

Direction and vertical position	East side shear span		West side shear span	
	Position from East end support		Position from West end support	
	At 0 mm (mm)	At 890 mm (mm)	At 0 mm (mm)	At 890 mm (mm)
(1)	(2)	(3)	(4)	(5)
North top	+0.83	+0.93	+0.77	+0.67
North bottom	+0.82	+0.63	+0.71	+0.52
South bottom	+0.85		+1.10	

(d) Longitudinal strain in plate at mid-span

The longitudinal strains at different depths of the plate are shown in Figs. 8-123 to 8-126. The strain in Fig. 8-123 at the top of the plate is very close to zero. This suggests that the neutral axis in the plate lies very close to the top of the plate and, as such, the strains at the other depths of the plate are in tension, as can be seen in their respective figures. The strains at the different depths and at the maximum shear load are given in Table 8.34.

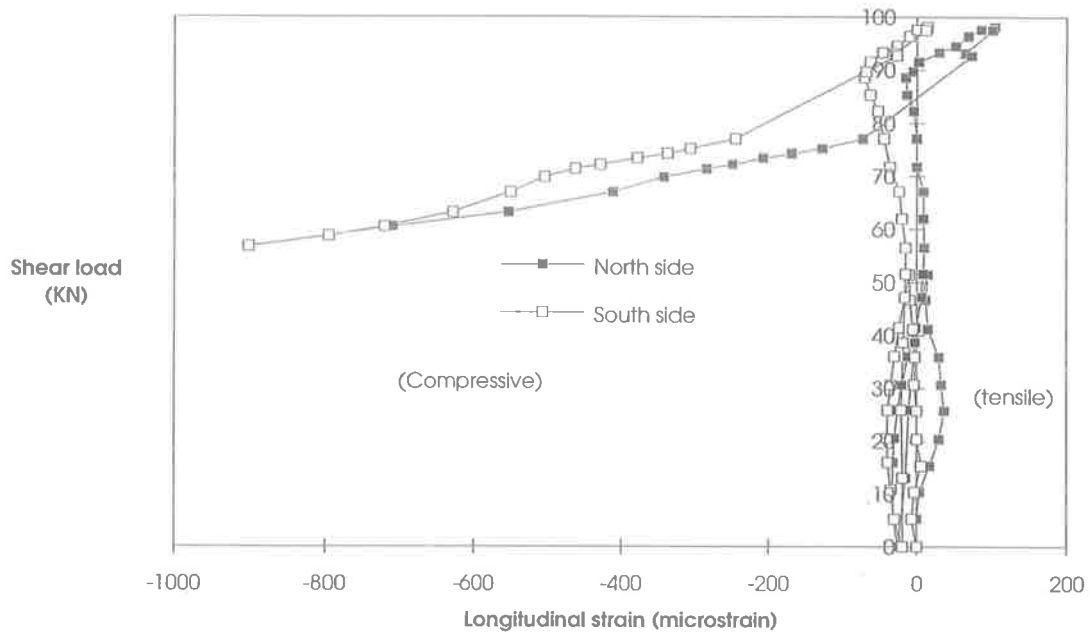

Fig. 8-123 Longitudinal strain at 5mm from plate top (Beam B24)

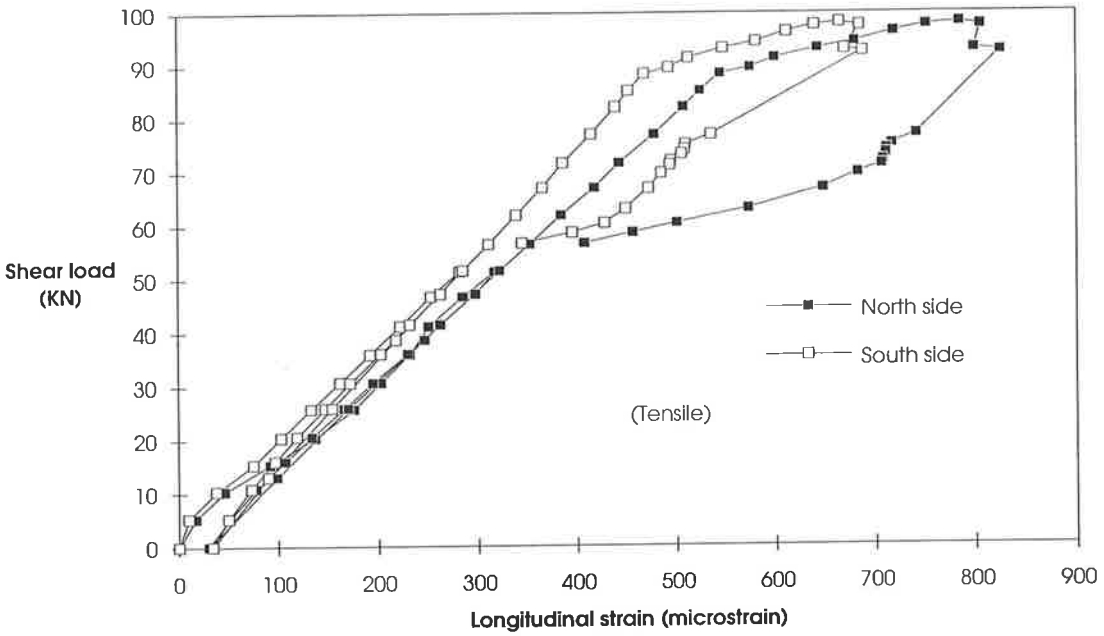

Fig. 8-124 Longitudinal strain at 50 mm from plate top (Beam B24)

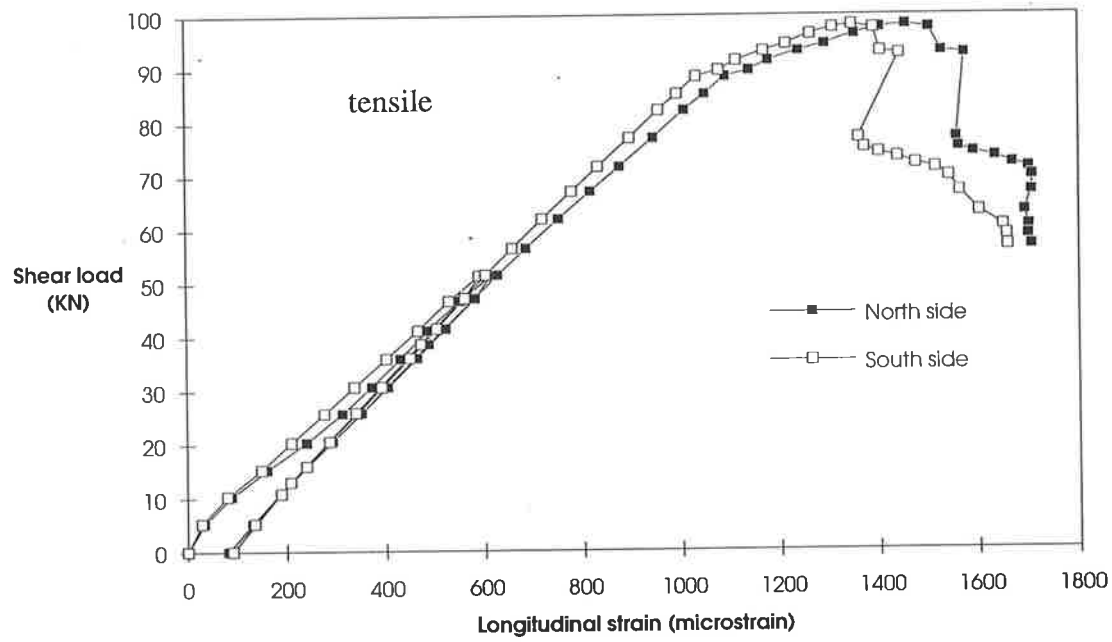

Fig. 8-125 Longitudinal strain at 95 mm from plate top (Beam B24)

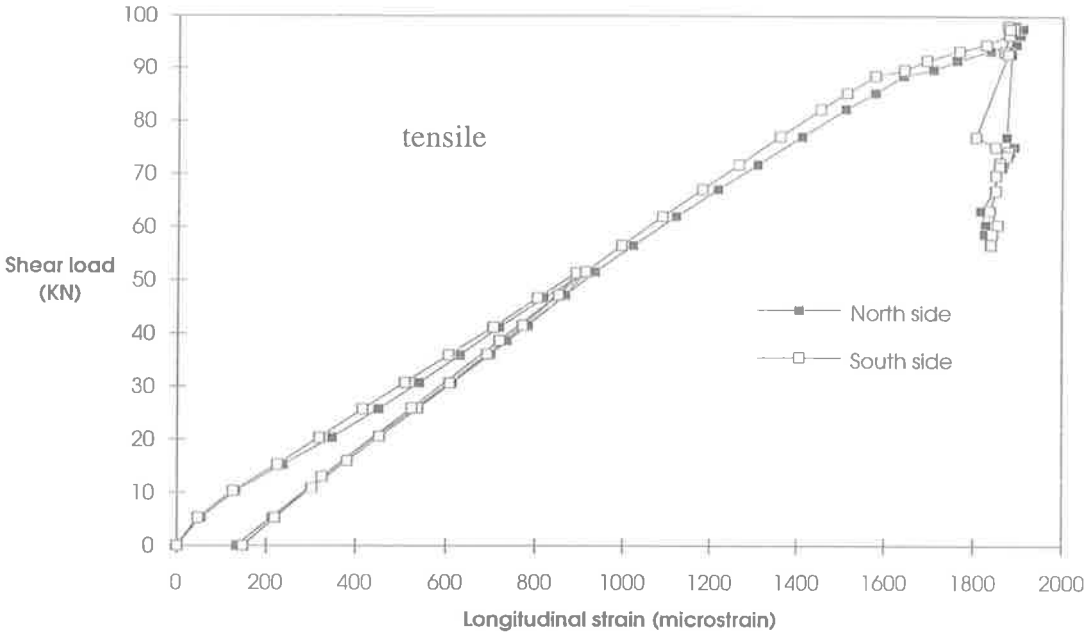

Fig. 8-126 Longitudinal strain at 140 mm from plate top (Beam B24)

Table 8.34 Strain in plate at mid-span (Beam B24)

Location from plate top	North side (microstrain)	South side (microstrain)
(1)	(2)	(3)
5 mm	+104	+14
50 mm	+785	+665
95 mm	+1456	+1348
140 mm	+1893	+1877

(e) Strain profiles in the concrete and plate at mid-span

The strain profiles in the RC beam and the plate at the mid-span at various load steps are shown in Figs. 8-127 to 8-131. The behaviour of the strain profiles can be seen to be similar to the previous tests.

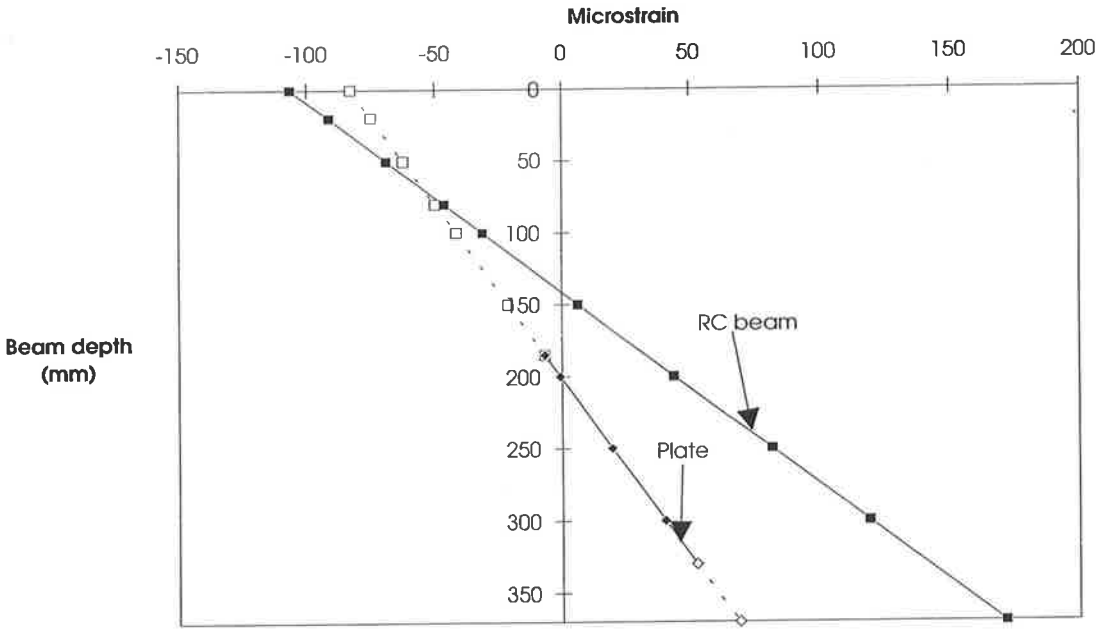

Fig. 8-127 Strain profiles at applied load of 10 kN (Beam B24)

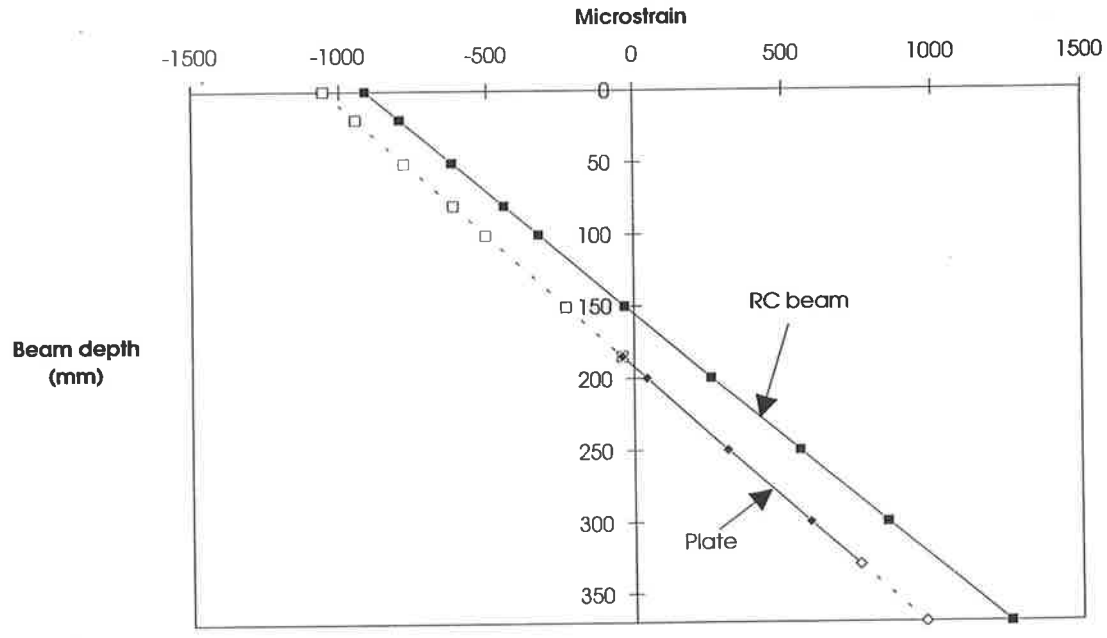

Fig. 8-128 Strain profiles at applied load of 77 kN (Beam B24)

Table 8.35 Forces in one side plate (Beam B24)

Applied Load (kN)	N-A position y_{np} (mm)	Compressive force		Tensile force		Resultant force	
		P_{comp} (kN)	x (mm)	P_{ten} (kN)	y (mm)	P_{plate} (kN)	z (mm)
1	2	3	4	5	6	7	8
10.0	16.52	0.07	5.51	4.07	102.17	4.00	103.80
51.8	9.36	0.20	3.12	44.54	99.79	44.34	100.25
77.4	7.20	0.17	2.40	62.42	99.07	62.25	99.33
154.1	7.27	0.33	2.43	119.11	99.09	118.78	99.36
186.0	5.78	0.27	1.93	156.64	98.59	156.37	98.76
196.0	-1.17	0	0	176.31	96.08	176.31	96.08

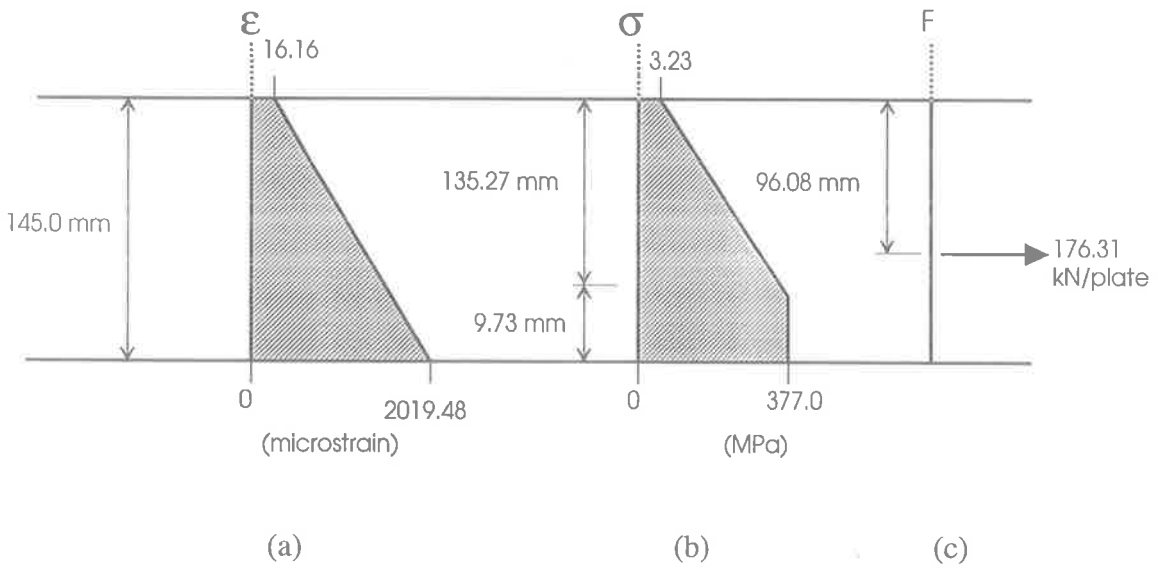

Fig. 8-132 Strain-stress-force distribution in plate (Beam B24)

Figure 8-133 shows the relationship between the longitudinal force in the plate per side and the shear load. The variation is almost linear up to the shear load of 88 kN. The longitudinal shear force in the plate is 176.31 kN per side at the maximum shear load and it stays almost the same when the shear load reduces to about 92 kN. However, longitudinal shear force in plate then reduces with further reduction of shear load.

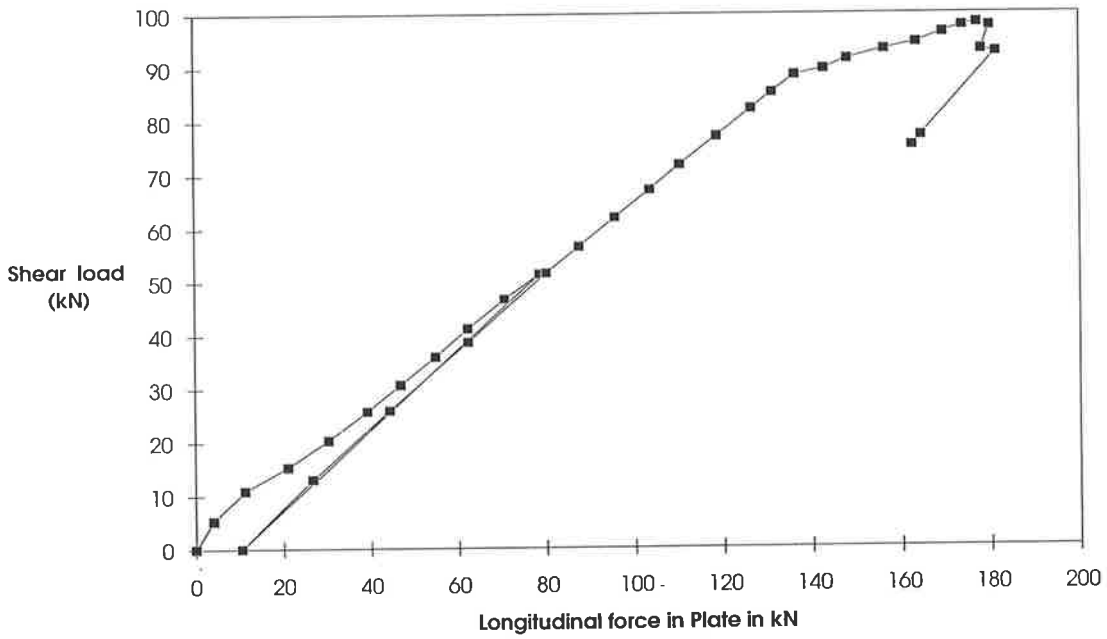

At each of the side plate

Fig. 8-133 Longitudinal force in plate per side (Beam B24)

(g) Moment-curvature relationship

Figure 8-134 shows the relationship between the moment and the curvature of the concrete and plate elements. It can be seen that the curvature in the plate is less than that of the RC beam. The curvature in the RC beam increases more rapidly than that of the plate. The maximum moment was 181.48 kNm.

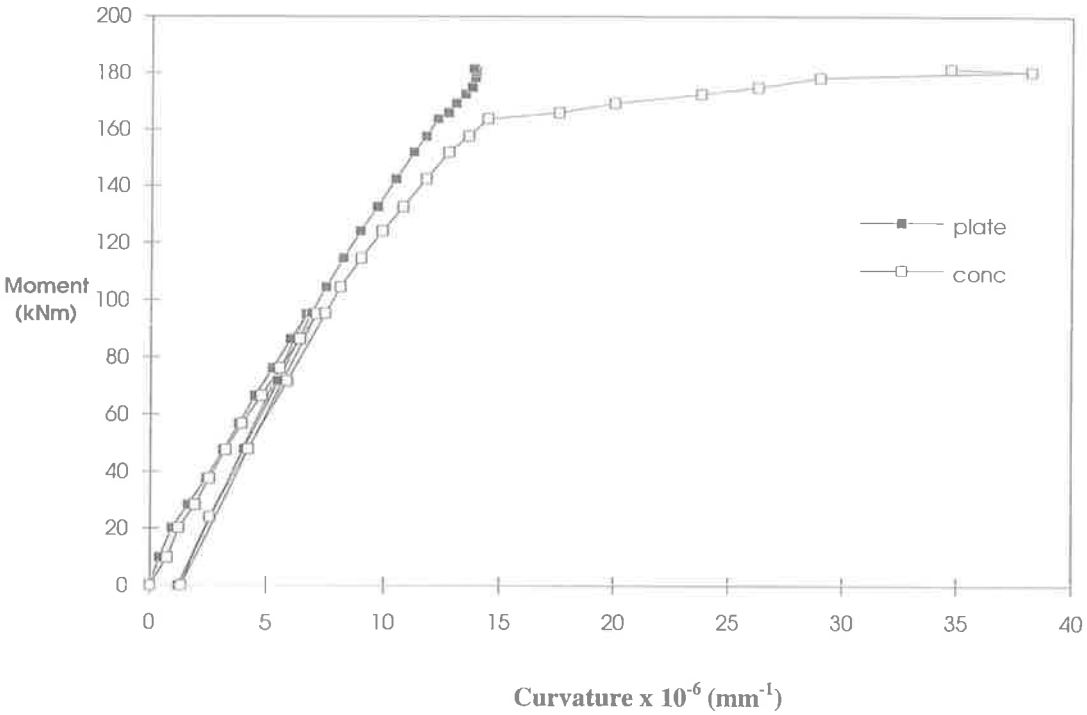

Fig. 8-134 Moment curvature plot (Beam B24)

8.4.6.3 Series 3: Full depth plated beam

This series is consisted of two plated beams C11 and C12. Their specifications are described in Sect. 8.4.1.3. The main variation in this series is the degree of shear connection. The bolt positions and instrumentation are given in Sects. 8.4.1.3 and. 8.4.4 respectively.

8.4.6.3.1 Test 6 : Full depth plated beam C11

It was anticipated in the test that buckling would occur at the top of the plate. As this is not a parameter considered in this research, clamps were used to prevent buckling as shown in P8.54. The clamps were only hand tight to ensure that they did not increase the longitudinal shear strength between the plates and the RC beam.

The load was applied to the beam in two cycles. In the first cycle, the increment of applied load was 10 kN. The onset of buckling was noticed in the south side of the plate at 80 kN of applied load (shear load of 40 kN). Buckling was prevented by tightening the clamp. The first cycle of loading was completed at 130 kN of applied load (shear load of 65 kN) and load was taken off gradually to zero.

In the second cycle, the increment of applied load was 20 kN until 100 kN, then 10 kN until 190 kN after which the load increments were replaced by increments of 1 mm deflection. The onset of buckling in the plate that is, significant separation of the plate from the RC beam, was noticed at an applied load of 204 kN (shear load of 102 kN), so that the number of clamps was increased, as shown in P8.55. At an applied load of 213 kN (shear load of 106.5 kN), the onset of buckling occurred in between the bolts of the S-W shear span. It was realised that the plate needed to be clamped at the level of the top bolts. As such, the top strain gauges on both the sides of the beam were ruined when the plate was clamped at this position. A photograph of the clamp can be seen in P8.56.

The maximum applied load was 220.40 kN (shear load of 110.2 kN), after which the load started to drop off, and spalling was noticed at an applied of 214.90 kN (shear load of 107.45 kN). Flexural failure of the beam is shown in P8.57 when much buckling in the

plate had occurred. The amount of buckling increased as the applied load was reduced further.

(a) Load deflection behaviour

Figure 8-135 shows the load-deflection curve of the beam. It can be seen in the figure that the variation is linear up to point A (at about 94 kN of shear load). The stiffness of the beam then reduces and the shear load gradually increases to the maximum of 110.2 kN at point B. The strength of the beam then reduces and the beam failed in flexure at point C. It should be mentioned that the buckling in the plate occurred at about point A and continued thereafter.

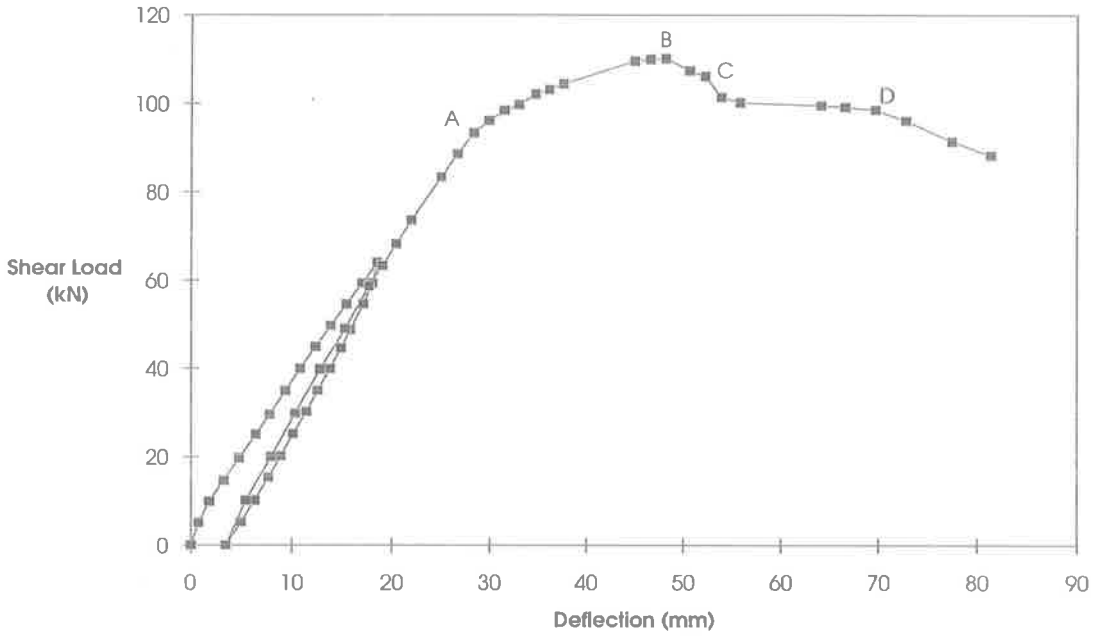

Fig. 8-135 Load-deflection curve (Beam C11)

(b) Vertical slip

The variations of vertical slip with the shear load at different positions are shown in Figs. 8-136 to 8-138. The variation of vertical slip near the support bolt, shown in Fig. 8-136, and at the bolt nearest to the mid-span, shown in Fig. 8-138, have similar shapes but are in the opposite direction. This shows that the relative movement of the plate near the support is downwards with respect to the RC beam whereas it is upwards at the bolt near mid-span. The vertical slip near mid-shear-span in Fig. 8-137 shows that the magnitude of the vertical slip is very small and changes sign at high load levels. This suggests that the position of the LVDT was very close to the position where vertical slip changes its direction. The vertical slips at the maximum shear load are given in Table 8.36.

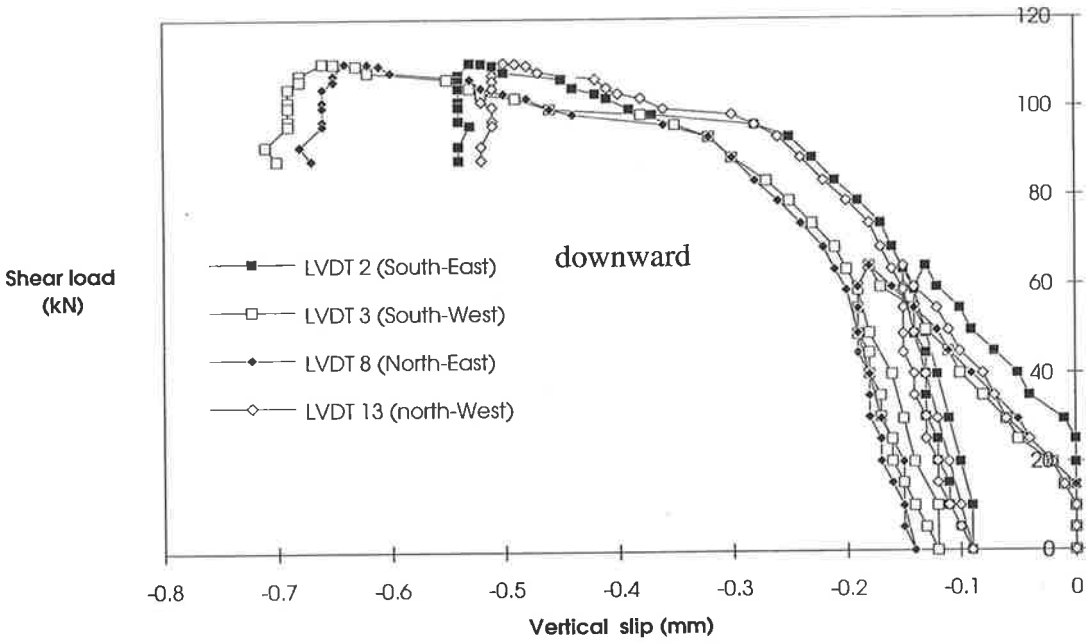

Fig. 8-136 Vertical slip near support bolt (Beam C11)

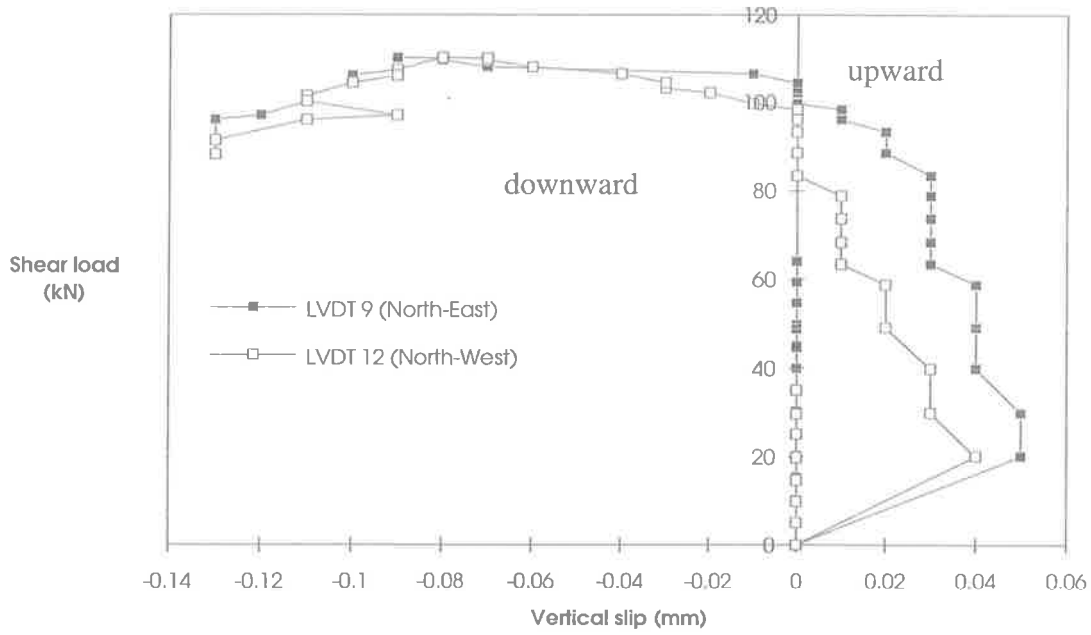

Fig. 8-137 Vertical slip near mid-shear span (Beam C11)

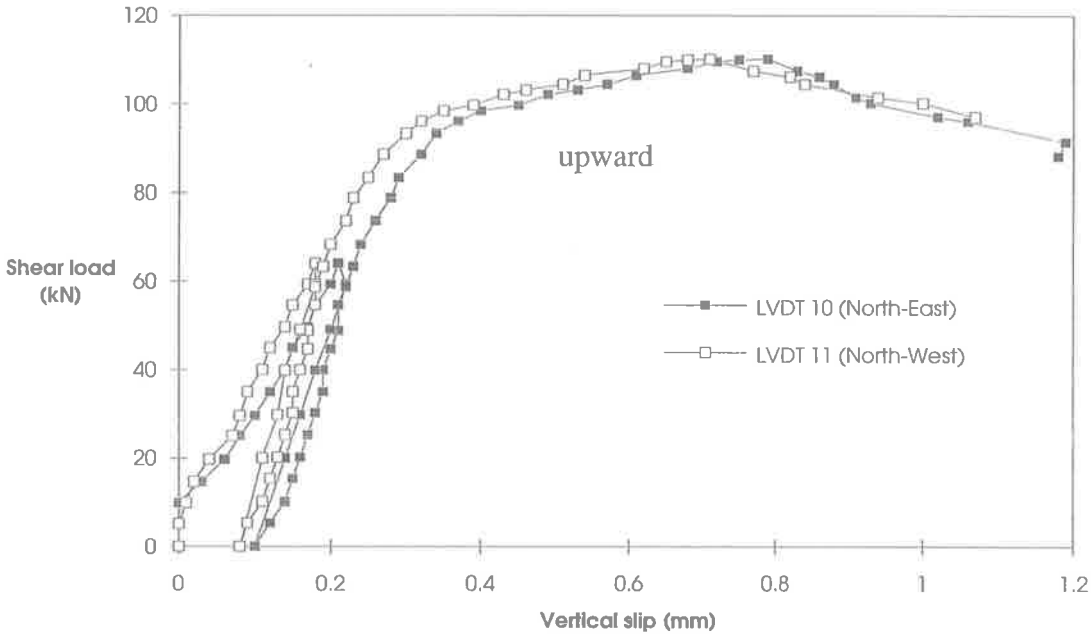

Fig. 8-138 Vertical slip at end bolt of shear span (Beam C11)

It can be seen in Table 8.36 that the vertical slip changes direction from downwards near the supports to upward near the mid-span, as to be expected. The vertical slips at the

end bolt of shear span are roughly the same magnitude being slightly larger at the bolt near mid-span.

Table 8.36 Vertical slip at the maximum shear load (Beam C11)

Direction	East shear span (Distance from East end support)			West shear span (Distances from West end support)		
	At 120 mm	At 860 mm	At 1600 mm	At 120 mm	At 860 mm	At 1600 mm
	(mm)	(mm)	(mm)	(mm)	(mm)	(mm)
(1)	(2)	(3)	(4)	(5)	(6)	(7)
North side	-0.64	-0.09	+0.79	-0.50	-0.08	+0.71
South side	-0.53			-0.66		

(c) Longitudinal slip

The variation of the longitudinal slip along the plate are shown in Figs. 8-139 to 8-142. The variation at all the positions can be seen to be similar. The longitudinal slips at the maximum shear load are given in Table 8.37.

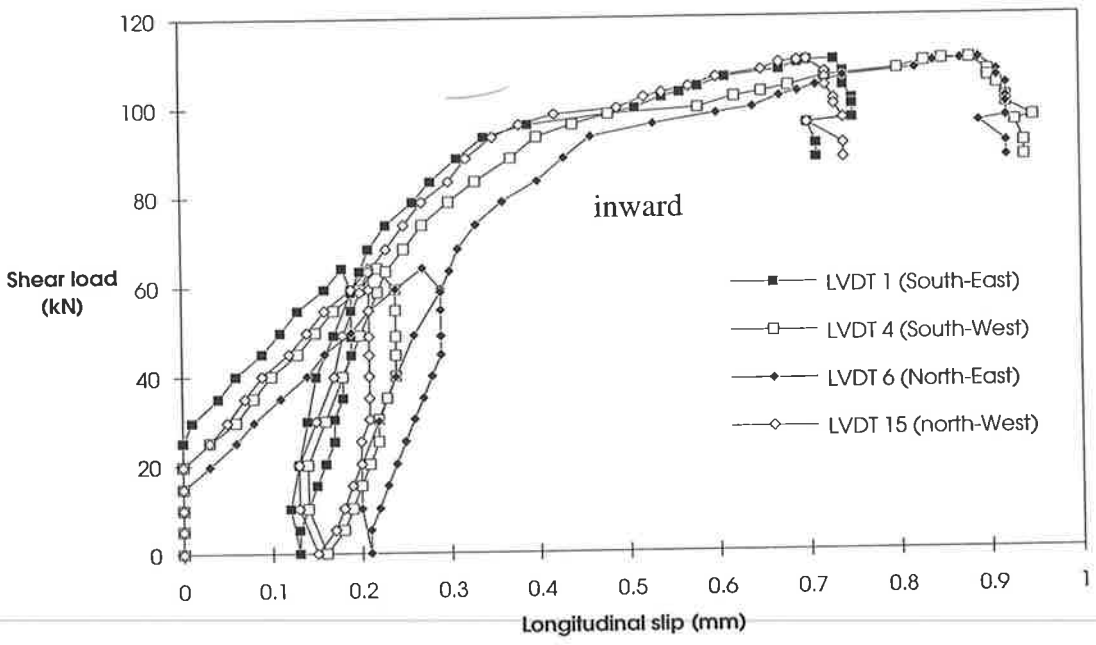

Fig. 8-139 Longitudinal slip at bottom bolt level over support (Beam C11)

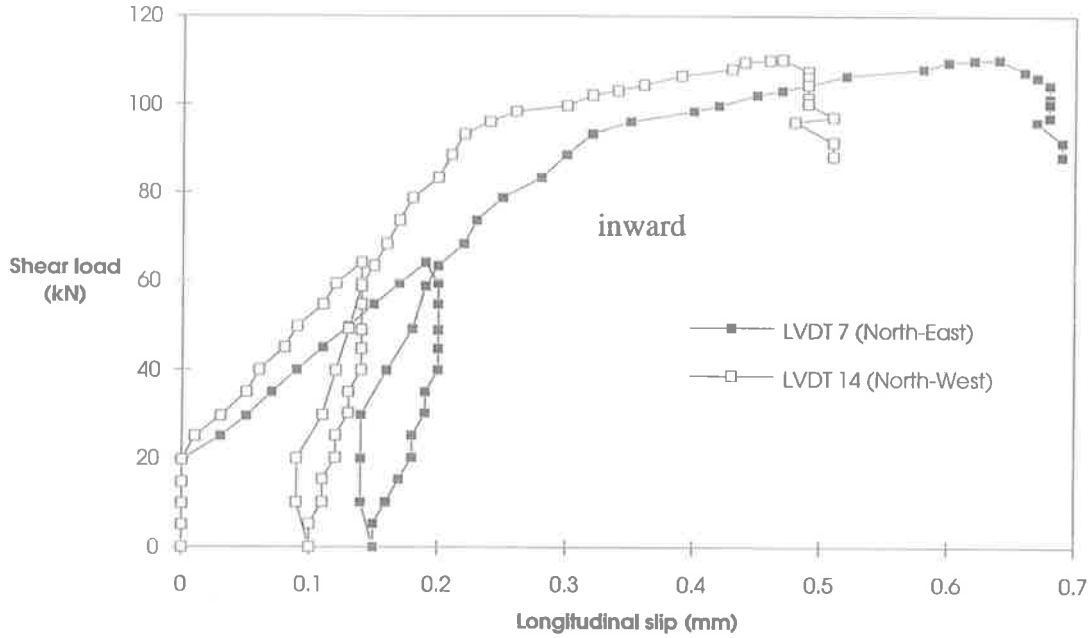

Fig. 8-140 Longitudinal slip at top bolt level over support (Beam C11)

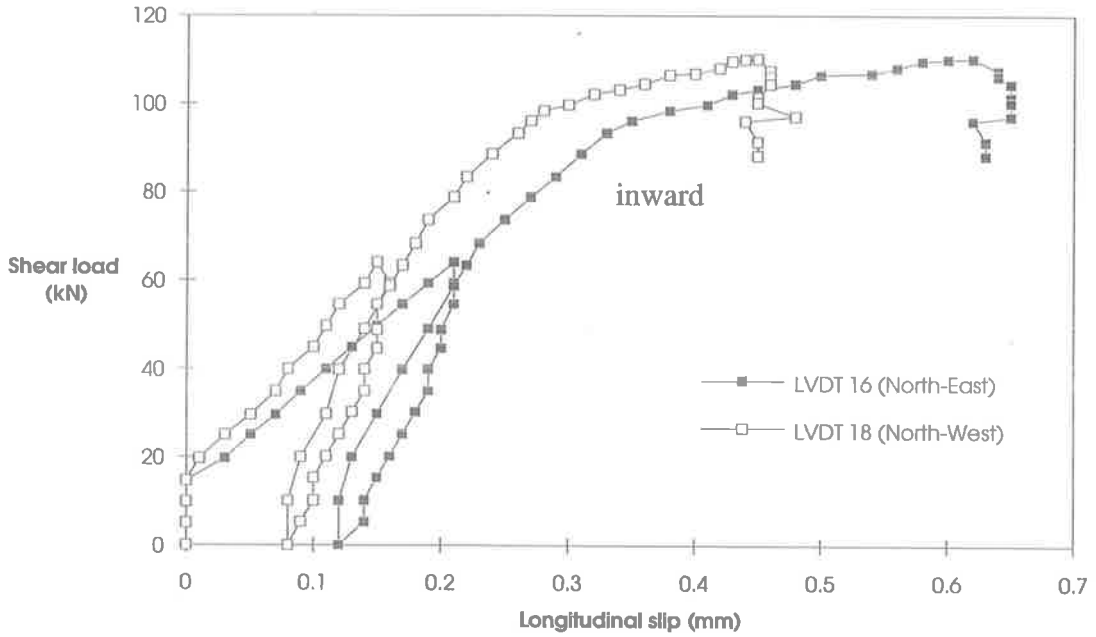

Fig. 8-141 Longitudinal slip at top bolt level near mid-shear span (Beam C11)

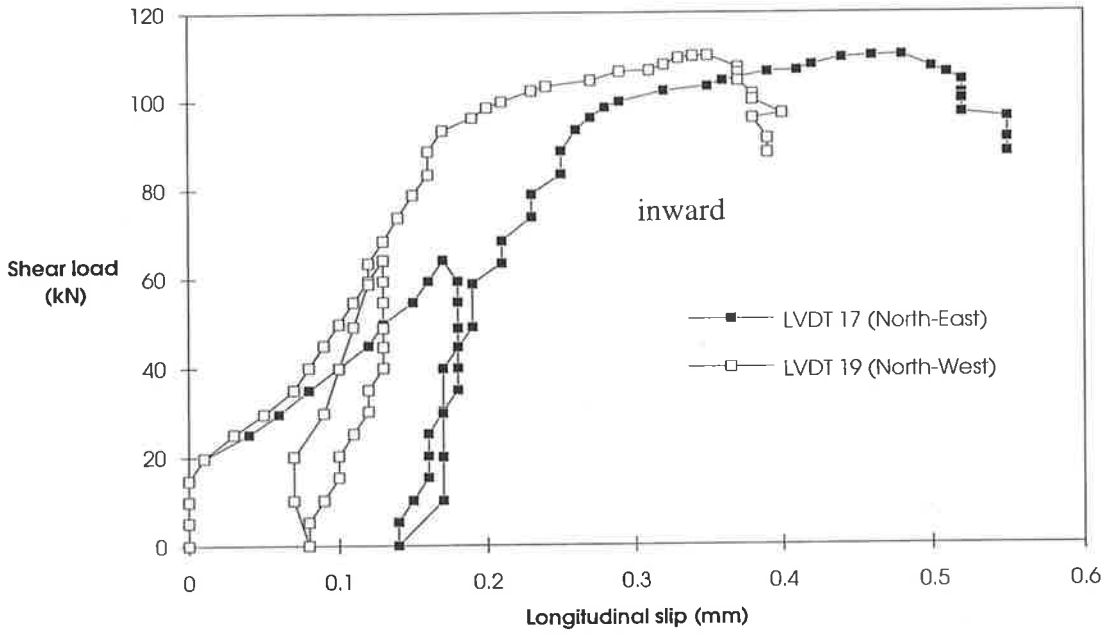

Fig. 8-142 Longitudinal slip at bottom bolt level near mid-shear span (Beam C11)

It can be seen in Table 8.37 that the maximum longitudinal slip occurs at the supports. The longitudinal slip at the bottom bolt level over the support is higher than that of the top bolt level, however, the situation near the mid-shear span is the reverse.

Table 8.37 Longitudinal slip at the maximum shear load (Beam C11)

Direction and vertical position	East side shear span		West side shear span	
	Position from East end support		Position from West end support	
	At 0 mm (mm)	At 830 mm (mm)	At 0 mm (mm)	At 830 mm (mm)
(1)	(2)	(4)	(5)	(6)
North top	+0.64	+0.62	+0.47	+0.45
North bottom	+0.89	+0.48	+0.70	+0.35
South bottom	+0.73		+0.88	

(d) Longitudinal strain in plate at mid-span

The variation of the longitudinal strain with the shear load at different depths of the plate are shown in Figs. 8-143 to 8-146. The electrical strain gauges at 50 mm depth were ruined at a shear load of 106 kN when the plates were clamped to prevent buckling. As such, the variations of strain after the shear load of 106 kN cannot be seen in Fig. 8-143. The longitudinal strains at the maximum shear load are given in Table 8.38.

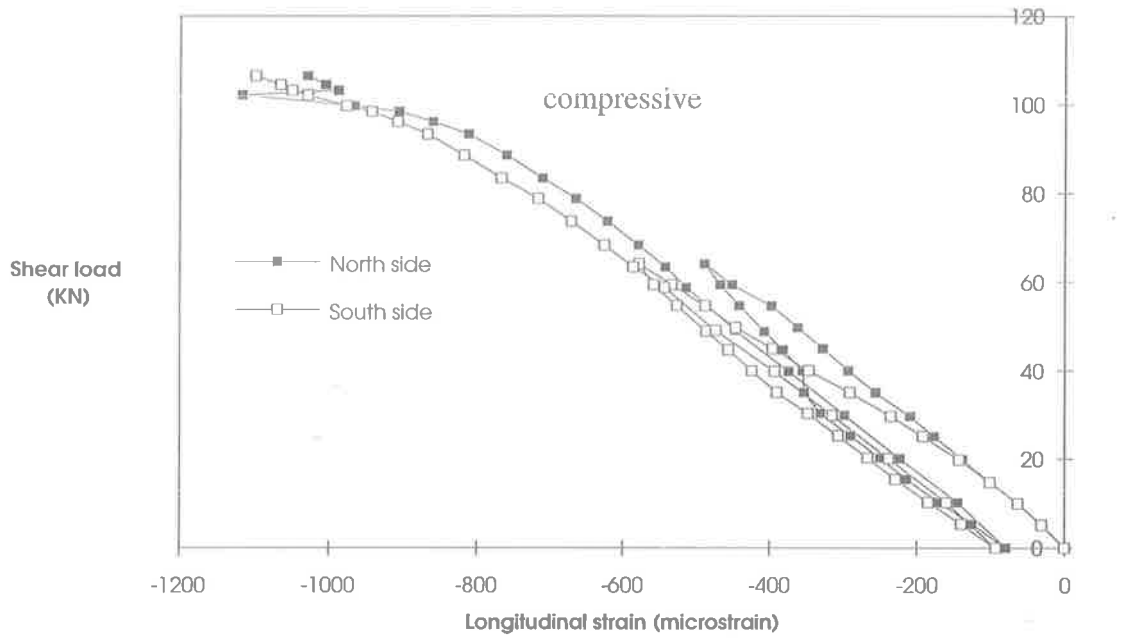

Fig. 8-143 Longitudinal strain at 50 mm level from plate top (Beam C11)

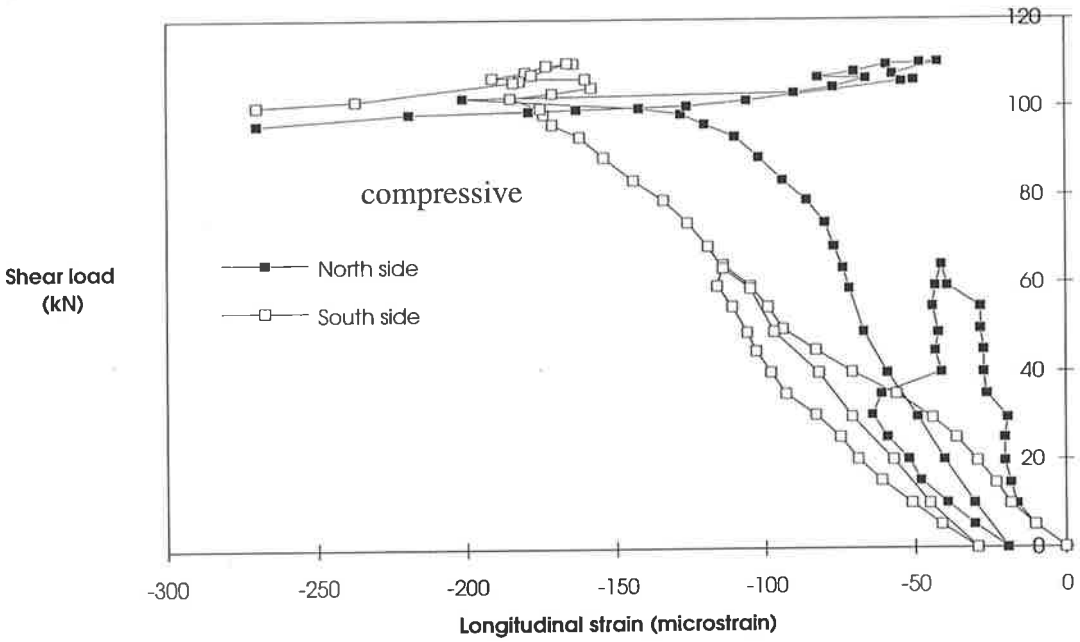

Fig. 8-144 Longitudinal strain at 113 mm from plate top (Beam C11)

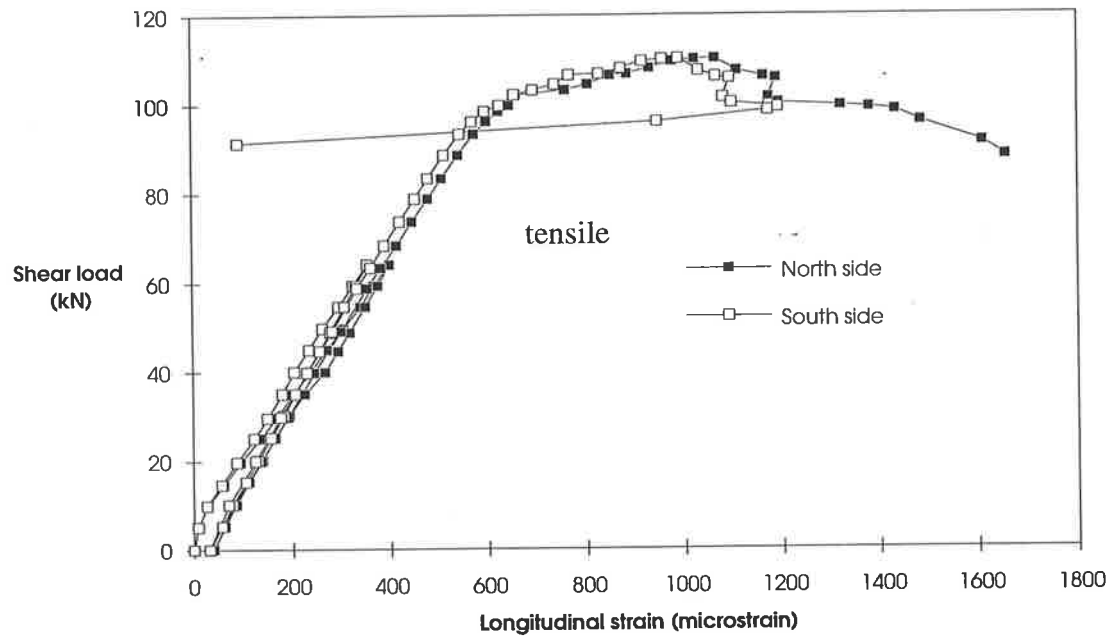

Fig. 8-145 Longitudinal strain at 176 mm from plate top (Beam C11)

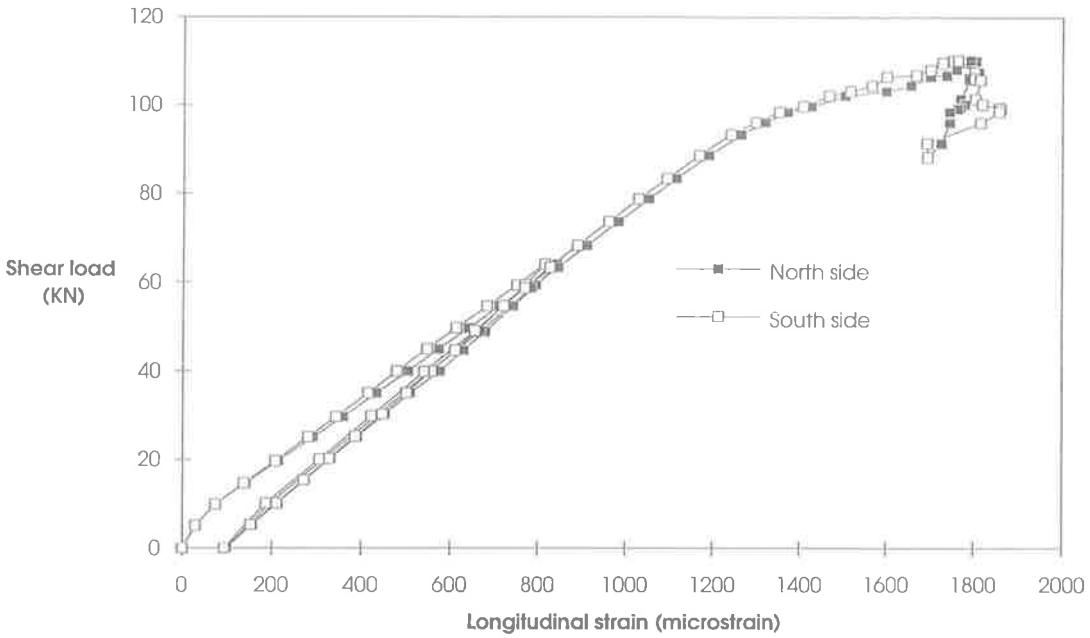

Fig. 8-146 Longitudinal strain at 240 mm from plate top (Beam C11)

Table 8.38 Strain in plate at mid-span (Beam C11)

Location from plate top	North side (microstrain)	South side (microstrain)
(1)	(2)	(3)
50 mm	-	-
113 mm	-42	-166
176 mm	+1066	+990
240 mm	+1792	+1763

(e) Longitudinal forces in each of the side plate at mid-span

The compressive forces and the tensile forces in one side plate and their locations are given in Table 8.39. It can be seen in Col. 2 that the neutral axis depth in the plate is higher than that was seen in shallow plated beam and therefore, the compressive force is higher. This causes the lateral displacement of the plate that was described before.

The strain and stress distribution in the mid-span of the plate at the maximum shear load are shown in Fig. 8-147. It can be seen in (b) that a large part of the plate is in compression and the remainder is in tension. Also only a small part of the tensile section is fully yielded whereas no part in the compressive area is fully yielded. The location of the resultant force is shown in (c).

Table 8.39 Forces in one side plate at mid-span (Beam C11)

Applied Load (kN)	n-a position y_{np} (mm)	Compressive force P_{comp} (kN)	Compressive force x (mm)	Tensile force P_{ten} (kN)	Tensile force y (mm)	Resultant force P_{plate} (kN)	Resultant force z (mm)
1	2	3	4	5	6	7	8
20.0	137.67	8.15	45.89	9.98	239.22	1.83	1101.5
80.0	124.97	40.23	41.66	70.17	234.99	29.94	494.81
118.7	124.41	61.65	41.47	109.20	234.80	47.56	485.41
157.7	125.62	86.43	41.87	147.99	235.21	61.57	506.60
199.5	126.64	120.98	42.21	199.94	235.21	78.97	530.88
220.40	118.14	122.45	39.38	242.95	229.85	120.50	423.40

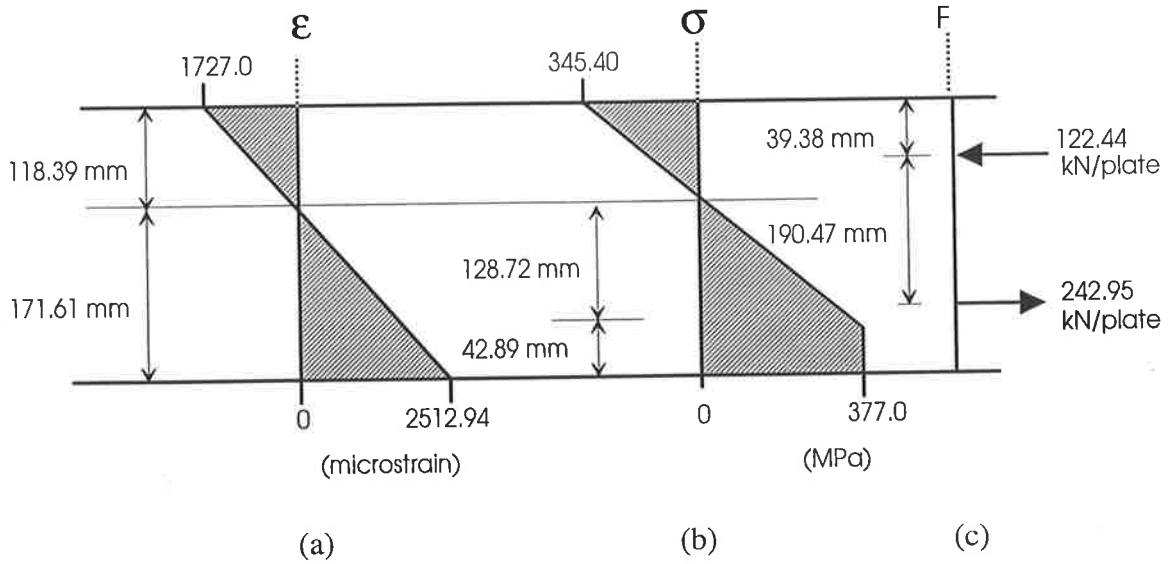

Fig. 8-147 Strain-stress-force distribution in plate (Beam C11)

Figure 8-148 shows the variation of longitudinal force in the plate per side with shear load. It can be seen that the variation of longitudinal force and shear load is linear up to about 100 kN of shear load. The longitudinal force in the plate then increases rapidly with the increase of shear load. The maximum longitudinal force at the maximum shear load was 120.50 kN per side.

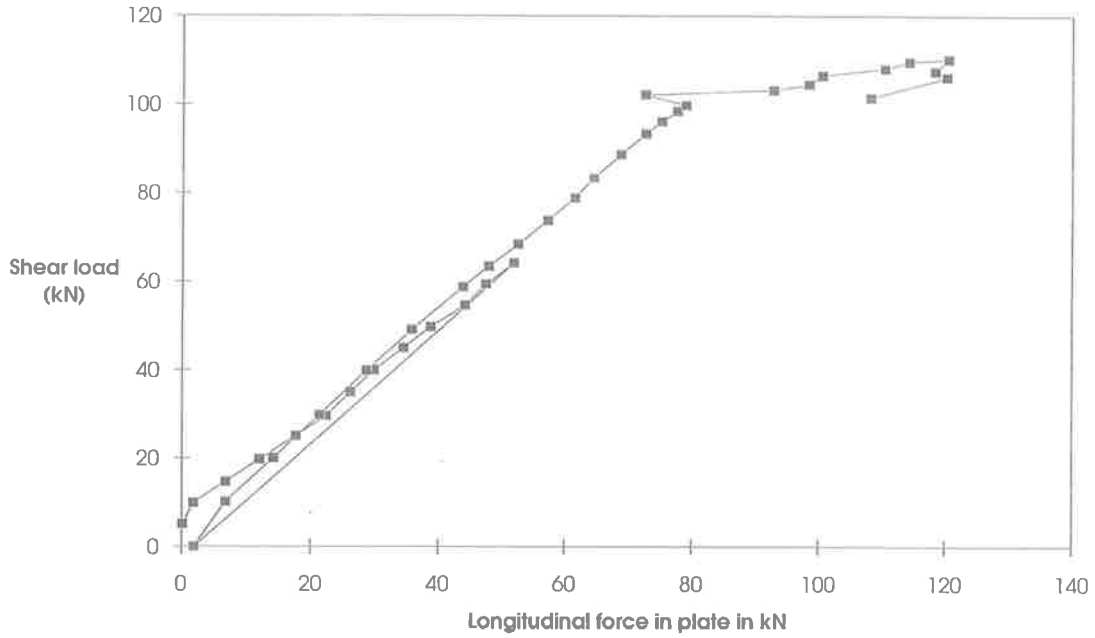

At each of the side plate

Fig. 8-148 Longitudinal shear force in plate per side (Beam C11)

(f) Curvature in the plate

The variation of curvature in the plate at mid-span is given in Fig. 8-149. It can be seen that the curvature varies almost linearly up to the maximum applied moment. Also, at or near the maximum applied moment, the increment of curvature is very small or the curvature stays at almost the same.

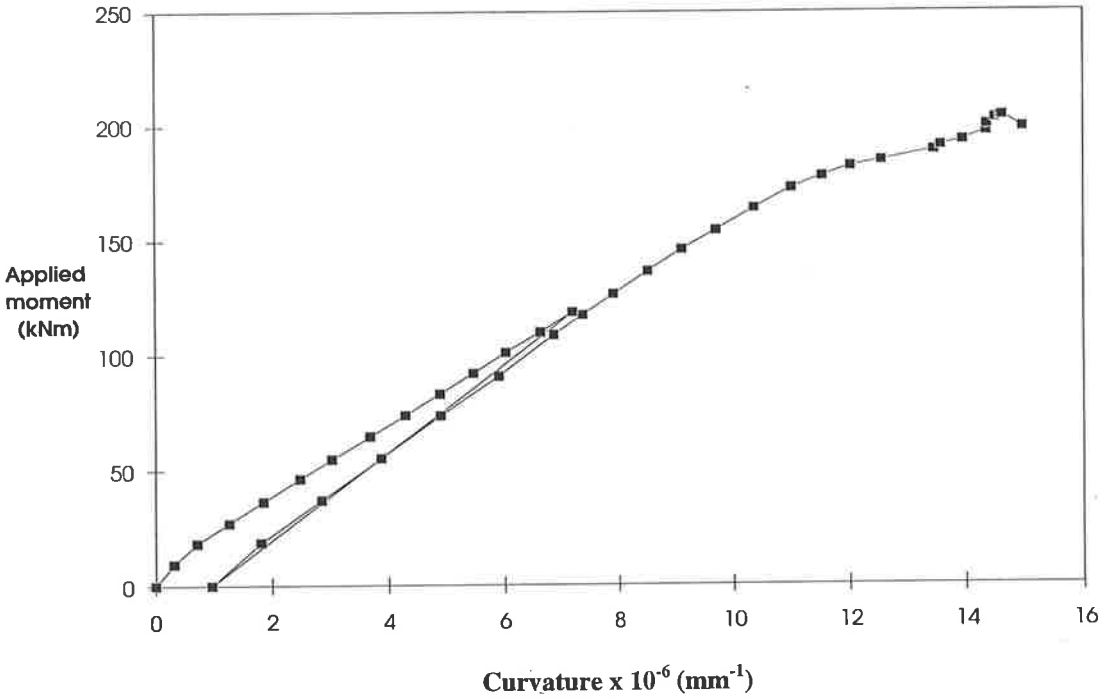

Fig. 8-149 Curvature in the plate (Beam C11)

8.4.6.3.2 Test 7 : Full depth plated beam C12

Unlike beam C11, the plate was first clamped to the RC beam at the position of the top bolt level for this test, as shown in P8.58. The load was applied to the beam in two cycles. In the first cycle, the increment of applied load was 10 kN. At about 20.5 kN of applied load, flexural cracks formed. As the load increased further, more flexural cracks formed and propagated behind the plate. At 100 kN of applied load, the first cycle was completed and the load was gradually taken off to zero.

In the second cycle, the load increment was 25 kN up to a total load of 100 kN, after which the load increments were replaced by increments of 2 mm deflection up to a total load of 200 kN and then increments of deflection of 1 mm. A ripping crack appeared below the plate at the position of the north-east corner bolt at 116 kN of applied load (shear load of 58 kN), as shown in P8.59. At this stage, the onset of buckling in the plate was noticed and this increased with the applied load. As such the clamps were tightened to minimize the buckling. Ripping cracks at the position of the other three corner bolts were noticed at 191.7 kN of load (shear load of 95.9 kN), as shown in P8.60, P8.61 and P8.62 respectively. Spalling occurred at 218.4 kN of applied load (shear load of 109.2 kN).

The maximum load was equal to 220.60 kN (shear load of 110.3 kN), after which the load started to drop. At 214.7 kN of load (shear load of 107.4 kN), large buckling of the side plates at the mid-span in the south side was evident. At 188.10 kN (shear load of 94.05 kN), the beam failed in flexure, as shown in P8.63, at which point there occurred large buckling in the plate, as shown in P8.64. This buckling in the plate further increased as the applied load reduced and at 187.4 kN of load (shear load of 93.7 kN) the clamps were bent due to the buckling forces and the experiment was stopped. The photograph in P8.65 shows the amount of buckling when the clamps were removed.

(a) Load deflection behaviour

Figure 8-150 shows the load-deflection behaviour of the beam. The variation of shear load and deflection is linear up to point A (at about 92 kN of shear load). The stiffness of the beam then reduces and the shear load increases up to the maximum at point B (shear load

of 110.3 kN), after which the strength reduces and the beam failed in flexure at point C. The buckling in the plate was extensive when the applied load was reduced.

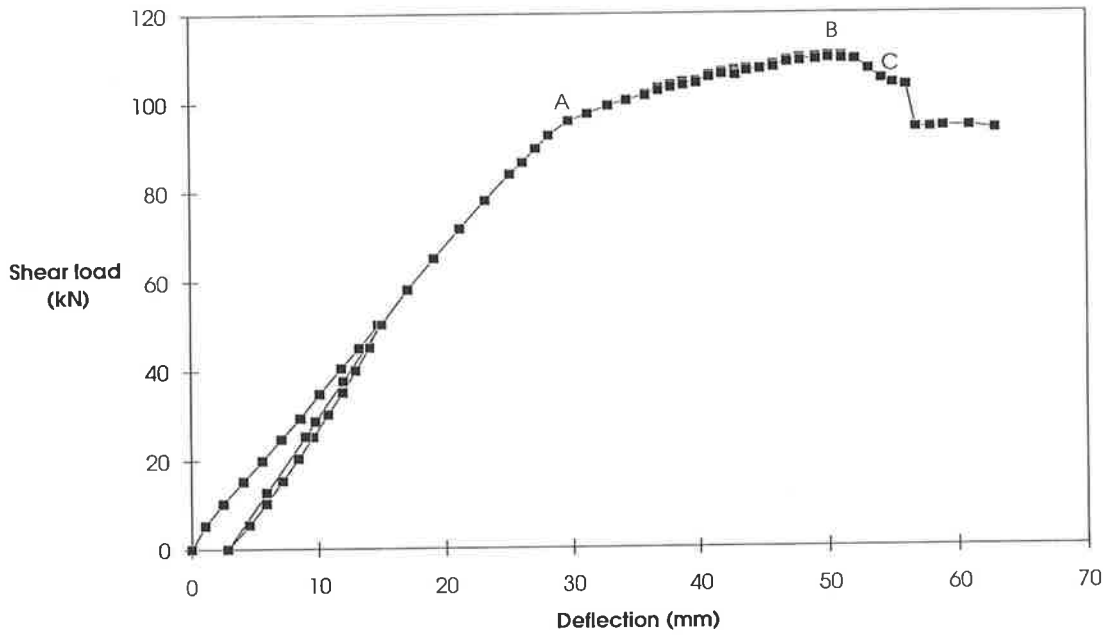

Fig. 8-150 Load-Deflection curve (Beam C12)

(b) Longitudinal slip

The longitudinal slip at the support and at the levels of the bottom bolt and top bolt are shown in Figs. 8-151 and 8-152 respectively. The longitudinal slips near the mid-shear-span at the top and bottom bolt levels are shown in Figs. 8-153 and 8-154 respectively. It can be seen in Fig. 8-153 that the longitudinal slip in LVDT 18 abruptly changes at the shear load region of 65-85 kN. This probably happened due to the buckling in the plate. The longitudinal slip at the maximum shear load is given in Table 8.40.

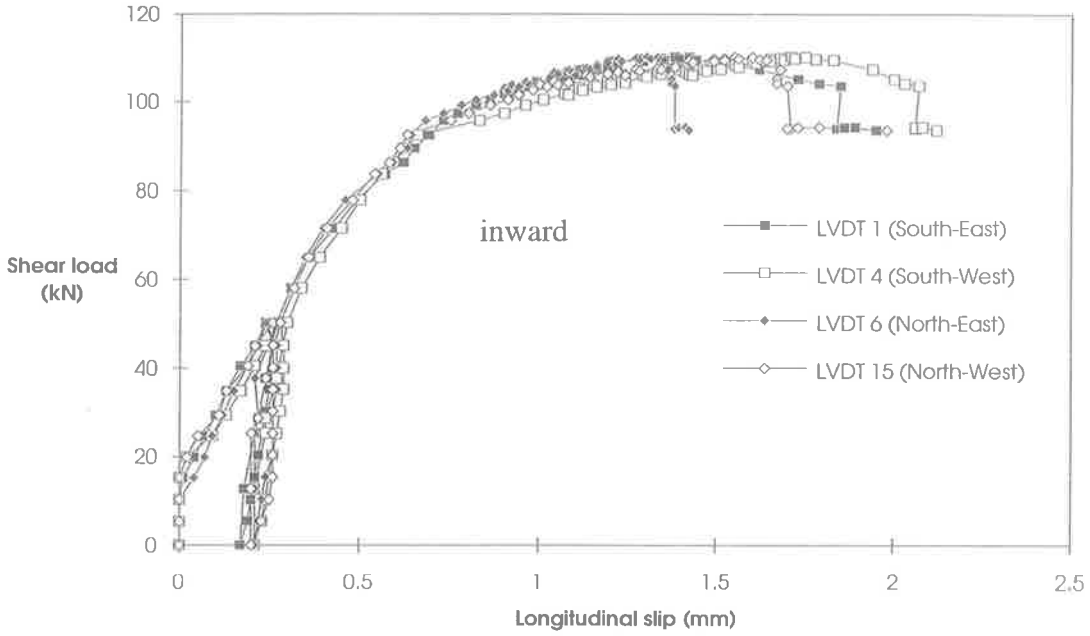

Fig. 8-151 Longitudinal slip at bottom bolt level over the support (Beam C12)

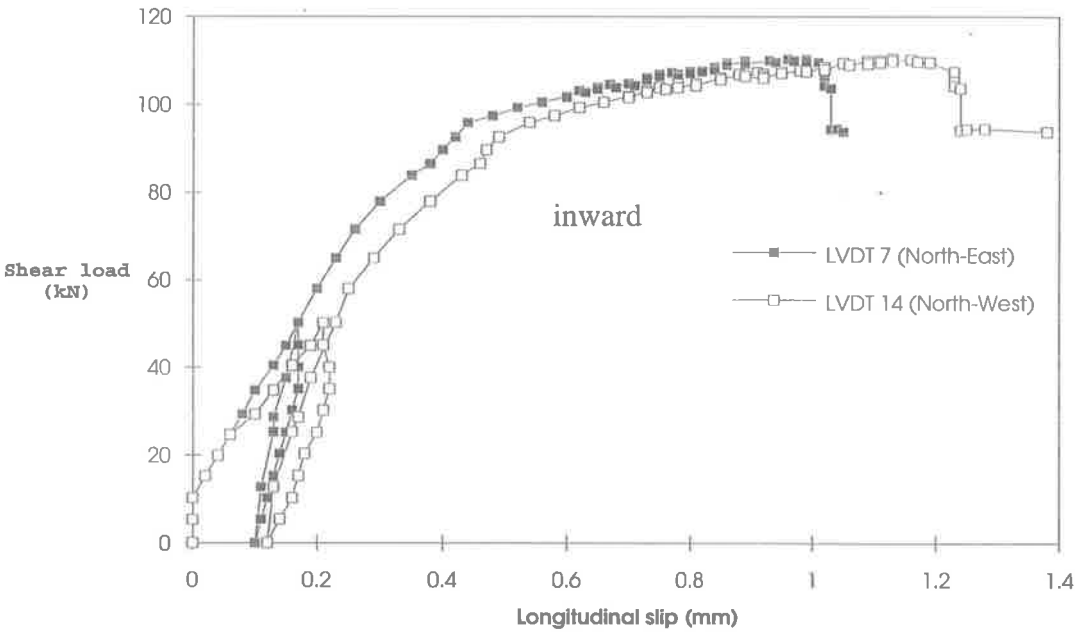

Fig. 8-152 Longitudinal slip at top bolt level over the support (Beam C12)

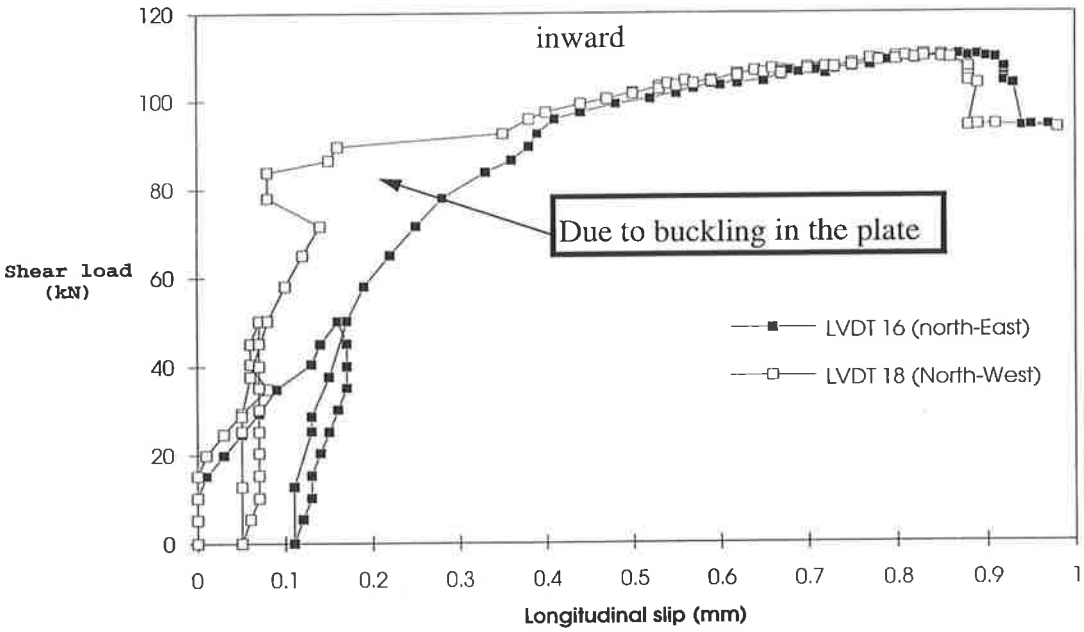

Fig. 8-153 Longitudinal slip at top bolt level near mid-shear span (Beam C12)

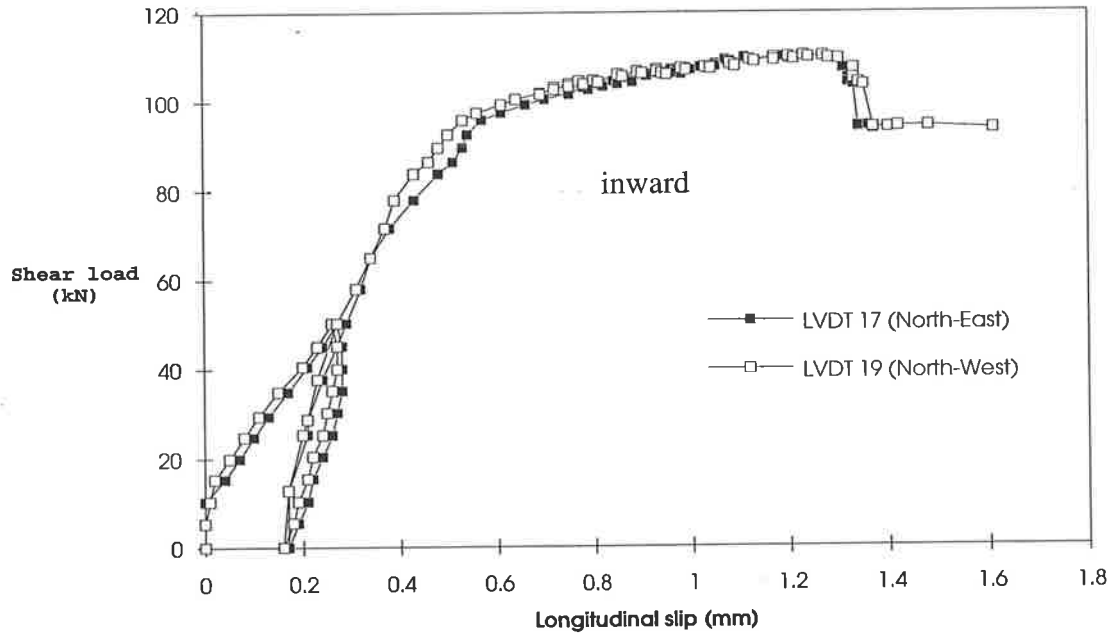

Fig. 8-154 Longitudinal slip at bottom bolt level near mid-shear span (Beam C12)

It can be seen in Table 8.40 that the longitudinal slips are largest at the supports. Also the longitudinal slip is higher at the level of bottom bolts than at the top bolts.

Table 8.40 Longitudinal slip at maximum shear load (Beam C12)

Direction and vertical position	East side shear span		West side shear span	
	Position from East end support		Position from West end support	
	At 0 mm (mm)	At 800 mm (mm)	At 0 mm (mm)	At 800 mm (mm)
(1)	(2)	(4)	(5)	(6)
North top	+0.96	+0.85	+1.11	+0.83
North bottom	+1.30	+1.23	+1.55	+1.23
South bottom	+1.38		+1.71	

(c) Vertical slip

The variations of vertical slip near the support bolts, near the mid-shear-span bolts and at the bolts nearest to the mid-span are shown in Figs. 8-155 to 8-157 respectively. The vertical slip is in opposite directions at the support and nearest to the mid-span. It can be seen in Fig. 8-156 that the variation is similar to the previous figures, but the magnitude of the slip is very small. The vertical slip at the maximum shear load is given in Table 8.41.

It can be seen in Table 8.41 that the maximum vertical slip occurs at the bolts nearest mid-span of the shear span. Also, the direction of vertical slip changes from downwards near the support to upwards at the bolts nearest mid-span.

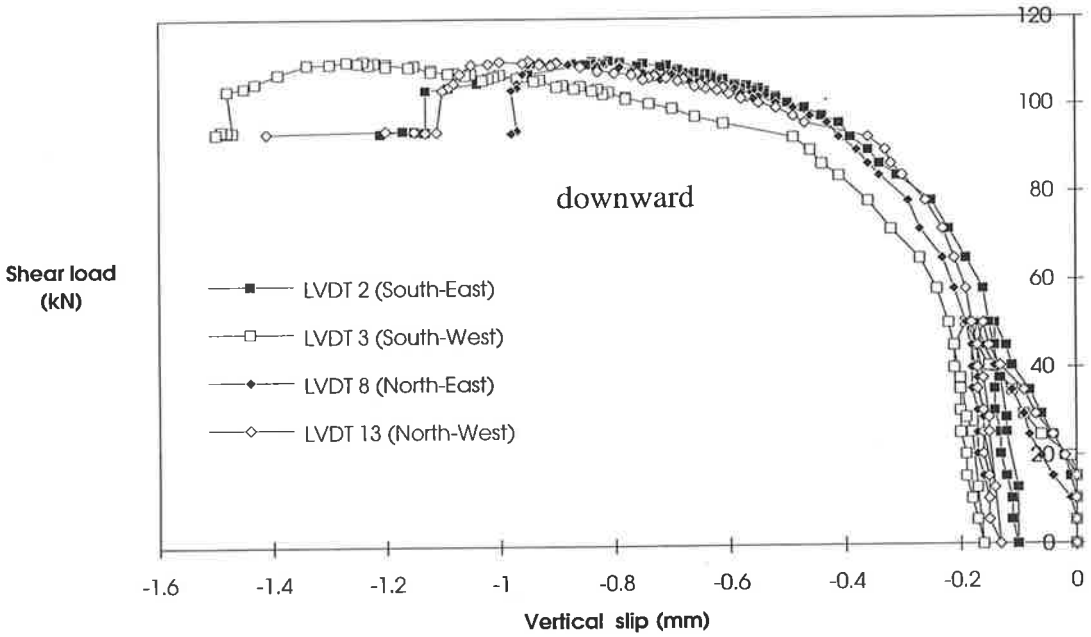

Fig. 8-155 Vertical slip at the bolt near support (Beam C12)

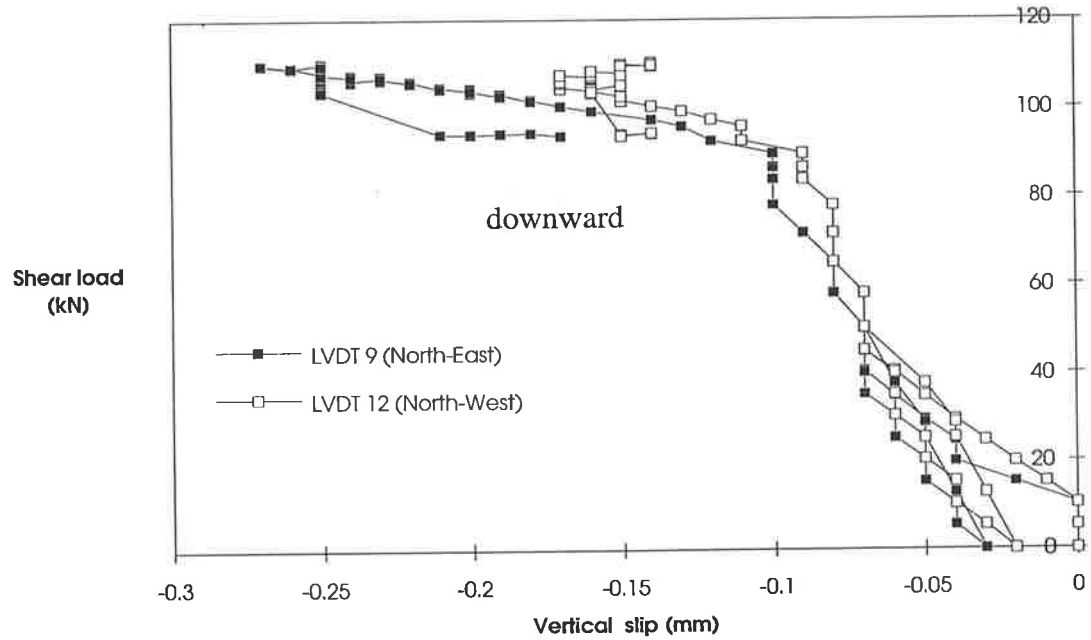

Fig. 8-156 Vertical slip near mid-shear span (Beam C12)

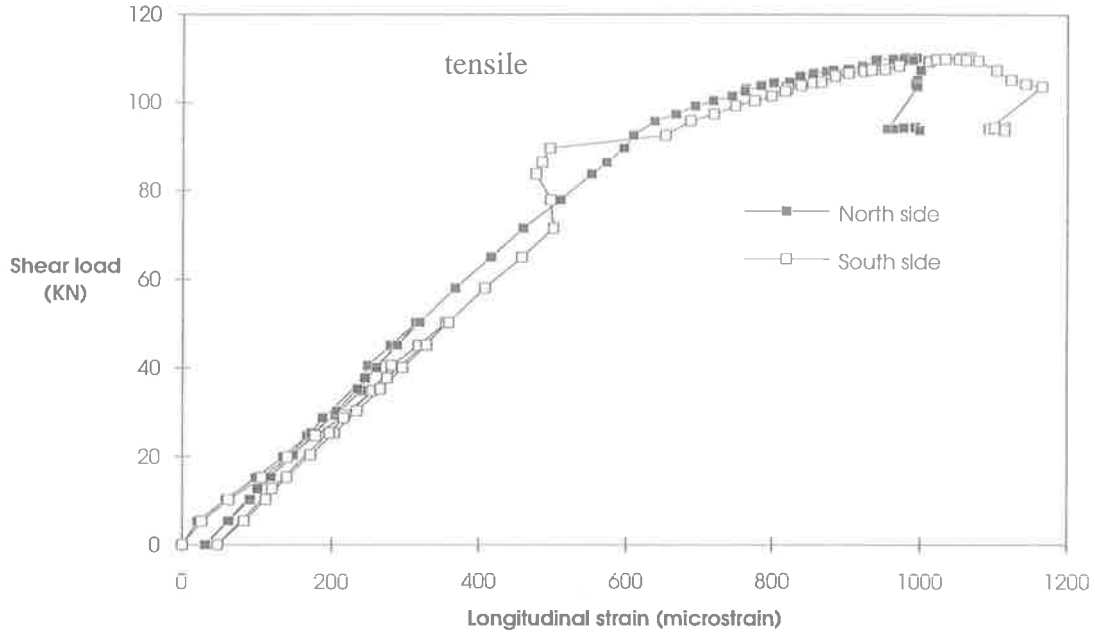

Fig. 8-160 Longitudinal strain at 191.7 mm from plate top (Beam C12)

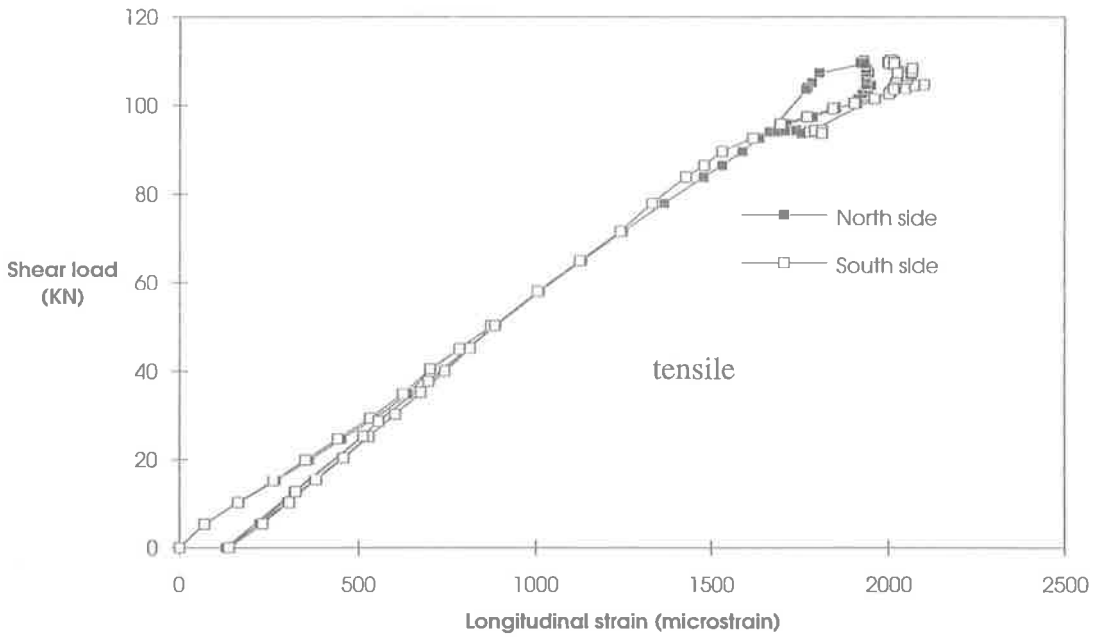

Fig. 8-161 Longitudinal strain at 285 mm from plate top (Beam C12)

Table 8.42 Strain in plate at mid-span (Beam C11)

Location from plate top	North side (microstrain)	South side (microstrain)
(1)	(2)	(3)
5 mm	-1803	-1876
98.3 mm	-422	-434
191.7 mm	+979	+1056
285 mm	+1933	+2006

(e) Longitudinal forces in each of the side plate at the mid-span

The compressive forces and the tensile forces in one side plate and their locations at various load steps are given in Table 8.43. The behaviour is the same as described for the beam C11. The strain and stress profiles in the plate at the mid-span and at the maximum shear load is shown in Fig. 8-162. It can be seen in (b) that a large part of the plate is in compression whereas the remainder is in tension. Only one-seventh of the tensile part is fully yielded and no part in the compression is fully yielded. The location of the resultant forces are shown in (c).

Table 8.43 Forces in one side plate at mid-span (Beam C12)

Applied Load (kN)	n-a position y_{np} (mm)	Compressive force		Tensile force		Resultant force	
		P_{comp} (kN)	x (mm)	P_{ten} (kN)	y (mm)	P_{plate} (kN)	z (mm)
1	2	3	4	5	6	7	8
10	134.97	4.90	44.99	6.47	238.32	1.57	843.67
40	125.20	20.77	41.73	35.90	235.06	1.52	498.97
80.9	131.82	47.55	43.94	68.47	237.27	20.92	676.60
130.0	128.53	70.95	42.84	111.97	236.18	41.02	570.57
172.9	138.77	120.28	48.26	142.86	239.59	22.58	1269.5
200.9	126.48	114.26	42.16	190.80	235.44	76.54	523.98
220.6	132.07	145.57	44.02	203.98	236.43	58.41	716.00

8.4.6.4 Qualitative comparison of results of plated beam tests

The load-deflection curves of the beams in Series 2 and Series 3 are compared in Figs. 8-165 and 8-166. It can be seen in Fig. 8-165 that the plated beams B11 to B24 in Series 2 had higher strengths and stiffness than the unplated beam A11. The stiffness of the plated beams are found to be similar but their strengths are different. The highest strength was achieved in beam B11, where the degree of shear connection was the highest. But the ductility of the beam B11 is less than the other beams. Beams B12 and B13 had almost the same degree of shear connection, but the bolts were placed in two rows and in a single row, respectively. Between them, B13 achieved a higher strength with a larger plateau than beam B12. Furthermore, beam B13 had also larger plateau than all the other beams.

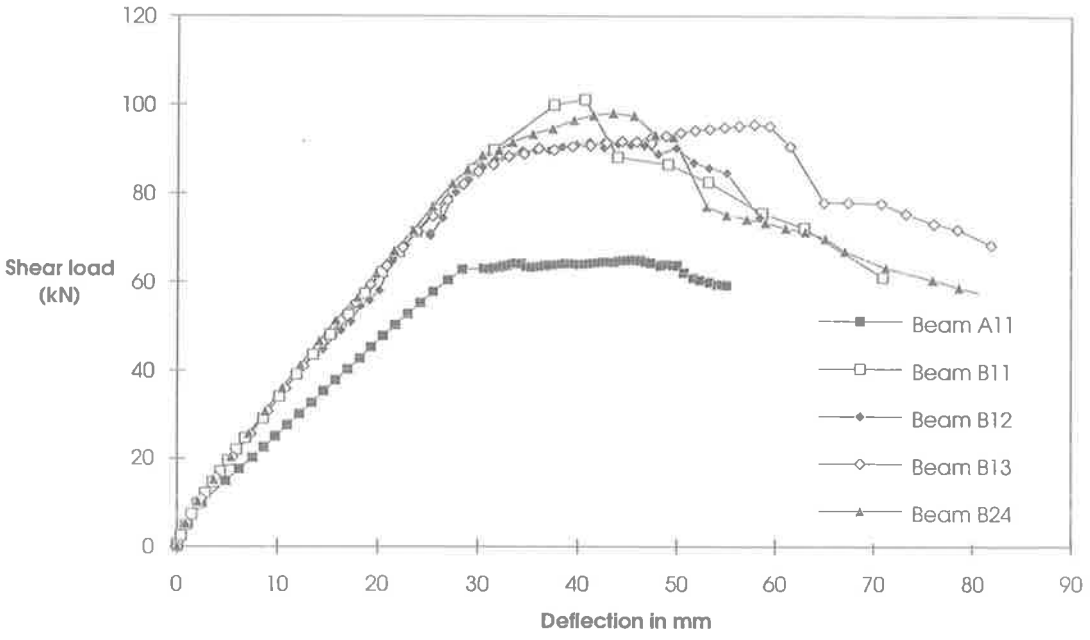

Fig. 8-165 Comparison of the plated beams in Series 2

It can be seen in Fig. 8-166 that the strength and stiffness of beams C11 and C12 are almost identical and substantially larger than the unplated beam A11. The reason is that the strength of this type of plated beam with full depth plates is not highly dependent on

the degree of shear connection (Oehlers and Bradford, 1995). Furthermore, the ductility of the plated beams are found to be fairly large as compared to the unplated beam.

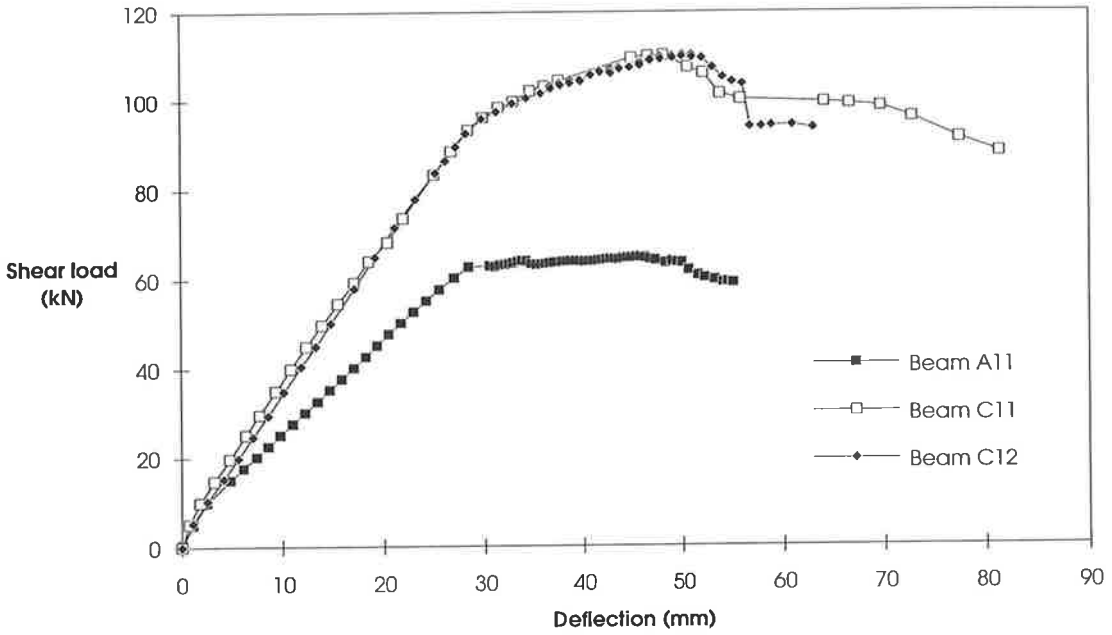

Fig. 8-166 Comparison of the plated beams in Series 3

The theoretical and experimental flexural capacities of the beams are tabulated in Table 8.44. The theoretical and the experimental increase of flexural capacity due to the plates are given in Col. 7 and 9 respectively. It is to be mentioned that the plated beam B24 has been compared with the unplated beam A21 as they both were from the same pour of concrete.

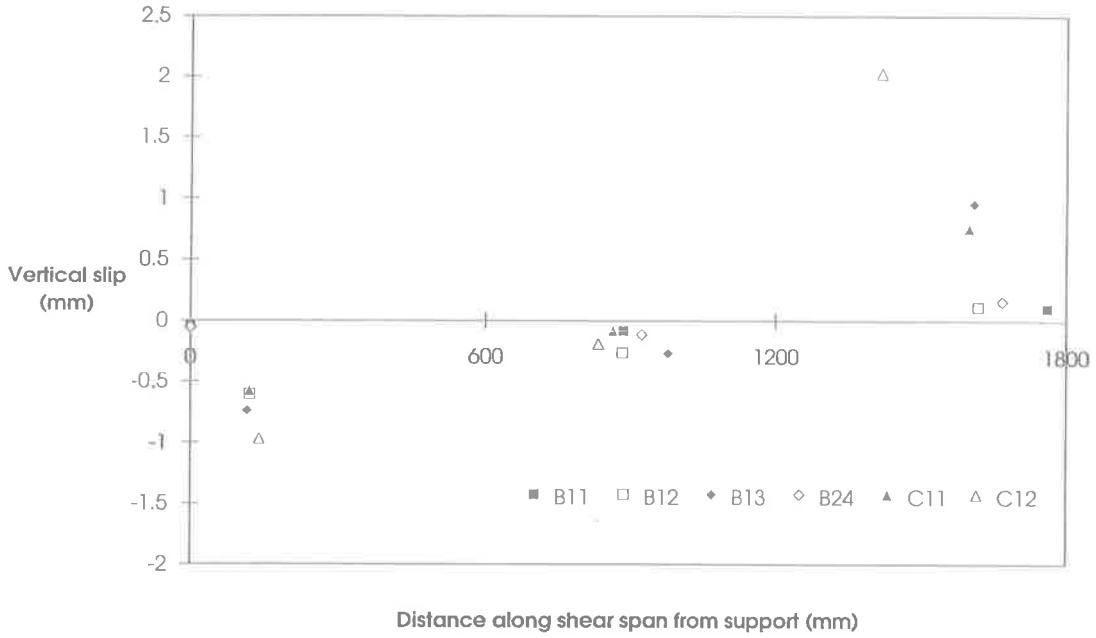

Fig. 8-168 Vertical slip

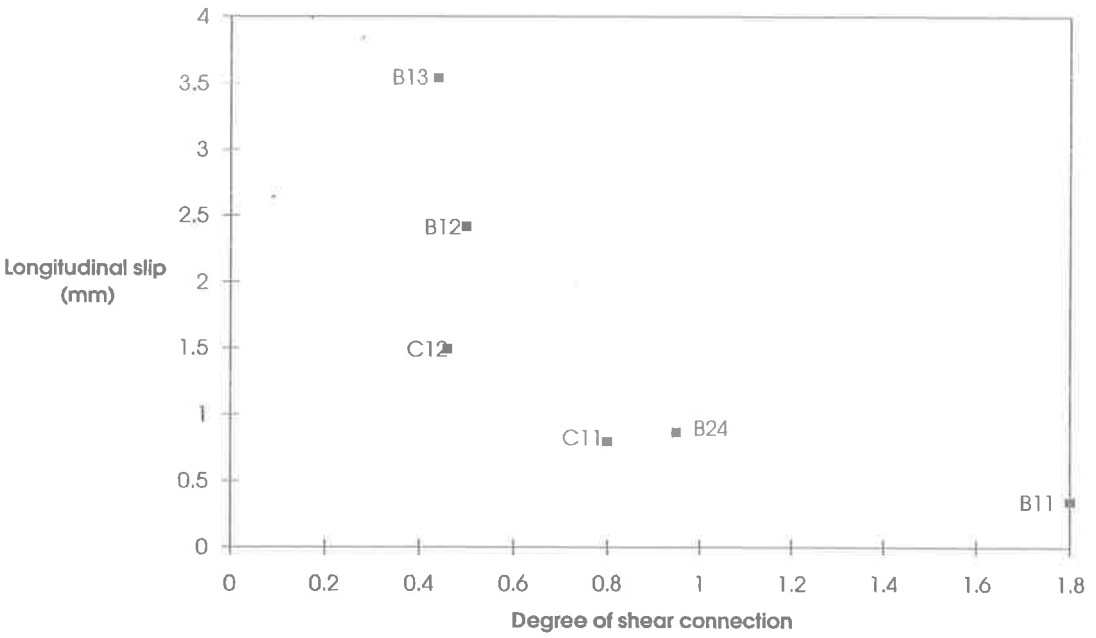

Fig. 8-169 Longitudinal slip

8.4.6.5 Summary of plated beam tests

Total eight beams were tested among which two were unplated and six were plated. The variation of the plated beams were the depths of the plate, the degree of shear connection and the number of row of bolts. The load-deflection behaviour, the distribution of vertical and longitudinal slip, the strain profile of the concrete element and the plate element, the forces in the plate element and the curvature in the concrete element and the plate element have been presented. The major observation was that the vertical slip causes the difference between the curvature of the elements, which also affect the rigid plastic flexural strengths. Moreover, the strengths of the almost full depth plated beams were found same for different degree of shear connection. Also, the experimental investigation showed that the strength of plated beam can be affected due to buckling in the plate.

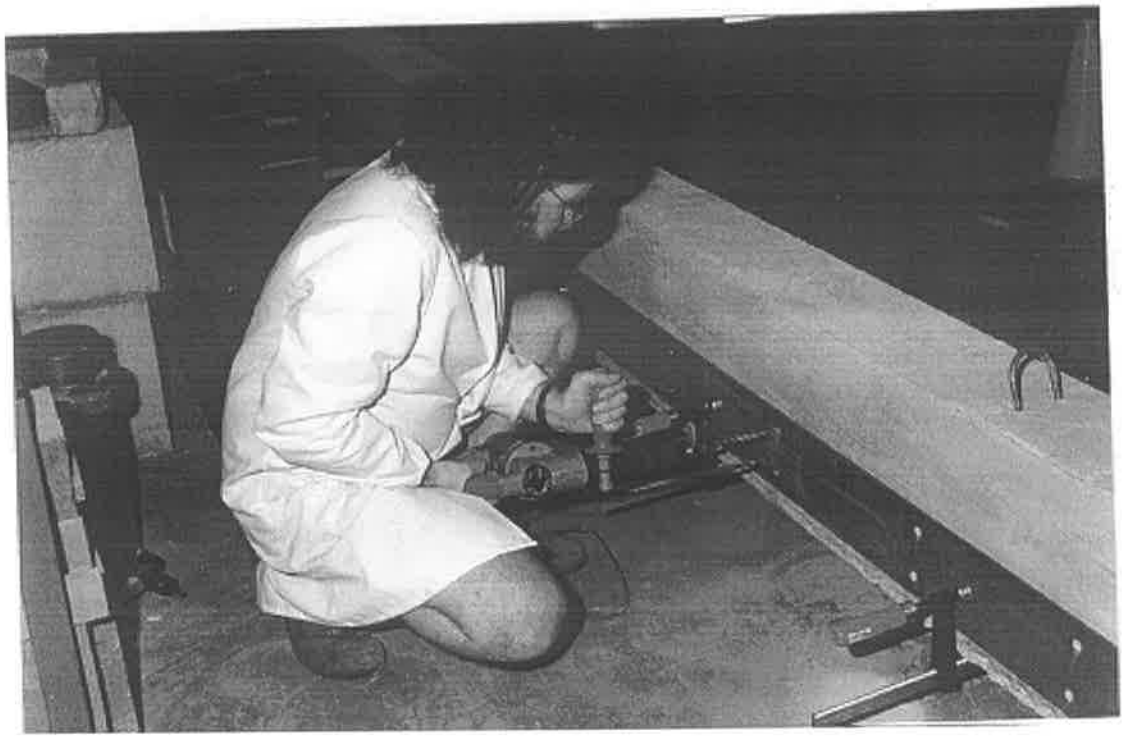

P8.6 Drilling into concrete and plate

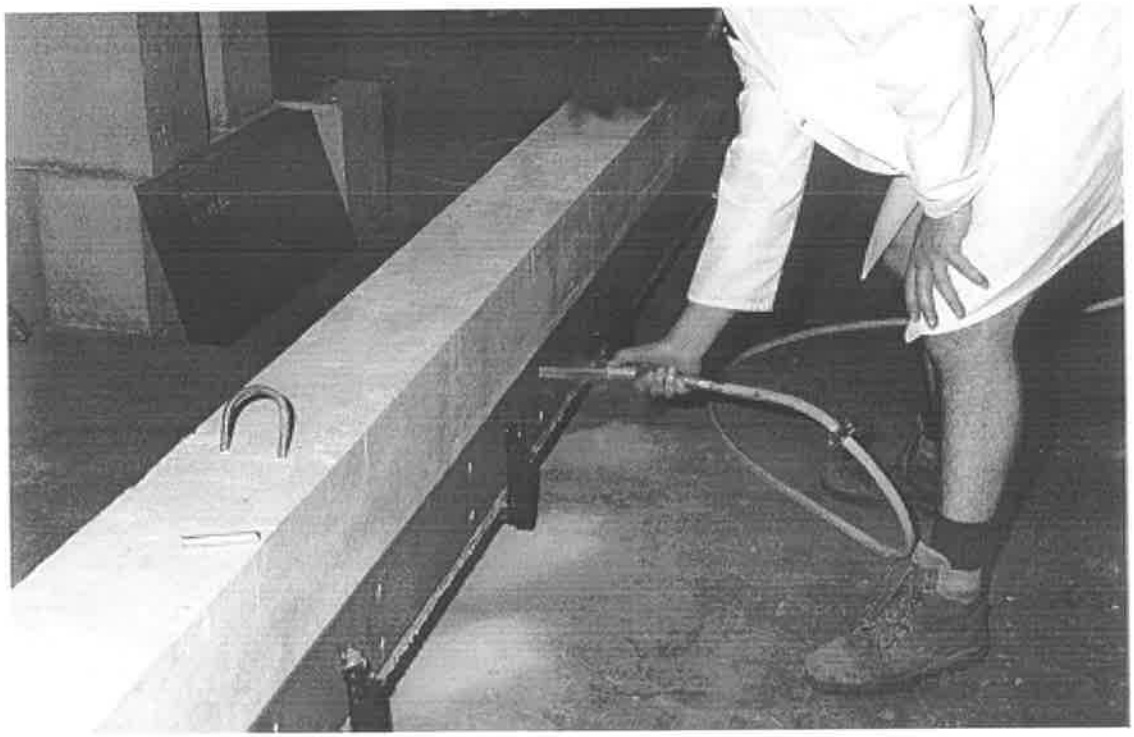

P8.7 Clearing dust from concrete hole

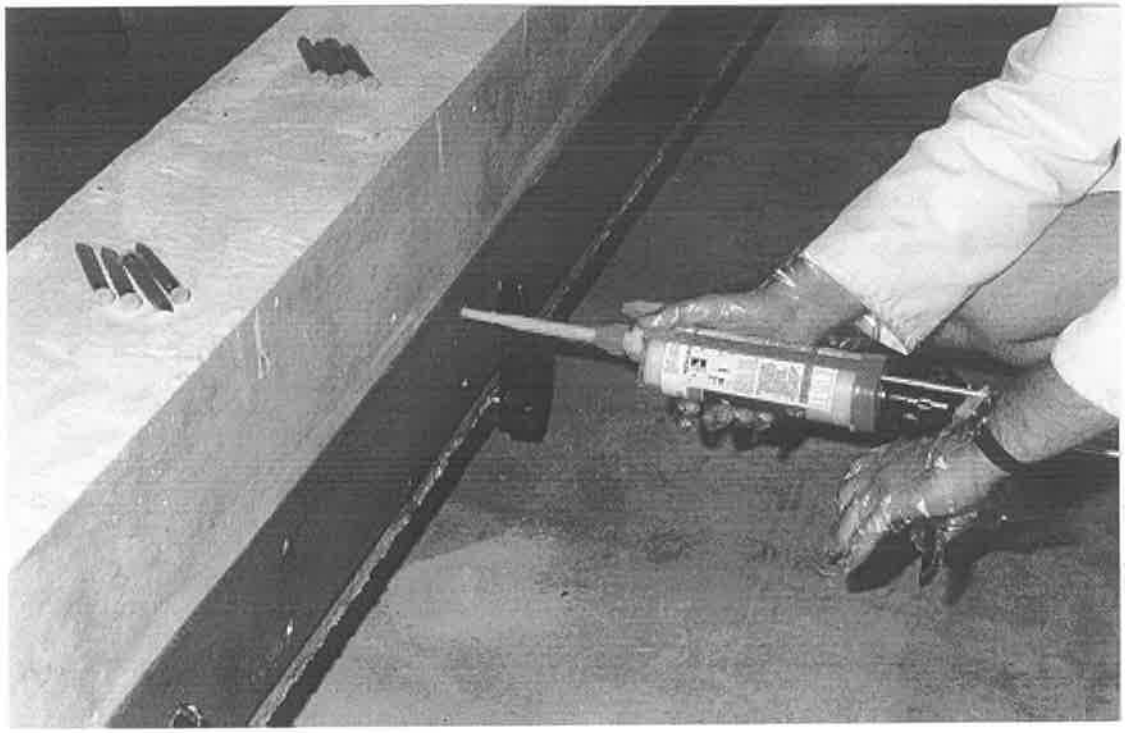

P8.8 Injection of glue into concrete hole

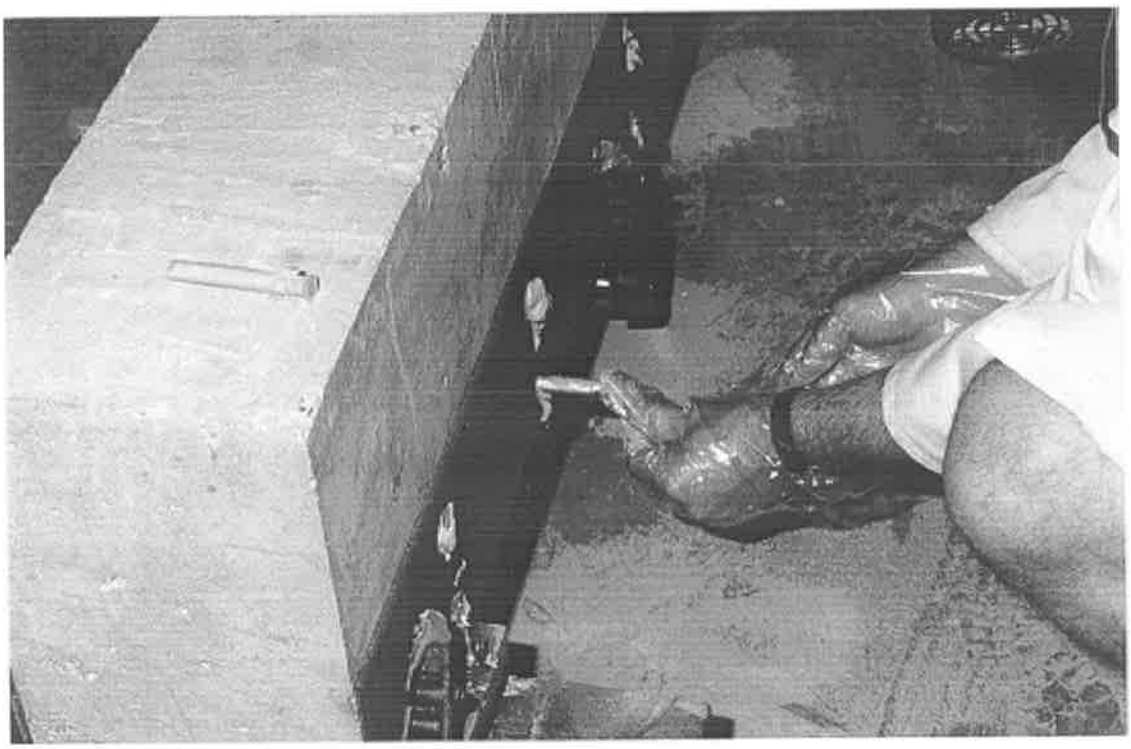

P8.9 Insertion of HIS adhesive bolt

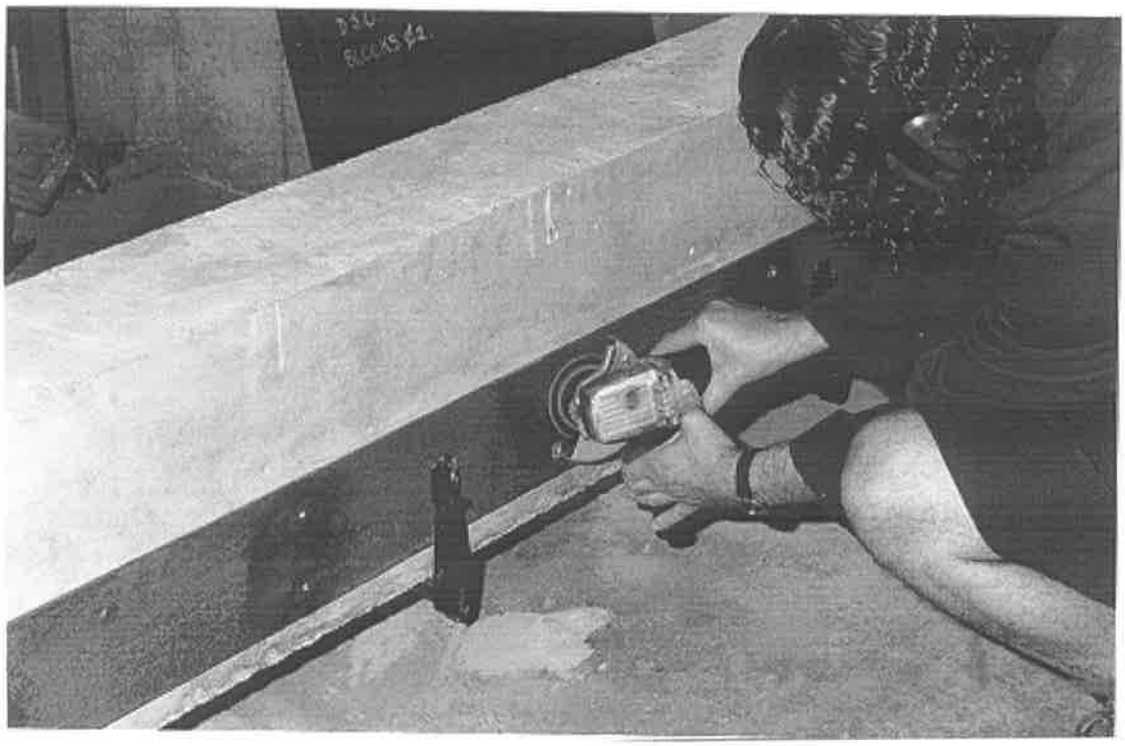

P8.10 Cleaning glue over plate

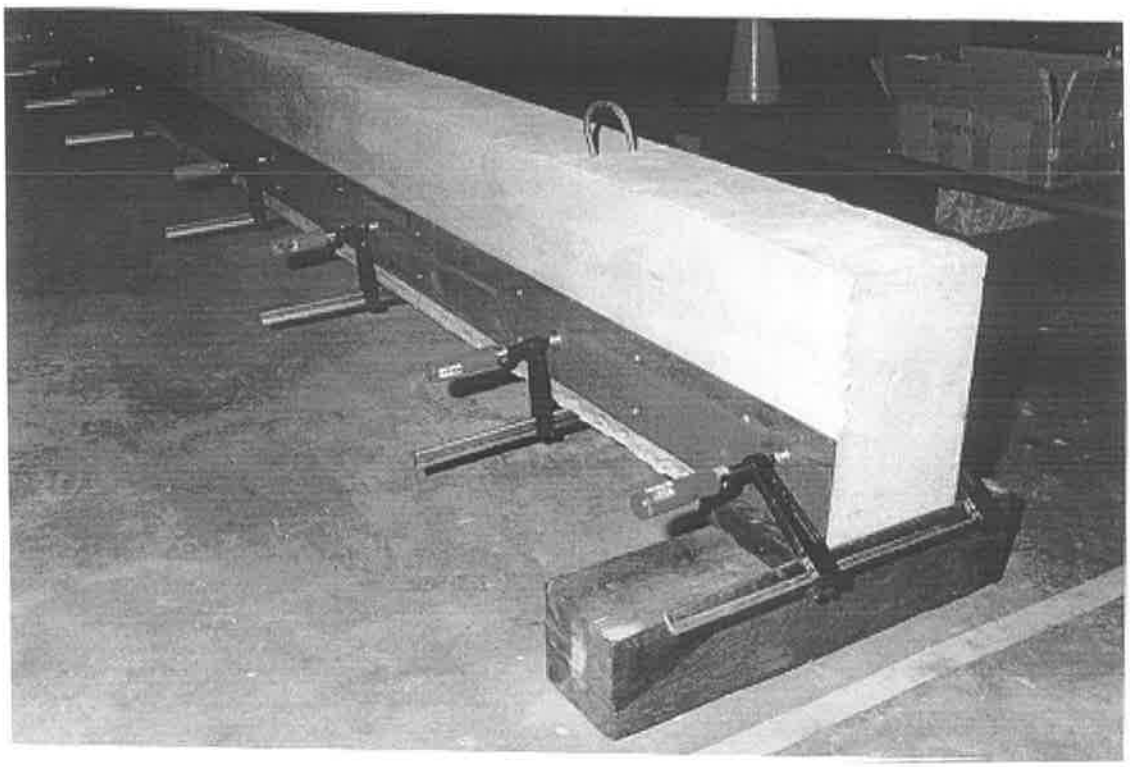

P8.11 Curing of glue

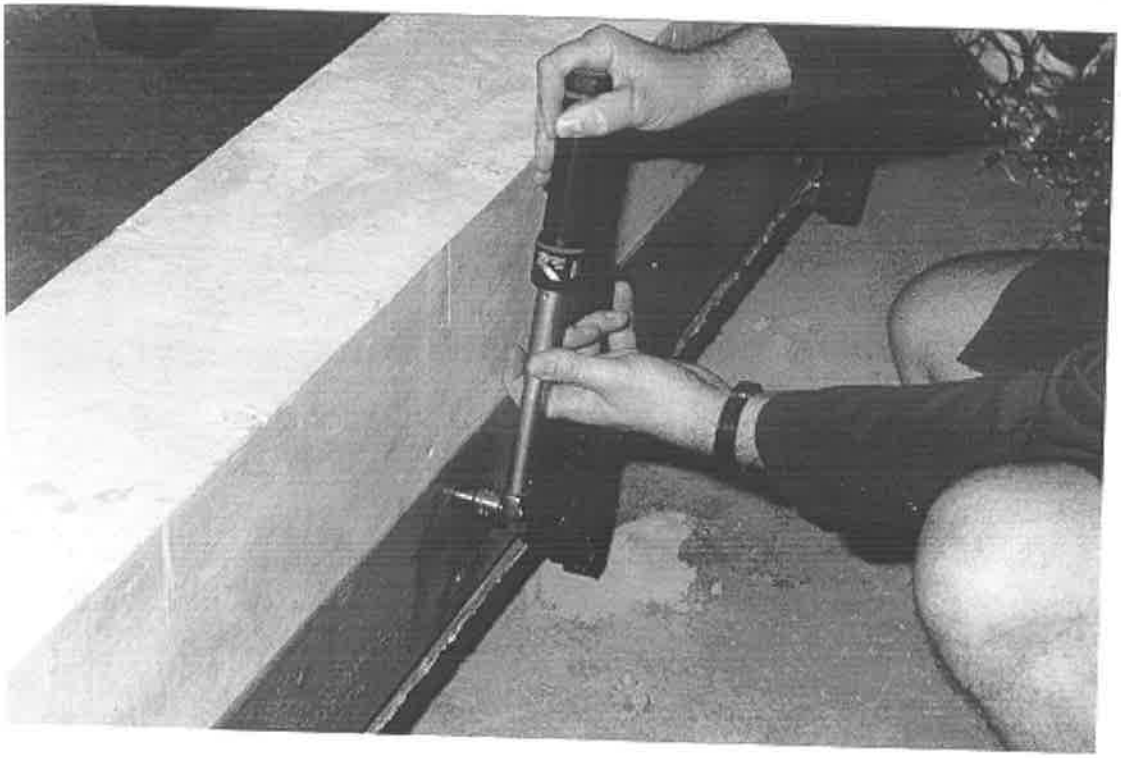

P8.12 Tightening of Set screw into bolt

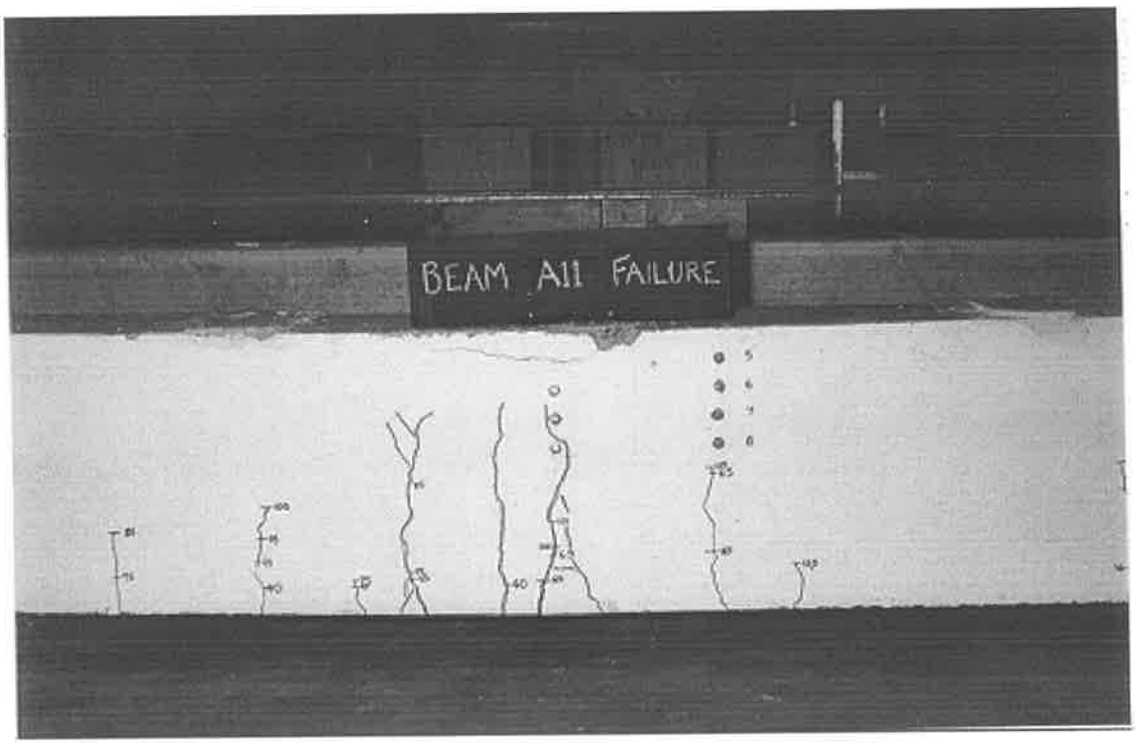

P8.13 Flexural failure of beam A11

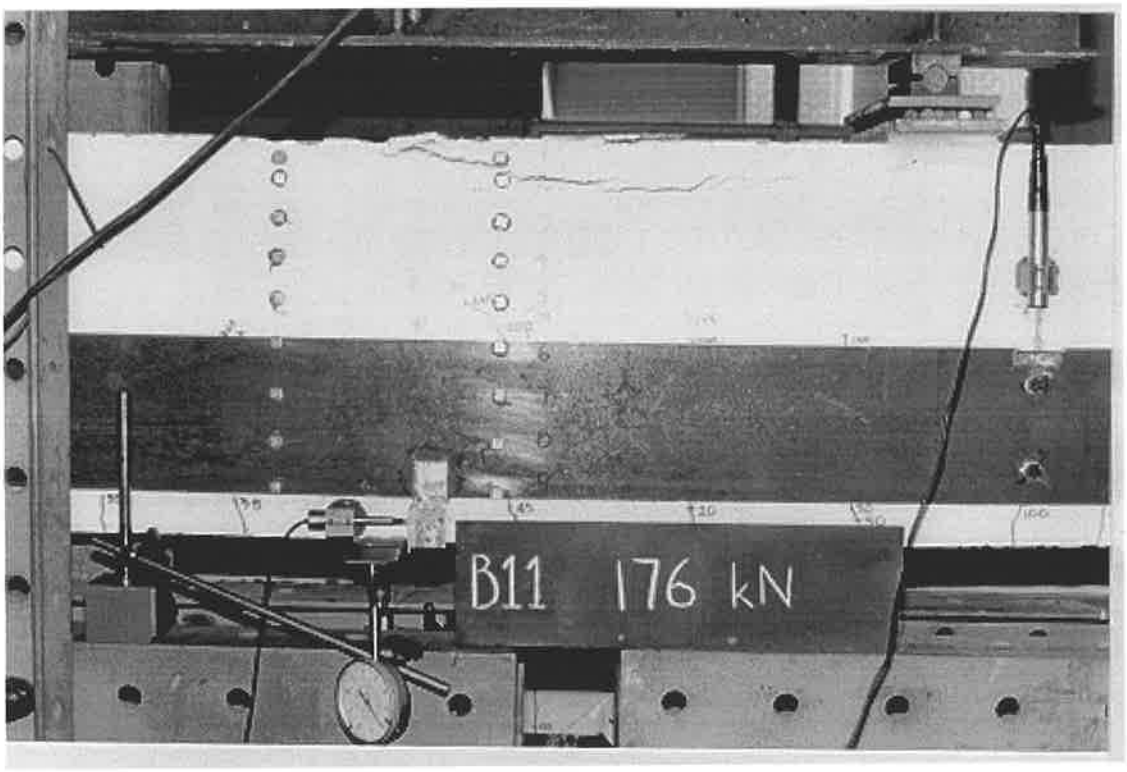

P8.16 Flexural failure of beam B11

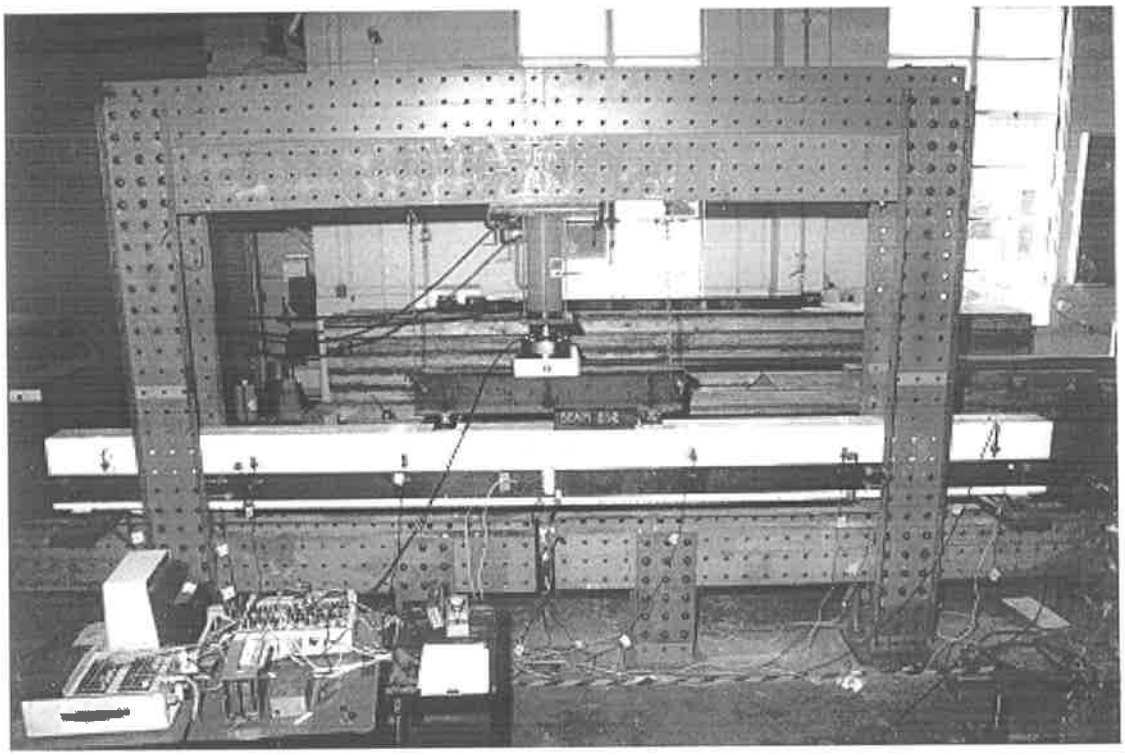

P8.17 Test set up of beam B12

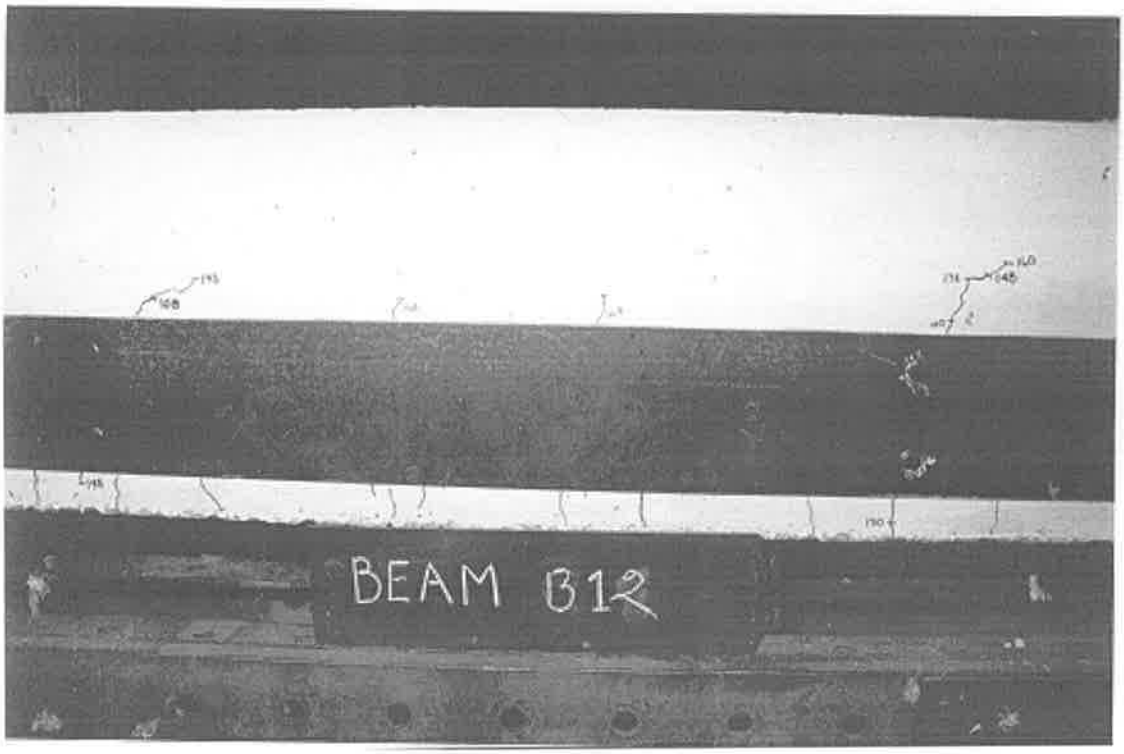

P8.18 Cracks appeared above plate at 90 kN of applied load in beam B12

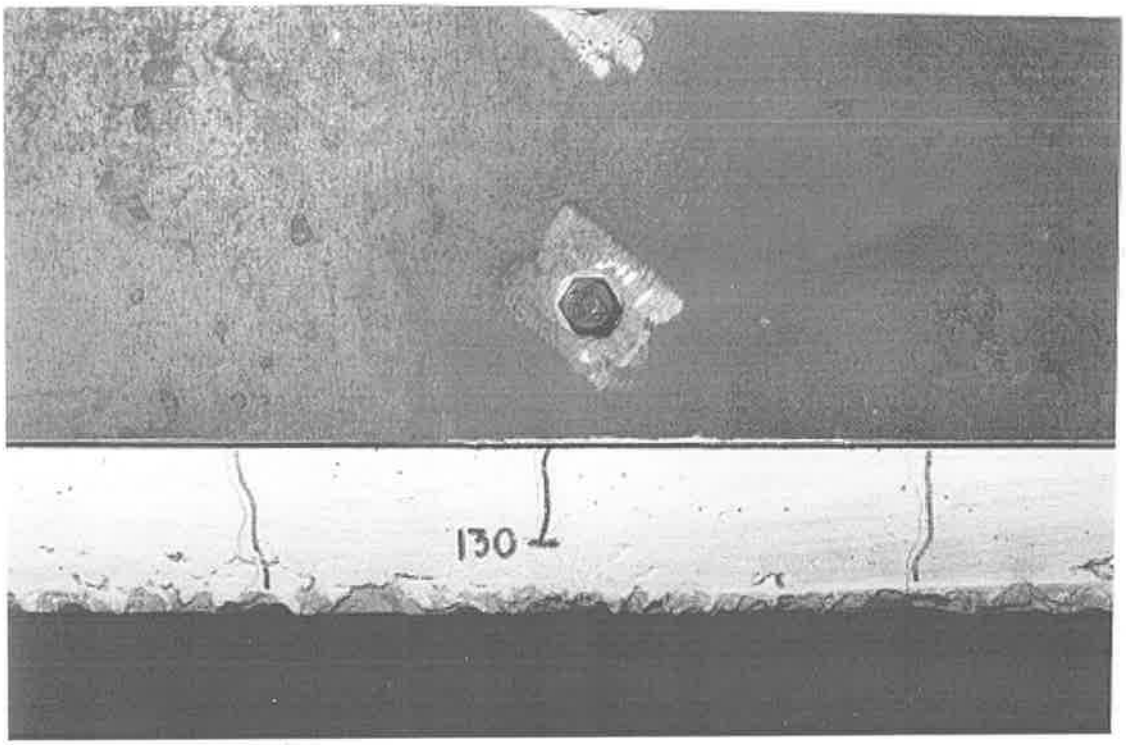

P8.19 Cracks at the position of bolt in beam B12

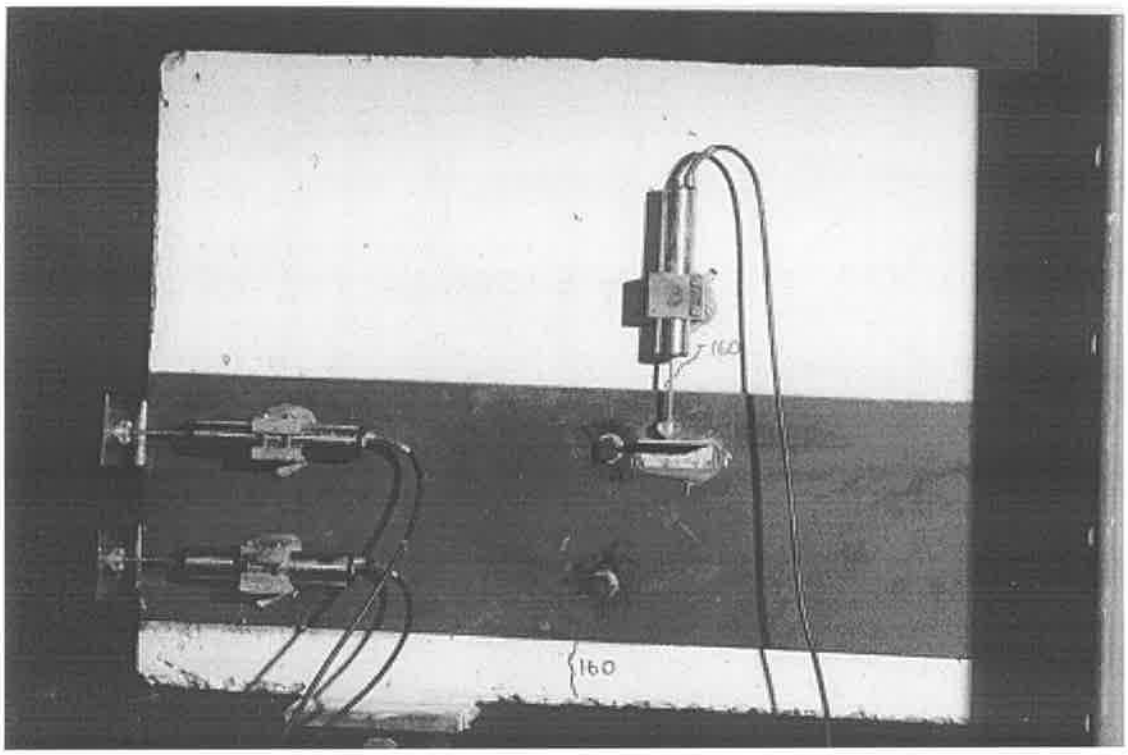

P8.20 Cracks at the position of bolt near support in beam B12

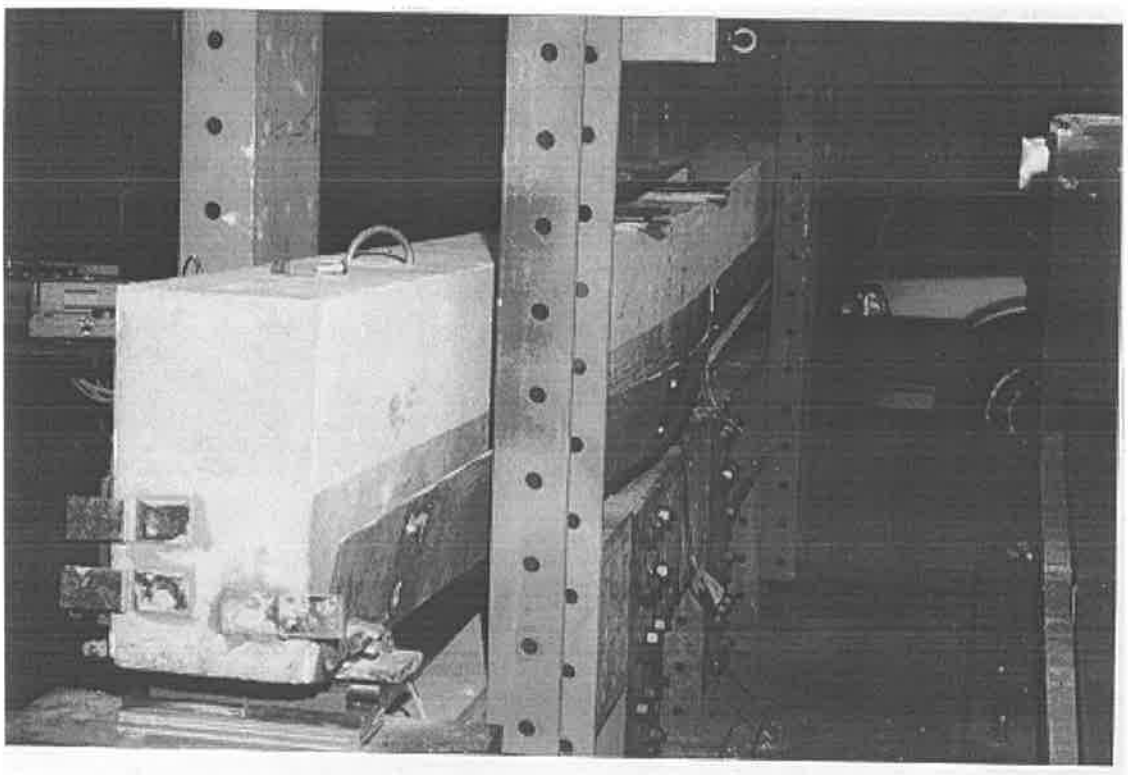

P8.21 Plate pulled out in beam B12

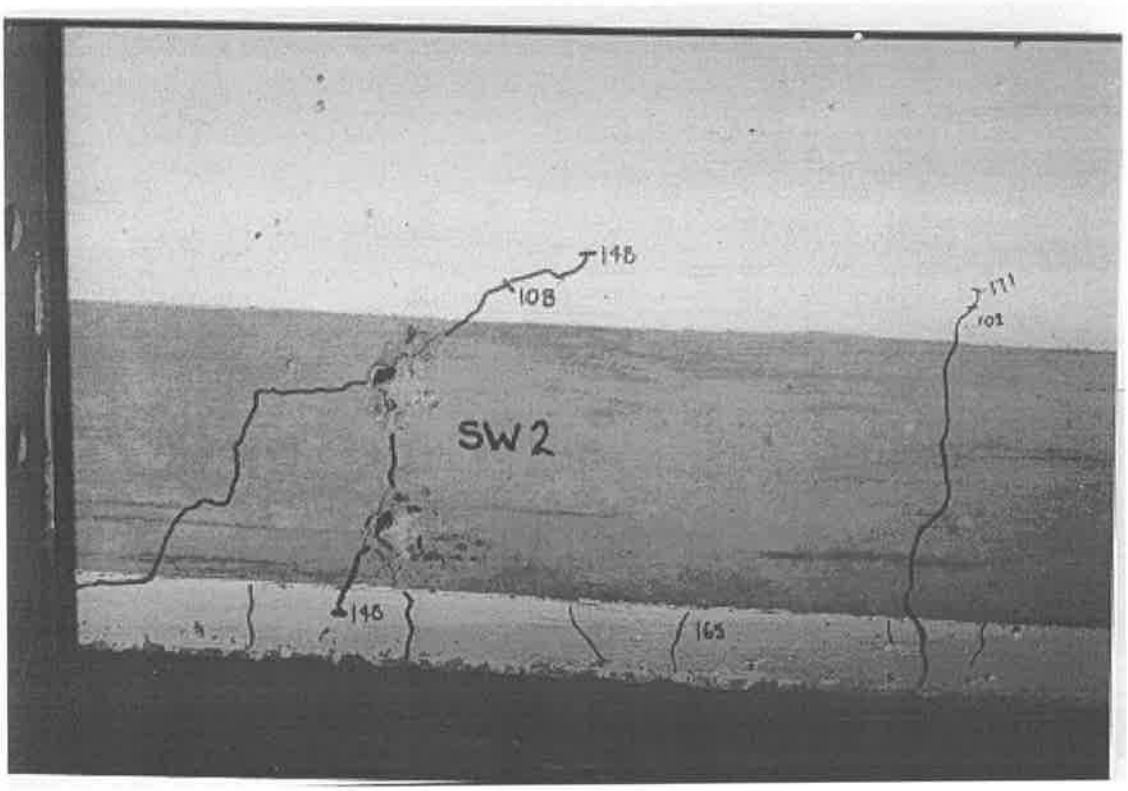

P8.22 Cracks at the middle of South-West shear span (Beam B12)

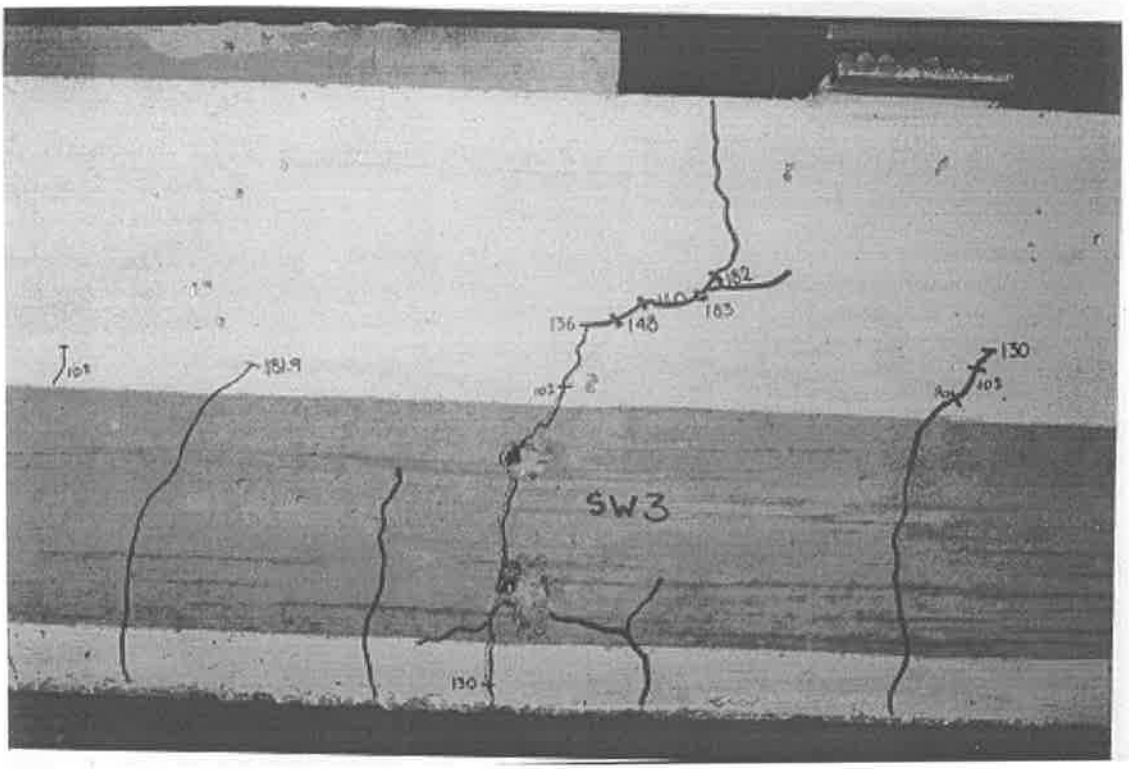

P8.23 Cracks near to the applied load at South-West shear span (Beam B12)

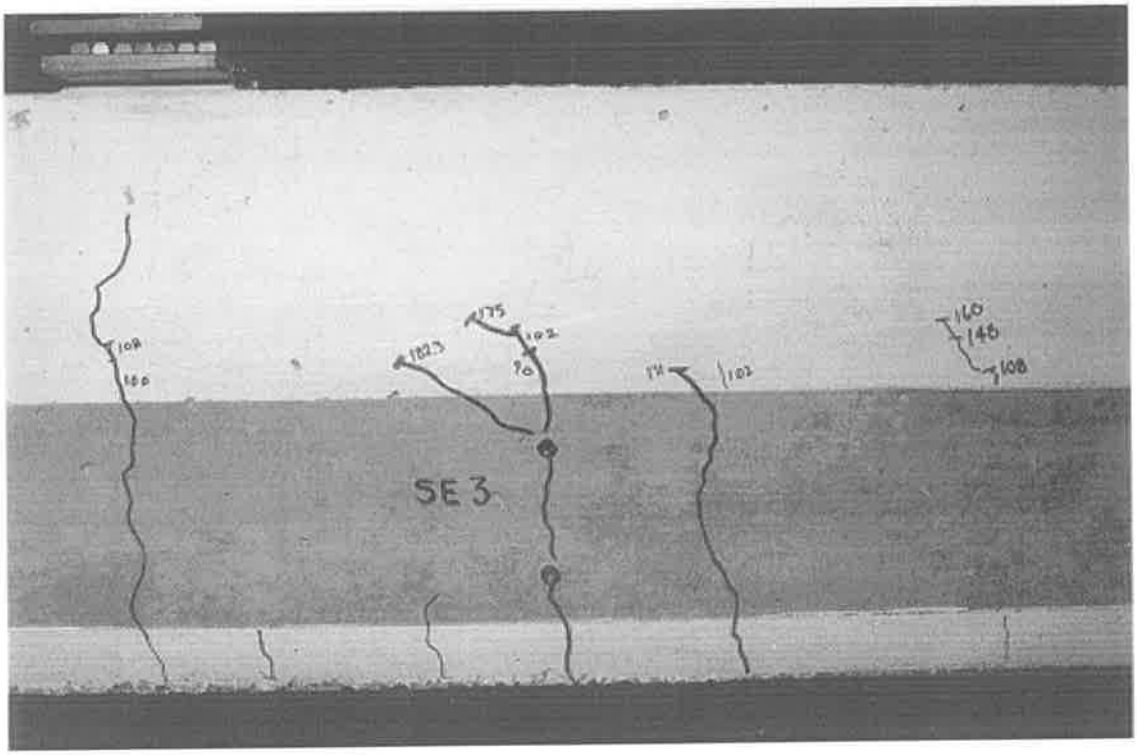

P8.24 Cracks near to applied load at South-East shear span (Beam B12)

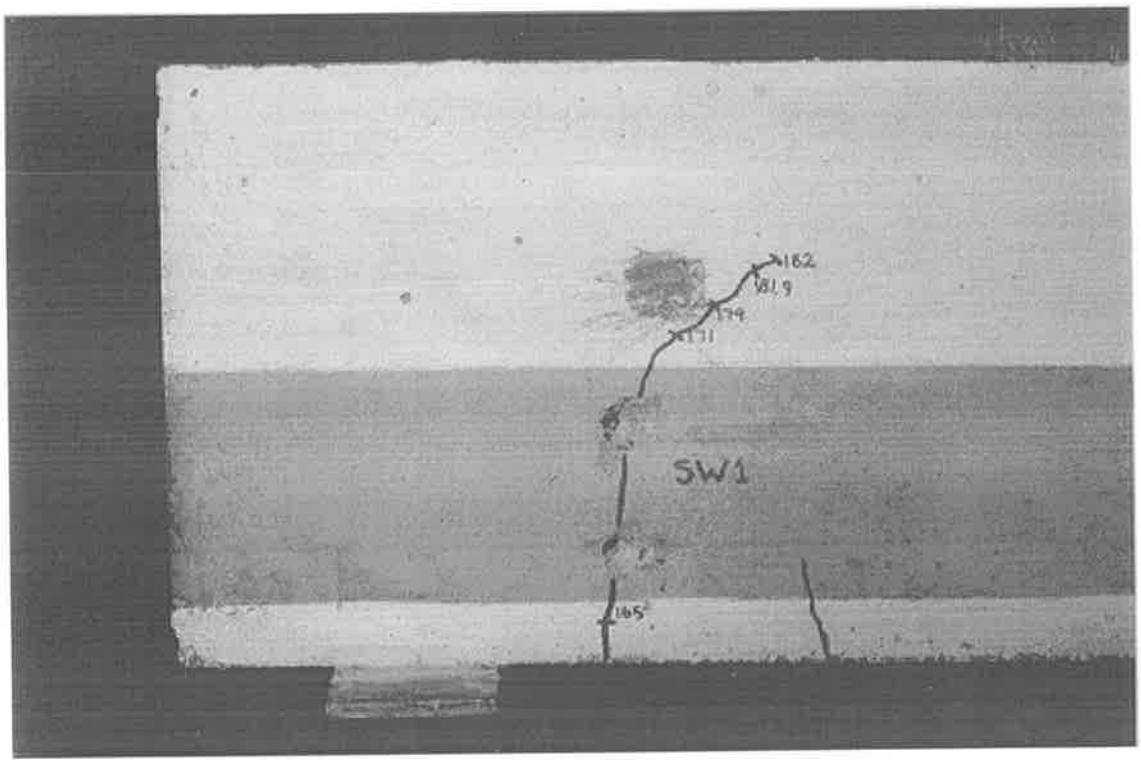

P8.25 Cracks near to support at South-West shear span (Beam B12)

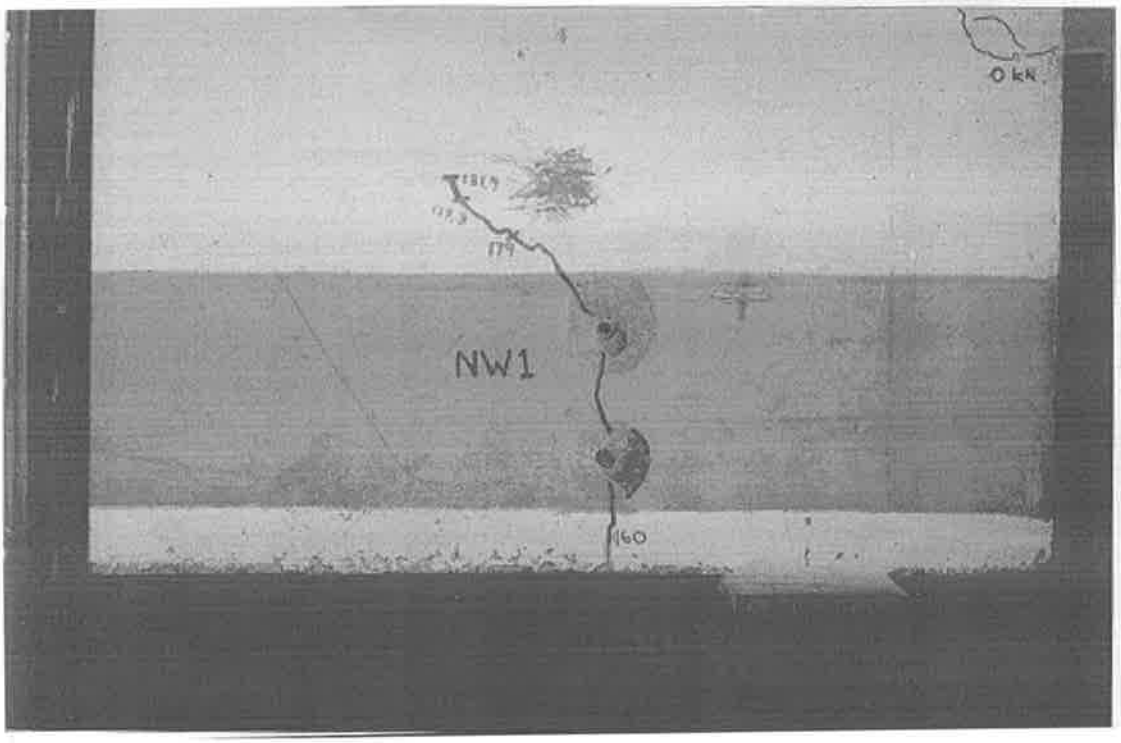

P8.28 Cracks near to support at North-West shear span (Beam B12)

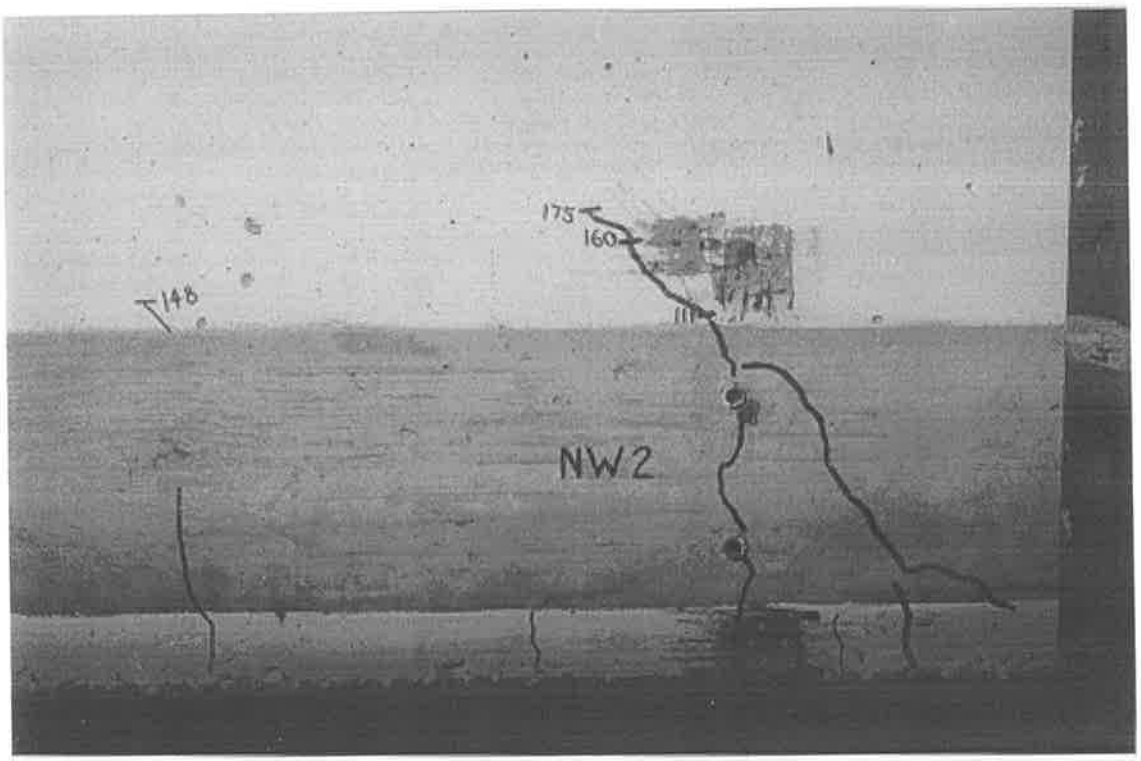

P8.29 Cracks at the middle of North-West shear span (Beam B12)

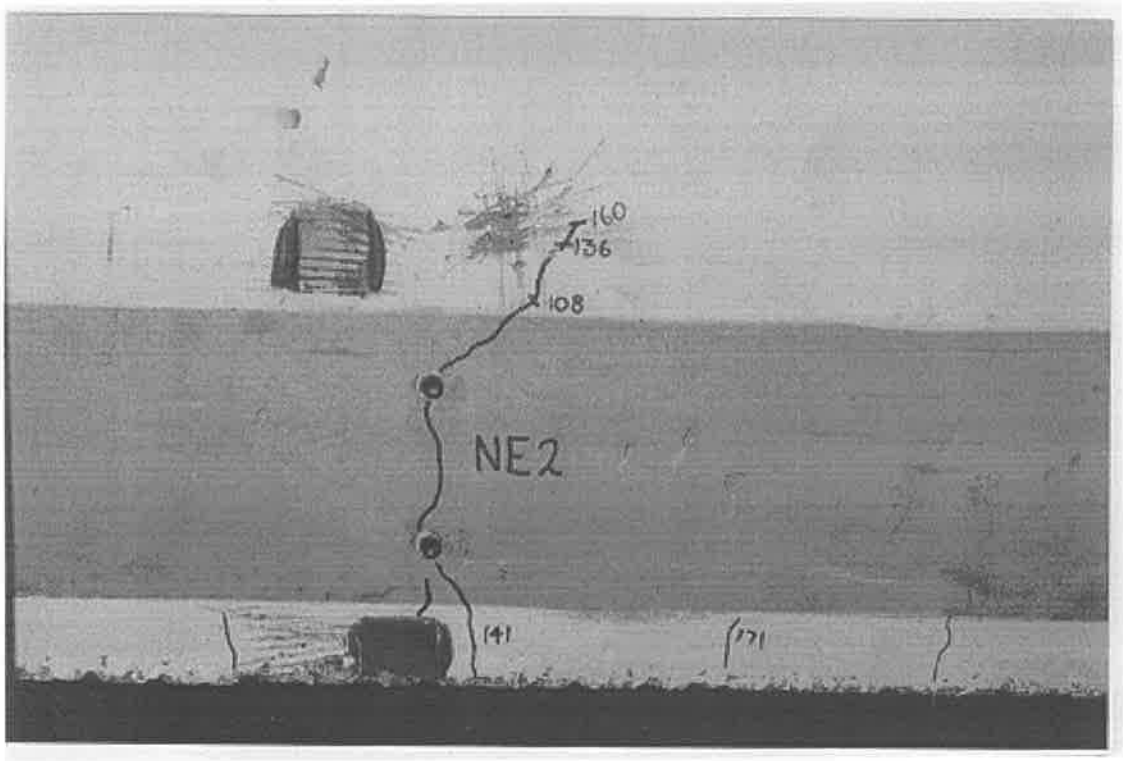

P8.32 Cracks at the middle of North-East shear span (Beam B12)

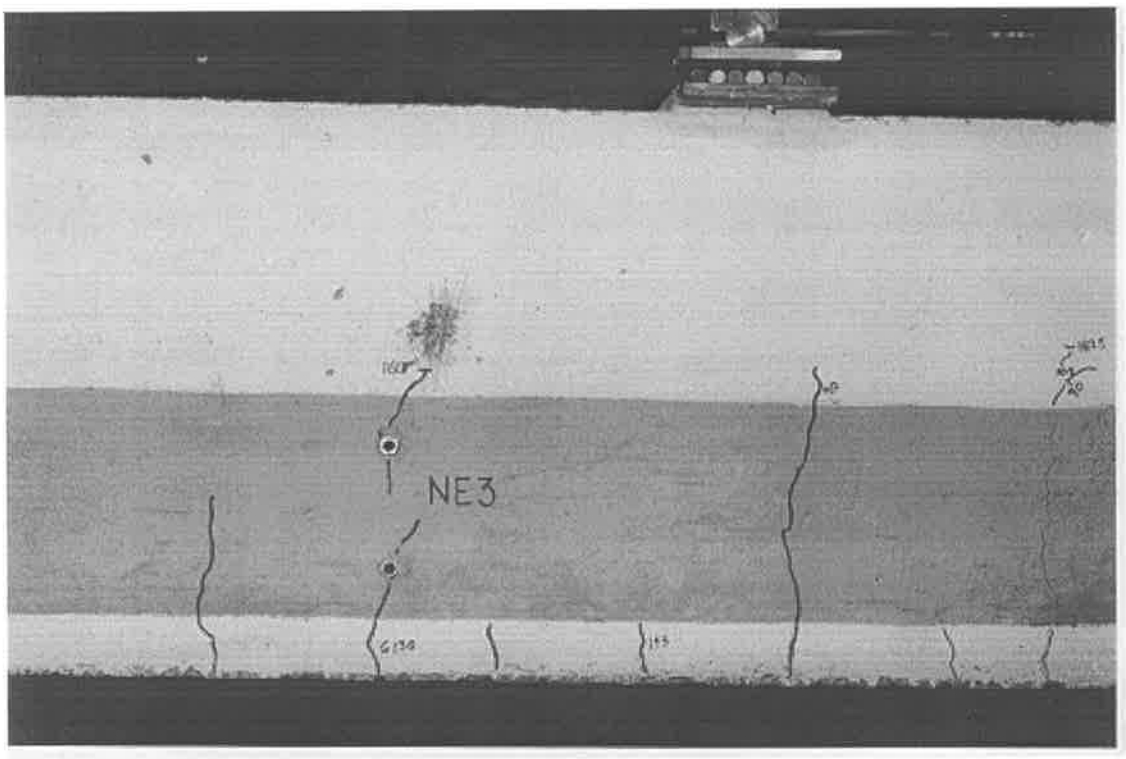

P8.33 Cracks near to applied load at North-East shear span (Beam B12)

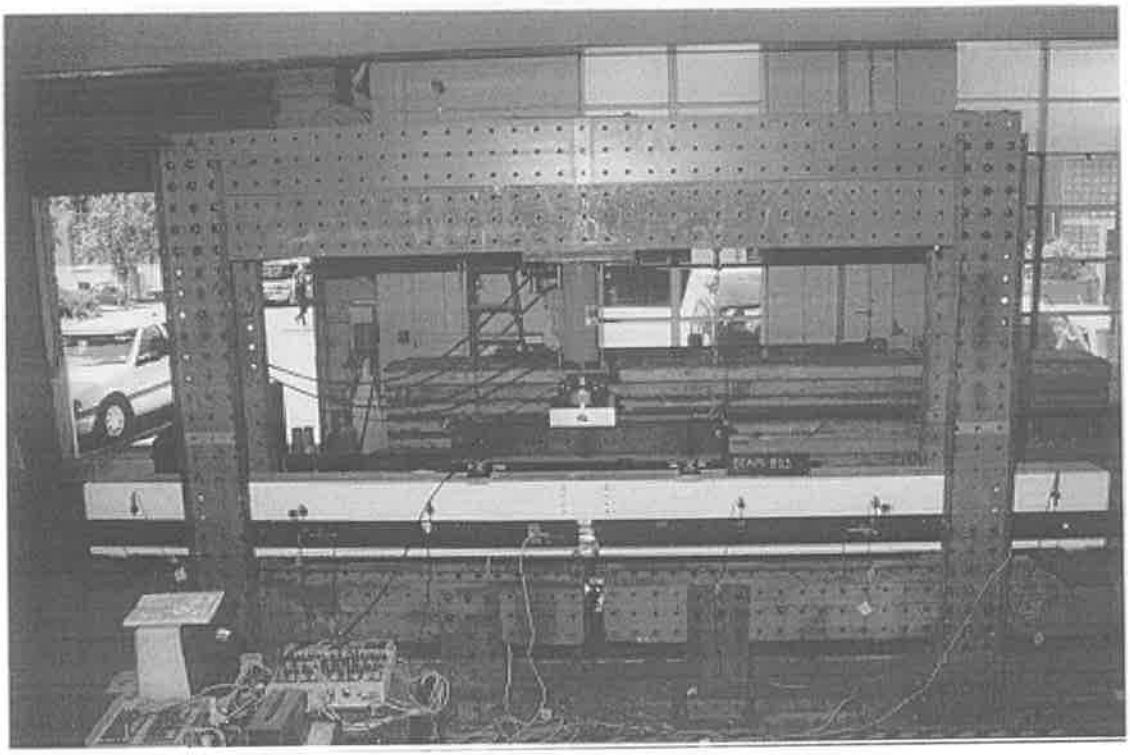

P8.34 Test set up of beam B13

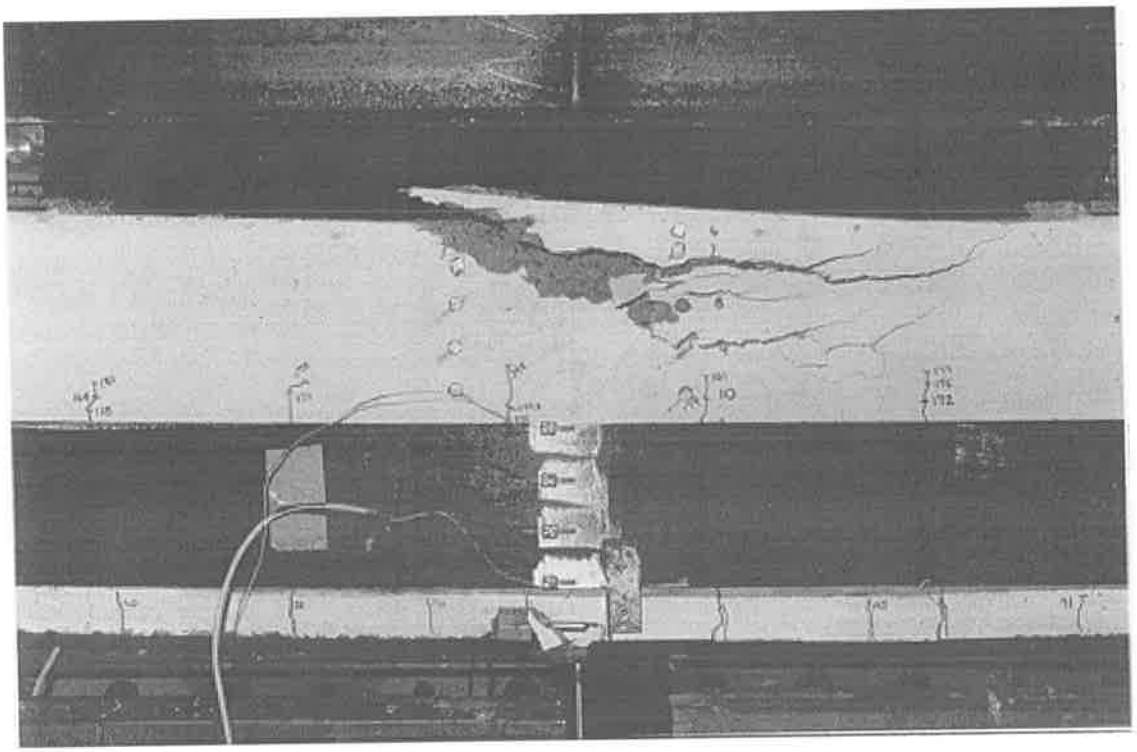

P8.35 Flexural failure of beam B13

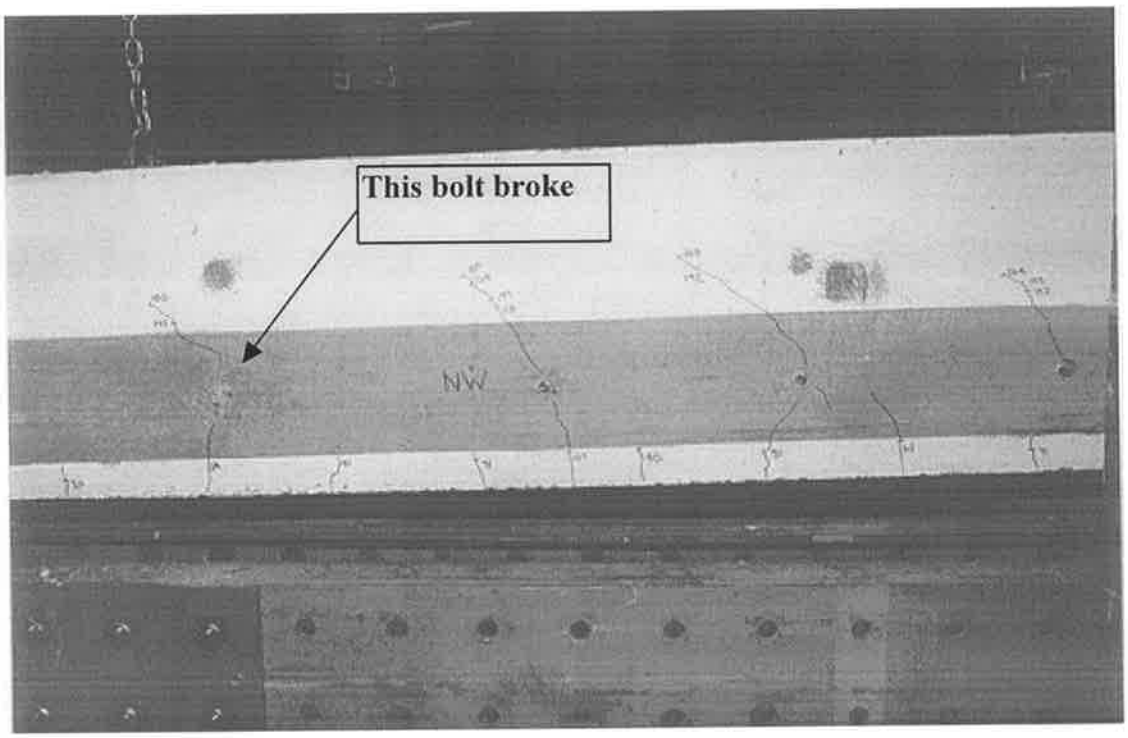

P8.36 Cracks at North-West shear span (Beam B13)

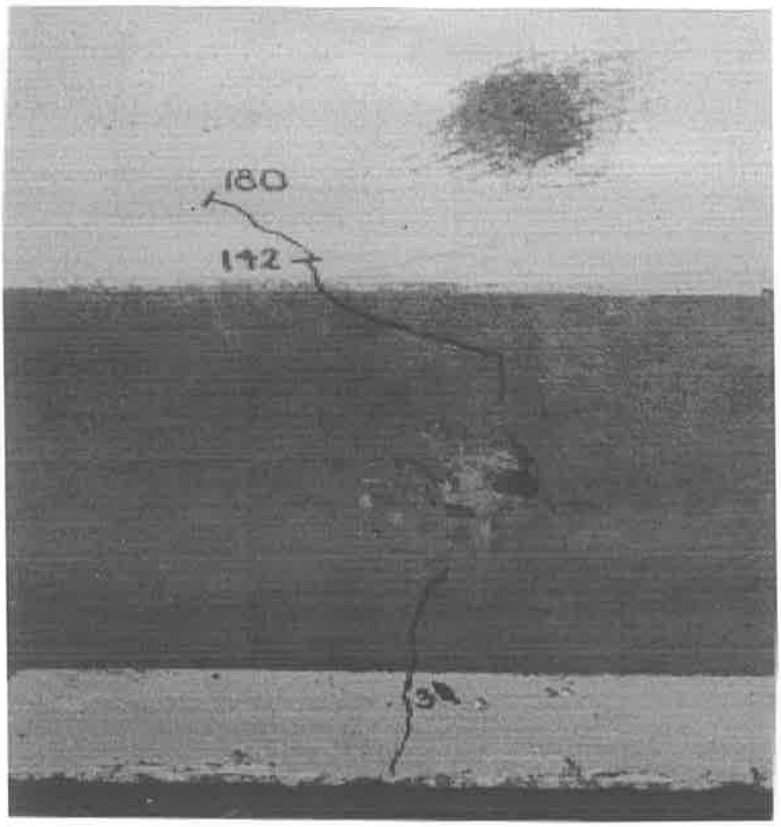

P8.37 Crushed concrete surrounding the broken bolt (Beam B13)

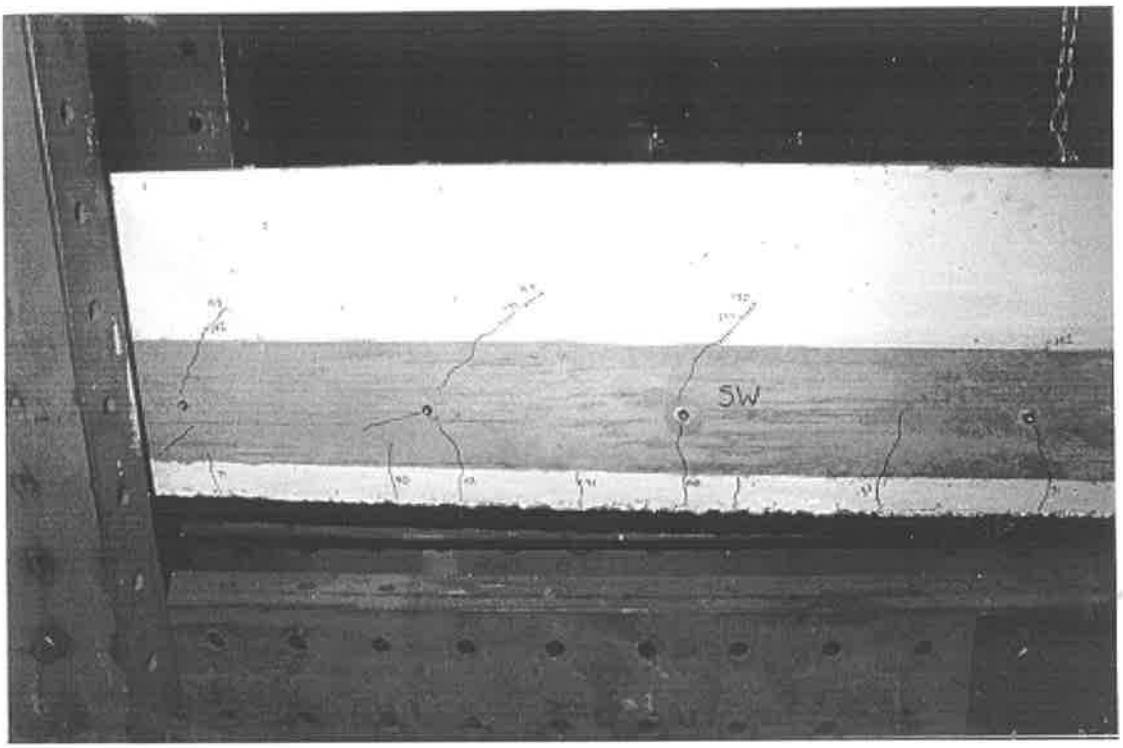

P8.40 Cracks at South-West shear span (Beam B13)

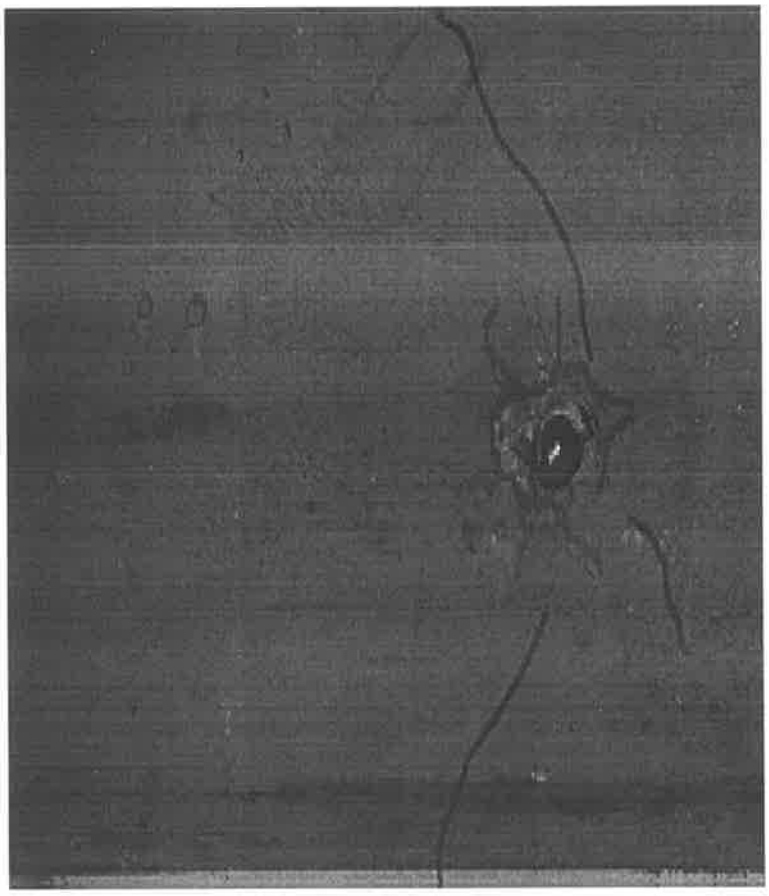

P8.41 Damaged concrete surrounding bolt (Beam B13)

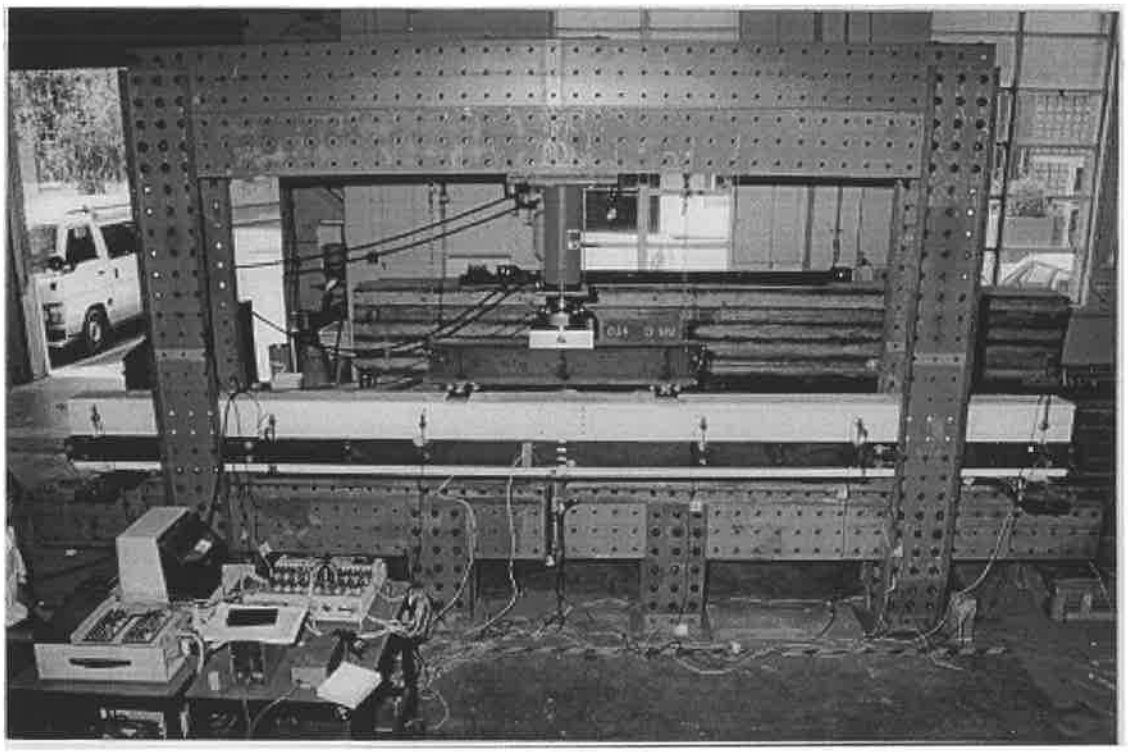

P8.42 Test set up of beam B24

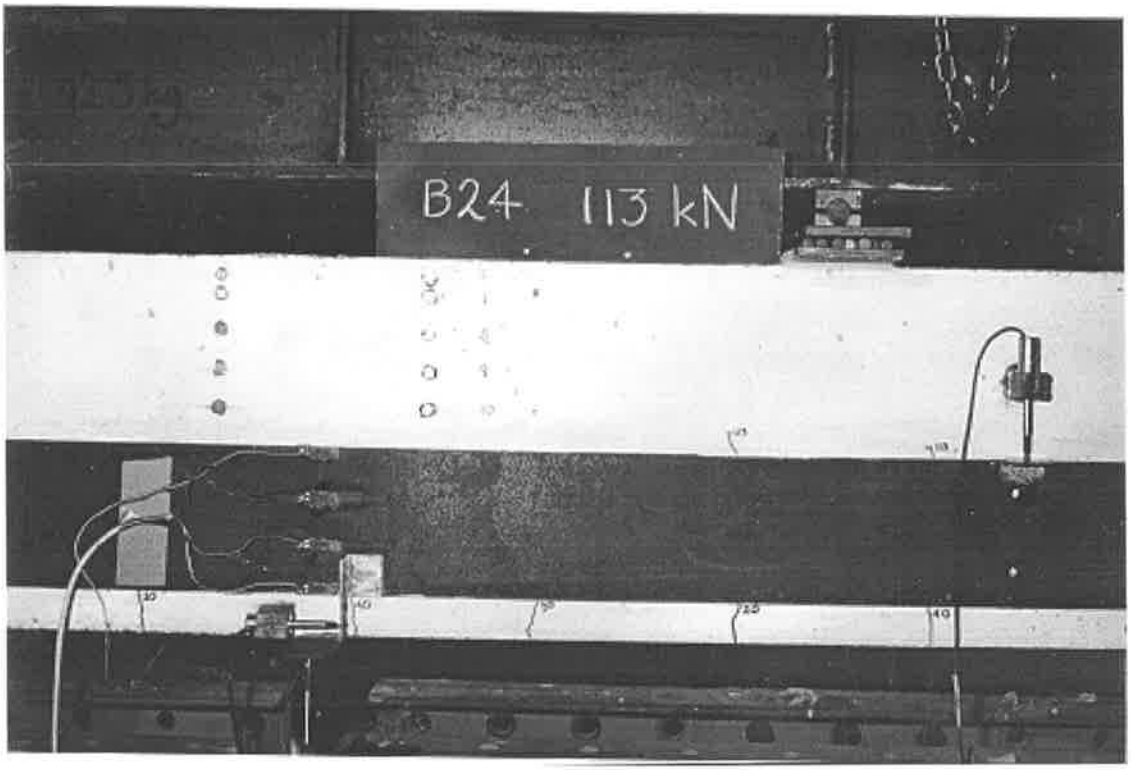

P8.43 Flexural crack in beam B24

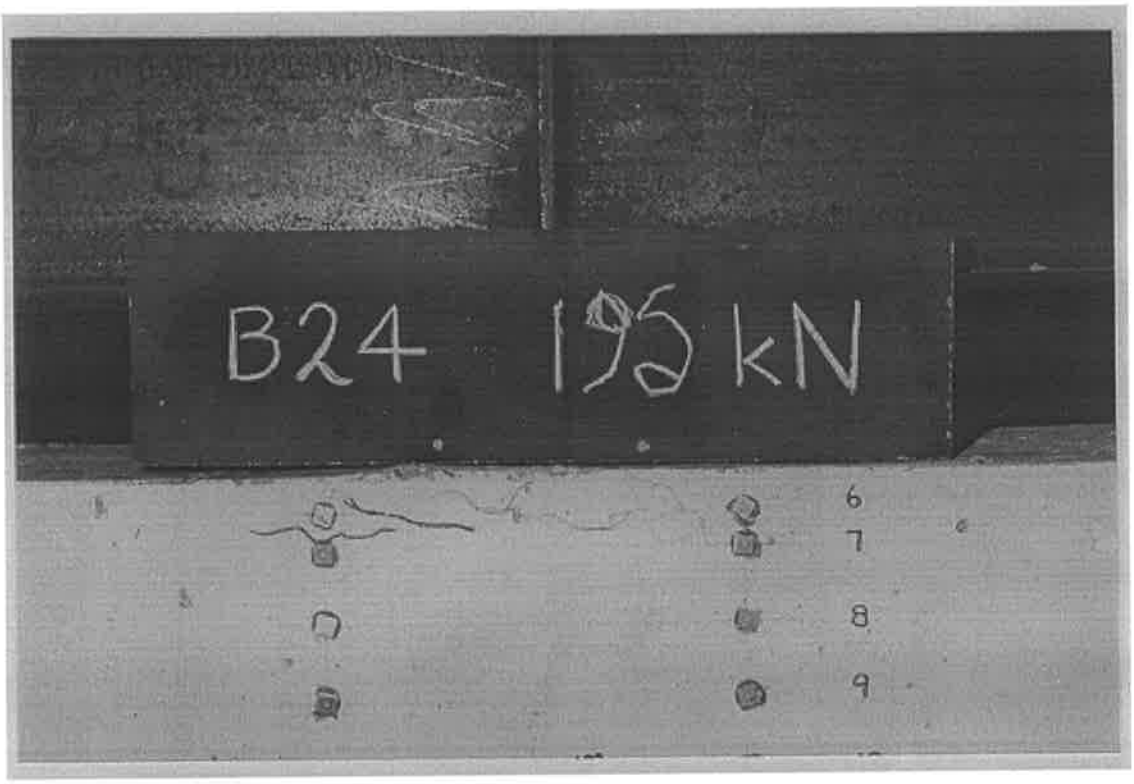

P8.44 Flexural failure of beam B24

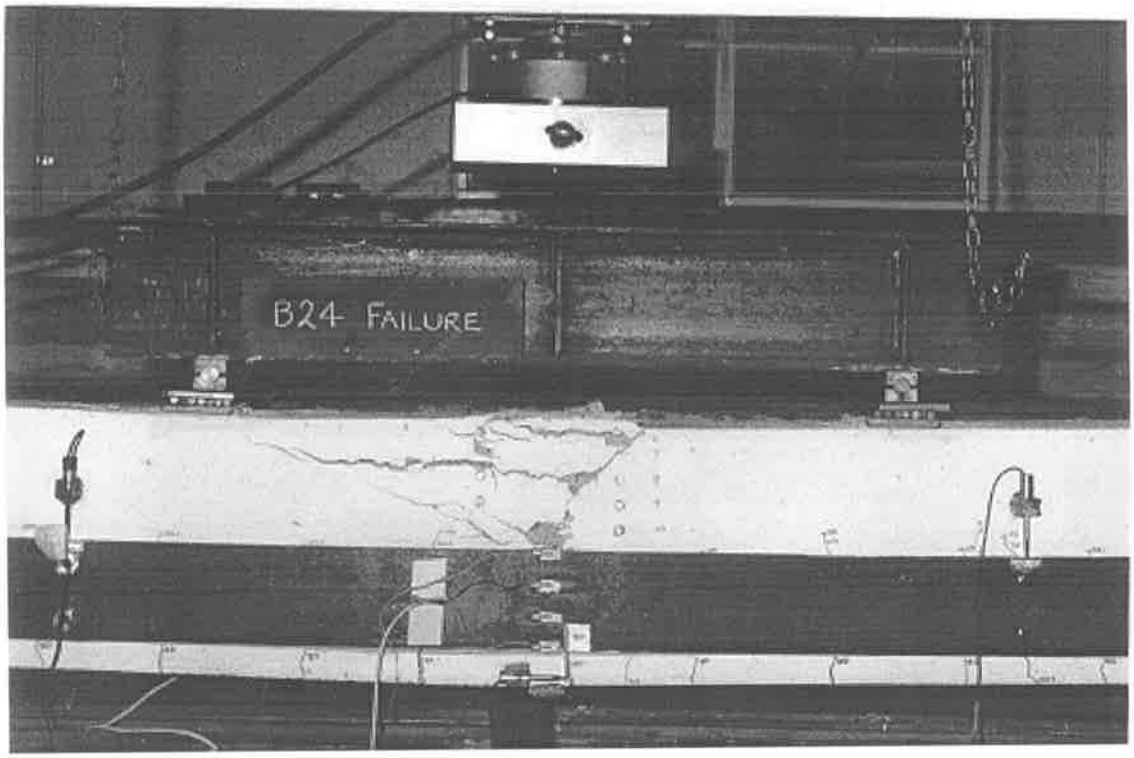

P8.45 Flexural failure of beam B24

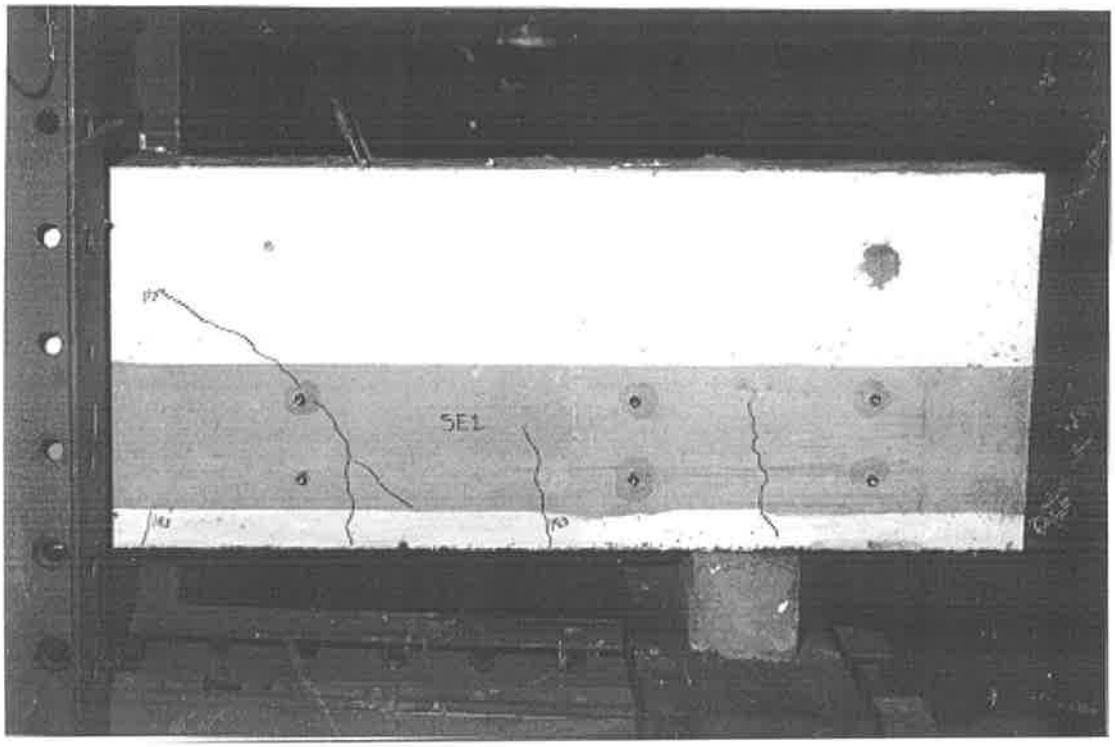

P8.48 Cracks near to support at South-East shear span of beam B24

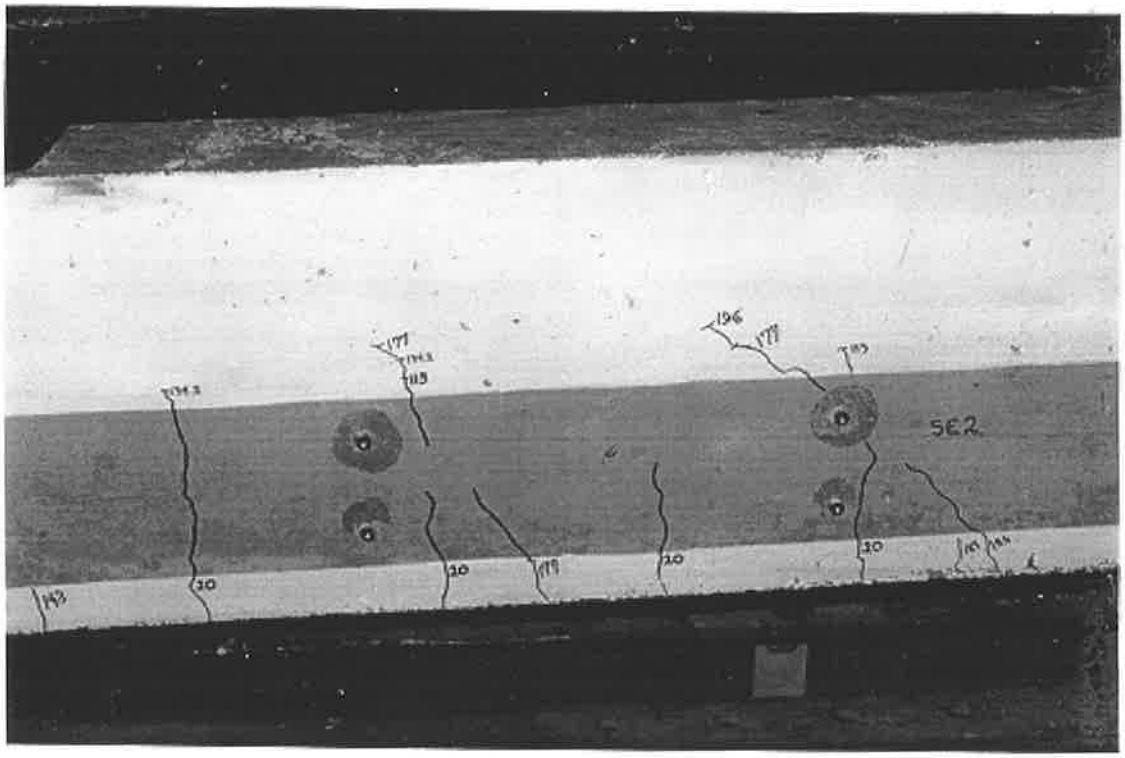

P8.49 Cracks near to applied load at South-East shear span of beam B24

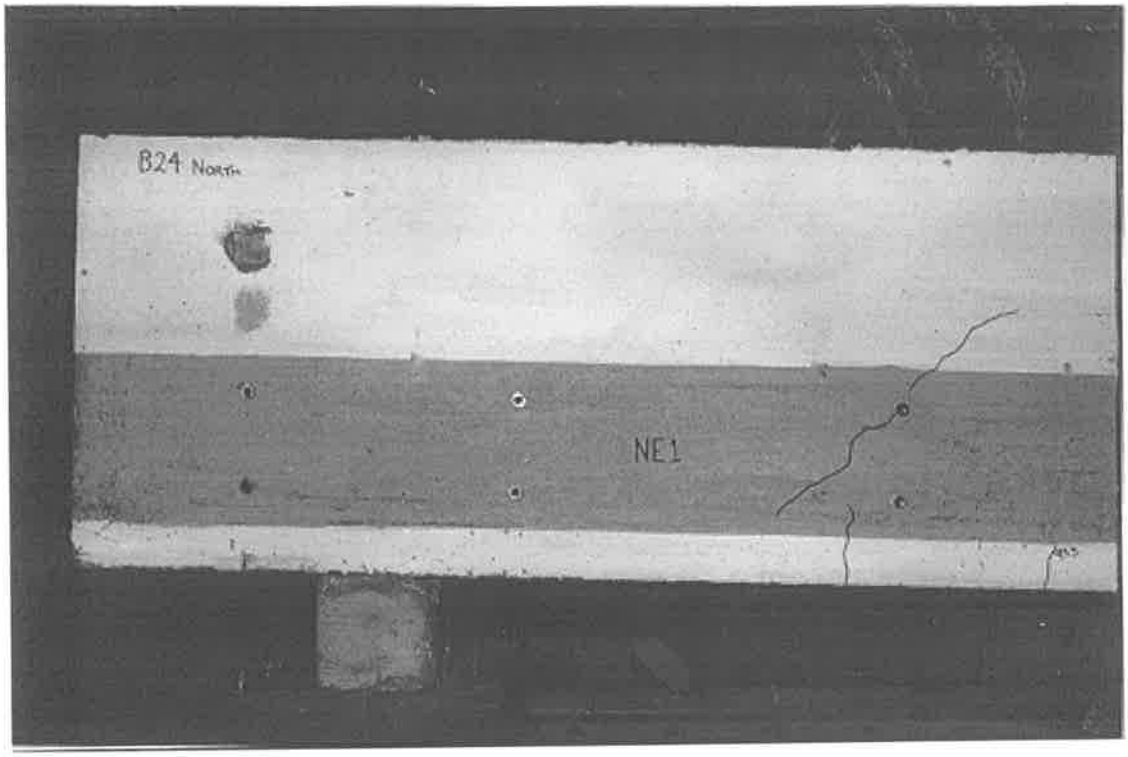

P8.50 Cracks near to the support at North-East shear span of beam B24

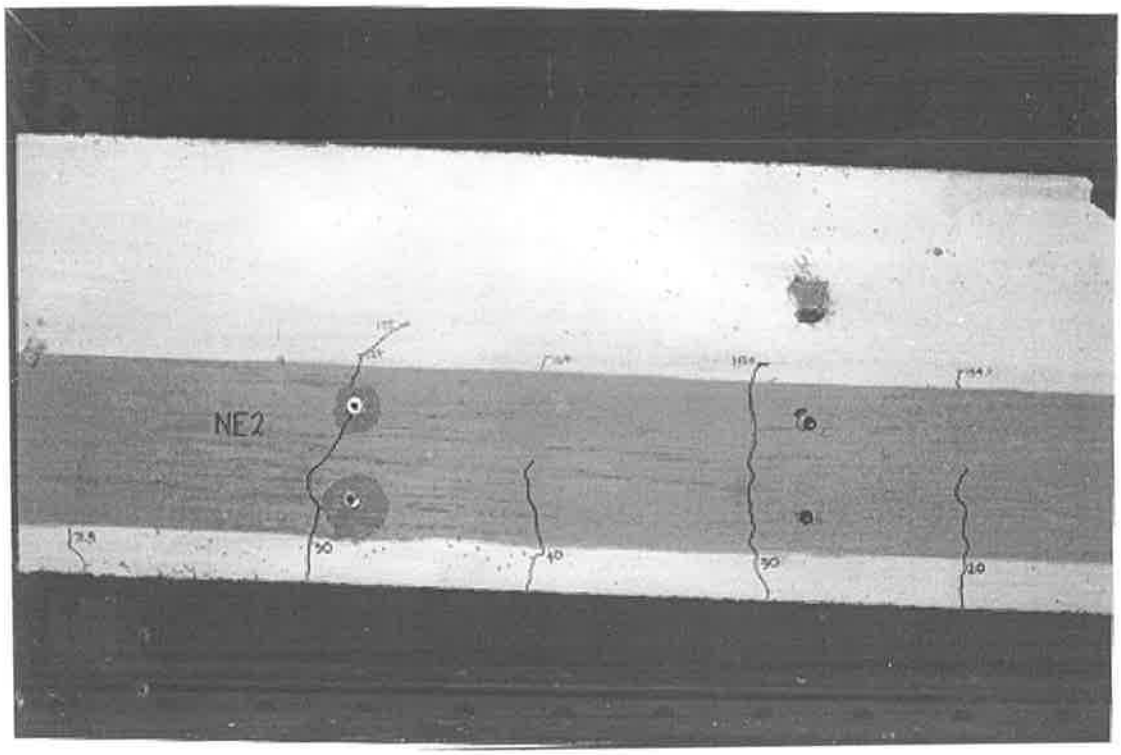

P8.51 Cracks near to the applied load at North-East shear span of beam B24

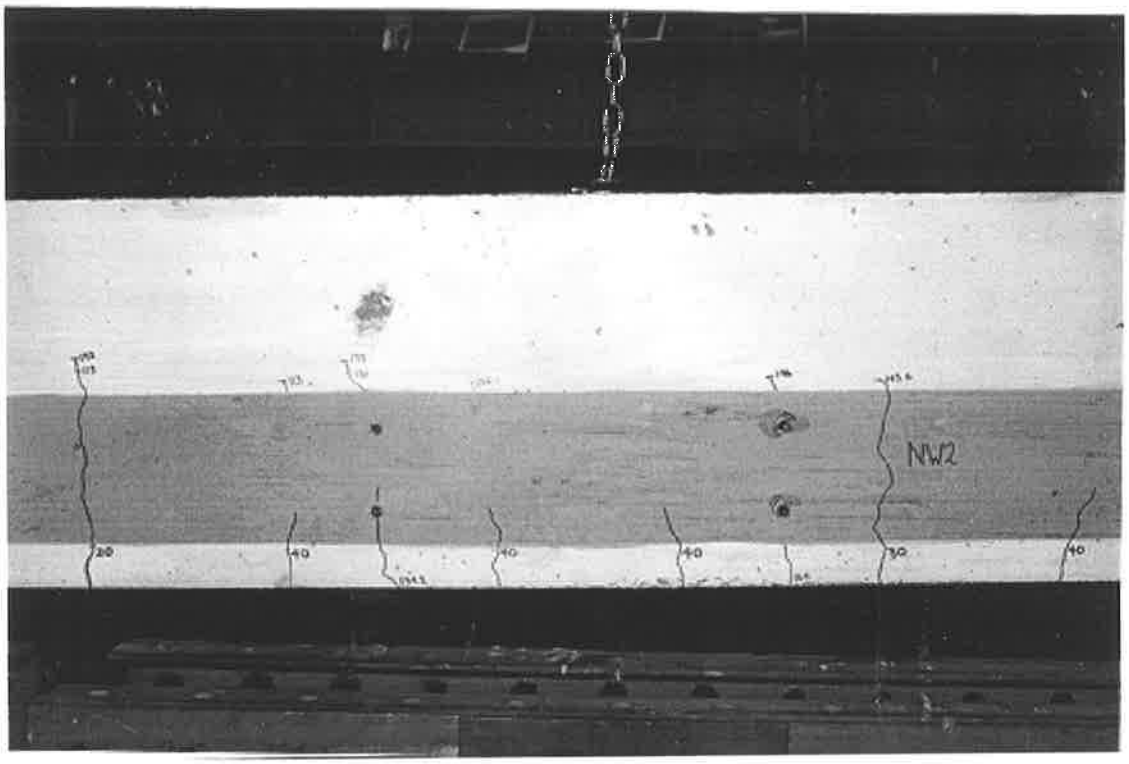

P8.52 Cracks near to applied load at North-West shear span of beam B24

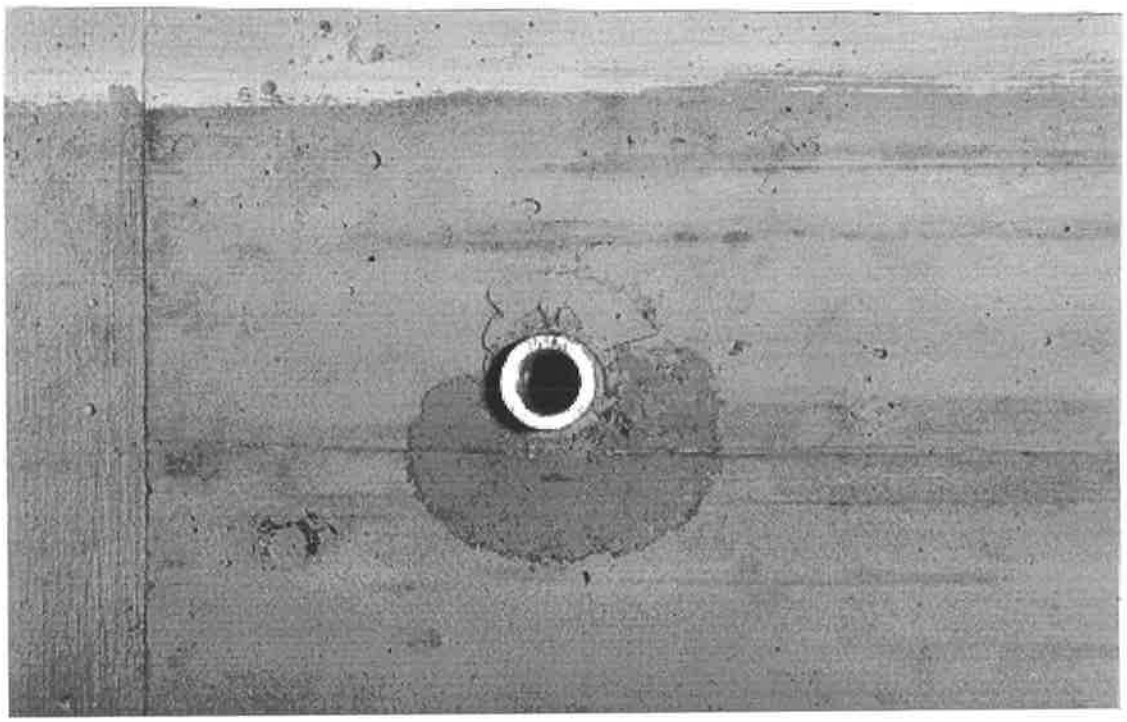

P8.53 Concrete surrounding bolt crushed in beam B24

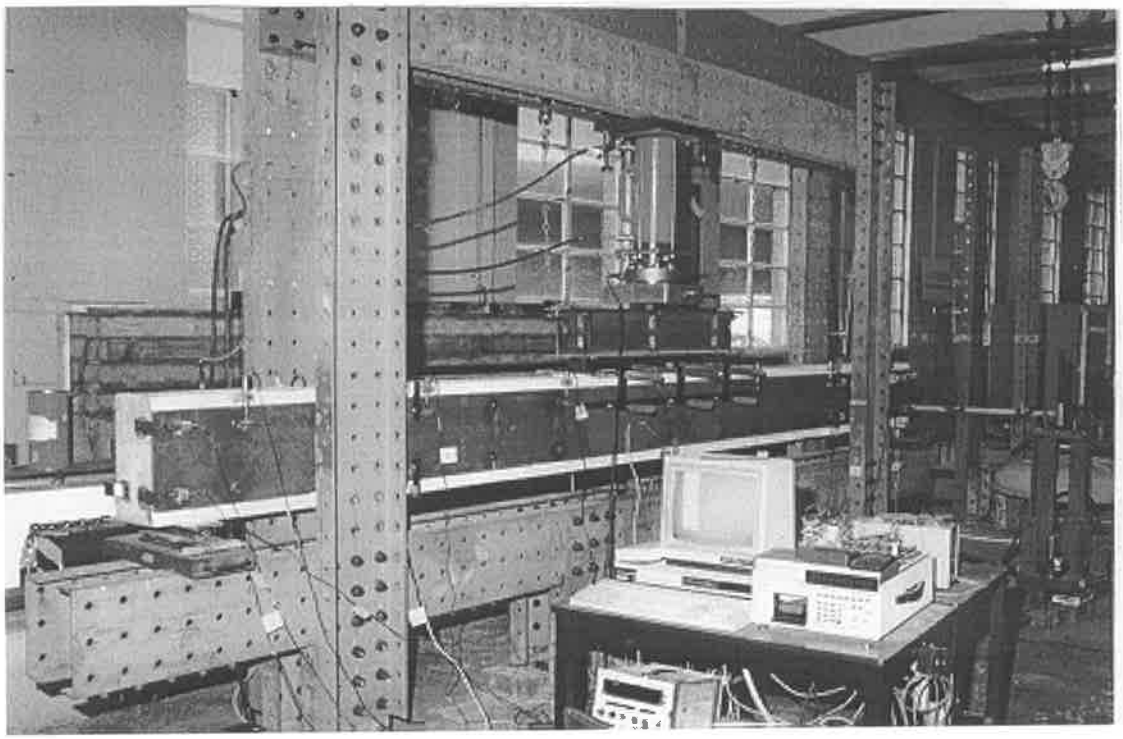

P8.54 Test set up of beam C11

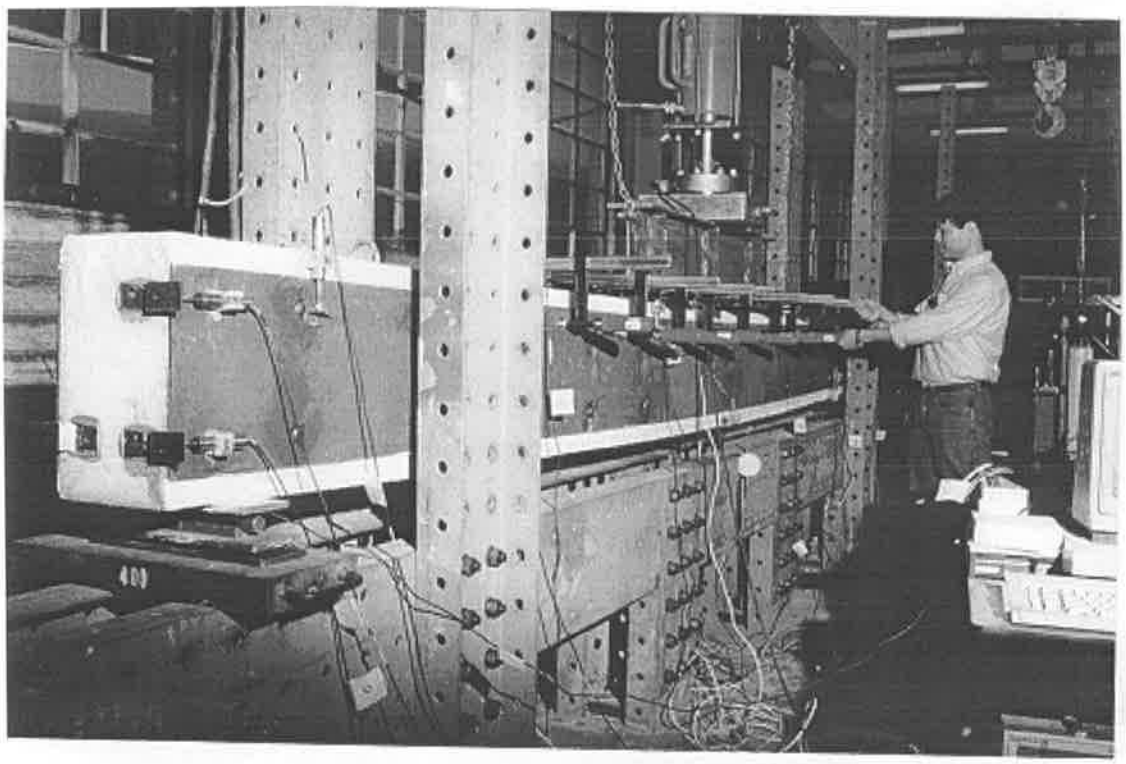

P8.55 Number of clamps increased in beam C11

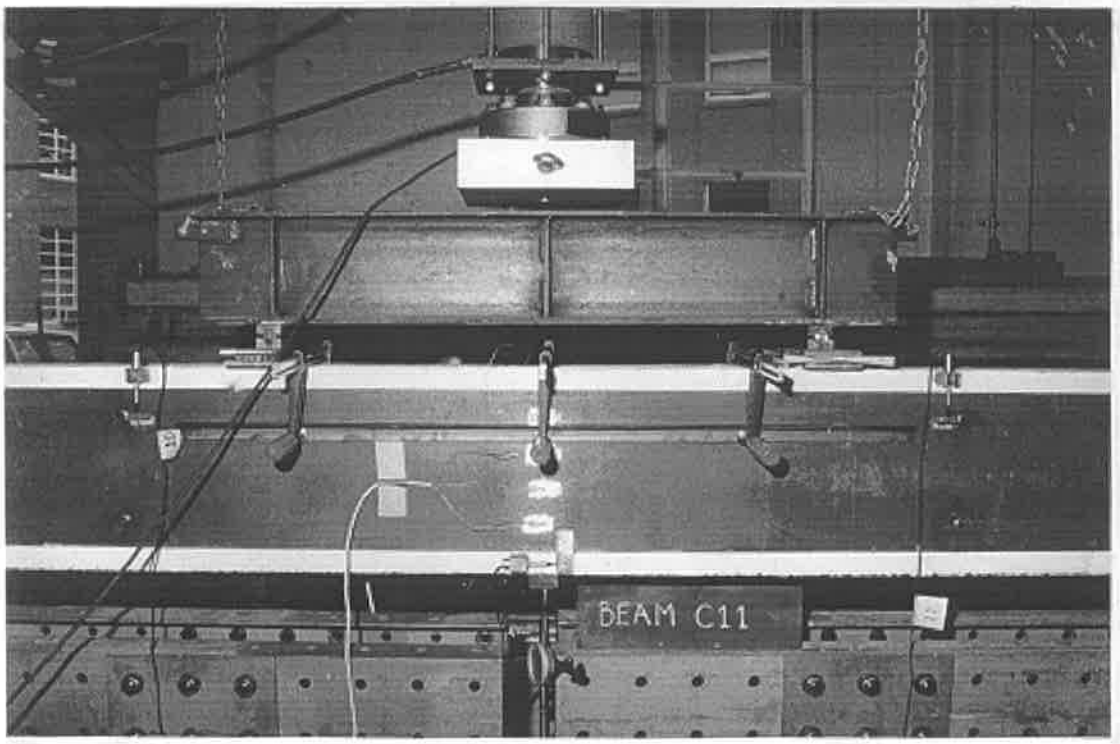

P8.56 Position of clamp changed (Beam C11)

P8.57 Flexural failure of beam C11

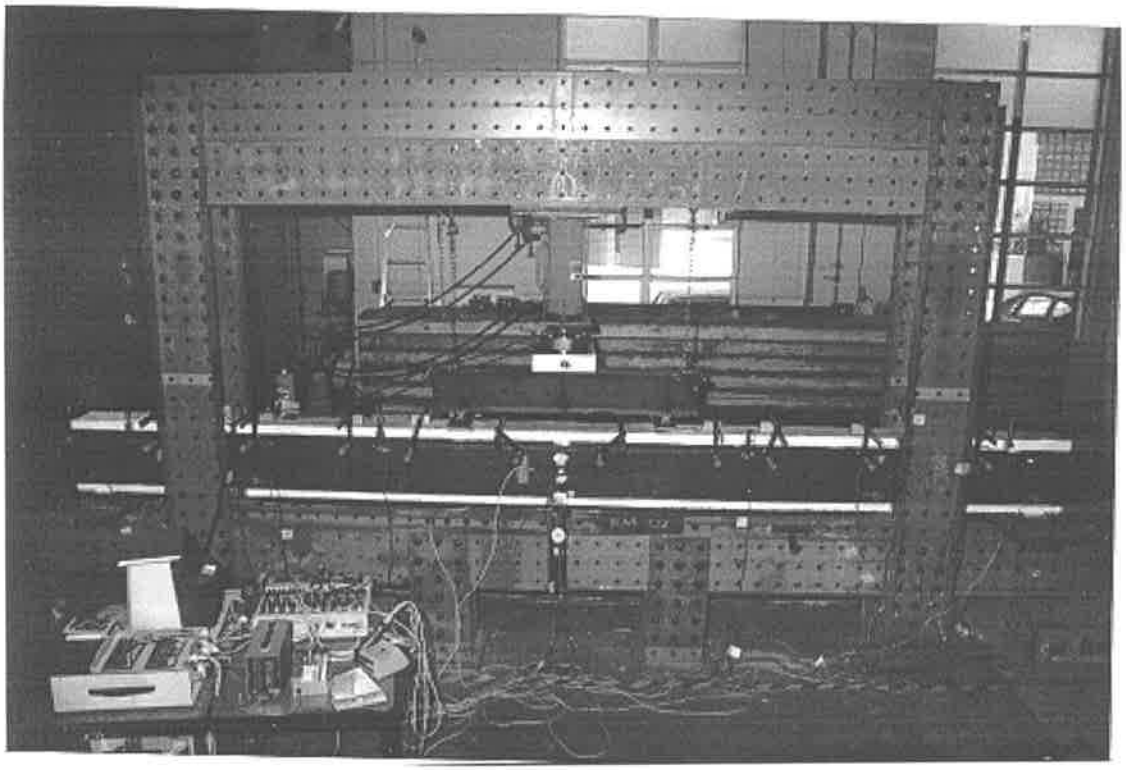

P8.58 Test set up of beam C12

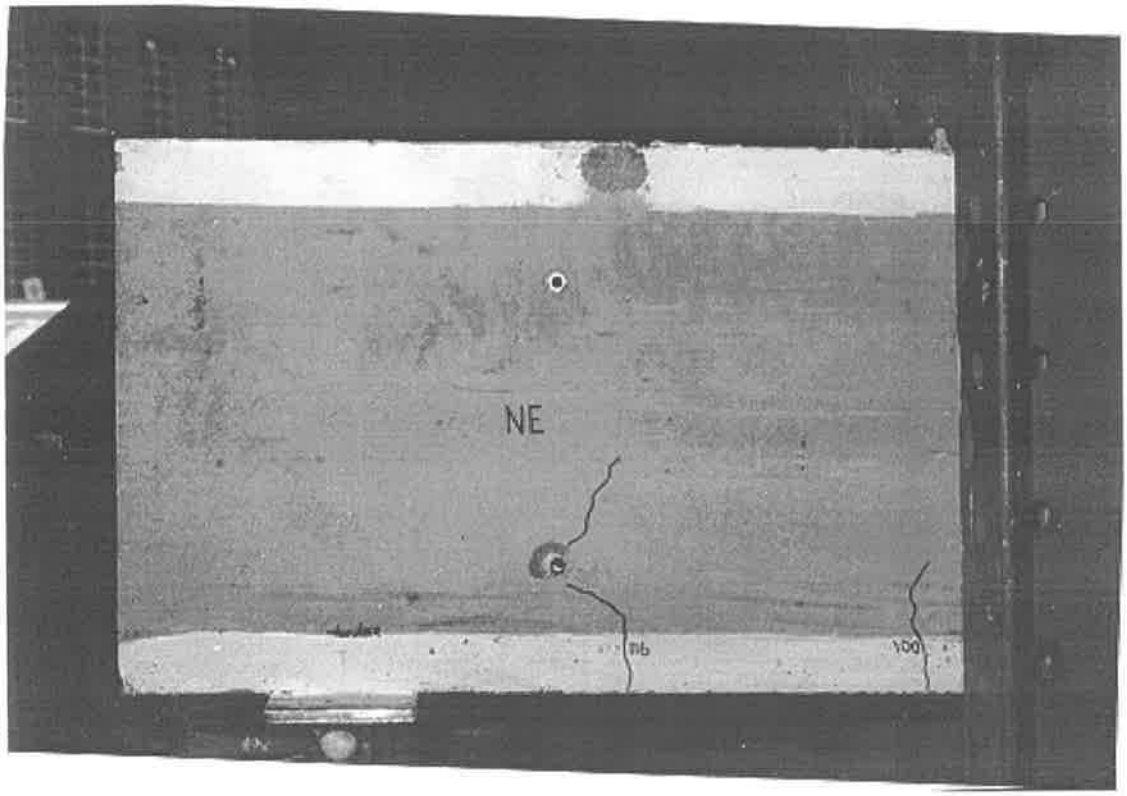

P8.59 Ripping crack in North-East shear span (Beam C12)

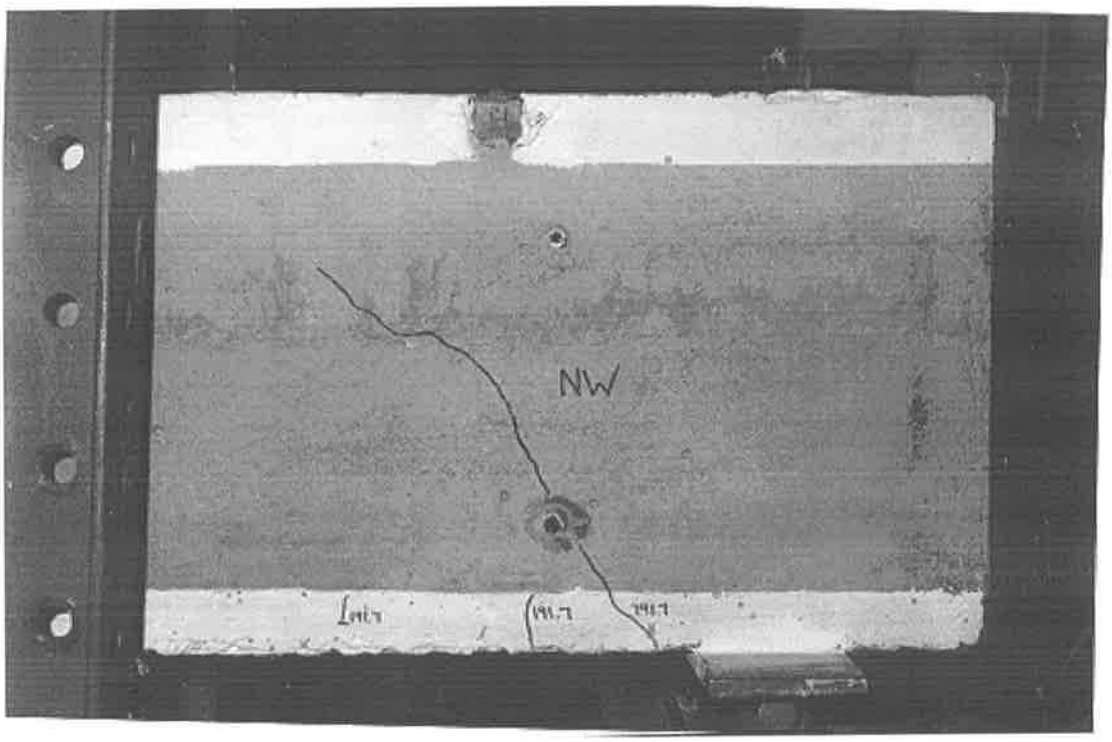

P8.60 Ripping crack in North-West shear span (Beam C12)

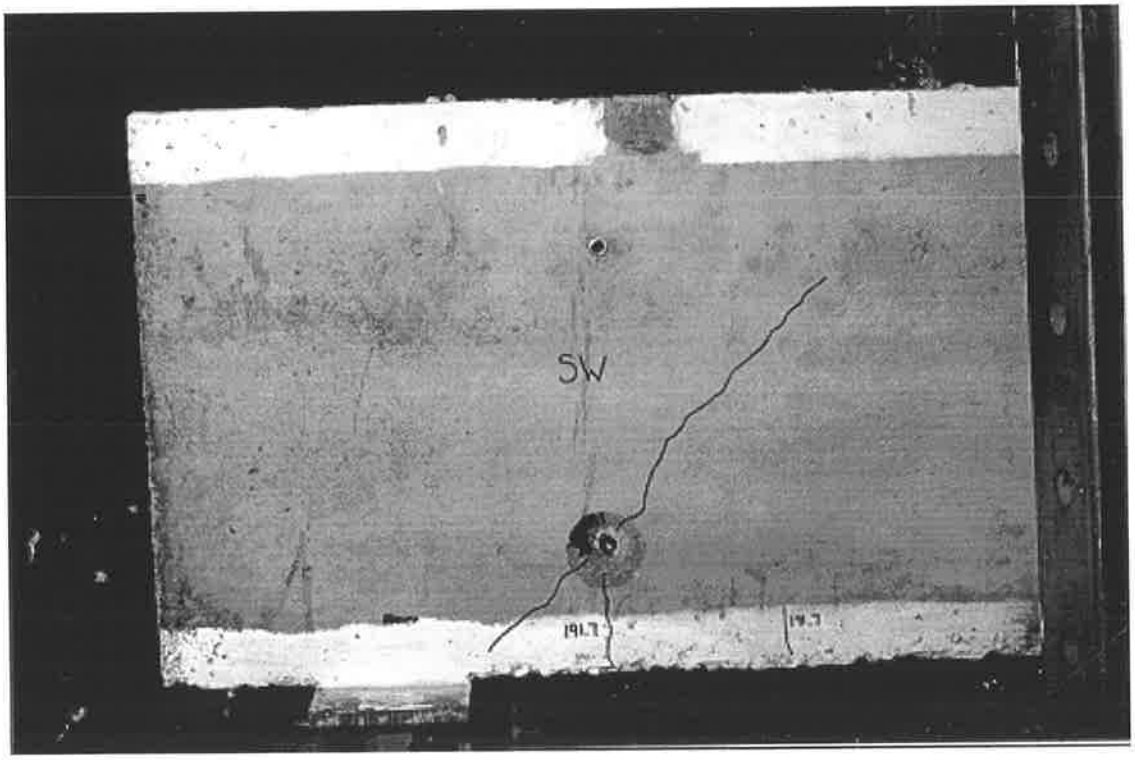

P8.61 Ripping crack in South-West shear span (Beam C12)

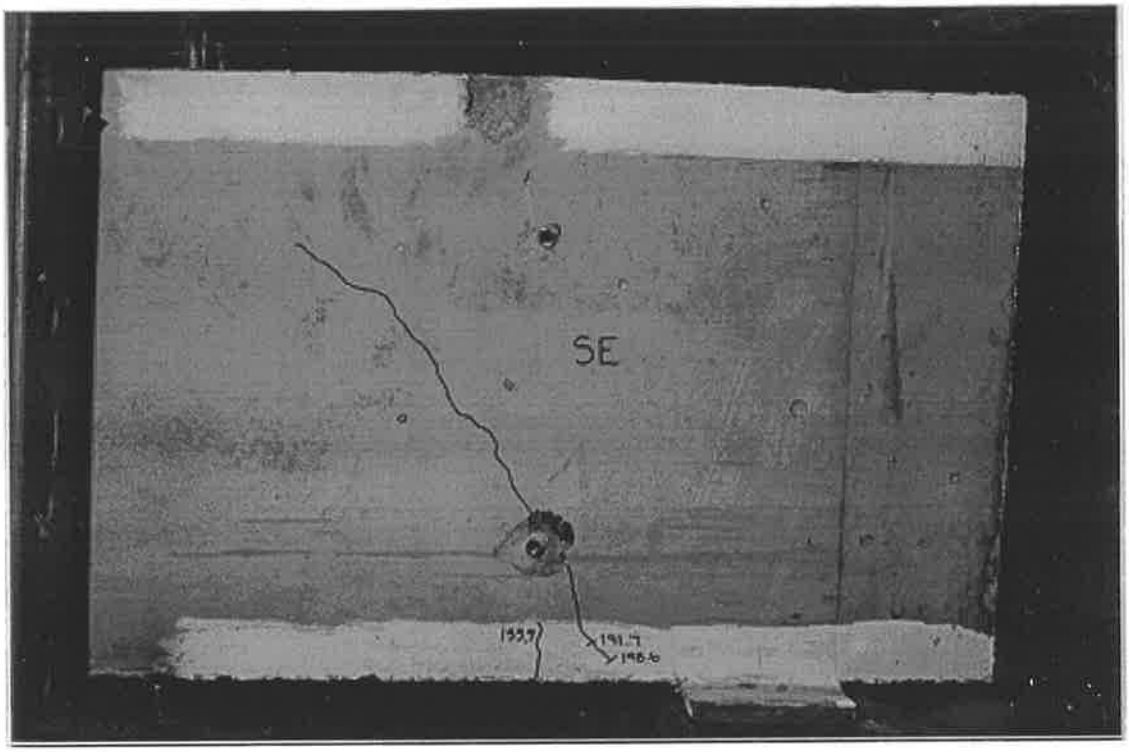

P8.62 Ripping crack in South-East shear span (Beam C12)

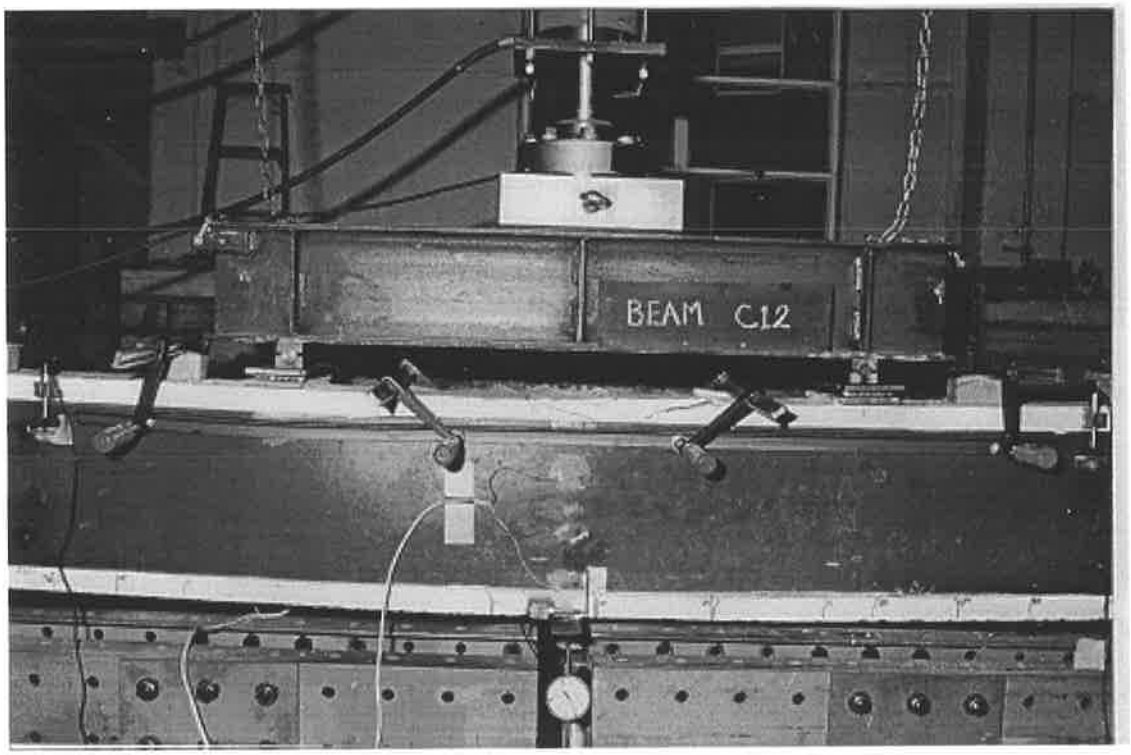

P8.63 Flexural failure of beam C12

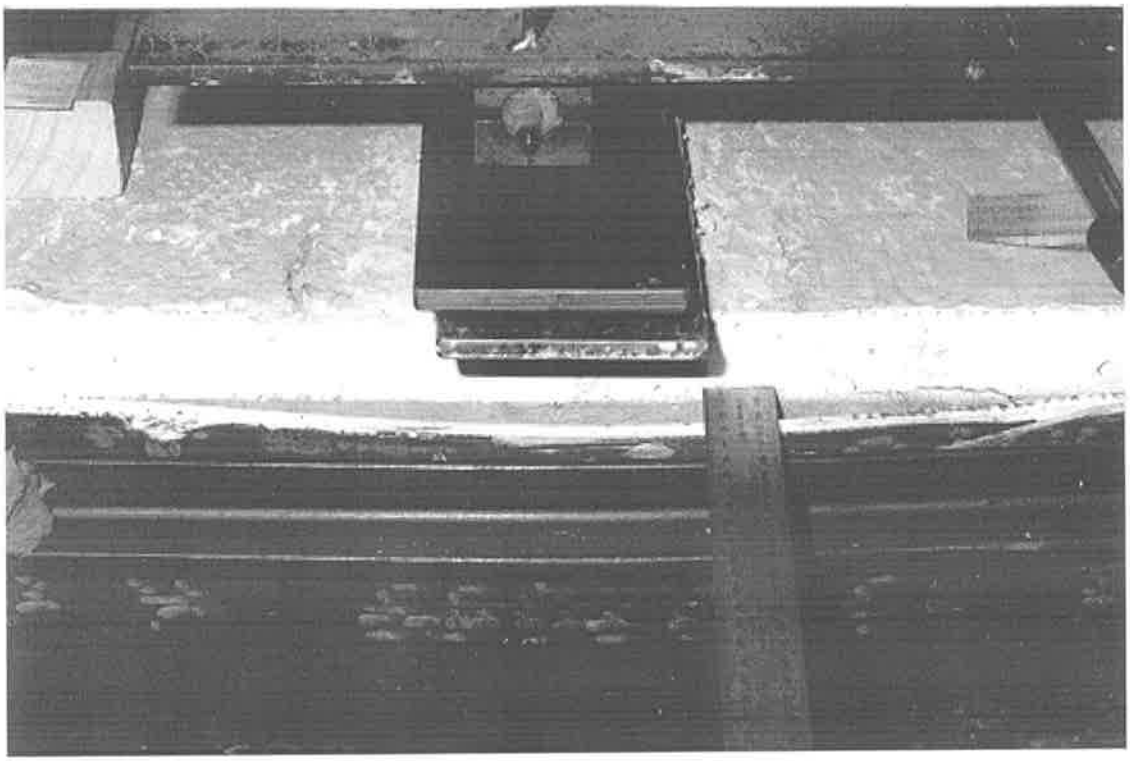

P8.64 Buckling in the plate during test (Beam C12)

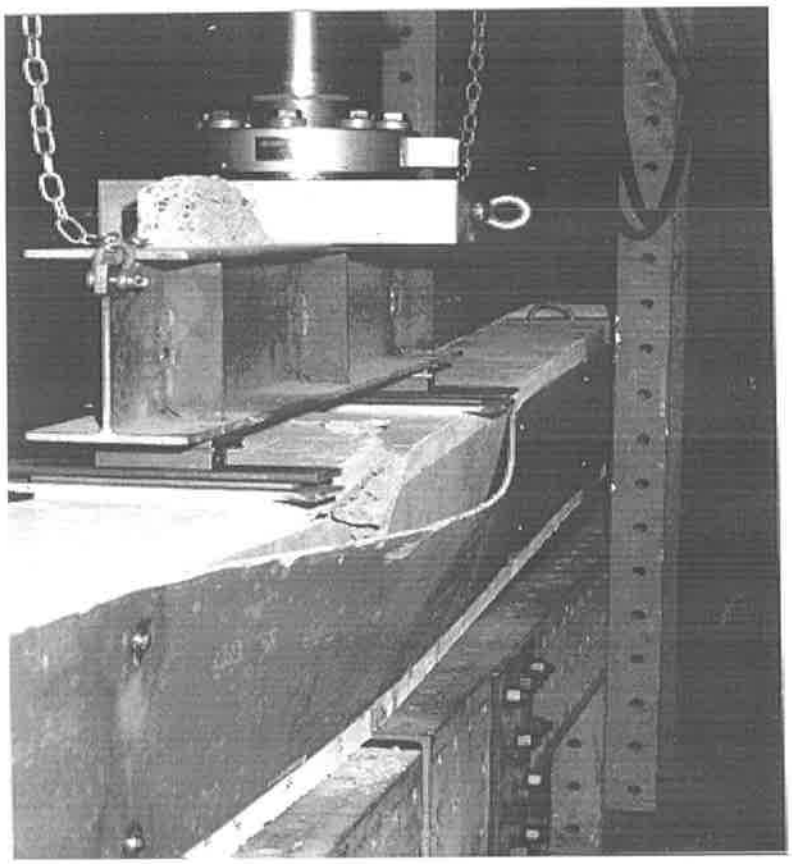

P8.65 Buckling in the plate when clamps were removed

Chapter Nine

Analysis and Design for Vertical Slip

9.1 INTRODUCTION

The theory of vertical shear forces and vertical slip have been described in Chapter 4 and it was shown that the vertical slip can reduce the rigid plastic flexural capacity of plated beams. Mathematical equations were developed to quantify the vertical shear forces and vertical slips in side plated beams. In doing this, it was assumed that the concrete and plate elements were linear-elastic and that the shear connectors were elastic-plastic. In Chapter 5, non-linear computer models were then described to determine the distribution of vertical shear forces and vertical slips. Among these, computer model 3 was developed to study the vertical slip only. This computer model and the theory of Chapter 4 will be used in this chapter to analyse the experimental beams. Furthermore, a mechanism for resisting vertical shear forces in the side plated beams will be described. This will then be used to develop a design procedure that allows for vertical slip.

9.2 ANALYSIS OF PLATED BEAMS BY COMPUTER MODEL 3

The computer model 3 from Chapter 5 will be used in this section to analyse the experimental beams. The basic assumptions of this computer model is that the bolted shear connectors are infinitely stiff in the longitudinal direction but flexible in the vertical direction. Therefore, the side plated beam has no longitudinal slip between the elements, that is full longitudinal full-interaction exists, but has vertical slip, that is vertical partial-interaction exists.

9.2.1 Limitations of the analysis

This computer model has the following limitations:

(a) The computer model can be applied only to beams having one line of connectors as longitudinal full interaction can occur only at one point when there is vertical partial interaction. Therefore, in the case of the beams having two line of connectors, they will be considered to be positioned in one line.

(b) Due to longitudinal full interaction, the connectors will transfer higher longitudinal forces into the elements than occurs in practice.

(c) The slip of a bolted shear connector has a vertical component and a horizontal component, as shown in Fig. 9-1. Therefore, the bolts exhibit a resultant shear forces as shown. However, the slip measured in the push test in Sect. 8.3 is also the resultant slip. As such, the load and slip in the load-slip curve of a push test are the resultant force and the resultant slip, as in Fig. 9-1. Therefore, the use of the push-test load-slip curve only to determine the vertical stiffness of connectors in beams will over estimate the stiffness when the connector is behaving plastically.

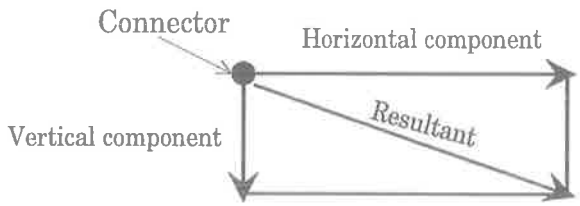

Fig. 9-1 Resultant slip of the bolted connection

9.2.2 Beam analysis

The plate in the simply supported plated beam in Fig. 9-2 has the longitudinal shear forces and the vertical shear forces, as shown. These forces are applied to the plate element. The resultant of these forces are P and V, respectively, and are shown in Fig. 9-3. The distance between the resultant vertical shear forces is L. In this section, the variations of V and L

will be determined by using computer model 3 and the results will be compared with the mathematical model in eqn. (4.7). The shear connector load-slip curve that will be used in these analyses will be discussed in the following section.

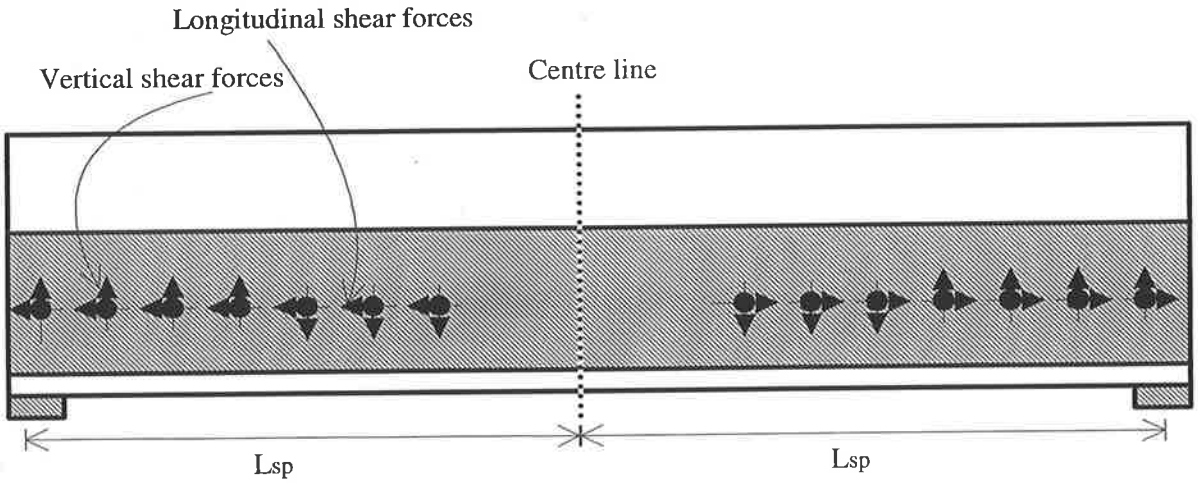

Fig. 9-2 Simply supported plated beam

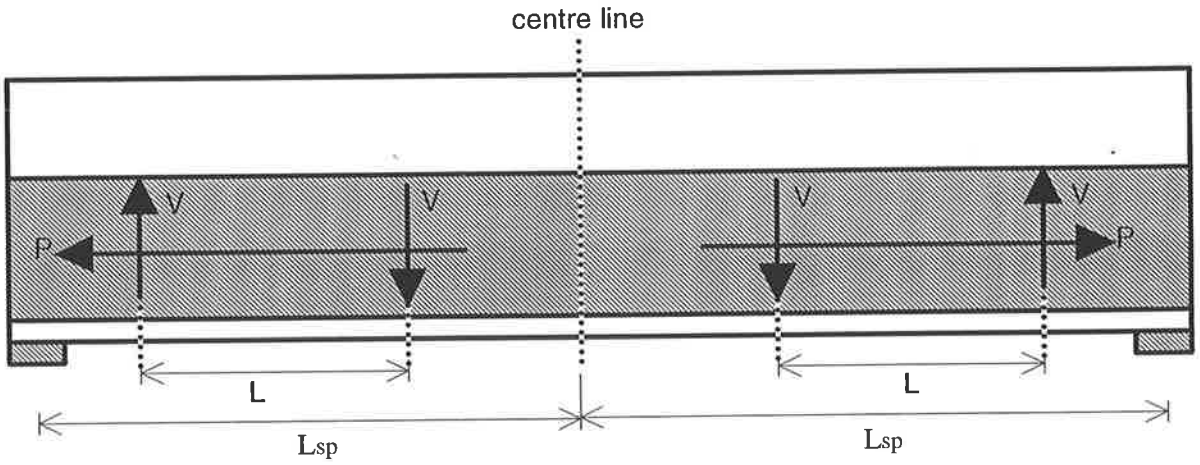

Fig. 9-3 Resultant forces in the side plated beam

9.2.2.1 Load-slip characteristics of bolted shear connector

The average of the different push test results in Table 8.16 of the bolted shear connector is represented as O-A-B-C-D in Fig. 9-4, which has a K_{si} of 46670 N/mm. Due to the limitation (c) in Sect. 9.2.1, a different curve as represented by O-B-C-D, which has K_{si} of 14000 N/mm will be used as an approximation.

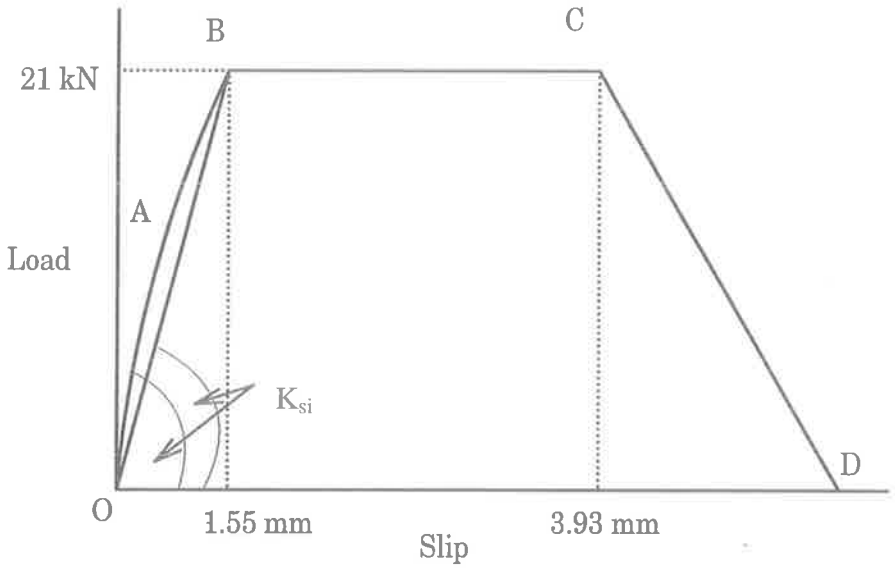

Fig. 9-4 Idealised load-slip curve of the bolted connection

9.2.2.2 Comparison of results of computer model with mathematical model

In this section, the results of computer model 3 will be compared with the vertical full interaction mathematical model in eqn. (4.7). First, the experimental beam B13 is simulated using a connector stiffness, K_{si}, of 46670 N/mm and then a K_{si} of 14000 N/mm. The calculated computer moments VL will be referred to as $(VL)_{comp}$. Then, using eqn. (4.7), VL will be calculated. This theoretical moment VL will be referred to as $(VL)_{cr}$ when $(EI)_c$ in eqn. (4.7) is for the cracked concrete section, and $(VL)_{uncr}$ when $(EI)_c$ in eqn. (4.7) is for the uncracked concrete section. The magnitude of P_{shear} in eqn. (4.7) is taken from the

computer analysis. The results are tabulated in Table 9.1 for different M/M_{max}, where M is the applied moment and M_{max} is the experimental moment capacity of the beam.

It can be seen in Col. 6 of Table 9.1 that the change in the stiffness of the shear connectors has little effect on the magnitude of $(VL)_{comp}$. Also, it can be seen that the results obtained by using the cracked concrete section in Col. 4 are much closer to the computer result in Col. 6 than those using the uncracked concrete section in Col. 5. It is therefore, the value of K_{si} will be taken as 14000 N/mm in the beam analysis in the following section. Also, $(EI)_c$ in eqn. (4.7) will be taken for cracked concrete section whenever used further in this chapter.

Table 9.1 Analysis of beam B13

		Mathematical model			Computer
K_{si} (N/mm)	$\frac{M}{M_{max}}$	P_{shear} (kN)	$(VL)_{cr}$ (kNm)	$(VL)_{uncr}$ (kNm)	$(VL)_{comp}$ (kNm)
1	2	3	4	5	6
46670	0.30	51.29	1.93	0.78	1.08
	0.60	193.24	3.26	1.46	3.52
	0.90	320.50	4.69	2.17	6.47
16534	0.30	51.29	1.93	0.78	1.00
	0.60	193.24	3.26	1.46	3.30
	0.90	320.50	4.69	2.17	5.99

9.2.2.3 Analysis of Beams B11, B13 and B24

In this section, beams B11, B13 and B24 in Sect. 8.4 will be analysed using the computer model 3. These beams have the degrees of shear connection of 1.75, 0.43 and 0.91 respectively. The analyses will be done for two-point loads as in the experiments (this will be referred to as point loads) and then for uniform distributed loads (which will be referred to as UDL). In all the computer simulations, the connectors are positioned at the mid-depth of the plate.

The variations of L/L_{sp} (where L is the distance between the resultant vertical shear forces and L_{sp} is the shear span as in Fig. 9.3) are shown in Figs. 9-5, 9-9 and 9-13 for beams B13, B24 and B11 respectively. It can be seen that there is a big divergence in L/L_{sp} between the point loads and the UDL loads at low load levels, but they converge at high load levels.

The variation of V in beam B13 is shown in Fig. 9-6. It can be seen that V for the point loads and the UDL loads are very close at the very low loads but the difference increases as the load increases. Also, the variation of V is almost linear for both loading conditions. A similar variation occurs for VL in Fig. 9-7.

The variations of V and VL for beam B24 are shown in Figs. 9-10 and 9-11 respectively and those for beam B11 are shown in Figs. 9-14 and 9-15 respectively. The variations are similar to those already described for beam B13.

The variations of vertical slip along the shear span at the experimental moment capacity of the beam B13 is shown in Fig. 9-8. In the case of point loads, the variation is almost linear and the vertical slip is maximum at the end bolts of the shear span. Also, the vertical slip changes direction almost near the mid-shear span. This variation of vertical slip is similar to that found in the experiment, as was shown in Fig. 8-168. However, in the case of a UDL, the vertical slip along the shear span varies almost linearly from the support to near the mid-shear span, as shown in Fig. 9-8, after which vertical slip stays almost the same. The variation of vertical slip for beam B24 is shown in Fig. 9-12, and for beam B11 is shown in Fig. 9-16 which are similar to that found for beam B13.

The magnitudes of L/L_{sp}, V and VL at the maximum load for the different beams are tabulated in Table 9.2. It can be seen that the magnitude of L/L_{sp} of different beams at maximum loads are very close to each other both for UDL and point loads. In general, L/L_{sp} can be considered as 0.66. Furthermore, it can be seen that the magnitude of V given in Col. 4 and VL given in Col. 5 increases as the degree of shear connection increases, when there is a point load. In the case of a UDL, the magnitude of V and VL are found to be less when the degrees of shear connection is the highest.

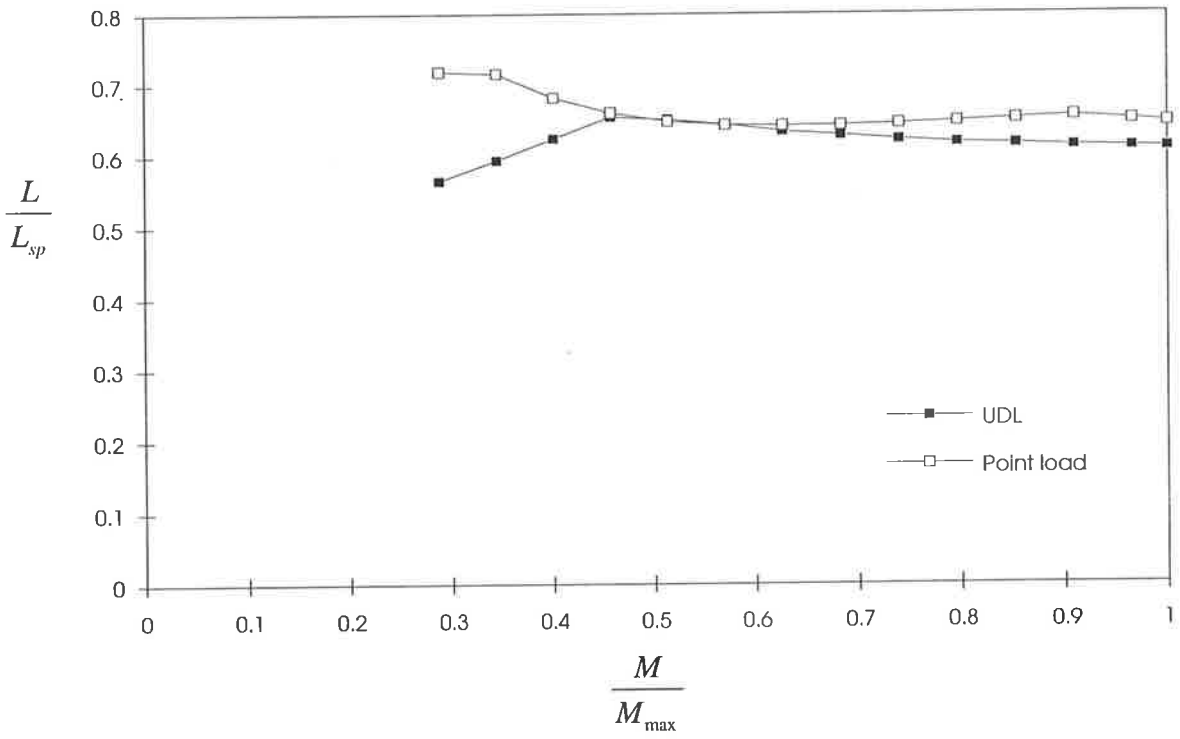

Fig. 9-5 Variation of L for Beam B13

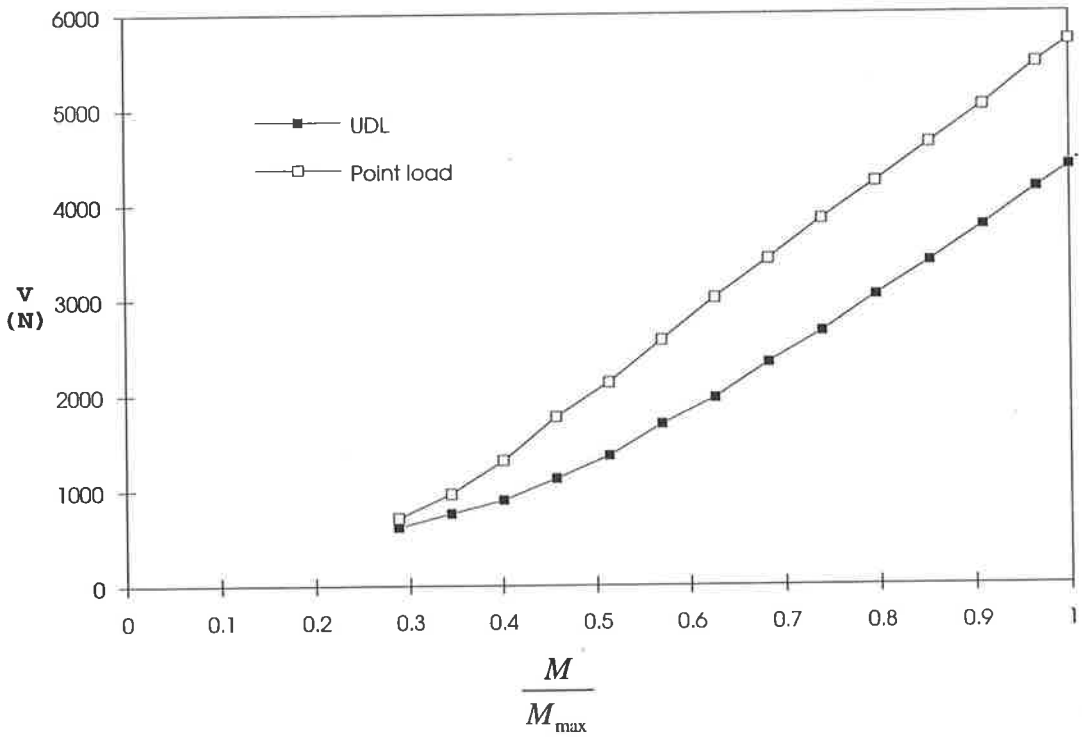

Fig. 9-6 Variation of V for Beam B13

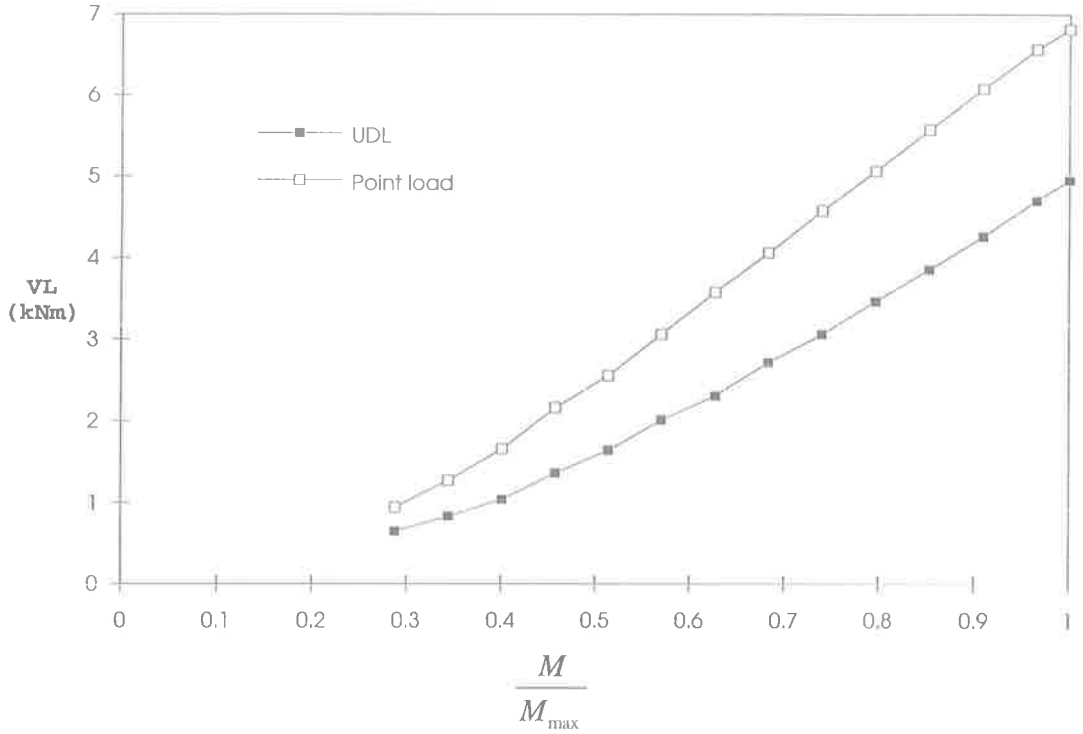

Fig. 9-7 Variation of VL for Beam B13

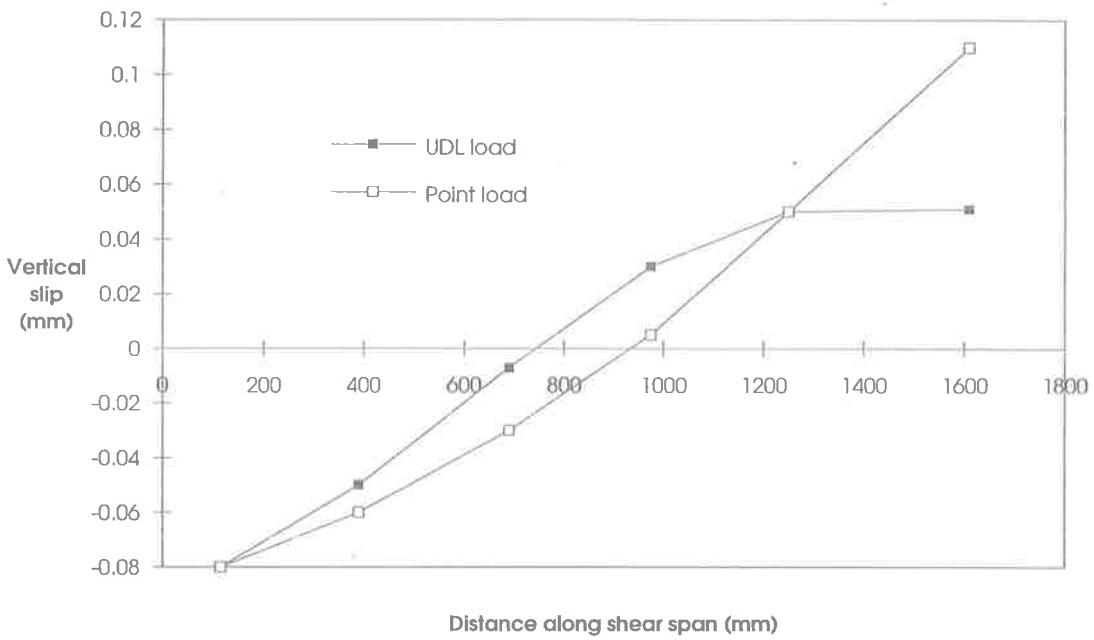

Fig. 9-8 Distribution of vertical slip at experimental capacity for Beam B13

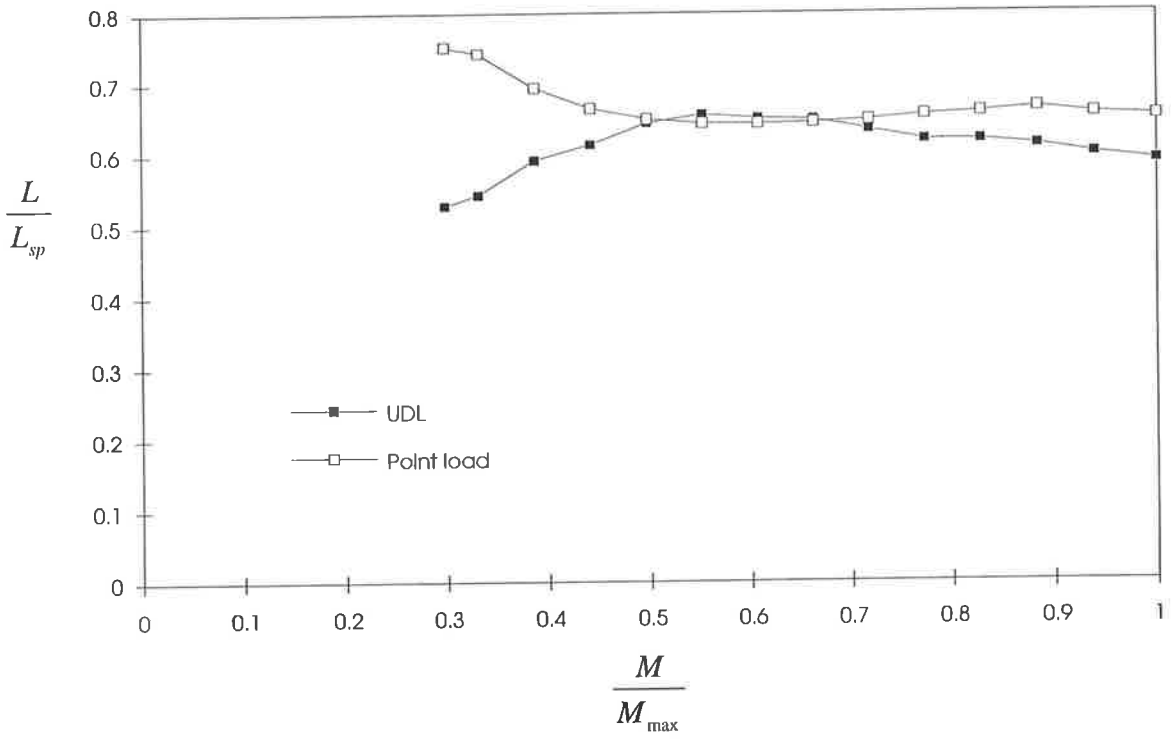

Fig. 9-9 Variation of L for Beam B24

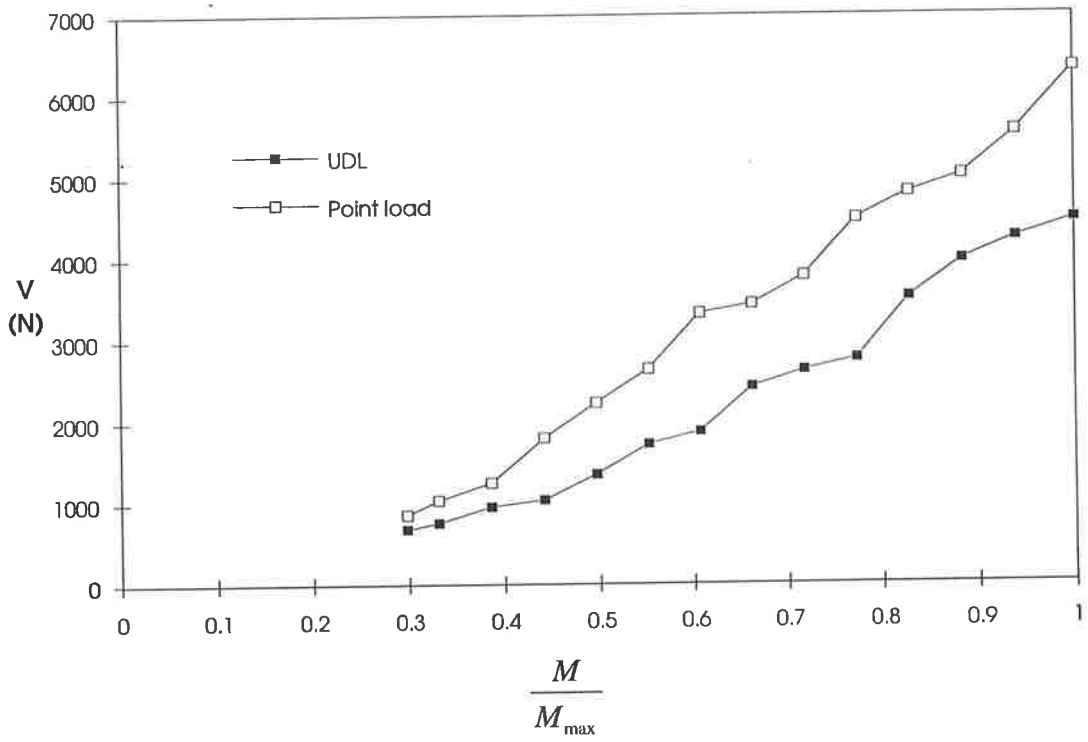

Fig. 9-10 Variation of V for Beam B24

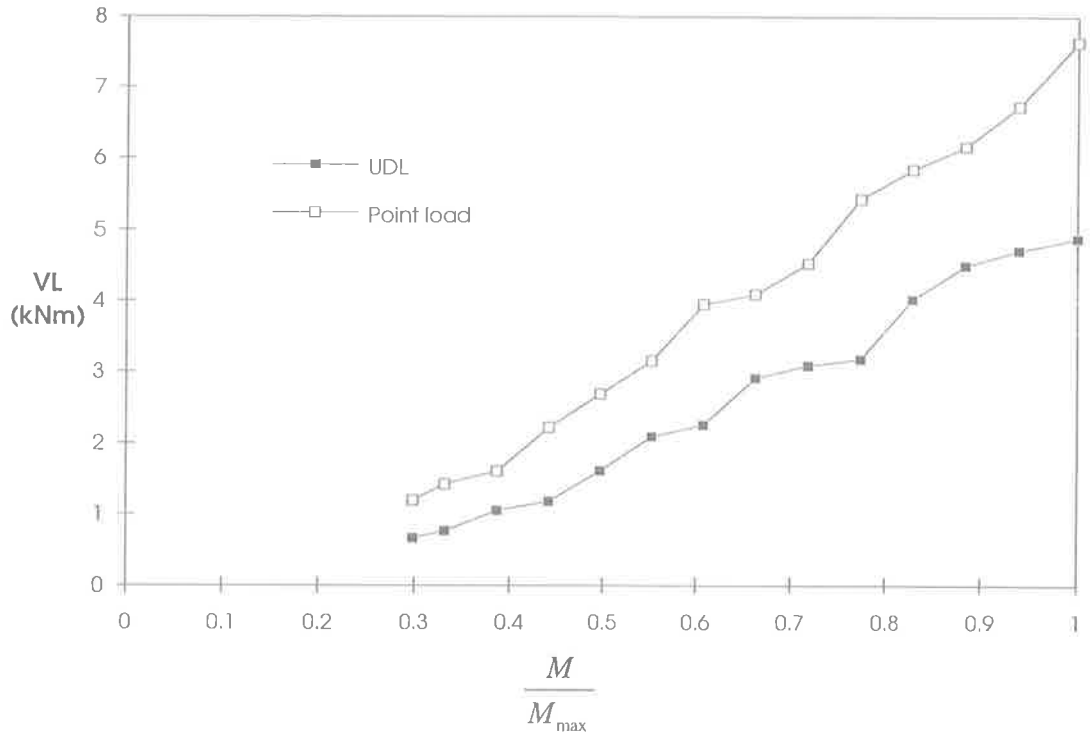

Fig. 9-11 Variation of VL for Beam B24

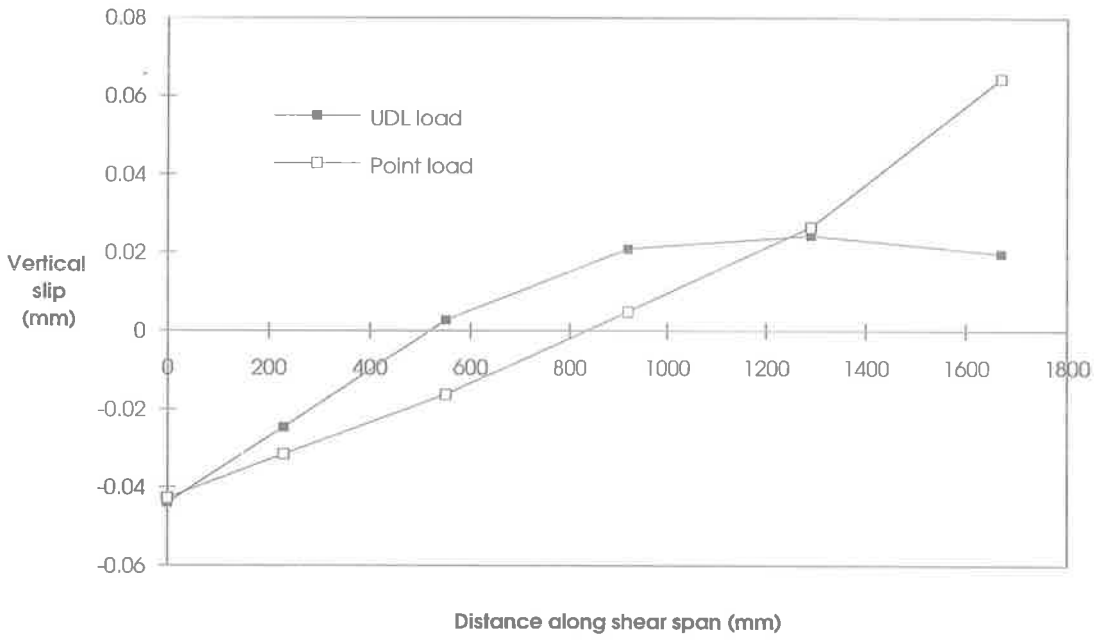

Fig. 9-12 Distribution of vertical slip at experimental capacity for Beam B24

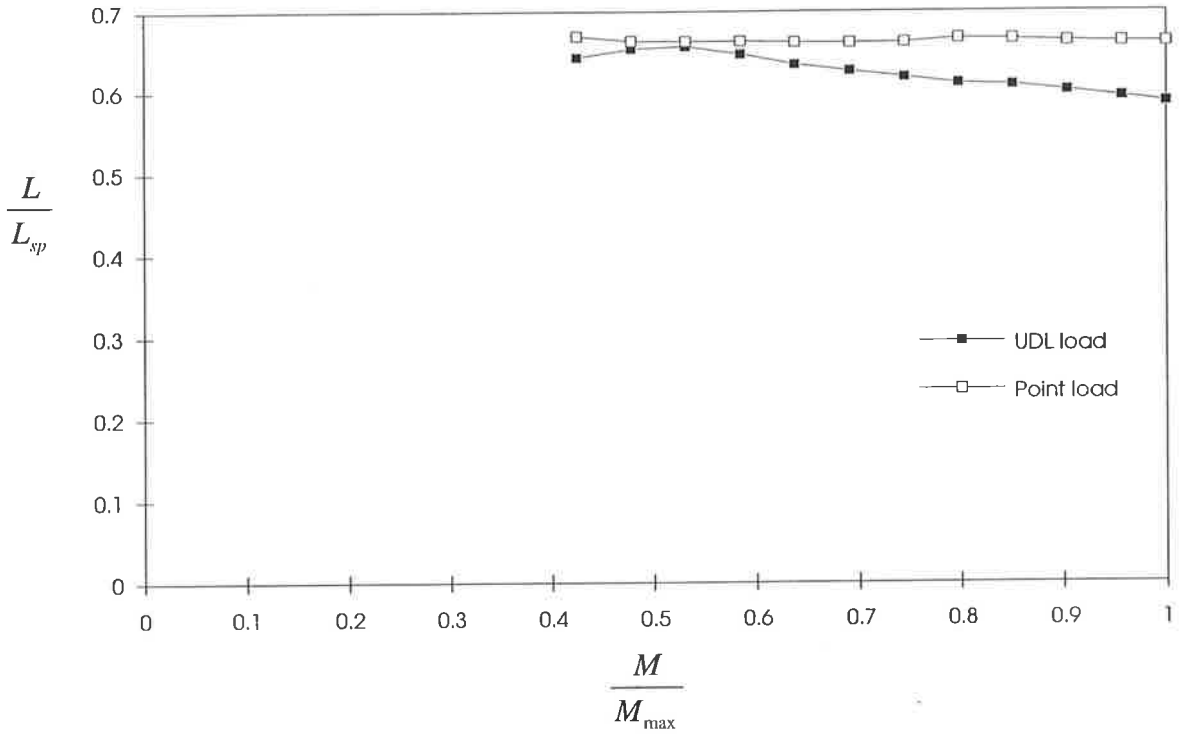

Fig. 9-13 Variation of L for Beam B11

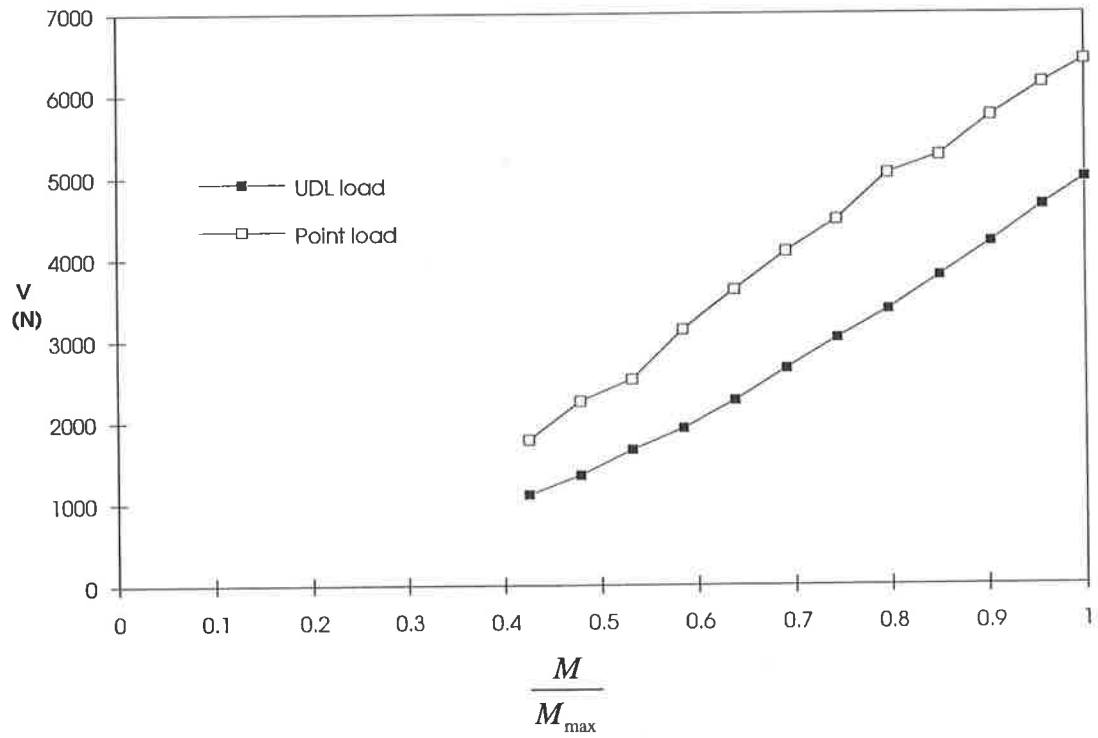

Fig. 9-14 Variation of V for Beam B11

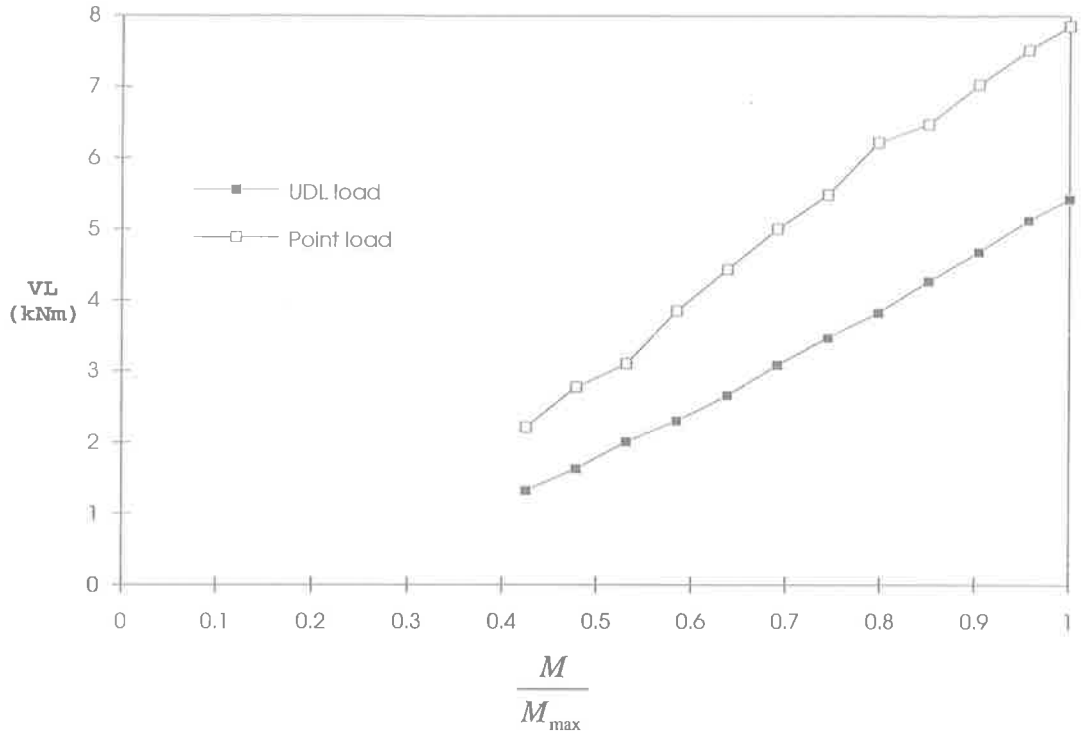

Fig. 9-15 Variation of VL for Beam B11

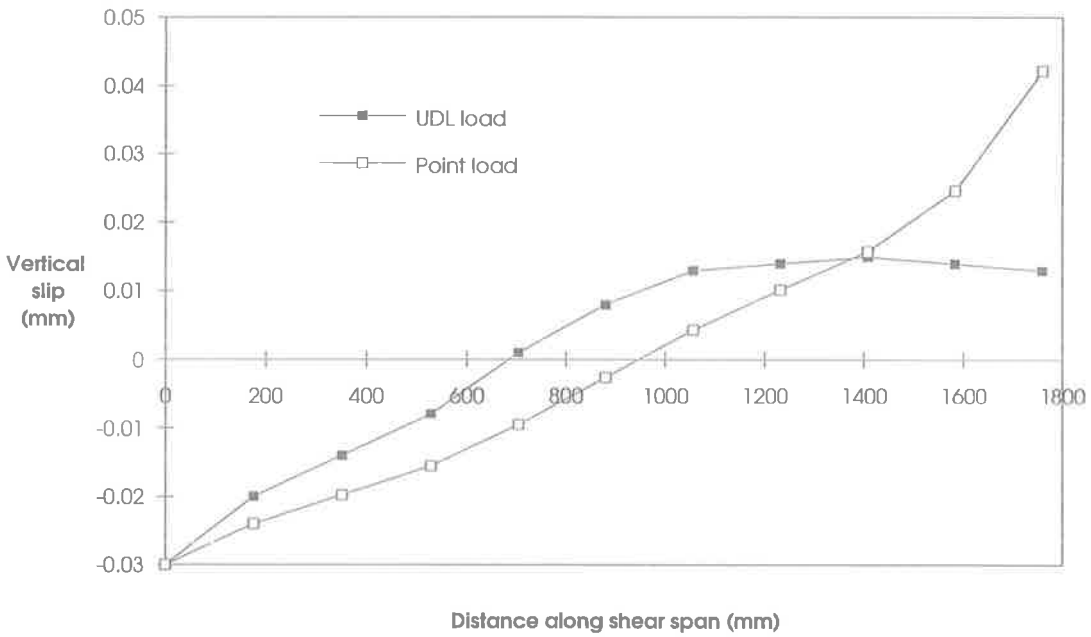

Fig. 9-16 Distribution of vertical slip at experimental capacity for Beam B11

Table 9.2 Results of computer analysis at maximum load

		Two-point load			UDL load		
Beam no.	η	$\frac{L}{L_{sp}}$	V (kN)	VL (kNm)	$\frac{L}{L_{sp}}$	V (kN)	VL (kNm)
1	2	3	4	5	6	7	8
Beam B13	0.43	0.64	5.70	6.81	0.61	4.39	4.95
Beam B24	0.91	0.65	6.33	7.64	0.60	4.47	4.88
Beam B11	1.75	0.66	6.42	7.85	0.59	4.98	5.42

9.3 MECHANISM OF RESISTING VERTICAL SHEAR FORCES

Two possible mechanisms can be found to resist VL in the side plates of the beam. In one mechanism, the bolted shear connectors can resist VL by their position as described in Sect. 4.5. In the other mechanism, a portion of the plate of depth h_f can be used to resist VL, as shown in Fig. 9-17, and, hence, the remainder of the plate of depth, $(h - 2h_f)$, can take the longitudinal shear forces P as shown. The later mechanism will be used in this section to analyse the experimental beams.

In these analyses, first VL is calculated from eqn. (4.7). In this equation, P_{shear} is taken as equal to the bond force, F_b, that is obtained from a rigid plastic analysis, and M is taken as the rigid plastic ultimate flexural capacity of the beam M, which are given in Cols. 3 and 4 respectively in Table 9.3, detailed calculations of which is given in Appendix-D. The magnitudes of VL for different beams are given in Col. 5 in Table 9.3. The following equation is then used to determine the depth, h_f in Fig. 9-17.

$$VL = 2h_f f_{yp} t_p (h - h_f) \quad \text{.....(9.1)}$$

If the calculated h_f from eqn. (9.1) is greater than the vertical position of the bolts, h_b in Fig. 9-14, then the following equation is used that allows for the presence of the bolt holes.

$$VL = 2(h - h_b) f_{yp} t_p (h - h_f - h_b) \quad \text{.....(9.2)}$$

Thus, the depth h_f is obtained that is required to resist VL, with the remainder of the plate's internal forces used to calculate the longitudinal shear forces, P, in Fig. 9-17, which is given in Col. 6 of Table 9.3. It is worth noting that the axial strength of the plate in all the plated beams was 656 kN.

The strain-stress and force distributions in the plate of different beams were obtained from the experimental work at the maximum load and have been given in Chapter 8. These are used to calculate the experimental moment in the plate element, $(M_{plate})_{expt}$, at the mid-depth of plate and the experimental longitudinal shear force in the plate element, $(P)_{expt}$. The results are tabulated in Cols. 7 and 8 in Table 9.3 respectively.

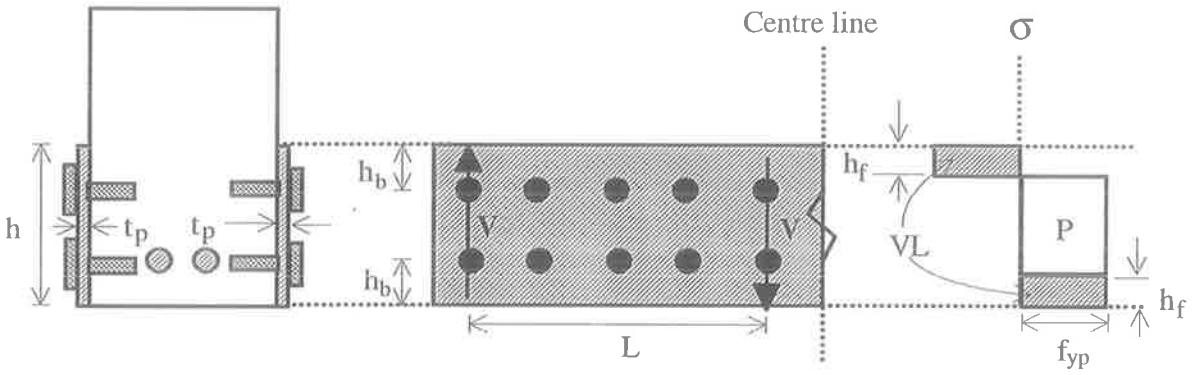

Fig. 9-17 Flexure induced by vertical shear forces

The ratios of $VL/(M_{plate})_{expt}$ are plotted in Fig. 9-18. It can be seen that all the values lie significantly below the line of $VL/(M_{plate})_{expt} = 1$. Again, when the longitudinal forces P from the theoretical analysis are compared to $(P)_{expt}$ from experimental analysis, variations are found to be very high in all the beams except beam B11 which was designed with full-interaction full-shear-connection. This happens as the plate elements are considered to be fully yielded in the theoretical analysis, as shown in Fig. 9-19, whereas the plates did not fully yield in the experiments, as can be seen in Chapter 8.

Table 9.3 Comparison of theoretical VL with experimental results

Beam no.	η	F_b (kN)	M (kNm)	VL (kNm)	P (kN)	$(M_{plate})_{expt}$ (kNm)	$(P)_{expt}$ (kN)
1	2	3	4	5	6	7	8
B11	1.75	542.88	226.62	6.12	452.40	7.33	433.48
B12	0.48	259.08	197.29	6.74	442.18	9.84	215.40
B13	0.43	259.08	198.53	6.79	441.36	13.58	241.72
B24	0.91	492.48	219.22	6.13	452.03	8.31	352.62
C11	0.77	431.80	255.34	57.97	706.83	67.09	241.00
C12	0.46	259.08	245.74	59.64	688.10	66.69	116.82

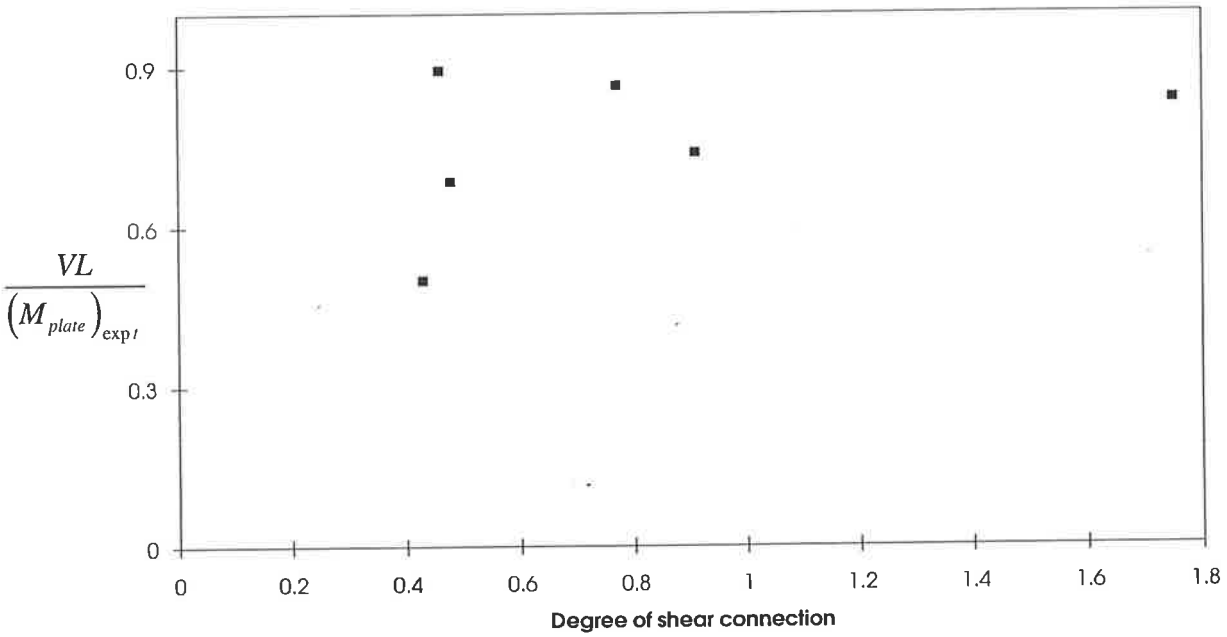

Fig. 9-18 Variation of $VL/(M_p)_{expt}$ with degree of shear connection of all beams

9.4 DESIGN PROCEDURE FOR VERTICAL SHEAR FORCE AND VERTICAL SLIP

From the theoretical analysis and the experimental work, it can now be concluded that side plated beams cannot be designed using the conventional rigid plastic method as the plate in the plated beam do not yield fully. As such, the difference in curvature between the steel

plate and the concrete element, as shown in Fig. 9-19, need to be considered in the design. When the difference between the curvature and the neutral axis separation, h_{na}, are known, then the corresponding stress profile can be known and thereby the flexural capacity of plated beam can be determined.

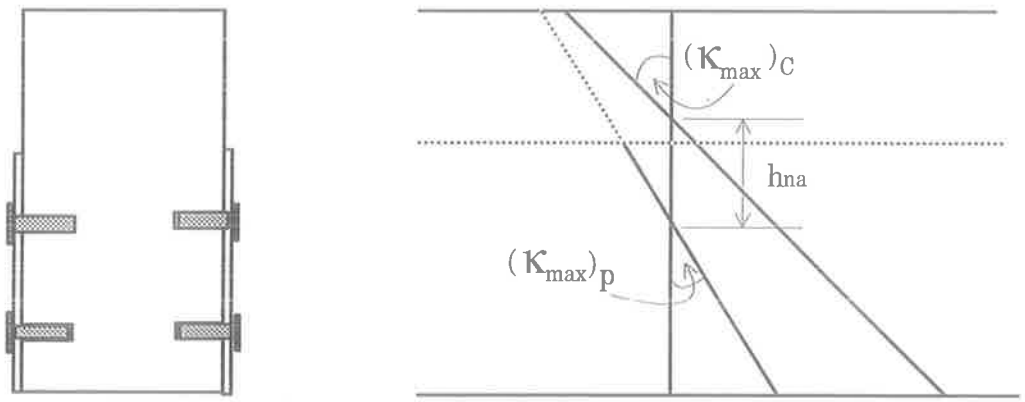

Fig. 9-19 Strain distribution in the plated beam

The fundamental equation for the vertical slip in beams subjected to a point load has been given in eqn. (4.22). This equation can further be modified in terms of curvature as given below (detail derivation is given in Appendix-F)

$$L\left[\frac{F-V-qh_{na}}{(EI)_c}-\frac{V}{(EI)_p}\right]=\left[(\kappa_{max})_c-(\kappa_{max})_p\right] \quad \text{.....(9.3)}$$

When the curvatures of the elements are equal, that is when there is vertical full interaction, then the right hand side of eqn. (9.3) becomes zero and eqn. (9.3) becomes eqn. (4.7), which was derived previously at the condition of vertical full interaction. Equation (9.3) can be used to determine VL for a known difference in curvature. As a first approximation, L can be taken as 2/3 of the shear span of the beam as found in Sect. 9.2.2.3 and thus V can be determined. This can be used in eqn. (4.28) to determine the number of connectors to maintain the specified curvature in the plated beam.

For a uniform distributed load, the modified equation is:

$$L\left[\frac{0.625wL - V - qh_{na}}{(EI)_c} - \frac{V}{(EI)_p}\right] = \left[1.25(\kappa_{max})_c - (\kappa_{max})_p\right] \quad \text{.....(9.4)}$$

(detail derivation is given in Appendix-F). It should be mentioned that eqn. (9.4) will not become eqn. (4.7) when the curvatures are equal. The reason is that eqn. (9.4) was developed by considering a curvilinear moment distribution due to the applied load, and a linear moment distribution due to vertical shear forces in the plate and a linear moment distribution due to uniform distribution of shear flow. This assumption gives a different constant value for curvilinear variation and linear variation during the integration process and, hence, cannot be eliminated. The same modified equation (9.4) can be found for the beam in Fig. 4-7 (detail derivation is given in Appendix-F).

9.5 SUMMARY

Computer model 3 which was developed specifically for vertical slip has been used in this chapter to analyses the plated beams. It has been described that the load-slip curve obtained from the push test gives the resultant slip and resultant load. It is therefore, a less stiffer load-slip curve than that obtained from experiment was used in the computer model to analysis the plated beams for vertical slip. Firstly, the results between mathematical model and the computer model have been compared and very good correlation was found. The side plated beams then analysed by computer model 3 for the experimental loading condition and for the uniform loading condition. An alternative mechanism have been described to resist vertical shear force and then a design procedure to allow for vertical slip has been described.

Chapter Ten

Concluding Remarks

10.1 INTRODUCTION

The general objective of the present study has been to deepen knowledge in the area of bolting plates to the sides of reinforced concrete beams. The work presented in this thesis has been extensive and many interesting problems have emerged during the time of the work. Some important concepts were looked at but others could not be tackled due to limitations of time. In this chapter, some concluding remarks will be made regarding both the theoretical and experimental works that have presented, and then proposals for future research will be suggested.

10.2 EXPERIMENTAL WORK

The following list represents a summary of the important findings from the experimental work.

A) The HIS adhesive bolted shear connector shown in Fig. 8-4(e) was found to be the most suitable connector for the plated beams as this shear connection system has a large plastic plateau in the load-slip curve.

B) The maximum increase in flexural capacity obtained for the shallow plated beam B11 was 55% which had the degree of shear connection of 1.75.

C) When the degree of shear connections in the deep plated beams C11 and C12 were 0.70 and 0.42 respectively, there were almost no difference in flexural strength. This indicated

that the flexural strength of deep plated beams is not very sensitive to the degree of shear connection.

D) The side plate does not unduly affect the ductility of the RC beam and can increase it. However, ductility can be affected by the degrees of shear connection in the plated beams.

E) None of the plate elements in the plated beams was yielded fully at the maximum load, even when the degree of shear connection was 1.75. It was found that near the maximum applied load, the curvature in the concrete element increases rapidly, whereas the curvature in the plate element stays almost constant which prevents the plate from being fully yielded.

F) The difference between the curvature of the plate element and the reinforced concrete element was found to be very small at low applied load levels, but increased at high applied load levels. As the vertical slip depends on the difference between the curvatures of the elements, it is also small at low load levels and increases rapidly at high load levels. Vertical slip was found to be at a maximum at the ends of each shear span.

G) The tests showed that the compression zone of the plate element is susceptible to buckling. Furthermore, the plates that buckled induced axial tensile loads in the shear connectors which caused fracture of the connectors.

H) None of the shear connectors induced longitudinal splitting, which suggests that their design, which was based on the theory of splitting in concrete beams, was adequate. Ripping cracks were observed but had no adverse effect on the flexural strength of the beam.

I) The experimental flexural capacities indicate that conventional rigid plastic design methods cannot be used for side plated beams. Existing rigid plastic techniques have to be adapted to allow for the difference in curvature.

10.3 THEORETICAL STUDY

The following list presents a summary of the major theoretical studies contained within the research:

A) Mathematical models have been developed using a combination of linear elastic and linear elastic-plastic theory, in order to quantify the resultant vertical shear forces and their lever arms at the conditions of vertical full interaction and vertical partial interaction.

B) Four non-linear computer models have been described for the following combinations of vertical and longitudinal interaction: vertical and longitudinal full interaction; longitudinal partial interaction but vertical full interaction; longitudinal full interaction but vertical partial interaction; and longitudinal and vertical partial interaction.

C) The full interaction computer analysis showed that the ductility of side plated beams first decreases and then increases as the height of the plate increases.

D) The full interaction computer analysis also showed that the γ factor that is used in design of reinforced concrete beams cannot be used in the rigid plastic analysis of side plated beams as the γ factor leads to an under estimation of the longitudinal bond force. Therefore, a new value of γ has been proposed specifically for the rigid plastic analysis of side plated beams.

E) The vertical partial interaction computer model has been used to analysis the shallow plated beams and then a design procedure for vertical slip has been developed.

10.4 FUTURE RESEARCH NEEDS

The following additional research is needed to provide design tools to practicising engineers:

A) The mathematical models for vertical shear forces and vertical slip have been developed by considering the materials as primarily linear elastic. These mathematical models need to be calibrated using the computer simulations to allow for material non-linearity.

B) The design rules for side plated beams require neutral axis separation and hence a mathematical model needs to be developed to find this separation h_{na}.

C) The elastic-plastic mathematical model of maximum longitudinal slip needs to be further adapted to allow for the difference between the curvatures of the elements in order to prevent connector fracture.

D) Design rules are required to avoid buckling in the side plated beams. Hence, further research is required in this area.

References

Al-Sulaimani, G. J., Sharif, A., Basunbul, A. I., et al, (1994), *Shear Repair for Reinforced Concrete by Fiber Glass Plate Bonding*, ACI Structural Journal, Vol. 91, No. 3, Jul-Aug, P458-464.

AS 3600, (1988), *Concrete Structures*, Standards Association of Australia.

AS 1012, (1993), *Methods of Testing Concrete*, Standards Association of Australia.

AS 1391, (1991), *Methods for Tensile Testing of Metals*, Standards Association of Australia.

Bazant, Z. P. and Oh, B. H., (1984), *Deformation of Progressively Cracking Reinforced Concrete Beams*, ACI Journal, Vol. 81, No. 3, May-June, P268-278.

Burnet, M. J., (1996), *Partial Interaction Design of Composite Steel and Concrete Flexural Members*, Ph.D Thesis in Preparation, Department of Civil and Environmental Engineering, The University of Adelaide.

Davies, O. L. and Goldsmith, P. L., (1980), *Statistical Methods in Research and Production*, Fourth Revised Edition, Longman Group Ltd., London.

Gilbert, R. I. and Warner, R. F., (1978), *Tension Stiffening in Reinforced Concrete Slabs*, Journal of the Structural Division, ASCE, Vol. 104, No. ST12, Dec, P1885-1900.

Hilti Manual, (1993a), *Fastening Technology Manual - Product Information*, Hilti B3.1, Issue 7, Hilti (Australia) Pty. Ltd.

Hilti Manual, (1993b), *Fastening Technology Manual - Product Information*, Hilti B3.2, Issue 7, Hilti (Australia) Pty. Ltd.

Johnson, R. P., and Molenstra, N., (1991), *Partial Shear Connection in Composite Beams for Buildings*, Proc. of Instn. of Civ. Engrs., London, England, Part 2, 91(Dec.), P679-704.

Jones, R., Swamy, R. N. and Charif, A., (1988), *Plate Separation and Anchorage of Reinforced Concrete Beams Strengthen by Epoxy-Bonded Steel Plates*, The structural Engineer, Vol. 66, No. 5, March, P85-94.

Johnson, R. P., (1994), *Composite Structures of Steel and Concrete, Volume 1, Beams, Slabs, Columns and Frames for buildings*, Second edition, Blackwell Scientific Publications, Oxford, London.

Johnson, R. P. and Oehlers, D. J., (1982), *Design for Longitudinal Shear in Composite T-Beams*, Proc. Instn. of Civil Engineers, London, Part 2, Vol. 73, P147-170.

Kotsovos, M. D., (1984), *Behaviour of Reinforced Concrete Beams with a Shear Span to Depth Ratio between 1.0 and 2.5*, ACI Journal, Vol. 81, No.3, may-June, P279-286.

Luo, W, (1993), *Strengthening of Post-Tensioned and Reinforced Concrete Beams by Bonding External Steel Plates*, M.Sc. Engineering thesis, Department of Civil and Environmental Engineering, The University of Adelaide.

Mckenna, J. K. and Erki, M. A., (1994), *Strengthening of Reinforced Concrete Flexural Members using Externally Applied Steel Plates and Fiber Composites--a Survey,* Canadian Journal of Civil Engineering, 21, Feb., P16-24.

Newmark, N. M., Seiss, C. P. and Viest, I. M., (1951), *Tests and Analysis of Composite Beams with Incomplete Interaction*, Proc. Society for Experimental Stress Analysis, 9, No. 1, P75-92.

Oehlers, D. J., (1992), *Reinforced Concrete Beams with Plates Glued to their Soffit,* Journal of the Structural Division of the American Society of Civil Engineers, Aug., P2023-2038.

Oehlers, D. J., (1990), *Strengthening Reinforced Concrete Beams by Bonding Steel Plates to their Soffits*, Proc. of the Second National Structural Engineering Conference, Adelaide, Oct., P346-350.

Oehlers, D. J., (1995), *Rules for Bonding Steel Plates to Existing Reinforced Concrete Slabs*, Australian Civil Engineering Transactions, Vol. CE 37, No. 1, Feb., P15-20.

Oehlers, D. J. and Burnet M. J., (1994), *Strengthening and Stiffening Existing Reinforced Concrete Slabs by Bonding Steel Plates to their Tension Face*, Australasian Structural Engineering Conference, Sydney, Sept., P919-924.

Oehlers, D. J. and Wyatt, R., (1993), *Plated Corbels*, Australian Civil Engineering Transaction, Vol. 35, No. 3, Sept., P235-240.

Oehlers, D. J. and Moran, J. P., (1990), *Premature Failure of Externally Plated Reinforced Concrete Beams*, Journal of the Structural Division of the American Society of Civil Engineers, Vol. 116, No.4, April, P978-995.

Oehlers, D. J. and Bradford, M. A., (1995), *Composite Steel and Concrete - Structural Members, Fundamental Behaviour*, Pergamon Press, Oxford, UK.

Oehlers, D. J., Wright, H. D. and Burnet, M. J., (1994) *Flexural Strength of Profiled Beams*, Journal of Structural Engineering, ASCE, Vol. 120, No. 2, P379-393.

Oehlers, D. J. and Sved, G., (1995), *Composite Beams with Limited-Slip-Capacity Shear Connectors*, Journal of Structural Engineering, ASCE, Vol. 21, No. 6, June, P932-938.

Oehlers, D. J. and Johnson, R. P., (1987), *The Strength of Stud Shear Connections in Composite Beams*, The Structural Engineer, Vol. 65B, No. 2, June, P44-48.

Oehlers, D. J., (1989), *Splitting Induced by Shear Connectors in Composite Beams*, Journal of Structural Engineering, ASCE, Vol. 115, No.2, Feb, P341-362.

Pippard, A. J. S. and Barker, Sir J., (1962), *The Analysis of Engineering Structures*, Edward Arnold (Publishers) Ltd. London.

Parkinson, J., (1978), *Glue Solves a Sticky Problem for Gestetner*, New Civ. Engr., 310, Sep., P26-27.

Ramset Manual, (1992a), *Design Engineers' Manual, Trubolt, Masonry Anchors-2*, Ramset Fasteners (Australia) Pty. Limited.

Ramset Manual, (1992b), *Design Engineers' Manual, Dynabolt, Masonry Anchors-1*, Ramset Fasteners (Australia) Pty. Limited.

Swamy, R. N., Jones, R. and Bloxham, J. W., (1987), *Structural Behaviour of Reinforced Concrete Beams Strengthened by Epoxy Bonded Steel Plates*, The Structural Engineer, Vol. 65A, No. 2, Feb., P59-68.

Smith, S. T. and Bradford, M. A., (1995), *Ductility of Reinforced Concrete Beams with Side and Soffit Plates*, Proc. of 14th Australasian Conference on the Mechanics of Structure and Materials, Vol. 2, P428-432.

Toprac, A. A. and Dale, G. E. , (1967), *Composite Beams with a Hybrid Tee Steel Section*, Journal of the Structural Division, ASCE, No. ST5, P309-322.

Uy, B. and Bradford, M. A., (1995), *Ductility of Profiled Composite Beams, Part I: Experimental Study*, Journal of Structural Engineering, ASCE, May, Vol. 121, No. 5, P876-882.

Uy, B. and Bradford, M. A., (1995), *Ductility of Profiled Composite Beams, Part II: Analytical Study*, Journal of Structural Engineering, ASCE, May, Vol. 121, No. 5, P883-889.

Van Gemert, D. A., (1981), *Repairing of Concrete Structures by Externally Bonded Steel Plates*, Proc. ICP/RILEM/IBK Int. Symp. Plastic in Materials and Struct. Engrg., Prague, Czechoslovakia, P519-526.

Wyatt, R. and Oehlers, D. J., (1992), *Application of Composite Plated Beam Construction to Existing Bridge Corbels*, Rilem International Conference on Rehabilitation of concrete structures, Melbourne, August, P297-308.

Warner, R. F., (1969), *Biaxial Moment Thrust Curvature Relations*, Journal of the Structural Division, ASCE, Vol. 95, No. ST5, May, P923-940.

Warner, R. F., Rangan, B. V. and Hall, A. S., (1989), *Reinforced Concrete*, 3rd edition, Longman Cheshire, Melbourne, Australia.

Ziraba, N. Y., Baluch, H. M., Basunbul, A., et al, (1994), *Guide Lines towards the Design of Reinforced Concrete Beams with External Plates*, ACI Structural Journal, Nov.-Dec., P639-645.

Appendix A

Derivation of the Equations of Vertical Slip in Side Plated Beams

In this appendix, a detailed derivations of total vertical slip for UDL and for two point loads are given.

A.1 UDL loads

The side plated beam with a uniformly distributed load applied to the RC element is shown in Fig. A-1(a). The forces in the concrete element and that in the plate element are shown in (b) and (c) respectively, where P is the longitudinal shear force and V is the vertical shear force. Using the equilibrium eqn. (4.2), the moment in the concrete element at any point x can be expressed as follows

$$M_{conc}(x) = M(x) - M_{plate}(x) - P_{shear}(x)h_{na} \quad \text{.....(A.1)}$$

The parameters in eqn. (A.1) can be found from the forces in the concrete element, as shown in A-1(b), and can be written as

$$M_{conc} = \left(wLx - \frac{wx^2}{2}\right) - Vx - h_{na}qx \quad \text{.....(A.2)}$$

The relationship between the curvature and the moment is

$$\frac{d^2y}{dx^2} = \frac{M_{conc}}{(EI)_c} = \frac{\left(wLx - \frac{wx^2}{2}\right) - Vx - h_{na}qx}{(EI)_c} \quad \text{.....(A.3)}$$

Integrating eqn. (A.3), gives

$$\frac{dy}{dx} = \frac{1}{(EI)_c}\left[\left(wL\frac{x^2}{2} - \frac{wx^3}{6}\right) - \frac{Vx^2}{2} - h_{na}q\frac{x^2}{2}\right] + C \quad \text{.....(A.4)}$$

where C is the integration constant. As we are dealing with a simply supported symmetrically loaded beam, dy/dx = 0 at x = L. This gives,

$$C = -\frac{1}{(EI)_c}\left[\frac{wL^3}{3} - \frac{VL^2}{2} - h_{na}q\frac{L^2}{2}\right] \quad \text{.....(A.5)}$$

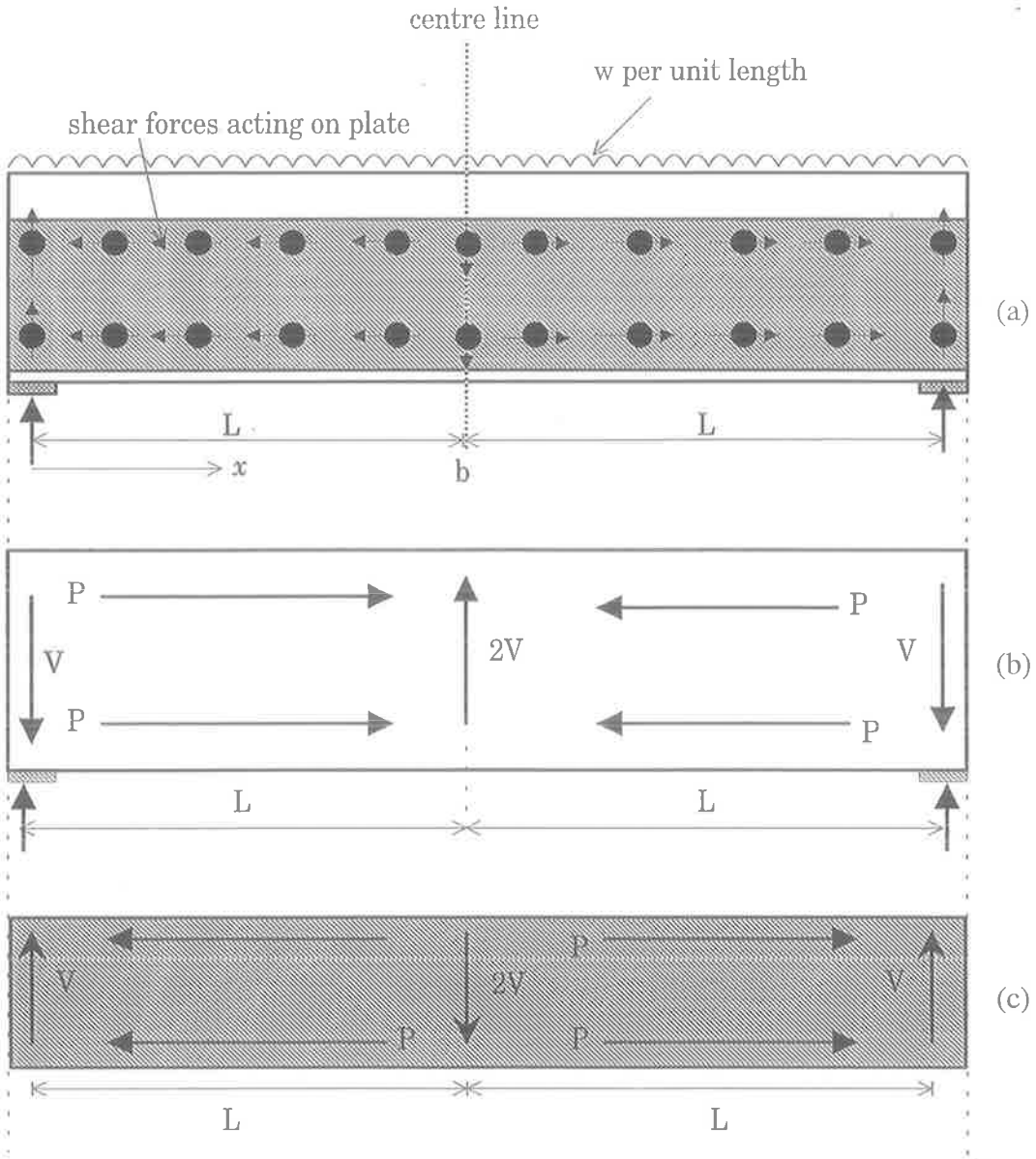

Fig. A-1 Plated beam with UDL

Inserting eqn. (A.5) into eqn. (A.4) gives

$$\frac{dy}{dx} = \frac{1}{(EI)_c}\left[\left(wL\frac{x^2}{2} - \frac{wx^3}{6}\right) - \frac{Vx^2}{2} - h_{na}q\frac{x^2}{2}\right] - \frac{1}{(EI)_c}\left[\frac{wL^3}{3} - \frac{VL^2}{2} - h_{na}q\frac{L^2}{2}\right]$$

.....(A.6)

Integrating eqn. (A.6) gives

$$y(x) = \frac{1}{(EI)_c}\left[\left(wL\frac{x^3}{6} - \frac{wx^4}{24}\right) - \frac{Vx^3}{6} - h_{na}q\frac{x^3}{6}\right] - \frac{1}{(EI)_c}\left[\frac{wL^3}{3} - \frac{VL^2}{2} - h_{na}q\frac{L^2}{2}\right]x + D$$

.....(A.7)

where, D is the constant of integration. At x = 0, y = 0, which gives D = 0 when substituting into eqn. (A.7). Then eqn. (A.7) can be written as follows

$$y(x) = \frac{1}{(EI)_c}\left[\left(wL\frac{x^3}{6} - \frac{wx^4}{24}\right) - \frac{Vx^3}{6} - h_{na}q\frac{x^3}{6}\right] - \frac{1}{(EI)_c}\left[\frac{wL^3}{3} - \frac{VL^2}{2} - h_{na}q\frac{L^2}{2}\right]x$$ .....(A.8)

Now eqn. (A.8) can be used to derive the deflection at x = L as follows.

$$\left(y_{x=L}\right)_c = -\frac{L^3}{3(EI)_c}\left[\frac{5}{8}wL - V - qh_{na}\right]$$ .....(A.9)

Assuming a linear variation in moment in the plate and following a similar procedure gives deflection of the plate element at x = L as follows, when the deflection at the support is zero.

$$\left(y_{x=L}\right)_p = -\frac{VL^3}{3(EI)_p}$$ .....(A.10)

The total vertical slip at x = L is given by

$$\left|(y_{x=L})_c\right| - \left|(y_{x=L})_p\right| = (s_v)_t \quad \text{.....(A.11)}$$

Inserting eqn. (A.9) and (A.10) into eqn. (A.11) gives

$$\frac{L^3}{3}\left[\frac{0.625wL - V - qh_{na}}{(EI)_c} - \frac{V}{(EI)_p}\right] = (s_v)_t \quad \text{.....(A.12)}$$

which is the general equation of total vertical slip of the plated beam in Fig. A-1(a).

A.2 Two Point Loads

The side plated beam with two point loads applied to the RC element is shown in Fig. A-2(a). The forces in the concrete element and that in the plate element are shown in (b) and (c) respectively. Applying Macaulay's method (Pippard and Barker, 1962), the moment in the concrete element in Fig. A-2(b) at any point x can be expressed as

$$M_{conc}(x) = Fx - F(x-L) - Vx + V(x-L) - qh_{na}x + qh_{na}(x-L) \quad \text{.....(A.13)}$$

Then, rearranging eqn. (A.13) gives

$$M_{conc}(x) = (F - V - qh_{na})x - (F - V - qh_{na})(x-L) \quad \text{.....(A.14)}$$

Equation (A.14) can be related to the curvatures as follows

$$\frac{d^2y}{dx^2} = \frac{M_{conc}(x)}{(EI)_c} = (F - V - qh_{na})\frac{x-(x-L)}{(EI)_c} \quad \text{.....(A.15)}$$

Integrating eqn. (A.15) gives

$$\frac{dy}{dx} = \frac{F - V - qh_{na}}{(EI)_c}\left[\frac{x^2}{2} - \frac{(x-L)^2}{2}\right] + C \quad \text{.....(A.16)}$$

where C is the constant of integration. At $x = L_1$, $dy/dx = 0$ and hence

$$C = \frac{F - V - qh_{na}}{2(EI)_c}\left[L^2 - 2LL_1\right] \quad \text{.....(A.17)}$$

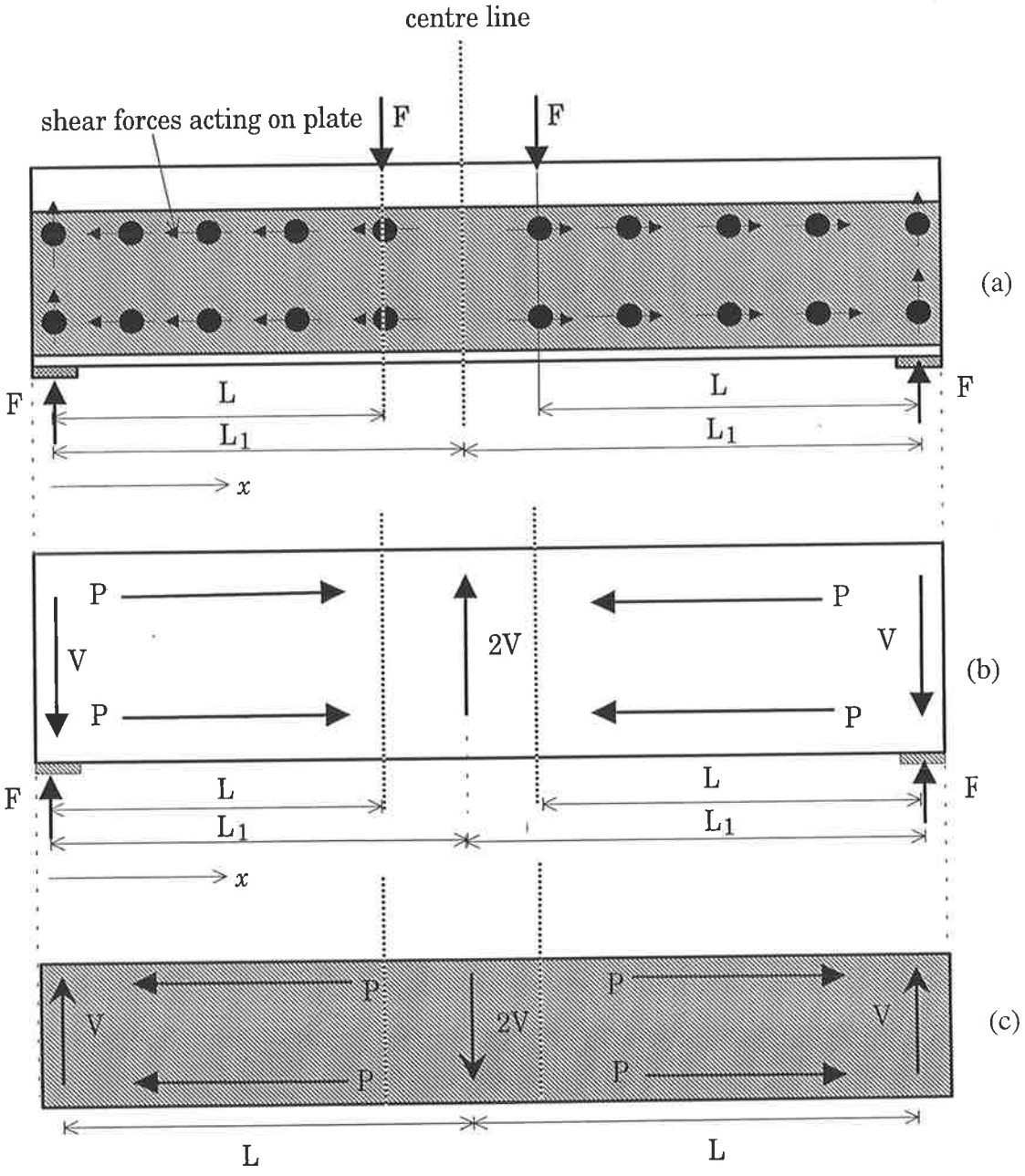

Fig. A-2 Plated beam with point loads

Inserting eqn. (A.17) into eqn. (A.16) gives

$$\frac{dy}{dx}=\frac{F-V-qh_{na}}{(EI)_c}\left[\frac{x^2}{2}-\frac{(x-L)^2}{2}\right]+\frac{F-V-qh_{na}}{2(EI)_c}\left[L^2-2LL_1\right] \quad \text{.....(A.18)}$$

Integrating eqn. (A.18) gives

$$y(x)=\frac{F-V-qh_{na}}{(EI)_c}\left[\frac{x^3}{6}-\frac{(x-L)^3}{6}\right]+\frac{F-V-qh_{na}}{2(EI)_c}\left[L^2-2LL_1\right]x+D\,. \quad \text{.....(A.19)}$$

where D is the constant of integration. At x = 0, y = 0 so, substituting into eqn. (A.18) gives D = 0. Then eqn. (A.19) can be written as

$$y(x)=\frac{F-V-qh_{na}}{(EI)_c}\left[\frac{x^3}{6}-\frac{(x-L)^3}{6}\right]+\frac{F-V-qh_{na}}{2(EI)_c}\left[L^2-2LL_1\right]x \quad \text{.....(A.20)}$$

Now, eqn. (A.20) can be used to derive the expression of deflection at x = L as follows

$$\left(y_{x=L}\right)_c=\frac{F-V-qh_{na}}{(EI)_c}\left[\frac{L^3}{6}+\frac{L^3-2L^2L_1}{2}\right] \quad \text{.....(A.21)}$$

Similarly, the following equation can be derived to give the deflection at x = L, when the deflection of the plate at the supports is zero, as shown in Fig. 4-7(c).

$$\left(y_{x=L}\right)_p=\frac{V}{(EI)_p}\left[\frac{L^3}{6}+\frac{L^3-2L^2L_1}{2}\right] \quad \text{.....(A.22)}$$

Inserting eqn. (A.21) and (A.22) into eqn. (A.11), gives the total vertical slip $(s_v)_t$ as follows.

$$\left[\frac{F-V-qh_{na}}{(EI)_c}-\frac{V}{(EI)_p}\right]\left[\frac{L^3}{6}+\frac{L^3-2L^2L_1}{2}\right]=\left(s_v\right)_t \quad \text{.....(A.23)}$$

Appendix-B

Experimental Material Properties

The material properties of the concrete, the reinforcement and the plate were obtained by testing several specimens. The test results of all the specimen are given in this appendix. All the tests were performed according to the Australian Standards AS1012 (1993) and AS1391(1991).

B.1 Concrete

There were five pours to cast the push-specimens and beam specimens with their associated concrete material properties. The concrete materials were tested to determine the material properties of the different pours at different ages. The results of individual sample tests are given in the following sections.

B.1.1 Concrete of Pour 1

The test results from cylinder specimens, cube specimens and the beam specimens are given in Tables B.1 to B.4 respectively.

Table B.1 Pour 1, Compression and Elastic modulus tests on cylinder specimens

Sample no.	Ultimate load, P_{max} (kN)	Comp-ressive strength, f_c (MPa)	Elastic modulus, E_c (MPa)	Weight (gm)	Size (mmxmm)	Density (kg/m^3)	Age (days)
1	2	3	4	5	6	7	8
1	403.5	50.36	-	3830.1	101.0x201.0	2378.38	133
2	394.5	49.23	-	3757.3	100.5x201.0	2356.45	133
3	446.0	55.56	44783.82	3830.0	100.5x201.0	2402.04	133
4	421.0	52.54	40460.63	3814.2	100.5x200.5	2398.10	133

Table B.2 Pour 1, Indirect tensile tests on cylinder specimens

Sample no.	Ultimate load, P_{max} (kN)	Indirect tensile strength, f_t (MPa)	Weight (gm)	Size (mmxmm)	Density (kg/m^3)	Age (days)
1	2	3	5	6	7	8
1	171.0	5.40	3830.5	100.5x200.5	2408.35	133
2	178.0	5.61	3827.2	100.5x201.0	2400.29	133

Table B.3 Pour 1, Compression tests on cube specimens

Sample no.	Ultimate load, P_{max} (kN)	Comp-ressive strength, f_{cu} (MPa)	Weight (gm)	Size (mm x mm x mm)	Density (kg/m^3)	Age (days)
1	2	3	5	6	7	8
1	611.0	59.89	2544.3	101.0x101.0x102.0	2445.26	133
2	593.0	58.13	2534.2	101.0x101.0x102.0	2435.56	133
3	529.0	51.86	2558.8	101.0x101.0x102.5	2447.20	133
4	555.0	54.40	2564.0	101.0x101.0x102.0	2464.20	133

Table B.4 Pour 1, Flexural tests on beam specimens

Sample no.	Ultimate load, P_{max} (kN)	Flexural strength, f_{cf} (MPa)	Weight (gm)	Size (mm x mm x mm)	Density (kg/m^3)	Age (days)
1	2	3	5	6	7	8
1	22.02	6.61	12492.6	500.0x100.0x100.0	2498.52	835
2	22.16	6.65	12449.8	500.0x100.0x100.0	2489.96	835
3	19.20	5.76	12378.3	500.0x100.0x100.0	2475.66	835

B.1.2 Concrete of Pour 2

The test results of the cylinder specimen, cube specimens and the beam specimens are given in Table B.5 to B.8 respectively.

Table B.5 Pour 2, Compression and Elastic Modulus tests on cylinder specimens

Sample no.	Ultimate load, P_{max} (kN)	Comp-ressive strength, f_c (MPa)	Elastic modulus, Ec (MPa)	Weight (gm)	Size (mmxmm)	Density (kg/m^3)	Age (days)
1	2	3	4	5	6	7	8
1	339.0	43.16	-	3740.6	100.0x200.5	2375.40	111
2	349.5	44.06	-	3677.6	100.5x200.5	2312.21	111
3	372.0	47.36	31727.67	3711.2	100.0x200.5	2356.73	111
4	356.5	44.94	33680.14	3688.9	100.5x200.0	2325.12	111

Table B.6 Pour 2, Indirect tesile tests on cylinder specimen

Sample no.	Ultimate load, P_{max} (kN)	Indirect tensile strength, f_t (MPa)	Weight (gm)	Size (mmxmm)	Density (kg/m^3)	Age (days)
1	2	3	5	6	7	8
1	129.0	4.07	3709.6	100.5x201.0	2326.53	111
2	128.2	4.07	3679.4	100.0x200.5	2336.53	111

Table B.7 Pour 2, Compression tests on cube specimens

Sample no.	Ultimate load, P_{max} (kN)	Comp-ressive strength, f_{cu} (MPa)	Weight (gm)	Size (mm x mm x mm)	Density (kg/m^3)	Age (days)
1	2	3	5	6	7	8
1	514.5	50.43	2480.6	101.0x101.0x102.0	2384.04	111
2	489.5	47.99	2466.7	101.0x101.0x102.0	2370.68	111
3	515.0	50.48	2482.8	101.0x101.0x102.0	2386.16	111
4	520.0	50.98	2483.5	101.0x101.0x102.0	2386.82	111

Table B.8 Pour 2, Flexural tests on beam specimens

Sample no.	Ultimate load, P_{max} (kN)	Flexural strength, f_{cf} (MPa)	Weight (gm)	Size (mm x mm x mm)	Density (kg/m^3)	Age (days)
1	2	3	5	6	7	8
1	18.80	5.64	12053.7	500.0x100.0x100.0	2410.74	832
2	19.24	5.77	12000.2	500.0x100.0x100.0	2400.04	832
3	16.90	5.07	12025.9	500.0x100.0x100.0	2405.18	832

B.1.3 Concrete of Pour 3

The test results are given in Tables B.9 to B.12. It can be seen in Table B.11 that that strength of sample no. 1 is much lower than the others. Also, the failure mode of this sample was different from others. This happened as the specimen was loaded eccentrically during the test due to the disturbance of the machine. Hence, it was excluded from the calculation of the average strength of Pour 3.

Table B.9 Pour 3, Compression and Elastic Modulus on cylinder specimens

Sample no.	Ultimate load, P_{max} (kN)	Comp-ressive strength, f_c (MPa)	Elastic modulus, E_c (MPa)	Weight (gm)	Size (mmxmm)	Density (kg/m^3)	Age (days)
1	2	3	4	5	6	7	8
1	366.6	45.75	43997.88	3762.5	101.0x200.0	2384.09	605
2	356.4	44.48	41128.45	3743.0	100.5x200.0	2359.22	605
3	369.8	46.15	42514.80	3710.3	101.0x201.0	2303.99	605
4	352.0	43.99	41466.49	3726.0	101.0x200.0	2325.31	605

Table B.10 Pour 3, Indirect tensile tests on cylinder specimen

Sample no.	Ultimate load, P_{max} (kN)	Indirect tensile strength, f_t (MPa)	Weight (gm)	Size (mmxmm)	Density (kg/m^3)	Age (days)
1	2	3	5	6	7	8
1	131.2	4.13	3761.0	101.0x200.0	2347.15	605
2	130.2	4.10	3736.8	101.0x200.0	2332.05	605

Table B.11 Pour 3, Compression tests on cube specimen

Sample no.	Ultimate load, P_{max} (kN)	Comp-ressive strength, f_{cu} (MPa)	Weight (gm)	Size (mm x mm x mm)	Density (kg/m^3)	Age (days)
1	2	3	5	6	7	8
1	254.8	24.98	2484.3	101.0x101.0x101.0	2411.24	605
2	398.0	38.63	2496.5	101.0x101.0x102.0	2399.32	605
3	378.8	36.69	2500.4	100.0x101.0x102.0	2427.10	605

Table B.12 Pour 3, Flexural tests on beam specimen

Sample no.	Ultimate load, P_{max} (kN)	Flexural strength, f_{cu} (MPa)	Weight (gm)	Size (mm x mm x mm)	Density (kg/m^3)	Age (days)
1	2	3	5	6	7	8
1	20.02	6.01	12191.8	500.0x100.0x100.0	2438.36	605
2	19.04	5.71	12117.1	500.0x100.0x100.0	2423.42	605
3	17.52	5.26	11895.8	500.0x100.0x100.0	2379.16	605

B.1.4 Concrete of Pour 4

The test results are given in Tables B.13 to B.16. It can be seen in Table B.13 that the strength of sample nos. 1 to 5 and 7 are much lower than the others. This happened due to eccentric loading of the specimens during the tests. A similar thing happened to the samples of 53 and 121 days of the cube specimens in Table B.15. All these specimens were excluded from the calculation of the average strength of Pour 4.

Table B.13 Pour 4, Compression tests and Elastic modulus tests on cylinder specimens

Sample no.	Ultimate load, P_{max} (kN)	Comp-ressive strength, f_c (MPa)	Elastic modulus, E_c (MPa)	Weight (gm)	Size (mmxmm)	Density (kg/m^3)	Age (days)
1	2	3	4	5	6	7	8
1	295.0	36.82	25000.0	3701.7	101.0x200.0	2309.70	53
2	268.4	33.50	21875.0	3721.1	101.0x200.0	2322.25	53
3	285.8	35.67	28571.0	3692.5	101.0x200.0	2604.40	53
4	265.2	33.10	26666.7	3718.6	101.0x200.0	2320.69	53
5	270.6	33.44	39333.0	3686.3	101.5x200.0	2277.92	121
6	420.5	51.96	39230.0	3695.3	101.5x200.0	2283.48	121
7	291.6	36.04	30000.0	3655.4	101.5x200.0	2258.83	121
8	394.0	48.69	39033.0	3709.3	101.5x200.0	2292.13	121
9	391.0	48.19	41333.0	3722.5	101.5x200.0	2300.29	121
10	361.5	44.68	-	3696.0	100.5x200.0	2329.69	143
11	383.0	47.33	-	3717.4	100.5x200.0	2343.08	143
12	411.0	51.29	-	3736.7	100.5x200.0	2355.25	143
13	414.5	51.73	40850.2	3708.7	100.5x200.0	2337.60	143
14	-	-	45656.1	3729.4	100.0x201.0	2362.39	143
15	-	-	41006.2	3748.3	100.0x200.0	2386.24	143

Table B.14 Pour 4, Indirect tensile tests on cylinder specimen

Sample no.	Ultimate load, P_{max} (kN)	Indirect tensile strength, f_t (MPa)	Weight (gm)	Size (mmxmm)	Density (kg/m^3)	Age (days)
1	2	3	5	6	7	8
1	131.0	4.13	3737.4	100.0x200.0	2379.30	53
2	132.8	4.19	3742.9	101.0x200.0	2335.85	53
3	128.8	4.04	3729.4	101.0x201.0	2315.85	144
4	134.5	4.24	3748.3	101.0x201.0	2327.59	144

Table B.15 Pour 4, Compression tests on cube specimen

Sample no.	Ultimate load, P_{max} (kN)	Comp-ressive strength, f_{cu} (MPa)	Weight (gm)	Size (mm x mm x mm)	Density (kg/m^3)	Age (days)
1	2	3	5	6	7	8
1	420.0	39.97	2522.6	102.5x102.5x102.5	2342.48	53
2	463.5	44.55	2532.3	102.0x102.0x102.0	2386.24	53
3	274.0	26.59	2481.4	101.5x102.0x101.5	2361.37	121
4	366.5	35.57	2509.5	101.5x101.5x101.0	2411.76	121
5	572.0	56.45	2510.2	101.5x100.0x100.0	2473.10	143
6	557.5	55.12	2496.1	101.0x100.0x101.0	2446.32	143

Table B.16 Pour 4, Flexural tests on beam specimen

Sample no.	Ultimate load, P_{max} (kN)	Flexural strength, f_{cf} (MPa)	Weight (gm)	Size (mm x mm x mm)	Density (kg/m^3)	Age (days)
1	2	3	5	6	7	8
1	20.48	6.14	11914.1	500.0x100.0x100.0	2382.82	53
2	20.36	6.11	11781.5	500.0x100.0x100.0	2356.30	53
3	20.22	6.10	11887.6	500.0x100.0x100.0	2377.52	53
4	20.86	6.26	11857.4	500.0x100.0x100.0	2371.48	220
5	20.74	6.22	11801.9	500.0x100.0x100.0	2360.38	220
6	22.86	6.86	11876.7	500.0x100.0x100.0	2375.34	220

B.1.5 Concrete of Pour 5

The test results are given in Tables B.17 to B.20.

Table B.17 Pour 5 Compression and Elastic Modulus tests on cylinder specimens

Sample no.	Ultimate load, P_{max} (kN)	Comp-ressive strength, f_c (MPa)	Elastic modulus, E_c (MPa)	Weight (gm)	Size (mmxmm)	Density (kg/m^3)	Age (days)
1	2	3	4	5	6	7	8
1	313.0	39.45	32804.66	3666.1	100.5x201.0	2299.25	109
2	366.0	46.14	32213.58	3692.2	101.0x202.0	2281.39	109
3	393.8	49.64	34715.61	3702.6	100.5x200.0	2333.75	109
4	349.0	44.05	-	3658.1	100.2x200.0	2319.53	109
5	347.0	43.74	-	3666.4	100.5x200.0	2310.94	117
6	346.5	43.67	35757.08	3693.7	100.5x200.0	2328.14	117
7	363.5	45.76	34715.61	3666.9	100.5x200.0	2311.25	117

Table B.18 Pour 5, Indirect tensile tests on cylinder specimen

Sample no.	Ultimate load, P_{max} (kN)	Indirect tensile strength, f_t (MPa)	Weight (gm)	Size (mmxmm)	Density (kg/m^3)	Age (days)
1	2	3	5	6	7	8
1	147.8	4.68	3684.2	100.5x200.0	2322.15	117
2	133.2	4.21	3682.1	100.5x200.0	2320.83	117

Table B.19 Pour 5, Compression tests on cube specimens

Sample no.	Ultimate load, P_{max} (kN)	Comp-ressive strength, f_{cu} (MPa)	Weight (gm)	Size (mm x mm x mm)	Density (kg/m^3)	Age (days)
1	2	3	5	6	7	8
1	548.0	53.19	2464.1	102.0x101.0x100.0	2391.86	109
2	543.0	52.87	2475.6	101.0x102.0x102.0	2355.91	109
3	542.5	53.18	2507.6	101.0x101.0x101.0	2433.85	109

Table B.20 Pour 5, Flexural tests on beam specimens						
Sample no.	Ultimate load, P_{max} (kN)	Flexural strength, f_{cf} (MPa)	Weight (gm)	Size (mm x mm x mm)	Density (kg/m^3)	Age (days)
1	2	3	5	6	7	8
1	23.08	6.92	12135.2	500.0x100.0x100.0	2427.04	117
2	20.60	6.18	12219.5	500.0x100.0x100.0	2443.90	117
3	20.38	6.14	12050.1	500.0x100.0x102.0	2362.76	117

B.2 Steel Reinforcement

The reinforcement used in the beams were from two different batches. Three samples from each batch were tested and the results are given in Table B.21.

Table B.21 Yield and ultimate strength of Y20 bar		
Beam specimen	Yield strength (MPa)	Ultimate strength (MPa)
1	2	3
Beam Series 1-3 (excluding beam B24 and A21)	438.89	528.00
	440.48	527.37
	449.71	529.60
Beam A21 and B24	442.08	534.37
	433.48	533.42
	421.39	514.32

B.3 Steel Plates

The plate used in the push specimens and the beam specimens were from three different batches. Three samples were tested for each of the batches. The results are given in Table B.22.

Table B.22 Yield and Ultimate strength of Plate

Plated beam	Push specimen	Yield stress (MPa)	Ultimate stress (MPa)
1	2	3	4
Series 2-3	-	380	442
		375	443
		377	442
-	Series 1-5 except Test P22	368	464
		369	465
		369	465
-	Test P22	314	449
		323	424
		324	440

Appendix-C

Push Tests Results of Bolted Shear Connector

The slip in the push tests in Sect. 8.3 was recorded at four corners of the push specimen, as shown in Fig. 8-7. The results at four different corners are presented in this appendix in Figs. C-1 to C-24. The numbers that are shown against the curves are the reference numbers of the respective LVDTs. When there is little variations in the four load-slip curves, the reference numbers of the LVDTs are not shown.

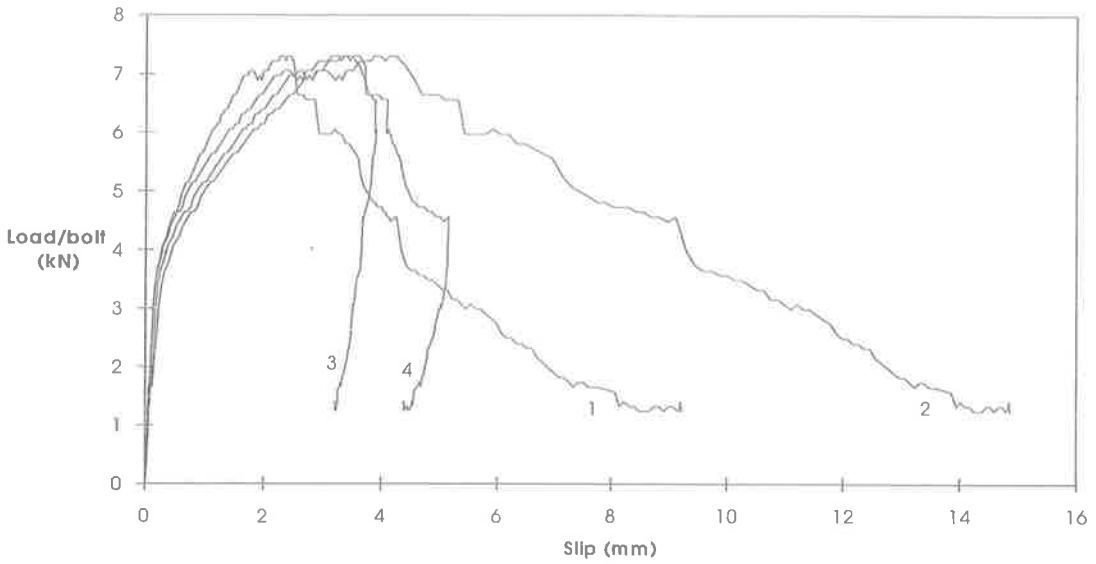

Fig. C-1 Push test P1: Dynabolt of 26 mm length

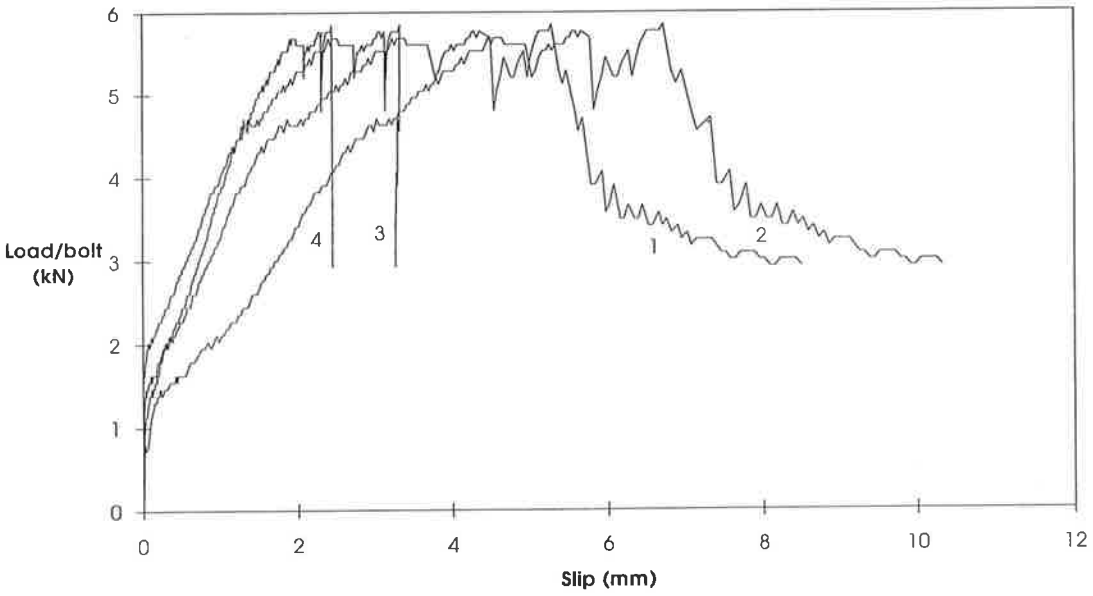

Fig. C-2 Push test P2: Dynabolt of 26 mm length

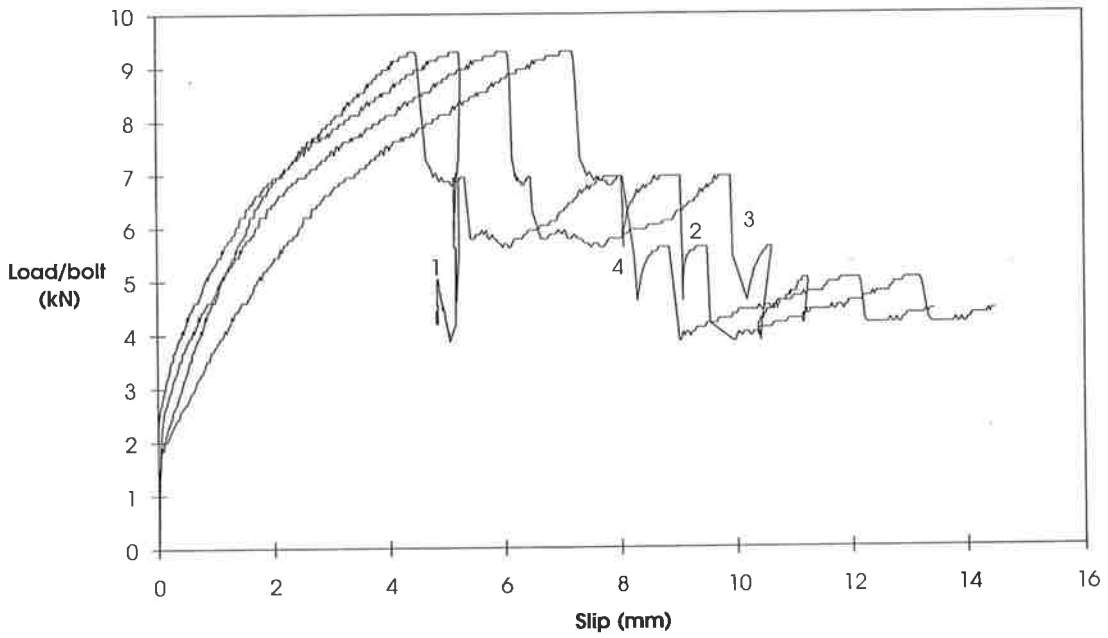

Fig. C-3 Push test P3 : Dynabolt of 38 mm length

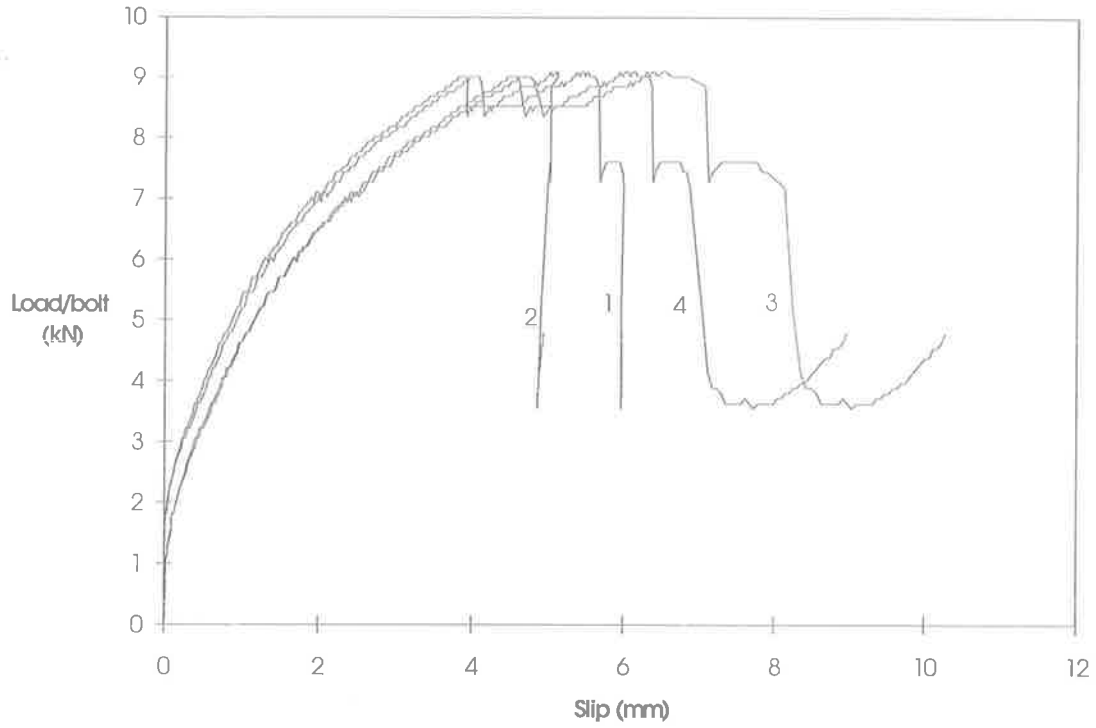

Fig. C-4 Push test P4: Dynabolt of 38 mm length

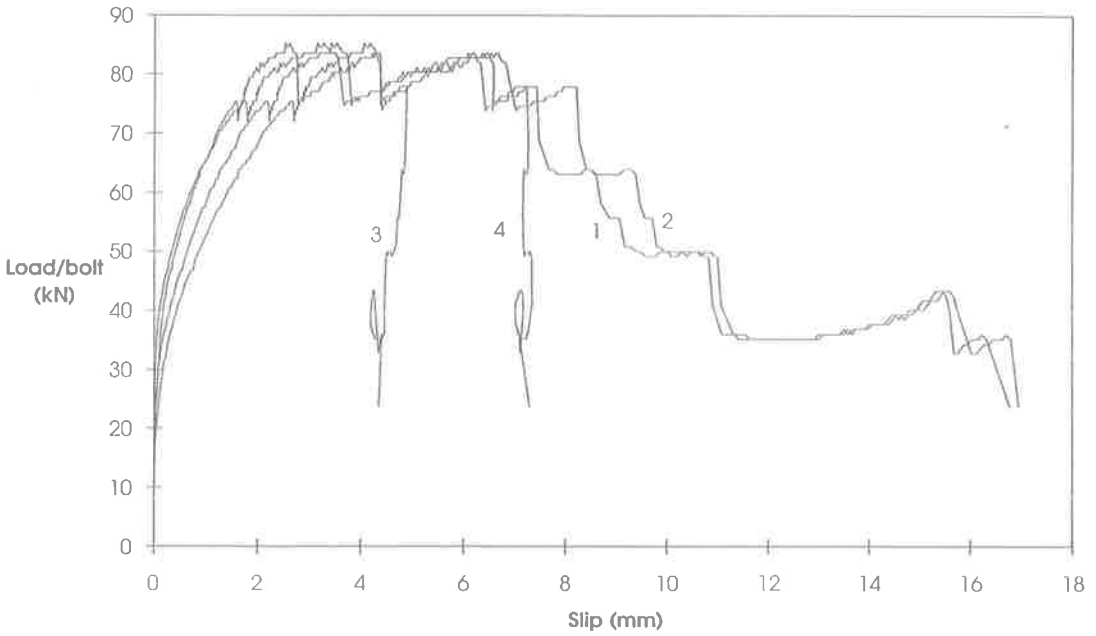

Fig. C-5 Push test P5: Dynabolt of 58 mm length

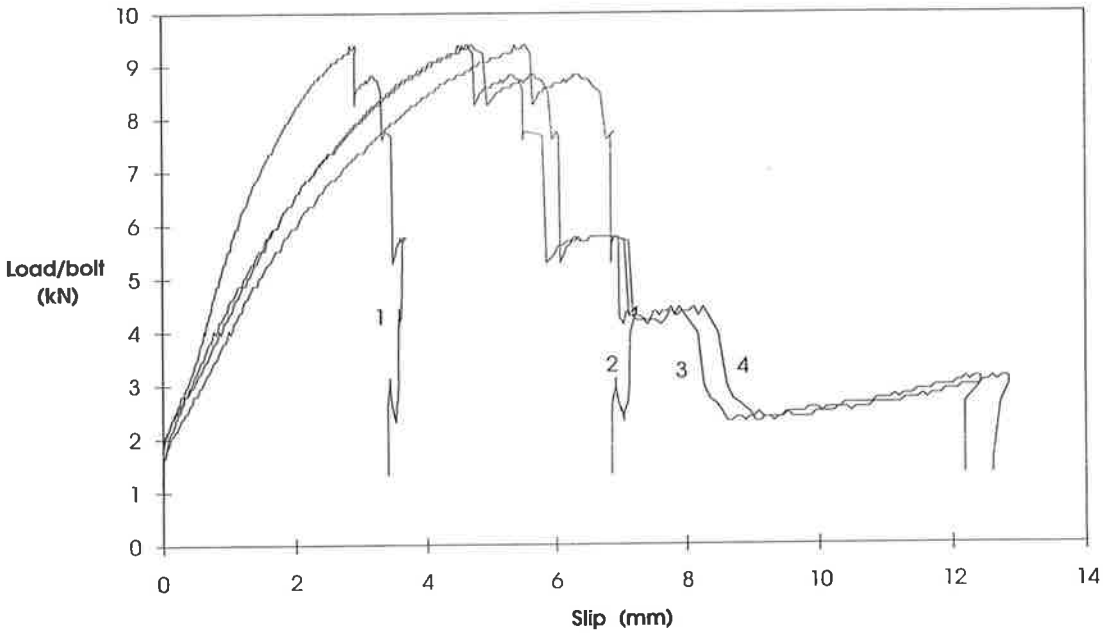

Fig. C-6 Push test P6: Dynabolt of 58 mm length

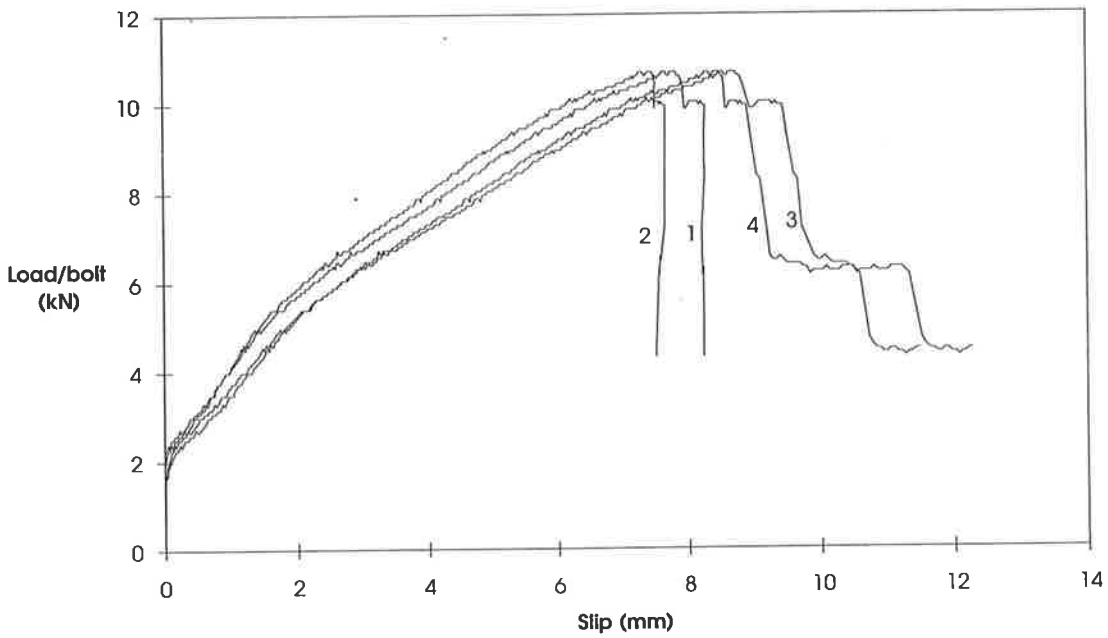

Fig. C-7 Push test P7: Dynabolt of 38mm length (2.5 mm clearance in plate)

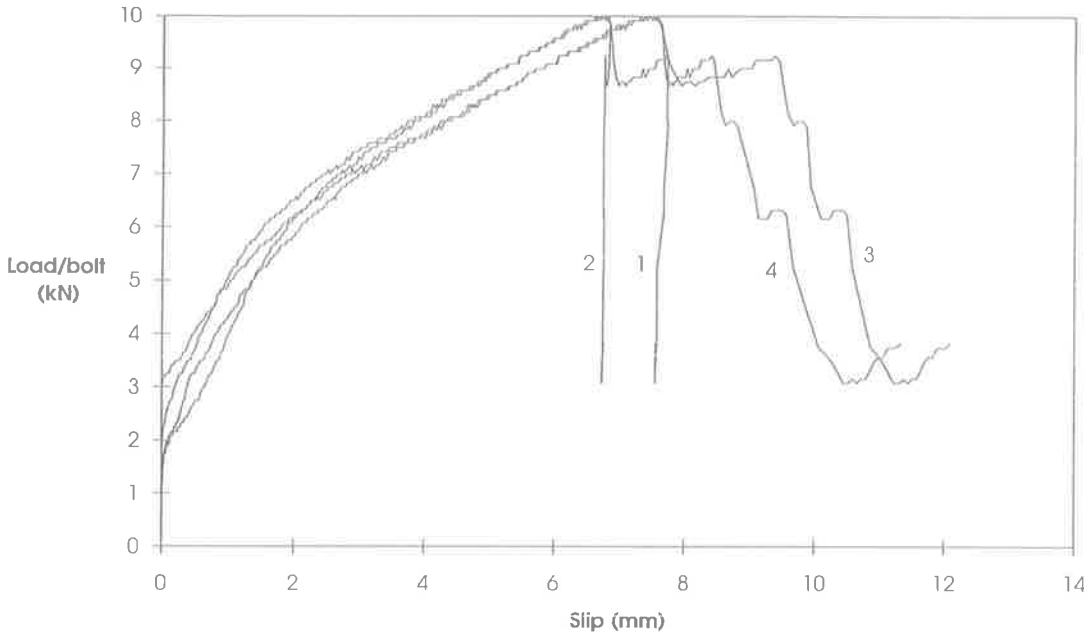

Fig. C-8 Push test P8: Dynabolt of 38 mm length (2.5m clearance in plate)

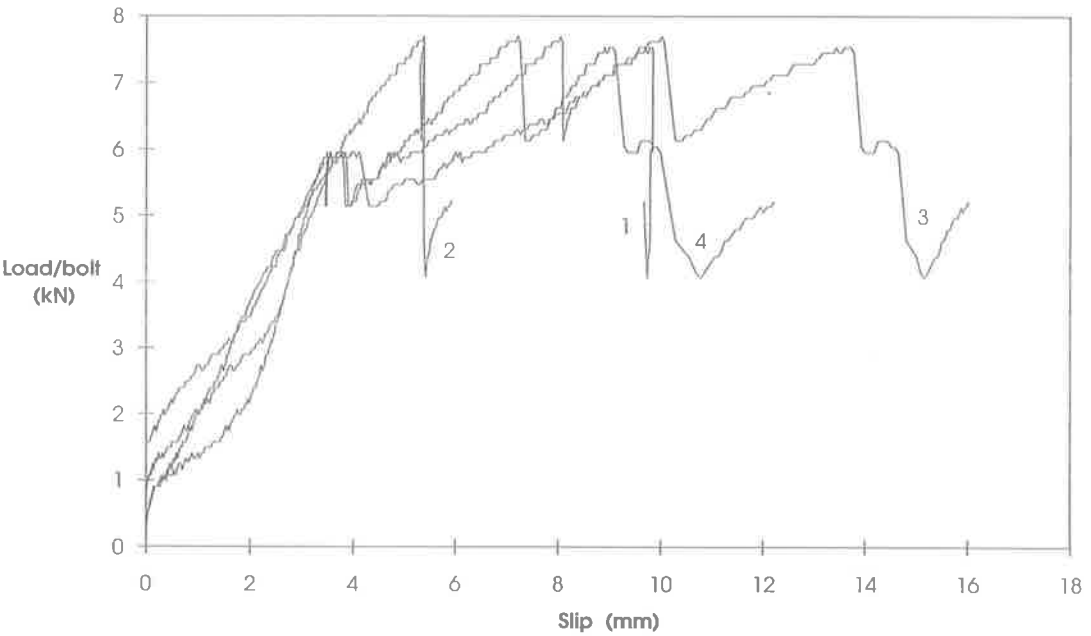

Fig. C-9 Push test P9: Dynabolt of 38 mm length (3.5 mm clearance in plate)

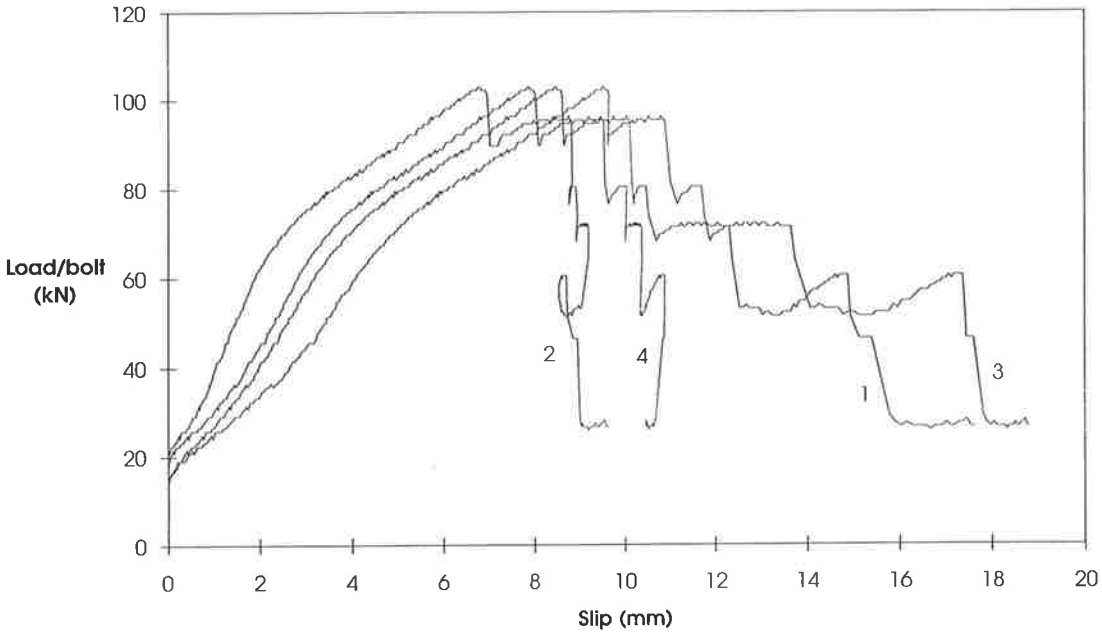

Fig. C-10 Test P10: Dynabolt of 38 mm length (3.5 mm clearance in plate)

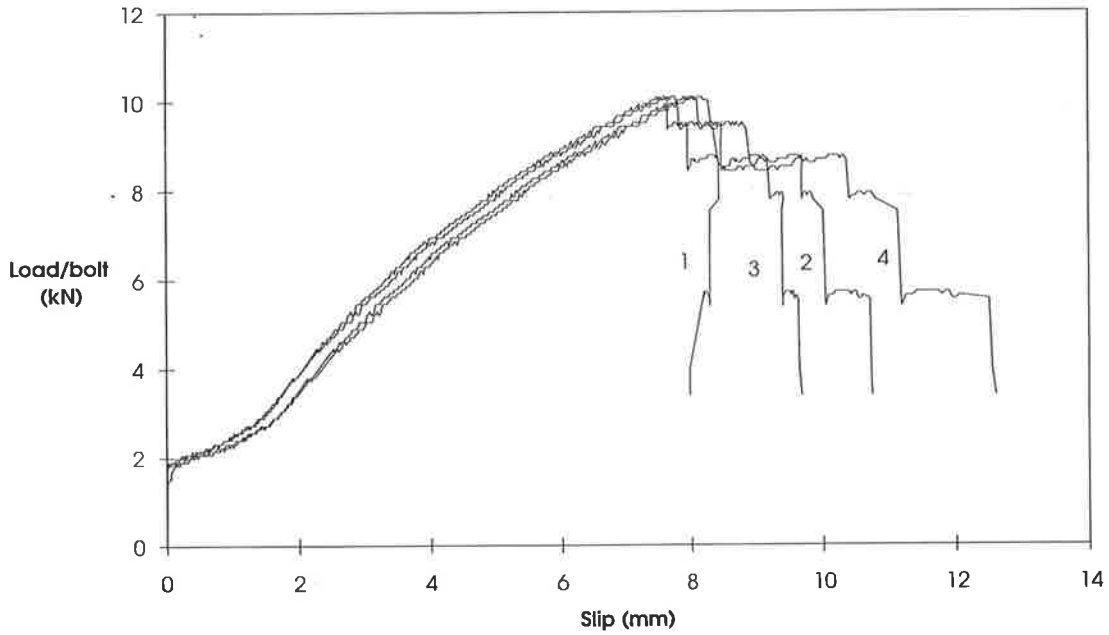

Fig. C-11 Push test P11: Dynabolt of 38 mm length (4.5 mm clearance in plate)

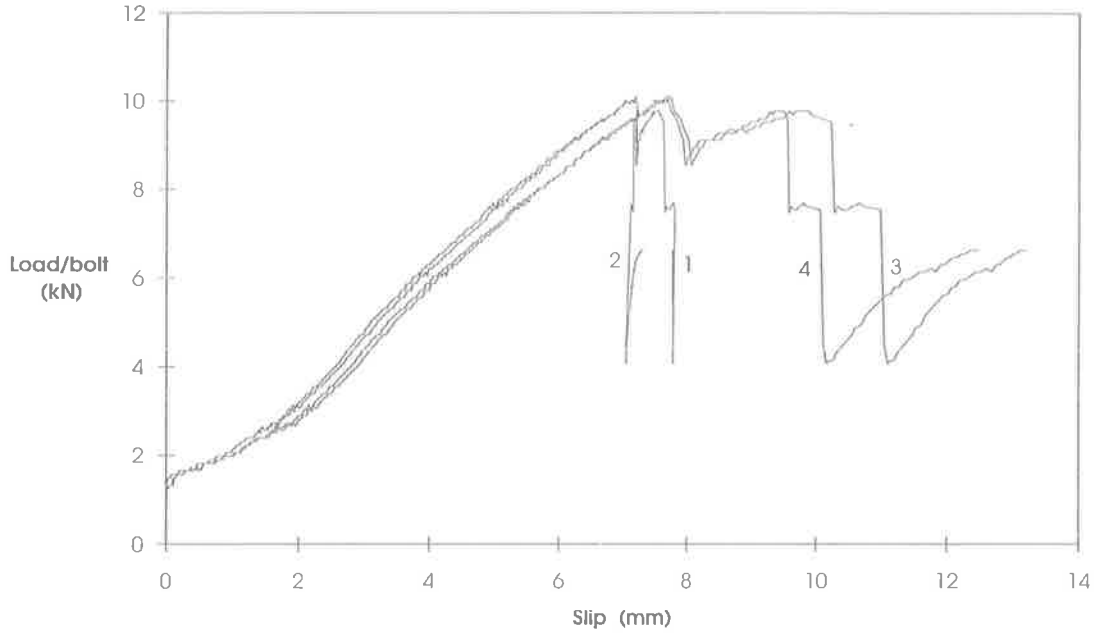

Fig. C-12 Push test P12: Dynabolt of 38 mm length (4.5 mm clearance in plate)

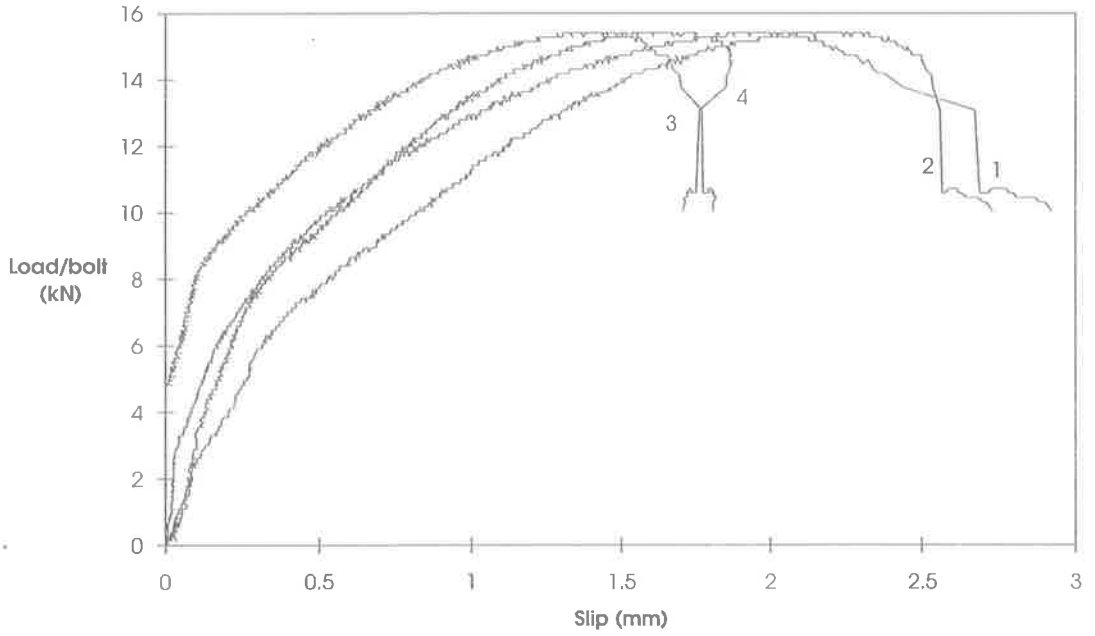

Fig. C-13 Push test P13: Trubolt

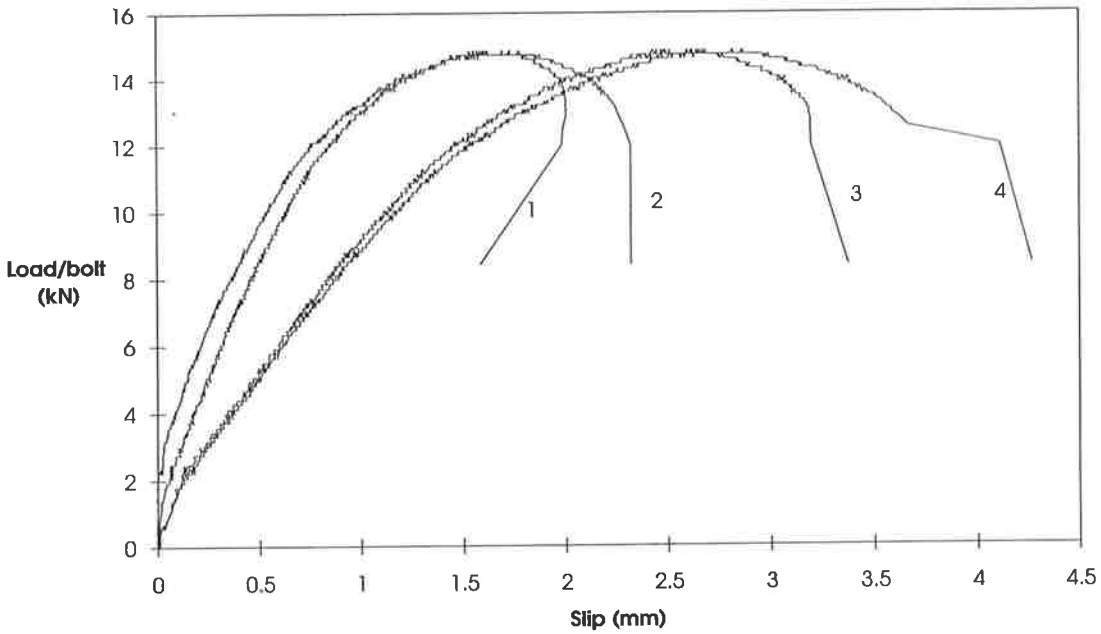

Fig. C-14 Push test P14: Glued Trubolt

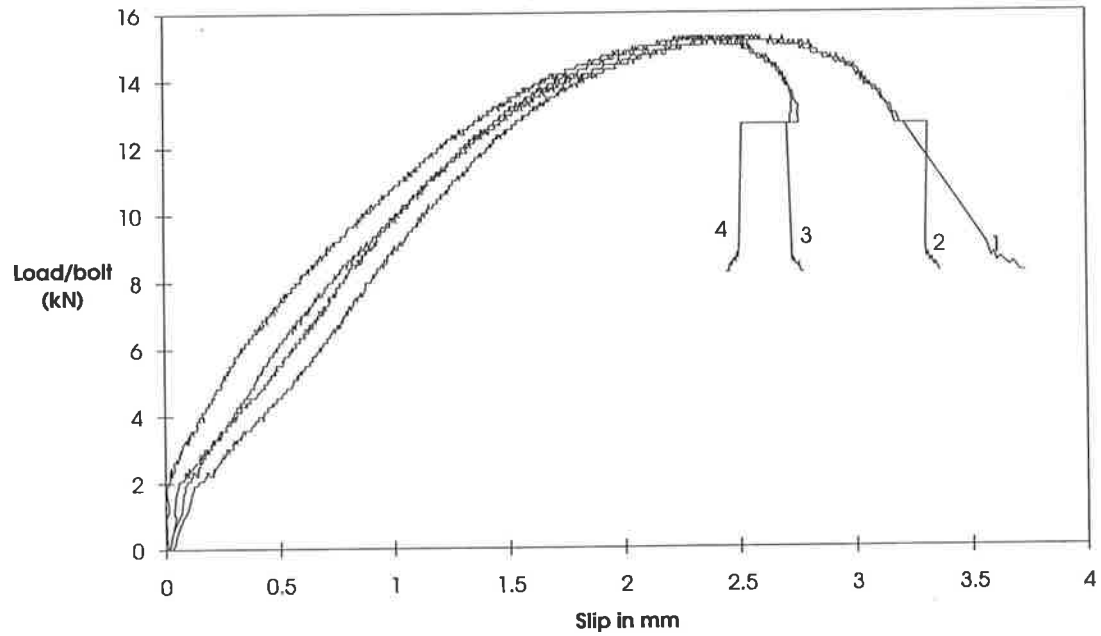

Fig. C-15 Push test P15: HSA bolt

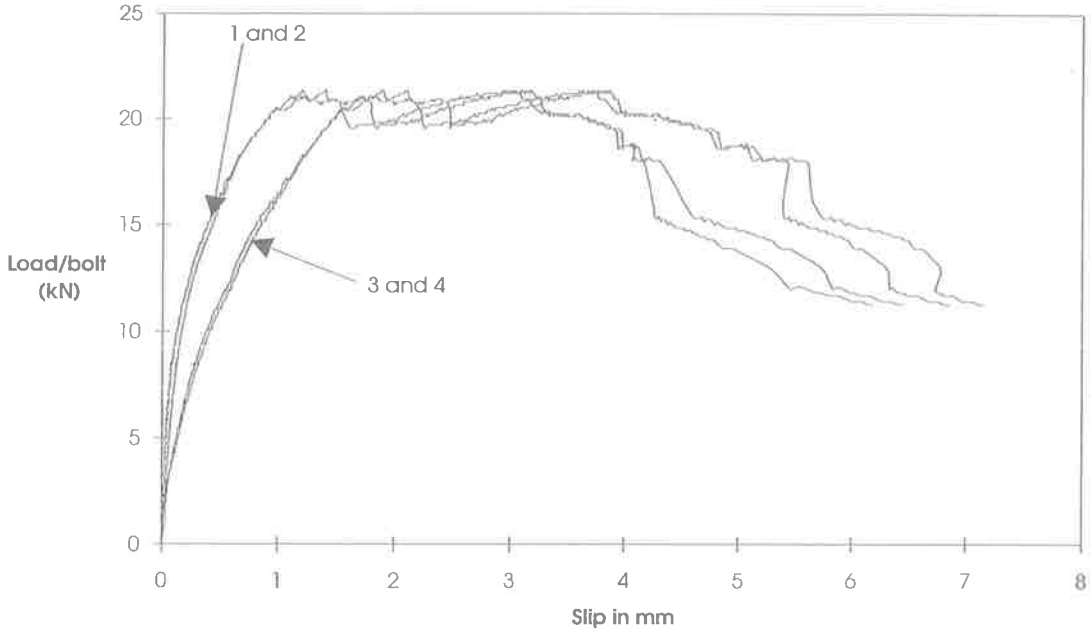

Fig. C-16 Push test P16: HIS adhesive bolt

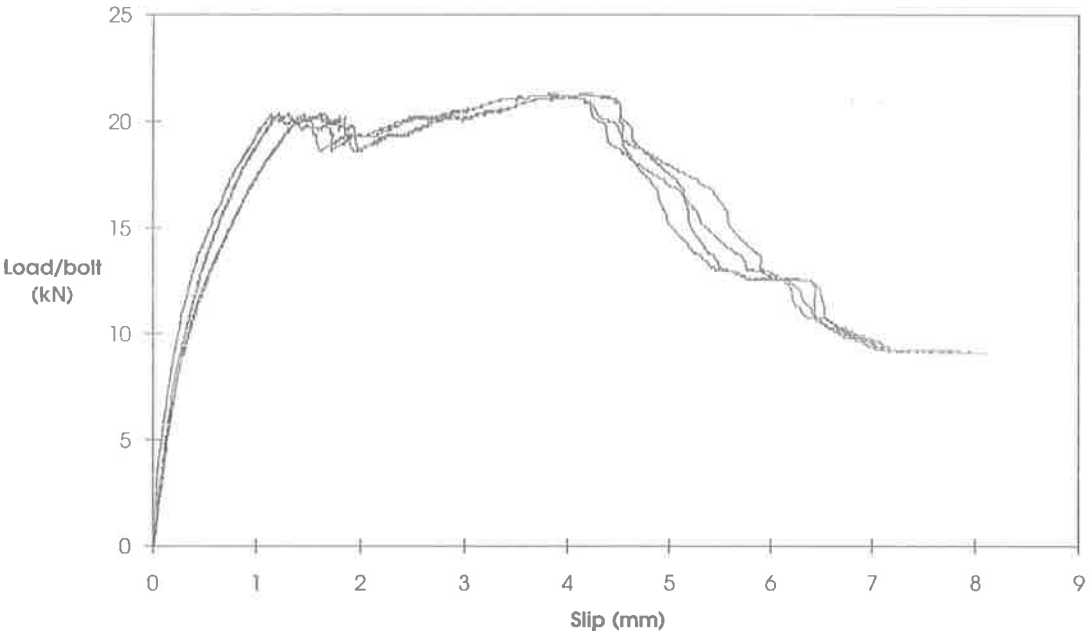

Fig. C-17 Push test P17: HIS adhesive bolt using Ramset glue

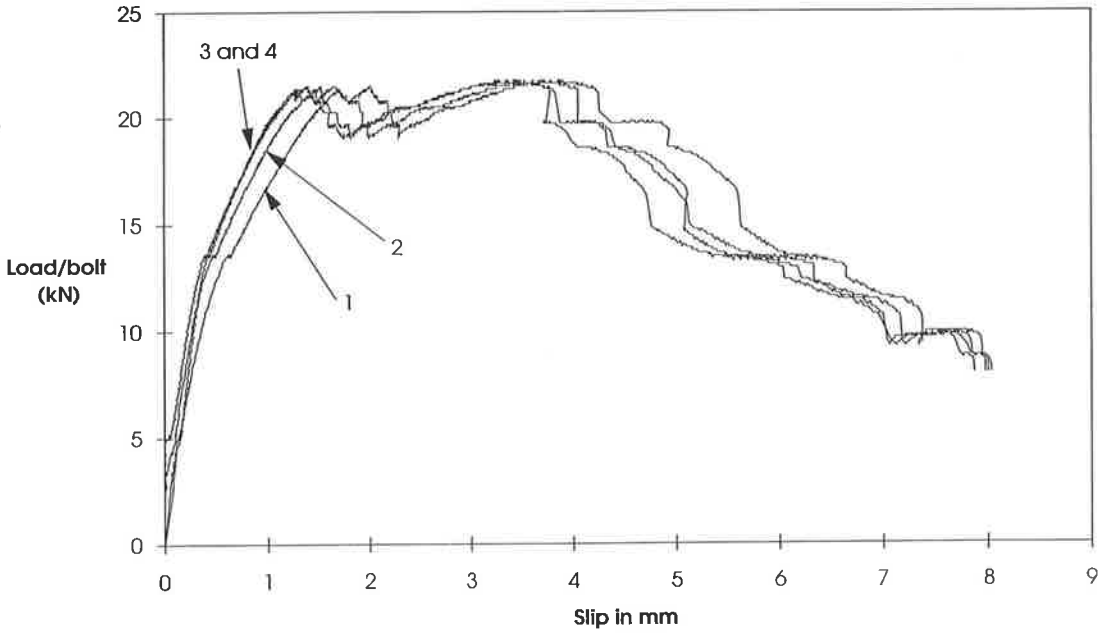

Fig. C-18 Push test P18: HIS adhesive bolt using Ramset glue

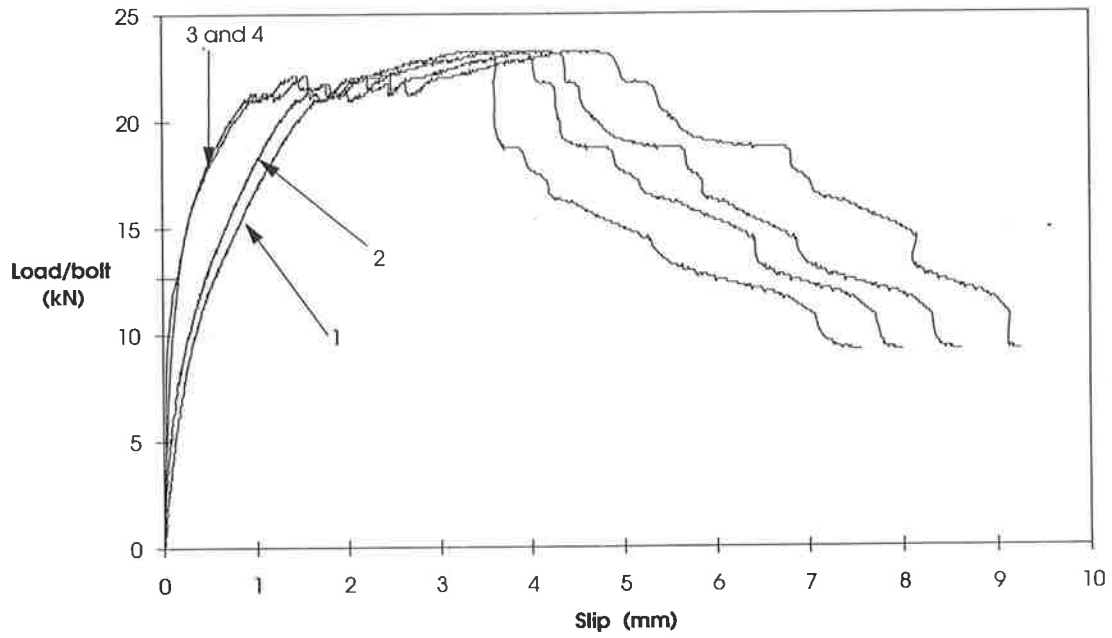

Fig. C-19 Push test P19: HIS adhesive bolt using Hilti glue

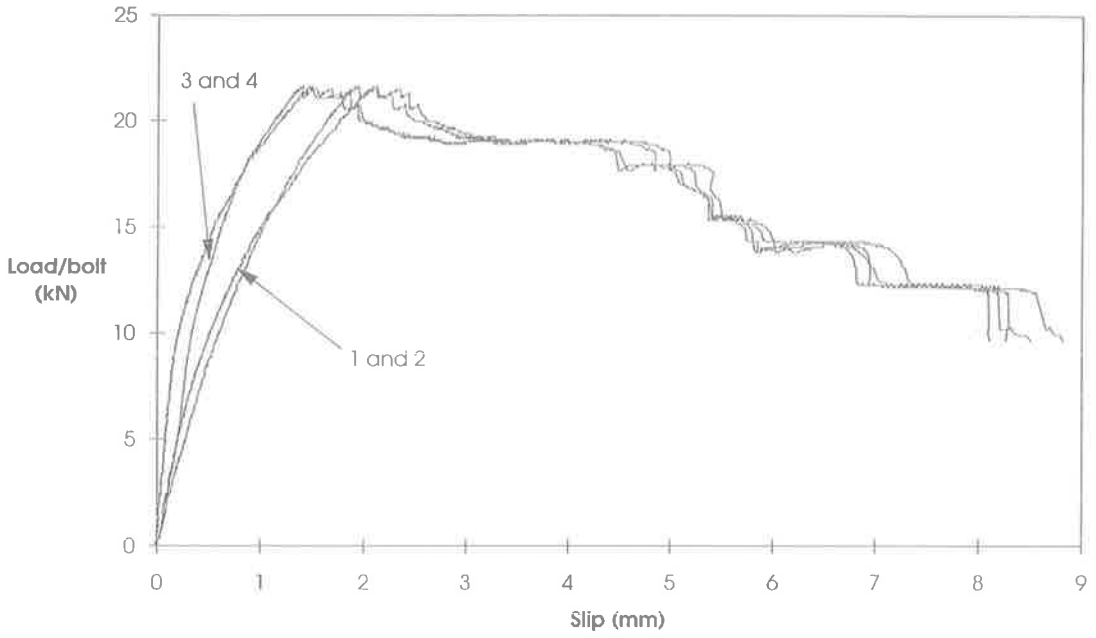

Fig. C-20 Push test P20: HIS adhesive bolt using no glue

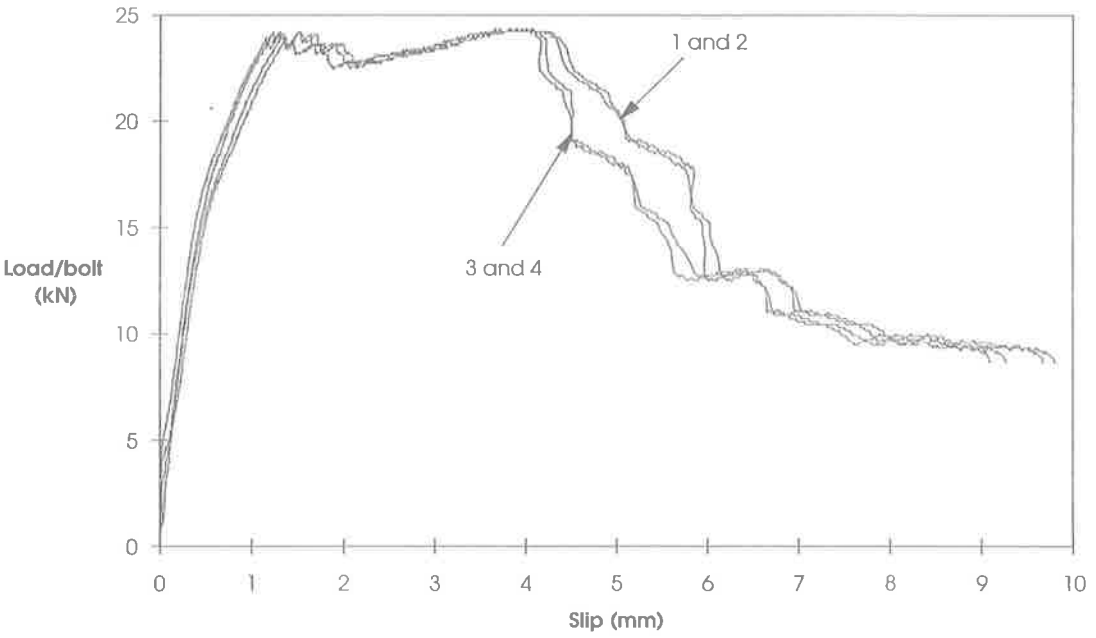

Fig. C-21 Test P21: HIS adhesive bolt with Ramset glue (Pour 4)

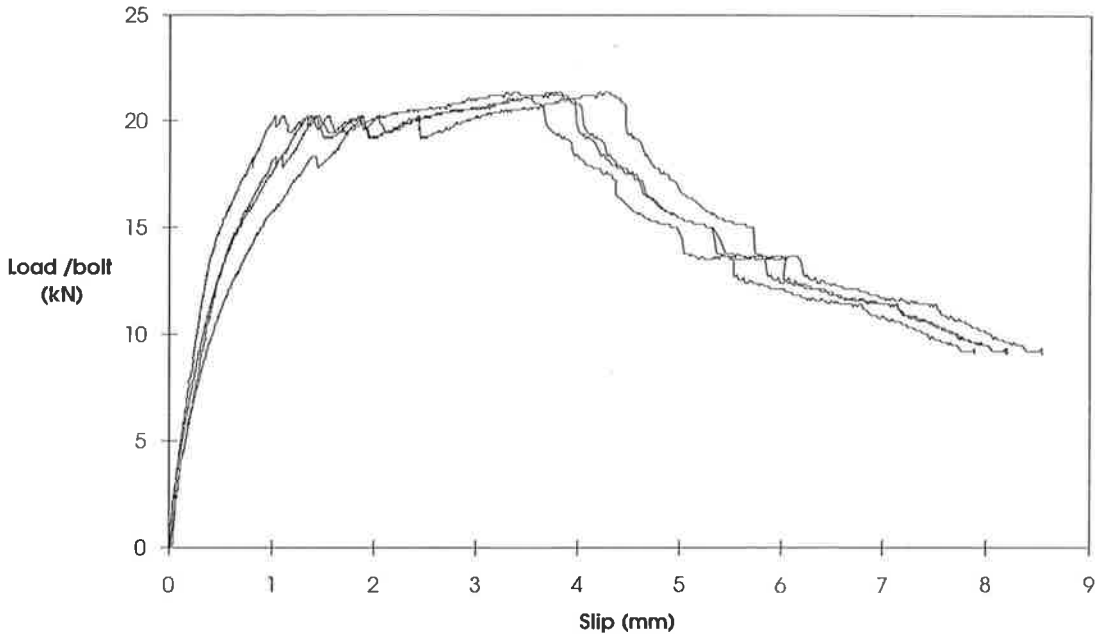

Fig. C-22 Test P22: HIS adhesive bolt with Ramset glue (Pour 4)

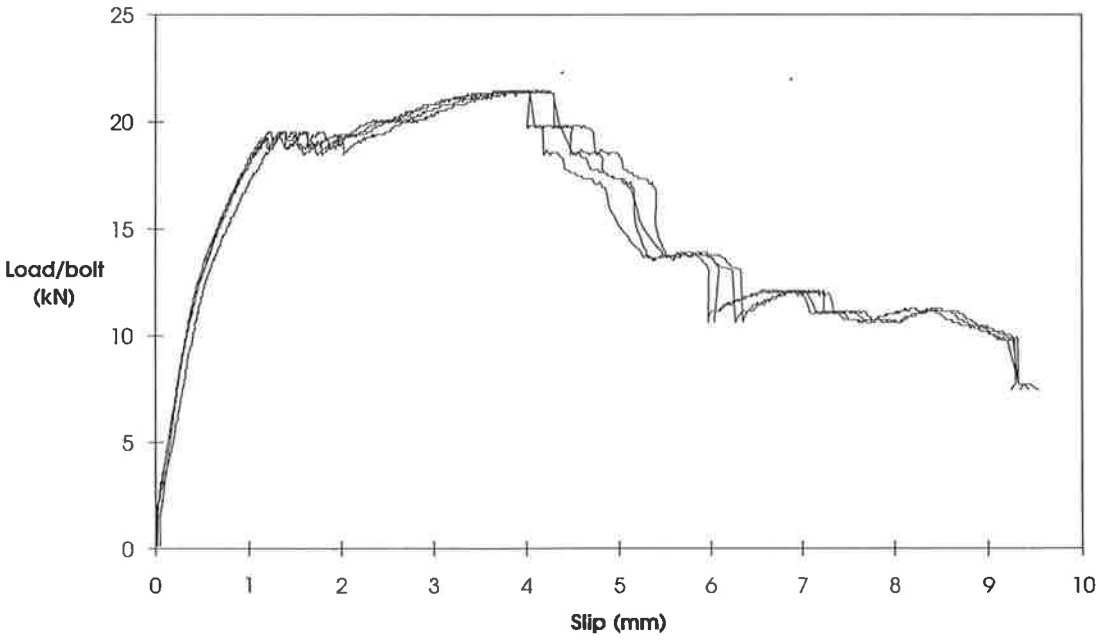

Fig. C-23 Push Test P23: HIS adhesive bolt with Ramset glue (Pour 5)

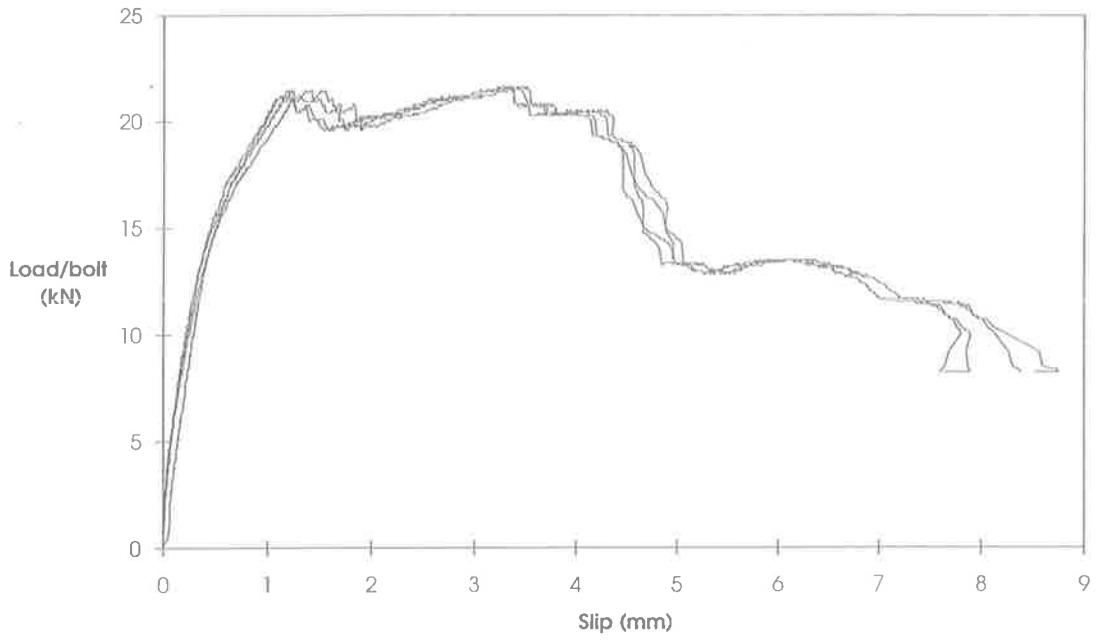

Fig. C-24 Push test P24: HIS adhesive bolt with Ramset glue (Pour 5)

Appendix D

Design of Experimental Beams using Rigid Plastic Method

The experimental beams in Chapter 8 are analysed in this appendix using the rigid plastic method. The procedure that was described in Sect. 3.2 has been used.

D.1 Series 1: Unplated Beams, A11 and A21

The design of unplated beams A11 and A21 has been shown in Fig. 8-30. The dimensions of the beams, the area and the location of the reinforcement are given below where the notations are given in Fig. D-1(a).

Width of RC beam	: b = 200 mm
Effective depth of RC beam	: d = 340 mm
Clear cover at top of the beam	: d1 = 40 mm
Area of tensile reinforcement	: A_{rt} = 942.6 mm^2
Area of compressive reinforcement	: A_{rc} = 226.4 mm^2

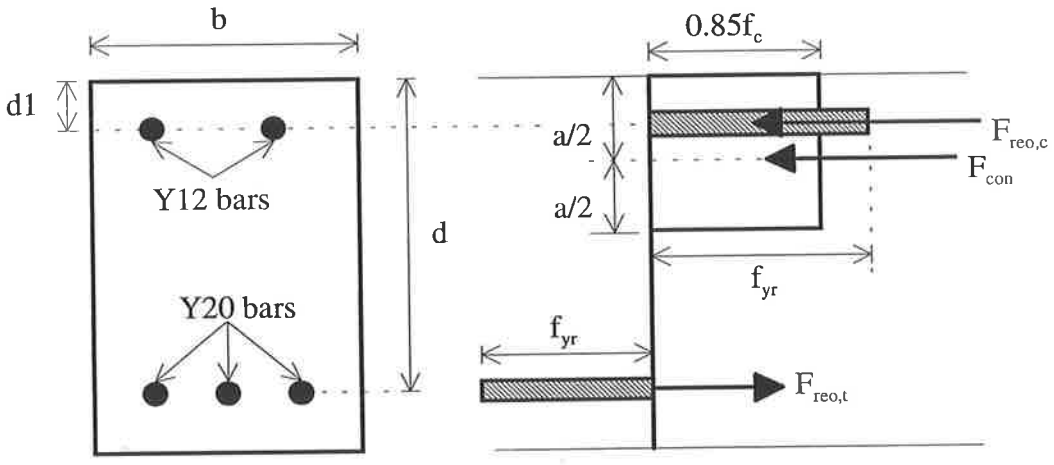

(a) RC beam (b) Stress profile

Fig. D-1 Analysis of unplated beam

The depth of the rectangular stress block, a in Fig. D-1(b) is

$$a = \frac{(A_{rt} - A_{rc})f_{yr}}{0.85 f_c b} \quad \text{.....(D.1)}$$

where, f_c = compressive strength of concrete and f_{yr} = yield strength of reinforcement. The compressive force in concrete, F_{con} in Fig. D-1(b) is

$$F_{con} = 0.85 f_c ab \quad \text{.....(D.2)}$$

The compressive force in top reinforcement, $F_{reo,c}$ is

$$F_{reo,c} = A_{rc} f_{yr} \quad \text{.....(D.3)}$$

The tensile force in bottom reinforcement, $F_{reo,t}$ is

$$F_{reo,t} = A_{rt} f_{yr} \quad \text{.....(D.4)}$$

The flexural capacity of the RC section, M is

$$M = F_{reo,t} d - F_{reo,c} d1 - F_{con} \frac{a}{2} \quad \text{.....(D.5)}$$

Equations (D.1) to (D.5) are solved using respective material properties of the beam A11 and A21 and the results are given in Table 8.1.

Table D.1 Results of unplated beam analysis (Beam A11 and A21)

Beam no.	f_c (MPa)	f_{yr} (MPa)	a mm	F_{con} (kN)	$F_{reo,c}$ (kN)	$F_{reo,t}$ (kN)	M (kNm)
1	2	3	4	5	6	7	8
Beam A11	49.2	443.0	37.9	317.3	100.3	417.6	131.9
Beam A21	45.5	432.0	40.0	309.4	978.0	407.2	128.3

D.2 Series 2: Shallow Plated Beam

In this section, the analysis of the shallow plated beams B11, B12, B13 and B24 are presented.

D.2.1 Analysis of beam B11

The cross-section of the shallow plated beam, B11 is shown in Fig. D-2(a). The parameters related to the RC part is same as the unplated beam in Sect. D.1 and those related to the plate element are given in Table D.2, where the notations are given in Fig. D-2(a) and (d). The cylinder strength of the concrete, f_c, the yield strength of reinforcement, f_{yr}, the yield strength of the plate, f_{yp} and the dowel strength of the bolted shear connector, D_{max} are given in Col. 6 to 9 respectively. The numbers of bolt in a shear span, m is given in Col. 10.

Table D.2 Geometry of plate and material properties of the elements of beam B11

	Plate element				Material properties				Nos. of bolt
Beam no.	t_p (mm)	D_b (mm)	h (mm)	h_o (mm)	f_c (MPa)	f_{yr} (MPa)	f_{yp} (MPa)	D_{max} (kN)	m (Nos)
1	2	3	4	5	6	7	8	9	10
Beam B11	6.0	12.5	145.0	185.0	49.2	443.0	377.0	21.59	44

The full-interaction analysis in Fig. D-2 is done as follows.

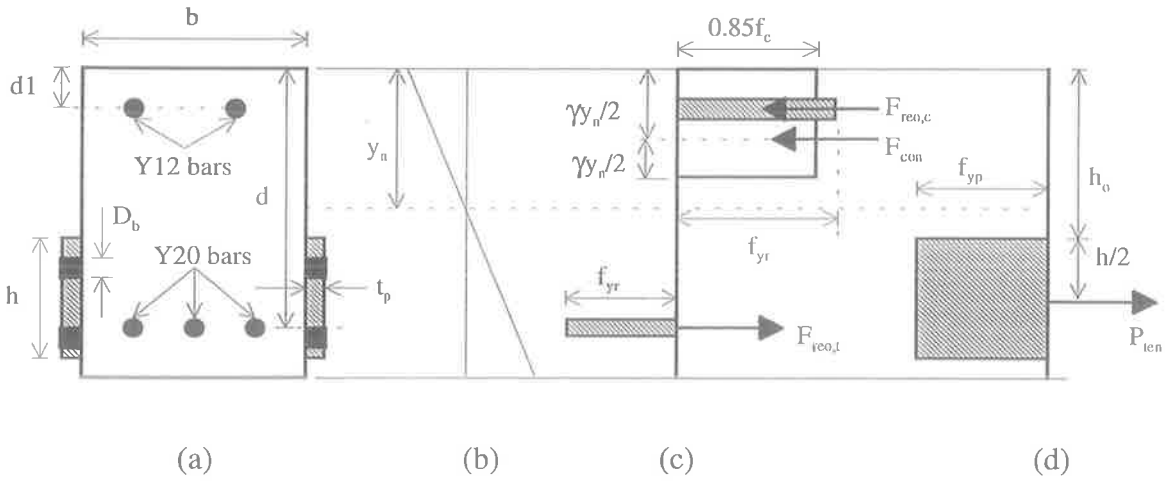

Fig. D-2 Full-shear connection and full-interaction analysis

The following equation has been used for γ, which was derived in Chapter 7 for the side plated beams.

$$\gamma = 0.997 - 0.00191(f_c - 28) \quad \text{.....(D.6)}$$

The compressive force in concrete, F_{con} in Fig. D-2(c) is

$$F_{con} = 0.85 f_c \gamma y_n b \quad \text{.....(D.7)}$$

The compressive force in top reinforcement, $F_{reo,c}$ is

$$F_{reo,c} = A_{rc} f_{yr} \quad \text{.....(D.8)}$$

The tensile force in bottom reinforcement, $F_{reo,t}$ is

$$F_{reo,t} = A_{rt} f_{yr} \quad \text{.....(D.9)}$$

The tensile force in plate, P_{ten} in Fig. D-2(d) is

$$P_{ten} = 2(ht_p - 2D_b t_p) f_{yp} \quad \text{.....(D.10)}$$

The neutral axis position, y_n in Fig. D-2(b) is

$$y_n = \frac{F_{reo,t} + P_{ten} - F_{reo,c}}{0.85 f_c \gamma b} \quad \text{.....(D.11)}$$

Using the definition in Chapter 3, the bond force, F_b is

$$F_b = P_{ten} \quad \text{.....(D.12)}$$

The flexural capacity, M is

$$M = -F_{con}\frac{\gamma y_n}{2} + F_{reo,t}d + P_{ten}\left(h_o + \frac{h}{2}\right) - F_{reo,c}d1 \quad \text{.....(D.13)}$$

The total longitudinal shear force of the bolted shear connection, P_{shear} in the shear span is

$$P_{shear} = mD_{\max} \quad \text{.....(D.14)}$$

Using the definition in Chapter 3, degree of shear connection, η is

$$\eta = \frac{P_{shear}}{F_b} \quad \text{.....(D.15)}$$

Equations (D.6) to (D.15) are solved for the beam B11 and the results are given in Table D.3.

Table D.3 Full-shear connection and full-interaction analysis of beam B11

Beam no.	y_n (mm)	F_{con} (kN)	$F_{reo,t}$ (kN)	$F_{reo,c}$ (kN)	P_{ten} (kN)	F_b (kN)	M (kNm)	m	P_{shear} (kN)	η
1	2	3	4	5	6	7	8	9	10	11
Beam B11	107.6	860.2	417.6	100.3	542.9	542.9	233.5	44	950.0	1.75

As the degree of shear connection is greater than 1 (Col. 11 of Table D.3), the full-shear connection full-interaction analysis is okay for the beam B11.

D.2.2 Analysis of beam B12

The cross-section and material properties of beam B12 are the same as beam B11, only the numbers of connectors, m is different. These are given in Table D.4.

Table D.4 Geometry of plate and material properties of the elements of beam B12

	Plate element				Material properties				Nos. of bolt
Beam no.	t_p (mm)	D_b (mm)	h (mm)	h_o (mm)	f_c (MPa)	f_{yr} (MPa)	f_{yp} (MPa)	D_{max} (kN)	m (Nos)
1	2	3	4	5	6	7	8	9	10
Beam B12	6.0	12.5	145.0	185.0	49.2	443.0	377.0	21.59	12

The full-shear connection and full-interaction analysis result of beam B12 are same as those for beam B11, as their design and material properties are the same. These are reproduced in Table D.5 for the beam B12.

Table D.5 Full-shear connection and full-interaction analysis of beam, B12

Beam no.	y_n (mm)	F_{con} (kN)	$F_{reo,t}$ (kN)	$F_{reo,c}$ (kN)	P_{ten} (kN)	F_b (kN)	M (kNm)	m	P_{shear} (kN)	η
1	2	3	4	5	6	7	8	9	10	11
Beam B11	107.6	860.2	417.6	100.3	542.9	542.9	233.5	12	259.0	0.48

The degree of shear connection is less than 1 (Col. 11 of Table D.5), so a partial shear connection analysis must be done for beam B12 as follows.

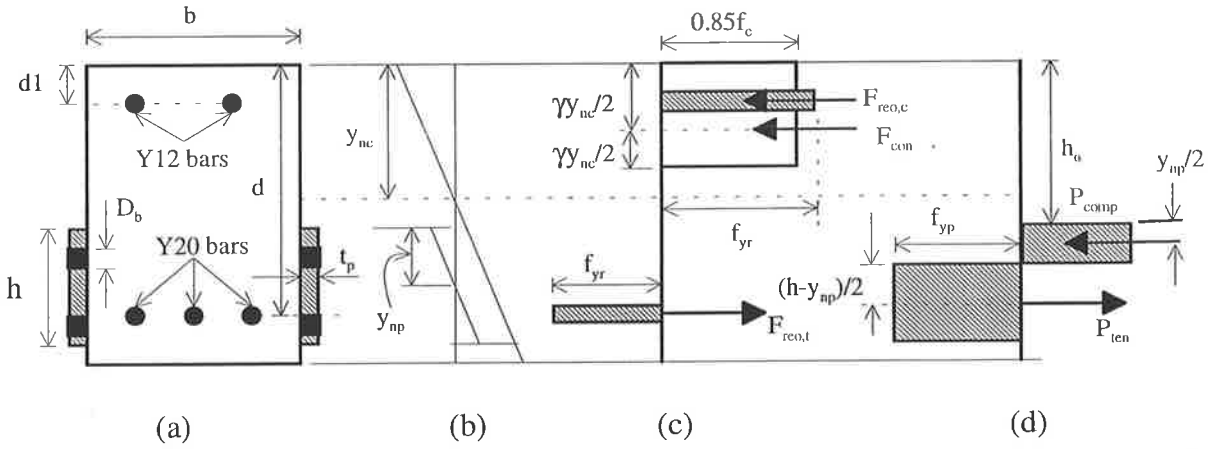

Fig. D-3 Partial-shear connection analysis

Neutral axis position in plate, y_{np} in Fig. D-3(b) is

$$y_{np} = \frac{2ht_p f_{yp} - P_{shear} x10^3}{4t_p f_{yp}} \quad \text{.....(D.16)}$$

The compressive force in plate, P_{comp} in Fig. D-3(d) is

$$P_{comp} = \left(2y_{np}t_p - 2D_b t_p\right) f_{yp} \quad \text{.....(D.17)}$$

The tensile force in plate, P_{ten} is

$$P_{ten} = \left(2\left(h - y_{np}\right)t_p - 2D_b t_p\right) f_{yp} \quad \text{.....(D.18)}$$

Neutral axis position in the concrete element, y_{nc} is

$$y_{nc} = \frac{P_{shear} x10^3 + F_{reo,t} - F_{reo,c}}{0.85 f_c \gamma b} \quad \text{.....(D.19)}$$

where $F_{reo,t}$ and $F_{reo,c}$ are given in eqns. (D.9) and (D.8) respectively. The compressive force of concrete, F_{con} in Fig. D-3(c) is

$$F_{con} = 0.85 f_c \gamma y_{nc} b \quad \text{.....(D.20)}$$

The flexural capacity, M is

$$M = -F_{con}\frac{\gamma y_{nc}}{2} + F_{reo,t}d + P_{ten}\left(h_o + y_{np} + \frac{h - y_{np}}{2}\right) - P_{comp}\left(h_o + \frac{y_{np}}{2}\right) - F_{reo,c}d1$$

.....(D.21)

The results of partial-shear connection analysis for the beam B12 are given in Table D.6.

Table D.6 Partial-shear connection analysis of beam B12

Beam no.	y_{nc} (mm)	F_{con} (kN)	$F_{reo,c}$ (kN)	$F_{reo,t}$ (kN)	y_{np} (mm)	P_{ten} (kN)	P_{comp} (kN)	M (kNm)
1	2	3	4	5	6	7	8	9
Beam B12	72.1	576.4	100.3	417.6	43.9	401.0	141.9	200.8

D.2.3 Analysis of beam B13

The cross-section of the beam is shown in Fig. D-4(a). The parameters of the RC part is the same as those given in Sect. D.1 for the unplated beams. The parameters related to the plate element, the material properties of the elements and the numbers of bolt are given in Table D.7.

Table D.7 Geometry of plate and material properties of the elements of beam B13

	Plate element				Material properties				Nos. of bolt
Beam no.	t_p (mm)	D_b (mm)	h (mm)	h_o (mm)	f_c (MPa)	f_{yr} (MPa)	f_{yp} (MPa)	D_{max} (kN)	m (Nos)
1	2	3	4	5	6	7	8	9	10
Beam B13	6.0	12.5	145.0	185.0	49.2	443.0	377.0	21.59	12

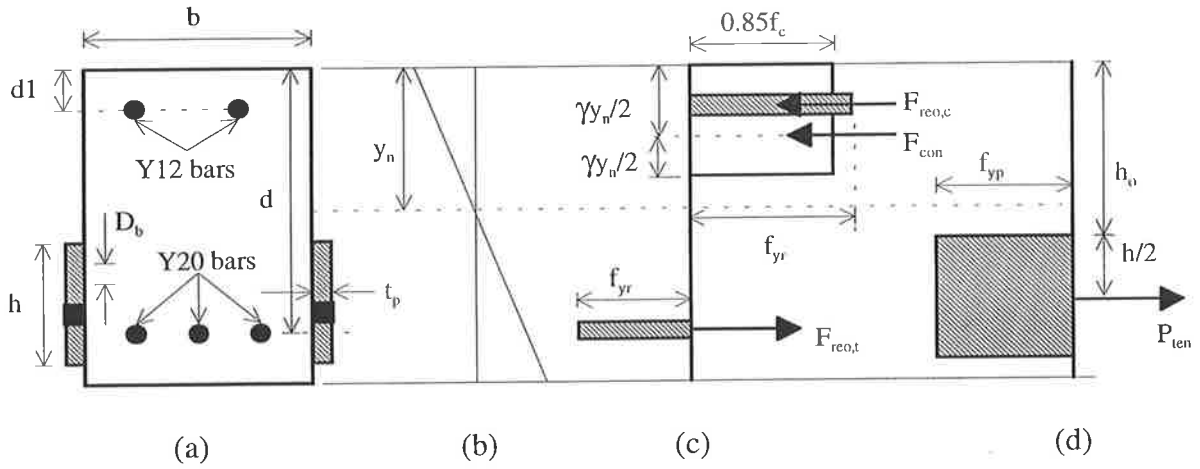

Fig. D-4 Full-shear connection full-interaction analysis

First, a full-shear connection and full-interaction analysis is done as shown in Fig. D-4. The equations of forces in the concrete element in (c) are same as those derived for beam B11. The tensile force in the plate element, P_{ten} in (d) is

$$P_{ten} = 2\left(ht_p - D_b t_p\right) f_{yp} \quad \text{.....(D.22)}$$

The equations for y_n, F_b, P_{shear} and η are the same as those described in Sect. D.2.1 for beam B11. The results are presented in Table D.8.

Table D.8 Full-shear connection and full-interaction analysis of beam B13

Beam no.	y_n (mm)	F_{con} (kN)	$F_{reo,t}$ (kN)	$F_{reo,c}$ (kN)	P_{ten} (kN)	F_b (kN)	m	P_{shear} (kN)	η
1	2	3	4	5	6	7	8	9	10
Beam B13	114.6	916.7	417.6	100.3	599.4	599.4	12	259.1	0.43

The degree of shear connection is less than 1 (Col. 10 of Table D.8), so the partial-shear connection analysis in Fig. D-5 needs to be done.

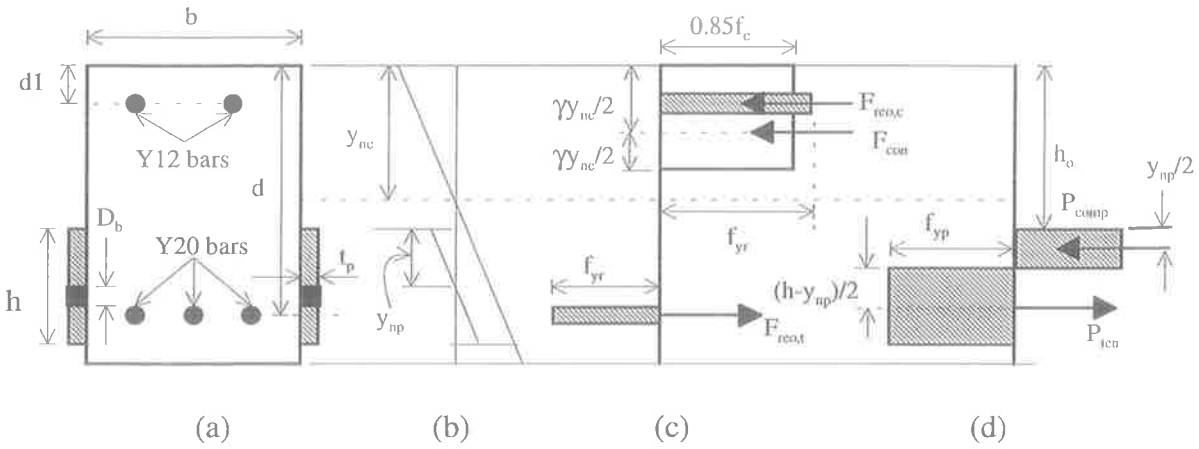

Fig. D-5 Partial-shear connection analysis

The equations of forces and neutral axis position of the concrete element in Fig. D-5(c) are the same as those given in Sect. D.2.2 for beam B12. The neutral axis position of the plate element, y_{np} is

$$y_{np} = \frac{2(ht_p - D_b t_p)f_{yp} - P_{shear}x10^3}{4t_p f_{yp}} \quad \text{.....(D.23)}$$

The compressive force in plate, P_{comp} is

$$P_{comp} = 2y_{np}t_p f_{yp} \quad \text{.....(D.24)}$$

and the equation of the tensile force in plate, P_{ten} is same as eqn. (D.17). Hence, eqn. (D.21) gives the flexural capacity, M. The results are tabulated in Table D.9.

Table D.9 Partial shear connection analsyis of beam B13

Beam no.	y_{nc} (mm)	F_{con} (kN)	$F_{reo,c}$ (kN)	$F_{reo,t}$ (kN)	y_{np} (mm)	P_{ten} (kN)	P_{comp} (kN)	M (kNm)
1	2	3	4	5	6	7	8	9
Beam B13	72.1	576.4	100.3	417.6	37.6	429.3	170.2	202.0

D.2.4 Analysis of beam B24

The cross-section of beam B24 is same as beam B11 (Fig. D-2(a)). The parameters related to the plate element, the material properties of different elements and the number of bolt in the shear span are given in Table D.10.

Table D.10 Geometries of plate and material properties of the elements of beam B24

	Plate element				Material properties				Nos. of bolt
Beam no.	t_p (mm)	D_b (mm)	h (mm)	h_o (mm)	f_c (MPa)	f_{yr} (MPa)	f_{yp} (MPa)	D_{max} (kN)	m (Nos)
1	2	3	4	5	6	7	8	9	10
Beam B24	6.0	12.5	145.0	185.0	45.5	432.0	377.0	20.52	24

The full-shear connection full-interaction analysis of beam B24 is done following the same equations of the beam B11. The results are given in Table D.11.

Table D.11 Full-shear connection and full-interaction analysis of beam B24

Beam no.	y_n (mm)	F_{con} (kN)	$F_{reo,t}$ (kN)	$F_{reo,c}$ (kN)	P_{ten} (kN)	F_b (kN)	M (kNm)	m	P_{shear} (kN)	η
1	2	3	4	5	6	7	8	9	10	11
Beam B24	127.5	950.0	407.2	97.8	542.9	542.9	219.9	24	492.5	0.91

The degree of shear connection is less than 1 (Col. 11 of Table D.11); hence partial shear connection analysis needs to be done using Fig. D-3 and following the same equations those were derived for the beam B12. The results are given in Table D.12.

Table D.12 Partial-shear connection analysis of beam B24

Beam no.	y_{nc} (mm)	F_{con} (kN)	$F_{reo,c}$ (kN)	$F_{reo,t}$ (kN)	y_{np} (mm)	P_{ten} (kN)	P_{comp} (kN)	M (kNm)
1	2	3	4	5	6	7	8	9
Beam B24	107.6	801.8	97.8	407.2	18.07	517.7	25.2	226.0

D.3 Series 3: Full depth plated beam

In this section, the analysis of deep plated beams C11 and C12 will be presented.

D.3.1 Beam C11

The cross-section of beam C11 is shown in Fig. D-6. The dimension and reinforcement of the RC part is same as the unplated beams, which has been given in Sect. D.1. The parameters related to the plate element, the material properties of different elements and the number of bolted shear connectors are given in Table D.13.

Table D.13 Geometries of plate and material properties of the elements of beam C11

	Plate element				Material properties				Nos. of bolt
Beam no.	t_p (mm)	D_b (mm)	h (mm)	h_o (mm)	f_c (MPa)	f_{yr} (MPa)	f_{yp} (MPa)	D_{max} (kN)	m (Nos)
1	2	3	4	5	6	7	8	9	10
Beam C11	6.0	12.5	290.0	40.0	49.2	443.0	377.0	21.59	20

First, a full-shear connection full-interaction analysis in Fig. D-6 is done. The equations of forces $F_{reo,c}$, $F_{reo,t}$ and F_{con} in (c) are the same as eqns. (D.8), (D.9) and (D.7) respectively. The compressive force in plate, P_{comp} is

$$P_{comp} = 2\left(\left(y_n - h_o\right)t_p - D_b t_p\right)f_{yp} \quad \text{.....(D.25)}$$

The tensile force in plate, P_{ten} is

$$P_{ten} = 2\left(\left(h + h_o - y_n\right)t_p - D_b t_p\right)f_{yp} \quad \text{.....(D.26)}$$

The position of neutral axis, y_n is

$$y_n = \frac{2f_{yp}t_p\left(h + 2h_o\right) + F_{reo,t} - F_{reo,c}}{0.85f_c\gamma b + 4t_p f_{yp}} \quad \text{.....(D.27)}$$

The bond force, F_b is

$$F_b = P_{ten} - P_{comp} \quad \text{.....(D.28)}$$

and hence, P_{shear} and η are derived from eqns. (D.14) and (D.15) respectively.

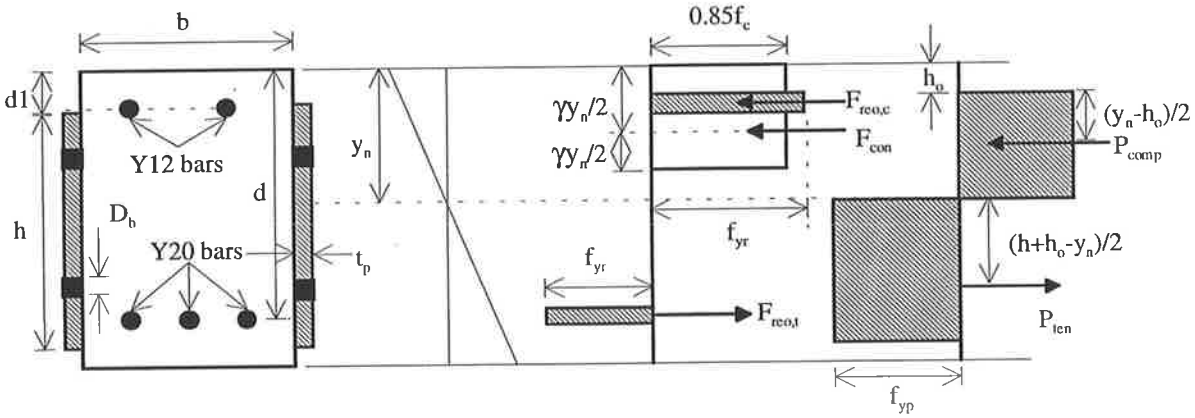

Fig.D-6 Full-shear connection full-interaction analysis of deep plated beam

The results of full-shear connection and full interaction analysis is given in Table D.14.

Table D.14 Full-shear connection and full-interaction analysis of beam C11

Beam no.	y_n (mm)	F_{con} (kN)	$F_{reo,t}$ (kN)	$F_{reo,c}$ (kN)	P_{ten} (kN)	P_{comp} (kN)	F_b (kN)	m	P_{shear} (kN)	η
1	2	3	4	5	6	7	8	9	10	11
Beam C11	116.8	934.2	417.6	100.3	907.9	291.0	616.9	20	431.8	0.70

The degree of shear connection is less than 1 (Col.11 of Table D.14); hence partial shear connection analysis will be done using Fig. D-7. The equations of beam B12 applies to beam C11, using Fig. D-7. The results are given in Table D.15.

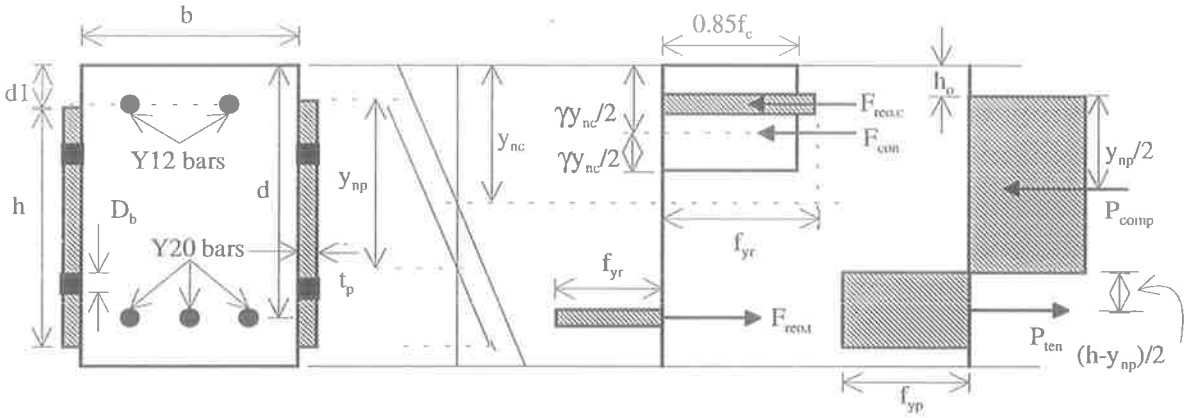

Fig. D-7 Partial-shear connection analysis

Table D.15 Partial-shear connection analysis of beam C11

Beam no.	y_{nc} (mm)	F_{con} (kN)	$F_{reo,c}$ (kN)	$F_{reo,t}$ (kN)	y_{np} (mm)	P_{ten} (kN)	P_{comp} (kN)	M (kNm)
1	2	3	4	5	6	7	8	9
Beam C11	93.68	749.1	100.3	417.6	97.3	815.3	383.5	260.9

D.3.2 Beam C12

The cross-section and material properties of the elements of beam C12 are same as the beam C11 in Fig. D-6(a). The parameters related to the plate element and material properties of different element are given in Table D.16. The number of bolt is given in Col. 10. This beam has the same full-shear connection full-interaction analysis results as beam C11, so those results are reproduced in Table D.17 for the beam C12.

Table D.16 Geometries of plate and material properties of the elements of beam C12

	Plate element				Material properties				Nos. of bolt
Beam no.	t_p (mm)	D_b (mm)	h (mm)	h_o (mm)	f_c (MPa)	f_{yr} (MPa)	f_{yp} (MPa)	D_{max} (kN)	m (Nos)
1	2	3	4	5	6	7	8	9	10
Beam C12	6.0	12.5	290.0	40.0	49.2	443.0	377.0	21.59	12

It can be seen that the degree of shear connection is less than 1 (Col. 11 of Table D.17), so a partial shear connection analysis is done using the Fig. D-7 and same equations of beam B12. The results of partial-shear connection analysis are given in Table D.18.

Table D.17 Full-shear connection and full-interaction analysis of beam C12

Beam no.	y_n (mm)	F_{con} (kN)	$F_{reo,t}$ (kN)	$F_{reo,c}$ (kN)	P_{ten} (kN)	P_{comp} (kN)	F_b (kN)	m	P_{shear} (kN)	η
1	2	3	4	5	6		7	9	10	11
Beam C12	116.8	934.2	417.6	100.3	907.9	291.0	616.9	12	259.1	0.42

Table D.18 Partial-shear connection analysis of beam C12

Beam no.	y_{nc} (mm)	F_{con} (kN)	$F_{reo,c}$ (kN)	$F_{reo,t}$ (kN)	y_{np} (mm)	P_{ten} (kN)	P_{comp} (kN)	M (kNm)
1	2	3	4	5	6	7	8	9
Beam C11	72.08	576.4	100.3	417.6	116.37	729.0	469.9	249.24

Appendix-E

Derivation of axial forces in the plate

In this appendix, the procedure that has been used to calculate the forces in the plate will be described. This is a very simple and similar procedure to that which was described in Sect. 2.5. The material properties of the plate are examined and then the procedure is given.

E.1 Stress-strain relationship of plate

The following stress-strain relationship of the plate is considered in the calculation of the stress distribution of the plate. The yield stress of the plate, f_{yp} = 377 MPa, is found experimentally in Sect. 8.2.3. The elastic modulus of plate, E_p is taken as 200,000 Mpa, a typical value for steel.

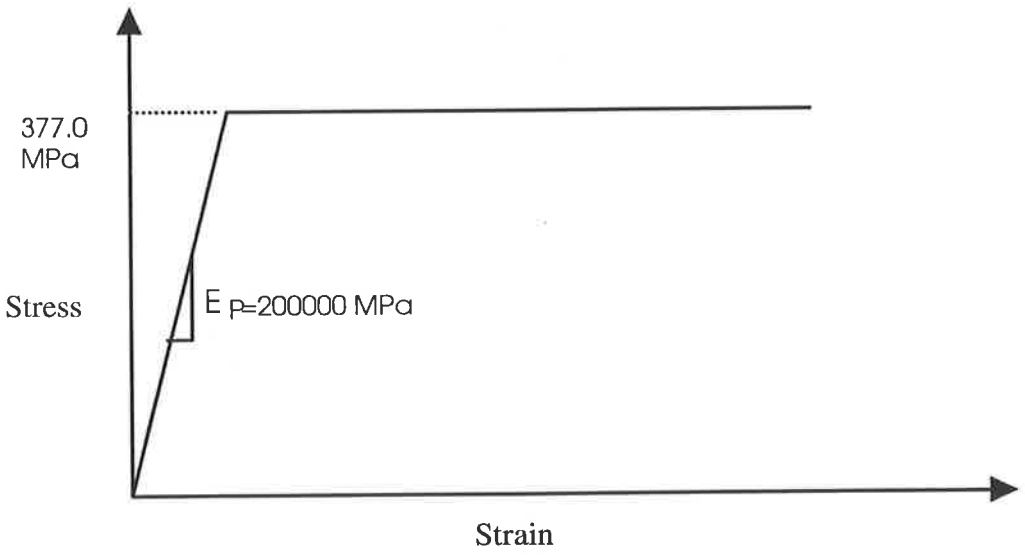

Fig. E-1 Stress-strain relationship of plate

E.2 Procedure of calculation

The strain distribution of the plate in Fig. E-2(b) is divided into 40 slices. Then strain is calculated at mid-depth of each slice. This is then used to calculate the stress in the slice from Fig. E-1 which is assumed to be act throughout the depth of the slice. This is used to calculate the force in the slice.

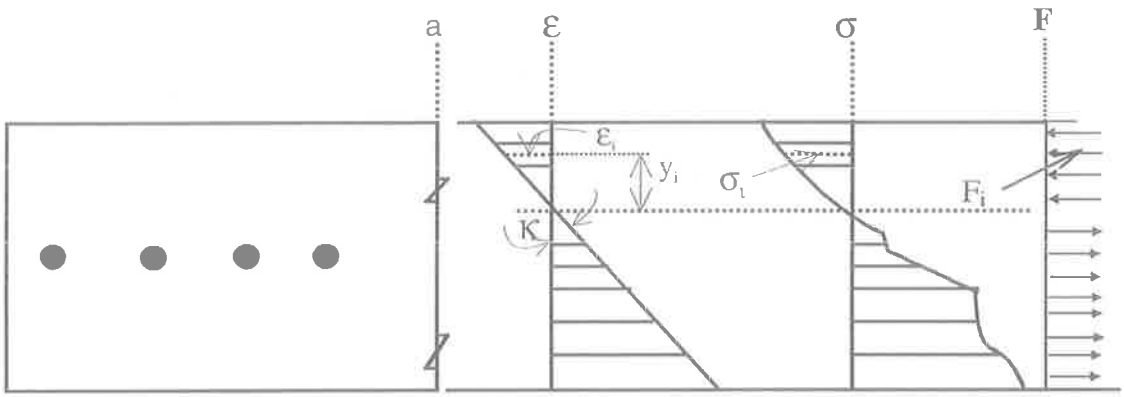

(a) Plate element **(b) Strain** **(c) Stress** **(d) Force**

Fig. E-2 Forces in the plate

Let us consider that ε_i is the strain and σ_i is the stress at the i-th slice, which gives the force in the slice F_i as

$$F_i = \sigma_i t_p d \quad \text{.....(E.1)}$$

where t_p is the thickness of the plate and d is the depth of each slice. Then, summing up the forces above neutral axis, gives the total compressive force in the plate, P_{comp}. The location of P_{comp} can be determined by equating the summation of moment contribution of each slice force above neutral axis at top of the plate to the moment contribution of resultant compressive force P_{comp} at top of the plate. In the same way, the resultant tensile force P_{ten} and its location can be determined by considering the slices below neutral axis. The resultant force in the plate is the summation of all slice forces above and below the neutral axis. Its location can be determined by equating the summation of moment contribution of all the slice forces to the moment contribution of the resultant force at any particular level.

Appendix F

Equations of Vertical Slip in terms of Curvature

In this appendix, equations of vertical slip will be derived for different loading conditions in terms of the curvature of the elements of side plated beam.

F.1 Point Load

The plated beam with an applied point load in Fig. F-1(a) will be analysed in this section. The variation of curvature in the concrete element and that in the plate element are shown in (b) and (c) respectively.

Let us first consider the curvature of concrete element in Fig. F-1(b). The general equation for the linear variation of curvature is

$$\kappa(x) = ax + b \quad \text{.....(F.1)}$$

where a is the slope of the line and b is a constant. At the support the curvature is zero, hence $\kappa(0) = 0$ when x = 0 and therefore, b = 0. Then, eqn. (F.1) is simply

$$\kappa(x) = ax \quad \text{.....(F.2)}$$

Equation (F.2) can be written as

$$\frac{d^2y}{dx^2} = \kappa(x) = ax \quad \text{.....(F.3)}$$

Integrating eqn. (F.3), we get

$$\frac{dy}{dx} = a\frac{x^2}{2} + C \quad \text{.....(F.4)}$$

where C is a constant of integration. As we are dealing with a symmetrically loaded simply supported beam, at x = L, dy/dx = 0 and therefore

$$c = -\frac{aL^2}{2} \qquad \text{.....(F.5)}$$

Inserting eqn. (F.5) into eqn. (F.4), we can write

$$\frac{dy}{dx} = a\frac{x^2}{2} - a\frac{L^2}{2} \qquad \text{.....(F.6)}$$

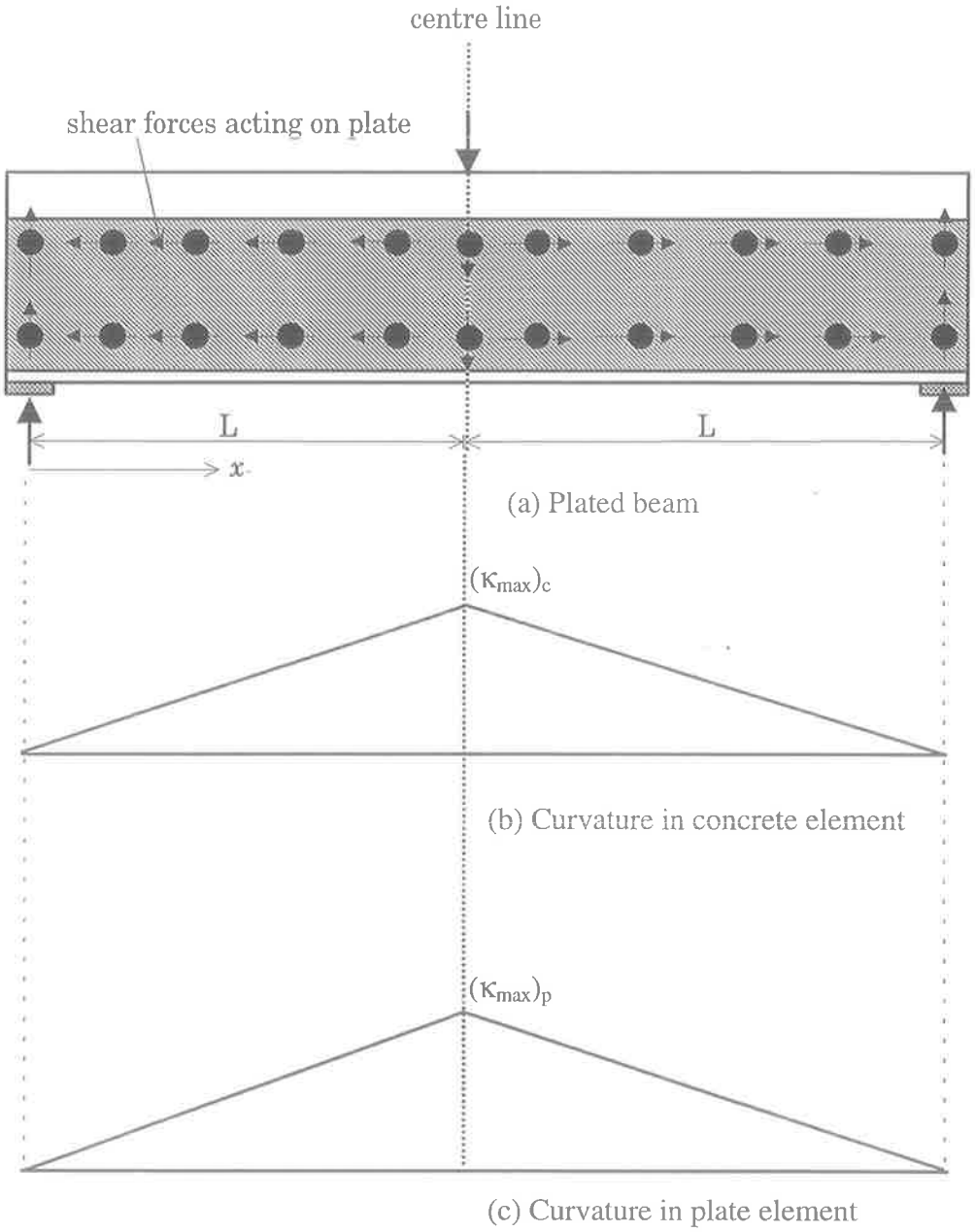

Fig. F-1 Curvature in the plated beam

Again, integrating eqn. (F.6) gives

$$y(x) = a\frac{x^3}{6} - a\frac{L^2 x}{2} + D \quad \text{.....(F.7)}$$

where D is the constant of integration. At x = 0, y(0) = 0 and therefore, D =0. Hence

$$y(x) = a\frac{x^3}{6} - a\frac{L^2 x}{2} \quad \text{.....(F.8)}$$

The deflection at x = L can be given by

$$\left(y_{x=L}\right)_c = -\frac{aL^3}{3} \quad \text{.....(F.9)}$$

We know that for a simply supported beam, curvature is maximum at the mid-span. Hence, considering $\kappa(x) = (\kappa_{max})_c$ at x = L in eqn. (F.2) gives

$$a = \frac{\left(\kappa_{max}\right)_c}{L} \quad \text{.....(F.10)}$$

Inserting eqn. (F.10) into eqn. (F.9) we get

$$\left(y_{x=L}\right)_c = -\left(\kappa_{max}\right)_c \frac{L^2}{3} \quad \text{.....(F.11)}$$

By following similar approach for the curvature in the plate element in Fig. F-1(c), following equation is derived when the deflection of the plate at the support is zero.

$$\left(y_{x=L}\right)_p = -\left(\kappa_{max}\right)_p \frac{L^2}{3} \quad \text{.....(F.12)}$$

The total vertical slip at x = L is

$$\left|\left(y_{x=L}\right)_c\right| - \left|\left(y_{x=L}\right)_p\right| = \left(s_v\right)_t \quad \text{.....(F.13)}$$

Inserting eqn. (F.11) and (F.12) gives

$$(s_v)_t = \frac{L^2}{3}\left[(\kappa_{max})_c - (\kappa_{max})_p\right] \quad \text{.....(F.14)}$$

Equation (F.14) gives the total vertical slip in the plated beam from a known curvature of the elements. Equation (4.22) gives the total vertical slip in the plated beam from the known loading condition. Hence, from eqn. (F.14) and eqn. (4.22), we get

$$L\left[\frac{F - V - qh_{na}}{(EI)_c} - \frac{V}{(EI)_p}\right] = \left[(\kappa_{max})_c - (\kappa_{max})_p\right] \quad \text{.....(F.15)}$$

from which the vertical shear forces in the plated beam can be calculated from the known curvature in the elements.

F.2 UDL loads

The plated beam in Fig. F-2(a) with an applied UDL will be analysed in this section. The variations of curvature in the concrete element and in the plate element are shown in (b) and (c) respectively.

The general equation of the curvature of the concrete element in Fig. F-2(b) can be expressed as

$$\kappa(x) = ax^2 + bx + c \quad \text{.....(F.16)}$$

where a, b and c are the constant of the curve. At x = 0, the curvature is zero and hence C =0. Therefore, eqn. (F.16) can be written as

$$\kappa(x) = ax^2 + bx \quad \text{.....(F.17)}$$

The condition of maximum curvature can be used in eqn. (F.17) to get the constants. This is done by using the following differential equation

$$\frac{d\kappa(x)}{dx} = 0 \quad \text{.....(F.18)}$$

which gives

$$2ax + b = 0 \quad \text{.....(F.19)}$$

Equation (F.19) is valid at x = L, so

$$b = -2aL \quad \text{.....(F.20)}$$

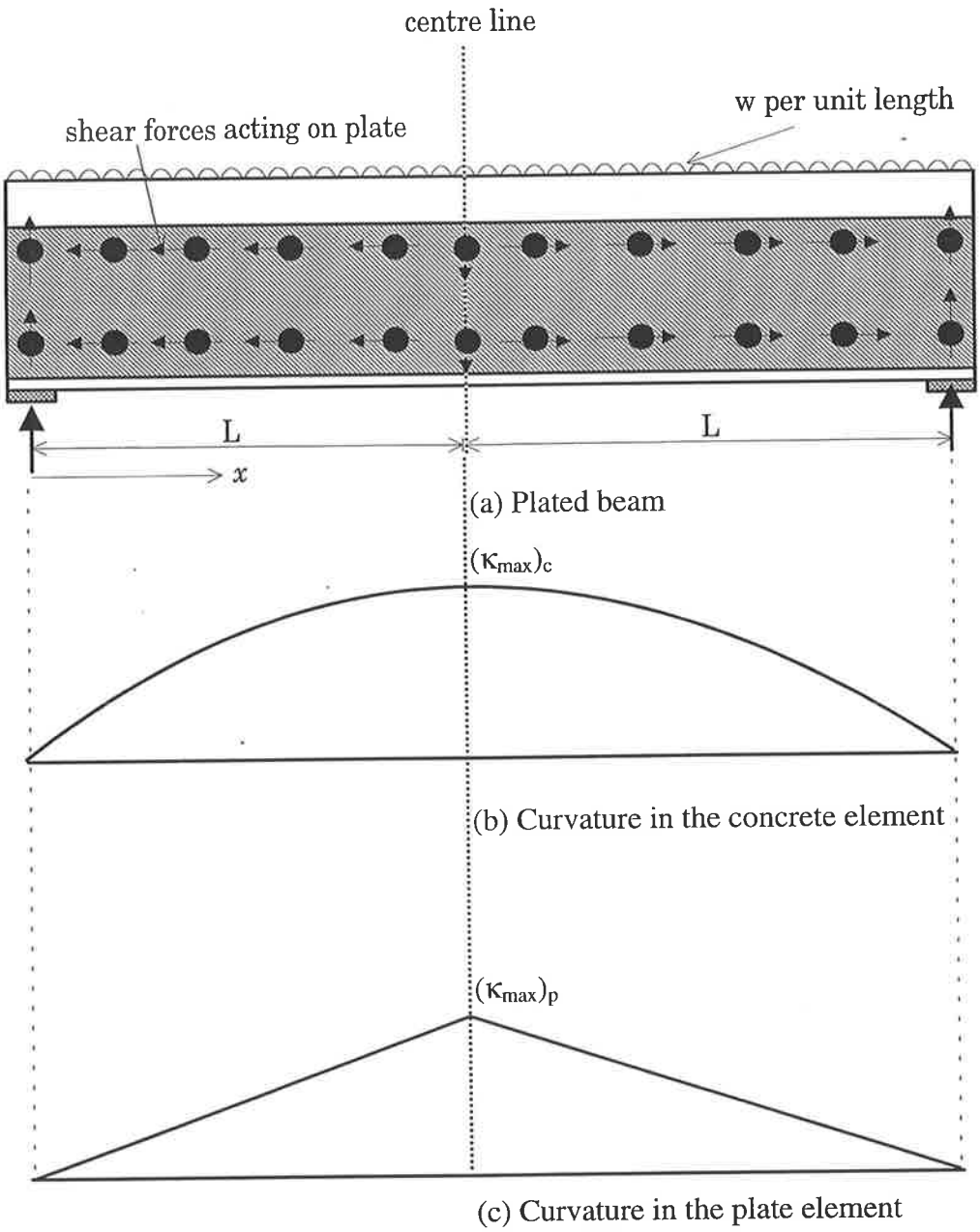

Fig. F-2 Curvatures in the plated beam

Inserting eqn. (F.20) into eqn. (F.17) gives

$$\kappa(x) = ax^2 - 2aLx \quad \text{.....(F.21)}$$

which can be written as

$$\frac{d^2y}{dx^2} = ax^2 - 2aLx \quad \text{.....(F.22)}$$

Integrating eqn. (F.22) gives

$$\frac{dy}{dx} = \frac{ax^3}{3} - aLx^2 + C \quad \text{.....(F.23)}$$

where C is a constant. At x = L, dy/dx = 0 and hence

$$C = \frac{2aL^3}{3} \quad \text{.....(F.24)}$$

Inserting eqn. (F.24) into eqn. (F.23) gives

$$\frac{dy}{dx} = \frac{ax^3}{3} - aLx^2 + \frac{2aL^3}{3} \quad \text{.....(F.25)}$$

Integrating eqn. (F.25) gives

$$y(x) = \frac{ax^4}{12} - \frac{aLx^3}{3} + \frac{2aL^3x}{3} + D \quad \text{.....(F.26)}$$

where D is a constant. At x = 0, y = 0 and hence D = 0 and therefore, eqn. (F.26) becomes

$$y(x) = \frac{ax^4}{12} - \frac{aLx^3}{3} + \frac{2aL^3x}{3} \quad \text{.....(F.27)}$$

which can be used to derive the deflection at x = L as follows.

$$\left(y_{x=L}\right)_c = \frac{5}{12}aL^4 \quad \text{.....(F.28)}$$

Now, the constant a in eqn. (F.28) can be evaluated considering $\kappa(x) = \left(\kappa_{max}\right)_c$ and x = L in eqn. (F.21), which gives

$$a = -\frac{(\kappa_{max})_c}{L^2} \quad \text{.....(F.29)}$$

and then eqn. (F.28) becomes

$$(y_{x=L})_c = -\frac{5}{12} L^2 (\kappa_{max})_c \quad \text{.....(F.30)}$$

By following a similar procedure for the linear variation of curvature in the plate element in Fig. F-2(c), the deflection in the plate element at x = L can be obtained as

$$(y_{x=L})_p = -\frac{L^2}{3} (\kappa_{max})_p \quad \text{.....(F.31)}$$

when the deflection of the plate element at the support is zero as shown in Fig. 4-7(c). Then total vertical slip of eqn. (F.13) is given by

$$(s_v)_t = \frac{5L^2}{12} (\kappa_{max})_c - \frac{L^2}{3} (\kappa_{max})_p \quad \text{.....(F.32)}$$

Another equation of total vertical slip in terms of the loads in the beam has been given in eqn. (4.29). Equating eqn. (F.32) and eqn. (4.29) gives

$$L\left[\frac{0.625wL - V - qh_{na}}{(EI)_c} - \frac{V}{(EI)_p}\right] = \left[1.25(\kappa_{max})_c - (\kappa_{max})_p\right] \quad \text{.....(F.33)}$$

which can be used to derive the vertical shear forces in the plated beam from the known curvature in the elements.

F.3 Two point loads

A side plated beam with a two point applied load is shown in Fig. F-3(a). It can be seen that there is no bolted shear connectors within the constant moment region. The curvatures in the concrete element and plate element are shown in Fig. (b) and (c) respectively.

Applying Macaulay's method (Pippard and Barker 1962), the general equation of curvature in the concrete element in Fig. F-3(b) can be written as

$$\kappa(x) = ax - a(x - L) \quad \text{.....(F.34)}$$

where a is the slope of the line up to length L. Equation (F.34) can be written as

$$\frac{d^2y}{dx^2} = ax - a(x - L) \quad \text{.....(F.35)}$$

Integrating eqn. (F.35) gives

$$\frac{dy}{dx} = \frac{ax^2}{2} - a\frac{(x-L)^2}{2} + C \quad \text{.....(F.36)}$$

where C is the constant. At x = L_1, dy/dx = 0 and hence

$$C = \frac{a\left(L^2 - 2LL_1\right)}{2} \quad \text{.....(F.37)}$$

Inserting eqn. (F.37) into eqn. (F.36) gives

$$\frac{dy}{dx} = \frac{ax^2}{2} - a\frac{(x-L)^2}{2} + \frac{a\left(L^2 - 2LL_1\right)}{2} \quad \text{.....(F.38)}$$

Integrating eqn. (F.38) gives

$$y(x) = \frac{ax^3}{6} - a\frac{(x-L)^3}{6} + \frac{a\left(L^2 - 2LL_1\right)x}{2} + D \quad \text{.....(F.39)}$$

where D is the constant. At x = 0, y = 0 and hence D = 0 and then eqn. (F.39) can be written as

$$y(x) = \frac{ax^3}{6} - a\frac{(x-L)^3}{6} + \frac{a\left(L^2 - 2LL_1\right)x}{2} \quad \text{.....(F.40)}$$

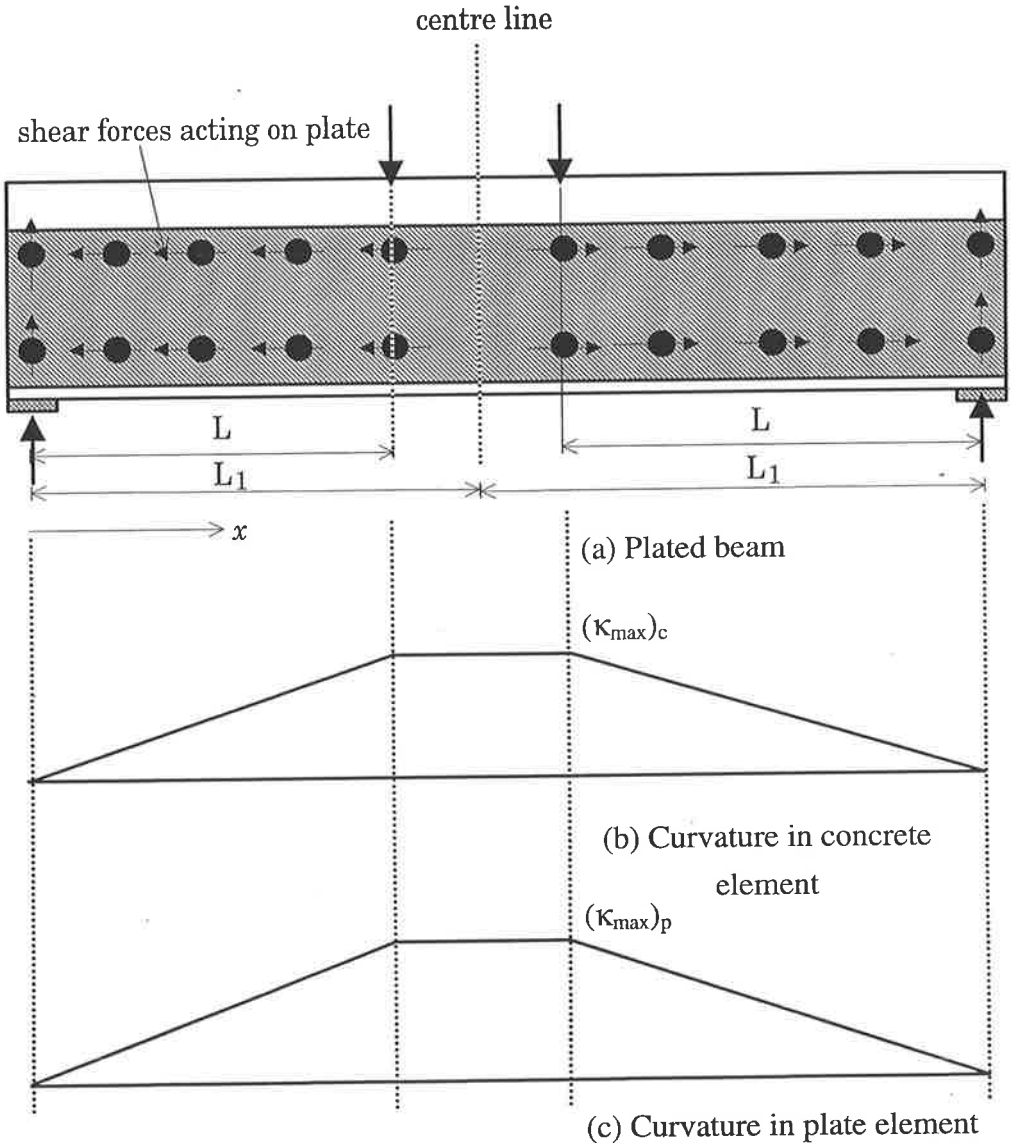

Fig. F-3 Curvatures in the plated beam

Then the deflection at x = L is

$$\left(y_{x=L}\right)_c = aL\left[\frac{L^2}{6}+\frac{L^2-2LL_1}{2}\right] \quad \text{.....(F.41)}$$

The constant a in eqn. (F.41) can be determined by putting $\kappa(x)=\left(\kappa_{\max}\right)_{conc}$ and x = L in eqn. (F.34) which gives

$$a=\frac{\left(\kappa_{\max}\right)_c}{L} \quad \text{.....(F.42)}$$

Inserting eqn. (F.42) into eqn. (F.41) gives

$$(y_{x=L})_c = (\kappa_{max})_c \left[\frac{L^2}{6} + \frac{L^2 - 2LL_1}{2} \right] \quad \text{.....(F.43)}$$

By following a similar procedure for the plate element, we get the following equation when the deflection of the plate element at the support is zero, as shown in Fig. 4-7(c).

$$(y_{x=L})_p = (\kappa_{max})_p \left[\frac{L^2}{6} + \frac{L^2 - 2LL_1}{2} \right] \quad \text{.....(F.44)}$$

Now eqn. (F.43) and eqn. (F.44) can be used in eqn. (F.13) to find the total vertical slip as follows.

$$(s_v)_t = \left[(\kappa_{max})_c - (\kappa_{max})_p \right] \left[\frac{L^2}{6} + \frac{L^2 - 2LL_1}{2} \right] \quad \text{.....(F.45)}$$

Another equation of total vertical slip has been given in eqn. (4.30). Equating eqn. (F.45) and eqn. (4.30) gives

$$L \left[\frac{F - V - qh_{na}}{(EI)_c} - \frac{V}{(EI)_p} \right] = \left[(\kappa_{max})_c - (\kappa_{max})_p \right] \quad \text{.....(F.46)}$$

which can give the total vertical shear forces in the plated beam from the known curvature in the elements.